UNIVERSITÉ DU LUXEMBOURG

PhD-FSTM-2022-031
The Faculty of Science, Technology and Medicine

DISSERTATION

Defence held on 12/04/2022 in Esch-Sur-Alzette

to obtain the degree of

DOCTEUR DE L'UNIVERSITÉ DU LUXEMBOURG

EN BIOLOGIE

by

Mathis WOLTER
Born on 13 December 1988 in Ettelbruck (Luxembourg)

EXCESSIVE MICROBIAL MUCIN FORAGING INDUCED BY DIETARY FIBER DEPRIVATION MODULATES SUSCEPTIBILITY TO INFECTIOUS AND AUTOIMMUNE DISEASES

Dissertation defence committee

Dr. Mahesh S. Desai, Dissertation Supervisor
Group Leader, Eco-Immunology and Microbiome, Luxembourg Institute of Health

Dr. Alexander Skupin, Chairman
Associate Professor, University of Luxembourg

Dr. Richard Grencis, Vice Chairman
Professor, University of Manchester

Dr. Gerard Eberl
Professor, Institut Pasteur, Paris

Dr. Eric Martens,
Professor, University of Michigan

LUXEMBOURG INSTITUTE OF HEALTH

RESEARCH DEDICATED TO LIFE

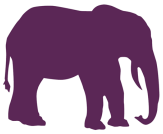

CORE

MULTI-ANNUAL THEMATIC RESEARCH PROGRAMME

Luxembourg National Research Fund

FULBRIGHT

National Institutes of Health

Turning Discovery Into Health

The work in this thesis was supported by the Luxembourg Research Fund (CORE grant number: C15/BM/10318186), the National Institute of Health (Grant number: GM099513) and by a Fulbright grant for Visiting Scholars from the Commission for Educational Exchange between the United States of America, Belgium and Luxembourg.

Affidavit

I hereby confirm that the PhD Thesis entitled "EXCESSIVE MICROBIAL MUCIN FORAGING INDUCED BY DIETARY FIBER DEPRIVATION MODULATES SUSCEPTIBILITY TO INFECTIOUS AND AUTOIMMUNE DISEASES" has been written independently and without any other sources than cited.

All animal experiments were performed according to the "Règlement Grand-Ducal du 11 janvier 2013 relatif à la protection des animaux utilisés à des fins scientifiques", based on Directive 2010/63/EU on the protection of animals used for scientific purposes. All necessary ethical approvals were obtained as appropriate by the Animal Experimentation Ethics Committee of the University of Luxembourg or the Animal Welfare Structure of the Luxembourg Institute of Health and by the Luxembourgish Ministry of Agriculture, Viticulture, and Rural Development or by University Committee for the Use and Care of Animals of the University of Michigan.

Name: Mathis WOLTER

Luxembourg, the 28th July 2022

Acknowledgements

I would like to thank everyone who supported me during my PhD thesis.

First of all I would like to thank Assoc. Prof. Dr. Mahesh Desai, my PhD supervisor, and Prof. Dr. Markus Ollert, for giving me the opportunity to research such an interesting topic at the Luxembourg Institute of Health.

I would also like to thank the members of my thesis supervision committee (CET), Assoc. Prof. Dr. Alexander Skupin, Dr. Jacques Zimmer, and Assoc. Prof. Dr. Mahesh Desai.

I am grateful to Assoc. Prof. Dr. Alexander Skupin, Assoc. Prof. Dr. Mahesh Desai, Prof. Dr Gerard Eberl, Prof. Dr. Eric Martens and Prof. Dr. Richard Grencis for agreeing to form my Dissertation Defence Committee, and to Prof. Dr. Markus Ollert and Dr. Jacques Zimmer who agreed to serve as experts in an advisory capacity.

A special thanks to Prof. Dr. Eric Martens for inviting me to work with him at the University of Michigan and the continuous collaboration.

I also gratefully acknowledge the collaboration with Prof. Dr. Richard Grencis.

Additionally, I would like to thank all of the members of the Eco-Immunology & Microbiome Group at the LIH, Dr. Alex Steimle, Dr. Marie Boudaud, Mareike Neumann, Dr. Amy Parrish, Erica Grant, Stéphanie Willieme and Alessandro De Sciscio for their advice and support.

Many thanks to my wife Ania for her encouragement and patience.

Abstract

The gastrointestinal (GI) mucus layer is a protective and lubricating hydrogel of polymer-forming glycoproteins that covers our intestinal epithelium. This mucus layer serves as an interface between the intestinal epithelium and environment as well as a as first line of defense against the potentially harmful microorganisms. While the GI mucus layer closer to the gut epithelium is highly condensed and acts as a physical barrier for invading microorganisms, further away from the epithelium, proteolytic degradation makes it loose. This looser part of the mucus layer serves as an attachment site and a nutrient source for some commensal gut bacteria. The molecular mechanisms that drive the mucus–microbe interactions are emerging and are important to understand the functional role of the gut microbiome in health and disease. Previous work by my research group showed that a dietary fiber-deprived gut microbiota erodes the colonic mucus barrier and enhances susceptibility to a mucosal pathogen *Citrobacter rodentium*, a mouse model for human *Escherichia coli* infections. In this PhD thesis, I studied role of the gut mucus layer in the context of various other infectious and autoimmune diseases by inducing the natural erosion of the mucus layer by dietary fiber deprivation. In order to unravel the mechanistic details in the intricate interactions between diet, mucus layer and gut microbiome, I leveraged our previously established gnotobiotic mouse model hosting a synthetic human gut microbiota of fully characterized 14 commensal bacteria (14SM). I employed three different types of infectious diseases for the following reasons: 1) attaching and effacing (A/E) pathogen (*C. rodentium*), to better understand which commensal bacteria aid in enhancing the pathogen susceptibility when a fiber-deprived gut microbiota erodes the mucus barrier; 2) human intracellular pathogens (*Listeria monocytogenes* and *Salmonella* Tyhimurium) to investigate, whether like the A/E pathogen,

erosion of the mucus layer could affect the infection dynamics; and 3) a mouse nematode parasite – *Trichuris muris*, which is a model for the human parasite *Trichuris trichiura* – to study how changes in the mucin–microbiome interactions drive the worm infection, as mucins play an important role in worm expulsion. In my thesis, I used various combinations of 14SM by dropping out individual or all mucin-degrading bacteria from the microbial community to show that, in the face of reduced dietary fiber, the commensal gut bacterium *Akkermansia muciniphila* is responsible for enhancing susceptibility to *C. rodentium*, most likely by eroding the protective gut mucus layer. For my experiments with intracellular pathogens (*L. monocytogenes* and *S.* Tyhimurium), I found that dietary fiber deprivation provided protection against the infection by both *L. monocytogenes* and *S.* Typhimurium. This protective effect against the pathogens was driven directly by diet and not by the microbial erosion of the mucus layer, since a similar protective effect was observed in both gnotobiotic and germ-free mice. Finally, for the helminth model, I showed that that fiber deprivation-led elevated microbial mucin foraging promotes clearance of the parasitic worm by shifting the host immune response from a susceptible, Th1 type to a resistant, Th2 type. In the context of autoimmune disease, I focused on inflammatory bowel disease (IBD). Although IBD results from genetic predisposition, the contribution of environmental triggers is thought to be crucial. Diet–gut microbiota interactions are considered to be an important environmental trigger, but the precise mechanisms are unknown. As a model for IBD, I employed IL-10$^{-/-}$ mice which are known to spontaneously develop IBD-like colitis in conventional mice. Using our 14SM gnotobiotic mouse model, I showed that in a genetically susceptible host, microbiota-mediated erosion of the mucus layer following dietary fiber deprivation is sufficient to induce lethal colitis. Furthermore, my results show that this effect was clearly dependent on interaction all three factors: microbiome, diet and genetic susceptibility. Leaving out only one of these factors eliminated the lethal phenotype. The novel findings arising from my PhD thesis will help the scientific community to enhance our understanding of the functional role of mucolytic bacteria and the GI mucus layer in shaping our health. Overall, given a reduced consumption of dietary fiber in industrialized countries

compared to developing countries, my results have profound implications for potential treatment and prevention strategies by leveraging diet to engineer the gut microbiome, especially in the context of personalized medicine.

Contents

List of Figures

1. Introduction

1.1 The colonic mucus layer

1.1.1 The structure of the colonic mucus layer

In order to sustain life, organisms need a clear separation from the environment and potential harmful organisms [1]. Outside of our body the skin fulfills this function, however, the need to actively interact with our environment on the inside of our body—for example in the form of gas exchange and nutrient uptake—requires a more dynamic solution [1]. Accordingly, these surfaces are generally covered by a protective and lubricating mucus layer which is mainly composed of mucins, highly glycosylated proteins [2]. These mucins are generally divided into transmembrane mucins and gel-forming or polymer-forming mucins [1,2]. As the name implies, transmembrane mucins are attached to the cell membrane of enterocytes and cover the apical side of the epithelium [2]. Their primary function is cell protection, but in contrast to polymer-forming mucins they are not part of the gel-like mucus layer [2]. Polymer-forming mucins are secreted by goblet cells which are highly abundant in the crypts of the colon where the mucin MUC2 is predominantly produced [2–4]. The MUC2 glycoproteins consist of a protein core which mainly incorporates PTS domains, highly repetitive domains consisting of proline, serine and threonine [5, 6], (Fig. 1.1). In the case of MUC2 the protein core is composed of approximately 5200 amino acids [3, 7], the protein core is glycosylated in the Golgi apparatus, most often by *O*-glycosylation by attachment of an *N*-acetylgalactosamine to the hydroxyl groups of threonine and serine resulting in the basal structure called Tn antigen [6, 7]. The Tn antigen structure can then be further extended by the successive action of many different glycosyltransferases,

resulting in complex and often branched *O*-glycan chains which constitute up to 80% of the mucin biomass [8]. These glycan chains are often terminally capped with glycan residues such as fucose, sialic acid or *N*-Acetylgalactosamine [1]. The extensive glycosylation protects the protein core from proteases and heavily contributes to the biophysical properties of mucin, with the glycan's high affinity to water, leading to the gel-like properties of mucin [1]. Different MUC2 glycoproteins are linked by disulfide bonds between their C- and N-termini, resulting in flat, net-like polymers which arrange in sheets forming the 50-200 µm thick, stratified mucus layer (Fig. 1.1) [5]. The part of the colonic mucus layer which is closely attached to the epithelium is highly condensed and nearly impenetrable to bacteria [5, 9]. Endogenous protease activity causes the mucus layer to expand more the further it is from the epithelium resulting in a 4 to 5-fold increase in volume [5]. Bacteria can penetrate this looser mucus, creating a natural reservoir for the commensal bacteria living in our gut [5, 10].

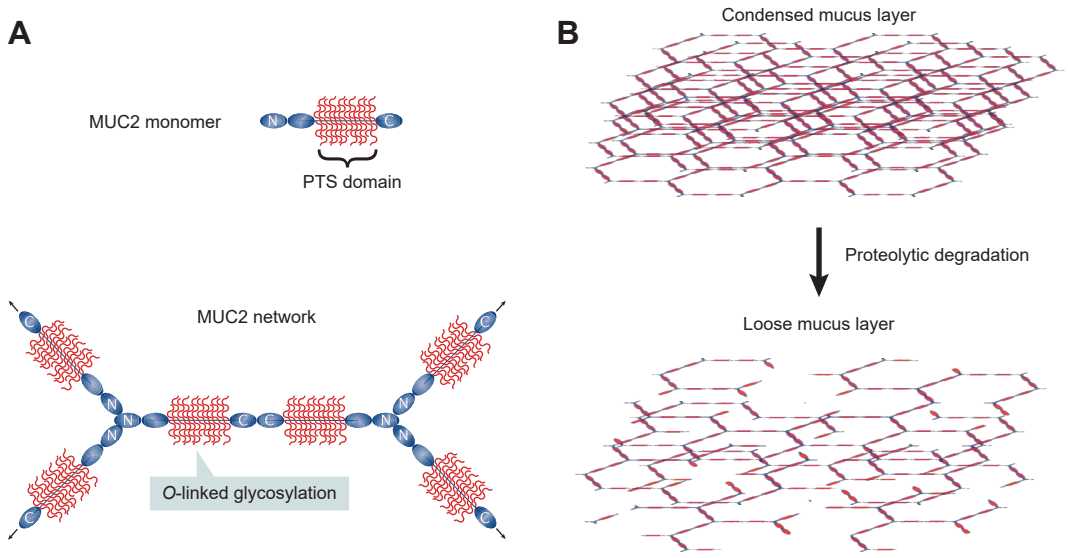

Figure 1.1 – **Mucus layer structure.** (A) MUC2 is the major constituent of the gut mucus layer. Its monomers are composed of a protein core which is mainly composed of PTS domains, highly repetitive amino acid chains rich in proline, serine and threonine. The PTS domains are highly glycosylated mostly by *O*-linked glycosylation. The C- and N-termini of the monomers are rich on cysteine allowing crosslinking by disulfide bonds resulting in its characteristic flat, net-like structure. Adapted from Martens et al., [6]. (B) The mucins are highly condensed upon secretion from goblet cells, but endogenous protease activity results in a looser layer further from the epithelium. Adapted from Johansson et al., [5].

1.1.2 Mucus-gut bacteria interactions

The functions of the colonic mucus is manifold: as a hydrogel it hydrates the epithelium and acts as lubricant, improving the passage of food and debris through the gastrointestinal tract and protecting the epithelium from mechanical damage [2, 11, 12]. Furthermore it protects the epithelium from dehydration and against chemical damage [13–16]. However the gut mucus layer also serves as interface between the intestinal epithelium and the environment and as such serves as first line of defense against potentially harmful microorganisms. In this context, the mucus layer serves as physical barrier preventing attachment of bacteria to the epithelium [12, 17] and can prevent biofilm formation [17, 18]. Additionally, the gut

mucus barrier serves also as locus for the intricate interactions of bacteria and the host immune system and consequently is as reservoir for immune mediators such as IgA [19], Reg3γ [20] or Dual oxidase 2, an important source of hydrogen peroxide [21]. Interestingly, bacteriophages also bind to the host mucins, providing another layer of protection against potential harmful bacteria [22]. However, interactions between mucus and bacteria are not limited to the protective role of the gut mucus. Many of the commensal bacteria living in our gut inhabit the looser part of the mucus layer where it serves as attachment site and potential nutrient source [5, 23, 24]. Given they have the proper enzymatic capabilities, the gut mucus layer can serve as nutrient source for these bacteria and other commensal bacteria which scavenge the glycan residues released by these so-called mucolytic bacteria [24, 25]. Mucolytic bacteria can be divided into mucin specialists and mucin generalists. Mucin specialist, such as *Akkermansia muciniphila* or *Barnesiella intestinihomis*, are specialized and thus depended on the utilization of mucin glycans [26, 27]. In contrast mucin generalists such as *Bacteroides caccae* or *Bacteroides thetaiotaomicron* have a wide variety of other carbohydrate degrading activities and are capable of, but not completely dependent on, mucin degradation [26, 28]. By creating this living niche for the commensal bacteria, the host receives a plethora of benefits in turn. The commensal bacteria compete with invading bacteria for nutrients, produce bacteriocins and secondary bile acids which can inhibit pathogens, and their fermentation of both dietary fiber and mucins results in host-beneficial short-chain fatty acids (SCFAs) [29–31]. Furthermore, commensal bacteria and their products are essential for the integrity of gut mucus layer, as the absence of bacteria results in a decreased number of mucus-filled goblet cells, as well as, a thinner, more penetrable mucus layer with an altered glycosylation [26, 32, 33]. In conclusion, mucus-bacteria interactions are highly varied, bi-directional and highly context-dependent. Broadly speaking, the mucus layer protects the host from potential pathogens, but at the same time hosts commensal bacteria, in turn commensal bacteria produce host-beneficial metabolites while pathogens try to avoid or penetrate the mucosal barrier in order to infect the host.

1.2 The human gut microbiome

1.2.1 The definition of microbiome and microbiota

Microbial communities are defined as multi-species assemblages, in which (micro-)organisms interact with each other in a contiguous environment [34] and a microbiome is considered a specific type of microbial community with distinct properties, functions and interactions with its environment. Over time, many different definitions have been given, but they often fail to capture the full complexity of the microbiome often limiting the definition to the metagenome or the community of microorganisms without capturing the host and environment factors which must be considered an integral component of the microbiome [35]. In the frame of the Microbiome Support project, a panel of international experts convened with the purpose to propose consensus definition based on the current knowledge of the microbiome [35]. They suggested the use of the original microbiome definition put forward by Whipps et al, [36] and extending it by clearly defining the difference between microbiome and microbiota (Fig. 1.2). The microbiota being defined as "the assembly of microorganisms belonging to the different kingdoms", encompassing Prokaryotes (Bacteria & Archaea) and Eukaryotes (Protozoa, Fungi and Algae), but not viruses, phages, plasmids and mobile genetic elements as they are usually not considered living microorganisms [35]. In contrast the microbiome is defined as "a characteristic microbial community occupying a reasonable well-defined habitat which has distinct physio-chemical properties" [35]. As such it does not only encompass the microorganisms, but also the functional aspects of the microbiota, such as structural components and metabolites, as well as, viruses, phages, plasmids and mobile genetic elements [35]. Finally, the surrounding macro-ecosystems are also considered, which includes environmental factors which are crucial for the functioning and health of the microbial ecosystem (e.g. the eukaryotic hosts) [35].

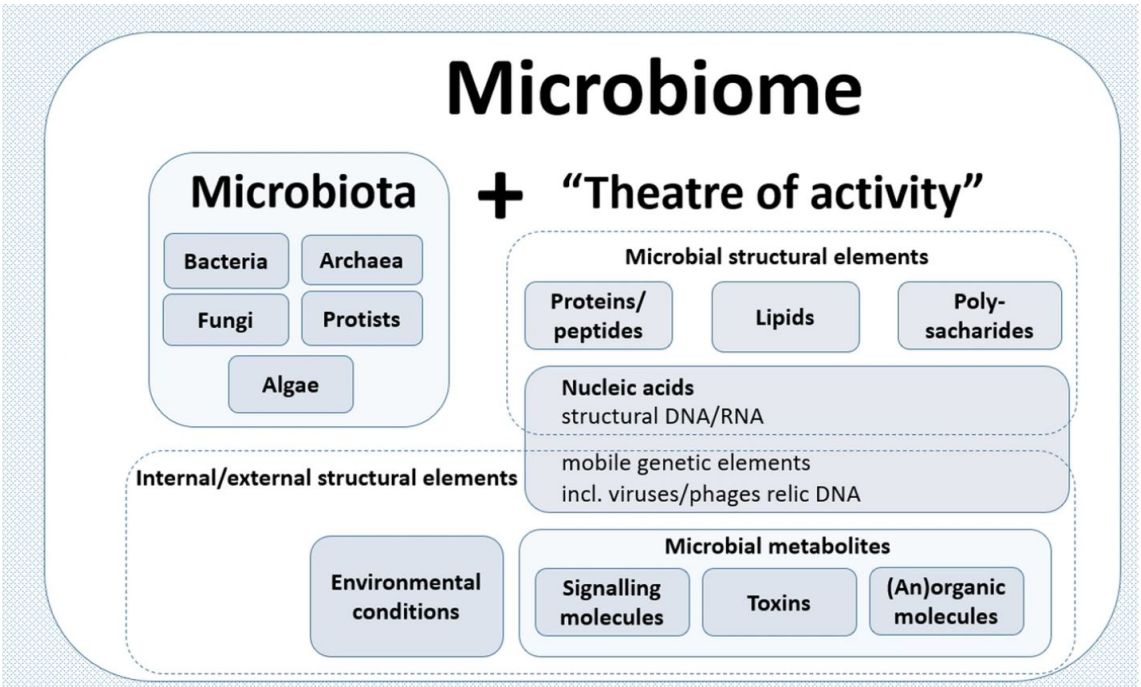

Figure 1.2 – **Schematic figure of the microbiota and microbiome definition.** The microbiota is the assembly of microorganisms belonging to the different kingdoms. In contrast, the microbiome includes the so-called "theatre of activity" of the microbiota in its definition, meaning it includes microbial, internal and external structure elements [35].

1.2.2 The characterization of the human gut microbiota

The estimated ratio of human cells to bacteria residing on our body is 1:1.3 and of all the human body sites the colon is the far most densely populated harboring around 10^{13}–10^{14} bacteria [37]. The initial microbiome is mostly established very selectively by exposure to the maternal microbiome and the microbiome becomes fairly quickly resilient to changes even in infants [38]. The pioneering work of the human microbiome project, has established that the microbial flora of a healthy, human adult is generally dominated by the phyla *Firmicutes* and Bacteroidetes (Fig. 1.3) [39]. Nonetheless contact with other humans or species, environmental stimuli as well as lifestyle choices shape the microbiome short-term, long-term and throughout generations [40–42]. As such, there exists a substantial amount of interpersonal variation in addition to a less pronounced temporal variation [43].

Despite extensive efforts to characterize the human gut microbiome in detail and to identify stable microbial patterns in the form of enterotypes and core microbiomes [44, 45], it has become apparent that phyla are an insufficient level of characterization in the context of human health and disease [46, 47]. As a result, the focus has shifted partially towards a more precise taxonomic classifications, but above all towards characterization of metabolic functions in order to better grasp the complexity of the human gut microbiome [47, 48].

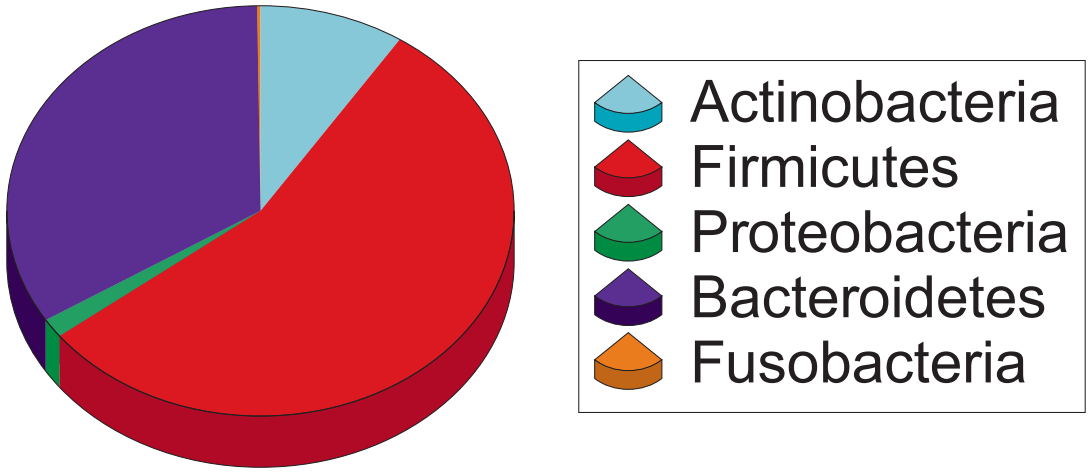

Figure 1.3 – **The average colonic microbiome composition of a healthy human adult.** The colonic microbiome of a healthy human adult is dominated by the phyla *Bacteroidetes* and *Firmicutes*, but the individual composition is highly variable and depends on a number environmental factors. Adapted from Cho et al. [49]

1.2.3 Leveraging diet to engineer our gut microbiome

Of all environmental factors, diet is the most significantly associated with our gut microbiome composition. Considering the essential role of our microbiome in shaping our health and disease, this raises the question how exactly diet-microbiome interactions affect the host and if these interactions could be leveraged to our benefit. The following part of the introduction consists of a comprehensive perspective article in which we consolidate knowledge about diet-microbiome interactions and their impact on host immunity with a focus on autoimmune diseases. By understanding the impact of individual dietary components on

the metabolic output of the gut microbiome as well as the host physiology, we can explore diet-based methods and concepts to treat or prevent autoimmune disease aiming to return a disrupted gut microbiome back to a functionally health state. Finally, we discuss how personalized dietary intervention could optimize existing or conceptual microbiome-modulating tools such as fecal microbiota transplantation, probiotics and orthogonal niche.

Personal contributions: I share the co-first authorship of this review published in Nature Reviews Gastroenterology & Hepatology with E. Grant. I had significant contributions concerning the design, initial outline and abstract of the perspective, including the coordination of the different authors and the consolidating, refinement and revision of the different sections. I contributed the dietary fat metabolism section and the diet-assisted therapies chapter. Finally, I also contributed the concept and drawing of Figure 2, parts of the introduction, challenges and future directions and conclusion sections.

Leveraging diet to engineer the gut microbiome

Mathis Wolter, Erica T. Grant, Marie Boudaud, Alex Steimle, Gabriel V. Pereira, Eric C. Martens and Mahesh S. Desai

Abstract | Autoimmune diseases, including inflammatory bowel disease, multiple sclerosis and rheumatoid arthritis, have distinct clinical presentations but share underlying patterns of gut microbiome perturbation and intestinal barrier dysfunction. Their potentially common microbial drivers advocate for treatment strategies aimed at restoring appropriate microbiome function, but individual variation in host factors makes a uniform approach unlikely. In this Perspective, we consolidate knowledge on diet–microbiome interactions in local inflammation, gut microbiota imbalance and host immune dysregulation. By understanding and incorporating the effects of individual dietary components on microbial metabolic output and host physiology, we examine the potential for diet-based therapies for autoimmune disease prevention and treatment. We also discuss tools targeting the gut microbiome, such as faecal microbiota transplantation, probiotics and orthogonal niche engineering, which could be optimized using custom dietary interventions. These approaches highlight paths towards leveraging diet for precise engineering of the gut microbiome at a time of increasing autoimmune disease.

Autoimmune diseases are characterized by an immune system that erroneously attacks healthy host cells; examples include multiple sclerosis, type 1 diabetes mellitus (T1DM), rheumatoid arthritis, systemic lupus erythematosus (SLE) and inflammatory bowel disease (IBD). During the past century, the incidence of autoimmune diseases has overtaken that of infectious diseases in industrialized countries[1], reflecting their growing public health burden globally. The onset and progression of these multifactorial disorders is commonly thought to be influenced by genetics[2,3], environmental factors (for example, diet[4] or pathogen exposure[5]) and the microbiome[6]. Existing treatments focus on dampening the immune response, which can be problematic owing to the potential increased risk of infection or cancer[7]. In the past decades, it has become clear that autoimmune diseases are also characterized by distinct, 'dysbiotic' gut microbiomes, which represent a departure from a stable, 'healthy' state[6]. Furthermore, the likelihood of a patient with IBD or rheumatoid arthritis responding to treatment can be predicted by the patient's gut microbiome composition, function or drug metabolism[8–10], presenting an alternative target for treatment. The gut microbiome modulates innate and adaptive immunity in mammalian hosts, either directly or via diet-derived metabolites[11–13]; thus, there is interest in prevention or management of various autoimmune diseases, including multiple sclerosis[14] and IBD[15], by altering the gut microbiota composition or its activity.

The intimate link between diet, the gut microbiome and host health is reflected in their correlated trends throughout human history, as depicted in FIG. 1. Although there is substantial heterogeneity in global diet patterns[16], meat consumption and food processing has generally risen over time, with marked increases in the Neolithic period (ca. 10,000–4,500 BCE) and at the start of the Industrial Revolution (ca. 1760–1840)[17], whereas intake of diverse plant-sourced foods has decreased[17]. When comparing the gut microbiomes of individuals in modern hunter-gatherer communities with those of individuals in industrialized societies, changes have been observed in microbial functional capacity; for example, in the abundance of genes encoding microbial carbohydrate-active enzymes (CAZymes)[18,19]. CAZymes are enzymes responsible for the breakdown, modification or synthesis of glycoconjugates, oligosaccharides and polysaccharides, which are found abundantly encoded in the human gut microbiome[20]. Changes in the abundance of various types of CAZymes reflect the selective pressures of the host's diet on the gut microbial community. However, the lack of causal data in humans makes it impossible to conclude that the modernization of diet is the primary driver of these changes; other factors such as changing exposure to antibiotics and infectious diseases cannot be ruled out. Nonetheless, the observation that dietary shifts correlate with the rise of autoimmune diseases[21] has prompted the formulation of diets aimed at restoring immune homeostasis, such as the autoimmune protocol (AIP) diet, a version of the paleo diet designed to aid in the treatment of various autoimmune diseases through avoidance of foods that may trigger gut inflammation[22,23]. These diets embrace the compelling concept of an 'evolutionary mismatch'[17] between humans and the modern environment. Proponents of this hypothesis argue that humans evolved under a drastically different dietary environment and modern diseases are a result of our maladaptation to the current environment. Modern, Western-style diets, for example, do not adequately support a diverse and resilient microbiome[24], leading to irregular antigen detection and improper immune development.

Nevertheless, it is prudent to caution against the fallacy that what is considered 'natural' is unquestionably good for health. Although early evidence supports the ability of the AIP diet to reduce transcriptional markers of inflammation[25] in patients with IBD, incorporation of this diet into treatment of other autoimmune diseases lags behind. Well-designed investigations and peer-reviewed findings are needed to understand the effect of a paleo-like diet on disease progression in other contexts. Furthermore, global societies have advanced considerably since

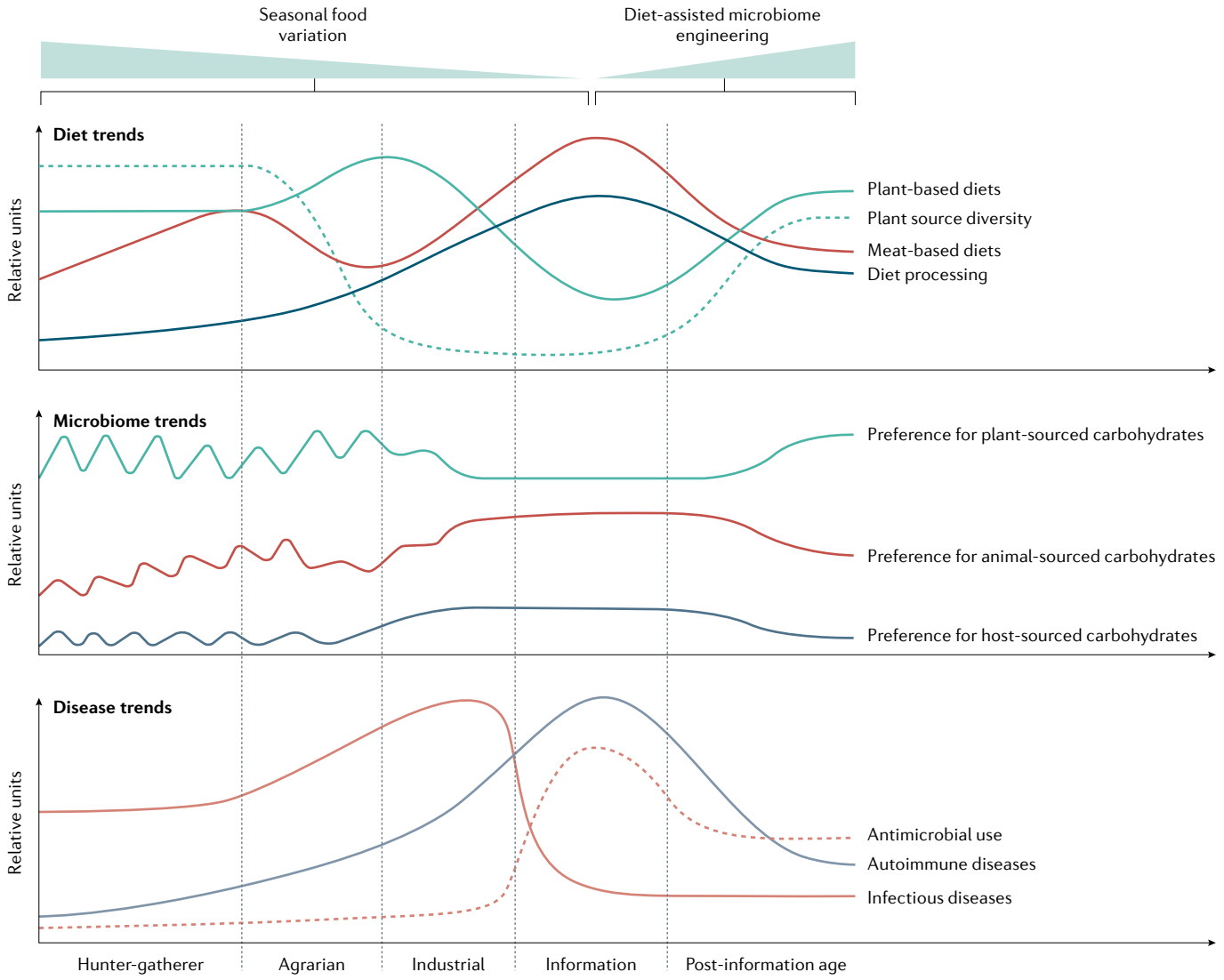

Fig. 1 | **Temporal trends in human host, the gut microbiome and diet.** The social and technological revolutions that accompany each historic period (hunter-gatherer, agrarian, industrial, information and post-information age) mark major shifts in diet, microbial activity and disease. Adapted from various reports, this graphical illustration presents trends in diet proportionally, in the absence of actual intake estimates during these periods, including the relatively high meat consumption of many, though not all, hunter-gatherer societies[235,236], the rise of cereals in the agricultural revolution[237], the decrease in diversity of plant-food sources and the rise in food processing[17]. The estimation of the gut microbiome carbohydrate preference is based on the abundance of genes encoding carbohydrate-active enzymes (CAZymes) specific to a particular carbohydrate source (plant, animal or host mucin). The carbohydrate preferences are based on data collected from the Hadza people, a modern hunter-gatherer society with fluctuating CAZyme abundances, based on seasonal food availability[19]. The Hadza community is used as a proxy for the ancestral microbiome because their lifestyle is presumed to have been least altered by overall dietary shifts accompanying the social ages[19]. Carbohydrate preferences of present-day microbiomes are estimated from the Human Microbiome Project, similarly adapted from Smits et al.[19]. Disease trends appear to be associated with concomitant changes in gut microbiome enzymatic capacity and diet. Historic and predicted trends in infectious disease burden[1] are displayed, with increases accompanying the agricultural revolution and population growth[237] before being largely quelled by antibiotics[26]. Meanwhile, the burden of autoimmune disease similarly rises through history, tracking complex dietary and microbial changes. Based on existing and emerging insights, we predict where each of these trends may settle, as we gain the ability to manipulate these factors for optimal health.

the Palaeolithic era of hunter-gatherers owing to domestication of crops based on yield, improved sanitation and longevity, as well as the discovery of antibiotics[26] and the associated decreased infectious disease burden[1]. Some of these changes might contribute to disease by removing normal exposure to microorganisms. This concept is summarized in the hygiene hypothesis[5,12], which postulates that the rise in autoimmune diseases and related inflammatory disorders might be the result of a hyper-hygienic environment — especially in early life — and that this lack of exposure to microorganisms prevents the normal development of immune tolerance. However, the path to optimizing human health is not as simple as mirroring the diet of our ancestors or increasing our exposure to microorganisms. Ultimately, our past and present environments are fundamentally and perhaps irreversibly distinct; therefore, the goal of dietary interventions targeting the microbiome should not be to return to an ancestral state, but rather to manipulate our microbiomes and optimize host health in a directed adaptation to an increasingly industrialized world (FIG. 1).

The approach to autoimmune disease treatment is shifting to capitalize on the

integration of multiomics data and the recognition that humans are highly individualized holobionts, which, after thousands of years of co-evolution, cannot truly be considered independent of our microbial inhabitants[27]. Although clinicians point to the need for further translational research in this area[28], existing evidence from genome-wide association studies and animal models suggests that autoimmune diseases might share a common underlying mechanism, namely the impairment of intestinal barrier function, colloquially termed 'leaky gut'[29], which leads to atypical external antigen detection and subsequent immune dysregulation[12,13,30,31] (FIG. 2). The increasingly apparent linkage between diet, the gut microbiome and host health underscores the potential to use personalized therapeutic diets to modulate the gut microbiome for improved autoimmune disease treatment efficacy. Concerted efforts by researchers and clinicians are needed to understand how diet and gut microbiome interactions influence individual responses to therapies[32] and to exploit the available tools for eventual manipulation of the gut microbiome in support of existing therapies[33]. Indeed, aside from biological agents or synthetic drugs, preclinical research and clinical trials for new autoimmune disease therapies largely aim to target or restructure the gut microbiome, restore intestinal barrier function or affect both using nutritional interventions[7].

In this Perspective, we consider the potential for leveraging diet and individual dietary components to counteract autoimmune disease progression via microbiome engineering. Although this term is largely used in the context of synthetic biology applications, which focus on genetic engineering to modify physiological processes[34], we use it here to encompass the alteration of the complex gut microbiome community or its metabolic output based on mechanistic knowledge of the interactions and environmental factors involved to achieve a more disease-resistant, homeostatic microbiome. We will not cover

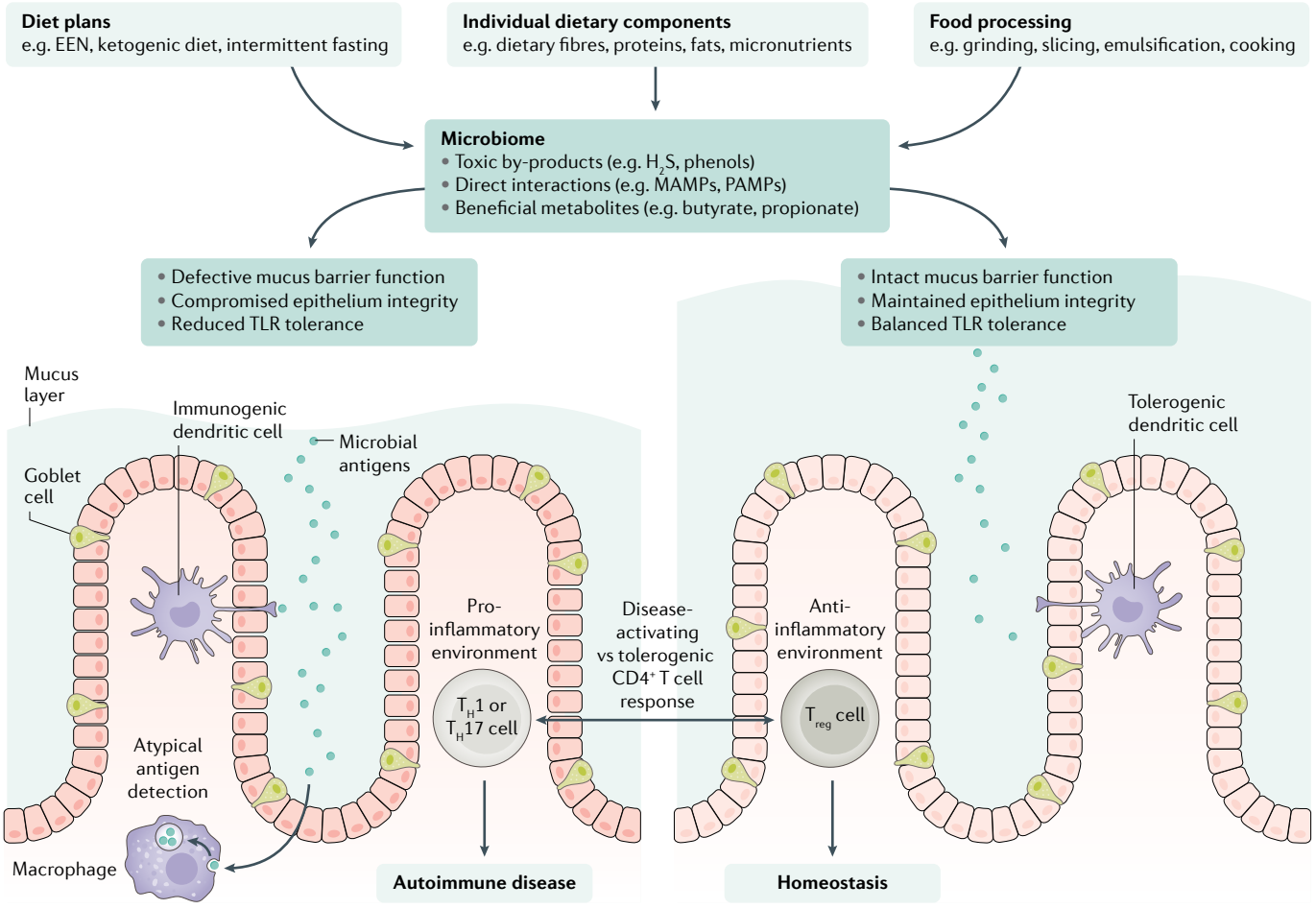

Fig. 2 | **Diet–gut microbiome–host axis in autoimmune diseases and homeostasis.** Common themes underlie the emergence of autoimmune diseases including underlying patterns of gut microbiome perturbation and intestinal barrier dysfunction, as studied in animal models[12,13,30]. Whole diet plans, such as exclusive enteral nutrition (EEN), individual dietary components or modifications in the form of food processing, can exert an influence on the composition and metabolic output of the gut microbiota. In turn, the gut microbiota directly (for example, through microorganism-associated molecular patterns (MAMPs) or pathogen-associated molecular patterns (PAMPs)) or indirectly (for example, through the production of metabolites) influences the local innate pro-inflammatory or anti-inflammatory response and adaptive immunity. Impaired barrier function via a degraded mucus barrier or weak tight junctions could contribute to atypical antigen detection by antigen presenting cells such as dendritic cells and macrophages. Toll-like receptor (TLR) tolerance, which can be modulated by the gut microbiome[48], also plays a part in mediating disease severity for diverse autoimmune diseases as inadequate TLR activation by commensal bacteria can contribute to immune dysregulation[14,47]. Finally, among patients with autoimmune disease, circulating $CD4^+$ T cell populations tend to be skewed towards disease-activating T helper 1 (T_H1) cells or T helper 17 (T_H17) cells, rather than tolerogenic regulatory T (T_{reg}) cells, whose differentiation is influenced by microbial metabolites such as butyrate[50] or propionate[96].

applications of the term in other settings, such as industry or agriculture. Despite restricting our focus to autoimmune diseases, our perspectives of diet-mediated microbiota manipulation approaches could be broadly relevant to other conditions in which gut microbiota modulate the progression of disease, including colorectal cancer[35], cardiometabolic diseases[36] and neurodegenerative diseases[37].

Gut microbiota and host immunity

In the gut, the immunological balancing act of responding appropriately to microbial threats but tolerating commensal microorganisms and self-antigens is especially relevant in early life, a window in which the colonizing microbiota and the host immune system interact, priming for pro-inflammatory or anti-inflammatory predispositions with potential lifelong health consequences[38–40]. Early-life factors such as caesarean delivery, formula feeding and use of antibiotics might disturb this process, as shown in a cohort of 43 infants[41], and have been implicated in several autoimmune diseases in a mouse model[42], with correlative evidence derived from 10,913 stool metagenomes in a cohort of 783 children with early-onset T1DM[43]. Exposure to human milk oligosaccharides in breast milk during infancy supports the colonization with *Bifidobacterium* spp., which dominate the early-life gut microbiome, producing fucose, acetate, pyruvate and 1,2-propanediol to support expansion of the microbiota through cross-feeding, and encouraging immune tolerance towards commensal bacteria[44,45].

After transitioning to a solid food diet, usually beginning at ~6 months of age in humans, the bacterial community expands considerably, producing a larger quantity and variety of metabolites (for example, butyrate, which facilitates the maturation of the colonic mucus barrier[46] and counteracts growth of bacteria with high pathogenic potential[47]). In a study involving 149 healthy volunteers, lipopolysaccharide (LPS) — a major component of the outer membrane of Gram-negative bacteria — dampened innate immune processes by inducing Toll-like receptor 4 (TLR4) tolerance[48]. Improper TLR stimulation by microbial antigens might also influence the progression of autoimmune disease and offer clues for its remediation, as demonstrated in a mouse model of SLE over-expressing TLR7 (REF.[47]). In this model, lupus progression was alleviated using resistant starch supplementation to shift microbial metabolic output and taxonomic composition[47] (TABLE 1). Relatedly, in a mouse model of multiple sclerosis, stimulation of TLR2 by administration of bacterial lipoproteins decreased disease severity[49]. In translating these findings to a 26-person patient cohort, it was observed that half of the patients with multiple sclerosis exhibited enhanced TLR2 sensitivity[49]. These findings suggest that microorganism-associated molecular patterns that are derived from the gut microbiome are important regulators of TLR signalling, which contribute to a tolerogenic gut environment (FIG. 2).

Microbial-driven dysregulation of the adaptive immune response has also been found in patients with autoimmune diseases. For example, when compared with healthy controls, a cohort of 71 patients with multiple sclerosis reportedly had higher abundances of *Akkermansia muciniphila* and *Acinetobacter calcoaceticus*, bacteria with dubious roles in gut homeostasis that might further contribute to immune dysregulation by stimulating differentiation of T helper 1 (T_H1) cells, but not regulatory T (T_{reg}) cells, in vitro[14]. Commensal microbiota in the mammalian gut, especially *Clostridium* clusters IV and XIVa, which metabolize dietary fibres into butyrate to induce T_{reg} cell development, have been inversely correlated with colitis severity in a mouse model[50]. Typically, patients with autoimmune disease exhibit decreased abundances of tolerogenic IL-10-producing $CD25^+FOXP3^+$ T cells and an increased abundance of autoreactive, effector T cell subsets such as T_H1 cells and T_H17 cells, which shift the ratio of T_{reg} cells to effector T cells away from a homeostatic state level[51] (FIG. 2). These alterations might further contribute to increased intestinal permeability via excess production of pro-inflammatory cytokines, such as TNF and IL-17, which modulate the expression of tight-junction proteins, as demonstrated in mouse models[52] and in patients with multiple sclerosis[53,54]. The intricate role of microorganisms in mediating barrier function and immunity has been reviewed elsewhere by Zhang et al.[55], who further detail common immune pathways elucidated from mouse models for various autoimmune diseases. The potentially shared underlying drivers for autoimmune disease encourages the pursuit of gut microbiome engineering through dietary intervention[56] or microbiota modulation strategies (discussed below)[57,58] to shift the gut microbiome towards a functionally diverse 'healthy' state (FIG. 2).

Diet and the gut microbiome

Diet can directly affect the gut microbiota, modulating its composition or metabolic output in a manner that might promote disease or foster a homeostatic state[59–62]. For example, Vangay et al.[63] employed 16S rRNA gene sequencing to document alterations in the gut microbiota in a cross-sectional study of 550 Thai immigrants (including first- and second-generation immigrants) to the US and healthy controls. Among a subset of 19 individuals, they also documented longitudinal changes to the microbiome, which became more pronounced with longer duration of residence and compounded across generations[63]. Food diversity decreased, while the percentage of calories derived from protein, sugars and fats rose. These dietary shifts explained 16.8% of the observed microbial changes, including reduced microbial diversity and, in many cases, a tenfold increase in the number of *Bacteroides* strains relative to *Prevotella*, which might also account for the loss of genes corresponding to fibre-degrading enzymes[63]. Although health outcomes of these microbial shifts were not investigated in this study, the observed changes have elsewhere been associated with increased susceptibility to chronic diseases that are more prevalent in the Western world and highlight the role of the microbiome as a mediator of the diet–disease axis[21].

Dietary carbohydrate fermentation. In a daily sampling study in 34 healthy human participants[64], diet, as assessed using multiple 24-h food recalls, accounted for 44% of the variation in microbiome composition, with another third of the variation explained by factors such as gender, BMI and age. Among the major food groups analysed, grain and fruit fibres showed the strongest correlation with microbial composition. It is therefore unsurprising that plant polysaccharides[65], most of which fall under the definition of dietary fibre, are commonly investigated in the context of disease prevention or progression. Over the past decades, substantial strides have been made in understanding the microbiome-mediated role of dietary fibres in disease; the evidence linking fibre with disease is further discussed in BOX 1.

In the competitive and metabolically mercurial mammalian gut environment, fibre-degrading commensals such as *Bacteroides cellulosilyticus*, *Bacteroides thetaiotaomicron* and *Bacteroides ovatus* are adept at producing the appropriate CAZymes to exploit the available substrate[66]. This activity is complemented by complex cross-feeding processes amongst the gut microbiota that use intermediate oligosaccharides to generate host-beneficial short-chain fatty acids (SCFAs) such as

Table 1 | **Evidence of dietary effects on gut microbiome and host biomarkers in autoimmune diseases**

Diet or dietary component	Study model	Autoimmune disease type	Effect on autoimmune disease	Effect on gut microbiome	Effect on host biomarkers	Refs
Diet plans						
Intermittent fasting	Mouse	EAE (MS)	↓EAE score	↑Bacterial richness, Prevotellaceae, Bacteroidaceae, Lactobacillaceae, pathways in ketone and glutathione synthesis and degradation	↑T_{reg} cells ↓LPS biosynthesis, leptin, T_H17 cells	101
EEN	Human, meta-analysis	Crohn's disease	↑Remission ↓Disease score	↑Lachnospiraceae, Rikenellaceae, Coriobacteriaceae ↓Enterococcaceae, Ruminococcae, Enterobacteriaceae, Prevotellaceae, Veillonellaceae, Bifidobacteriaceae	↓CRP, faecal calprotectin	99
CDED	Human	Crohn's disease	↑Remission ↓Disease score	↑*Oscillibacter*, *Roseburia* ↓Proteobacteria, *Haemophilus*, *Veillonella*, *Bifidobacterium*, *Prevotella*, *Anaerostipes*	↑Proportion of patients with normal intestinal permeability ↓CRP, faecal calprotectin	98
SCD	Human	IBD	↑Remission ↓Disease score	NA	↓CRP and sedimentation rate, albumin normalization	139
Low FODMAP	Human RCT	IBD	↓Disease score	↑Propionate production pathway ↓*Bifidobacterium*, *Faecalibacterium prausnitzii*, acetyl-CoA to acetate pathway	No change in inflammatory markers	140
Paleo	Human, cross-sectional	NA	NA	↑*Hungatella*	↑Serum TMAO ↓Intake of dietary RS	219
AIP	Human	IBD	↑Remission ↓Disease score	NA	↓CRP (NS), faecal calprotectin (NS)	22
Ketogenic	Mouse, human	NA	NA	↑Fermentative capacity ↓*Bifidobacterium*, *Lactobacillus*	↑Ketone bodies, β-hydroxybutyrate ↓T_H17 cells	124
High vegetable/low protein	Human	MS	↑Remission ↓Disease score	↑Lachnospiraceae, *Coprococcus eutactus*, *Ruminococcus lactaris*, *Roseburia intestinalis* No change in α-diversity	↓T_H17 cells	220
Monosaccharides						
High-sugar diet	Mouse	DSS-induced colitis (IBD)	↑Colitis	↑Verrucomicrobiaceae, Porphyromonadaceae ↓α-Diversity, Prevotellaceae Lachnospiraceae, Anaeroplasmataceae	↑Intestinal permeability, pro-inflammatory cytokines, BMDM reactivity to LPS ↓Total SCFA, acetate	221
Artificial sweetener	Mouse	SAMP1/YitFc ileitis (Crohn's disease)	No change	↑Proteobacteria	↑Ileal myeloperoxidase reactivity	222
Milk oligosaccharides						
GOS	Human, crossover	NA	NA	↑*Bifidobacterium* ↓*Ruminococcus*, *Synergistes*, *Dehalobacterium*, *Holdemania*	↓Butyrate (NS), *Bacteroides* predicts OGTT	73
2′-Fucosyl lactose	Mouse	(IBD)	↓Colitis	↑*Ruminococcus gnavus* ↓*Bacteroides acidifaciens*, *Bacteroides vulgatus*	↑Acetate, propionate, valerate, TGFβ, occludin ↓iNOS, IL-1β, IL-6	223
Plant polysaccharides						
Dietary fibre	Mouse	T cell transfer colitis (IBD)	↓Colitis	No change in microbial load or Clostridiales abundance, metabolic changes between high-fibre and low-fibre diets presumed based on butyrate output	↑T_{reg} cells, caecal and luminal butyrate, *Foxp3* histone H3 acetylation	94
	Human, RCT meta-analysis	NA	NA	↑*Bifidobacterium*, *Lactobacillus* No change in α-diversity	↑Faecal butyrate FOS and GOS drove microbial shifts	72

Table 1 (cont.) | **Evidence of dietary effects on gut microbiome and host biomarkers in autoimmune diseases**

Diet or dietary component	Study model	Autoimmune disease type	Effect on autoimmune disease	Effect on gut microbiome	Effect on host biomarkers	Refs
Plant polysaccharides (cont.)						
Cellulose	Mouse	EAE, OSE (MS)	↓Incidence, delayed onset, no change in EAE score	↑*Desulfovibrio*, *Parabacteroides*, *Pseudoflavonifractor*, *Oscillibacter*, valine/leucine/isoleucine biosynthesis ↓*Parasutterella*, *Coprobacillus*, *Lactobacillus*, Saccharibacteria (TM7)	↑LCFA, T_H2 cells ↓Butyrate, muricholic acid, T_H1 cells	224
FOS	Human, crossover	NA	NA	↑*Bifidobacterium* ↓*Phascolarctobacterium*, *Enterobacter*, *Turicibacter*, *Coprococcus*, *Salmonella*	↓Butyrate *Bacteroides* predicts OGTT	73
ITF	Human, RCT	Ulcerative colitis	↑Remission ↓Colitis	↑*Faecalibacterium*, *Dialister* (correlated with colitis reduction)	↑Total SCFA, butyrate ↓Faecal calprotectin	74
Long-chain ITF	Mouse	NOD (T1DM)	↓T1DM incidence	↑Ruminococcaceae, *Lactobacillus* ↓Bacteroidetes	↑Total SCFA, occludin, claudin-2, β-defensin-1, CRAMP, T_{reg} cells ↓T_H17 cells	225
Psyllium	Mouse	DSS-induced, T cell transfer colitis (IBD)	↓Colitis	↑α-Diversity ↓Microbial density	↑Butyrate, T_{reg} cells ↓IL-6, faecal LCN-2, intestinal permeability	105
RS	Mouse	TLR7.1 Tg (SLE)	↓Lupus-related mortality	↑Clostridiales, *Bifidobacterium*, *Bacteroides acidifaciens*, *Streptococcus*, *Anaeroplasma*, *Bilophila* ↓*Lactobacillus*, *Allobaculum*, AF12, Erysipelotrichaceae, *Turicibacter*	↑SCFA ↓T_H17 cells, $CD44^+$ T cells, neutrophils, type I IFN expression Dose-dependent SCFA inhibition of *Lactobacillus reuteri*	47
Yeast β-glucan	Mouse	NOD (T1DM)	↓T1DM incidence	↑*Akkermansia*, *Parabacteroides*, *Dysgonomonas*, carbohydrate metabolism (pathways inferred with PICRUSt) ↓*Blautia*, *Oscillospira*, terpenoid/polyketide metabolism (pathways inferred with PICRUSt)	↑T_{reg} cells, *Il10*, *Tnf*, *Il6*, *Il1β*, *Raldh1*	226
SCFA						
Propionate	Human	MS	↑Remission ↓Disease score	↑Anaerobic bacterial load ↓Aerobic bacteria	↑T_{reg} cells and suppressive capacity, IL-10 ↓T_H17 cells	96
Butyrate	Mouse	AIA (RA)	↓Arthritis	↑*Allobaculum*, *Bifidobacterium*, Rhodospirillaceae, Trp-metabolizing bacteria, serotonin metabolite production	↑AhR-dependent gene transcription, IL-10, Bregs ↓TNF, IL-6, MCP-1, T_H17 cells, plasmablasts, germinal centre B cells	227
	Mouse	(IBD)	↓Colitis	↑α-Diversity (NS), Lactobacillaceae, Erysipelotrichaceae ↓IgA-coated bacteria, Prevotellaceae	↓TNF, IL-6, infiltration of inflammatory cells in colonic mucosa, acetate	228
Proteins and amino acids						
Casein	Mouse	DSS-induced colitis (IBD)	↑Colitis	↑Microbial density, *Staphylococcus*, *Enterococcus*, *Streptococcus*, *Escherichia coli*, Peptostreptococcaceae, *Odoribacter*, *Akkermansia*, Ruminococcaceae ↓α-Diversity	↑Intestinal permeability, activation of colonic Ly-6Chi monocytes, IL-6, TNF, LCN-2, TGFβ, IL-1β, iNOS	105,106
Wheat gluten	Mouse	DSS-induced colitis (IBD)	↓Colitis (relative to casein)	↑Coriobacteriaceae, *Enterococcus*, Lachnospiraceae, *Staphylococcus*, Erysipelotrichaceae, *E. coli*	↑SCFA, BCAA, and phenylalanine	106

Table 1 (cont.) | **Evidence of dietary effects on gut microbiome and host biomarkers in autoimmune diseases**

Diet or dietary component	Study model	Autoimmune disease type	Effect on autoimmune disease	Effect on gut microbiome	Effect on host biomarkers	Refs
Proteins and amino acids (cont.)						
No tryptophan	Mouse	EAE (MS)	↓EAE score	↑Actinobacteria, Proteobacteria, Firmicutes ↓α-Diversity, Bacteroidetes, *Akkermansia*, *Lactobacillus*, *Barnesiella*	↓IL-10 secretion after restimulation, T_H1 cells, plasma leptin	115
Tryptophan	Mouse	DSS-induced colitis (IBD)	↓Colitis	NA	↑*Il22*, *Stat3* ↓*Il6*, *Tnfa*, *Il1β*, *Ccl2*, *Cxcl1*, *Cxcl2*	113
	Mouse	TC (SLE)	↑SLE	↑*Paraprevotella*, *Lactobacillus*, Prevotellaceae	↑Anti-dsDNA IgG ↓Serum Trp, serotonin (relative to WT)	229
Dietary fats						
Saturated fats	Mouse	*Il10*$^{-/-}$, DSS-induced colitis (IBD)	↑Colitis	↑Bacteroidetes, *Bilophila wadsworthia* ↓α-Diversity, Firmicutes	↑T_H1 mucosal response due to change in bile acid production	116
Omega-3 PUFA	Human crossover	NA	NA	↑*Roseburia*, SCFA-producers (NS) ↓*Coprococcus* No change in α-diversity or β-diversity	↑Red blood cell fatty acids	128
Phytochemicals						
Resveratrol	Mouse	TNBS-induced colitis (IBD)	↓Colitis	↑*Ruminococcus gnavus*, *Akkermansia* ↓*Bacteroides acidifaciens*	↑i-Butyric acid, T_{reg} cells ↓T_H1 and T_H17 cells	230
Micronutrients						
Dietary haem	Mouse	DSS-induced colitis (IBD)	↑Colitis	↑Enterobacteriaceae ↓α-Diversity, Firmicutes Non-beneficial functional shifts	↑Genes related to haem release, uptake, and export ↓Butyrate	231
Iron sulfate	Human	IBD and anaemic controls	↓Anaemia No change in colitis	↑*Bifidobacterium* ↓*Faecalibacterium prausnitzii*, *Ruminococcus bromii*, *Dorea*, *Collinsella aerofaciens*	↑Faecal iron, phosphatidylglycerol, palmitate and derivatives	232
Salt (NaCl)	Mouse	DSS-induced colitis (IBD)	↑Colitis	↑Lachnospiraceae, *Oscillospira*, fatty acid metabolism, lysine degradation, arginine/proline metabolism ↓*Lactobacillus*, Clostridiales, fructose/mannose metabolism (pathways inferred with PICRUSt)	↑T_H17 cells, *Ract*, *Gnb1*, *Il7/Il1rap*, *Map2k1*, *Mapk3* ↓Butyrate, lactic acid (NS), *Ccl3*, *Alox15*	233
	Mouse	EAE (MS)	↑EAE score	↑*Parasutterella* ↓*Lactobacillus* (also in healthy humans), *Oscillibacter*, *Pseudoflavonifractor*, *Clostridium* XIVa, *Johnsonella*, *Rothia*	↑T_H17 cells, *Il17a*, *Rorc*, *Csf2* ↓Faecal ILA, IIA (Trp metabolites)	234
Food processing						
P80, CMC	Mouse	*Il10*$^{-/-}$ (IBD)	↑Colitis	↑*Ruminococcus gnavus*, *Akkermansia*, *Bilophila*, *Helicobacter* ↓Bacteroidales	↑LCN-2, bile acid levels, intestinal permeability	141

AIA, adjuvant-induced arthritis; AIP, autoimmune protocol; AhR, aryl hydrocarbon receptor; BCAA, branched chain amino acids; BMDM, bone marrow-derived macrophages; Bregs, regulatory B cells; CDED, Crohn's disease exclusion diet; CMC, carboxymethylcellulose; CRAMP, cathelicidin-related antimicrobial peptide; CRP, C-reactive protein; DSS, dextran-sulfate-sodium; EAE, experimental autoimmune encephalomyelitis; EEN, exclusive enteral nutrition; FODMAP, fermentable oligosaccharides, disaccharides, monosaccharides and polyols; FOS, fructooligosaccharides; GOS, galacto-oligosaccharides; IBD, inflammatory bowel disease; ILA, indole-3-lactic acid; iNOS, inducible nitric oxide synthase; ITF, inulin-type fructans; LCFA, long-chain fatty acid; LCN-2, lipocalin-2; LPS, lipopolysaccharide; MCP-1, monocyte chemoattractant protein-1; MS, multiple sclerosis; NA, not applicable; NOD, non-obese diabetic mice; NS, not significant; OGTT, oral glucose tolerance test; OSE, opticospinal encephalomyelitis; P80, polysorbate 80; PICRUSt, phylogenetic investigation of communities by reconstruction of unobserved states; PUFA, polyunsaturated fatty acid; RA, rheumatoid arthritis; RALDH1, retinal dehydrogenase 1; RCT, randomized controlled trial; RS, resistant starch; SCD, specific carbohydrate diet; SCFA, short-chain fatty acids; SLE, systemic lupus erythematosus; T1DM, type 1 diabetes mellitus; TC, triple congenic lupus-prone mice; TGFβ, transforming growth factor-β; T_H, T helper; TLR, Toll-like receptor; TMAO, trimethylamine *N*-oxide; TNBS, trinitrobenzenesulfonic acid; TNF, tumour necrosis factor; T_{reg}, regulatory T; Trp, tryptophan; WT, wild type.

Box 1 | **Dietary fibre and autoimmune diseases**

During an observation period from 1966 to 1971, Burkitt found an absence of non-infectious colonic diseases among African people consuming a fibre-rich diet and conceived the 'fibre hypothesis', which postulates that the refining of carbohydrates and consequent decrease in fibre content underlies many modern, emerging diseases[238,239]. Shortly after, Aries et al. found differences in faecal bacteria between people from England and people from Uganda, and suggested that low fibre consumption allows the expansion of microorganisms that degrade bile salts into carcinogenic compounds[240]. Sequencing-based technologies solidified this microbial link, with low microbial gut diversity continually observed in association with inflammatory diseases. In a study among children from a West African village ($n = 15$) who consumed nearly twice as much fibre as the 'healthy' Western cohort ($n = 15$), De Filippo et al. observed increased microbial diversity and fourfold higher butyrate and propionate levels[127]. In 2015, O'Keefe et al. swapped the diets of African Americans and rural Africans in a 2-week food exchange, and demonstrated the reciprocal effects of a high-fat, low-fibre Western diet and a high-fibre, low-fat African diet in inducing changes in carbohydrate fermentation, butyrate generation and secondary bile acid synthesis[35]. The mechanistic rationale for the protective effects of fibre are largely attributed to the immunoregulatory[4,12,13], barrier-enforcing[70,105] and microbiota-modifying[92] properties of the short-chain fatty acid fermentation end products. Although initially studied in the context of colorectal cancer, the list of diseases that may be prevented or ameliorated through defined fibre supplementation has grown to include autoimmune diseases, such as multiple sclerosis and type 1 diabetes mellitus[224,225].

butyrate and propionate[67]. Improved understanding of the precise relationships between complex variations in fibre chemistry and the corresponding selective pressures in the gut will enable more precise diet-based manipulation of gut microbiome activity[68–70]. The use of dietary interventions to engineer the microbiome is currently hampered by study design limitations, diet recall reporting bias and uncontrolled confounding factors[71], as well as by the differences in how individual microbiomes respond to a specific type of fibre. Encouragingly, randomized controlled trials involving fibre supplementation successfully alter microbial composition or activity[72–74] (TABLE 1) and although microbiome changes in individuals are typically heterogeneous, responses to specific fibre structures have been shown to be surprisingly consistent. For example, in a dose–response trial, maize type IV resistant starch (RS4) enriched *Eubacterium rectale* among all ten participants, whereas tapioca RS4 universally favoured the growth of *Parabacteroides distasonis*[56]. Numerous studies have investigated the effects of defined dietary fibre interventions on the gut microbiomes of healthy adults with varied effects depending on the fibre type[72]; however, mechanistically oriented, multiomics research must be prioritized over traditional intervention studies that only consider downstream physiological outcomes, such as disease remission. The resulting studies should help decipher the role of individual fibre types on gut microbial physiology to explain variations in intervention efficacy and more accurately predict host health relevance[75,76]. To this end, culture libraries based on human faecal isolates or complete communities can be utilized to define and manipulate microbiome activity in vitro and in gnotobiotic or human microbiome-associated (HMA) mouse models[77,78] (FIG. 3). These investigations are critical for identifying microbial targets for potential manipulation, especially considering high-powered reports that the strongest microbiome–diet associations are observed for microorganisms that are uncultured and/or are poorly characterized[36].

Prebiotics and postbiotics. Prebiotics, as defined by the International Scientific Association for Probiotics and Prebiotics, are substrates characterized by their selective utilization by host microorganisms and their resulting health benefits[79]. Using a gnotobiotic mouse model, fibre-deprived gut microbiota were found to target host mucin glycans as an energy source, leading to reduction of the intestinal mucus barrier and increased susceptibility to the enteric pathogen *Citrobacter rodentium*[70]. However, a cocktail of 14 different purified prebiotics, or other polysaccharides with high solubility instead of complex plant fibres, was unable to prevent degradation of the colonic mucus barrier when fed to mice[70]. Furthermore, Singh et al.[80] found surprisingly that enrichment of foods with purified soluble fibres (for example, inulin, fructooligosaccharides or pectin) can result in hepatocellular carcinoma in mice with pre-existing perturbed microbial communities. These findings suggest that additional parameters, such as amount, solubility and the complex-branched form of natural dietary fibre or raw fibre concentrates, as found in whole-food products, might warrant consideration to exert optimum effects. We should evaluate the effect of natural polysaccharides from whole foods in treating host intestinal inflammation so that the next generation of prebiotics can take into account their accessibility to the gut microbiota. Continued investigations into the effects of defined fibre types in the context of inflammatory diseases and the use of high-quality randomized trials are essential to provide actionable, substantiated tools for leveraging the microbiota-mediated effects of diet on autoimmune diseases[81].

Interestingly, a high-fibre diet administered in a 17-week randomized, prospective study in 39 healthy volunteers altered CAZyme profiles; however, butyrate levels did not change significantly in response to the intervention[82]. Instead, the amount of fibre consumed was strongly correlated with total stool carbohydrates, suggesting that the participants' gut microbiota was not able to completely degrade the fibres in the diet. These findings caution that blindly increasing fibre intake might not translate to increased SCFA generation if the fibre-degrading pathways are saturated. In a prospective cohort study in which 170,776 women were followed for 26 years, fruit-derived and vegetable-derived fibres were inversely associated with Crohn's disease incidence, although this was curiously not the case for other fibre sources or for ulcerative colitis incidence[83]. Another study following 401,326 participants over 7 years found no association between IBD incidence and fibre intake[84]. These findings hint that differences in the underlying microbiome, specifically the ability to degrade fibres to generate SCFAs, might be a better predictor of disease incidence than diet alone. To this end, a study in 127 patients with ulcerative colitis revealed that patients exhibited a decreased abundance of key butyrate-producing bacteria, *Roseburia hominis* and *Faecalibacterium prausnitzii*, compared with healthy controls, and that the abundance of these bacteria was inversely correlated with disease activity[85], a finding that was independently corroborated in a targeted analysis of bacteria inhabiting colonic mucosal brushings[86]. Collectively, these observations suggest that impaired microbial SCFA production might precede active disease among patients with ulcerative colitis.

Given these associations and the role of SCFAs in maintaining immune homeostasis and intestinal barrier

function[87], there is interest in capitalizing on the beneficial host-modulating effects of microorganism-derived metabolites, encompassed in the term 'postbiotics'[88,89]. For example, the fermentation of dietary fibre by primary degraders such as *Bifidobacterium* spp. yields acetate and other intermediate products before it is converted into butyrate by defined subsets of colonic bacteria[90]. In mouse and human cell lines, insufficient butyrate can cause the mucin-producing goblet cells to switch from β-oxidation to anaerobic glycolysis, which negatively affects goblet cell differentiation and the synthesis of MUC2, a glycoprotein constituting the majority of the colonic mucus layer[91]. This metabolic shift also increases oxygen and nitrate availability[92], setting off a positive feedback loop whereby increased oxygen disfavours obligate anaerobes, the main producers of SCFAs[93]. Additionally, butyrate can bind to G protein-coupled receptors (for example, GPR41, GPR43 and GPR109A), downregulating inflammatory cytokine transcription and promoting T_{reg} cell differentiation, as demonstrated in transgenic mouse models[87,94]. Propionate, another important SCFA, is involved in gluconeogenesis in the liver, promotion of satiety and cholesterol reduction[95]. In a proof-of-concept study, 143 patients with multiple sclerosis who were given propionate supplementation with existing therapies attained remission as well as an increase in functionally competent T_{reg} cells, countered

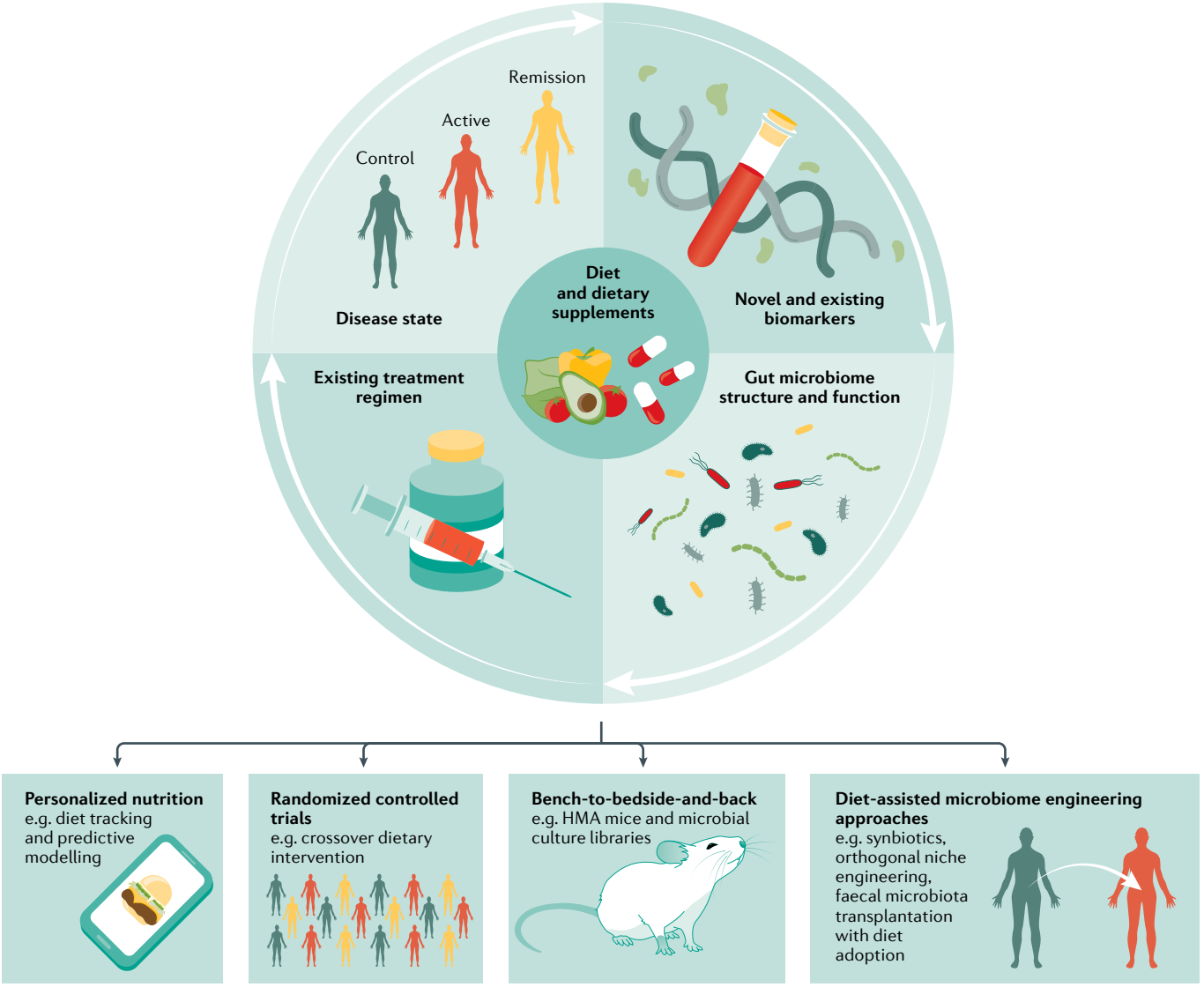

Fig. 3 | **Approaches for personalized application of gut microbiome engineering tools.** The optimal usage of gut microbiome engineering tools involves consideration of the disease state, disease-specific biomarkers, gut microbiome structure and function, and the existing treatment regimen, which should inform the choice of approach and should be monitored regularly. By incorporating these factors, possible approaches for customized therapeutic diet development include: personalized nutrition, characterized by diet tracking, individualized diet recommendations and response prediction; and randomized controlled trials involving human cohorts, such as crossover diet interventions to determine effective diets to attain remission at an individual or subgroup level. Additionally, a bench-to-bedside-and-back approach — the cyclical process of translating findings from the laboratory bench to the patient bedside through novel or adapted therapies and then returning to the bench to refine or build on the insights gained in the clinical setting — can be applied. For example, human microbiome-associated (HMA) rodent models colonized with patient and control stool samples can be used to screen different diet compositions or supplements in an animal model. This approach can be maximized by deriving culture libraries from these samples from patients and healthy controls to identify and characterize unique bacterial isolates. When possible, other diet-assisted microbiome engineering approaches can also be applied for targeted manipulation of the gut microbiome.

by a decrease in T_H1 and T_H17 cells[96]. Although the mechanisms of microbiome modulation in this supplementation are unclear, the transcriptomic profiles of gut microbiomes from responding patients corresponded to genes positively correlated with T_{reg} induction, while genes negatively correlated with T_{reg} cell induction were supressed, with the opposite trend observed in non-responding patients[96].

Exclusion or elimination diets. Optimizing SCFA production through the microbiome might hold promise as a conjunctive treatment strategy; however, the iterative process of evaluating host and microbial biomarkers (measurable biochemical or physiological indicators of disease state) must be adapted to account for the disease state as, during active disease, many patients with IBD report distension and excess gas after consuming high-fibre foods[97]. Although complex carbohydrates might be contraindicated during active periods of disease or surgical intervention, they might still play a part in preventing or in prolonging remission periods. Various exclusion or elimination diets, such as exclusive enteral nutrition (EEN) or partial enteral nutrition (PEN)[23,98,99] (BOX 2), typically prescribed for patients with IBD, should not neglect fibre altogether, but rather exploit forthcoming research under states of active disease or remission. EEN and PEN, for example, are popular therapeutic diets that lack fibre and are capable of inducing remission in 80–90% of patients with Crohn's disease[100]. Although not associated with a consistent taxonomic shift in all patients, EEN appears to increase Crohn's disease remission rates by altering the metabolic output of the colonic microbiota to fermentation of proteins rather than carbohydrates[100]. The mechanistic effects of this functional shift on disease outcomes are not fully elaborated; it remains unclear which of the following permits remission: the exclusion of fibre, lack of another dietary component, the decrease in bacterial density or diversity, or some combination of these.

Alternatively, the observed protective effect of intermittent fasting on multiple sclerosis progression via gut ecosystem remodelling[101] might also provide insights into the success of EEN therapy. By considering microbiome-mediated mechanisms involved in the success of these elimination diets, we might be able to refine dietary interventions. Such adaptations might be important for increasing patient compliance and sustained remission, as the EEN formula diet is challenging to maintain for long periods and might even be harmful in patients with Crohn's disease when used in conjunction with antibiotics[68]. Following induction of remission, it might be advisable to selectively complement EEN with well-tolerated fibre mixes, as proposed in the Crohn's disease exclusion diet (CDED)[98] (BOX 2). In a randomized control trial among 78 children with Crohn's disease, CDED resulted in decreased levels of Proteobacteria and inflammation and remission was maintained in a higher proportion of patients than among those receiving EEN alone[98]. In support of this finding, *Il10*$^{-/-}$ mice with active colitis were given EEN with a defined fibre mix, which decreased disease activity and colitis. This finding was also accompanied by increased $CD4^+FOXP3^+$ T_{reg} cell populations in the lamina propria, increased total SCFA levels in the caecum, and various other indications of restored barrier function[102], encouraging the consideration of whether specific fibres might be advisable in patients with active inflammation.

Nonetheless, the focus of interventions should not be limited to carbohydrates. As shown in TABLE 1, numerous diets and dietary components share the ability to affect host health in a microbiota-dependent manner. Although a link between the Western diet — characterized by high intake of fat, protein, sugar, salt and processed foods — and accompanying microbial changes that contribute to autoimmune disease development is becoming clear[21,103], disentangling the mechanisms to design therapeutic diets is less than straightforward. The studies described in TABLE 1 point to the fact that, among readily modifiable factors that influence the gut microbiome, diet stands out as a potentially powerful tool in the directed modification of the microbiome towards a healthy state.

Protein putrefaction. Dietary protein, another key macronutrient, can also be subjected to bacterial fermentation, producing key metabolites that affect host function and bacterial composition. During digestion, dietary proteins are first hydrolysed into peptides by host enzymes and free amino acids are absorbed in the small intestine. Unabsorbed peptides and amino acids can reach the colon, where they are fermented by commensal microorganisms to produce an estimated 17–38% of colonic SCFAs, based on in vitro and in vivo measurements[104]. Protein degradation by gut microbiota provides essential free amino acids to the host and branched-chain fatty acids (BCFAs) can serve as an alternative energy source for colonocytes. However, this process can be detrimental for the local intestinal environment owing to the release of toxic

Box 2 | Diets for therapeutic applications

Most diets that show promise in therapeutic applications seek to ameliorate inflammation in the gut by avoiding certain foods, with pronounced effects on the gut microbiome (see TABLE 1). We also recommend expert reviews for further details, mainly in the context of inflammatory bowel disease (IBD)[241–243] or irritable bowel syndrome[244].

- Autoimmune protocol diet: based on the paleo diet, this regimen emphasizes consumption of nutrient-rich, fresh or fermented foods and elimination of food groups that might trigger inflammation. Gradual reintroduction of specific foods during the maintenance phase varies according to individual food tolerances.
- Exclusive or partial enteral nutrition (EEN or PEN): a liquid elemental (amino acid-based), semi-elemental (oligopeptides) or polymeric (whole protein-based) formula diet administered with no solid food (EEN) or restricted intake (PEN) for 1–3 months to decrease food antigen exposure and promote intestinal healing.
- Crohn's disease exclusion diet (CDED): tailored to induce remission among patients with Crohn's disease, this whole-food diet is administered along with a PEN diet to decrease exposure to dietary components that might negatively affect host immunity, intestinal barrier function and/or the microbiome.
- Specific carbohydrate diet (SCD): originally developed for the treatment of coeliac disease, this diet is commonly used to aid in the treatment of IBD and allows most fruits, some vegetables, nuts, meats and eggs, while avoiding all grains, table sugar, food additives and most dairy products.
- Low FODMAP diet: this diet emphasizes restriction of fermentable oligosaccharides, disaccharides, monosaccharides and polyols (FODMAP) and operates in phases — elimination, reintroduction and maintenance — to identify foods that trigger disease symptoms and facilitate development of a personalized diet.
- Ketogenic: this low-carbohydrate, high-fat diet encourages ketosis, a metabolic state in which fat, rather than glucose, is degraded for energy generation. The production of ketone bodies was shown to deplete bifidobacteria and to reduce levels of pro-inflammatory T helper 17 cells[124].

metabolic by-products such as ammonia, hydrogen sulfide and phenols, which increase epithelial permeability in mice[105] and decrease cell viability in vitro[104]. In a mouse model of IBD, protein of animal origin exacerbated colitis through pro-inflammatory monocytes, which was not observed for a diet rich in plant protein or in germ-free mice, suggesting that microbial metabolites of the animal protein drive excess inflammation[106]. Thus, personalizing protein type or source (for example, gluten or casein) to the microbiota composition of individual patients is essential to limit production of inflammatory metabolites[107] (TABLE 1).

It is important to consider that different protein sources such as soy might not be as readily degraded in the small intestine, and therefore increased substrate reaches the colon where it can be fermented[107]. Furthermore, the effect of specific proteins on the microbiome and metabolic products varies because not all proteins are equally suited to fermentation and not all bacteria are equipped with appropriate enzymatic pathways. For instance, although all amino acids undergo ammonia-releasing deamination, only branched-chain amino acids (valine, leucine and isoleucine) yield BCFAs[108]; sulfated amino acids favour the expansion of sulfate-reducing bacteria to provide hydrogen sulfide, a process elevated in patients with ulcerative colitis[109]; and aromatic amino acids are preferentially fermented by *Enterobacter* spp. and *Escherichia* spp. to produce phenols, according to metabolic models using human microbiome data[110]. Tryptophan, for example, is an essential aromatic amino acid that is mostly metabolized by host enzymes; however, it can also be metabolized by the gut microbiota through the well-characterized indole pathway[111]. Its metabolites provide ligands for the host aryl hydrocarbon receptors that reduce the expression of pro-inflammatory cytokines and chemokines and promote production of IL-22, which stimulates epithelial cells to release antimicrobial peptides that regulate microbiome growth in mice[112,113]. Consistent with these immunometabolic processes, dietary tryptophan supplementation or tryptophan-producing *Lactobacillus* strains alleviate experimental colitis in various mouse models[112–114]. Conversely, dietary tryptophan might exacerbate experimental autoimmune encephalomyelitis (EAE), a preclinical mouse model of multiple sclerosis, by increasing the amount of circulating autoreactive $CD4^+$ T cells and facilitating their migration through the blood–brain barrier[115]. Thus, although dietary tryptophan has been proposed as a therapeutic strategy to alleviate colitis in patients with IBD[112,113], its microbiota-mediated effects might be organ-specific and disease-specific.

Dietary fat metabolism. Besides being a potential nutrient source of gut microorganisms, dietary fat also changes the microbial composition through increased host bile acid production[116,117], which can promote growth of commensals with high pathogenic potential[118], such as *Bilophila wadsworthia*[116,117]. The gut microbiota compositional alterations induced by dietary fat can also modulate the abundance of microbial-derived secondary bile acids[119]. For example, the consumption of walnuts, which are rich in unsaturated fats, enriched *Faecalibacterium*, *Roseburia* and *Clostridium* in the gut of healthy adults, which led to a reduction in microbial-derived, pro-inflammatory secondary bile acids[119].

Moreover, it has been shown in mice that high-fat diets can also influence host health by increasing exposure to LPS, which can induce the host pro-inflammatory TLR4 signalling pathway[120], resulting in a low-grade systemic inflammation termed metabolic endotoxaemia[121]. This metabolic endotoxaemia might have a profound impact on the onset of autoimmune activity (FIG. 2), considering the strong correlation between LPS levels and disease severity observed in patients with IBD, as well as the demonstrated link between LPS and T1DM[122]. The detailed mechanisms linking elevated LPS exposure to disease remain to be fully elucidated; however, based on mouse studies, it is probably multifactorial, including: increased abundance of Gram-negative bacteria[120], an altered source of LPS with more potent immunogenicity[122,123]; a decrease in bacteria that inhibit LPS-induced inflammation such as bifidobacteria[120,124]; and host factors such as increased intestinal permeability owing to direct effects of the fats or microbial activities[125].

Undefined high-fat diets are commonly used in human microbiome studies, nevertheless, the specific type of dietary fat has a major effect on the gut microbiota and host health outcomes[126]. Although Western high-fat diets support detrimental microbial shifts[4,35,127], numerous examples of beneficial microbial changes exist for defined fat types, such as ω-3 polyunsaturated fatty acids[128] (TABLE 1) or complex fat sources such as walnuts[119,129]. Additionally, in one study that did not assess clinical parameters, patients with multiple sclerosis exhibited restored levels of bacteria including *Eubacterium rectale* and *Faecalibacterium prausnitzii*, which are considered reflective of a proper fermentation capacity, after 6 months on a ketogenic diet (low in carbohydrates and high in fat)[130] (BOX 2). In a similarly microbiome-dependent manner, a ketogenic diet alleviated colitis compared with a low-carbohydrate diet in a dextran sodium sulfate (DSS)-induced colitis mouse model[131]. Furthermore, the production of ketone bodies on a ketogenic diet, specifically β-hydroxybutyrate, was shown to deplete bifidobacteria and reduce levels of T_H17 cells in humans[124], and a similar ketogenic diet-induced reduction of T_H17 cells was observed in children with autoimmune epilepsy[132] (FIG. 2). These findings challenge the blanket classification of high-fat diets as pro-inflammatory, but underscore the need for further studies of how specific dietary fats modulate the gut microbiome or host–microbiome interactions (for example, by directly altering the immune system that then feeds back to the gut microbiome and vice versa). The analysis of specific types of fat and their effects on the microbiome is key to using dietary fats to precisely engineer our microbiome.

Food processing. Food processing, which has generally increased over the course of human history (FIG. 1), encompasses a range of practices that might be thermal (for example, cooking or puffing), mechanical (for example, grinding, slicing or whipping) or chemical (for example, hydrogenation or emulsification), or involve the use of additives[133]. These manipulations usually serve to increase shelf life or improve appearance or taste[133]. Food processing might also saturate nutrient digestion in the small intestine, with poorly defined consequences on resource availability for the colonic microbiota[134].

Cooking, one of the earliest examples of food processing, has a major effect on nutrient digestibility, as demonstrated by Carmody et al. using controlled feeding studies in mice and humans[135]. They found that consumption of starch-rich raw tubers disrupts gut microbial physiology, lowering bacterial abundance and upregulating microbial pathways for xenobiotic metabolism, relative to cooked tubers[135]. These findings point to possible opportunities to mine raw foods for components with therapeutic applications, as microbial xenobiotic metabolism can be beneficial to the host or toxic, or it

can modify pharmaceuticals, depending on the gut microbiome composition[136]. Another study found that subjecting whole wheat flour to cooking–freezing cycles substantially increased the percentage of resistant starch, which led to increased propionate and *Bifidobacterium* levels during in vitro fermentation[137]. The increased bioavailability or chemical alteration of nutrients due to these temperature cycles are seldom factors in diet design, yet such processes might warrant closer consideration in light of findings that raw, cooked and frozen foods can affect the microbiome in disparate ways[135,137].

Targeted food modification using additives — typically for the purpose of preservation, colour or texture modification, or taste enhancement — has increased dramatically in the past century, and is thought to partially explain the correlated rise in autoimmunity by impairing tight junction integrity and increasing intestinal permeability, as reviewed by Lerner and Matthias[138]. Indeed, the avoidance of processed foods is common to many exclusion or elimination diets used to mediate autoimmune disease progression, including the AIP diet[22,23], the specific carbohydrate diet[23,139] and the low fermentable oligosaccharides, disaccharides, monosaccharides and polyols (FODMAP) diet[23,140] (BOX 2). In a mouse model with genetic susceptibility to colitis, exposure to two common emulsifiers, carboxymethyl cellulose and polysorbate 80, increased mucus layer permeability, increased bacterial adherence to the mucosa and favoured a more pro-inflammatory microbial community[141]. Carboxymethyl cellulose is chemically derived from cellulose and structurally considered a fibre, thus, it contributes to the dietary fibre content on nutritional labels in Europe[142]. This might mislead consumers who are aiming to increase their dietary fibre intake based on the labelled value. Safety assessment of such additives by regulatory agencies has also not incorporated the potential microbiota-mediated health effects, ostensibly because this body of research is relatively new. However, studies in animal models and patient cohorts[138,141,143] suggest food additives might be more damaging than current regulations imply, highlighting the need to consider their effects on the microbiome as well as the host.

Overall, a growing body of research highlights the effect of carbohydrates, fats, proteins, phytochemicals (Supplementary Box 1), micronutrients (Supplementary Box 2) and food additives on microbiome composition and metabolic output. With the explosion of sequencing technologies in the past decades, we are able to uncover deeper insights into the complex communities within our gut and the part they play in health and disease, but our ability to act on this new knowledge lags behind. Adaptive, personalized research approaches and tools are needed to develop tailored diet plans or identify potential microbial targets to promote remission among patients with autoimmune diseases.

Microbiota modulation approaches

As low microbial diversity has been observed in patients diagnosed with various autoimmune diseases[130], enriching diversity is a commonly suggested strategy with the potential to maximize health benefits of the human gut microbiome[65]. However, the oversimplification that a 'healthy' microbiome is synonymous with a highly diverse microbiome might mask potential biomarkers or signals from underlying drivers of disease. We echo Brüssow's caution against reliance on diversity metrics to label a microbiota as 'dysbiotic' in the context of disease without exploring the underlying mechanisms[144]. Approaches based on maximizing beneficial microbial physiology — the realized metabolic or physical properties of a microorganism — and minimizing detrimental effects could avoid this pitfall, provided the proper physiological targets can be defined. To this end, machine-learning approaches are powerful tools to exploit existing metagenomic and metabolomic data in the context of autoimmune diseases[145]. Such targets can also offer opportunities to personalize interventions based on genetics, environmental factors and the underlying microbial community present within an individual.

Existing research in patient cohorts and animal models supports the use of tailored diets or specific dietary components to modulate the gut microbiota and host response in various disease contexts (TABLE 1). Numerous host factors, including genetics[2,3] and the pre-existing gut microbiota composition[80], can influence how individuals respond to a diet. In light of the growing evidence of personalized gut microbiota-associated responses to diet or therapies[61,64,146–148], we must actively incorporate a more dynamic approach (FIG. 3) into current treatment regimens for autoimmune diseases, using knowledge of mechanisms underlying disease or remission states to maximize the success of existing diet-based therapies in a given individual. In personalized nutrition[32], for example, individuals might track their diet and, by incorporating relevant covariates such as disease state, treatment regimen, the microbiome and other biomarkers, predictive modelling tools could be used to suggest foods to consume or avoid for a particular outcome. In a landmark study in 800 healthy humans, Zeevi et al. designed a machine-learning algorithm to recommend custom diets by accounting for individual health metrics strongly associated with glucose response[146]. Extension of this model to a cohort of 100 individuals similarly permitted the targeted reduction of glucose responses, suggesting that the design of such diets can be streamlined by accounting for a set of personalized factors. The ability to design custom diets to elicit a desired change in glucose levels is only the tip of the iceberg; in extending this work to other, non-metabolic diseases, mechanistic insights should inform the selection of biomarkers to develop personalized dietary recommendations.

Approaches to improving our understanding of diet–microbiome interactions in health and disease might involve human cohorts that are provided with a diet or dietary component to stratify patients by response (FIG. 3), while also incorporating relevant factors to assist in understanding differences in intervention efficacy. To this end, adaptive platform trials[149] hold promise to further the treatment of autoimmune diseases as the iterative process of testing treatment options to identify subsets of responders is built into the trial design. However, to generate mechanistic knowledge, studies in mouse models remain indispensable to validate or inspire translational efforts in humans. Such a strategy would enable deeper insights into the diet–microbiome–host axis and the identification of new intervention options[150]. For practicality, many studies infer gut microbiota composition according to taxa detected in faecal samples, yet fine-scale variations in host features and microbial physiology along the gastrointestinal tract might be highly relevant in homeostasis[151]. For example, bacteria inhabiting the mucus or colonic crypts, such as *Akkermansia muciniphila* or *Acinetobacter* spp., have been implicated in multiple sclerosis[14] and pathogen-induced colitis[70], yet their abundance is likely to be lower in faeces-derived microbiome profiles than their actual abundance in the colonic mucosa[151]. However, investigations of the microbial communities at clinically relevant sites, such as the colonic mucosa,

require invasive biopsies, and therefore mouse models could be useful to readily study spatial heterogeneity in gut microbial compositions. Critically, no single method is sufficient to understand disease drivers and improve health outcomes; it is essential to exploit the use of all relevant model organisms, systems (for example, *in silico*, in vitro or in vivo) and approaches (for example, reductionist or ecological).

Diet-assisted therapies

There are a number of emerging technologies that aim to manipulate the gut microbiome towards a functionally healthy state by introducing bacteria harbouring new or lost beneficial functions or by eliminating bacteria harbouring detrimental functions. A subset of these techniques, such as faecal microbiota transplantation (FMT)[152] or orthogonal niche engineering[153,154], show high potential to be used in combination with specific diets or dietary supplementation to address some of their limitations or to potentially amplify their effect (FIG. 3). The addition of specific diets to these techniques adds another modifiable variable, potentially providing a higher degree of control of the system and improving the ability to deal with personalized responses. Here, we introduce and discuss emerging methods to engineer the gut microbiome in the context of autoimmune diseases, which have been explored in combination with diet or dietary supplementation.

Faecal microbiota transplantation and diet. Although the mechanisms underlying successful FMT are still not completely resolved, this procedure has the potential to be used more effectively in conjunction with specific diets or dietary supplements. FMT seeks to re-establish a diverse and homeostatic microbiota composition by transferring faecal material from a healthy donor to the gastrointestinal tract of a recipient with a perturbed gut microbiome. This procedure was first used for the treatment of chronic, recurrent gastrointestinal *Clostridioides difficile* infection (CDI), consistently leading to reversal in up to 90% of patients with CDI who were treated with FMT[155]. While patient studies utilizing FMT for the treatment of some autoimmune diseases such as T1DM[156], multiple sclerosis[157], coeliac disease[158] and rheumatoid arthritis[159] are just emerging, the use of FMT for treatment of ulcerative colitis[160–163], Crohn's disease[164,165], liver diseases[166,167], metabolic disorders[168] or neurological pathologies[169] has shown mixed outcomes compared with its effectiveness in CDI. Nevertheless, the hypothesis remains valid that certain microbiota compositions might worsen or precipitate certain diseases, including sub-forms of IBD[170]. Although possible pitfalls and the reasons underlying the mixed outcomes following FMT are well documented[171–173], here we focus on the potential role of diet in the success of FMT.

Given the remarkable influence of diet on the microbiome, as demonstrated by the study results presented in TABLE 1, the effect of the recipient's nutritional habits on the success and persistence of the transplant is a potentially important topic. Although largely unexplored, there are two intuitive approaches: the recipient's diet could be designed to replicate the donor's diet, thereby maximizing the transfer fidelity of the donor's microbiota; or the recipient could consider a diet supporting the implantation of potentially beneficial bacteria, such as a CDED diet or inulin-type fructan supplementation to support SCFA-producing *Roseburia* or *Faecalibacterium* spp., respectively[74,98]. One randomized clinical trial comparing the effectiveness of FMT with or without pectin supplementation in 20 patients with active ulcerative colitis suggested that supplementation with pectin might improve the persistence of the transplanted microbiota[152]; however, at this time, research in humans that addresses whether dietary interventions could be devised to improve the effectiveness of FMT is scarce. Further studies involving a sufficient number of patients and suitable controls are needed to better understand the potential for diet to enhance FMT success. FMT alone might be partially sufficient to provide disease-alleviating properties[174] or to induce remission[160], yet feeding mice a high-fibre diet combined with FMT resulted in additive beneficial effects on the microbiome composition and SCFA output in an emphysema mouse model[175]. The observation in a mouse model of obesity that the beneficial and disease-alleviating effects of the gut microbiome can be transmitted by FMT (for example, from a donor eating a phytochemical-rich diet) to recipients on a high-fat or high-sucrose diet[176] also raises the question of whether modifying the donor's diet, rather than just the recipient's diet, should be investigated further. Finally, in cases where the donor gut microbiota composition is not known, the ability to design FMT-supporting diets might be limited. As such, the use of defined bacterial cultures derived from the stool of healthy donors should be considered[177,178].

Probiotic–diet combinations and synbiotics. Independent of FMT, the direct administration of a single microbial strain or a consortium of strains, such as the probiotic preparation VSL#3 (REF.[179]), to the pre-existing gut microbiota is a widely explored therapeutic option for IBD[178,180,181]. When administering probiotics there are two major considerations: the first, and probably the most important, is the microbial composition of the probiotic; and the second is the choice of the food matrix or encapsulation in which the probiotic should be delivered. The oral administration of either a single probiotic species or a community has been extensively explored. This approach has proven effective in various mouse models of experimental IBD as well as in patients with ulcerative colitis, but not in patients with Crohn's disease, as defined by prolonged remission or active induction of remission[180,181]. As the application and potential of probiotics to treat autoimmune diseases, especially IBD, has been reviewed in detail elsewhere[180–183], here we discuss their combination with dietary supplementation as well as their delivery matrix.

The matrix in which the microorganisms are delivered can have different forms, most commonly either a food matrix, such as yogurt, cereal bars and juices[184], or an encapsulation in a protective emulsion or biopolymer[185]. The choice of delivery matrix is essential as major limitations in the use of probiotics are bacterial viability during passage through the gastrointestinal tract[186] and colonization resistance, which is the property of the endogenous microbial community to prevent colonization of novel bacteria previously not present in the microbiota[147,187–189]. As nutrient limitation is one of the central mechanisms behind colonization resistance[189] and, as discussed previously, diet-based nutrient availability can have a major effect on the gut microbiome, the choice of food or drink in which the probiotic is delivered can have a considerable influence on the viability and sustained engraftment of the probiotic strain[190]. This process is not only due to the nutrient availability, but also due to the environmental stress factors, such as pH, oxygen and temperature during production and storage, as well as the high acidity of the stomach and presence of bile acids in the intestine during passage through the gastrointestinal tract[190]. Although the most extensively studied food matrices are dairy products, there has been an effort to explore different food matrices such as cereals, fruits, vegetables and meat-based products[184].

Alternatively, prebiotics and probiotics can be combined into so-called synbiotics, which can be defined either as complementary or as synergistic. Complementary synbiotics consist of prebiotics and probiotics that elicit health benefits independent of each other, while synergistic synbiotics aim to maximize the beneficial functionalities of the probiotic[57]. The rationales behind the synergistic design are that: the prebiotic can improve the survivability of the probiotic against environmental stress; the probiotic assures the capability of the gut microbiome to metabolize the prebiotic in a beneficial way; and the prebiotic can support the engraftment of the probiotic bacteria into the host microbiome by opening up a new nutrient niche[57,185]. Although human studies using synbiotics are just starting to emerge, certain combinations have been found to be effective and have been used to treat patients with autoimmune diseases. In the context of IBD, bifidobacteria and lactobacilli have shown promise in combination with psyllium[191], fructooligosaccharides[192] and inulin[193,194]. Similarly, a mixture of *Lactobacillus acidophilus*, *Lactobacillus casei* and *Bifidobacterium bifidum* supplemented with inulin led to beneficial effects in patients with rheumatoid arthritis[195] and the combination of *Lactobacillus sporogenes* with maltodextrin and fructooligosaccharide was beneficial in patients with T1DM[196]. Another way to improve viability and colonization is the encapsulation of the bacteria in a protective emulsion or biopolymer[185]. Such encapsulation not only protects the bacteria from environmental hazards and potentially enables site-specific release[197], but it also opens up the possibility to create complex synbiotic constructs by encapsulating the bacteria in prebiotic-containing matrices; for example, alginate–inulin–xanthan gum[198] or poly(lactic-co-glycolic acid)-alginate capsules[199].

Orthogonal niche engineering. Orthogonal niche engineering is an evolution of the synbiotics concept in that the microorganism–substrate relationship is leveraged for a sustained engraftment of bacteria in the host microbiota[153,154]. Although the prebiotics portion of synbiotics generally consists of common nutrients, in orthogonal niche engineering, unused or uncommon nutrients are leveraged to create an exclusive niche for the stable engraftment of the bacteria into the host microbiota[153,154]. As an example, the ability to degrade porphyran, a seaweed polysaccharide, was used to stably engraft a human commensal bacterium into a mouse gut[153,154]. Although studies are currently limited to mice, the use of these uncommon metabolic pathways allows the engrafted bacteria to be precisely manipulated by either intermittent or constant dietary supplementation[153,154] (Supplementary Figure 1). While the ability of the human gut microbiome to degrade seaweed is more pervasive than initially assumed[200,201], orthogonal niche engineering holds substantial promise for overcoming the challenge of a sustained engraftment of bacteria in the gut microbiome, especially considering the wide range of potential genes to harness[201]. New niches, such as agarose, porphyran or carrageenan degradation[201], could be harnessed to help engraft beneficial bacteria that are either wild type, a modified version of the original strain, or a different strain in which the genes involved in utilizing the orthogonal nutrient have been transferred. A conceptual application of orthogonal niche engineering would be screening for bacteria with beneficial functional capacities lost during industrialization (FIG. 1), which remain relevant for our modern lifestyle and for reintroducing them in the human gut (Supplementary Figure 1). An example of such a lost bacterium would be the well-studied probiotic *Lactobacillus reuteri*[202,203] whose immunomodulatory effects on SLE and multiple sclerosis have been studied in mouse models[204,205]. Another conceptual application is the introduction of rare nutrient utilization pathways in recombinant bacteria designed to produce therapeutic compounds, such as IL-10 (REF.[206]) or defensin-5 (REF.[207]) for IBD treatment. The use of uncommon nutrient utilization pathways could allow precise manipulation of the dose and duration of the colonization, enabling the treatment to be tailored specifically to the needs of an individual patient. However, the long-term tractability of this approach might be challenging as continuous feeding can lessen the activity of the implanted bacteria over time[153]. One possible explanation of this phenomenon is that such feeding might encourage niche partitioning, whereby the implanted bacteria are confined to colonic crypts via IgA-binding, and access to the substrate is reduced[153]. Additionally, there is a risk of spreading the trait to other gut bacteria by horizontal gene transfer[208], which could lead to a reduced specificity or a completely altered response.

Challenges and future directions

In a meta-analysis of epidemiological studies and long-term clinical trials, Reynolds et al. calculated a reduction of up to 30% in the incidence and mortality of non-communicable disease among individuals consuming 25–29 g per day of dietary fibre[209]. Furthermore, the dose-dependent relationship between fibre consumption and the incidence of non-communicable diseases, such as coronary heart disease, stroke, type 2 diabetes mellitus and colorectal cancer, suggests that increased levels of fibre intake might confer greater protection against disease[209]. Thus, while we focus on autoimmune diseases, the implications and study approaches described and discussed could be extended to cardiometabolic diseases[36] or colorectal cancer[35], the latter of which critically contributed to the foundation of early hypotheses surrounding fibre (BOX 1).

Although there have been promising advances in connecting diet and the microbiome to autoimmune diseases (TABLE 1), the mechanisms of these interactions are not completely resolved. For example, individuals with a high relative abundance of *Prevotella copri* appear to be more susceptible to rheumatoid arthritis[210], and varied diet plans, including a vegan, gluten-free diet and fasting, have shown effectiveness in reducing the severity of this disease[211]. The connection, if any, between these observations remains equivocal[212], despite decades of work to identify diet and microbial involvement in rheumatoid arthritis[213]. Although frustrating, it is important to realize that this field of research concerns highly complex interactions with numerous variables, such as emerging interactions within the gut microbiome, which are further influenced by the host genome, immune system and a multitude of lifestyle factors, each of which might be incompletely characterized. Nonetheless, there is strong interest in understanding these dynamics to offer new treatment options; therefore, upcoming research should be conducted with the dual aims of identifying both general and subpopulation-specific biomarkers to inform optimal treatment and resolving underlying mechanisms behind the variable responses to proposed interventions.

With the refinement of available tools, the microbiome field could shift from correlation-based studies towards those aimed at uncovering mechanisms, enabling the development of new microbiome-focused treatment options. To this end, cultured human live therapeutics, such as those using a defined commensal consortium[178], are demonstrating great potential to precisely

regulate immunity and effectively inhibit disease progression. New and existing biotech companies have emerged or adapted to develop innovative synthetic microbial consortia and engineered bacteria approved for various therapeutic applications[214,215]. Nonetheless, we face a number of challenges in the realization of diet-driven manipulation of the gut microbiome in disease. The resilience of the human gut microbiome, which is a favourable attribute under healthy conditions[216], means that when translating findings from mouse models into humans, the effects of an intervention might be less pronounced than expected[217]. Furthermore, the relative stability of the gut microbiome could thwart efforts to exert a lasting change in composition or function in, for example, patients with autoimmune diseases, especially if the underlying drivers of a stable diseased state are not addressed. Although diet can be an effective tool in eliciting microbial changes, the cessation of that diet typically results in a reversion to the former microbial state[218]. Thus, interventions might need to be continuous, which introduces the additional challenge of ensuring compliance with the regimen. By coupling dietary interventions with other microbiome-modulating approaches, the changes might be more stable; however, this prediction remains to be investigated. In the case of orthogonal niche engineering, for example, the stability of the human microbiome could also be an asset because, if successful engraftment of novel strains can be achieved, the change might be more persistent than a dietary intervention alone. Additionally, repeated sampling of a stable community should reduce the background noise from typical microbial fluctuations, revealing disease-specific signatures. By understanding the baseline microbiome, it might indeed be easier to propose and test effective treatments in an individual patient. Thus, as methods evolve, studies translating valuable mechanistic knowledge from animal models to humans or expanding it to less-studied diseases are critical to refine the application of diet in microbiome engineering.

Conclusions

The idea that microbiota-driven barrier dysfunction underlies various autoimmune diseases encourages closer inspection of these functional changes for the restoration of beneficial host–microbiome interactions. Researchers and clinicians must account for the fact that numerous host, environmental and even temporal factors might determine the 'perfect' microbiome on an individual basis and actively incorporate a more dynamic, tailored approach into current treatment regimens. By implementing precision medicine approaches and an appreciation of the underlying mechanisms driving disease, we can improve the success of existing treatments. We are at the cusp of the microbiome engineering age, but to make this transition effectively, we must prioritize research on personalized responses to dietary interventions and the precise mechanisms shaping the microbiome.

Mathis Wolter[1,2,5], *Erica T. Grant*[1,2,5], *Marie Boudaud*[1], *Alex Steimle*[1], *Gabriel V. Pereira*[3], *Eric C. Martens*[3] *and Mahesh S. Desai*[1,4]✉

[1]*Department of Infection and Immunity, Luxembourg Institute of Health, Esch-sur-Alzette, Luxembourg.*

[2]*Faculty of Science, Technology and Medicine, University of Luxembourg, Esch-sur-Alzette, Luxembourg.*

[3]*University of Michigan Medical School, Ann Arbor, MI, USA.*

[4]*Odense Research Center for Anaphylaxis, Department of Dermatology and Allergy Center, Odense University Hospital, University of Southern Denmark, Odense, Denmark.*

[5]*These authors contributed equally: Mathis Wolter, Erica T. Grant.*

✉*e-mail: mahesh.desai@lih.lu*

https://doi.org/10.1038/s41575-021-00512-7
Published online 27 September 2021

1. Bach, J. F. The effect of infections on susceptibility to autoimmune and allergic diseases. *N. Engl. J. Med.* **347**, 911–920 (2002).
2. Markle, J. G. M. et al. Sex differences in the gut microbiome drive hormone-dependent regulation of autoimmunity. *Science* **339**, 1084–1088 (2013).
3. Inshaw, J. R. J., Cutler, A. J., Burren, O. S., Stefana, M. I. & Todd, J. A. Approaches and advances in the genetic causes of autoimmune disease and their implications. *Nat. Immunol.* **19**, 674–684 (2018).
4. Thorburn, A. N., Macia, L. & Mackay, C. R. Diet, metabolites, and "western-lifestyle" inflammatory diseases. *Immunity* **40**, 833–842 (2014).
5. Bach, J. F. The hygiene hypothesis in autoimmunity: the role of pathogens and commensals. *Nat. Rev. Immunol.* **18**, 105–120 (2018).
6. Levy, M., Kolodziejczyk, A. A., Thaiss, C. A. & Elinav, E. Dysbiosis and the immune system. *Nat. Rev. Immunol.* **17**, 219–232 (2017).
7. Fugger, L., Jensen, L. T. & Rossjohn, J. Challenges, progress, and prospects of developing therapies to treat autoimmune diseases. *Cell* **181**, 63–80 (2020).
8. Ananthakrishnan, A. N. et al. Gut microbiome function predicts response to anti-integrin biologic therapy in inflammatory bowel diseases. *Cell Host Microbe* **21**, 603–610.e3 (2017).
9. Doherty, M. K. et al. Fecal microbiota signatures are associated with response to ustekinumab therapy among Crohn's disease patients. *mBio* **9**, e02120-17 (2018).
10. Scher, J. U., Nayak, R. R., Ubeda, C., Turnbaugh, P. J. & Abramson, S. B. Pharmacomicrobiomics in inflammatory arthritis: gut microbiome as modulator of therapeutic response. *Nat. Rev. Rheumatol.* **16**, 282–292 (2020).
11. Zheng, D., Liwinski, T. & Elinav, E. Interaction between microbiota and immunity in health and disease. *Cell Res.* **30**, 492–506 (2020).
12. Wasko, N. J., Nichols, F. & Clark, R. B. Multiple sclerosis, the microbiome, TLR2, and the hygiene hypothesis. *Autoimmun. Rev.* **19**, 102430 (2020).
13. Ruff, W. E., Greiling, T. M. & Kriegel, M. A. Host–microbiota interactions in immune-mediated diseases. *Nat. Rev. Microbiol.* **18**, 521–538 (2020).
14. Cekanaviciute, E. et al. Gut bacteria from multiple sclerosis patients modulate human T cells and exacerbate symptoms in mouse models. *Proc. Natl Acad. Sci. USA* **114**, 10713–10718 (2017).
15. Khalili, H. et al. The role of diet in the aetiopathogenesis of inflammatory bowel disease. *Nat. Rev. Gastroenterol. Hepatol.* **15**, 525–535 (2018).
16. Willett, W. et al. Food in the Anthropocene: the EAT–Lancet Commission on healthy diets from sustainable food systems. *Lancet* **393**, 447–492 (2019).
17. Cordain, L. et al. Origins and evolution of the Western diet: health implications for the 21st century. *Am. J. Clin. Nutr.* **81**, 341–354 (2005).
18. Kaoutari, A. E., Armougom, F., Gordon, J. I., Raoult, D. & Henrissat, B. The abundance and variety of carbohydrate-active enzymes in the human gut microbiota. *Nat. Rev. Microbiol.* **11**, 497–504 (2013).
19. Smits, S. A. et al. Seasonal cycling in the gut microbiome of the Hadza hunter-gatherers of Tanzania. *Science* **357**, 802–806 (2017).
20. Lombard, V., Golaconda, R. H., Drula, E., Coutinho, P. & Henrissat, B. BT2824 – the carbohydrate-active enzymes database (CAZy) in 2013. *Nucleic Acids Res* **42**, D490–D495 (2014).
21. Manzel, A. et al. Role of 'western diet' in inflammatory autoimmune diseases. *Curr. Allergy Asthma Rep.* **14**, 404 (2014).
22. Konijeti, G. G. et al. Efficacy of the autoimmune protocol diet for inflammatory bowel disease. *Inflamm. Bowel Dis.* **23**, 2054–2060 (2017).
23. Damas, O. M., Garces, L. & Abreu, M. T. Diet as adjunctive treatment for inflammatory bowel disease: review and update of the latest literature. *Curr. Treat. Options Gastroenterol.* **17**, 313–325 (2019).
24. Sonnenburg, E. D. et al. Diet-induced extinctions in the gut microbiota compound over generations. *Nature* **529**, 212–215 (2016).
25. Chandrasekaran, A. et al. The autoimmune protocol diet modifies intestinal RNA expression in inflammatory bowel disease. *Crohns Colitis 360* **1**, otz016 (2019).
26. Klein, E. Y. et al. Global increase and geographic convergence in antibiotic consumption between 2000 and 2015. *Proc. Natl Acad. Sci. USA* **115**, e3463–e3470 (2018).
27. Postler, T. S. & Ghosh, S. Understanding the holobiont: how microbial metabolites affect human health and shape the immune system. *Cell Metab.* **26**, 110–130 (2017).
28. Camilleri, M. Leaky gut: mechanisms, measurement and clinical implications in humans. *Gut* **68**, 1516–1526 (2019).
29. Paray, B. A., Albeshr, M. F., Jan, A. T. & Rather, I. A. Leaky gut and autoimmunity: an intricate balance in individuals health and the diseased state. *Int. J. Mol. Sci.* **21**, 9770 (2020).
30. Li, B., Selmi, C., Tang, R., Gershwin, M. E. & Ma, X. The microbiome and autoimmunity: a paradigm from the gut–liver axis. *Cell. Mol. Immunol.* **15**, 595–609 (2018).
31. Márquez, A. et al. Meta-analysis of Immunochip data of four autoimmune diseases reveals novel single-disease and cross-phenotype associations. *Genome Med.* **10**, 97 (2018).
32. Kolodziejczyk, A. A., Zheng, D. & Elinav, E. Diet–microbiota interactions and personalized nutrition. *Nat. Rev. Microbiol.* **17**, 742–753 (2019).
33. Inda, M. E., Broset, E., Lu, T. K. & de la Fuente-Nunez, C. Emerging Frontiers in Microbiome Engineering. *Trends Immunol.* **40**, 952–973 (2019).
34. Ruder, W. C., Lu, T. & Collins, J. J. Synthetic biology moving into the clinic. *Science* **333**, 1248–1252 (2011).
35. O'Keefe, S. J. D. et al. Fat, fibre and cancer risk in African Americans and rural Africans. *Nat. Commun.* **6**, 6342 (2015).
36. Asnicar, F. et al. Microbiome connections with host metabolism and habitual diet from 1,098 deeply phenotyped individuals. *Nat. Med.* **27**, 321–332 (2021).
37. Parker, A., Fonseca, S. & Carding, S. R. Gut microbes and metabolites as modulators of blood-brain barrier integrity and brain health. *Gut Microbes* **11**, 135–157 (2020).
38. Cox, L. M. et al. Altering the intestinal microbiota during a critical developmental window has lasting metabolic consequences. *Cell* **158**, 705–721 (2014).

39. Al Nabhani, Z. et al. A weaning reaction to microbiota is required for resistance to immunopathologies in the adult. *Immunity* **50**, 1276–1288.e5 (2019).
40. Kalbermatter, C., Fernandez Trigo, N., Christensen, S. & Ganal-Vonarburg, S. C. Maternal microbiota, early life colonization and breast milk drive immune development in the newborn. *Front. Immunol.* **12**, 683022 (2021).
41. Bokulich, N. A. et al. Antibiotics, birth mode, and diet shape microbiome maturation during early life. *Sci. Transl. Med.* **8**, 343ra82 (2016).
42. Mahmoud, T. I. et al. Autoimmune manifestations in aged mice arise from early-life immune dysregulation. *Sci. Transl. Med.* **8**, 361ra137 (2016).
43. Vatanen, T. et al. The human gut microbiome in early-onset type 1 diabetes from the TEDDY study. *Nature* **562**, 589–594 (2018).
44. Lawson, M. A. E. et al. Breast milk-derived human milk oligosaccharides promote Bifidobacterium interactions within a single ecosystem. *ISME J.* **14**, 635–648 (2020).
45. Fanning, S. et al. Bifidobacterial surface-exopolysaccharide facilitates commensal-host interaction through immune modulation and pathogen protection. *Proc. Natl Acad. Sci. USA* **109**, 2108–2113 (2012).
46. Beaumont, M. et al. Gut microbiota derived metabolites contribute to intestinal barrier maturation at the suckling-to-weaning transition. *Gut Microbes* **11**, 1268–1286 (2020).
47. Zegarra-Ruiz, D. F. et al. A diet-sensitive commensal lactobacillus strain mediates TLR7-dependent systemic autoimmunity. *Cell Host Microbe* **25**, 113–127.e6 (2019).
48. D'Hennezel, E., Abubucker, S., Murphy, L. O. & Cullen, T. W. Total lipopolysaccharide from the human gut microbiome silences toll-like receptor signaling. *mSystems* **2**, e00046-17 (2017).
49. Fujiwara, M. et al. Enhanced TLR2 responses in multiple sclerosis. *Clin. Exp. Immunol.* **193**, 313–326 (2018).
50. Atarashi, K. et al. Induction of colonic regulatory T cells by indigenous Clostridium species. *Science* **331**, 337–341 (2011).
51. Ohkura, N. et al. Regulatory T cell-specific epigenomic region variants are a key determinant of susceptibility to common autoimmune diseases. *Immunity* **52**, 1119–1132.e4 (2020).
52. Lee, J. S. et al. Interleukin-23-independent IL-17 production regulates intestinal epithelial permeability. *Immunity* **43**, 727–738 (2015).
53. Cosorich, I. et al. High frequency of intestinal TH17 cells correlates with microbiota alterations and disease activity in multiple sclerosis. *Sci. Adv.* **3**, e1700492 (2017).
54. Buscarinu M. C. et al. Altered intestinal permeability in patients with relapsing–remitting multiple sclerosis: a pilot study. *Mult. Scler.* **23**, 442–446 (2017).
55. Zhang, X., Chen, B. D., Zhao, L. D. & Li, H. The gut microbiota: emerging evidence in autoimmune diseases. *Trends Mol. Med.* **26**, 862–873 (2020).
56. Deehan, E. C. et al. Precision microbiome modulation with discrete dietary fiber structures directs short-chain fatty acid production. *Cell Host Microbe* **27**, 389–404.e6 (2020).
57. Swanson, K. S. et al. The International Scientific Association for Probiotics and Prebiotics (ISAPP) consensus statement on the definition and scope of synbiotics. *Nat. Rev. Gastroenterol. Hepatol.* **17**, 687–701 (2020).
58. Hvas, C. L. et al. Fecal microbiota transplantation is superior to fidaxomicin for treatment of recurrent clostridium difficile infection. *Gastroenterology* **156**, 1324–1332.e3 (2019).
59. Carmody, R. N. et al. Diet dominates host genotype in shaping the murine gut microbiota. *Cell Host Microbe* **17**, 72–84 (2015).
60. Wu, G. D. et al. Comparative metabolomics in vegans and omnivores reveal constraints on diet-dependent gut microbiota metabolite production. *Gut* **65**, 63–72 (2016).
61. Venkataraman, A. et al. Variable responses of human microbiomes to dietary supplementation with resistant starch. *Microbiome* **4**, 33 (2016).
62. Sheflin, A. M., Melby, C. L., Carbonero, F. & Weir, T. L. Linking dietary patterns with gut microbial composition and function. *Gut Microbes* **8**, 113–129 (2017).
63. Vangay, P. et al. US immigration westernizes the human gut microbiome. *Cell* **175**, 962–972.e10 (2018).
64. Johnson, A. J. et al. Daily sampling reveals personalized diet-microbiome associations in humans. *Cell Host Microbe* **25**, 789–802.e5 (2019).
65. Makki, K., Deehan, E. C., Walter, J. & Bäckhed, F. The impact of dietary fiber on gut microbiota in host health and disease. *Cell Host Microbe* **23**, 705–715 (2018).
66. McNulty, N. P. et al. Effects of diet on resource utilization by a model human gut microbiota containing bacteroides cellulosilyticus WH2, a symbiont with an extensive glycobiome. *PLoS Biol.* **11**, e1001637 (2013).
67. Flint, H. J., Scott, K. P., Duncan, S. H., Louis, P. & Forano, E. Microbial degradation of complex carbohydrates in the gut. *Gut Microbes* **3**, 289–306 (2012).
68. Tanes, C. et al. Role of dietary fiber in the recovery of the human gut microbiome and its metabolome. *Cell Host Microbe* **29**, 394–407.e5 (2021).
69. Déjean, G. et al. Synergy between cell surface glycosidases and glycan-binding proteins dictates the utilization of specific beta(1,3)-glucans by human gut Bacteroides. *mBio* **11**, e00095-20 (2020).
70. Desai, M. S. et al. A dietary fiber-deprived gut microbiota degrades the colonic mucus barrier and enhances pathogen susceptibility. *Cell* **167**, 1339–1353.e21 (2016).
71. Ananthakrishnan, A. N. Epidemiology and risk factors for IBD. *Nat. Rev. Gastroenterol. Hepatol.* **12**, 205–217 (2015).
72. So, D. et al. Dietary fiber intervention on gut microbiota composition in healthy adults: a systematic review and meta-analysis. *Am. J. Clin. Nutr.* **107**, 965–983 (2018).
73. Liu, F. et al. Fructooligosaccharide (FOS) and galactooligosaccharide (GOS) increase Bifidobacterium but reduce butyrate producing bacteria with adverse glycemic metabolism in healthy young population. *Sci. Rep.* **7**, 11789 (2017).
74. Valcheva, R. et al. Inulin-type fructans improve active ulcerative colitis associated with microbiota changes and increased short-chain fatty acids levels. *Gut Microbes* **10**, 334–357 (2019).
75. Salyers, A. A., West, S. E. H., Vercellotti, J. R. & Wilkins, T. D. Fermentation of mucins and plant polysaccharides by anaerobic bacteria from the human colon. *Appl. Environ. Microbiol.* **34**, 529–533 (1977).
76. Chung, W. S. F. et al. Modulation of the human gut microbiota by dietary fibres occurs at the species level. *BMC Biol.* **14**, 3 (2016).
77. Goodman, A. L. et al. Extensive personal human gut microbiota culture collections characterized and manipulated in gnotobiotic mice. *Proc. Natl Acad. Sci. USA* **108**, 6252–6257 (2011).
78. Elzinga, J., van der Oost, J., de Vos, W. M. & Smidt, H. The use of defined microbial communities to model host-microbe interactions in the human gut. *Microbiol. Mol. Biol. Rev.* **83**, e00054-18 (2019).
79. Gibson, G. R. et al. Expert consensus document: the International Scientific Association for Probiotics and Prebiotics (ISAPP) consensus statement on the definition and scope of prebiotics. *Nat. Rev. Gastroenterol. Hepatol.* **14**, 491–502 (2017).
80. Singh, V. et al. Dysregulated microbial fermentation of soluble fiber induces cholestatic liver cancer. *Cell* **175**, 679–394.e22 (2018).
81. Yao, C. K. & Staudacher, H. M. The low-fibre diet: contender in IBD, or has it had its time? *Lancet Gastroenterol. Hepatol.* **4**, 339 (2019).
82. Wastyk, H. C. et al. Gut microbiota-targeted diets modulate human immune status. *Cell* **184**, 4137–4153 (2020).
83. Ananthakrishnan, A. N. et al. A prospective study of long-term intake of dietary fiber and risk of Crohn's disease and ulcerative colitis. *Gastroenterology* **145**, 970–977 (2013).
84. Andersen, V. et al. Fibre intake and the development of inflammatory bowel disease: a European prospective multi-centre cohort study (EPIC-IBD). *J. Crohns Colitis* **12**, 129–136 (2018).
85. Machiels, K. et al. A decrease of the butyrate-producing species Roseburia hominis and Faecalibacterium prausnitzii defines dysbiosis in patients with ulcerative colitis. *Gut* **63**, 1275–1283 (2014).
86. Earley, H., Lennon, G., Coffey, J. C., Winter, D. C. & O'Connell, P. R. Colonisation of the colonic mucus gel layer with butyrogenic and hydrogenotropic bacteria in health and ulcerative colitis. *Sci. Rep.* **11**, 7262 (2021).
87. Venegas, D. P. et al. Short chain fatty acids (SCFAs) mediated gut epithelial and immune regulation and its relevance for inflammatory bowel diseases. *Front. Immunol.* **10**, 277 (2019).
88. Wong, A. C. & Levy, M. New approaches to microbiome-based therapies. *mSystems* **4**, e00122-19 (2019).
89. Salminen, S. et al. The International Scientific Association of Probiotics and Prebiotics (ISAPP) consensus statement on the definition and scope of postbiotics. *Nat. Rev. Gastroenterol. Hepatol.* https://doi.org/10.1038/s41575-021-00440-6 (2021).
90. Baxter, N. T. et al. Dynamics of human gut microbiota and short-chain fatty acids in response to dietary interventions with three fermentable fibers. *mBio* **10**, e02566-18 (2019).
91. Sünderhauf, A. et al. Loss of mucosal p32/gC1qR/HABP1 triggers energy deficiency and impairs goblet cell differentiation in ulcerative colitis. *Cell. Mol. Gastroenterol. Hepatol.* **12**, 229–250 (2021).
92. Byndloss, M. X. et al. Microbiota-activated PPAR-γ signaling inhibits dysbiotic Enterobacteriaceae expansion. *Science* **357**, 570–575 (2017).
93. Zeng, M. Y., Inohara, N. & Nuñez, G. Mechanisms of inflammation-driven bacterial dysbiosis in the gut. *Mucosal Immunol.* **10**, 18–26 (2017).
94. Furusawa, Y. et al. Commensal microbe-derived butyrate induces the differentiation of colonic regulatory T cells. *Nature* **504**, 446–450 (2013).
95. Louis, P. & Flint, H. J. Formation of propionate and butyrate by the human colonic microbiota. *Environ. Microbiol.* **19**, 29–41 (2017).
96. Duscha, A. et al. Propionic acid shapes the multiple sclerosis disease course by an immunomodulatory mechanism. *Cell* **180**, 1067–1080.e16 (2020).
97. Cohen, A. B. et al. Dietary patterns and self-reported associations of diet with symptoms of inflammatory bowel disease. *Dig. Dis. Sci.* **58**, 1322–1328 (2013).
98. Levine, A. et al. Crohn's disease exclusion diet plus partial enteral nutrition induces sustained remission in a randomized controlled trial. *Gastroenterology* **157**, 440–450.e8 (2019).
99. Horwat, P. et al. Influence of enteral nutrition on gut microbiota composition in patients with Crohn's disease: a systematic review. *Nutrients* **12**, 2551 (2020).
100. Walton, C. et al. Enteral feeding reduces metabolic activity of the intestinal microbiome in Crohn's disease: an observational study. *Eur. J. Clin. Nutr.* **70**, 1052–1056 (2016).
101. Cignarella, F. et al. Intermittent fasting confers protection in CNS autoimmunity by altering the gut microbiota. *Cell Metab.* **27**, 1222–1235.e6 (2018).
102. Wang, H. et al. Dietary non-digestible polysaccharides ameliorate intestinal epithelial barrier dysfunction in IL-10 knockout mice. *J. Crohns Colitis* **10**, 1076–1086 (2016).
103. Richards, J. L., Yap, Y. A., McLeod, K. H., MacKay, C. R. & Marinō, E. Dietary metabolites and the gut microbiota: an alternative approach to control inflammatory and autoimmune diseases. *Clin. Transl. Immunol.* **5**, e82 (2016).
104. Macfarlane, G. T., Gibson, G. R., Beatty, E. & Cummings, J. H. Estimation of short-chain fatty acid production from protein by human intestinal bacteria based on branched-chain fatty acid measurements. *FEMS Microbiol. Lett.* **101**, 81–88 (1992).
105. Llewellyn, S. R. et al. Interactions between diet and the intestinal microbiota alter intestinal permeability and colitis severity in mice. *Gastroenterology* **154**, 1037–1046.e2 (2018).
106. Kostovcikova, K. et al. Diet rich in animal protein promotes pro-inflammatory macrophage response and exacerbates colitis in mice. *Front. Immunol.* **10**, 919 (2019).
107. Dallas, D. C. et al. Personalizing protein nourishment. *Crit. Rev. Food Sci. Nutr.* **57**, 3313–3331 (2017).
108. Portune, K. J. et al. Gut microbiota role in dietary protein metabolism and health-related outcomes: the two sides of the coin. *Trends Food Sci. Technol.* **57**, 213–232 (2016).
109. Gibson, G. R., Cummings, J. H. & Macfarlane, G. T. Growth and activities of sulphate-reducing bacteria in gut contents of healthy subjects and patients with ulcerative colitis. *FEMS Microbiol. Lett.* **86**, 103–111 (1991).
110. Sridharan, G. V. et al. Prediction and quantification of bioactive microbiota metabolites in the mouse gut. *Nat. Commun.* **5**, 5492 (2014).
111. Agus, A., Planchais, J. & Sokol, H. Gut microbiota regulation of tryptophan metabolism in health and disease. *Cell Host Microbe* **23**, 716–724 (2018).

112. Lamas, B. et al. CARD9 impacts colitis by altering gut microbiota metabolism of tryptophan into aryl hydrocarbon receptor ligands. *Nat. Med.* **22**, 598–605 (2016).
113. Islam, J. et al. Dietary tryptophan alleviates dextran sodium sulfate-induced colitis through aryl hydrocarbon receptor in mice. *J. Nutr. Biochem.* **42**, 43–50 (2017).
114. Kepert, I. et al. D-tryptophan from probiotic bacteria influences the gut microbiome and allergic airway disease. *J. Allergy Clin. Immunol.* **139**, 1525–1535 (2017).
115. Sonner, J. K. et al. Dietary tryptophan links encephalogenicity of autoreactive T cells with gut microbial ecology. *Nat. Commun.* **10**, 4877 (2019).
116. Devkota, S. et al. Dietary-fat-induced taurocholic acid promotes pathobiont expansion and colitis in Il10−/− mice. *Nature* **487**, 104–108 (2012).
117. Watanabe, M., Fukiya, S. & Yokota, A. Comprehensive evaluation of the bactericidal activities of free bile acids in the large intestine of humans and rodents. *J. Lipid Res.* **58**, 1143–1152 (2017).
118. Casadevall, A. The pathogenic potential of a microbe. *mSphere* **2**, e00015-17 (2017).
119. Holscher, H. D. et al. Walnut consumption alters the gastrointestinal microbiota, microbially derived secondary bile acids, and health markers in healthy adults: a randomized controlled trial. *J. Nutr.* **148**, 861–867 (2018).
120. Kim, K. A., Gu, W., Lee, I. A., Joh, E. H. & Kim, D. H. High fat diet-induced gut microbiota exacerbates inflammation and obesity in mice via the TLR4 signaling pathway. *PLoS ONE* **7**, e47713 (2012).
121. Cani, P. D. et al. Improvement of glucose tolerance and hepatic insulin sensitivity by oligofructose requires a functional glucagon-like peptide 1 receptor. *Diabetes* **55**, 1484–1490 (2006).
122. Vatanen, T. et al. Variation in microbiome LPS immunogenicity contributes to autoimmunity in humans. *Cell* **165**, 842–853 (2016).
123. Steimle, A. et al. Weak agonistic LPS restores intestinal immune homeostasis. *Mol. Ther.* **27**, 1974–1991 (2019).
124. Ang, Q. Y. et al. Ketogenic diets alter the gut microbiome resulting in decreased intestinal Th17 cells. *Cell* **181**, 1263–1275.e16 (2020).
125. Lam, Y. Y. et al. Effects of dietary fat profile on gut permeability and microbiota and their relationships with metabolic changes in mice. *Obesity* **23**, 1429–1439 (2015).
126. Wolters, M. et al. Dietary fat, the gut microbiota, and metabolic health—a systematic review conducted within the MyNewGut project. *Clin. Nutr.* **38**, 2504–2520 (2019).
127. De Filippo, C. et al. Impact of diet in shaping gut microbiota revealed by a comparative study in children from Europe and rural Africa. *Proc. Natl Acad. Sci. USA* **107**, 14691–14696 (2010).
128. Watson, H. et al. A randomised trial of the effect of omega-3 polyunsaturated fatty acid supplements on the human intestinal microbiota. *Gut* **67**, 1974–1983 (2018).
129. Tindall, A. M., McLimans, C. J., Petersen, K. S., Kris-Etherton, P. M. & Lamendella, R. Walnuts and vegetable oils containing oleic acid differentially affect the gut microbiota and associations with cardiovascular risk factors: follow-up of a randomized, controlled, feeding trial in adults at risk for cardiovascular disease. *J. Nutr.* **150**, 806–817 (2020).
130. Swidsinski, A. et al. Reduced mass and diversity of the colonic microbiome in patients with multiple sclerosis and their improvement with ketogenic diet. *Front. Microbiol.* **8**, 1141 (2017).
131. Kong, C. et al. Ketogenic diet alleviates colitis by reduction of colonic group 3 innate lymphoid cells through altering gut microbiome. *Signal. Transduct. Target. Ther.* **6**, 154 (2021).
132. Ni, F.-F. et al. The effects of ketogenic diet on the Th17/Treg cells imbalance in patients with intractable childhood epilepsy. *Seizure* **38**, 17–22 (2016).
133. Monteiro, C. A. et al. Ultra-processed foods: what they are and how to identify them. *Public. Health Nutr.* **22**, 936–941 (2019).
134. Zinöcker, M. K. & Lindseth, I. A. The western diet–microbiome–host interaction and its role in metabolic disease. *Nutrients* **10**, 365 (2018).
135. Carmody, R. N. et al. Cooking shapes the structure and function of the gut microbiome. *Nat. Microbiol.* **4**, 2052–2063 (2019).
136. Koppel, N., Rekdal, V. M. & Balskus, E. P. Chemical transformation of xenobiotics by the human gut microbiota. *Science* **356**, eaag2770 (2017).
137. Arcila, J. A. & Rose, D. J. Repeated cooking and freezing of whole wheat flour increases resistant starch with beneficial impacts on in vitro fecal fermentation properties. *J. Funct. Foods* **12**, 230–236 (2015).
138. Lerner, A. & Matthias, T. Changes in intestinal tight junction permeability associated with industrial food additives explain the rising incidence of autoimmune disease. *Autoimmun. Rev.* **14**, 479–489 (2015).
139. Obih, C. et al. Specific carbohydrate diet for pediatric inflammatory bowel disease in clinical practice within an academic IBD center. *Nutrition* **32**, 418–425 (2016).
140. Cox, S. R. et al. Effects of low FODMAP diet on symptoms, fecal microbiome, and markers of inflammation in patients with quiescent inflammatory bowel disease in a randomized trial. *Gastroenterology* **158**, 176–188.e7 (2020).
141. Chassaing, B. et al. Dietary emulsifiers impact the mouse gut microbiota promoting colitis and metabolic syndrome. *Nature* **519**, 92–96 (2015).
142. Stephen, A. M. et al. Dietary fibre in Europe: current state of knowledge on definitions, sources, recommendations, intakes and relationships to health. *Nutr. Res. Rev.* **30**, 149–190 (2017).
143. Logan, M. et al. Analysis of 61 exclusive enteral nutrition formulas used in the management of active Crohn's disease — new insights into dietary disease triggers. *Aliment. Pharmacol. Ther.* **51**, 935–947 (2020).
144. Brüssow, H. Problems with the concept of gut microbiota dysbiosis. *Microb. Biotechnol.* **13**, 423–434 (2020).
145. Volkova, A. & Ruggles, K. V. Predictive metagenomic analysis of autoimmune disease identifies robust autoimmunity and disease specific microbial signatures. *Front. Microbiol.* **12**, 621310 (2021).
146. Zeevi, D. et al. Personalized nutrition by prediction of glycemic responses. *Cell* **163**, 1079–1094 (2015).
147. Zmora, N. et al. Personalized gut mucosal colonization resistance to empiric probiotics is associated with unique host and microbiome features. *Cell* **174**, 1388–1405.e21 (2018).
148. Korem, T. et al. Bread affects clinical parameters and induces gut microbiome-associated personal glycemic responses. *Cell Metab.* **25**, 1243–1253.e5 (2017).
149. The Adaptive Platform Trials Coalition Adaptive platform trials: definition, design, conduct and reporting considerations. *Nat. Rev. Drug Discov.* **18**, 797–807 (2019).
150. Holzinger, D., Kessel, C., Omenetti, A. & Gattorno, M. From bench to bedside and back again: translational research in autoinflammation. *Nat. Rev. Rheumatol.* **11**, 573–585 (2015).
151. Donaldson, G. P., Lee, S. M. & Mazmanian, S. K. Gut biogeography of the bacterial microbiota. *Nat. Rev. Microbiol.* **14**, 20–32 (2016).
152. Wei, Y. et al. Pectin enhances the effect of fecal microbiota transplantation in ulcerative colitis by delaying the loss of diversity of gut flora. *BMC Microbiol.* **16**, 255 (2016).
153. Kearney, S. M., Gibbons, S. M., Erdman, S. E. & Alm, E. J. Orthogonal dietary niche enables reversible engraftment of a gut bacterial commensal. *Cell Rep.* **24**, 1842–1851 (2018).
154. Shepherd, E. S., Deloache, W. C., Pruss, K. M., Whitaker, W. R. & Sonnenburg, J. L. An exclusive metabolic niche enables strain engraftment in the gut microbiota. *Nature* **557**, 434–438 (2018).
155. Quraishi, M. N. et al. Systematic review with meta-analysis: the efficacy of faecal microbiota transplantation for the treatment of recurrent and refractory Clostridium difficile infection. *Aliment. Pharmacol. Ther.* **46**, 479–493 (2017).
156. de Groot, P. et al. Faecal microbiota transplantation halts progression of human new-onset type 1 diabetes in a randomised controlled trial. *Gut* **70**, 92–105 (2021).
157. Engen, P. A. et al. Single-arm, non-randomized, time series, single-subject study of fecal microbiota transplantation in multiple sclerosis. *Front. Neurol.* **11**, 978 (2020).
158. Van Beurden, Y. H. et al. Serendipity in refractory celiac disease: full recovery of duodenal villi and clinical symptoms after fecal microbiota transfer. *J. Gastrointest. Liver Dis.* **25**, 385–388 (2016).
159. Zeng, J. et al. Fecal microbiota transplantation for rheumatoid arthritis: a case report. *Clin. Case Rep.* **9**, 906–909 (2021).
160. Costello, S. P. et al. Effect of fecal microbiota transplantation on 8-week remission in patients with ulcerative colitis: a randomized clinical trial. *JAMA* **321**, 156–164 (2019).
161. Moayyedi, P. et al. Fecal microbiota transplantation induces remission in patients with active ulcerative colitis in a randomized controlled trial. *Gastroenterology* **149**, 102–109.e6 (2015).
162. Paramsothy, S. et al. Multidonor intensive faecal microbiota transplantation for active ulcerative colitis: a randomised placebo-controlled trial. *Lancet* **389**, 1218–1228 (2017).
163. Rossen, N. G. et al. Findings from a randomized controlled trial of fecal transplantation for patients with ulcerative colitis. *Gastroenterology* **149**, 110–118.e4 (2015).
164. Vaughn, B. P. et al. Increased intestinal microbial diversity following fecal microbiota transplant for active Crohn's disease. *Inflamm. Bowel Dis.* **22**, 2182–2190 (2016).
165. Cui, B. et al. Fecal microbiota transplantation through mid-gut for refractory Crohn's disease: safety, feasibility, and efficacy trial results. *J. Gastroenterol. Hepatol.* **30**, 51–58 (2015).
166. Philips, C. A. et al. Healthy donor fecal microbiota transplantation in steroid-ineligible severe alcoholic hepatitis: a pilot study. *Clin. Gastroenterol. Hepatol.* **15**, 600–602 (2017).
167. Mullish, B. H., McDonald, J. A. K., Thursz, M. R. & Marchesi, J. R. Fecal microbiota transplant from a rational stool donor improves hepatic encephalopathy: a randomized clinical trial. *Hepatol* **66**, 1354–1355 (2017).
168. Kootte, R. S. et al. Improvement of insulin sensitivity after lean donor feces in metabolic syndrome is driven by baseline intestinal microbiota composition. *Cell Metab.* **26**, 611–619.e6 (2017).
169. Kang, D. W. et al. Long-term benefit of microbiota transfer therapy on autism symptoms and gut microbiota. *Sci. Rep.* **9**, 5821 (2019).
170. Lloyd-Price, J. et al. Multi-omics of the gut microbial ecosystem in inflammatory bowel diseases. *Nature* **569**, 655–662 (2019).
171. Dailey, F. E., Turse, E. P., Daglilar, E. & Tahan, V. The dirty aspects of fecal microbiota transplantation: a review of its adverse effects and complications. *Curr. Opin. Pharmacol.* **49**, 29–33 (2019).
172. Wilson, B. C., Vatanen, T., Cutfield, W. S. & O'Sullivan, J. M. The super-donor phenomenon in fecal microbiota transplantation. *Front. Cell. Infect. Microbiol.* **9**, 2 (2019).
173. Knox, N. C., Forbes, J. D., Van Domselaar, G. & Bernstein, C. N. The gut microbiome as a target for IBD treatment: are we there yet? *Curr. Treat. Options Gastroenterol.* **17**, 115–126 (2019).
174. Burrello, C. et al. Therapeutic faecal microbiota transplantation controls intestinal inflammation through IL10 secretion by immune cells. *Nat. Commun.* **9**, 5184 (2018).
175. Jang, Y. O. et al. Fecal microbial transplantation and a high fiber diet attenuates emphysema development by suppressing inflammation and apoptosis. *Exp. Mol. Med.* **52**, 1128–1139 (2020).
176. Anhê, F. F. et al. Treatment with camu camu (Myrciaria dubia) prevents obesity by altering the gut microbiota and increasing energy expenditure in diet-induced obese mice. *Gut* **68**, 453–464 (2019).
177. Petrof, E. O. et al. Stool substitute transplant therapy for the eradication of Clostridium difficile infection: 'RePOOPulating' the gut. *Microbiome* **1**, 3 (2013).
178. Tanoue, T. et al. A defined commensal consortium elicits CD8 T cells and anti-cancer immunity. *Nature* **565**, 600–605 (2019).
179. Sood, A. et al. The probiotic preparation, VSL#3 induces remission in patients with mild-to-moderately active ulcerative colitis. *Clin. Gastroenterol. Hepatol.* **7**, 1202–1209 (2009).
180. Derwa, Y., Gracie, D. J., Hamlin, P. J. & Ford, A. C. Systematic review with meta-analysis: the efficacy of probiotics in inflammatory bowel disease. *Aliment. Pharmacol. Ther.* **46**, 389–400 (2017).
181. Ganji-Arjenaki, M. & Rafieian-Kopaei, M. Probiotics are a good choice in remission of inflammatory bowel diseases: a meta analysis and systematic review. *J. Cell. Physiol.* **233**, 2091–2103 (2018).
182. Shigemori, S. & Shimosato, T. Applications of genetically modified immunobiotics with high immunoregulatory capacity for treatment of inflammatory bowel diseases. *Front. Immunol.* **8**, 22 (2017).
183. Sales-Campos, H., Soares, S. C. & Oliveira, C. J. F. An introduction of the role of probiotics in human infections and autoimmune diseases. *Crit. Rev. Microbiol.* **45**, 413–432 (2019).

184. Flach, J., van der Waal, M. B., van den Nieuwboer, M., Claassen, E. & Larsen, O. F. A. The underexposed role of food matrices in probiotic products: reviewing the relationship between carrier matrices and product parameters. *Crit. Rev. Food Sci. Nutr.* **58**, 2570–2584 (2018).
185. Cassani, L., Gomez-Zavaglia, A. & Simal-Gandara, J. Technological strategies ensuring the safe arrival of beneficial microorganisms to the gut: from food processing and storage to their passage through the gastrointestinal tract. *Food Res. Int.* **129**, 108852 (2020).
186. Bezkorovainy, A. Probiotics: determinants of survival and growth in the gut. *Am. J. Clin. Nutr.* **73** (Suppl. 2), 399–405 (2001).
187. Maldonado-Gômez, M. X. et al. Stable engraftment of Bifidobacterium longum AH1206 in the human gut depends on individualized features of the resident microbiome. *Cell Host Microbe* **20**, 515–526 (2016).
188. Suez, J. et al. Post-antibiotic gut mucosal microbiome reconstitution is impaired by probiotics and improved by autologous FMT. *Cell* **174**, 1406–1423.e16 (2018).
189. Sorbara, M. T. & Pamer, E. G. Interbacterial mechanisms of colonization resistance and the strategies pathogens use to overcome them. *Mucosal Immunol.* **12**, 1–9 (2019).
190. Champagne, C. P., Gardner, N. J. & Roy, D. Challenges in the addition of probiotic cultures to foods. *Crit. Rev. Food Sci. Nutr.* **45**, 61–84 (2005).
191. Fujimori, S. et al. A randomized controlled trial on the efficacy of synbiotic versus probiotic or prebiotic treatment to improve the quality of life in patients with ulcerative colitis. *Nutrition* **25**, 520–525 (2009).
192. Amiriani, T. et al. Effect of Lactocare® synbiotic on disease severity in ulcerative colitis: a randomized placebo-controlled double-blind clinical trial. *Middle East. J. Dig. Dis.* **12**, 27–33 (2020).
193. Furrie, E. et al. Synbiotic therapy (Bifidobacterium longum/Synergy 1) initiates resolution of inflammation in patients with active ulcerative colitis: a randomised controlled pilot trial. *Gut* **54**, 242–249 (2005).
194. Steed, H. et al. Clinical trial: the microbiological and immunological effects of synbiotic consumption - a randomized double-blind placebo-controlled study in active Crohn's disease. *Aliment. Pharmacol. Ther.* **32**, 872–883 (2010).
195. Zamani, B., Farshbaf, S., Golkar, H. R., Bahmani, F. & Asemi, Z. Synbiotic supplementation and the effects on clinical and metabolic responses in patients with rheumatoid arthritis: a randomised, double-blind, placebo-controlled trial. *Br. J. Nutr.* **117**, 1095–1102 (2017).
196. Zare Javid, A., Aminzadeh, M., Haghighi-Zadeh, M. H. & Jamalvandi, M. The effects of synbiotic supplementation on glycemic status, lipid profile, and biomarkers of oxidative stress in type 1 diabetic patients. A placebo-controlled, double-blind, randomized clinical trial. *Diabetes Metab. Syndr. Obes.* **13**, 607–617 (2020).
197. Chen, L., Yang, T., Song, Y., Shu, G. & Chen, H. Effect of xanthan-chitosan-xanthan double layer encapsulation on survival of Bifidobacterium BB01 in simulated gastrointestinal conditions, bile salt solution and yogurt. *LWT Food Sci. Technol.* **81**, 274–280 (2017).
198. Fratianni, F. et al. Ability of synbiotic encapsulated Saccharomyces cerevisiae boulardii to grow in berry juice and to survive under simulated gastrointestinal conditions. *J. Microencapsul.* **31**, 299–305 (2014).
199. Cook, M. T., Tzortzis, G., Charalampopoulos, D. & Khutoryanskiy, V. V. Microencapsulation of a synbiotic into PLGA/alginate multiparticulate gels. *Int. J. Pharm.* **466**, 400–408 (2014).
200. Hehemann, J. H. et al. Transfer of carbohydrate-active enzymes from marine bacteria to Japanese gut microbiota. *Nature* **464**, 908–912 (2010).
201. Pudlo, N. A. et al. Extensive transfer of genes for edible seaweed digestion from marine to human gut bacteria. Preprint at *bioRxiv* https://doi.org/10.1101/2020.06.09.142968 (2020).
202. Walter, J., Britton, R. A. & Roos, S. Host-microbial symbiosis in the vertebrate gastrointestinal tract and the Lactobacillus reuteri paradigm. *Proc. Natl Acad. Sci. USA* **108**, 4645–4652 (2011).
203. Martínez, I. et al. The gut microbiota of rural Papua New Guineans: composition, diversity patterns, and ecological processes. *Cell Rep.* **11**, 527–538 (2015).
204. Mu, Q. et al. Control of lupus nephritis by changes of gut microbiota. *Microbiome* **5**, 73 (2017).
205. He, B. et al. Lactobacillus reuteri reduces the severity of experimental autoimmune encephalomyelitis in mice by modulating gut microbiota. *Front. Immunol.* **10**, 385 (2019).
206. De Moreno De Leblanc, A. et al. Evaluation of the biosafety of recombinant lactic acid bacteria designed to prevent and treat colitis. *J. Med. Microbiol.* **65**, 1038–1046 (2016).
207. Zeng, L. et al. An engineering probiotic producing defensin-5 ameliorating dextran sodium sulfate-induced mice colitis via Inhibiting NF-κB pathway. *J. Transl. Med.* **18**, 107 (2020).
208. Lerner, A., Matthias, T. & Aminov, R. Potential effects of horizontal gene exchange in the human gut. *Front. Immunol.* **8**, 1630 (2017).
209. Reynolds, A. et al. Carbohydrate quality and human health: a series of systematic reviews and meta-analyses. *Lancet* **393**, 434–445 (2019).
210. Scher, J. U. et al. Expansion of intestinal Prevotella copri correlates with enhanced susceptibility to arthritis. *eLife* **2**, e01202 (2013).
211. Kjeldsen-Kragh, J. et al. Controlled trial of fasting and one-year vegetarian diet in rheumatoid arthritis. *Lancet* **338**, 899–902 (1991).
212. Stoll, M. L. Genetics, Prevotella, and the pathogenesis of rheumatoid arthritis. *Lancet Rheumatol.* **2**, e375–e376 (2020).
213. Peltonen, R. et al. Faecal microbial flora and disease activity in rheumatoid arthritis during a vegan diet. *Br. J. Rheumatol.* **36**, 64–68 (1997).
214. Charbonneau, M. R., Isabella, V. M., Li, N. & Kurtz, C. B. Developing a new class of engineered live bacterial therapeutics to treat human diseases. *Nat. Commun.* **11**, 1738 (2020).
215. FitzGerald, M. J. & Spek, E. J. Microbiome therapeutics and patent protection. *Nat. Biotechnol.* **38**, 806–810 (2020).
216. Lloyd-Price, J., Abu-Ali, G. & Huttenhower, C. The healthy human microbiome. *Genome Med.* **8**, 51 (2016).
217. Schellekens, H. et al. Bifidobacterium longum counters the effects of obesity: partial successful translation from rodent to human. *EBioMedicine* **63**, 103176 (2021).
218. Fragiadakis, G. K. et al. Long-term dietary intervention reveals resilience of the gut microbiota despite changes in diet and weight. *Am. J. Clin. Nutr.* **111**, 1127–1136 (2020).
219. Genoni, A. et al. Long-term Paleolithic diet is associated with lower resistant starch intake, different gut microbiota composition and increased serum TMAO concentrations. *Eur. J. Nutr.* **59**, 1845–1848 (2020).
220. Saresella, M. et al. Immunological and clinical effect of diet modulation of the gut microbiome in multiple sclerosis patients: a pilot study. *Front. Immunol.* **8**, 1391 (2017).
221. Laffin, M. et al. A high-sugar diet rapidly enhances susceptibility to colitis via depletion of luminal short-chain fatty acids in mice. *Sci. Rep.* **9**, 12294 (2019).
222. Rodriguez-Palacios, A. et al. The artificial sweetener Splenda promotes gut proteobacteria, dysbiosis, and myeloperoxidase reactivity in Crohn's disease-like ileitis. *Inflamm. Bowel Dis.* **24**, 1005–1020 (2018).
223. Grabinger, T. et al. Alleviation of intestinal inflammation by oral supplementation with 2-fucosyllactose in mice. *Front. Microbiol.* **10**, 1385 (2019).
224. Berer, K. et al. Dietary non-fermentable fiber prevents autoimmune neurological disease by changing gut metabolic and immune status. *Sci. Rep.* **8**, 10431 (2018).
225. Chen, K. et al. Specific inulin-type fructan fibers protect against autoimmune diabetes by modulating gut immunity, barrier function, and microbiota homeostasis. *Mol. Nutr. Food Res.* **61**, 1601006 (2017).
226. Gudi, R. et al. Complex dietary polysaccharide modulates gut immune function and microbiota, and promotes protection from autoimmune diabetes. *Immunology* **157**, 70–85 (2019).
227. Rosser, E. C. et al. Microbiota-derived metabolites suppress arthritis by amplifying aryl-hydrocarbon receptor activation in regulatory B cells. *Cell Metab.* **31**, 837–851.e10 (2020).
228. Zhang, T. et al. Sodium butyrate reduces colitogenic immunoglobulin A-coated bacteria and modifies the composition of microbiota in IL-10 deficient mice. *Nutrients* **8**, 728 (2016).
229. Choi, S. C. et al. Gut microbiota dysbiosis and altered tryptophan catabolism contribute to autoimmunity in lupus-susceptible mice. *Sci. Transl. Med.* **12**, eaax2220 (2020).
230. Alrafas, H. R., Busbee, P. B., Nagarkatti, M. & Nagarkatti, P. S. Resveratrol modulates the gut microbiota to prevent murine colitis development through induction of Tregs and suppression of Th17 cells. *J. Leukoc. Biol.* **106**, 467–480 (2019).
231. Constante, M., Fragoso, G., Calvé, A., Samba-Mondonga, M. & Santos, M. M. Dietary heme induces gut dysbiosis, aggravates colitis, and potentiates the development of adenomas in mice. *Front. Microbiol.* **8**, 1809 (2017).
232. Lee, T. et al. Oral versus intravenous iron replacement therapy distinctly alters the gut microbiota and metabolome in patients with IBD. *Gut* **66**, 863–871 (2016).
233. Miranda, P. M. et al. High salt diet exacerbates colitis in mice by decreasing Lactobacillus levels and butyrate production. *Microbiome* **6**, 57 (2018).
234. Wilck, N. et al. Salt-responsive gut commensal modulates TH17 axis and disease. *Nature* **551**, 585–589 (2017).
235. Eaton, S. B. & Konner, M. Paleolithic nutrition: a consideration of its nature and current implications. *N. Engl. J. Med.* **312**, 283–289 (1985).
236. Cordain, L. et al. Plant-animal subsistence ratios and macronutrient energy estimations in worldwide hunter-gatherer diets. *Am. J. Clin. Nutr.* **71**, 682–692 (2000).
237. Diamond, J. Evolution, consequences and future of plant and animal domestication. *Nature* **418**, 700–707 (2002).
238. Burkitt, D. Related disease — related cause? *Lancet* **294**, 1229–1231 (1969).
239. Burkitt, D. P., Walker, A. R. P. & Painter, N. S. Dietary fiber and disease. *JAMA* **229**, 1068–1074 (1974).
240. Aries, V., Crowther, J. S., Drasar, B. S., Hill, M. J. & Williams, R. E. Bacteria and the aetiology of cancer of the large bowel. *Gut* **10**, 334–335 (1969).
241. Gu, P. & Feagins, L. A. Dining with inflammatory bowel disease: a review of the literature on diet in the pathogenesis and management of IBD. *Inflamm. Bowel Dis.* **26**, 181–191 (2020).
242. Sabino, J., Lewis, J. D. & Colombel, J. F. Treating inflammatory bowel disease with diet: a taste test. *Gastroenterology* **157**, 295–297 (2019).
243. Hou, J. K., Lee, D. & Lewis, J. Diet and inflammatory bowel disease: review of patient-targeted recommendations. *Clin. Gastroenterol. Hepatol.* **12**, 1592–1600 (2014).
244. Moayyedi, P., Simrén, M. & Bercik, P. Evidence-based and mechanistic insights into exclusion diets for IBS. *Nat. Rev. Gastroenterol. Hepatol.* **17**, 406–413 (2020).

Acknowledgements
This work was supported by the following grants in the laboratory of M.S.D.: Luxembourg National Research Fund (FNR) CORE grants (C15/BM/10318186 and C18/BM/12585940) to M.S.D.; M.B. was supported by a European Commission Horizon 2020 Marie Skłodowska-Curie Actions individual fellowship (897408); M.W. was supported by a Fulbright grant for Visiting Scholars from the Commission for Educational Exchange between the United States of America, Belgium and Luxembourg; E.T.G. was supported by the Luxembourg National Research Fund PRIDE (17/11823097) and the Fondation du Pélican de Mie et Pierre Hippert-Faber, under the aegis of the Fondation de Luxembourg. G.V.P. was supported by a fellowship from the W. Garfield Weston Foundation and E.C.M. acknowledges the financial support from National Institutes of Health (DK118024).

Author contributions
All authors have contributed to the writing and editing of the manuscript.

Competing interests
The authors declare no competing interests.

Peer review information
Nature Reviews Gastroenterology & Hepatology thanks R. Carmody and the other, anonymous, reviewers for their contribution to the peer review of this work.

Publisher's note
Springer Nature remains neutral with regard to jurisdictional claims in published maps and institutional affiliations.

Supplementary information
The online version contains supplementary material available at https://doi.org/10.1038/s41575-021-00512-7.

nature portfolio

https://doi.org/10.1038/s41575-021-00512-7

Supplementary information

Leveraging diet to engineer the gut microbiome

In the format provided by the authors and unedited

SUPPLEMENTARY INFORMATION

Supplementary Box 1 | Phytochemicals: spotlight on polyphenols

Phytochemicals are plant-derived secondary metabolites that, at appropriate doses, can exert health benefits by acting as prebiotics for the gut microbiota[S1]. In rodent models, it was demonstrated that phytochemicals induce stress resistance mechanisms in the host, such as autophagy induction and ROS inactivation[S1]. Although there is substantial variation between individuals, as little as 5% of phenols, polyphenols and tannins ingested in the diet are absorbed in the human small intestine[S2]. Consequently, phytochemicals accumulate in the colon where they are metabolized by microbial enzymes, influencing the gut microbiota community structure in a bidirectional manner. The exact effects vary depending on the underlying microbiome composition and the structure of the specific phytochemical[S1]; for example, urolithin A, a microbial metabolite derived from berry and pomegranate polyphenols, enhances intestinal barrier function by activating aryl hydrocarbon receptor (AhR)–NRF2-dependent pathways to upregulate epithelial tight junction proteins[S3]. Due to their anti-inflammatory and anti-oxidative properties, most studies examining the effects of phytochemicals in humans or animal models consider the direct effects of polyphenols — including flavonoids, phenolic acids, lignans and other plant-derived secondary metabolites — on the host and key signalling pathways[S4]. However, polyphenols might also represent an under-exploited opportunity to selectively modify the gut microbiome, as demonstrated through *in vitro* studies[S5] and studies in mouse models of metabolic[S6] or autoimmune diseases[S7] (**Table 1**). Indeed, various polyphenols, such as resveratrol, curcumin or epigallocatechin gallate, are being tested in clinical trials to assess their efficacy in treating autoimmune diseases such as vitiligo, ulcerative colitis and multiple sclerosis[S4]. Although the initial findings are promising, further translational studies are needed to define the effects of individual phytochemicals on the gut microbiome, particularly in the context of active disease.

Supplementary Box 2 | Micronutrient imbalances

Micronutrients are vitamins or minerals that are needed in small quantities to maintain health and are almost exclusively obtained through diet or dietary supplements[S8]. Micronutrients can exert a marked effect on microbial composition, as demonstrated in human microbiome-associated (HMA) mouse models and *in vitro* growth assays[S8]; hence, the intake of these vitamins or minerals might be a readily modifiable factor to alter the microbiome and facilitate treatment of autoimmune diseases.

Iron dysregulation and consequent host–microbiome imbalance might underlie many autoimmune diseases, as reviewed elsewhere[S9]. For example, IBD is often associated with iron deficiency[S10,S11], yet supplementation is problematic because it encourages expansion of commensals with high pathogenic potential, which have evolved specific strategies to acquire and assimilate iron[S12], as demonstrated in mice[S10] and patients with IBD[S11]. In a DSS-induced colitis mouse model, oral haem supplementation encouraged *Enterobacteriaceae* blooms and led to increased expression of inflammatory markers (that is, *Lcn2* and *Il6* transcripts) compared to untreated controls, while intra-peritoneal haem administration resulted in less weight loss due to colitis, decreased *Lcn2* mRNA, and reduced *Enterobacteriaceae* compared to untreated controls[S13] (**Table 1**). Luminal haem appears to favour potential pathogens and exacerbate inflammation, highlighting the need to consider the effects of iron on the gut microbiome and use alternative routes of administration to address anaemia, where possible. Indeed, among patients with IBD, intravenous administration was more effective at restoring serum ferritin-mediated iron storage and had a lower adverse effect on microbiota composition than oral administration[S11] (**Table 1**). Thus, it might be advisable to reduce oral iron intake through a custom diet plan and supplement iron intravenously, so as to discourage the expansion of disease-promoting gut microorganisms.

Salt provides two essential micronutrients for the maintenance of electrolyte balance and functioning of cell membrane transport systems: sodium cations and chloride anions. However, excess salt intake, also a characteristic of a Western diet, results in microbiota-dependent exacerbation of DSS-induced colitis[S14] and EAE[S15] (**Table 1**). Excessive salt intake consistently depletes *Lactobacillus* species and encourages expansion of pro-inflammatory T_H17 cells in mice and healthy humans[S15]. Many members of this genus produce immune-modulating metabolites, including butyrate and indole-3-lactic acid (ILA), which exert a dose-dependent reduction in T_H17 polarization of $CD4^+$ T cells[S15] (**FIG. 2**). Thus, replenishing lost *Lactobacillus* spp. by decreasing salt intake and/or continuous probiotic supplementation might hold therapeutic benefit for patients with autoimmune disease. Indeed, daily gavage of *Lactobacillus murinus* decreased T_H17 cells and ameliorated EAE among mice on a high salt diet[S15]. The dynamics between salt and *Lactobacillus* spp. demonstrate

that, while dietary alterations might independently modify the microbiome in the prevention or promotion of autoimmune disease, there is great potential to use diet in combination with other live therapeutics.

Supplementary Figure 1 | Orthogonal niche engineering allows targeted manipulation of the microbiome

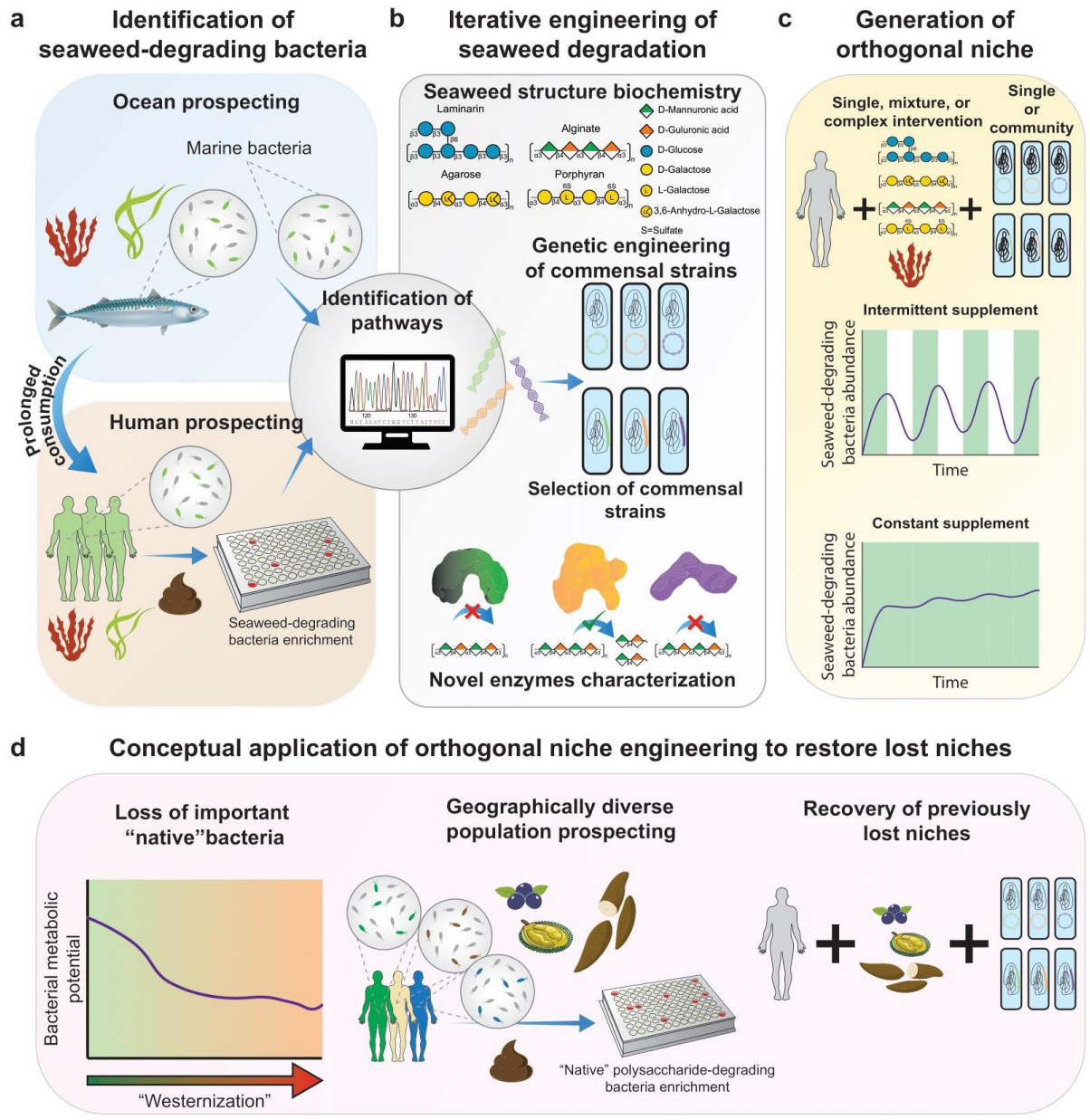

Supplementary Figure 1 Legend. Harnessing rare nutrient metabolism (e.g. seaweed degradation) allows generation of previously untapped niches in the human gut, allowing stable engraftment of bacteria. (a) This approach utilizes the identification of seaweed-degrading bacteria through culture-dependent and culture-independent methods in the marine environment (blue panel) and individuals who traditionally consume seaweed (brown panel). The prolonged consumption of seaweed and ocean-derived nutrients by certain individuals led to the acquisition of seaweed-degrading genes by

commensal bacteria, potentially through DNA exchange with marine microbes. (b) The iterative engineering step of this process would start with identification of these seaweed-degrading pathways using sequencing approaches. The further combination of understanding polysaccharide chemical structures and discovery of novel enzymes can lead to better genetic engineering of commensal bacteria or selection of commensal strains that possess the metabolic capability to degrade specific seaweed polysaccharides, e.g. porphyran and agarose. (c) The generation of an orthogonal niche can be achieved through different approaches, i.e. supplementation with a seaweed-related polysaccharide(s) or untreated seaweed in combination with a single strain or a community of bacteria that target the substrate(s). While the long-term stability of these systems has to be further investigated, especially in the context of horizontal gene transfer, this approach allows direct manipulation of the engrafted bacteria by “pulsing” the intervention regimen, e.g. intermittent supplementation, or by maintaining constant supplement, driving to different outcomes (yellow panel). (d) Furthermore, orthogonal niche engineering could be used to restore previously lost niches in the human gut by prospecting nutrients uniquely consumed by diverse populations.

SUPPLEMENTARY REFERENCES

S1. Martel, J., Ojcius, D. M., Ko, Y. F. & Young, J. D. Phytochemicals as Prebiotics and Biological Stress Inducers. *Trends in Biochemical Sciences* (2020) doi:10.1016/j.tibs.2020.02.008.

S2. Clifford, M. N. Diet-derived phenols in plasma and tissues and their implications for health. *Planta Medica* (2004) doi:10.1055/s-2004-835835.

S3. Singh, R. *et al.* Enhancement of the gut barrier integrity by a microbial metabolite through the Nrf2 pathway. *Nat. Commun.* (2019) doi:10.1038/s41467-018-07859-7.

S4. Khan, H. *et al.* Polyphenols in the treatment of autoimmune diseases. *Autoimmunity Reviews* (2019) doi:10.1016/j.autrev.2019.05.001.

S5. Lakes, J. E., Richards, C. I. & Flythe, M. D. Inhibition of Bacteroidetes and Firmicutes by select phytochemicals. *Anaerobe* (2020) doi:10.1016/j.anaerobe.2019.102145.

S6. Roopchand, D. E. *et al.* Dietary polyphenols promote growth of the gut bacterium Akkermansia muciniphila and attenuate high-fat diet-induced metabolic syndrome. *Diabetes* (2015) doi:10.2337/db14-1916.

S7. Alrafas, H. R., Busbee, P. B., Nagarkatti, M. & Nagarkatti, P. S. Resveratrol modulates the gut microbiota to prevent murine colitis development through induction of Tregs and suppression of Th17 cells. *J. Leukoc. Biol.* (2019) doi:10.1002/JLB.3A1218-476RR.

S8. Hibberd, M. C. *et al.* The effects of micronutrient deficiencies on bacterial species from the human gut microbiota. *Sci. Transl. Med.* (2017) doi:10.1126/scitranslmed.aal4069.

S9. Kell, D. B. & Pretorius, E. No effects without causes: the Iron Dysregulation and Dormant Microbes hypothesis for chronic, inflammatory diseases. *Biol. Rev.* (2018) doi:10.1111/brv.12407.

S10. Ellermann, M. *et al.* Dietary iron variably modulates assembly of the intestinal microbiota in colitis-resistant and colitis-susceptible mice. *Gut Microbes* **11**, 32–50 (2019).

S11. Lee, T. *et al.* Oral versus intravenous iron replacement therapy distinctly alters the gut microbiota and metabolome in patients with IBD. *Gut* **66**, 863–871 (2016).

S12. Choby, J. E. & Skaar, E. P. Heme Synthesis and Acquisition in Bacterial Pathogens. *J. Mol. Biol.* (2016) doi:10.1016/j.jmb.2016.03.018.

S13. Constante, M., Fragoso, G., Calvé, A., Samba-Mondonga, M. & Santos, M. M. Dietary heme induces gut dysbiosis, aggravates colitis, and potentiates the development of adenomas in mice. *Front. Microbiol.* **8**, 1809 (2017).

S14. Miranda, P. M. *et al.* High salt diet exacerbates colitis in mice by decreasing Lactobacillus levels and butyrate production. *Microbiome* **6**, 57 (2018).

S15. Wilck, N. *et al.* Salt-responsive gut commensal modulates TH17 axis and disease. *Nature* (2017) doi:10.1038/nature24628.

1.2.4 The 14SM gnotobiotic mouse model

The complex nature of the gut microbiome makes it a challenging research topic. Lack of data standardization, proper coordination and collaboration remain problems [50]. Furthermore, translating descriptive research into medical interventions or industrial applications has proven challenging due to the large compositional complexity of the microbiome and high interpersonal variability [51]. Shedding light on the detailed mechanisms underlying the complex interaction of the microbiome with itself and its environment remains challenging, but vital to better translate our knowledge into applications. One potential approach to address these highly complex challenges is to employ gnotobiotic mouse models. These are germ-free mice in which defined bacterial communities are assembled. The use of these defined communities, consisting of a limited number of often fully characterized bacteria, allows it to better track the functional mechanisms underlying the bacterial community dynamics. For this purpose, we chose employ the previously designed 14-member synthetic human gut microbiota (14SM) in this work [26]. This synthetic microbiota consists of 14 fully characterized commensal human bacteria. The members of which have been chosen to represent the normal phylogenetic distribution of the human gut, with *Bacteroidetes* and *Firmicutes* being the most abundant species and also including *Actinobacteria*, *Proteobacteria* and *Verrucomicrobiota* (Fig. 1.4) .

Furthermore, important metabolic capabilities were considered, such as plant and host glycan degradation, sulfate reduction and acetogenesis. In addition to being fully sequenced, the carbohydrate utilization capabilities of each of the 14 bacteria has been determined by growth assay (Fig. 1.5). For this purpose, minimal media was used with one of 42 plant- or animal-derived mono- and polysaccharides as sole carbon source. It should be noted that 4 of the 14 bacteria were capable of degrading mucus *O*-glycans (Fig. 1.5). *Akkermansia muciniphila* and *Barnesiella intestinihominis* are mucin specialists while *Bacteroides thetaiotaomicron* and *Bacteroides caccae* are mucin generalists (Fig. 1.5).

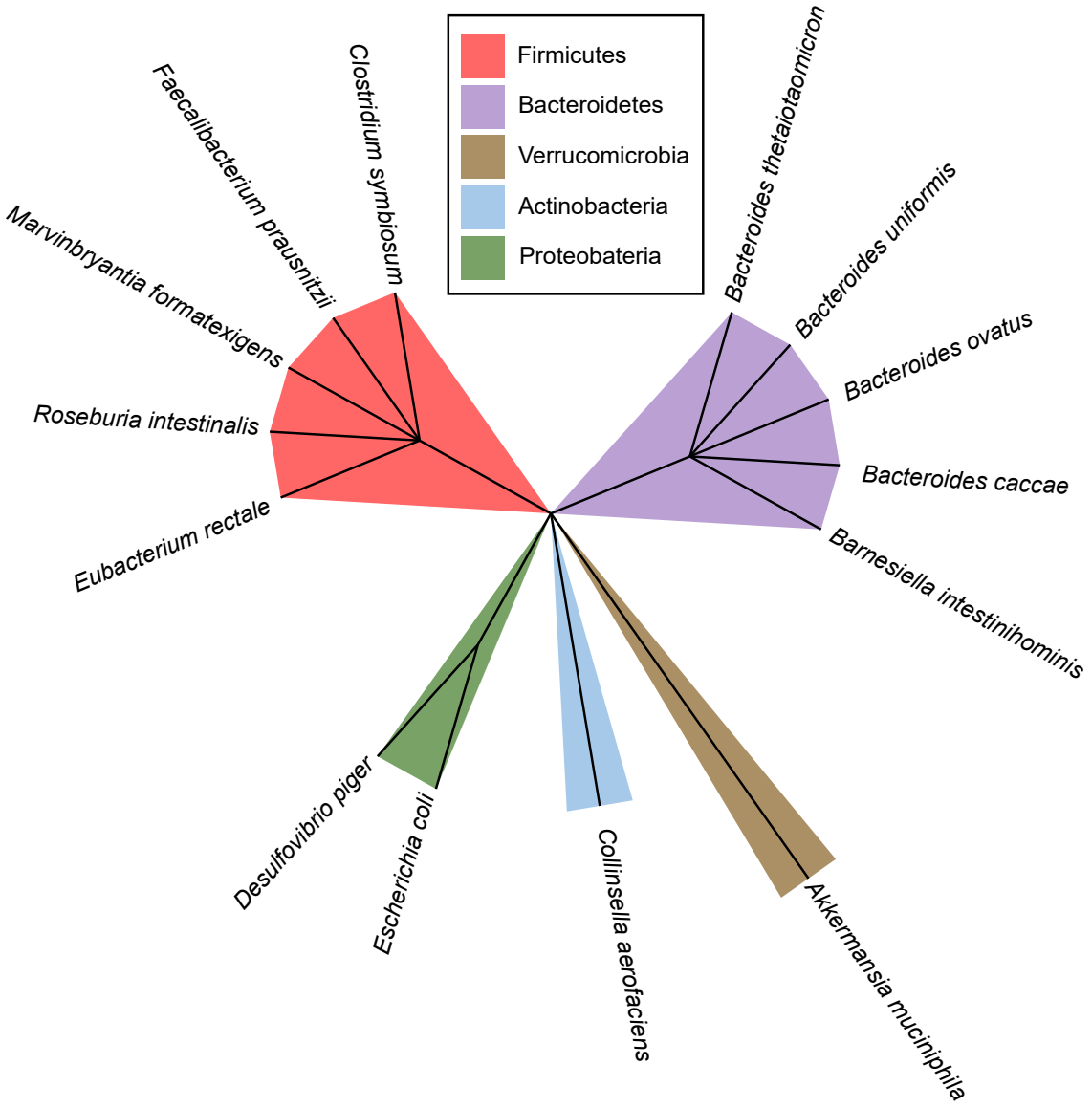

Figure 1.4 – **Composition of the 14SM community.** The members of the 14SM have been chosen to represent the normal phylogenetic distribution found in the human gut, but metabolic capabilities were also considered.

The 14SM has been shown to be highly responsive to dietary fiber deprivation (Fig. 1.6 A). A lack of dietary fiber leads to a reduction of typical fiber degraders such as *Eubacterium rectale* and *Bacteroides ovatus*, while mucin-degrading bacteria such as *A. muciniphila* and *B. caccae* drastically expand (Fig. 1.6 A). These shifts in bacterial abundance also led to an overall increased mucolytic activity of the gut microbiome, resulting in a thinner mucus layer (Fig. 1.6 B). As such the

14SM model is an invaluable model in order to study the effect of natural mucus layer erosion in the context of different diseases.

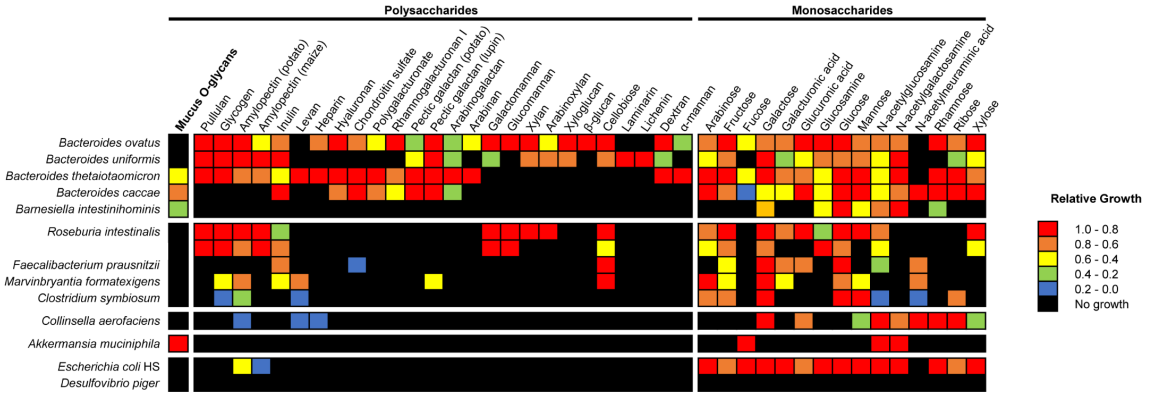

Figure 1.5 – **Results of carbohydrate growth assay of the 14SM community.** Together the 14SM community is able to degrade and grow on all carbon sources commonly found in the human gut. Adapted from Desai et al., [26].

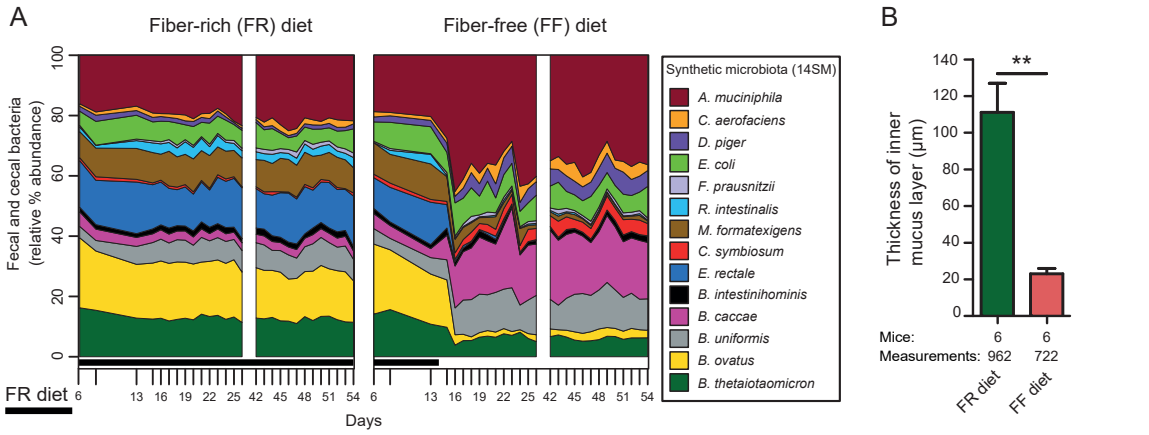

Figure 1.6 – **Dietary fiber deprivation leads to an expansion of the mucus-degrading bacteria of the 14SM resulting in the natural erosion of the gut mucus layer.** (A) Dietary-fiber deprivation causes the microbiome composition drastically to shift as assessed by 16S rRNA gene sequencing. Typical fiber-degrading bacteria reduce in abundance, while mucus-degrading bacteria expand. (B) As a result of the expansion of the mucus-degrading bacteria, the hosts gut mucus layer is eroded, resulting in a thinner mucus layer. Adapted from Desai et al., [26].

Bibliography

[1] Hansson GC. 2020. Mucins and the Microbiome. Annu Rev Biochem.

[2] Johansson ME V, Sjövall H, Hansson GC. 2013. The gastrointestinal mucus system in health and disease. Nat Rev Gastroenterol Hepatol 10:352–61.

[3] Gum JR, Hicks JW, Toribara NW, Siddiki B, Kim YS. 1994. Molecular Cloning of Human Intestinal Mucin (MUC2) cDNA: Identification of the Amino Terminus and Overall Sequence Similarity to Prepro-Von Willebrand Factor. J Biol Chem 269:2440–2446.

[4] Ambort D, Johansson MEV, Gustafsson JK, Nilsson HE, Ermund A, Johansson BR, Koeck PJB, Hebert H, Hansson GC. 2012. Calcium and pH-dependent packing and release of the gel-forming MUC2 mucin. Proc Natl Acad Sci U S A https://doi.org/10.1073/pnas.1120269109.

[5] Johansson ME V, Larsson JMH, Hansson GC. 2011. The two mucus layers of colon are organized by the MUC2 mucin, whereas the outer layer is a legislator of host-microbial interactions. Proc Natl Acad Sci U S A 108 Suppl:4659–65.

[6] Martens EC, Neumann M, Desai MS. 2018. Interactions of commensal and pathogenic microorganisms with the intestinal mucosal barrier. Nat Rev Microbiol 16:457–470.

[7] Hansson GC, Johansson MEV. 2010. The inner of the two Muc2 mucin-dependent mucus layers in colon is devoid of bacteria. Gut Microbes https://doi.org/10.4161/gmic.1.1.10470.

[8] Larsson JMH, Karlsson H, Sjövall H, Hansson GC. 2009. A complex, but uniform O-glycosylation of the human MUC2 mucin from colonic biopsies analyzed by nanoLC/MSn. Glycobiology https://doi.org/10.1093/glycob/cwp048.

[9] Johansson ME V., Phillipson M, Petersson J, Velcich A, Holm L, Hansson GC. 2008. The inner of the two Muc2 mucin-dependent mucus layers in colon is devoid of bacteria. Proc Natl Acad Sci 105:15064–15069.

[10] Raimondi S, Musmeci E, Candeliere F, Amaretti A, Rossi M. 2021. Identification of mucin degraders of the human gut microbiota. Sci Rep https://doi.org/10.1038/s41598-021-90553-4.

[11] Pelaseyed T, Zäch M, Petersson ÅC, Svensson F, Johansson DGA, Hansson GC. 2013. Unfolding dynamics of the mucin SEA domain probed by force spectroscopy suggest that it acts as a cell-protective device. FEBS J https://doi.org/10.1111/febs.12144.

[12] Cone RA. 2009. Barrier properties of mucus. Adv Drug Deliv Rev.

[13] Desai MA, Mutlu M, Vadgama P. 1992. A study of macromolecular diffusion through native porcine mucus. Experientia https://doi.org/10.1007/BF01923598.

[14] Liu L, Tian C, Dong B, Xia M, Cai Y, Hu R, Chu X. 2021. Models to evaluate the barrier properties of mucus during drug diffusion. Int J Pharm.

[15] Larhed AW, Artursson P, Björk E. 1998. The influence of intestinal mucus components on the diffusion of drugs. Pharm Res https://doi.org/10.1023/A:1011948703571.

[16] Bakshani CR, Morales-Garcia AL, Althaus M, Wilcox MD, Pearson JP, Bythell JC, Burgess JG. 2018. Evolutionary conservation of the antimicrobial function of mucus: A first defence against infection. npj Biofilms Microbiomes.

[17] Kavanaugh NL, Zhang AQ, Nobile CJ, Johnson AD, Ribbeck K. 2014. Mucins suppress virulence traits of Candida albicans. MBio https://doi.org/10.1128/mBio.01911-14.

[18] Co JY, Cárcamo-Oyarce G, Billings N, Wheeler KM, Grindy SC, Holten-Andersen N, Ribbeck K. 2018. Mucins trigger dispersal of Pseudomonas aeruginosa biofilms. npj Biofilms Microbiomes https://doi.org/10.1038/s41522-018-0067-0.

[19] Rogier EW, Frantz AL, Bruno MEC, Kaetzel CS. 2014. Secretory IgA is concentrated in the outer layer of colonic mucus along with gut bacteria. Pathogens https://doi.org/10.3390/pathogens3020390.

[20] Vaishnava S, Yamamoto M, Severson KM, Ruhn KA, Yu X, Koren O, Ley R, Wakeland EK, Hooper L V. 2011. The antibacterial lectin RegIIIγ promotes the spatial segregation of microbiota and host in the intestine. Science (80-) https://doi.org/10.1126/science.1209791.

[21] Sommer F, Bäckhed F. 2015. The gut microbiota engages different signaling pathways to induce Duox2 expression in the ileum and colon epithelium. Mucosal Immunol https://doi.org/10.1038/mi.2014.74.

[22] Almeida GMF, Laanto E, Ashrafi R, Sundberg LR. 2019. Bacteriophage adherence to mucus mediates preventive protection against pathogenic bacteria. MBio https://doi.org/10.1128/mBio.01984-19.

[23] Pelaseyed T, Hansson GC. 2020. Membrane mucins of the intestine at a glance. J Cell Sci https://doi.org/10.1242/JCS.240929.

[24] Koropatkin NM, Cameron EA, Martens EC. 2012. How glycan metabolism shapes the human gut microbiota. Nat Rev Microbiol.

[25] Bunesova V, Lacroix C, Schwab C. 2018. Mucin Cross-Feeding of Infant Bifidobacteria and Eubacterium hallii. Microb Ecol https://doi.org/10.1007/s00248-017-1037-4.

[26] Desai MS, Seekatz AM, Koropatkin NM, Kamada N, Hickey CA, Wolter M, Pudlo NA, Kitamoto S, Terrapon N, Muller A, Young VB, Henrissat B, Wilmes P, Stappenbeck TS, Núñez G, Martens EC. 2016. A Dietary Fiber-Deprived Gut Microbiota Degrades the Colonic Mucus Barrier and Enhances Pathogen Susceptibility. Cell 167:1339-1353.e21.

[27] van Passel MWJ, Kant R, Zoetendal EG, Plugge CM, Derrien M, Malfatti SA, Chain PSG, Woyke T, Palva A, de Vos WM, Smidt H. 2011. The genome of Akkermansia muciniphila, a dedicated intestinal mucin degrader, and its use in exploring intestinal metagenomes. PLoS One 6:e16876.

[28] Martens EC, Chiang HC, Gordon JI. 2008. Mucosal Glycan Foraging Enhances Fitness and Transmission of a Saccharolytic Human Gut Bacterial Symbiont. Cell Host Microbe 4:447–457.

[29] Van Herreweghen F, De Paepe K, Roume H, Kerckhof FM, Van de Wiele T. 2018. Mucin degradation niche as a driver of microbiome composition and Akkermansia muciniphila abundance in a dynamic gut model is donor independent. FEMS Microbiol Ecol https://doi.org/10.1093/femsec/fiy186.

[30] Hino S, Mizushima T, Kaneko K, Kawai E, Kondo T, Genda T, Yamada T, Hase K, Nishimura N, Morita T. 2020. Mucin-Derived O-Glycans act as endogenous fiber and sustain mucosal immune homeostasis via short-Chain fatty acid production in rat cecum. J Nutr https://doi.org/10.1093/jn/nxaa097.

[31] Ducarmon QR, Zwittink RD, Hornung BVH, van Schaik W, Young VB, Kuijper EJ. 2019. Gut Microbiota and Colonization Resistance against Bacterial Enteric Infection. Microbiol Mol Biol Rev https://doi.org/10.1128/mmbr.00007-19.

[32] Johansson MEV, Jakobsson HE, Holmén-Larsson J, Schütte A, Ermund A, Rodríguez-Piñeiro AM, Arike L, Wising C, Svensson F, Bäckhed F, Hansson GC. 2015. Normalization of host intestinal mucus layers requires long-term microbial colonization. Cell Host Microbe https://doi.org/10.1016/j.chom.2015.10.007.

[33] Petersson J, Schreiber O, Hansson GC, Gendler SJ, Velcich A, Lundberg JO, Roos S, Holm L, Phillipson M. 2011. Importance and regulation of the colonic mucus barrier in a mouse model of colitis. Am J Physiol - Gastrointest Liver Physiol https://doi.org/10.1152/ajpgi.00422.2010.

[34] Konopka A. 2009. What is microbial community ecology. ISME J https://doi.org/10.1038/ismej.2009.88.

[35] Berg G, Rybakova D, Fischer D, Cernava T, Vergès MCC, Charles T, Chen X, Cocolin L, Eversole K, Corral GH, Kazou M, Kinkel L, Lange L, Lima N, Loy A, Macklin JA, Maguin E, Mauchline T, McClure R, Mitter B, Ryan M,

Sarand I, Smidt H, Schelkle B, Roume H, Kiran GS, Selvin J, Souza RSC de, Van Overbeek L, Singh BK, Wagner M, Walsh A, Sessitsch A, Schloter M. 2020. Microbiome definition re-visited: old concepts and new challenges. Microbiome.

[36] Whipps J, Lewis K, Cooke R. 1988. Mycoparasitism and plant disease control, p. 161–187. In M, B (ed.), Fungi in Biological Control Systems. Manchester University Press.

[37] Sender R, Fuchs S, Milo R. 2016. Revised Estimates for the Number of Human and Bacteria Cells in the Body. PLoS Biol https://doi.org/10.1371/journal.pbio.1002533.

[38] Korpela K, Costea P, Coelho LP, Kandels-Lewis S, Willemsen G, Boomsma DI, Segata N, Bork P. 2018. Selective maternal seeding and environment shape the human gut microbiome. Genome Res https://doi.org/10.1101/gr.233940.117.

[39] Turnbaugh PJ, Ley RE, Hamady M, Fraser-Liggett CM, Knight R, Gordon JI. 2007. The Human Microbiome Project. Nature.

[40] David LA, Maurice CF, Carmody RN, Gootenberg DB, Button JE, Wolfe BE, Ling A V, Devlin AS, Varma Y, Fischbach MA, Biddinger SB, Dutton RJ, Turnbaugh PJ. 2014. Diet rapidly and reproducibly alters the human gut microbiome. Nature 505:559–63.

[41] Sonnenburg ED, Smits SA, Tikhonov M, Higginbottom SK, Wingreen NS, Sonnenburg JL. 2016. Diet-induced extinctions in the gut microbiota compound over generations. Nature 529:212–215.

[42] Uhr GT, Dohnalová L, Thaiss CA. 2019. The Dimension of Time in Host-Microbiome Interactions. mSystems https://doi.org/10.1128/msystems.00216-18.

[43] Yatsunenko T, Rey FE, Manary MJ, Trehan I, Dominguez-Bello MG, Contreras M, Magris M, Hidalgo G, Baldassano RN, Anokhin AP, Heath AC, Warner B, Reeder J, Kuczynski J, Caporaso JG, Lozupone CA, Lauber C,

Clemente JC, Knights D, Knight R, Gordon JI. 2012. Human gut microbiome viewed across age and geography. Nature.

[44] Arumugam M, Raes J, Pelletier E, Paslier D Le, Yamada T, Mende DR, Fernandes GR, Tap J, Bruls T, Batto JM, Bertalan M, Borruel N, Casellas F, Fernandez L, Gautier L, Hansen T, Hattori M, Hayashi T, Kleerebezem M, Kurokawa K, Leclerc M, Levenez F, Manichanh C, Nielsen HB, Nielsen T, Pons N, Poulain J, Qin J, Sicheritz-Ponten T, Tims S, Torrents D, Ugarte E, Zoetendal EG, Wang J, Guarner F, Pedersen O, de Vos WM, Brunak S, Doré J, Weissenbach J, Ehrlich SD, Bork P, Antolín M, Artiguenave F, Blottiere HM, Almeida M, Brechot C, Cara C, Chervaux C, Cultrone A, Delorme C, Denariaz G, Dervyn R, Foerstner KU, Friss C, Guchte M van de, Guedon E, Haimet F, Huber W, Hylckama-Vlieg J van, Jamet A, Juste C, Kaci G, Knol J, Kristiansen K, Lakhdari O, Layec S, Roux K Le, Maguin E, Mérieux A, Minardi RM, M'rini C, Muller J, Oozeer R, Parkhill J, Renault P, Rescigno M, Sanchez N, Sunagawa S, Torrejon A, Turner K, Vandemeulebrouck G, Varela E, Winogradsky Y, Zeller G. 2011. Enterotypes of the human gut microbiome. Nature https://doi.org/10.1038/nature09944.

[45] Hamady M, Knight R. 2009. Microbial community profiling for human microbiome projects: Tools, techniques, and challenges. Genome Res.

[46] Costea PI, Hildebrand F, Manimozhiyan A, Bäckhed F, Blaser MJ, Bushman FD, De Vos WM, Ehrlich SD, Fraser CM, Hattori M, Huttenhower C, Jeffery IB, Knights D, Lewis JD, Ley RE, Ochman H, O'Toole PW, Quince C, Relman DA, Shanahan F, Sunagawa S, Wang J, Weinstock GM, Wu GD, Zeller G, Zhao L, Raes J, Knight R, Bork P. 2017. Enterotypes in the landscape of gut microbial community composition. Nat Microbiol https://doi.org/10.1038/s41564-017-0072-8.

[47] Zierer J, Jackson MA, Kastenmüller G, Mangino M, Long T, Telenti A, Mohney RP, Small KS, Bell JT, Steves CJ, Valdes AM, Spector TD, Menni C. 2018. The fecal metabolome as a functional readout of the gut microbiome. Nat Genet https://doi.org/10.1038/s41588-018-0135-7.

[48] Jovel J, Patterson J, Wang W, Hotte N, O'Keefe S, Mitchel T, Perry T, Kao D, Mason AL, Madsen KL, Wong GKS. 2016. Characterization of the gut microbiome using 16S or shotgun metagenomics. Front Microbiol https://doi.org/10.3389/fmicb.2016.00459.

[49] Cho I, Blaser MJ. 2012. The human microbiome: At the interface of health and disease. Nat Rev Genet.

[50] Proctor L. 2019. Priorities for the next 10 years of human microbiome research. Nature.

[51] Brüssow H. 2020. Problems with the concept of gut microbiota dysbiosis. Microb Biotechnol.

2. Scope and Aims

In this study I aimed to understand how the erosion of the colonic mucus layer affects disease susceptibility. For this purpose, we focus on two disease types, infectious diseases and autoimmune diseases. In the context of infectious disease we study *Citrobacter rodentium*, an attaching-and-effacing bacterial pathogen which is a murine model for enteropathogenic *Escherichia coli* infections. In the group of my supervisor Dr. Desai, we have previously shown that dietary-fiber deprived mice are more susceptible to *C. rodentium* and that this seems to be linked to an excessive mucus foraging, but the exact mechanisms as well as the specific bacteria driving this phenotype remain to be determined. As second infectious disease model, we study the intracellular food pathogens *Listeria monocytogenes* and *Salmonella enterica* serovar Typhimurium. It remains unknown if the susceptibility to intracellular pathogens would be majorly affected by the natural erosion of the mucus layer as only the initial infection dynamics should be affected. Finally, I study the intestinal parasite *Trichuris muris*, a murine model for *Trichuris trichuria* infections. *T. muris* is not only a valuable study model for Th1 and Th2 immune responses, host mucin secretion plays a key role in the clearance of the infection. In the context of autoimmune diseases, we use the IL-10$^{-/-}$ mouse model to study if an eroded mucus layer might affect the susceptibility to inflammatory bowel disease.

The specific aims of this study were:

1. Gaining insight into how dietary-fiber deprivation induced mucosal foraging can affect infectious diseases by:
    - Understanding which bacteria drive the increased susceptibility to *C. rodentium* as a result from excessive mucin foraging.

- Determining if mucosal erosion alters colitis-susceptibility to intracellular pathogens such as *L. monocytogenes* and *S.* Typhimurium.
- Determining how excessive mucosal foraging affects the host's immune response to the intestinal parasitic worm *T. muris*.

2. Gaining insight into how dietary fiber-deprivation induced mucosal foraging can affect susceptibility to autoimmune diseases such as inflammatory bowel disease.

3. Akkermansia muciniphila expansion under dietary-fiber deprivation increases susceptibility to attaching and effacing pathogen

3.1 Rationale

The first infectious disease we investigated was the attaching and effacing pathogen *Citrobacter rodentium*, a murine model for enteropathogenic *E. coli* infections. For its infection, this pathogen, which is normally self-limiting, needs to bypass the gut mucus layer in order to attach to the host epithelium. This makes *C. rodentium* a perfect model to study the protective role of the gut mucus layer. We have previously shown, that during dietary fiber deprivation, the host's mucus layer is eroded, resulting in an increased *C. rodentium* susceptibility. However, the role of the specific mucolytic bacteria and the detailed mechanisms leading to the increased host susceptibility remain open. Here we leveraged our gnotobiotic model to determine that *A. muciniphila* a sole mucolytic species is sufficient to generate the pathogen susceptible phenotype resulting of dietary fiber-deprivation. We furthermore show that this phenotype is not due to immunomodulatory properties of *A. muciniphila*, but probably due to the erosion of the gut mucus layer by *A. muciniphila*. This erosion most likely facilitates access of the enteric pathogen to the host tissue, thus increasing host susceptibility. However,

additional interactions between *A. muciniphila* and *C. rodentium* which increase susceptibility can't be excluded.

Personal contributions: I am first author of this paper draft and as such had significant contributions to the design, the execution, the data analysis, as well as, the drafting of this paper. I performed all the animal experiments, including husbandry for the animals in Luxembourg (over half of the total mouse number). I performed the experiments and analysis of all experiments in Figure 1 with the exception of the SCFA measurements. I additionally performed and analyzed all experiment for Figure 2 except the determination of the histological disease score (Figure 2E). The experiments for Figure 3 were performed by me with the help of my colleagues, while the data analysis was performed by my colleagues. Furthermore, I drafted the initial manuscript.

3.2 Results

Akkermansia muciniphila expansion under dietary-fiber deprivation increases susceptibility to *attaching and effacing pathogen*

Mathis Wolter[a,b], Marie Boudaud[a], Nicholas A. Pudlo[c], Kathryn A. Eaton[c], Gabriel V. Pereira[c], Eric C. Martens[c] and Mahesh S. Desai[a,d,*]

[a]*Department of Infection and Immunity, Luxembourg Institute of Health, Esch-sur-Alzette, Luxembourg*

[b]*Faculty of Science, Technology and Medicine, University of Luxembourg, Esch-sur-Alzette, Luxembourg*

[c]*Department of Microbiology and Immunology, University of Michigan Medical School, Ann Arbor, Michigan, USA*

[d]*Odense Research Center for Anaphylaxis, Department of Dermatology and Allergy Center, Odense University Hospital, University of Southern Denmark, Odense, Denmark*

[*]Corresponding author: Mahesh S. Desai, mahesh.desai@lih.lu

Abstract

The gut mucus layer is the first layer of defense against invading pathogens. We have previously shown that dietary fiber-deprivation causes the gut microbiome to excessively forage this protective barrier and increase susceptibility to the enteric pathogen *C. rodentium*. Here we leverage our 14-member synthetic human gut microbiota model to deduce which bacteria or function is responsible for the altered susceptibility. By dropping out different mucolytic bacteria from our synthetic community, we were able to show that, during dietary fiber deprivation, *A. muciniphila* alone was sufficient to make the host vulnerable to the enteric pathogen. This most likely due to the observed erosion of the gut mucus layer by *A. muciniphila*, enabling the pathogen to easily access the host tissue. Study of both host immune response and *C. rodentium* gene transcript was unable to provide insight into other mechanisms by which *A. muciniphila* could alter the host's susceptibility. Our study provides novel insight into the role of mucolytic bacteria during the development of pathogen infections, furthermore we show that depending on the dietary context, *A. muciniphila,* a commensal bacterium often considered as probiotic, can increase pathogen susceptibility.

Introduction

The gut mucus layer is the protective and lubricating layer of mucin glycoproteins covering our intestinal epithelium which is an integral part of the mucosal immune system (*1*). Amongst the many functions of the gut mucus layer is the protection against bacterial infection (*1*). The colonic mucus layer is mainly composed of Mucin-2 (MUC2) which are secreted in a greatly condensed form by goblet cells lining the gut epithelium and highly abundant in the crypts of the colon (*2*). Upon secretion the MUC2 glycoprotein will expand forming a nearly impenetrable, net-like structure covering the epithelium (*3*). The gut bacteria will erode the outer edges of this structure, resulting in a looser layer further in the lumen which hosts many of the members of the gut microbiota (*3*). This complex structure makes the mucus layer not only an important physical barrier, but also an interface between microbiota and immune system (*4*). Furthermore, the mucin glycoproteins can serve as important nutrient source for the gut microbiome (*5*). The degradation of the gut mucus by mucolytic bacteria—bacteria with the enzymatic capabilities to degrade the complex mucin glycoproteins—releases glycan residues which can be metabolized by either the mucolytic bacteria themselves or other members of the gut microbiota (*5*–*7*). The use of these host-derived glycoproteins seems to be particularly important in the absence of dietary fiber, which is one of the main nutrient sources of the gut microbiota (*8*).

Dietary fiber are long chained polysaccharides, which are non-digestible by the human enzymes (*9*). In contrast to the host, gut commensals have been shown to collectively possess an extensive repertoire of enzymes dedicated to the degradation of even the most complex of these fibers (*10*). The bacterial degradation of dietary fibers results in short-chain fatty acids (SCFAs) which are crucial for the maintenance of the host intestinal homeostasis (*11*). Hence, the beneficial properties of dietary fiber are not limited to their physical benefits in the form of fecal bulking and improved laxation (*12*), but they are also essential for the health of the gut microbiota and by extension for the host's health (*13*). Nonetheless, dietary fiber intake in many industrialized countries remains below the recommended intake for adults of 25g/day (*14*). As dietary fibers represent the main nutrient source of the gut microbiota, a lack thereof causes the microbiota to shift towards a more mucolytic composition which can result in an excessive scavenging of the gut mucus layer (*8*, *15*). The potential danger of an excessive mucus foraging in the context of enteric infections has been demonstrated using a variety of mouse models (*8*, *15*, *16*). For example, infections with *Citrobacter rodentium*, a murine model for enteropathogenic *Escherichia coli* infections, are usually self-limiting, but genetic ablation of the Muc2 gene results in lethal infections (*16*). In support of this, we have shown that the natural erosion of the gut mucus layer by a lack of dietary fiber consumption drastically increases the susceptibility to *C. rodentium* in both gnotobiotic and specific pathogen-free mice (*8*, *15*). However, the detailed mechanisms underlying excessive mucus erosion and increased pathogen susceptibility are still not fully elucidated. Here we leverage our well characterized 14-member

synthetic human gut microbiota in a gnotobiotic mouse model to elucidate which specific bacteria or functions are responsible for increasing pathogen susceptibility in the absence of fiber. Considering that the increased *C. rodentium* susceptibility is characterized by a thin mucus layer phenotype, we decided to focus on the mucolytic members of our 14SM community. Using this approach, we were able to show that *A. muciniphila* by itself is the major contributor to the *C. rodentium* susceptible phenotype.

Presence of mucolytic bacteria during dietary fiber deprivation does not influence the induced microbiota composition shifts, but affects SCFA and low-grade inflammation profiles.

We colonized age-matched germ-free Swiss-Webster mice which fed a fiber-rich (FR) diet, that is a normal mouse chow, with different synthetic microbiota (SM) **(Fig. 1A)**. All of the different SMs were based on the 14-member synthetic human gut microbiota which we previously described (*8*, *17*). As we wished to study the importance of the mucin-degrading bacteria in promoting susceptibility to *C. rodentium* we dropped out different mucolytic bacteria from this community in order design four new SMs (Fig. 1B). The 10SM contained none of 4 mucolytic bacteria present in the 14SM; *Akkermansia muciniphila*, *Barnesiella intestinihominis*, *Bacteroides caccae* and *Bacteroides thetaiotaomicron* (Fig. 1B). The 11SM contains only the mucin specialist *A. muciniphila*, while the 12SM contains both mucin generalists, *B. caccae* and *B. thetaiotaomicron* **(Fig. 1B)**. Finally, the 13SM contains all the mucin-degrading bacteria except for *A. muciniphila*. Initial colonization of the different SM was verified by qPCR using primers specific to each of the 14 bacterial strains as previously described (*17*). Mice were maintained for 14 days on the FR diet before half of the mice in each experimental group were switched to a fiber-free (FF) diet **(Fig. 1A)**. Forty days after the diet switch some of the mice were sacrificed to collect the presented pre-infection readouts, while the remaining were infected with approximately 10^9 CFU *C. rodentium* **(Fig. 1A)**. The mice were monitored up to 10 days post-infection (DPI) before they were sacrificed to collect final readouts **(Fig. 1A)**. The relative abundance of different members of the SM was determined for each group prior to the infection **(Fig. 1C)**. Throughout the different groups two major shifts can be observed when comparing the FR groups to the FF groups. There is an expansion of the mucolytic bacteria *A. muciniphila* and/or *B. caccae* (except in the 10SM group) and a reduction of typical fiber-degrading bacteria such as *Eubacterium rectale* and *Bacteroides ovatus* **(Fig. 1C-D)**. Interestingly, the community compositions do not seem to majorly shift between the different SMs with the dropping out of certain bacteria being mostly filled up by the equal expansion of the other bacteria **(Fig. 1C)**. This highlights that even without the mucolytic bacteria the SM are a fairly stable community. While we have previously shown that the 14SM community is characterized by a thinner mucus layer (*8*),

here we wished to assess if the erosion of the mucus layer also results in a higher penetrability **(Fig. 1E)**. We were able to show a significant increase in the penetrability of the gut mucus layer of the 14SM FF group compared to the FR group **(Fig. 1E)**. In contrast, the penetrability of both 13SM groups is similar to each other. **(Fig. 1E)**. As microbial produced SCFAs are essential for the maintenance of the mucosal barrier integrity (*18*), we assessed their concentration in the cecal content of the mice. Acetic acid concentrations were generally identical between the FR and the FF groups, in contrast propionic acid and butyric acid showed SM dependant changes. Propionic acid concentration was increased on the FR diet in both the 14SM and the 11SM group, while butyric acid was increased under FF conditions in the 14SM and 13SM group, but under FR conditions in the 11SM group **(Fig. 1F)**. Surprisingly, the 11SM data hints that in the presence of dietary fiber *A. muciniphila*, a mucin-specialist, might be involved in both the propionic and butyric acid synthesis. However, as this trend is not observed under FF conditions and *A. muciniphila* has a carbohydrate degrading activity specialized on host mucin degradation (*8*), the presence of a cross-feeding effect with one of the fiber-degrading specialists can be hypothesized. Furthermore, the lack of a similar trend in the butyrate production in the 14SM groups hints that this potential niche is overtaken by one of the other mucin-degrading bacteria. Considering the role of SCFA in maintaining the host intestinal homeostasis (*11*) we suspected that shifts in SCFA production might induce low levels of inflammation in the host. We therefore measured pre-infection fecal lipocalin-2 (LCN-2) concentration, as a biomarker for low-grade inflammation (*19*) **(Fig. 1G)**. Both the 14SM and the 13SM groups showed a significant increase in LCN-2 on the fiber-free diet with the 10SM group showing a nearly significant trend **(Fig. 1E)**. Looking at the colon shortening, another indicator for inflammation, we can see that all the groups except the 11SM and 10SM groups show a significant shortening of the colon on the FF diet **(Fig. 1F).** However, there does not seem any clear link with the SCFA concentrations and the inflammation levels assessed by LCN2 or colon length.

A. muciniphila ***is responsible for increased*** **C. rodentium** ***susceptibility during fiber-deprivation***

Leveraging our gnotobiotic model with the 5 different SMs, we set out to determine the presence of which bacteria are responsible for increasing the susceptibility to *C. rodentium* during fiber-deprivation. After the 40 days feeding period, we infected each group with *C. rodentium* and observed them for 10 days post infection. We were able to reproduce the previously described (*8*) susceptible phenotype in the 14SM model, however, while *C. rodentium* load was highly elevated in the FF group **(Fig. 2A)**, none of the mice in the 14SM group suffered from lethal colitis. Similarly, to the 14SM group the 11SM group showed drastically increased *C. rodentium* levels, while the 12SM and 10SM group only slightly elevated levels during 1-2 days on the FF diet and the 13SM group

showed no difference between both diet groups **(Fig. 2A)**. The weight loss after the infection mostly reflects this trend, with the 14SM and 11SM groups showing a significant weight loss on the FF diet, however, surprisingly also the 10SM group shows a weight loss during fiber-deprivation **(Fig. 2B)** and the same significant trends can be observed for fecal LCN-2 at the end of the infection **(Fig. 2C)**. In contrast, the colon lengths after the infection are reflective of their pre-infection status, with the 14SM, 13SM and 12SM showing a significant shortening on the FF diet **(Fig. 2D)**. Histological analysis of the cecum tissue confirms the strong level of inflammation during fiber-deprivation in the 14SM and 10SM group, however, surprisingly there seems to be also some inflammation in the 13SM group on the FF diet compared to the FR diet **(Fig. 2E)**. This observation is out of line with any of the other readouts from the 13SM group **(Fig. 2)**. The increased markers of inflammation in the absence of a high *C. rodentium* load in the FF-fed 10SM group **(Fig. 2)**, might be reflective of the pre-infection status were LCN-2 levels were already increased **(Fig. 1G)**. This might suggest that a complete lack of mucolytic bacteria could potentially disturb the host homeostasis during fiber-deprivation. This could be potentially explained by the lack of butyric acid production on the FF diet, which is present in the FF-fed 14SM and 13SM groups **(Fig. 1F)**. Overall, our data shows that the increased susceptibility to *C. rodentium* during dietary-fiber deprivation seems to be caused by the presence of a single bacteria: *A. muciniphila*. While the presence of all mucin-degrading bacteria seems to exacerbate this effect, the lack of *A. muciniphila* is sufficient to avoid the excessive vulnerability to *C. rodentium* on the FF diet. As *A. muciniphila* abundance is heavily modulated by the presence of dietary fiber, we decided to supplement the FF diet with 7.5% of the dietary fiber acetylated galactoglucomannan (AcGGM). We intended to rescue the vulnerable 14SM phenotype by supplementing this prebiotic. Unfortunately, AcGGM did have not have any impact on the outcome of the infection (Data not shown).

Exploration of host immune response and pathogen transcriptome does not offer a mechanism by which* A. muciniphila *could impact the pathogen susceptibility.

The presence of *A. muciniphila* during fiber deprivation appears to increase the penetrability of the mucus barrier **(Fig. 1E)**. This might explain the increased *C. rodentium* susceptibility under FF conditions, however *A. muciniphila* has also been studied for its potential immunomodulatory properties (*20–22*), offering another possible explanation. The expansion of it on the FF diet might have repercussions on the host immune response, thus explaining the increased *C. rodentium* susceptibility. As already the initial expansion of *C. rodentium* is heavily affected by dietary fiber deprivation we chose to assess the immune cell populations at 3 days post infection using fluorescence-activated cell sorting (FACS). Overall, the different immune cell populations show very similar trends, although there are barely any significant changes observed **(Fig. 3A and Fig. S1)**.

The RORγt positive T helper cell population (CD4+ RORγt+) is significantly decreased in the 13SM FF diet group compared to the FR group, while it does not show any significant differences in the 14SM group **(Fig. 3A)**. As T helper cells play an essential role in the clearance of *C. rodentium* (*23*), this could be a potential explanation for the susceptible phenotype. Additionally, Foxp3+ cytotoxic T cells (CD8+ Foxp3+) are significantly increased in both FF group **(Fig. 3A)**.

In order to further investigate the role of *A. muciniphila* in modulating pathogen susceptibility we investigated both mouse host and *C. rodentium* transcripts in both diet groups of the 13SM and 14SM mice. Similarly, to the FACS data there was a certain degree of variability in the host transcript data which is why no distinct clustering by group could be observed in the PCoA plot **(Fig. 3B)**. In contrast *C. rodentium* transcript showed clear clustering based on diet and SM **(Fig. 3C)**. Analysis of the host transcripts showed only a limited number of genes differentially expressed in the different group. In the diet comparisons of the 13SM group 27 genes were differentially expressed of which 19 were upregulated in the FR group and 8 in the FF group **(Fig. 3D)**. In the comparison of the 14SM group 9 were upregulated during the FR diet and 13 during the FF diet **(Fig. 3D)**. As the 14SM FF group was the only group showing a clear increase in susceptibility, we compared the 13SM FR, 13SM FF and 14SM FR groups together to the 14SM FF group. Unfortunately, only 3 genes were upregulated in the 14SM FF group and none in the other group **(Fig. 3D)**. Overall, the differentially regulated host genes do not hint to why FF-fed 14SM mice are more susceptible to *C. rodentium*. In contrast to the host transcriptome data, there were more differences observed in the *C. rodentium* transcriptome. Comparison of the diet in the 13SM group, showed 57 genes upregulated in the FR group and 16 upregulated in the FF group **(Fig. 3E)**. In the 14SM group 13 were upregulated in the FR group and 9 in the FF **(Fig. 3E)**. Finally comparing all other groups to the 14SM FF group, 4 genes were downregulated in the 14SM FF group **(Fig. 3E)**. While there are some intriguing observations in the transcript data of *C. rodentium*, in particular the expression of a number of phage-type genes in the 13SM FR group, none of the upregulated genes offers a good explanation for the altered pathogen infectiousness **(Fig. 3E)**. Especially, considering that none of the genes in the LEE pathogenic island of *C. rodentium* was upregulated under any conditions.

Overall our data strongly supports the notion of an increased pathogen susceptibility induced by the presence of *A. muciniphila* under fiber-free conditions: Based on our collected readouts the most likely explanation for this is the erosion of the mucus layer by *A. muciniphila* offering *C. rodentium* an improved physical access to the host tissue.

Discussion

Until recently, the health benefits of dietary fibers have been attributed mainly to their physical properties resulting in increased fecal bulking and improved laxation (*12*, *24*), as well as the increased production of short-chain fatty acids resulting from their degradation by the our gut microbiota (*13*, *25*). However, dietary fiber consumption is also indispensable to avoid a dysbiosis of our gut microbiota. Using both gnotobiotic and SPF mouse models, we have previously shown that dietary fiber deprivation leads to a functional shift of the gut microbiota toward mucin degradation, which causes an erosion of the gut mucus layer as well as an increase in pathogen susceptibility (*8*, *15*).

Here, we leverage our gnotobiotic mouse model, hosting a defined and fully characterized synthetic human gut microbiota, to specifically manipulate the gut microbiota in order to study the functional interactions between host, diet, microbiota and pathogens. Thus, we were able to provide further insight in how fiber-deprivation can lead to an increased susceptibility to attaching and effacing pathogens. We show that the expansion of the mucus specialist *A. muciniphila* is inducing the increased susceptibility under fiber-deprivation **(Figure 2)**. This is a particularly important observation as *A. muciniphila* is regarded as potential probiotic bacterium (*22*, *26*). However, it has to be noted that in our model *A. muciniphila* seems to only have a limited impact on the host immune response and pathogen transcriptome **(Figure 3).** It has been reported that potential host beneficial transcripts are upregulated under mucin-depleted conditions (*27*), however, we could not observe a similar health benefit related to *A. muciniphila*. Our data reveals that during dietary fiber deprivation, *A. muciniphila* excessively degrades the gut mucus layer, thus most likely improving *C. rodentium* access to the host tissue allowing it to more easily infect the host. Our work offers the invaluable insight that under specific dietary conditions, *A. muciniphila* can increase infection susceptibility to attaching and effacing pathogen. This is an especially important consideration when designing probiotic therapies using this commensal bacterium.

Material and Methods

Ethical statement.

All animal experiments were performed in Luxembourg were performed according to the “Règlement Grand-Ducal du 11 janvier 2013 relatif à la protection des animaux utilisés à des fins scientifiques”, based on Directive 2010/63/EU on the protection of animals used for scientific purposes, and approved by the Animal Experimentation Ethics Committee of the University of Luxembourg and by the Luxembourgish Ministry of Agriculture, Viticulture, and Rural Development (national authorization no. LUPA 2019/52). All animal experiments in the United States were approved by the University of Michigan, University Committee for the Use and Care of Animals.

Experimental design and dietary treatment.

For the infection experiments, 6- to 8-week-old, age-matched, germ-free (GF) Swiss-Webster mice were housed in ISOcages with up to five animals per cage. These experiments were performed in two different facilities, one facility being in Luxembourg, the other in the USA. Results were reproduced independent of the location of the facility. Light cycles consisted of 12 h of light and sterile water, and diets were provided ad libitum. Mice were gavaged with 0.2 ml of one of the 5 synthetic human gut microbiota on two consecutive days. The gavage mix was prepared as described previously (*8*, *17*), except that depending on the specific SM some of the strains were not added to the gavage mix. Before and 14 days following the initial gavage, all mice were maintained on a standard mouse chow which we refer to as a fiber-rich (FR) diet. Afterwards, half of the gavaged and half of the GF mice per SM group were switched randomly to a fiber-free (FF) diet, while the rest were maintained on the FR diet. Instead of dietary fibers from plant sources, the FF contains increased glucose levels (*8*). All mice were maintained for 40 days on their respective diets and fecal samples were collected as represented in Figure 1A. After their 40-day feeding period mice were either euthanized for pre-infection readouts or infected with ~10^9 CFUs of *C. rodentium*. After infection mice were observed daily. Mice dedicated for FACS analysis were euthanized 3-4 days after infection while the remaining mice were observed for up to 10 days post infection before they were euthanized. In the USA mice were euthanized by CO2 asphyxiation followed by cervical dislocation, while mice in Luxembourg were euthanized directly by cervical dislocation. Colons were excised and immediately processed for FACS or bead penetration assay measurements or stored in Methacarn fixative for histological assessment. Cecal contents were flash frozen before being stored at −80°C for subsequent SCFA measurements or RNA extraction. Cecal tissue was processed using RNA later before being stored at -80°C for subsequent RNA extraction.

Animal diets.

The fiber-rich diet was a standard, autoclaved rodent chow (LabDiet, St. Louis, MO, USA; catalog no. 5013). The fiber-free diet has been manufactured and irradiated by SAFE Diets (Augy, France) according to the TD.140343 diet formulation, a modified version of the Harlan.TD08810 diet (Envigo, Indianapolis, IN, USA) described previously (*8*). The fiber-free diet lacks dietary fiber, which has been compensated by an increased glucose content; note that this diet also contains crystalline cellulose, although it cannot be degraded by any member of the SMs.

Cultivation and administration of the SM

All SM-constituent strains were cultured and intragastrically gavaged as described previously (*17*), however, some of the strains were not included depending on the specific SM (see Fig 1B).

Colon length measurements

Colon length was measured by taking pictures of the colons in their histology cassettes, followed by length measurements with ImageJ using the cassette size as reference.

Ex vivo *mucus layer penetrability assessment*

The penetrability of the gut mucus layer was assessed with the help of fluorescent beads as described previously (*28*).

DNA extraction

DNA was extracted by phenol-chloroform extraction, followed by the purification using a DNeasy Blood and Tissue Kit (Qiagen, USA) according to the following protocol:
Samples were put in screw-cap tubes and ~250 µl glass beads (Sigma G1277, acid washed 212-300 µl), 500 µl of Buffer A (200mM NaCl, 200 mM Tris, 200mM EDTA), 210 µl of 20% SDS and 500 µl of Phenol:Chloroform (1:1). The mixture was then bead beaten for 2 minutes at room temperature. The samples were then centrifuged for 3 minutes at 18000 rcf at 4°C and the aqueous phase was recovered. 500 µl Phenol: Chloroform (1:1) were added to the recovered sample and mixed by inversion. The samples were then centrifuged once more centrifuged for 3 minutes at 18000 rcf at 4°C and the aqueous phase was recovered. A final time 500 µl Phenol: Chloroform (1:1) were added to the recovered sample and mixed by inversion. The samples were centrifuged a third time for 3 minutes at 18000 rcf at 4°C and the aqueous phase was recovered. 1/10 volume of 3 M sodium acetate and 1 volume of isopropanol were added to the recovered phase and mixed by inversion. Next, the samples were placed for 20 minutes at -80°C in order to precipitate the DNA. In order to recover the DNA, the samples were centrifuged at 4°C for 20 minutes at maximum speed and the pellet was recovered. The pellet was washed using 1ml of room temperature 70% ethanol. To recover the pellet the sample was centrifuged for 3 minutes at max speed at room temperature. The supernatant was removed and the pellet dried for ~1 hour. Next the pellet was resuspended in 100 µl ddH2O and further purified by using the DNeasy Blood & Tissue Kit (QIAGEN, USA) according to manufacturer's instruction.

RNA extraction from mesenteric lymph nodes and colonic tissue

To extract the RNA from mesenteric lymph nodes and colonic tissue, 1 ml of TRIzol was added to the 50–100 mg of the respective tissue and samples were incubated overnight at –20°C. Samples were homogenized using a RETSCH Mixer Mill MM 400 by adding a 5 mm autoclaved metal bead to each sample and then homogenizing them for 8 mins at 30 Hz. In order to pellet the undissolved tissue, samples were centrifuged at 18000 × g for 10 min at 4°C. The entire supernatant was

transferred to a new tube to which 200 µl of chloroform was added followed by shaking for 10–15 seconds. Samples were incubated for 2–3 minutes at room temperature and then centrifuged at 12000 × g for 15 minutes at 4°C. The aqueous phase was transferred to a new tube containing 600 µl of chloroform, then shaken for 10–15 seconds followed by a 2-3 incubation at room temperature and a centrifugation at 12000 × g for 15 minutes at 4°C. The aqueous phase was recovered and 500 µl of isopropanol were added before mixing the resulting solution vigorously. The solution was incubated for 10 min at room temperature before being centrifuged at 12000 × g for 10 min at 4°C. The supernatant was discarded and the pellet was resuspended in 1 ml of ice-cold 75% ethanol by vortexing briefly. The sample was centrifuged for 5 minutes at 7500 × g at 4°C. The supernatant was discarded and the pellet was air-dried for 10 minutes before being resuspended in 50 µl RNase-free water. To assure the pellet was fully resuspended, it was incubated for 15 minutes at 56°C. The resulting solution was treated with DNAse I for 30 minutes at 37°C. Afterwards, 1 µl of 0.5M EDTA was added and the DNAse was heat-inactivated at 65°C for 10 minutes. The resulting RNA was further purified using the RNeasy Mini kit (Qiagen, Hilden, Germany) which was used according to the manufacturer's instruction. The integrity of the eluted RNA was assessed using an Agilent 2100 Bioanalyzer system and the RNA was stored at -80°C.

RNA-Seq

RNA extracted from samples at 3 DPI were utilized for performing RNA-Seq. Illumina Stranded Total RNA Prep with Ribo-Zero Plus was used to prepare the RNA sequencing library according to the reference guide's instructions. Sequencing was performed using NovaSeq 6000 SP Reagent Kit v1.5 (Illumina, San Diego, CA, USA) on an Illumina NovaSeq 6000 system.

RNA-Seq analysis

Transcriptome reads were cleaned up using kneaddata (https://github.com/biobakery/kneaddata) analysis and transcript quantification was performed using Salmon (*29*). Transcripts not appearing at least once on average across all samples were removed from subsequent analysis. Differential expression analysis was performed using DESeq2 1.30.1 with default parameters and *p*-value adjustment using the Benjamini-Hochberg method. Significant genes were identified based on adjusted *p*-value < 0.05. Pathway analysis was also performed using the enrichGO function of clusterProfiler 3.18.1(*30*) in R to identify upregulated pathways using Gene Ontology (GO) terms for biological processes.

Histological disease scoring

Histological disease scoring was performed by Prof. Kathryn A. Eaton from the University of Michigan Medical School according to a modified version of the Meira et al, 2008 protocol (*31*).

Quantification of bacterial relative abundance.

Initial colonization of the SM was verified using phylotype-specific qPCR primers as described previously (*17*). Subsequent analysis of the relative abundance was performed by 16S rRNA gene sequencing as described previously (*8*).

C. rodentium *culturing and enumeration.*

C. rodentium was cultivated using LB medium and enumerated using kanamycin containing LB-agar plates as described previously (*8*).

Intestinal fatty acid analysis.

Thirty to 100 mg of flash-frozen cecal content from uninfected mice, which were kept for 40 days on the FR or FF diet, was used for the fatty acid analysis. Per 50 mg of the samples, 500 µl MilliQ water containing 2 mM 2-ethylbutyric acid as an internal standard and 1.4-mm ceramic beads (5 beads per tube) were added. Homogenization was performed for 30 s at 6,000 rpm at 0 to 5°C (Precellys24 homogenizer, catalog no. P000669-PR240-A; Bertin Technologies, Montigny-le-Bretonneux, France), and the resulting homogenate was then centrifuged at 21,000 × g for 5 min at 4°C. Further processing of the sample homogenate and measurements were performed as previously described using gas chromatography-mass spectrometry (GC-MS) (*32*)

Immune cell profiling of colonic lamina propria.

Immune cell profiling was performed on infected mice by excising the colons and placing them in Hanks' balanced salt solution (HBSS) with phenol red and without calcium and magnesium (Lonza, Basel, Switzerland; catalog no. BE10-543F). Lamina propria cells were extracted using a lamina propria dissociation kit (catalog no. 130-097-410; Miltenyi Biotec, Bergisch Gladbach, Germany) according to the manufacturer's instructions.

Statistical analyses.

Statistical analysis was performed using Prism 8.1.1. (GraphPad Software, Inc., San Diego, CA, USA) or using Excel for some of the student T-tests. Statistical significances are represented by asterisks as follows: *, $P < 0.05$; **, $P < 0.01$; ***, $P < 0.001$; and ****, $P < 0.0001$. Unless otherwise specified in the figure legend, for normal distributed values, unpaired two-tailed t tests were used, while for nonnormal distributed values, a Mann-Whitney test was used. The specific test and the number of animals used for each experiment are detailed in the figure legends.

References

1. P. Paone, P. D. Cani, Mucus barrier, mucins and gut microbiota: The expected slimy partners? *Gut* (2020), , doi:10.1136/gutjnl-2020-322260.

2. E. E. L. Nyström, B. Martinez-Abad, L. Arike, G. M. H. Birchenough, E. B. Nonnecke, P. A. Castillo, F. Svensson, C. L. Bevins, G. C. Hansson, M. E. V. Johansson, An intercrypt subpopulation of goblet cells is essential for colonic mucus barrier function. *Science* (2021), doi:10.1126/science.abb1590.

3. M. E. V. Johansson, M. Phillipson, J. Petersson, A. Velcich, L. Holm, G. C. Hansson, The inner of the two Muc2 mucin-dependent mucus layers in colon is devoid of bacteria. *Proceedings of the National Academy of Sciences*. **105**, 15064–15069 (2008).

4. D. Zheng, T. Liwinski, E. Elinav, Interaction between microbiota and immunity in health and disease. *Cell Research* (2020), , doi:10.1038/s41422-020-0332-7.

5. S. Raimondi, E. Musmeci, F. Candeliere, A. Amaretti, M. Rossi, Identification of mucin degraders of the human gut microbiota. *Scientific Reports* (2021), doi:10.1038/s41598-021-90553-4.

6. C. Belzer, L. W. Chia, S. Aalvink, B. Chamlagain, V. Piironen, J. Knol, W. M. de Vos, Microbial metabolic networks at the mucus layer lead to diet-independent butyrate and vitamin B12 production by intestinal symbionts. *mBio* (2017), doi:10.1128/mBio.00770-17.

7. E. H. Crost, G. Le Gall, J. A. Laverde-Gomez, I. Mukhopadhya, H. J. Flint, N. Juge, Mechanistic insights into the cross-feeding of Ruminococcus gnavus and Ruminococcus bromii on host and dietary carbohydrates. *Frontiers in Microbiology* (2018), doi:10.3389/fmicb.2018.02558.

8. M. S. Desai, A. M. Seekatz, N. M. Koropatkin, N. Kamada, C. A. Hickey, M. Wolter, N. A. Pudlo, S. Kitamoto, N. Terrapon, A. Muller, V. B. Young, B. Henrissat, P. Wilmes, T. S. Stappenbeck, G. Núñez, E. C. Martens, A Dietary Fiber-Deprived Gut Microbiota Degrades the Colonic Mucus Barrier and Enhances Pathogen Susceptibility. *Cell*. **167**, 1339-1353.e21 (2016).

9. H. Trowell, Definition of dietary fiber and hypotheses that it is a protective factor in certain diseases. *American Journal of Clinical Nutrition* (1976), , doi:10.1093/ajcn/29.4.417.

10. E. C. Martens, E. C. Lowe, H. Chiang, N. A. Pudlo, M. Wu, N. P. McNulty, D. W. Abbott, B. Henrissat, H. J. Gilbert, D. N. Bolam, J. I. Gordon, Recognition and degradation of plant cell wall polysaccharides by two human gut symbionts. *PLoS biology*. **9**, e1001221 (2011).

11. D. P. Venegas, M. K. De La Fuente, G. Landskron, M. J. González, R. Quera, G. Dijkstra, H. J. M. Harmsen, K. N. Faber, M. A. Hermoso, Short chain fatty acids (SCFAs)mediated gut epithelial and immune regulation and its relevance for inflammatory bowel diseases. *Frontiers in Immunology* (2019), , doi:10.3389/fimmu.2019.00277.

12. D. P. Burkitt, A. R. P. Walker, N. S. Painter, Effect of Dietary Fibre on Stools and Transit-Times, and Its Role in the Causation of Disease. *The Lancet*. **300**, 1408–1411 (1972).

13. K. Makki, E. C. Deehan, J. Walter, F. Bäckhed, The Impact of Dietary Fiber on Gut Microbiota in Host Health and Disease. *Cell Host and Microbe*. **23**, 705–715 (2018).

14. European Food Safety Authority, Scientific Opinion on Dietary Reference Values for carbohydrates and dietary fibre. *EFSA Journal*. **8**, 1–77 (2010).

15. M. Neumann, A. Steimle, E. T. Grant, M. Wolter, A. Parrish, S. Willieme, D. Brenner, E. C. Martens, M. S. Desai, Deprivation of dietary fiber in specific-pathogen-free mice promotes susceptibility to the intestinal mucosal pathogen Citrobacter rodentium. *Gut Microbes*. **13** (2021), doi:10.1080/19490976.2021.1966263.

16. K. S. B. Bergstrom, V. Kissoon-Singh, D. L. Gibson, C. Ma, M. Montero, H. P. Sham, N. Ryz, T. Huang, A. Velcich, B. B. Finlay, K. Chadee, B. A. Vallance, Muc2 protects against lethal infectious colitis by disassociating pathogenic and commensal bacteria from the colonic mucosa. *PLoS Pathogens*. **6**, e1000902 (2010).

17. A. Steimle, A. De Sciscio, M. Neumann, E. T. Grant, G. V. Pereira, H. Ohno, E. C. Martens, M. S. Desai, Constructing a gnotobiotic mouse model with a synthetic human gut microbiome to study host–microbe cross talk. *STAR Protocols*. **2**, 100607 (2021).

18. R. Corrêa-Oliveira, J. L. Fachi, A. Vieira, F. T. Sato, M. A. R. Vinolo, Regulation of immune cell function by short-chain fatty acids. *Clinical and Translational Immunology*. **5**, e73 (2016).

19. B. Chassaing, G. Srinivasan, M. A. Delgado, A. N. Young, A. T. Gewirtz, M. Vijay-Kumar, Fecal Lipocalin 2, a Sensitive and Broadly Dynamic Non-Invasive Biomarker for Intestinal Inflammation. *PLoS ONE*. **7**, e44328 (2012).

20. Z. W. Luo, K. Xia, Y. W. Liu, J. H. Liu, S. S. Rao, X. K. Hu, C. Y. Chen, R. Xu, Z. X. Wang, H. Xie, Extracellular vesicles from akkermansia muciniphila elicit antitumor immunity against prostate cancer via modulation of CD8+ T cells and macrophages. *International Journal of Nanomedicine* (2021), doi:10.2147/IJN.S304515.

21. E. Ansaldo, L. C. Slayden, K. L. Ching, M. A. Koch, N. K. Wolf, D. R. Plichta, E. M. Brown, D. B. Graham, R. J. Xavier, J. J. Moon, G. M. Barton, Akkermansia muciniphila induces intestinal adaptive immune responses during homeostasis. *Science* (2019), doi:10.1126/science.aaw7479.

22. F. Ashrafian, S. Keshavarz Azizi Raftar, A. Shahryari, A. Behrouzi, R. Yaghoubfar, A. Lari, H. R. Moradi, S. Khatami, M. D. Omrani, F. Vaziri, A. Masotti, S. D. Siadat, Comparative effects of alive and pasteurized Akkermansia muciniphila on normal diet-fed mice. *Scientific Reports* (2021), doi:10.1038/s41598-021-95738-5.

23. C. Mullineaux-Sanders, J. Sanchez-Garrido, E. G. D. Hopkins, A. R. Shenoy, R. Barry, G. Frankel, Citrobacter rodentium–host–microbiota interactions: immunity, bioenergetics and metabolism. *Nature Reviews Microbiology*. **17**, 701–715 (2019).

24. J. H. Cummings, "The effect of dietary fiber on fecal weight and composition" in *CRC Handbook of Dietary Fiber in Human Nutrition, Third Edition* (2001).

25. E. D. Sonnenburg, J. L. Sonnenburg, Starving our microbial self: The deleterious consequences of a diet deficient in microbiota-accessible carbohydrates. *Cell Metabolism*. **20**, 779–786 (2014).

26. Q. Zhai, S. Feng, N. Arjan, W. Chen, A next generation probiotic, Akkermansia muciniphila. *Critical Reviews in Food Science and Nutrition* (2019), , doi:10.1080/10408398.2018.1517725.

27. J. Shin, J. R. Noh, D. H. Chang, Y. H. Kim, M. H. Kim, E. S. Lee, S. Cho, B. J. Ku, M. S. Rhee, B. C. Kim, C. H. Lee, B. K. Cho, Elucidation of akkermansia muciniphila probiotic traits driven by mucin depletion. *Frontiers in Microbiology* (2019), doi:10.3389/fmicb.2019.01137.

28. B. O. Schroeder, G. M. H. Birchenough, M. Ståhlman, L. Arike, M. E. V. Johansson, G. C. Hansson, F. Bäckhed, Bifidobacteria or Fiber Protects against Diet-Induced Microbiota-Mediated Colonic Mucus Deterioration. *Cell Host and Microbe*. **23**, 27-40.e7 (2018).

29. R. Patro, G. Duggal, M. I. Love, R. A. Irizarry, C. Kingsford, Salmon provides fast and bias-aware quantification of transcript expression. *Nature Methods* (2017), doi:10.1038/nmeth.4197.

30. G. Yu, L. G. Wang, Y. Han, Q. Y. He, ClusterProfiler: An R package for comparing biological themes among gene clusters. *OMICS A Journal of Integrative Biology*. **16**, 284–287 (2012).

31. L. B. Meira, J. M. Bugni, S. L. Green, C.-W. Lee, B. Pang, D. Borenshtein, B. H. Rickman, A. B. Rogers, C. A. Moroski-Erkul, J. L. McFaline, D. B. Schauer, P. C. Dedon, J. G. Fox, L. D. Samson, DNA damage induced by chronic inflammation contributes to colon carcinogenesis in mice. *Journal of Clinical Investigation* (2008), doi:10.1172/jci35073.

32. K. Greenhalgh, J. Ramiro-Garcia, A. Heinken, P. Ullmann, T. Bintener, M. P. Pacheco, J. Baginska, P. Shah, A. Frachet, R. Halder, J. V. Fritz, T. Sauter, I. Thiele, S. Haan, E. Letellier, P. Wilmes, Integrated In Vitro and In Silico Modeling Delineates the Molecular Effects of a Synbiotic Regimen on Colorectal-Cancer-Derived Cells. *Cell Reports*. **27**, 1621-1632.e9 (2019).

Figure 1. Dietary fiber-deprivation induced microbiota shifts are independent of the presence of mucus degraders. (A) Experimental timeline. Age-matched 6-8 week old germ-free Swiss-Webster mice were gavaged with one of the different synthetic gut microbiota (SM) on three consecutive days. These mice were maintained for 14 days on the fiber-rich (FR) diet, after which half of them were switched to a fiber-free diet. The mice were maintained for 40 days on their respective diets before they were infected with *Citrobacter rodentium*. After infection mice were closely observed for up to ten days. (B) Venn diagram representing the different synthetic microbiota composition (10SM, 11SM, 12SM, 13SM and 14SM) (C) Relative abundance of the gut bacteria as determined by 16S rRNA gene sequencing of stools of uninfected mice. (D) Relative proportion of fiber- and mucus-degrading bacteria in each of the groups. (E) *Ex vivo* mucus layer penetrability assessment on uninfected mice. AUC of the normalized bead penetrability was determined for each mouse. Error bars represent SEM; unpaired two-tailed t-test (F) Cecal short-chain fatty acid (SCFA) concentrations of uninfected mice. Error bars represent SEM; unpaired two-tailed t-test (G) Fecal lipocalin-2 (LCN-2) concentration of uninfected mice. Error bars represent SEM; unpaired two-tailed t-test (H) Colon length of uninfected mice. Error bars represent SEM; unpaired two-tailed t-test. ns, non-significant; *p<0.05; **p<0.01; ***p<0.001; ****p<0.0001.

Figure 2. *Akkermansia muciniphila* is the driving force behind the increased *Citrobacter rodentium* susceptibility during dietary fiber deprivation. (A) Fecal *C. rodentium* load of gnotobiotic Swiss-Webster mice during the 10 days of infection. Error bars represent SEM; unpaired two-tailed t-test. (B) Maximum weight loss reached during the infection with *C. rodentium*. Error bars represent SEM; unpaired two-tailed t-test. (C) Fecal LCN-2 concentration of infected mice on the final day of their infection. Error bars represent SEM; unpaired two-tailed t-test. (D) Colon length of infected mice at the final day of their infection. Error bars represent SEM; unpaired two-tailed t-test. (E) Histological determined disease score of infected mice at the final day of their infection. Error bars represent SEM; unpaired two-tailed t-test. ns, non-significant; *p<0.05; **p<0.01; ***p<0.001; ****p<0.0001.

Figure 3. Neither the observed host immune response nor *C. rodentium* gene expression explain the role of *A. muciniphila* in increasing pathogen susceptibility during the FF diet.
(A) Significant altered immune cell population of mice at 3 days post infection as determined by fluorescence-activated cell sorting (FACS). Error bars represent SEM; unpaired two-tailed t-test; *p<0.05; **p<0.01; ***p<0.001; ****p<0.0001. (B) PCoA plot of the mouse transcripts at 3 DPI separated by experimental group. (C) PCoA plot of the *C. rodentium* transcripts at 3DPI separated by experimental group. The two different diets were compared in both 13SM and 14SM groups. Additionally, the combination of the groups 13SM FR, 13SM FF and 14SM FR were compared to 14SM FF group in order to deduce which genes might be responsible for altering *C. rodentium* susceptibility. (D) Volcano plot of the genes expressed by the mouse host at 3 DPI. (E) Volcano plot of the genes expressed by *C. rodentium* at 3 DPI. The two different diets were compared in both 13SM and 14SM groups. Additionally, the combination of the groups 13SM FR, 13SM FF and 14SM FR were compared to 14SM FF group in order to deduce which genes might be responsible for altering *C. rodentium* susceptibility.

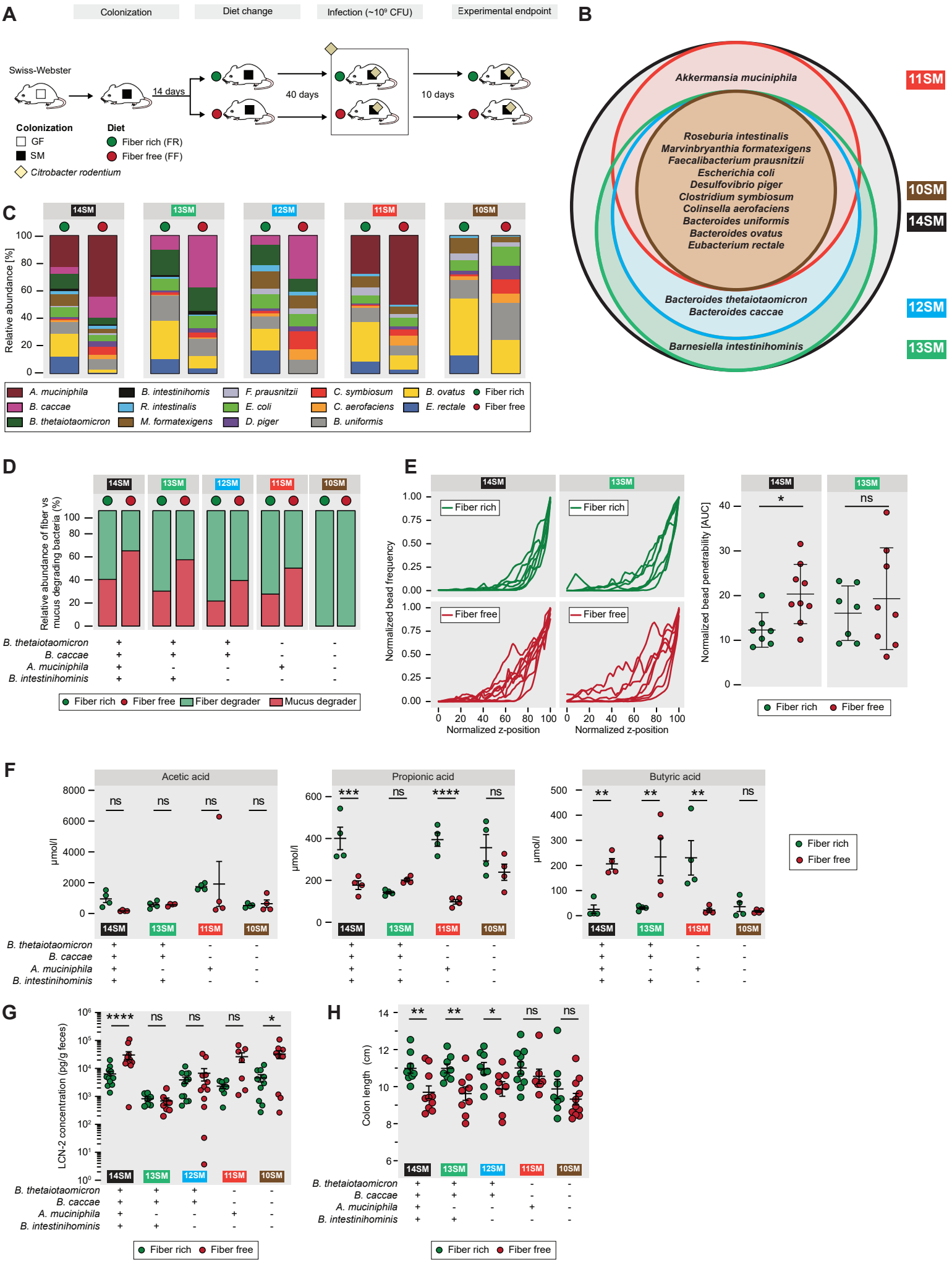
A
Colonization
Diet change
Infection (~10⁹ CFU)
Experimental endpoint
Swiss-Webster
14 days
40 days
10 days
Colonization
GF
SM
Diet
Fiber rich (FR)
Fiber free (FF)
Citrobacter rodentium
B
Akkermansia muciniphila
Roseburia intestinalis
Marvinbryanthia formatexigens
Faecalibacterium prausnitzii
Escherichia coli
Desulfovibrio piger
Clostridium symbiosum
Colinsella aerofaciens
Bacteroides uniformis
Bacteroides ovatus
Eubacterium rectale
Bacteroides thetaiotaomicron
Bacteroides caccae
Barnesiella intestinihominis
11SM
10SM
14SM
12SM
13SM
C
14SM
13SM
12SM
11SM
10SM
Relative abundance [%]
A. muciniphila
B. caccae
B. thetaiotaomicron
B. intestinihominis
R. intestinalis
M. formatexigens
F. prausnitzii
E. coli
D. piger
C. symbiosum
C. aerofaciens
B. uniformis
B. ovatus
E. rectale
Fiber rich
Fiber free
D
Relative abundance of fiber vs mucus degrading bacteria (%)
B. thetaiotaomicron
B. caccae
A. muciniphila
B. intestinihominis
Fiber rich
Fiber free
Fiber degrader
Mucus degrader
E
Normalized bead frequency
Normalized z-position
Normalized bead penetrability [AUC]
*
ns
F
Acetic acid
Propionic acid
Butyric acid
µmol/l
ns
***
****
**
G
LCN-2 concentration (pg/g feces)
****
H
Colon length (cm)

Figure 1

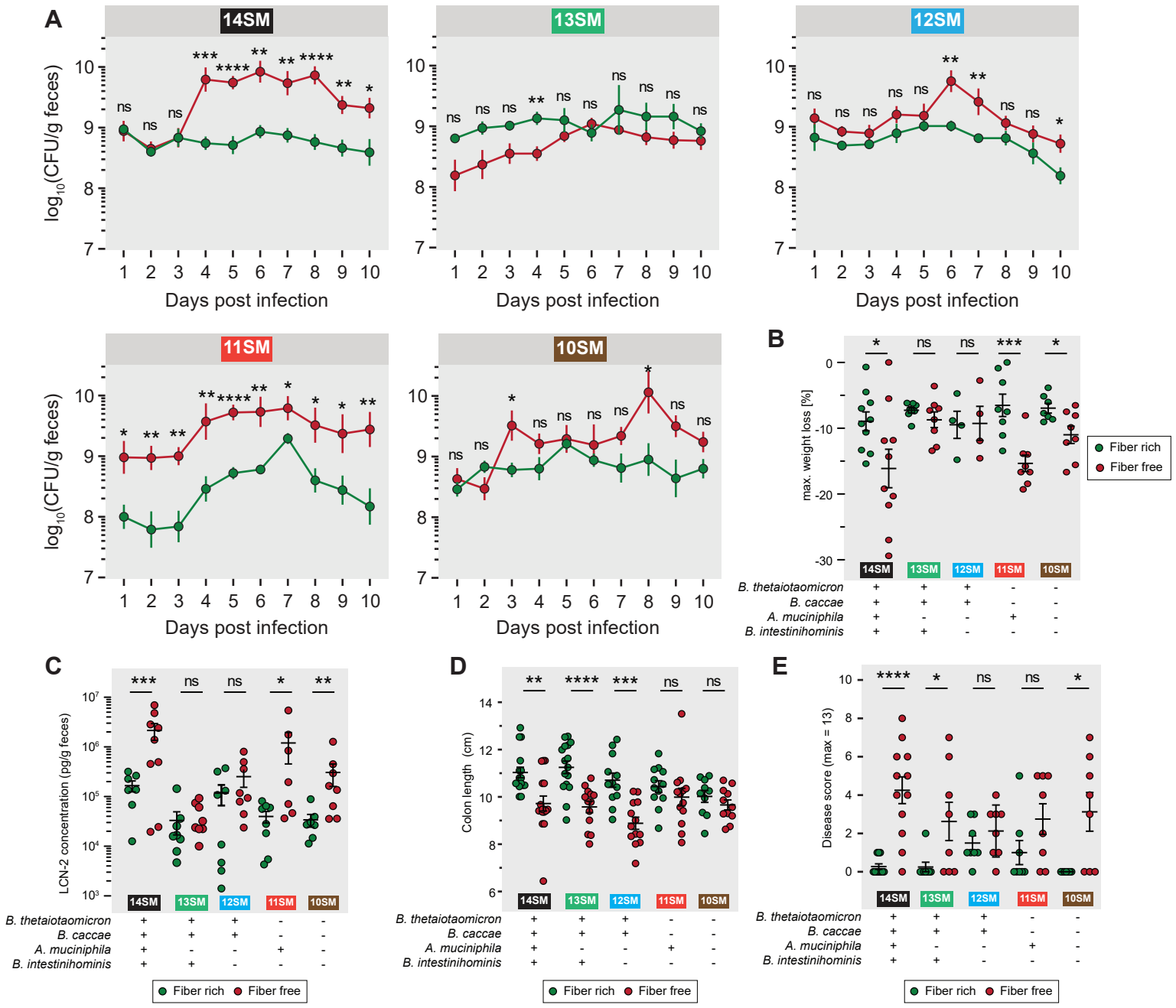
A
14SM
13SM
12SM
11SM
10SM
log10(CFU/g feces)
Days post infection
B
max. weight loss [%]
Fiber rich
Fiber free
B. thetaiotaomicron
B. caccae
A. muciniphila
B. intestinihominis
C
LCN-2 concentration (pg/g feces)
D
Colon length (cm)
E
Disease score (max = 13)

Figure 2

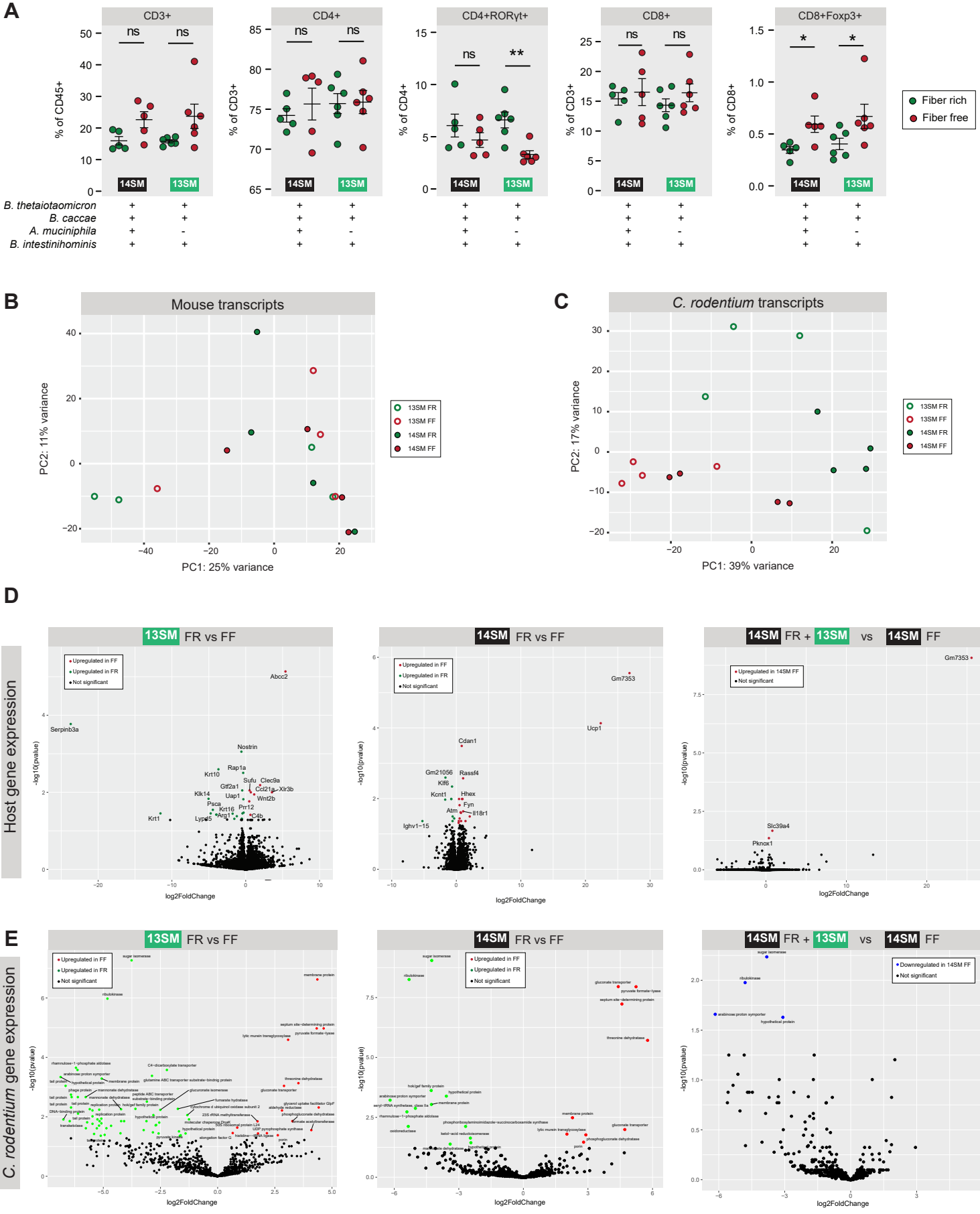
A
CD3+
CD4+
CD4+RORγt+
CD8+
CD8+Foxp3+
% of CD45+
% of CD3+
% of CD4+
% of CD3+
% of CD8+
ns
**
*
14SM
13SM
Fiber rich
Fiber free
B. thetaiotaomicron
B. caccae
A. muciniphila
B. intestinihominis
B
Mouse transcripts
PC2: 11% variance
PC1: 25% variance
13SM FR
13SM FF
14SM FR
14SM FF
C
C. rodentium transcripts
PC2: 17% variance
PC1: 39% variance
D
Host gene expression
13SM FR vs FF
14SM FR vs FF
14SM FR + 13SM vs 14SM FF
Upregulated in FF
Upregulated in FR
Upregulated in 14SM FF
Downregulated in 14SM FF
Not significant
-log10(pvalue)
log2FoldChange
Abcc2
Serpinb3a
Nostrin
Rap1a
Krt10
Sufu
Clec9a
Gtf2a1
Ccl21a
Xlr3b
Klk14
Uap1
Wnt2b
Psca
Prr12
Krt16
Arg1
C4b
Krt1
Lyz1
Gm7353
Ucp1
Cdan1
Gm21056
Rassf4
Klf6
Kcnt1
Hhex
Fyn
Atm
Il18r1
Ighv1-15
Slc39a4
Pknox1
E
C. rodentium gene expression

Figure 3

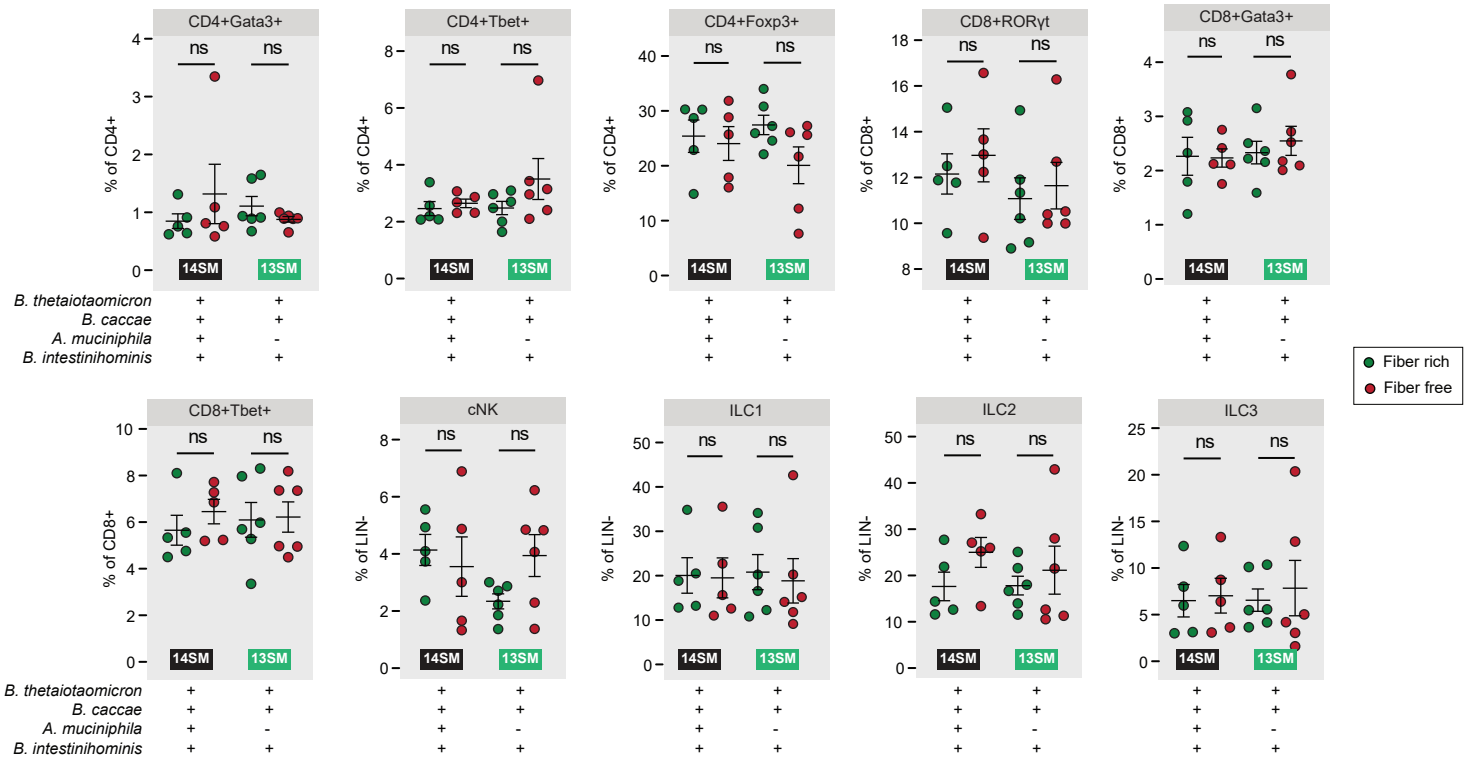

Figure S1: Non-significant altered immune cell population of mice infected for 3 days determined by FACS. ns, non-significant

4. Dietary Modulation Alters Susceptibility to *Listeria monocytogenes* and *Salmonella* Typhimurium with or without a Gut Microbiota

4.1 Rationale

The second type of infectious diseases we investigated were the classical models for intracellular food pathogens *Listeria monocytogenes* and *Salmonella enterica* serovar Typhimurium. Despite all the improvements concerning food safety, infections with foodborne pathogens remain highly prevalent as highlighted in my research paper below. Given the importance of the gut microbiome in modulating the susceptibility to these pathogens, the capability of dietary fiber in changing the microbial community and the importance of the gut mucus barrier as first line of defense against invading pathogens, we decided to investigate how the diet-microbiome-mucin interaction could shape the susceptibility to these pathogens. At most, the early infection dynamics of these intracellular pathogens should be affected by a thin gut mucus layer. As such, it was especially interesting to investigate whether the fiber deprivation-induced erosion of the mucus layer would affected them in a noticeable way. By using our 14SM gnotobiotic mouse we were able to show that dietary fiber, but not the mucus layer, modulates either the host's susceptibility, the virulence of these pathogens, or both. In contrast to our

results with *C. rodentium*, mice deprived of dietary fiber were protected from infections with both pathogens, compared to mice fed the fiber-rich diet. However, we observed the same effect of diet on germfree mice, suggesting that the susceptibility is directly driven by the diet itself even in the absence of the gut microbiome and accordingly independent of the erosion of the mucus layer. Furthermore, this study is a perfect example for showing the importance of germ-free controls, as our conclusions would have been likely misinterpreted in the absence of these controls.

Personal contributions: I am first author of this research paper published in mSystems and as such had significant contributions to the design, the execution, the data analysis, as well as, the drafting of this paper. With the partial support of other members of my group, I performed all the animal experiments, including husbandry, with the exception of those for the CyTOF and SCFA data (Fig 2A&C) which were performed by Amy Parrish. I performed the experiments and analysis of all experiments with the exception glycan-degrading enzyme activity assay (Fig. 1E), the SCFA analysis (Fig. 2A) and the CyTOF analysis (Fig 3C). With the exception of the glycan-degrading enzyme activity assay (Fig. 1E) and the CyTOF gating plots (top panel Fig 2C) all figures were drafted by me. I drafted the initial manuscript and performed the majority of the revisions.

4.2 Results

AMERICAN SOCIETY FOR MICROBIOLOGY | mSystems®

OBSERVATION

Dietary Modulation Alters Susceptibility to *Listeria monocytogenes* and *Salmonella* Typhimurium with or without a Gut Microbiota

Mathis Wolter,[a,b] Alex Steimle,[a] Amy Parrish,[a,b] Jacques Zimmer,[a] Mahesh S. Desai[a,c]

[a]Department of Infection and Immunity, Luxembourg Institute of Health, Esch-sur-Alzette, Luxembourg
[b]Faculty of Science, Technology and Medicine, University of Luxembourg, Esch-sur-Alzette, Luxembourg
[c]Odense Research Center for Anaphylaxis, Department of Dermatology and Allergy Center, Odense University Hospital, University of Southern Denmark, Odense, Denmark

ABSTRACT Food safety has considerably improved worldwide, yet infections with foodborne human enteric pathogens, such as *Listeria* spp. and *Salmonella* spp., still cause numerous hospitalizations and fatalities. Since dietary alterations, including fiber deficiency, might impact the colonization resistance mediated by the gut microbiome, studying the diet–microbiome–pathogen axis holds promise in further understanding the pathogenesis mechanisms. Using a gnotobiotic mouse model containing a 14-member synthetic human gut microbiota (14SM), we have previously shown that dietary fiber deprivation promotes proliferation of mucin-degrading bacteria, leading to a microbiome-mediated erosion of the colonic mucus barrier, which results in an increased susceptibility toward the rodent enteric pathogen *Citrobacter rodentium*. Here, we sought to understand how a low-fiber diet affects susceptibility to *Listeria monocytogenes* and *Salmonella enterica* serovar Typhimurium by using our 14SM gnotobiotic mouse model in BALB/c and C57BL/6 mouse backgrounds, respectively. Intriguingly, and in contrast to our results with *C. rodentium*, we observed that depriving mice of dietary fiber protected them from infections with both pathogens, compared to mice fed a standard chow. The microbiome delayed the overall pathogenicity compared to the onset of disease observed in germfree control mice. Nevertheless, we observed the same effect of diet on germfree mice, suggesting that the susceptibility is directly driven by the diet itself even in the absence of the gut microbiome. Our study points out an important observation, namely, that dietary fiber plays a crucial role in either the host's susceptibility, the virulence of these pathogens, or both. It would be judicious to design and interpret future studies on this basis.

IMPORTANCE The human enteric pathogens *Listeria monocytogenes* and *Salmonella* Typhimurium are employed as classical models in rodent hosts to understand the pathogenesis mechanisms of foodborne pathogens. Research in the past decade has stressed the importance of the gut microbial composition in modulating susceptibility to these pathogens. The results of our study—using gnotobiotic mice and germfree control animals—additionally suggest that the dietary fiber components can dominate the impact of enteropathogenic virulence over the pathogenicity-modulating properties of the gut microbiome. The significance of our research is that there is a need to carefully choose a certain chow when performing the enteropathogen-associated mouse experiments and to cautiously match the rodent diets when trying to replicate experiments across different laboratories. Finally, our data underscore the importance of using germfree control animals to study these pathogens, as our findings would have been prone to misinterpretation in the absence of these controls.

KEYWORDS colonic mucus layer, dietary fiber, gut microbiota, *Listeria monocytogenes*, pathogen susceptibility, *Salmonella* Typhimurium

Editor John F. Rawls, Duke University School of Medicine

Address correspondence to Mahesh S. Desai, mahesh.desai@lih.lu.

Received 9 June 2021
Accepted 18 October 2021
Published 2 November 2021

The gut microbiome confers colonization resistance against invading pathogens by nutrient competition and by maintaining the host's immune homeostasis and the mucosal barrier's integrity (1). However, a deficiency of dietary fiber might negatively affect these host-beneficial properties of the microbiome (2). Since dietary fiber consumption in Western countries is below the recommended intake of 25 to 35 g per day (3), such dietary habits might contribute to the observed incidence of enteric pathogen infections in the Western world. Using a well-characterized 14-member synthetic human gut microbiota (14SM) in gnotobiotic mice, we previously demonstrated that dietary fiber deprivation leads to an increase in the mucin-degrading activity of the gut microbiome, which excessively erodes the colonic mucus barrier (4). We further showed that the reduced mucus barrier enhances susceptibility to infection with *Citrobacter rodentium* (4), a rodent pathogen used to model human enteropathogenic and enterohemorrhagic *Escherichia coli* infections (5). Since the intestinal mucus barrier is a first line of innate defense (1), here, we hypothesized that diet-induced mucus erosion might also increase susceptibility to other enteric pathogens.

Food safety has increased considerably in recent years, yet foodborne enteric pathogens, such as *Listeria* spp. and *Salmonella* spp., remain a major source of disease, even in industrialized countries (6, 7). Since dietary alterations, including fiber deficiency, might alter colonization resistance by the gut microbiome to enteric pathogens (1), understanding the interconnections in the diet–microbiome–pathogen axis might help to shed light on hitherto unexplored pathogenesis mechanisms. It has previously been shown that mice lacking the *Muc2* gene, which encodes the major constituent glycoprotein of the colonic mucus layer, are more susceptible to *Listeria monocytogenes* and *Salmonella enterica* serovar Typhimurium infections (8, 9). Notably, a similar increase in susceptibility was observed for *C. rodentium* in *Muc2*$^{-/-}$ mice (10), a result that we could recapitulate in wild-type, fiber-deprived mice with a reduced mucus barrier (4). Thus, we leveraged our 14SM gnotobiotic model to investigate how dietary fiber deprivation and/or an eroded mucus barrier affects the host's susceptibility toward infections with the intracellular enteric pathogens *L. monocytogenes* and *S.* Typhimurium.

For this purpose, we employed BALB/c and C57BL/6 mice for infections with *L. monocytogenes* and *S.* Typhimurium, respectively; the choice of the host strains for each pathogen is based on previous studies (12–14). We colonized 6- to 10-week-old, germfree (GF) mice with the 14SM community and confirmed colonization of all 14 strains by quantitative PCR (qPCR) using strain-specific primers as described previously (4, 15). For 6 days after colonization, the mice were kept on a standard mouse chow, which we call a fiber-rich (FR) diet. After 6 days, half of the mice were switched to a fiber-free (FF), high-sugar diet. After an additional 20 days, BALB/c mice were infected via intragastric gavage with 10^9 CFU of *L. monocytogenes* and C57BL/6 mice were infected with 10^8 CFU of *S.* Typhimurium. The infection progress was monitored for up to 10 days (Fig. 1A). As a control for the 14SM-colonized mice, age- and sex-matched GF BALB/c and C57BL/6 mice were used. These GF controls were also fed either the FR or the FF diet before being subjected to *L. monocytogenes* and *S.* Typhimurium infection (Fig. 1A).

Throughout the feeding period before the pathogen infection, neither FR diet- nor FF diet-fed mice exhibited any obvious physiological abnormalities, irrespective of whether they were 14SM colonized or not. Fiber deprivation significantly altered the gut microbiota compositions of BALB/c and C57BL/6 mice (Fig. 1B). Infection of C57BL/6 mice caused severe diarrhea, making the analysis of their fecal matter impossible. Thus, analysis of the gut microbiota of infected mice could be performed only for BALB/c mice, which showed that the infection majorly influenced the microbiota composition (Fig. 1B). All bacterial members within the 14SM that shifted in response to the diet switch were further affected by the infection with the pathogen (Fig. 1C). In line with our previously published study with 14SM-colonized Swiss Webster mice (4), fiber deprivation increased the relative abundances of mucin-degrading bacteria, such as *Akkermansia muciniphila* and *Bacteroides caccae* (4), whereas the abundances of the

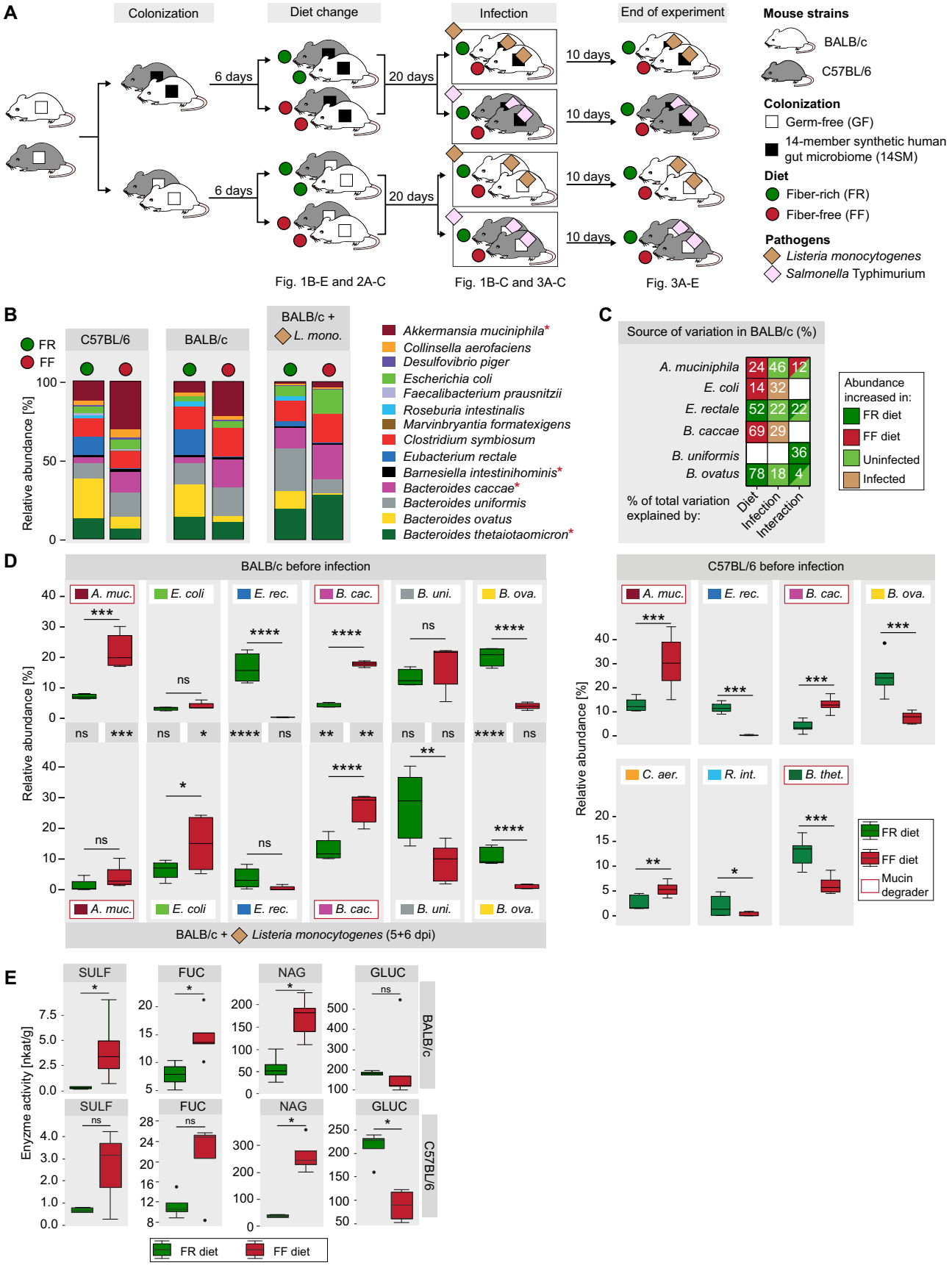

FIG 1 Fiber deprivation increases the abundance and activity of mucin-degrading gut bacteria in both BALB/c and C57BL/6 mice. (A) Experimental timeline. Half of the 6- to 10-week-old, age-matched, GF BALB/c and C57BL/6 mice were gavaged with the 14-member gut microbiota (14SM) on two

(Continued on next page)

fiber-degrading strains, such as *Bacteroides ovatus* and *Eubacterium rectale* (4), significantly decreased (Fig. 1D). Interestingly, the significantly increased abundance of *A. muciniphila* owing to the FF diet is nullified by its reduced abundance following the infection (Fig. 1C and D).

Unlike with *C. rodentium*, the primary infection site of the intracellular pathogens *L. monocytogenes* and *S.* Typhimurium is the small intestine and not the colon (12, 16). Nevertheless, a recent study highlighted the role of the colon as the main site for establishing the systemic spread of *L. monocytogenes* in *Muc2*$^{-/-}$ mice (8). Accordingly, the expansion of mucin-degrading commensals in FF diet-fed mice (Fig. 1D) prompted us to investigate the activities of certain bacterial mucin glycan-degrading enzymes, which can be used as a proxy for the microbiome-mediated erosion of the mucus barrier (17). Using fecal samples, we detected increased activities of key mucin glycan-degrading bacterial enzymes (18), such as sulfatase (SULF), α-fucosidase (FUC), and β-*N*-acetylglucosaminidase (NAG), in FF diet-fed BALB/c and C57BL/6 mice compared to those in FR diet-fed mice (Fig. 1E), although in BALB/c mice, the trends were not significant for SULF and FUC. On the other hand, the activity of β-glucosidase (GLU)—an enzyme that indicates microbial plant fiber metabolism (19)—significantly decreased in FF diet-fed C57BL/6 mice (Fig. 1E). Overall, while activities were less pronounced in C57BL/6 mice, our results suggest that fiber deprivation leads to increased activities of enzymes essential for mucin glycan degradation (Fig. 1E). We have previously shown using Swiss Webster mice that the increased mucin-degrading bacteria and the microbial enzymes that target the colonic mucins result in a reduced mucus barrier (4); therefore, here, we suspect a similar mucus barrier reduction in the C57BL/6 and BALB/c mice.

We then analyzed the short-chain fatty acid (SCFA) concentrations, as they serve as important regulators of mucosal barrier integrity (20). Nevertheless, despite the significant changes in microbial composition and activity, butyrate was the only SCFA with a significantly altered concentration (Fig. 2A). As low butyrate levels indicate an impaired mucosal barrier (20) and considering the suggested diet-induced impairment of the colonic mucus layer (Fig. 1E), we determined potential diet-induced colonic inflammation via detection of fecal lipocalin-2 (LCN-2) levels, which is considered a biomarker for low-grade inflammation (21). Significantly increased levels of LCN-2 were observed only in FR diet-fed GF BALB/c mice, not in their FF diet-fed counterparts (Fig. 2B). In contrast, in our previous study, 14SM-colonized Swiss Webster mice showed increased LCN-2 levels when fed the FF diet (4), suggesting that dietary fiber-mediated colonic baseline inflammation is likely dependent on the rodent genetic background. Furthermore, we detected higher concentrations of LCN-2 in 14SM-colonized and FF diet-fed mice than in their GF counterparts (Fig. 2B). However, when we assessed the local immune phenotype by time-of-flight mass cytometry (CyTOF)-based profiling of CD8^{+}, Th1, and NK immune cell populations in the colonic lamina propria of uninfected 14SM-colonized BALB/c mice, all of these immune cells were increased in the FF diet-fed mice (Fig. 2C). These data indicate an over-

FIG 1 Legend (Continued)
consecutive days, while the other half were maintained GF. Six days after the gavage, half of the mice from the GF and 14SM groups continued on the FR diet, while the other half were switched to the FF diet. The mice were maintained on their respective diets for 20 days, and then the BALB/c mice were infected with *Listeria monocytogenes* and the C57BL/6 mice were infected with *Salmonella* Typhimurium, after which the mice were observed for another 10 days. (B) Relative bacterial abundances before infection and for BALB/c mice after infection, determined by qPCR on DNA extracted from fecal pellets. While some low-abundance bacteria might not be visible in the figure, all 14 bacteria were detected. Red asterisks denote known mucin-degrading bacteria. (C) Sources of variation of the bacterial relative abundances in BALB/c mice, with consideration of the two variables, diet and infection status, determined by two-way ANOVA. The percentage of total variation due to diet, infection with *L. monocytogenes*, or the interaction of these two factors is represented in each cell. The trend of the shift in the abundance by a given factor is represented by the color of each cell. (D) Members of the 14SM whose abundance significantly changed due to diet, determined in BALB/c mice before and after the infection with *L. monocytogenes* and in C57BL/6 before infection with *S.* Typhimurium. Significance labels between the top and bottom panels represent comparisons between a given group before and after infection. For the Tukey box plot, BALB/c mice were analyzed by two-way ANOVA with a Tukey-Kramer *post hoc* test and C57BL/6 mice were analyzed by a Mann-Whitney test. (E) Glycan-degrading enzyme activities of the gut microbiome in stool samples determined by *p*-nitrophenyl glycoside-based enzyme assays. Sulfatase (SULF), α-fucosidase (FUC), and β-*N*-acetyl-glucosaminidase (NAG) are key mucin-degrading enzymes, while β-glucosidase (GLUC) serves as a control for general glycan-degrading activity. Tukey box plot values were determined by the Wilcoxon rank sum test. There were 5 BALB/c mice/group. For the C57BL/6 mice, there were 7 GF FR mice per group; for the other groups, there were 8 mice per group. ns, nonsignificant; *, $P < 0.05$; **, $P < 0.01$; ***, $P < 0.001$; ****, $P < 0.0001$. *L. mono.*, *L. monocytogenes*; *A. muc.*, *A. muciniphila*; *E. rec.*, *E. rectale*; *B. cac.*, *B. caccae*; *B. uni.*, *Bacteroides uniformis*; *B. ova.*; *Bacteroides ovatus*; *C. aer.*, *Collinsella aerofaciens*; *R. int.*, *Roseburia intestinalis*; *B. thet.*, *Bacteroides thetaiotaomicron*.

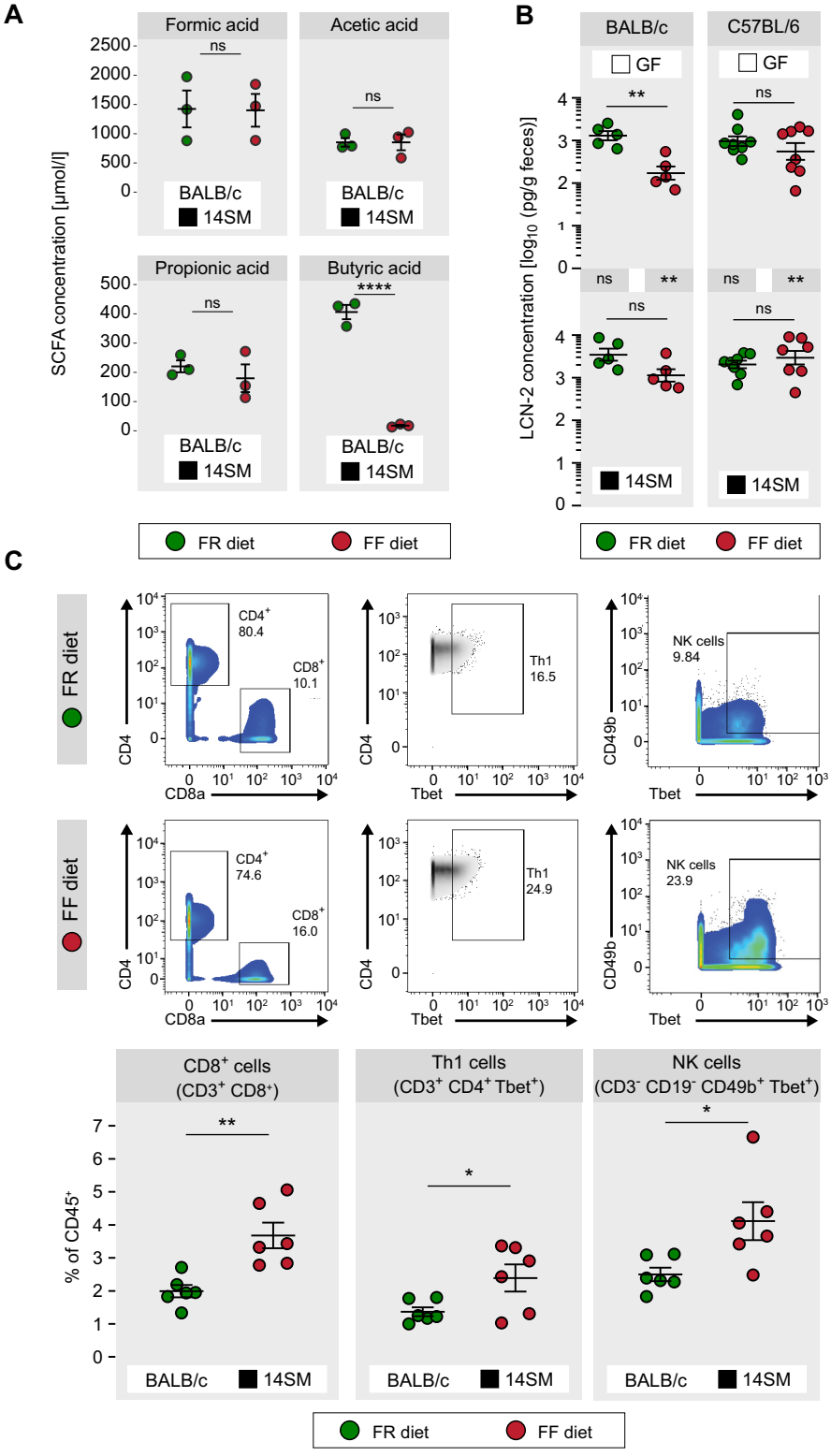

FIG 2 Fiber deprivation can prime the host against infection. (A) Short-chain fatty acid concentrations in cecal contents of uninfected BALB/c mice. Error bars represent standard errors of the means (SEM) from an unpaired, two-tailed *t* test (n = 3 mice/group). (B) Fecal LCN-2 levels determined by ELISA on the day before the pathogen infection. Significance labels between the top and bottom panels represent comparisons between GF and 14SM mice of a given dietary group. Error bars represent SEM from a two-way ANOVA with a Tukey-Kramer *post hoc* test. There were 5 BALB/c mice/group. For C57BL/6 mice, there were 7 GF FR diet-fed mice per group; in other groups, there were 8 mice per group. (C) $CD8^+$, Th1, and NK immune cell populations in colonic lamina propria of uninfected BALB/c mice determined using time of flight mass cytometry (CyTOF). Gating plots (top) show percentages of

(Continued on next page)

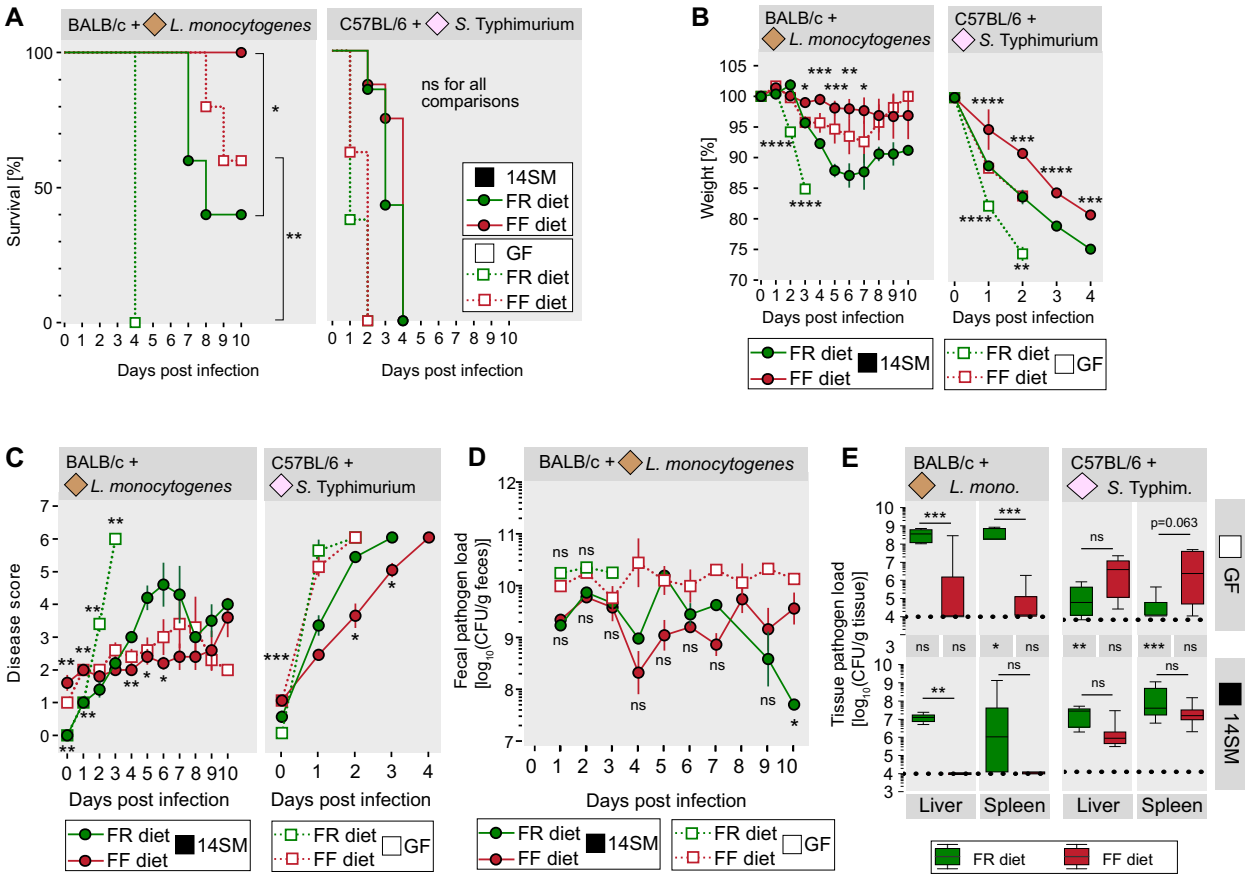

FIG 3 Fiber deprivation protects against *L. monocytogenes* and *S.* Typhimurium with or without the presence of a gut microbiota. (A) Survival curve of enteropathogen-infected mice determined by a log rank test between both diets of the GF or 14SM group. (B) Weight change of the enteropathogen-infected mice. The day 0 value was determined immediately before the gavage. Error bars represent SEM as determined by an unpaired, two-tailed *t* test between both diets of the GF (bottom significance labels) or 14SM (top significance labels) group; comparisons are not significant when the significance is not displayed. (C) Average disease scores attributed to each enteropathogen-infected group. The day 0 value was determined immediately before the gavage. Error bars represent SEM as determined by a Mann-Whitney test between both diets of the GF (top significance labels) or 14SM (bottom significance labels) group; comparisons are not significant when the significance is not displayed. (D) Fecal *L. monocytogenes* loads of BALB/c mice during the 10 days of infection. Depending on the sampling day, 1 to 5 samples per group were obtained and evaluated. The fecal *S.* Typhimurium load in C57BL/6 mice could not be determined, as the mice did not consistently provide fecal material due to the severe disease. Tukey box plot values are from an unpaired, two-tailed *t* test. (E) Pathogen loads of liver and spleen tissues on the day that each mouse was euthanized. Samples below the measurable threshold of 10^4 CFU (dotted black line) were considered 10^4. Significance labels between the top and bottom panels represent comparisons between GF and 14SM mice of a given dietary group. Tukey box plot values were determined by two-way ANOVA with a Tukey-Kramer *post hoc* test. There were 5 BALB/c mice per group. For the C57BL/6 group, there were 7 GF FR diet-fed mice per group; for other groups, there were 8 mice per group. Green, FR diet-fed mice; red, FF diet-fed mice; smooth lines, 14SM mice; dotted lines, GF mice. ns, nonsignificant; *, $P < 0.05$; **, $P < 0.01$; ***, $P < 0.001$; ****, $P < 0.0001$.

all increased type 1 inflammatory immune response under FF diet conditions, which seems to be regulated independently of the LCN-2 pathways.

After a 20-day feeding period, we infected both mouse strains with their respective pathogens (Fig. 1A). Body weight and disease scores of all mouse groups were assessed daily for up to 10 days postinfection (dpi). The lethality of *L. monocytogenes*-infected GF FR diet-fed BALB/c mice reached 100% by 4 dpi, while their FF diet-fed counterpart provided a significantly higher survival rate (Fig. 3A). Similarly, 14SM-colonized FF diet-fed BALB/c mice had a significantly higher survival rate than their FR diet-fed counterparts,

FIG 2 Legend (Continued)

cells of the previously gated population (the percentage of $CD3^+$ cells for $CD8^+$ cells, the percentage of $CD4^+$ cells for Th1 cells, and the percentage of $CD19^-$ cells for NK cells). In contrast, dot plots (bottom) are represented as percentages of all $CD45^+$ cells. Error bars represent SEM from an unpaired, two-tailed *t* test (n = 6/mice group, two independent experiments). ns, nonsignificant; *, $P < 0.05$; **, $P < 0.01$; ***, $P < 0.001$; ****, $P < 0.0001$.

TABLE 1 Scoring system used to determine the disease severity of mice[a]

Category	Score
Body wt	
5–10% wt loss	1
11–15% wt loss	2
16–20% wt loss	3
≥20% wt loss	HEP
Pinched skin/dehydration	4
Coat condition	
Coat slightly unkempt	1
Slight piloerection	2
Marked piloerection	4
Body function	
Tachypnea	3
Dyspnea	5
Environment	
Loose stools or diarrhea	1
Blood in diarrhea	HEP
Behaviors	
Tense and nervous on handling	3
Markedly distressed on handling, e.g., shaking, vocalizing, aggressive	4
Locomotion	
Slightly abnormal gait/posture	1
Markedly abnormal gait/posture	4
Significant mobility problems or reluctance to move	HEP
Procedure-specific indicator	
Conjunctivitis	4
Implementation of HEP	
Total score	≥6

[a]Mice reaching the humane endpoint (HEP) were scored the maximum score of 6.

and intriguingly, all 14SM-colonized FF diet-fed BALB/c mice survived the infection (Fig. 3A). In accordance with previous reports stating that mice harboring an intestinal microbiota are less susceptible to *L. monocytogenes* infections than GF mice (11), 14SM-colonized BALB/c mice generally provided increased survival compared to that of the GF controls fed the same diet (Fig. 3A). In line with the course of the survival curves, weight loss in FR diet-fed and *L. monocytogenes*-infected BALB/c mice, either 14SM colonized or GF, was significantly higher than in the corresponding FF diet-fed groups (Fig. 3B). Daily assessed disease scores for all four *L. monocytogenes*-infected BALB/c mouse groups (Fig. 3C; see Table 1 for the disease-scoring scheme) underscore that susceptibility to *L. monocytogenes* infection is more dependent on the fiber content of the diet itself than on the microbiome. Interestingly, fecal *L. monocytogenes* loads did not significantly differ between both diets of the GF and 14SM groups, except at the final time point in the 14SM group (Fig. 3D), hinting at a faster clearance in 14SM FR diet-fed mice. Systemic dissemination of *L. monocytogenes* in BALB/c mice was assessed by the detection of CFU in liver and spleen (Fig. 3E). Unlike with the fecal pathogen levels, both FR diet-fed groups showed significantly increased dissemination of *L. monocytogenes* into the liver compared to that of their FF diet-fed counterparts (Fig. 3E). Similarly, dissemination into the spleen was significantly higher in GF FR diet-fed mice than in the FF diet-fed controls (Fig. 3E). These results suggest that feeding mice a fiber-free diet does not affect the growth of *L. monocytogenes* but hinders its translocation across the intestinal epithelium.

In contrast to *L. monocytogenes*-infected BALB/c mice, all *S.* Typhimurium-infected C57BL/6 mice died within 4 days of infection (Fig. 3A). There were no significant

differences in survival rates between FR diet-fed and FF diet-fed GF mice or between 14SM-colonized mice fed the two different diets (Fig. 3A). Despite no significant differences in survival between *S.* Typhimurium-infected C57BL/6 mice fed different diets, weight loss in FR diet-fed 14SM-colonized mice, as well as in FR diet-fed GF C57BL/6 mice, was significantly increased compared to that of their FF diet-fed 14SM-colonized or GF mice (Fig. 3B). Disease scores of all mice reached the maximum possible score of 6 (Fig. 3C). Notably, GF mice were more susceptible to *S.* Typhimurium infection than 14SM-colonized mice, and FR diet-fed 14SM mice provided significantly higher disease scores than FF diet-fed 14SM-colonized mice. No significant differences in levels of dissemination of *S.* Typhimurium into the liver or spleen were detected (Fig. 3E). Interestingly, dissemination into the spleen and liver was significantly higher in 14SM-colonized mice than in GF mice (Fig. 3E).

Our data suggest that fiber deprivation has a protective effect against *L. monocytogenes* infections and to a reduced extent against *S.* Typhimurium. In contrast to Swiss Webster mice infected with cecum- and colon-targeting *C. rodentium* (4) and to *Muc2*$^{-/-}$ mice (8, 9), elevated microbial mucin degradation in BALB/c and C57BL/6 mice, as a consequence of fiber deprivation, did not promote susceptibility to the two enteropathogens. One potential explanation is that even a microbially eroded colonic mucus layer still provides sufficient protection to prevent the colon from becoming the locus for the systemic spread of these pathogens; alternatively, the direct effects of diet might simply dominate the impact of an eroded mucus layer. Overall, we determined a direct impact of dietary fiber components on host susceptibility to enteropathogenic infections, which seems to be rooted in a heightened translocation efficiency. Considering the potential cytotoxic environment resulting from the increased type 1 inflammatory immune response in the uninfected, FF diet-fed BALB/c mice compared to that of the FR diet-fed BALB/c mice (Fig. 2C), we hypothesize that this priming of the immune system provides protection against subsequent infection. Specifically, CD8^{+} T cells are known to play a crucial role in clearing *L. monocytogenes* infections (22, 23), and their increased percentage in the FF diet-fed 14SM-colonized mice (Fig. 2C) might at least partially explain why this group of mice is better protected from the infection.

Apparently, the 14SM could not protect the mice via colonization resistance, although the microbiome delayed the overall disease course and the pathogen load. Furthermore, we cannot exclude the possibility that the fiber types present in our FR diets promote pathogen virulence. Based on the ingredients provided by the supplier for this chow, β-glucans and arabinoxylans appear to be the dominant fibers. Indeed, a study in guinea pigs showed that supplementation with the dietary fibers pectin and inulin significantly increased the translocation of *L. monocytogenes* into the liver and spleen (24). However, this study also shows that supplementation with galacto-oligosaccharides and xylo-oligosaccharides decreased the translocation (24), indicating a fiber source-specific virulence modulation of *L. monocytogenes*. In this context, increased fiber consumption has previously been linked to both increased and decreased susceptibility (13, 25, 26) to *S.* Typhimurium infections, indicating that not only the presence or absence of dietary fiber in a mouse chow determines enteropathogen susceptibility but also the source or type of fiber is an essential factor. Despite many advantages of gnotobiotic mouse studies (27), the potential absence of interactions between specific commensal bacteria and pathogens such as *Prevotella* spp. with *L. monocytogenes* (14) or *Mucispirillum schaedleri* with *S.* Typhimurium (28) must be considered a limitation of our 14SM model. Moreover, gnotobiotic models might fail to provide a real-life picture of colonization resistance provided by a complex microbiome against both *L. monocytogenes* and *S.* Typhimurium infections (11, 12). Another potential caveat in comparing results obtained from our FR and FF diets might be the higher amount of glucose in the FF diet, especially given that the main infection site of these pathogens is the small intestine (4). It is difficult to disentangle the effect of low fiber and high glucose; although we showed that the fecal load of *L. monocytogenes* was unaffected by the diet, we cannot fully exclude the potential effect of sugar on the infectiousness of the pathogens.

The intriguing, direct impact of dietary fiber on the increased susceptibility to enteropathogenic infections of mice calls attention to the need to give due importance to designing diets in mouse studies. Thus, mouse studies investigating the underlying mechanisms of enteropathogen infections should involve a critical assessment of the animal chow compositions across different laboratories. Our observation might have been overlooked in the absence of GF control groups, highlighting the importance of such controls when studying enteropathogenesis mechanisms. At a broader level, our observational study suggests that even given the high potential of dietary modulations via fiber supplementation for the benefit of human health (29), studies should be performed carefully, considering the underlying microbiota composition and acknowledging potential downfalls due to unexpected side effects.

Ethical statement. All animal experiments were performed according to the "Règlement Grand-Ducal du 11 janvier 2013 relatif à la protection des animaux utilisés à des fins scientifiques" (30), based on Directive 2010/63/EU on the protection of animals used for scientific purposes (31), and approved by the Animal Experimentation Ethics Committee of the University of Luxembourg and by the Luxembourgish Ministry of Agriculture, Viticulture, and Rural Development (national authorization no. LUPA 2020/27 and LUPA 2019/50). The mice were housed in ISOcages under gnotobiotic conditions in accordance with the recommendations stated by the Federation of European Laboratory Animal Science Associations (FELASA).

Experimental design and dietary treatment. For the infection experiments, 6- to 10-week-old, age-matched, male, germfree (GF) BALB/c (n = 20, 5 per group) and C57BL/6N (n = 31; GF fiber-rich [FR] group, 7 per group; other groups, 8 per group) were housed in ISOcages with up to five animals per cage. Similarly, 6-week-old, female, GF BALB/c mice were housed in ISOcages for time of flight mass cytometry (CyTOF) and short-chain fatty acid (SCFA) measurements (n = 12; 6 mice per group for CyTOF, 3 mice per group for SCFA analysis). Light cycles consisted of 12 h of light and sterile water, and diets were provided *ad libitum*. The GF status of the mice was confirmed by aerobic and anaerobic microbial culturing of fecal samples. As per the groupings (Fig. 1A), the relevant mice were gavaged with 0.2 ml of a 14-member synthetic human gut microbiota (14SM) gavage mix on two consecutive days. The gavage mix was prepared as described previously (15). Before and 6 days following the gavage, all mice were maintained on a standard mouse chow which we refer to as a fiber-rich (FR) diet. Afterwards, half of the gavaged and half of the GF mice were switched randomly to a fiber-free (FF) diet, while the rest were maintained on the FR diet. In contrast to the FR diet, the FF diet does not contain dietary fiber from plant sources but instead contains increased glucose levels (4). All mice in the infection groups were maintained for 20 days on their respective diets, while mice from the SCFA and CyTOF measurement groups were maintained for 40 days on their respective diets. Fecal samples were collected once a week during this period. After their 40-day feeding period, mice from the SCFA and CyTOF groups were euthanized by cervical dislocation. Colons were excised and immediately processed for CyTOF measurements (see the details below). Cecal contents from three mice per group were collected and flash frozen before being stored at −80°C for subsequent SCFA measurements (see the details below). After their 20-day feeding period, mice from the infection group were infected with their respective pathogens; BALB/c mice were infected with *L. monocytogenes*, and the C57BL/6N mice were infected with *S.* Typhimurium. The mice were infected by oral gavage and without any sort of pretreatment, such as antibiotics or fasting. Following the infection, the mice were observed for up to 10 days on their respective diets, and fecal samples were collected daily for all possible mice. Upon reaching the humane endpoint or the end of the 10-day observation time, mice were euthanized by cervical dislocation. Livers and spleens were collected to determine pathogen load and spleen weight. Cecal contents were flash frozen and stored at −80°C for LCN-2 measurements (see the details below). Due to the rapid disease development, it was not possible to reliably obtain fecal material during the course of the *S.* Typhimurium infection because

of the severe symptoms; accordingly, we could not compare CFU counts from feces between these groups.

Animal diets. The fiber-rich diet was a standard, autoclaved rodent chow (LabDiet, St. Louis, MO, USA; catalog no. 5013). The fiber-free diet was manufactured and irradiated by SAFE Diets (Augy, France) according to the TD.140343 diet formulation, which is a modified version of the Harlan.TD08810 diet (Envigo, Indianapolis, IN, USA) described previously (4). The resulting fiber-free diet lacks all dietary fiber and has an increased glucose content to compensate for the lack of fiber; note that this diet contains crystalline cellulose, although it cannot be degraded by any of the 14SM members.

Colonization with 14SM. All 14SM-constituent strains were cultured and intragastrically gavaged as described previously (15).

Quantification of bacterial relative abundance. The colonization of individual strains in the 14-member synthetic microbiota was confirmed using phylotype-specific qPCR primers as described previously (15), and the relative abundances of individual microbial strains were computed using the same qPCR protocol (15).

Pathogen culturing and enumeration. Both *Listeria monocytogenes* (Murray et al.) Pirie (ATCC BAA-679) and *Salmonella enterica* subsp. *enterica* (ex Kauffmann and Edwards) Le Minor and Popoff serovar Typhimurium (strain SL1344, DSM 24522) were grown aerobically in Luria-Bertani (LB) broth. They were grown overnight at 37°C by continuous two-dimensional vortexing in culture tubes using a Skyline RM-2L Intelli mixer at 40 rpm. Cultures were then spun down by centrifugation for 10 min at 5,000 rcf and resuspended in LB broth to reach the appropriate number of CFU for gavage. BALB/c mice were infected with 10^9 CFU of *L. monocytogenes*, and C57BL/6 mice were infected with 10^8 CFU of *S.* Typhimurium. Fecal CFU enumeration was performed as described previously (4), with the modification of the selective media, which differed by strain. Tissue was processed in the same manner, except that the homogenization was performed using a tissue grinder. *L. monocytogenes* was plated on Oxford agar plates, while *S.* Typhimurium was plated on streptomycin-containing (50 μg/ml) LB agar plates.

Mouse disease scoring. A project-specific scoring system based on the FELASA guidelines for reporting clinical signs in laboratory animals (32) was used to determine the mouse disease score. This scoring system is shown in Table 1.

Intestinal fatty acid analysis. Thirty to 100 mg of flash-frozen cecal content from uninfected BALB/c mice, which were kept for 40 days on the FR or FF diet, was used for the fatty acid analysis. Per 50 mg of the samples, 500 μl MilliQ water containing 2 mM 2-ethylbutyric acid as an internal standard and 1.4-mm ceramic beads (5 beads per tube) were added. Homogenization was performed for 30 s at 6,000 rpm at 0 to 5°C (Precellys24 homogenizer, catalog no. P000669-PR240-A; Bertin Technologies, Montigny-le-Bretonneux, France), and the resulting homogenate was then centrifuged at 21,000 $\times$ *g* for 5 min at 4°C. Further processing of the sample homogenate and measurements were performed as previously described using gas chromatography-mass spectrometry (GC-MS) (33).

Immune cell profiling of colonic lamina propria. For the immune cell profiling, uninfected BALB/c mice were kept for 40 days on the FR or FF diet. Colons were excised and placed in Hanks' balanced salt solution (HBSS) with phenol red and without calcium and magnesium (Lonza, Basel, Switzerland; catalog no. BE10-543F). Lamina propria cells were extracted using a lamina propria dissociation kit (catalog no. 130-097-410; Miltenyi Biotec, Bergisch Gladbach, Germany) according to the manufacturer's instructions. Cell staining for mass cytometry acquisition was performed according to the method of Guerin et al. (34). Briefly, a total of 3.0×10^6 cells per sample were pelleted into individual 15-ml Falcon tubes and stained with 5 μM cisplatin for 5 min. Cells were washed, and cell surface staining mix containing preconjugated antibodies (Fluidigm, South San Francisco, CA, USA) was added for 30 min at room temperature. Cells were washed twice with flow cytometry (FACS) staining buffer and then fixed using the FOXP3 Fix/Perm kit (eBioscience, San Diego, CA, USA) for 45 min at 4°C, followed by a permeabilization wash. The intracellular staining mix was added to the cells for 30 min at room temperature. Samples were washed twice with FACS buffer, and then pellets were resuspended in cell-ID intercalator-

IR in MaxPar fixation solution (Fluidigm, South San Francisco, CA, USA). On the day of acquisition, samples were washed twice with 1× phosphate-buffered saline (PBS) and then twice with deionized water. Samples were resuspended in deionized water at 0.5×10^6 cells/ml with 10% calibration beads (EQ Four Element calibration beads; Fluidigm) and then acquired on the Helios mass cytometer (Fluidigm). Samples were kept at 4°C for a maximum of 5 days before acquisition. Flow cytometry standard (FCS) files were normalized before being imported into FlowJo (BD, Franklin Lakes, NJ, USA). The data were cleaned to remove in the following order beads, doublets, DNA^-, dead cells, and $CD45^-$ cells. $CD8^+$ T cells were gated on $CD3^+$ $CD8^+$ cells. Th1 T cells were gated on $CD3^+$ $CD4^+$ $Tbet^+$ cells. NK cells were gated on $CD19^-$ $CD3^-$ $CD49b^+$ $Tbet^+$ cells.

Lipocalin ELISA. Samples for the lipocalin enzyme-linked immunosorbent assay (ELISA) were prepared as described previously (4) and measured using the mouse lipocalin-2/NGAL DuoSet ELISA R&D system (Bio-Techne, Minneapolis, MN, USA; catalog no. DY1857) according to the manufacturer's instructions.

Detection of bacterial glycan-degrading enzyme activities. The enzymatic activities of sulfatase, α-fucosidase, β-*N*-acetyl-glucosaminidase, and β-glucosidase were determined using *p*-nitrophenyl glycoside-based enzyme assays from fecal samples as described previously (17).

Statistical analyses. Statistical analysis was performed using Prism 8.1.1. (GraphPad Software, Inc., San Diego, CA, USA), except for the bacterial glycan-degrading enzyme activities, for which R Studio (version 4.0.2) with the "kruskal.test" function within the dplyr package (version 1.0.2) and the "compare_means" function in the ggpubr package (version 0.4.0) was used. Statistical significances are represented by asterisks as follows: *, $P < 0.05$; **, $P < 0.01$; ***, $P < 0.001$; and ****, $P < 0.0001$. Unless otherwise specified in the figure legend, for normal distributed values, unpaired two-tailed *t* tests were used, while for non-normal distributed values, a Mann-Whitney test was used. For multiple comparisons, a two-way analysis of variance (ANOVA) with a Tukey-Kramer *post hoc* test was performed in Prism. The specific test and the number of animals used for each experiment are detailed in the figure legends.

SUPPLEMENTAL MATERIAL

Supplemental material is available online only.

FIG S1, EPS file, 2 MB.

TABLE S1, DOCX file, 0.02 MB.

ACKNOWLEDGMENTS

This work was supported by Luxembourg National Research Fund (FNR) CORE grants (C15/BM/10318186 and C18/BM/12585940) to M.S.D. and an FNR AFR individual Ph.D. fellowship to A.P. (11602973).

We thank Pascale Cossart and Olivier Dussurget from the Pasteur Institute in Paris for their support and for providing us with the *Listeria monocytogenes* strain used in this work. We also thank Christian Jäger, Xiangyi Dong, and Floriane Gavotto from the LCSB Metabolomics Platform for their support with the SCFA analysis.

We declare that we have no competing interests.

M.S.D. supervised the study and obtained research funding; M.W., J.Z., and M.S.D. designed the study; M.W., A.S., and A.P. performed the experiments; M.W. and M.S.D. wrote the original manuscript draft; and M.W., A.S., A.P., J.Z., and M.S.D. reviewed and edited the manuscript.

REFERENCES

1. Martens EC, Neumann M, Desai MS. 2018. Interactions of commensal and pathogenic microorganisms with the intestinal mucosal barrier. Nat Rev Microbiol 16:457–470. https://doi.org/10.1038/s41579-018-0036-x.
2. Makki K, Deehan EC, Walter J, Bäckhed F. 2018. The impact of dietary fiber on gut microbiota in host health and disease. Cell Host Microbe 23:705–715. https://doi.org/10.1016/j.chom.2018.05.012.
3. European Food Safety Authority. 2010. Scientific opinion on dietary reference values for carbohydrates and dietary fibre. EFSA J 8:1462. https://doi.org/10.2903/j.efsa.2010.1462.
4. Desai MS, Seekatz AM, Koropatkin NM, Kamada N, Hickey CA, Wolter M, Pudlo NA, Kitamoto S, Terrapon N, Muller A, Young VB, Henrissat B, Wilmes P, Stappenbeck TS, Núñez G, Martens EC. 2016. A dietary fiber-deprived gut

microbiota degrades the colonic mucus barrier and enhances pathogen susceptibility. Cell 167:1339–1353.e21. https://doi.org/10.1016/j.cell.2016.10.043.
5. Collins JW, Keeney KM, Crepin VF, Rathinam VAK, Fitzgerald KA, Finlay BB, Frankel G. 2014. Citrobacter rodentium: infection, inflammation and the microbiota. Nat Rev Microbiol 12:612–623. https://doi.org/10.1038/nrmicro3315.
6. de Noordhout CM, Devleesschauwer B, Angulo FJ, Verbeke G, Haagsma J, Kirk M, Havelaar A, Speybroeck N. 2014. The global burden of listeriosis: a systematic review and meta-analysis. Lancet Infect Dis 14:1073–1082. https://doi.org/10.1016/S1473-3099(14)70870-9.
7. Parisi A, Sarkar K, Blacker BF, Reiner RC, Hay SI, Nixon MR, Dolecek C, James SL, Mokdad AH, Abebe G, Ahmadian E, Alahdab F, Alemnew BTT, Alipour V, Bakeshei FA, Animut MD, Ansari F, Arabloo J, Asfaw ET, Bagherzadeh M, Bassat Q, Belayneh YMM, Carvalho F, Daryani A, Demeke FM, Demis ABB, Dubey M, Duken EE, Dunachie SJ, Eftekhari A, Fernandes E, Fard RF, Gedefaw GA, Geta B, Gibney KB, Hasanzadeh A, Hoang CL, Kasaeian A, Khater A, Kidanemariam ZT, Lakew AM, Malekzadeh R, Melese A, Mengistu DT, Mestrovic T, Miazgowski B, Mohammad KA, Mohammadian M, Mohammadian-Hafshejani A, Nguyen CT, Nguyen LH, Nguyen SH, Nirayo YL, Olagunju AT, Olagunju TO, GBD 2017 Non-Typhoidal Salmonella Invasive Disease Collaborators JD, et al. 2019. The global burden of non-typhoidal salmonella invasive disease: a systematic analysis for the Global Burden of Disease Study 2017. Lancet Infect Dis 19:1312–1324. https://doi.org/10.1016/S1473-3099(19)30418-9.
8. Zhang T, Sasabe J, Hullahalli K, Sit B, Waldor MK. 2021. Increased Listeria monocytogenes dissemination and altered population dynamics in Muc2-deficient mice. Infect Immun 89:e00667-20. https://doi.org/10.1128/IAI.00667-20.
9. Zarepour M, Bhullar K, Montero M, Ma C, Huang T, Velcich A, Xia L, Vallance BA. 2013. The mucin muc2 limits pathogen burdens and epithelial barrier dysfunction during Salmonella enterica serovar Typhimurium colitis. Infect Immun 81:3672–3683. https://doi.org/10.1128/IAI.00854-13.
10. Bergstrom KSB, Kissoon-Singh V, Gibson DL, Ma C, Montero M, Sham HP, Ryz N, Huang T, Velcich A, Finlay BB, Chadee K, Vallance BA. 2010. Muc2 protects against lethal infectious colitis by disassociating pathogenic and commensal bacteria from the colonic mucosa. PLoS Pathog 6:e1000902. https://doi.org/10.1371/journal.ppat.1000902.
11. Becattini S, Littmann ER, Carter RA, Kim SG, Morjaria SM, Ling L, Gyaltshen Y, Fontana E, Taur Y, Leiner IM, Pamer EG. 2017. Commensal microbes provide first line defense against Listeria monocytogenes infection. J Exp Med 214:1973–1989. https://doi.org/10.1084/jem.20170495.
12. Barthel M, Hapfelmeier S, Quintanilla-Martínez L, Kremer M, Rohde M, Hogardt M, Pfeffer K, Rüssmann H, Hardt WD. 2003. Pretreatment of mice with streptomycin provides a Salmonella enterica serovar Typhimurium colitis model that allows analysis of both pathogen and host. Infect Immun 71:2839–2858. https://doi.org/10.1128/IAI.71.5.2839-2858.2003.
13. Wotzka SY, Kreuzer M, Maier L, Arnoldini M, Nguyen BD, Brachmann AO, Berthold DL, Zünd M, Hausmann A, Bakkeren E, Hoces D, Gül E, Beutler M, Dolowschiak T, Zimmermann M, Fuhrer T, Moor K, Sauer U, Typas A, Piel J, Diard M, Macpherson AJ, Stecher B, Sunagawa S, Slack E, Hardt WD. 2019. Escherichia coli limits Salmonella Typhimurium infections after diet shifts and fat-mediated microbiota perturbation in mice. Nat Microbiol 4:2164–2174. https://doi.org/10.1038/s41564-019-0568-5.
14. Rolhion N, Chassaing B, Nahori MA, de Bodt J, Moura A, Lecuit M, Dussurget O, Bérard M, Marzorati M, Fehlner-Peach H, Littman DR, Gewirtz AT, Van de Wiele T, Cossart P. 2019. A Listeria monocytogenes bacteriocin can target the commensal Prevotella copri and modulate intestinal infection. Cell Host Microbe 26:691–701.e5. https://doi.org/10.1016/j.chom.2019.10.016.
15. Steimle A, De Sciscio A, Neumann M, Grant ET, Pereira GV, Ohno H, Martens EC, Desai MS. 2021. Constructing a gnotobiotic mouse model with a synthetic human gut microbiome to study host–microbe cross talk. STAR Protoc 2:100607. https://doi.org/10.1016/j.xpro.2021.100607.
16. Radoshevich L, Cossart P. 2018. Listeria monocytogenes: towards a complete picture of its physiology and pathogenesis. Nat Rev Microbiol 16:32–46. https://doi.org/10.1038/nrmicro.2017.126.
17. Steimle A, Grant ET, Desai MS. 2021. Quantitative assay to detect bacterial glycan-degrading enzyme activities in mouse and human fecal samples. STAR Protoc 2:100326. https://doi.org/10.1016/j.xpro.2021.100326.
18. Tailford LE, Crost EH, Kavanaugh D, Juge N. 2015. Mucin glycan foraging in the human gut microbiome. Front Genet 5:81. https://doi.org/10.3389/fgene.2015.00081.
19. Cairns JRK, Esen A. 2010. β-Glucosidases. Cell Mol Life Sci 67:3389–3405. https://doi.org/10.1007/s00018-010-0399-2.
20. Corrêa-Oliveira R, Fachi JL, Vieira A, Sato FT, Vinolo MAR. 2016. Regulation of immune cell function by short-chain fatty acids. Clin Transl Immunol 5:e73. https://doi.org/10.1038/cti.2016.17.
21. Chassaing B, Srinivasan G, Delgado MA, Young AN, Gewirtz AT, Vijay-Kumar M. 2012. Fecal lipocalin 2, a sensitive and broadly dynamic non-invasive biomarker for intestinal inflammation. PLoS One 7:e44328. https://doi.org/10.1371/journal.pone.0044328.
22. D'Orazio SEF. 2019. Innate and adaptive immune responses during Listeria monocytogenes infection. Microbiol Spectr 7:GPP3-0065-2019. https://doi.org/10.1128/microbiolspec.GPP3-0065-2019.
23. Lara-Tejero M, Pamer EG. 2004. T cell responses to Listeria monocytogenes. Curr Opin Microbiol 7:45–50. https://doi.org/10.1016/j.mib.2003.12.002.
24. Ebersbach T, Jørgensen JB, Heegaard PM, Lahtinen SJ, Ouwehand AC, Poulsen M, Frøkiær H, Licht TR. 2010. Certain dietary carbohydrates promote Listeria infection in a guinea pig model, while others prevent it. Int J Food Microbiol 140:218–224. https://doi.org/10.1016/j.ijfoodmicro.2010.03.030.
25. Ten Bruggencate SJM, Bovee-Oudenhoven IMJ, Lettink-Wissink MLG, Katan MB, Van Der Meer R. 2004. Dietary fructo-oligosaccharides and inulin decrease resistance of rats to salmonella: protective role of calcium. Gut 53:530–535. https://doi.org/10.1136/gut.2003.023499.
26. Petersen A, Heegaard PMH, Pedersen AL, Andersen JB, Sørensen RB, Frøkiær H, Lahtinen SJ, Ouwehand AC, Poulsen M, Licht TR. 2009. Some putative prebiotics increase the severity of Salmonella enterica serovar Typhimurium infection in mice. BMC Microbiol 9:245. https://doi.org/10.1186/1471-2180-9-245.
27. Martín R, Bermúdez-Humarán LG, Langella P. 2016. Gnotobiotic rodents: an in vivo model for the study of microbe-microbe interactions. Front Microbiol 7:409. https://doi.org/10.3389/fmicb.2016.00409.
28. Herp S, Brugiroux S, Garzetti D, Ring D, Jochum LM, Beutler M, Eberl C, Hussain S, Walter S, Gerlach RG, Ruscheweyh HJ, Huson D, Sellin ME, Slack E, Hanson B, Loy A, Baines JF, Rausch P, Basic M, Bleich A, Berry D, Stecher B. 2019. Mucispirillum schaedleri antagonizes Salmonella virulence to protect mice against colitis. Cell Host Microbe 25:681–694.e8. https://doi.org/10.1016/j.chom.2019.03.004.
29. Wolter M, Grant ET, Boudaud M, Steimle A, Pereira GV, Martens EC, Desai MS. Leveraging diet to engineer the gut microbiome. Nat Rev Gastroenterol Hepatol https://doi.org/10.1038/s41575-021-00512-7.
30. Agriculture, Viticulture, and Rural Development. 2013. Règlement Grand-Ducal du 11 janvier 2013 relatif à la protection des animaux utilisés à des fins scientifiques. J Grand Duchy Luxembourg https://legilux.public.lu/eli/etat/leg/rgd/2013/01/11/n2/jo.
31. European Union. 2010. Directive 2010/63/EU of the European Parliament and of the Council of September 22, 2010, relating to the protection of animals used for scientific purposes. European Union, Brussels, Belgium. https://eur-lex.europa.eu/eli/dir/2010/63/oj.
32. Fentener van Vlissingen JM, Borrens M, Girod A, Lelovas P, Morrison F, Torres YS. 2015. The reporting of clinical signs in laboratory animals: FELASA Working Group Report. Lab Anim 49:267–283. https://doi.org/10.1177/0023677215584249.
33. Greenhalgh K, Ramiro-Garcia J, Heinken A, Ullmann P, Bintener T, Pacheco MP, Baginska J, Shah P, Frachet A, Halder R, Fritz JV, Sauter T, Thiele I, Haan S, Letellier E, Wilmes P. 2019. Integrated in vitro and in silico modeling delineates the molecular effects of a synbiotic regimen on colorectal-cancer-derived cells. Cell Rep 27:1621–1632.e9. https://doi.org/10.1016/j.celrep.2019.04.001.
34. Guerin CL, Guyonnet L, Goudot G, Revets D, Konstantinou M, Chipont A, Chocron R, Blandinieres A, Khider L, Rancic J, Peronino C, Debuc B, Cras A, Knosp C, Latremouille C, Capel A, Ollert M, Diehl JL, Jansen P, Planquette B, Sanchez O, Gaussem P, Mirault T, Carpentier A, Gendron N, Smadja DM. 2021. Multidimensional proteomic approach of endothelial progenitors demonstrate expression of KDR restricted to CD19 cells. Stem Cell Rev Rep 17:639–651. https://doi.org/10.1007/s12015-020-10062-1.

Supplementary table 1. Comparison of major experimental parameters and readouts between the present study and our previously published work (4).

	Listeria monocytogenes	*Salmonella* Typhimurium	*Citrobacter rodentium*
Experimental parameters			
Mouse Model	BALB/c	C57BL/6N	Swiss Webster
Pathogen infection dose	10^9 CFUs	10^8 CFUs	10^9 CFUs
Selective culture medium	Oxford Agar	LB-agar with 50 µg/ml Streptomycin	LB-agar with 50 µg/ml Kanamycin
Fiber-rich (FR) diet	Autoclaved rodent chow (LabDiet, 5013)	Autoclaved rodent chow (LabDiet, 5013)	Autoclaved rodent chow (LabDiet, 5010)
FR diet manufacturer	LabDiet (St. Louis, Missouri, USA)	LabDiet (St. Louis, Missouri, USA)	LabDiet (St. Louis, Missouri, USA)
Fiber-free (FF) diet	TD.140343 (4)	TD.140343 (4)	TD.140343 (4)
FF diet manufacturer	SAFE diets (Augy, France)	SAFE diets (Augy, France)	Envigo (Indianapolis, Indiana, USA)
Mouse facility location	Luxembourg Institute of Health, Esch-Sur-Alzette, Luxembourg	Luxembourg Institute of Health, Esch-Sur-Alzette, Luxembourg	University of Michigan, Ann Arbor, Michigan, USA
Microbiome profiling method	qPCR using strain-specific primers	qPCR using strain-specific primers	16S rRNA gene Illumina sequencing and qPCR using strain-specific primers.
Organic acid and SCFA measurements	GC-MS	GC-MS	HPLC
Readouts			
Microbiome composition	Yes	Only before infection	Yes
Carbhoydrate growth profiles of 14SM	No	No	Yes
Carbohydrate-active enzymes gene expression	No	No	Yes
Carbohydrate-active enzyme activity	Yes	Yes	Yes
SCFA concentrations	Yes	No	Yes
LCN-2 concentration	Yes	Yes	Yes
Profiling of immune cell populations	Yes	No	No
Colonic mucus layer thickness measurements	No	No	Yes
Expression of genes involved in colonic mucus production	No	No	Yes
Host cecal transcriptome profile	No	No	Yes
Colon length	Not shown (not significant for all comparisons)	Not shown (not significant for all comparisons)	Yes
Survival	Yes	Yes	Yes
Weight	Yes	Yes	Yes

Disease score	Yes	Yes	No
Fecal pathogen load	Yes	No	Yes
Tissue pathogen load	Yes	Yes	No
Histopathological scoring	No	No	Yes
Localization of pathogen in colon	No	No	Yes

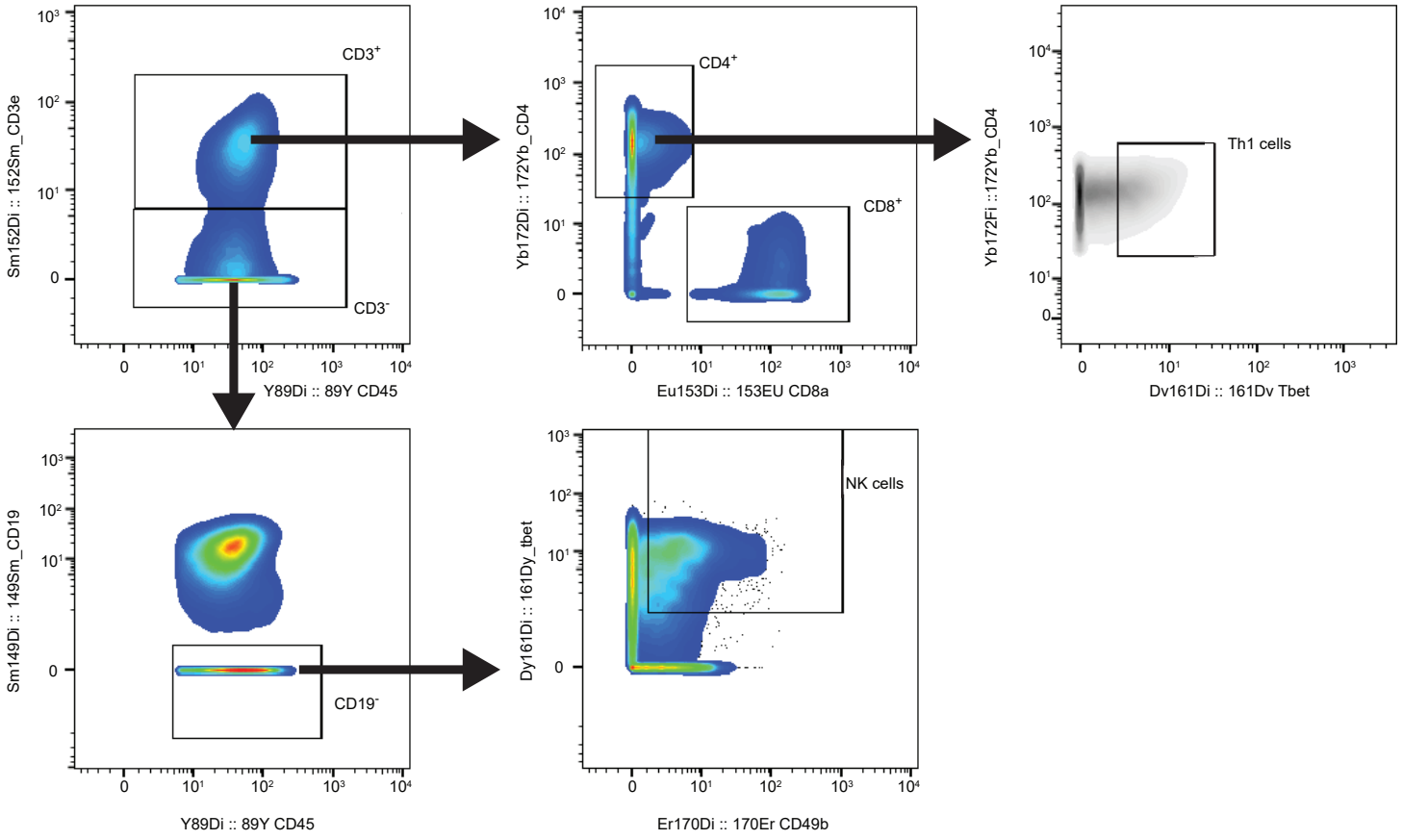

FIG S1 CyTOF gating strategy using FlowJo. Data was cleaned to remove in the following order: beads, doublets, DNA$^-$, dead cells and CD45$^-$. Cells were first gated on CD3. The CD3$^+$ population was then gated on CD8 and CD4 to select the CD8 cells (CD3$^+$ and CD8$^+$) and the CD4$^+$ population was gated on Tbet to select for Th1 cells (CD3$^+$, CD4$^+$ and Tbet$^+$). The initial CD3$^-$ population was gated on CD19 and the CD19$^-$ population was gated on Tbet and CD49b to select for NK cells (CD3$^-$, CD19$^-$, Tbet$^+$ and CD49b$^+$).

5. Increased gut microbial mucin foraging promotes clearance of parasitic worm

5.1 Rationale

The third type of infectious disease I targeted was non-bacterial infection: *Trichuris muris*, a model for soil-transmitted helminth infections. Such infections remain highly relevant, especially in developing countries. However, these parasites are also invaluable study models due to their capacity to subvert the host immune response. By using *T. muris* both Th1 and Th2 immune responses can be studied as the induced type of immune response is dependent on the infectious dose. Moreover, an important landmark in the clearance of *T. muris* infections is a Th2-driven secretion of mucins by colonic goblet cells. Finally, *T. muris* strongly interacts with the gut microbiota, hatching only in the presence of bacteria and modulating the abundance of the commensal bacteria after hatching. However, the mechanisms of how microbiota-mucin-host interactions alter susceptibility to helminths remain to be fully elucidated. Therefore, we decided that *T. muris* is an invaluable model to include in our study of how microbial induced erosion of the gut mucus layer might affect disease susceptibility. Here we confirmed a previous observation, that similarly to the infectious dose, the dietary fiber content of the host diet can modulate *T. muris* susceptibility by altering the host immune response. However, we go a step further and link the altered host response during fiber-deprivation to the mucin-degrading generalists of the gut microbiota and

potentially to a microbiota-induced alteration of the glycosylation of the gut mucus layer.

Personal contributions: I am first author of this research paper which has been submitted to Gastroenterology. As such I had significant contributions to the design, the execution, the data analysis, as well as, the drafting of this paper. With the partial support of other members of my group, I performed all the animal experiments, including husbandry. I performed the experiments and analysis of all experiments in Figure 1 except Figure 1D where I had help from a collaborator. Furthermore, I performed the majority of the experiments for Figure 4 and the analysis for Figure 3, 4 and 5 as well as the supplemental figures. I drafted all of the figures with the exception of Figure 2A and was responsible for the interpretation of the most of the data. Furthermore, I drafted the initial manuscript and performed a majority of the revisions.

5.2 Results

Increased gut microbial mucin foraging promotes clearance of a parasitic worm

Short title: *Nematodes and gut microbial mucin foraging*

Mathis Wolter[a,b], Erica T. Grant[a,b], Amy Parrish[a,b], Alessandro De Sciscio[a], Seona Thompson[c,d], Marie Boudaud[a], Jean-Jacques Gerardy[e,f], Michel Mittelbronn[e,f,g,h,i,j], David J. Thornton[c,d], Andrew J. Macpherson[k,l,m], Richard K. Grencis[c,d] and Mahesh S. Desai[a,n,*]

[a]*Department of Infection and Immunity, Luxembourg Institute of Health, Esch-sur-Alzette, Luxembourg*

[b]*Faculty of Science, Technology and Medicine, University of Luxembourg, Esch-sur-Alzette, Luxembourg*

[c]*Lydia Becker Institute for Immunology and Inflammation. Faculty of Biology, Medicine and Health, University of Manchester, Manchester, United Kingdom*

[d]*Wellcome Centre for Cell Matrix Research, Faculty of Biology, Medicine and Health, University of Manchester, Manchester, United Kingdom*

[e]*National Center of Pathology, Laboratoire National de Santé, Dudelange, Luxembourg*

[f]*Luxembourg Center of Neuropathology, Dudelange, Luxembourg*

[g]*Luxembourg Centre for Systems Biomedecine, University of Luxembourg, Esch-sur-Alzette, Luxembourg*

[h]*Department of Cancer Research, Luxembourg Institute of Health, Luxembourg, Luxembourg*

[i]*Faculty of Science, Technology and Medecine, University of Luxembourg, Esch-sur-Alzette*

[j]*Department of Life Science and Medicine, University of Luxembourg, Esch-sur-Alzette, Luxembourg*

[k]*Department of Visceral Surgery and Medicine, Bern University Hospital, University of Bern, Bern, Switzerland*

[l]*Maurice Müller Laboratories, Department for Biomedical Research, University of Bern, Bern, Switzerland*

[m]*CMPG, Institute of Ecology and Evolution, University of Bern, Bern, Switzerland*

[n]*Odense Research Center for Anaphylaxis, Department of Dermatology and Allergy Center, Odense University Hospital, University of Southern Denmark, Odense, Denmark*

[*]Corresponding author: Mahesh S. Desai, mahesh.desai@lih.lu

Grant support

This work was supported by the following grants in the laboratory of M.S.D.: Luxembourg National Research Fund (FNR) CORE grants (C15/BM/10318186 and C18/BM/12585940) to M.S.D.; FNR PRIDE (17/11823097) and the Fondation du Pélican de Mie et Pierre Hippert-Faber, under the aegis of the Fondation de Luxembourg grants to E.T.G.; FNR AFR individual PhD fellowship to A.P. (11602973); and European Commission Horizon 2020 Marie Skłodowska-Curie Actions individual fellowship to M.B. (897408). MM thanks the Luxembourg National Research Fond (FNR) for the support (FNR PEARL P16/BM/11192868 grant). The Wellcome Trust supports work of R.K.G and S.T. (Z10661/Z/18/Z; 203128A/Z/16/Z) and D.J.T (203128A/Z/16/Z).

Correspondence

Mahesh S. Desai, PhD

Luxembourg Institute of Health

Department of Infection and Immunity

29, rue Henri Koch, L-4354 Esch-sur-Alzette

Luxembourg

Tel: +352 26970-389

Fax: +352 26970-390

Email: mahesh.desai@lih.lu

Disclosures

M.S.D. works as a consultant and an advisory board member at Theralution GmbH, Germany.

Author Contributions

M.S.D. supervised the study and obtained research funding; M.W., D.J.T., R.K.G. and M.S.D. conceived and designed the study; M.W., E.T.G., A.P., A.D.S., and S.T. performed the experiments; M.W., E.T.G., R.K.G., A.P. and M.B. analyzed the data; J.-J. G. and M.M. prepared slides for histology; A.J.M. supplied germ-free mice; M.W. and M.S.D. primarily

wrote the manuscript with input from E.T.G and A.P. All authors reviewed and approved the manuscript.

Data Transparency Statement

All data, study materials and analytical methods will be made available to other researchers upon request.

Abstract

BACKGROUND & AIMS

Host-secreted gastrointestinal mucus plays a key role in the expulsion of intestinal nematode parasites. A balance between mucin secretion by the host and the gut microbial mucin foraging is essential to maintain the intestinal homeostasis, yet little is known about how changes in the mucin–microbiome interactions affect worm infection. Here, we aimed to examine how increased mucin foraging activity by the microbiome changes the course of the parasitic infection by modulating the host immune responses.

METHODS

We employed a gnotobiotic mouse model containing a 14-member synthetic human gut microbiota that facilitates functional interpretations, including diet-driven manipulation of the microbiota toward mucin foraging. We infected the mice with a robust murine nematode, *Trichuris muris*, that closely resembles human infection with *Trichuris trichiura*. We investigated the temporal dynamics of worm infection including worm burden and the host immune responses, and connected these readouts to the microbial changes and metabolic activity toward mucin foraging.

RESULTS

The microbial mucin foraging was further increased during worm infection only in mice with pre-enhanced mucin degrading capacity. The elevated mucin foraging coincides with a shift in host immune responses from susceptible (chronic, Th1 type) to resistant (acute, Th2 type), which promotes worm clearance. The relative abundances of mucin-generalist bacteria drammatically increased during worm clearance, but not during worm retention.

CONCLUSIONS

These results point to a mechanism whereby skewing the metabolic activity of the microbiome toward mucin glycoproteins promotes resistance to worm infection. Our study documents a clinically-relevant, novel link in the microbiome–parasite–host immune axis, which is important prerequisite knowledge in treating parasitic infections.

Keywords

Mucin; gut microbiome; nematode; *Trichuris muris*

Introduction

Chronic infections by intestinal parasitic worms (helminths) are common in animals and humans, especially in developing countries, where the infections are associated with high morbidity[1]. Due to their ability to subvert the host immune response, helminths make an invaluable model to study the host immunomodulatory mechanisms[2]. In this context, the murine parasite *Trichuris muris*—a relevant biological model for the closely related human parasite *Trichuris trichiura*—has been extensively investigated[3]. *T. muris* is an especially attractive model as either a susceptible (chronic, Th1 type) or resistant (acute, Th2 type) immune response is triggered, depending on the infectious dose[3,4]. Low-dose infections in mice, which are more reflective of the naturally-occurring chronic infections[5], are generally characterized by a Th1 response resulting in long-term worm infections and chronic colitis. On the other hand, high-dose infections, which are employed as a laboratory model, are generally characterized by an acute Th2 response leading to worm clearance and tissue repair[3].

Since they occupy the same host environment, it is no surprise that enteric parasites such as helminths strongly interact with the gut microbiome[6,7]. Although these interactions may lead to the suppression of either the gut microbiome or the helminth[6–8], in case of *T. muris*, bacterial–helminth crosstalk is essential for worm hatching, as the parasite eggs fail to hatch and establish in germ-free environments[9,10]. Once the worm has settled in the intestinal epithelium, the bacterial–helminth dynamics appear mainly unidirectional, with helminths altering the microbiome composition through various mechanisms, including through helminth excretory-secretory products or host anti-microbial peptides, released in response to the parasite[11–15]. Furthermore, the helminths alter the nutrients available to the microbiome, indirectly influencing which bacteria proliferate[16]. The effect of the infection on host immunology has an additional impact on the microbiome, as the worms or their metabolic byproducts can alter toll-like receptor (TLR) expression profiles[17,18] or responsiveness of host immune cells to TLR ligands[19] and interfere with local IgA-production[17]. While the gastrointestinal (GI) mucins are essential for worm clearance[20–22] and the impacts of the helminth infection on the microbiome during worm clearance are documented at the broader level of microbial phylogeny[23–28], questions remain regarding how the mucus–microbiome interactions affect worm infection and the underlying host immune responses.

Worm expulsion during an acute response is largely driven by goblet-cell secreted gastrointestinal mucin that is tightly linked to the Th2-type immune response[22]. Along these lines, mice lacking the *Muc2* gene, which encodes the major glycoprotein of the GI mucus,

show a delayed clearance of *T. muris*[29] and *Muc5ac* deficient mice completely fail to clear the helminth[22]. In germ-free mice, the mucus layer expands upon exposure to gut bacteria, and the colonic mucin secretion by goblet cells is regulated by the gut microbial activity[30,31]. The balance between mucin secretion and its consumption by the gut microbes is critical for intestinal homeostasis[32,33]. We have previously shown that a disrupted balance, for example, excessive mucin foraging by a fiber-deprived microbiota leads to an increase in the gut microbial mucin foraging activity[31,34].

Here, we hypothesized that excessive mucin foraging by the microbiota alters the course of the parasite infection by modulating the immune response. To test this hypothesis, we employed a tractable 14-member synthetic human microbiota (14SM) characterized for the capability of individual members to degrade various glycans including mucin oligosaccharides[31,35]. In a longitudinal experimental setup, using C57BL/6 ex-germ-free mice with a homeostatic mucin-foraging 14SM, we induced a chronic *T. muris* infection. Simultaneously, using fiber-deprived diet as a precursor, we skewed 14SM toward excessive mucin foraging. We assessed the worm burden and immune outcome of infection. Moreover, our 14SM model combined with a longitudinal infection setup enabled us to understand specific microbial functional changes along the course of the infection in both homeostatic 14SM and 14SM skewed toward mucin foraging. Our findings suggest a mechanism through which the increased gut microbial mucin foraging promotes worm clearance by enhancing a Th2 immune response, which sheds a new light on the microbiome–parasite–host immune interactions.

Methods

Ethical statement

All animal experiments were performed according to the "Règlement Grand-Ducal du 11 janvier 2013 relatif à la protection des animaux utilisés à des fins scientifiques" based on Directive 2010/63/EU on the protection of animals used for scientific purposes, and approved by the Animal Experimentation Ethics Committee of the University of Luxembourg and by the Luxembourgish Ministry of Agriculture, Viticulture, and Rural Development (national authorization no. LUPA2020/02). The mice were housed in accordance with the recommendations stated by the Federation of European Laboratory Animal Science Associations (FELASA).

Experimental design and dietary treatment

18–23 weeks old C57BL/6 male mice (n=4–5 per group) were housed in ISOcages with up to five animals per cage. Sterile food and water were provided *ad libitum* and light cycles consisted of 12 hours. Before the administration of 14SM, the germ-free status of the mice was confirmed using aerobic and anaerobic culturing of stools samples. Mice were intragastrically gavaged with 0.2 ml of the 14SM gavage mix as described previously[35]. Before and for 6 days following the gavage, mice were maintained on a standard mouse chow, which we refer to as Fiber-rich (FR) diet. Afterwards, half of the mice (n=24) were assigned to a Fiber-free (FF) diet and the rest remained on the FR diet (n=23). Twenty days after the diet switch, the mice were infected by oral gavage with a high dose of approximately 450 eggs of *T. muris* strain E. Mice were observed for up to 30 days post-infection (DPI). On 13, 15, 20, 25 and 30 DPI, four to five mice per group were euthanized by cervical dislocation to determine worm counts and other final readouts. A small piece (~0.5 cm) of the cecum was fixed in methacarn fixative in order to determine goblet cell numbers. The remaining part of the cecum and 2 cm of the attached colon were frozen at –80 °C to determine *T. muris* worm burden. The remaining colonic tissue and mesenteric lymph nodes were stored in RNAprotect Tissue Reagent (Qiagen, Hilden, Germany; catalog no. 76106, according to the manufacturer's protocol). Serum of the euthanized mice was collected and stored at –80 °C.

Animal diets

The Fiber-rich diet was a standard autoclaved rodent chow (LabDiet, St. Louis, MO, USA; catalog no. 5013), while the Fiber-free diet was a custom diet manufactured and irradiated by SAFE Diets (Augy, France). The FF diet was manufactured as the previously described TD.140343 diet[31], which is a modified version of the Harlan.TD08810 diet from Envigo (Indianapolis, IN, USA).

14SM cultivation and quantification

All bacterial strains of the 14SM were cultured as previously described[35]. The colonization of the 14SM was confirmed using strain-specific qPCR primers and relative abundances of the individual bacteria were determined using the same qPCR protocol as described previously[35]. Samples from different dates were run on the same plates in order to avoid plate-specific confounders.

Parasitological techniques

T. muris maintenance and infection was performed as previously described[36]. Mice were orally infected with ~450 eggs and worm burdens were assessed by counting the number of worms present in the cecum and 2 cm of the attached colon as described previously[36]. Worm burdens on 13 and 15 DPI were excluded from the analysis as determining the burden during the early larval stages, where low worm numbers establish, is technically challenging and is unreliable. The researcher, S.T., who counted the worms, was blinded for both the individual time points and dietary groups.

Goblet cell counting

Goblet cell counting was performed on a small piece (~0.5 cm) of methacarn-fixed and Alcian blue-stained cecal tissue. To preserve the mucus within the intestinal samples, a modified direct pretreatment in 99% ethanol and toluene was performed, omitting the usual previous ascending ethanol steps before embedding the samples in paraffin. All samples were cut using a microtome at 3 µm thickness before performing automated HE (Tissue-Tek Prisma Plus and Film, Sakura, Alphen aan den Rijn, Netherlands) and Alcian blue (Artisan Link Pro Special Staining System, Dako, Glostrup, Denmark) staining according to the manufacturers' instructions. The numbers of goblet cells per crypt were counted and averaged for each individual mouse before the mean per experimental group was determined. The researcher, S.T., who counted the goblet cells, was blinded for both the individual time points and dietary groups.

ELISA

Lipocalin-2 ELISA was performed on stool samples using the lipocalin-2/NGAL DuoSet ELISA R&D system (Bio-Techne, Minneapolis, MN, USA; catalog no. DY1857) according to the manufacturer's instructions and samples were prepared as previously described[31]. MCPT1 concentration of serum samples was determined using the MCPT-1 (mMCP-1) Mouse Uncoated ELISA Kit from Invitrogen (Waltham, MA, United States, catalog. no. 88-7503-88) according to manufacturer's instructions. Serum ELISA for total IgG1 and IgE were performed by coating plates using 0.5 µg/µl rat α mouse IgE purified UNLB (Imtec Diagnostics, 1130-01) or rat α-mouse IgG1 purified UNLB (Imtec Diagnostics, Ardmore, OK, United States; catalog no. 1144-01) capture antibody diluted in 0.05 M carbonate/bicarbonate buffer (pH 9.6). Washing steps were performed using 1% Tween, 154 mM NaCl, 10 mM Trizma Base. Blocking of the plates was performed using 1% w/v of BSA in a TBS buffer (15 mM Trizma-

acetate, 136 mM NaCl & 2 mM KCl). Mouse IgG1 Isotype Control UNLB (Imtec Diagnostics, Ardmore, OK, United States; catalog no 0102-01) or Mouse IgE Isotype Control (UNLB), Southern Biotech (Imtec Diagnostics, Ardmore, OK, United States; catalog no 0114-01) served as controls. Serum samples were two-fold diluted using the aforementioned TBS buffer with 0.1% w/v Tween-20 and 1% BSA. The secondary antibody was Goat anti-mouse IgG1-AP, Southern Biotech (Imtec diagnostics, Ardmore, OK, United States; catalog no 1071-04) or Goat anti-mouse IgE-AP, Southern Biotech (Imtec diagnostics, Ardmore, OK, United States; catalog no 1110-04), respectively. The substrate solution consisting of 0.5 mg/ml phosphate substrate (Sigma-Aldrich, St. Louis, MO, United States; catalog no. S0642-200 TAB) in 1 mM AMP and 0.1 mM $MgCl_2 \bullet 6H_2O$ and plates were read at 405 nm using a SpectraMax ABS PLUS spectrophotometer (Molecular Devices, San Jose, CA, United States). A detailed protocol can be found in the supplementary methods section. Parasite specific IgG1 and IgG2c ELISA was performed as previously described[37].

LEGENDplex bead-based immunoassay

The LEGENDplex assay (BioLegend, San Diego, CA, USA) was performed on serum samples according to manufacturers' instruction.

Detection of bacterial glycan-degrading enzyme activities

The enzymatic activities of α-fucosidase, β-*N*-acetyl-glucosaminidase, and β-glucosidase in fecal samples were determined using *p*-nitrophenyl glycoside-based enzyme assays as described previously[38].

RNA extraction from mesenteric lymph nodes and colonic tissue and RT-qPCR

A detailed protocol can be found in the supplemental methods section.

RNA-Seq

RNA extracted from samples at 30 DPI were utilized for performing RNA-Seq. Illumina Stranded Total RNA Prep with Ribo-Zero Plus was used to prepare the RNA sequencing library according to the reference guide's instructions. Sequencing was performed using NovaSeq 6000 SP Reagent Kit v1.5 (Illumina, San Diego, CA, USA) on an Illumina NovaSeq 6000 system.

RNA-Seq analysis

Following adapter removal with Cutadapt[39], reads were mapped and gene counts were generated with STAR 2.7.9a[40]. Transcripts not appearing at least once on average across all samples were removed from subsequent analysis. Samples were normalized using the median of ratios method[41] supported by DESeq2[42] and one outlier was removed based on PC score using the prcomp function of the base R stats 4.0.2 package. Differential expression analysis was performed using DESeq2 1.30.1 with default parameters and *p*-value adjustment using the Benjamini-Hochberg method. Significant genes were identified based on adjusted *p*-value < 0.05. The expressed log-ratios for significant genes were imported into Ingenuity Pathway Analysis (Qiagen, Hilden, Germany) and analyzed considering all available reference datasets for mice. Pathway analysis was also performed using the enrichGO function of clusterProfiler 3.18.1[43] in R to identify upregulated pathways using Gene Ontology (GO) terms for biological processes. REVIGO[44] was employed to reduce redundancy in GO terms before visualisation.

Statistical analyses

Statistical analysis was performed using Prism 9.2.0. (GraphPad Software, Inc., San Diego, CA, USA), Statistical significances are represented by asterisks as follows: *, $p < 0.05$; **, $p < 0.01$; ***, $p < 0.001$; and ****, $p < 0.0001$. Unless otherwise specified in the figure legend, for normally distributed values, unpaired two-tailed t tests were used, while for non-normally distributed values, a Mann–Whitney test was used. For multiple comparisons, a two-way analysis of variance (ANOVA) with a Šidák post hoc test was performed in Prism. The specific test used for each experiment is detailed in the figure legends.

Results

Increased mucin-degrading bacteria coincides with altered worm infection dynamics

We colonized germ-free, C57BL/6 mice with a 14-member synthetic human microbiota (14SM). Successful colonization of each bacterial strain was checked by qPCR primers specific to each of the 14 bacterial strains as described previously[35]. Mice were maintained for six days on the Fiber-rich (FR) diet, which is a standard mouse chow, before half of the mice (n=24) were switched to a Fiber-free (FF) diet **(Fig. 1A)**. Twenty days after the diet switch, mice in both dietary groups were gavaged with a high dose of *T. muris* consisting of approximately 450 eggs from the same egg suspension **(Fig. 1A)**. Mice were monitored for up to 30 days post-infection (DPI) and, on 13, 15, 20, 25 and 30 DPI, 4–5 mice per group were sacrificed and cecum, colon and mesenteric lymph nodes (MLNs) were frozen in order to collect various experimental readouts **(Fig. 1A)**. In line with our published work[31,45], the FF diet allowed for proliferation of two dominant mucin-degrading bacteria *Akkermansia muciniphila* and *Bacteroides caccae* and reduction of two prominent fiber-degrading bacteria *Eubacterium rectale* and *Bacteroides ovatus* **(Fig. 1B)**. Throughout the experiment, none of the mice exhibited any obvious physiological abnormalities. While FF-fed mice were overall heavier compared to the FR-fed mice, the weights of both groups remained largely stable over time **(Fig. 1C)**.

Frozen cecal tissues, including the ascending colon containing their luminal contents, were defrosted and the worms were counted in a blinded fashion. Following the establishment of low level infections, during the early larval stages, the *T. muris* larvae are too small to allow reliable enumeration which is why the worm burdens were only assessed starting day 20 post infection. Infection of *T. muris* with a high egg number (~450) in conventional or specific-pathogen-free (SPF) mice, results in an acute infection, and only lower number of eggs (<40) result in a chronic infection[3]. In our synthetic human gut microbiota under standard dietary conditions (that is fed the FR diet), infection with a high number of eggs caused a low level infection resulting in a chronic infection. The reasons for this could be rooted in an initially skewed immune response in our gnotobiotic model or in the fact that our study uses a synthetic human gut microbiota, as opposed to the complete, native murine microbiota that may be more suitable for egg hatching of the naturally occurring murine whipworm or improving the ability of the larvae to establish in the gut. Considering that this a new model, it is particularly an important point because previous studies have shown that the gut bacteria are essential for effective egg hatching, as the eggs do not hatch in the absence of gut bacteria *in vitro* or in

germ-free mice[9,10]. Our results showed that, although the worm burdens were statistically insignificant between FR and FF groups on 20 and 25 DPI, subsequent infection dynamics statistically differed between both groups, with FF-fed mice clearing the pathogen by 30 DPI and FR-fed mice remaining chronically infected **(Fig. 1D)**.

In order to investigate whether the two distinct diets and/or the skewed gut microbiome composition toward mucin polymer degradation caused an altered baseline inflammation prior to infection with *T. muris*, we determined fecal lipocalin-2 (LCN-2) levels, which serves as a marker for low-grade inflammation[46]. There were no significant differences between FR and FF groups at day 0 **(Fig. 1E)**, which is in line with our previous results in C57BL/6 mice[45]. However, after the infection, the levels of LCN-2 were significantly higher in the FR group **(Fig. 1E)**. Since chronic *T. muris* infections are characterized by a Th1 response leading to colitis, the elevated LCN-2 in the FR group compared to the FF group is indicative of an early induction of a Th1 response in the FR group, because LCN-2 has been shown to be induced by the Th1 cytokines IFNγ and TNF-α[47]. Altogether, these results are supportive of the notion that the worm retention in FR-fed 14SM group is driven by a Th1 immune response and similarly the worm clearance in FF-fed 14SM group might be driven by a Th2 response.

Global transcriptomic analyses support chronic and acute outcomes of worm infection

In order to better understand the change in host immunological responses that drive differential *T. muris* infection dynamics, we analyzed the host colonic gene expression at 30 DPI **(Fig. 2, Fig. S1 and Table S1)**. We found numerous significant differences in the host transcriptome of FR- and FF-fed mice, as evident in the volcano plot showing the differentially expressed genes, with 147 and 184 genes upregulated in the FR- and FF-fed groups, respectively **(Fig 2A)**. Ingenuity Pathway Analysis (IPA) revealed that both the interferon signaling and Th1 pathways were upregulated in the FR-fed mice that had a homeostatic 14SM before infection **(Fig. 2B)**. These two pathways are characteristic of chronic *T. muris* infections[3], which was consistent with the failure to successfully clear the parasite among FR-fed mice **(Fig. 2B)**. In accordance with upregulation of the interferon signaling and Th1 pathways, related disease pathways—that is, diseases often associated with an increased Th1 response such as osteoarthritis, systemic lupus erythematosus and even neuroinflammation—were also upregulated as their gene expression profiles overlap with those of a Th1 response **(Fig. 2B)**.

A closer look at the Ingenuity-generated summary of the transcriptomic data using IPA, showed that indeed most of the genes upregulated under FR conditions during the chronic *T.*

muris infection are strongly linked to interferon signaling, which results in a Th1 response **(Fig. 2C)**. This Th1 response is potentially linked to the observed increase in antimicrobial responses that results in the activation of cytotoxic T cells, lymphopoiesis, increased apoptosis of macrophages and a reduced replication of viruses **(Fig. 2C)**. In contrast to this, the host transcriptomic response on the FF diet was not clearly characterized by an increased Th2-type response typical for an acute *T. muris* infection **(Fig. 2B)**. However, the moderate type 2 response might be a result of the chosen sample time point as the infection is mostly cleared by 30 DPI **(Fig. 1D)**. In line with this, the increased MSP-RON signaling in macrophage pathway hints at an increased Th2 response under FF conditions **(Fig. 2B),** as an activation of the MSP-RON pathway causes M2 macrophage polarization[48], which is associated with a Th2-type immune response against *T. muris*[49,50]. Furthermore, the upregulation of the white adipose tissue browning pathway is also in line with this observation, as M2 macrophage differentiation has been linked to adaptive thermogenesis[51]. The observed results are consistent with a major shift toward the Th1 pathway and a chronic infection in the FR-fed group, whereas the acute response observed in the FF-fed group seems most likely to be based on the Th2 immunity or a failure to generate the Th1 immunity.

Maintenance or moderate increase of Th2 immunity permits worm expulsion

In order to further support conclusions from our RNA-Seq data **(Fig. 2)**, we used RT-qPCR to investigate transcription of cytokines IFNγ, IL-13 and IL-4 in RNA extracted from MLNs and colon at different time points **(Fig. 3A)**. These three cytokines are indicative of whether *T. muris* infection leads to a Th1- (IFNγ) or a Th2-type response (IL-4 and IL-13)[50,52]. In accordance with the global transcriptome analysis **(Fig. 2)**, chronic infection in the FR-fed group was dominated by a Th1-type response, as exhibited by over 6-fold upregulation of IFNγ in the colon by 30 DPI **(Fig. 3A)**. Cytokine expression in the MLNs was even more pronounced, with IFNγ having an over 30-fold increase in the FR group at day 20 and dropping to a 6-fold increase at 30 DPI. IL-13 was only significantly upregulated in the MLNs of FF-fed mice at 20 DPI and IL-4 showed a significant increase in the MLNs of the FR group at D15 before being upregulated under FF conditions for the subsequent days **(Fig. 3A)**. We performed similar analysis of the cytokine transcripts of TNF-α, IL-5, IL-22 and IL-17a at 13 and 30 DPI, but only TNF-α showed significant changes, with upregulation in the colon of the FR group both at 13 and 30 DPI **(Fig. S2A**). No diet-independent shifts in cytokine production were found by analyzing the absolute cytokine data **(Fig. S3)**.

To lend support to our transcript data, we used the LEGENDplex bead-based immunoassay to determine the cytokine protein concentration in the serum samples of mice at 30 DPI. Only one of the detected Th1 cytokines, TNF-α, was significantly upregulated under FR conditions **(Fig. 3B)** and another Th1 cytokine, IFNγ, showed an upward trend with p=0.0587. Some of the detected cytokines showed a trend toward increased production under the FR conditions, hinting at a generally more active immune system during the chronic infection **(Fig. 3B and Fig. S2B)**. The expression of transcription factors GATA3 and Tbet **(Fig. S2C)** further supports these trends by showing significantly increased levels of Tbet expression in the colon of the FR group at 30 DPI and a significant increase in GATA3 in the MLN of the FF group at 20 DPI **(Fig. S2C)**.

Assessment of serum concentrations of total IgE and IgG1, both of which are reflective of the protective responses against helminths, such as *T. muris*, resulted in no significant changes, albeit a slightly increased trend was observed for both antibodies at 30 DPI but not at 25 DPI **(Fig. 3C)**. We then assessed parasite specific IgG1and IgG2, characteristic of Th2 and Th1 responses, respectively[53]. Chronic *T. muris* infections are usually characterized by significantly elevated serum levels of parasite-specific IgG2a/c and a low increase in parasite specific IgG1[53]. In contrast, protection against *T. muris* is characterized by high parasite specific IgG1 levels, but a lack of IgG2a/c[53]. Importantly, although there was no significant increase in total IgG1, *T. muris*-specific IgG1 and IgG2a/c showed clear significant differences at 30 DPI, but not at 25 DPI **(Fig. 3D)**. In accordance with the observed worm burdens **(Fig. 1D)**, we saw an increase in specific IgG1 in mice fed the FF diet, while we see an increase in specific IgG2a/c in mice fed the FR diet **(Fig. 3D)**. Despite a similar upward trend for both parasite-specific antibodies at 25 DPI in the two respective dietary groups, the differences were not significant **(Fig. 3D)**. Furthermore, we quantified MCPT1—a proxy for mast cell degranulation[54]—in sera at all time points (13, 15, 20, 25 and 30 DPI) and observed significantly increased MCPT1 concentration at 30 DPI in the FF-fed group that cleared the parasite **(Fig. 3E)**. These data are in line with an increased tendency of total IgE in the FF-fed group at 30 DPI. Moreover, these data support the known association of mucosal mast cells and protection against helminths[55,56] supporting the elevation of the type 2 immunity.

Overall, our transcript **(Fig. 2 and Fig. 3A)** and protein expression data **(Fig. 3B)** support that, mostly during the later stages of infection, the worm infection in mice containing a homeostatic 14SM induce a Th1-type immune response that is driven by an overall increase in IFNγ. On the other hand, absence of a similar increase in IFNγ, after the worm infection, in

mice with increased microbial mucin foraging, induces a Th2-type immune response, resulting in the successful clearance of *T. muris*. This heightened Th2 response seems to peak earlier compared to the Th1 response of the FR group and likely levels off by 30 DPI; thus, the 30 DPI transcriptomics data **(Fig. 2)** might not have fully captured the Th2 response. Since the gut microbiome is intimately connected to changes in the diet and the host immune responses, and since specific changes in the microbial taxa could contribute to the observed immune responses, we ventured to determine which bacteria change in their abundance during the course of the worm infection.

Mucin generalists increase during worm clearance, but not during worm retention

Although previous studies have reported noticeable changes in the gut microbial taxa in mice with conventional gut microbiota after worm infection, these changes are described at broader level of microbial taxonomy[23–28]. It also remains to be studied which precise microbial species respond most to worm infection particularly during a longitudinal course of the worm infection both during chronic and acute phases of infection. Better understanding such changes would aid in further exploration of the microbiota–worm–host immune system interactions. In this regard, our tractable, fully-characterized 14SM model[31] is well-suited to support functional interpretations of how the underlying microbial metabolism changes as the worms start to moult and are either expelled (acute infection) or remain persistent (chronic infection). Thus, we next investigated the fecal gut microbial compositions using specific qPCR primers for all five time points post infection (13, 15, 20, 25 and 30 DPI) in both dietary groups **(Fig. 4).** To facilitate comparison, we combined these data with the microbial compositions prior to worm infection in Fig. 1B (shown in Fig. 4 as day 0).

Throughout the experiment, the gut microbiome composition in the mice that had been FR-fed for 20 days prior to infection remained distinct from the composition of the FF-fed mice as seen in the principal coordinates analysis (PCoA) plots **(Fig. 4A)**. While the 14SM composition has been shown to be stable over time[31], here we show that infection with *T. muris* led to substantial changes in the gut microbiome composition within each dietary group **(Fig. 4A)**. These changes seemed to be more dynamic under FF conditions than under FR conditions, which is likely explained by the nature of the chronic infection under FR conditions and an acute infection in the FF conditions, but might also be reflective of the worm burden of individual mice **(Fig. 4A)**. Looking at the microbiome composition over the course of the infection, while diet impacts the initial colonization of the gut microbiome, the infection with

T. muris led to the bloom of some bacterial species and a decline of others **(Fig. 4B)**. Interestingly, some of these changes seem to revert to initial levels upon clearance of *T. muris* in the mice fed the FF diet **(Fig. 4A and 4B)**.

Most of the individual bacteria changed in relative abundance either in response to the early larval stages (L2 (~day 8/9)–L3 (~day 17)) of *T. muris* or in response to the later larval stages (L3–L4 (~day 23)) **(Fig. 4C)**. These infection-induced abundance changes seem to be reversible for most bacteria **(Fig. 4C)**. *Marvinbryantia formatexigens* appears to be an exception as it does not significantly change in relative abundance due to either diet or infection **(Fig. 4C)**. Considering that we observed that nearly all bacteria change in abundance during the early larval stages of *T. muris*, it is likely that the growing worms competitively take over certain nutrients. While the overall bacterial abundances are modulated by the diet composition, some bacteria such as *Collinsella aerofaciens* or *Escherichia coli* seemed unaffected by diet. It has been reported that tissue damage induced by *T. muris* might induce the hypoxia response gene HIF-1α[57]. The resulting increased oxygen availability might explain the diet-independent bloom of the facultative anaerobic *E. coli*, just after the infection **(Fig. 4C)**. Furthermore, other highly oxygen sensitive bacteria such as *Roseburia intestinalis* and *Faecalibacterium prausnitzii* dropped in abundance around the same time, while the more oxygen-resistant *Bacteroides* spp. remained largely unaffected **(Fig. 4C)**[58].

Among the bacteria with mucin-degrading capacities, we observed that the abundance of *B. caccae* and *Bacteroides thetaiotaomicron* increased in the FF-fed group during the course of the infection, but not in the FR-fed group **(Fig. 4C)**. The normalized average fold-change of the abundance of these two mucin-generalist bacteria (*B. caccae* and *B. thetaiotaomicron*)[31] significantly increased by 15 DPI and kept increasing until doubling their abundance at 20 DPI in the FF-fed group but not in the FR fed group **(Fig 4D)**. In contrast, the abundance of mucin specialist, *A. muciniphila* slightly decreased in the FF-fed group **(Fig 4C)**. Since being a mucin-generalist and being capable of removing sulfate linkages on mucins[59] as well as secreting M-60 like proteases that degrade the mucin protein backbone[31,32], *B. caccae* and *B. thetaiotaomicron* are more aggressive mucin foragers than *A. muciniphila*, especially in the absence of dietary fibers. These data suggest an overall increased mucin-foraging activity in the FF-fed group as the worms start to grow and moult. This is further supported by the halted expansion of the mucin-specialist *Barnesiella intestinihominis* at 15 DPI in the FF group **(Fig 4C)**. A sharp significant increase in the abundance of a sulfate-reducing bacterium *Desulfovibrio piger* on 20 DPI in the FF-fed group, but not in the FR-fed group, further supports

the increase in mucin-foraging, as this bacterium increasingly utilizes the released sulfate from microbial mucin foraging as an electron acceptor[60].

Intriguingly, even in the absence of fiber, a classical fiber-degrader *E. rectale* bloomed in the FF-fed group around 25 DPI, after being almost non-existent before this and finally became almost non-existent again on 30 DPI **(Fig. 4C)**. This coincides with the bloom of the mucin generalists **(Fig. 4C)**. A similar trend was observed for *E. rectale* in the FR-fed group **(Fig. 4C)**, with the abundance of *E. rectale* doubling in the FR-fed group as compared to its abundance at 0 DPI. We have previously shown that *E. rectale* is adept at growing on two mucosal monosaccharides, galactose and *N*-acetylglucosamine, but it fails to grow on mucin oligosaccharides[31]. A potential explanation for the dramatic increase in *E. rectale* is that, despite an absence of dietary fibers in the FF-fed group, simple mucin sugars that can be readily metabolized, such as galactose and *N*-acetylglucosamine, become readily available through the elevated mucin degradation in the FF-fed group at around 20 DPI by the two mucin generalists *B. caccae* and *B. thetaiotaomicron*. Considering that the expansion of *E. rectale* occurs under both diets, another supportive explanation is that the *T. muris*-secreted serine proteases, which can depolymerize mucin[21], may make these structurally complex glycoproteins accessible to bacteria that are otherwise unable to utilize them, such as *E. rectale*. The loss of exclusivity of this niche offers a potential explanation for the halted expansion of the mucin specialists, *A. muciniphila* and *B. intestinihominis* **(Fig. 4D)**. Collectively, these results strongly connect increased mucin-degrading bacterial activity to worm clearance in the FF-fed group. As mucin plays a key role in the clearance of *T. muris* infection, we next rationalized that enhanced mucolytic activity during infection leads to increased mucus turnover, meaning an increased cycle of mucin degradation and secretion, which could facilitate clearance of *T. muris* in the FF-fed mice.

Enhanced mucin–microbiome interactions promote worm clearance

Since we found that the worm clearance is strongly correlated to increased abundance of mucin-degrading generalist bacteria, we next set out to study how this altered microbial composition has a functional impact on the mucin-degrading activity. To assess this, we measured the enzyme activity of the key mucin-degrading bacterial enzymes β-*N*-acetylglucosaminidase (NAG) and α-fucosidase (FUC) before and at days 20 and 25 post-infection **(Fig. 5A)**. As a contrast to these key mucin-degrading enzymes, we similarly determined the activity of β-glucosidase (GLU), a microbial enzyme specific for plant

polysaccharides **(Fig. 5A)**. At day 0, NAG activity was higher under FF conditions; however, after the infection, the activity of this enzyme significantly rose by 25 DPI in mice resistant to persistent worm infection, but not in the mice where worm infection became chronic. A similar pattern was observed for FUC activity. In contrast, GLUC activity showed a significant increase in the resistant mice only at 20 DPI **(Fig. 5A)**. Comparing NAG and FUC activity **(Fig. 5A)** to the abundance of mucin-degrading bacteria **(Fig. 4C and D)**, we observed a delay between the increased abundance of mucin-generalist bacteria under FF conditions at 20 DPI and the increased activity of mucin-degrading enzymes at 25 DPI, possibly due to a slight delay in extracellular secretion of the enzymes into the feces. A potential explanation is the tight regulation of mucin-degrading enzymes, as observed for *B. thetaiotaomicron*[61]. The depolymerized mucin released by the serine proteases of *T. muris* might initially suppress the expression of the NAG and FUC until fiber-degrading bacteria such as *E. rectale* expand sufficiently to fully scavenge those glycans[61]. Looking at the strong increase in the relative abundance of some fiber-degrading bacteria, such as *E. rectale*, around 20 DPI, it is also possible that the absolute abundance of the mucin-degrading bacteria under FF conditions keeps increasing past 20 DPI, but that this continuous expansion is not observable in the relative abundance due to an even stronger expansion of other bacteria (**Fig 4C and D)**. In this case, the NAG and FUC enzyme activity might be reflective of the absolute, but not relative abundance of the mucin-degrading bacteria.

Since we found increased abundance of mucin-generalist bacteria and subsequently increased mucin-degrading enzyme activity during the course of worm clearance, but not during the course of worm retention, we questioned whether this is a result of underlying qualitative changes in mucin production in goblet cells or whether a compensatory response to increased mucin-foraging leads to qualitative changes in mucin secretion. To better understand the changes in mucin secretion, we performed blinded counting of goblet cells in small (~0.5 cm) pieces of cecal tissue that were preserved in methacarn fixative. The goblet cell counts revealed no significant changes in numbers throughout the experiment **(Fig. 5B)**. Furthermore, the expression of neither the gene *Muc2* nor the gene *Muc5ac*, which play an important role in worm clearance[62], were upregulated **(Tables S1–S3)**. However, since these transcripts do not necessarily reflect protein production, involvement of these mucins and/or other mechanisms (such as epithelial cell turnover), that contribute to host protection, cannot be ruled out.

Among the genes involved in the five most upregulated pathways in resistant mice, we identified several genes involved in glycoprotein synthesis and glycosylation **(Fig. 5C)**. This

is especially interesting as many of the upregulated genes are involved in the glycosylation of the colonic mucins[32,63,64]. For example, the expression of the glycosyltransferases *Fut2*, *St3gal6*, *C1galt1*, *Galnt3* and *Galnt4* or the sulfotransferase *Gal3st2* were upregulated in the resistant mice[32,63,64] **(Fig. 5C)**. Altered mucin glycosylation, in particular sulfation, has been linked to modified *T. muris* susceptibility[64]. Thus, altered glycosylation might be responsible for the improved clearance of *T. muris* in resistant mice. This is particularly intriguing considering that the microbiome has a major influence on the glycosylation of the Muc2 glycoprotein, the major constituent of the colonic mucus layer[63]. Furthermore, enhanced microbial mucin foraging could potentially increase interaction of the gut microbiome with the host mast cells, which could explain the observed increase in MCPT1 **(Fig. 3E)**. Altogether, our results suggest that the increased mucolytic activity of the gut microbiome under fiber deprivation (**Fig. 5A)** without the compensatory mucin production **(Fig. 5B)**, but with possible changes in mucin glycosylation **(Fig. 5C)**, aids in clearance of *T. muris*.

Discussion

Helminth infection models have been profoundly utilized to elucidate the underlying host responses for the past several decades, yet open questions remain about the mechanisms of how the intricate interactions between the gut microbiome and GI mucus affect worm infection dynamics including the host immune responses. Here, we shed insight into the role of bacterial mucin foraging in altering the host immune responses during the infection with *T. muris*. Using a diet reduced in fiber to increase bacterial mucin foraging in a gnotobiotic mouse model containing a 14-member synthetic human gut microbiota, our study supports a model in which the increased microbial mucolytic activity promotes Th2-driven worm clearance **(Fig. 6)**. Our results document an intricate link in the gut microbiome–parasite axis, suggesting a potential mechanism through which increased microbial mucin foraging could alter the host immune response to the worm.

Our study demonstrates that an IFNγ-dominated Th1 response, which has been shown to drive chronic *T. muris* infections, is characterized by a balanced fiber vs. mucin degradation, while successful clearance of the worm characterized by a type 2 response is potentially the result of increased microbial mucin foraging during worm infection **(Figs. 2, 3 and 6)**. A recent study by Myhill et al.[27] observed a similar IFNγ-driven shift from a Th2 toward a Th1 response when feeding SPF mice a high-fiber diet containing 10% inulin, however, this study did not provide an explanation for the underlying mechanisms. Using our 14SM model, a standard

mouse chow containing 3.8% dietary fiber and a diet deprived of fiber, we offer an explanation that the mucin–microbiome interactions driven by dietary changes alter the host immune responses and the worm infection dynamics **(Fig. 6)**. Despite the well-known specificity of parasites for their hosts, it is clear that *T. muris* is able to establish and develop in the intestine colonized by the synthetic, human 14SM for at least 30 days. It is well known that bacteria are important for *T. muris* worm hatching[9,10], although the specific bacterial members involved are not well known and it is possible that the selected bacteria in our synthetic human microbiota might not be ideal for inducing egg hatching, resulting in a lower level of infection than would normally be seen in SPF mice with a natural microflora. The system used here, however, does provide a chronic low-level infection characteristic of infections under natural conditions.

T. muris has been shown to broadly alter the host's gut microbiome composition[23–28], but our longitudinal characterization of the gut microbiome provides explicit details about how the microbial shifts are characterized by distinct phases and specific microbial species based on their functional roles **(Fig. 6)**. In resistant mice, the microbial functional changes during the worm infection and clearance are largely centered around microbial mucin foraging. During the early larval stages (L2–L3) around 13 to 15 DPI, we observed a major disruption of the gut microbiome composition, especially in the FF-fed group **(Fig. 4)**, which was characterized by a drastic expansion of *E. coli* on both diets as well as a decline of *A. muciniphila* in resistant mice. A similar expansion of *Enterobacteriaceae* (*E. coli*) and decline of *Akkermansia* (*A. muciniphila*) was observed following a high-dose infection of SPF mice fed an inulin-supplemented diet[27]. The second major shift in microbial abundances occurs around 20 to 25 DPI which coincides with the moulting of the worm from the L3 to the L4 larval stage **(Fig. 4)**. During this transition, the worm moves to occupy cells nearer to the top of the crypt, protruding into the lumen, thus most likely increasing its interaction with the gut microbiome[3]. In resistant mice, this shift is characterized by an increased abundance of the mucin generalists *B. caccae* and *B. thetaiotaomicron*, resulting in an overall increased mucolytic activity of the gut microbiome **(Figs. 4, 5A and 6)**. It is likely that the resulting secretion of M60-like proteases by mucin generalists and the *T. muris*-secreted serine proteases depolymerize the mucin backbone[21,31,32] generating new niches for other bacteria. This is reflected by the increased abundance of *D. piger*, which forages the released sulfate and the increased abundance of a strict fiber-degrader *E. rectale*, which can degrade the released mucin monosaccharides.

In contrast to the observations in *Muc2*$^{-/-}$ mice[29], in our model, increased microbial mucin foraging under fiber-deprived conditions did not delay the parasite clearance, but instead promoted the clearance. These results are not unexpected as genetic ablation of Muc2 largely destabilizes the mucus structure, whereas the increased microbial mucin foraging seems to either resist transition to a Th1 response and/or aids in a Th2 response. We could not detect an increase in goblet cell numbers/mucin production associated with this **(Fig. 5**B**)**. Nevertheless, we observed increased transcription of genes involved in mucin glycosylation **(Fig. 5C)**, which has been shown previously to alter susceptibility to *T. muris*[64]. Considering that the microbiome can directly influence mucin glycosylation[63], our results suggest that the fiber-deprived diet-induced changes in the microbiome might lead to an alteration in the glycosylation of the GI mucins, which aids in clearance of *T. muris*. One caveat being that the gene transcription was not assessed longitudinally, thus limiting interpretations considering the infection dynamics. However, even if indirectly assessed, these data support the hypothesis that excessive mucin degradation leads to closer interaction of the gut microbiome and the host mast cells, leading to their activation or accumulation, as evidenced by an increase in MCPT1 concomitant with worm clearance **(Figs. 3E and 6)**. Mast cells have been linked to *T. muris* clearance[56] and based on the work with another nematode—*Trichinella spiralis*—this might be related to a mast cell-dependent increase in epithelial permeability[65]. Therefore, an increase in MCPT1 offers an additional explanation as to why excessive mucin foraging renders mice resistant to *T. muris* infection. Finally, mast cell activation suppresses Th1 responses by decreasing IFNγ expression and increasing Th2 cytokine expression[55], which offers an additional explanation how excessive foraging of mucin could alter the host immune response. However, it is also likely that the strong IFNγ expression on the FR diet simply impairs the type 2 and later mast cell response.

Given the high morbidity associated with the parasitic infections in humans[1], our study has generated important prerequisite knowledge for clinical settings: 1) for treating parasitic infections – in the absence of co-infections, periodic fiber deprivation or fasting to boost microbial mucin foraging could be potentially employed in the clinic to manage worm infections; and 2) for harnessing the immunomodulatory properties of helminths for their potential therapeutic use in inflammatory disorders[66] or allograft rejection[67]. Further research is required about how the model proposed in our study **(Fig. 6)** could be translated into the clinic.

References

1. World Health Organization. Global Health Estimates 2020: Disease burden by Cause, Age, Sex, by Country and by Region, 2000-2019. 2020.

2. Douglas B, Oyesola O, Cooper MM, et al. Immune System Investigation Using Parasitic Helminths. Annu Rev Immunol 2021;39:639–665.

3. Klementowicz JE, Travis MA, Grencis RK. Trichuris muris: A model of gastrointestinal parasite infection. Semin Immunopathol 2012;34:815–828.

4. Yousefi Y, Haq S, Banskota S, et al. Trichuris muris model: Role in understanding intestinal immune response, inflammation and host defense. Pathogens 2021;10.

5. Colombo SAP, Grencis RK. Immunity to Soil-Transmitted Helminths: Evidence From the Field and Laboratory Models. Front Immunol 2020;11.

6. Zaiss MM, Harris NL. Interactions between the intestinal microbiome and helminth parasites. Parasite Immunol 2016;38:5–11.

7. Brosschot TP, Reynolds LA. The impact of a helminth-modified microbiome on host immunity review-article. Mucosal Immunol 2018;11:1039–1046.

8. Jaenike J, Unckless R, Cockburn SN, et al. Adaptation via symbiosis: Recent spread of a drosophila defensive symbiont. Science (80-) 2010;329:212–215.

9. Hayes KS, Bancroft AJ, Goldrick M, et al. Exploitation of the intestinal microflora by the parasitic nematode trichuris muris. Science (80-) 2010;328:1391–1394.

10. White EC, Houlden A, Bancroft AJ, et al. Manipulation of host and parasite microbiotas: Survival strategies during chronic nematode infection. Sci Adv 2018;4.

11. Hewitson JP, Harcus Y, Murray J, et al. Proteomic analysis of secretory products from the model gastrointestinal nematode Heligmosomoides polygyrus reveals dominance of Venom Allergen-Like (VAL) proteins. J Proteomics 2011;74:1573–1594.

12. Abner SR, Parthasarathy G, Hill DE, et al. Trichuris suis: Detection of antibacterial activity in excretory-secretory products from adults. Exp Parasitol 2001;99:26–36.

13. Su L, Su CW, Qi Y, et al. Coinfection with an intestinal helminth impairs host innate immunity against Salmonella enterica serovar typhimurium and exacerbates intestinal inflammation in mice. Infect Immun 2014;82:3855–3866.

14. Fricke WF, Song Y, Wang AJ, et al. Type 2 immunity-dependent reduction of segmented filamentous bacteria in mice infected with the helminthic parasite Nippostrongylus brasiliensis. Microbiome 2015;3:40.

15. Forman RA, DeSchoolmeester ML, Hurst RJM, et al. The Goblet Cell Is the Cellular Source of the Anti-Microbial Angiogenin 4 in the Large Intestine Post Trichuris muris Infection. PLoS One 2012;7.

16. Shea-Donohue T, Sullivan C, Finkelman FD, et al. The Role of IL-4 in Heligmosomoides polygyrus -Induced Alterations in Murine Intestinal Epithelial Cell Function. J Immunol 2001;167:2234–2239.

17. Harris JB, Podolsky MJ, Bhuiyan TR, et al. Immunologic responses to Vibrio cholerae in patients co-infected with intestinal parasites in Bangladesh. PLoS Negl Trop Dis 2009;3.

18. Kosik-Bogacka DI, Wojtkowiak-Giera A, Kolasa A, et al. Hymenolepis diminuta: Analysis of the expression of Toll-like receptor genes and protein (TLR3 and TLR9) in the small and large intestines of rats. Exp Parasitol 2014;145:61–67.

19. Zakeri A, Borji H, Haghparast A. Interaction Between Helminths and Toll-Like Receptors: Possibilities and Potentials for Asthma Therapy. Int Rev Immunol 2016;35:219–248.

20. Marillier RG, Michels C, Smith EM, et al. IL-4/IL-13 independent goblet cell hyperplasia in experimental helminth infections. BMC Immunol 2008;9.

21. Hasnain SZ, McGuckin MA, Grencis RK, et al. Serine Protease(s) Secreted by the Nematode Trichuris muris Degrade the Mucus Barrier. PLoS Negl Trop Dis 2012;6.

22. Hasnain SZ, Evans CM, Roy M, et al. Muc5ac: A critical component mediating the rejection of enteric nematodes. J Exp Med 2011;208:893–900.

23. Li RW, Wu S, Li W, et al. Alterations in the porcine colon microbiota induced by the gastrointestinal nematode Trichuris suis. Infect Immun 2012;80:2150–2157.

24. Broadhurst MJ, Ardeshir A, Kanwar B, et al. Therapeutic Helminth Infection of Macaques with Idiopathic Chronic Diarrhea Alters the Inflammatory Signature and Mucosal Microbiota of the Colon. PLoS Pathog 2012;8.

25. Holm JB, Sorobetea D, Kiilerich P, et al. Chronic Trichuris muris infection decreases diversity of the intestinal microbiota and concomitantly increases the abundance of lactobacilli. PLoS One 2015;10.

26. Houlden A, Hayes KS, Bancroft AJ, et al. Chronic Trichuris muris infection in C57BL/6 mice causes significant changes in host microbiota and metabolome: Effects reversed by pathogen clearance. PLoS One 2015;10.

27. Myhill LJ, Stolzenbach S, Mejer H, et al. Fermentable Dietary Fiber Promotes Helminth Infection and Exacerbates Host Inflammatory Responses. J Immunol 2020;204:3042–3055.

28. Rosa BA, Snowden C, Martin J, et al. Whipworm-Associated Intestinal Microbiome Members Consistent Across Both Human and Mouse Hosts. Front Cell Infect Microbiol 2021;11.

29. Hasnain SZ, Wang H, Ghia JE, et al. Mucin Gene Deficiency in Mice Impairs Host Resistance to an Enteric Parasitic Infection. Gastroenterology 2010;138:1763-1771.e5.

30. Johansson MEV, Jakobsson HE, Holmén-Larsson J, et al. Normalization of host intestinal mucus layers requires long-term microbial colonization. Cell Host Microbe 2015;18:582–592.

31. Desai MS, Seekatz AM, Koropatkin NM, et al. A Dietary Fiber-Deprived Gut Microbiota Degrades the Colonic Mucus Barrier and Enhances Pathogen Susceptibility. Cell 2016;167:1339-1353.e21.

32. Martens EC, Neumann M, Desai MS. Interactions of commensal and pathogenic microorganisms with the intestinal mucosal barrier. Nat Rev Microbiol 2018;16:457–470.

33. Parrish A, Boudaud M, Kuehn A, et al. Intestinal mucus barrier: a missing piece of the puzzle in food allergy. Trends Mol Med 2022;28:36–50.

34. Neumann M, Steimle A, Grant ET, et al. Deprivation of dietary fiber in specific-pathogen-free mice promotes susceptibility to the intestinal mucosal pathogen Citrobacter rodentium. Gut Microbes 2021;13.

35. Steimle A, Sciscio A De, Neumann M, et al. Constructing a gnotobiotic mouse model with a synthetic human gut microbiome to study host–microbe cross talk. STAR

Protoc 2021;2:100607.

36. Wakelin D. Acquired immunity to Trichuris muris in the albino laboratory mouse. Parasitology 1967;57:515–524.

37. Hayes KS, Cliffe LJ, Bancroft AJ, et al. Chronic Trichuris muris infection causes neoplastic change in the intestine and exacerbates tumour formation in APC min/+ mice. PLoS Negl Trop Dis 2017;11.

38. Steimle A, Grant ET, Desai MS. Quantitative assay to detect bacterial glycan-degrading enzyme activities in mouse and human fecal samples. STAR Protoc 2021;2:100326.

39. Martin M. Cutadapt removes adapter sequences from high-throughput sequencing reads. EMBnet.journal 2011;17:10.

40. Dobin A, Davis CA, Schlesinger F, et al. STAR: Ultrafast universal RNA-seq aligner. Bioinformatics 2013;29:15–21.

41. Anders S, Huber W. Differential expression analysis for sequence count data. Genome Biol 2010;11.

42. Love MI, Huber W, Anders S. Moderated estimation of fold change and dispersion for RNA-seq data with DESeq2. Genome Biol 2014;15.

43. Yu G, Wang LG, Han Y, et al. ClusterProfiler: An R package for comparing biological themes among gene clusters. Omi A J Integr Biol 2012;16:284–287.

44. Supek F, Bošnjak M, Škunca N, et al. Revigo summarizes and visualizes long lists of gene ontology terms. PLoS One 2011;6.

45. Wolter M, Steimle A, Parrish A, et al. Dietary Modulation Alters Susceptibility to Listeria monocytogenes and Salmonella Typhimurium with or without a Gut Microbiota. mSystems 2021;6:e00717-21.

46. Chassaing B, Srinivasan G, Delgado MA, et al. Fecal Lipocalin 2, a Sensitive and Broadly Dynamic Non-Invasive Biomarker for Intestinal Inflammation Bereswill S, ed. PLoS One 2012;7:e44328.

47. Zhao P, Elks CM, Stephens JM. The induction of lipocalin-2 protein expression in vivo and in vitro. J Biol Chem 2014;289:5960–5969.

48. Chaudhuri A. Regulation of macrophage polarization by RON receptor tyrosine kinase signaling. Front Immunol 2014;5.

49. Forman R, Logunova L, Smith H, et al. Trichuris muris infection drives cell-intrinsic IL4R alpha independent colonic RELMα+ macrophages. PLoS Pathog 2021;17.

50. Sorobetea D, Svensson-Frej M, Grencis R. Immunity to gastrointestinal nematode infections. Mucosal Immunol 2018;11:304–315.

51. Hallowell RW, Collins SL, Craig JM, et al. MTORC2 signalling regulates M2 macrophage differentiation in response to helminth infection and adaptive thermogenesis. Nat Commun 2017;8.

52. Deschoolmeester ML, Else KJ. Cytokine and chemokine responses underlying acute and chronic Trichuris muris infection. Int Rev Immunol 2002;21:439–467.

53. Else KJ, Entwistle GM, Grencis RK. Correlations between worm burden and markers of Th1 and Th2 cell subset induction in an inbred strain of mouse infected with Trichuris muris. Parasite Immunol 1993;15:595–600.

54. Kasakura K, Nagata K, Miura R, et al. Cooperative Regulation of the Mucosal Mast Cell–Specific Protease Genes Mcpt1 and Mcpt2 by GATA and Smad Transcription Factors. J Immunol 2020;204:1641–1649.

55. Mazzoni A, Siraganian RP, Leifer CA, et al. Dendritic Cell Modulation by Mast Cells Controls the Th1/Th2 Balance in Responding T Cells. J Immunol 2006;177:3577–3581.

56. Hayes KS, Grencis RK. Trichuris muris and comorbidities-within a mouse model context. Parasitology 2021;148:1774–1782.

57. Hayes KS, Hager R, Grencis RK. Sex-dependent genetic effects on immune responses to a parasitic nematode. BMC Genomics 2014;15.

58. Browne HP, Neville BA, Forster SC, et al. Transmission of the gut microbiota: Spreading of health. Nat Rev Microbiol 2017;15:531–543.

59. Luis AS, Jin C, Pereira GV, et al. A single sulfatase is required to access colonic mucin by a gut bacterium. Nature 2021;598:332–337.

60. Rey FE, Gonzalez MD, Cheng J, et al. Metabolic niche of a prominent sulfate-

reducing human gut bacterium. Proc Natl Acad Sci U S A 2013;110:13582–13587.

61. Rogers TE, Pudlo NA, Koropatkin NM, et al. Dynamic responses of Bacteroides thetaiotaomicron during growth on glycan mixtures. Mol Microbiol 2013;88:876–890.

62. Larsson JMH, Thomsson KA, Rodríguez-Piñeiro AM, et al. Studies of mucus in mouse stomach, small intestine, and colon. III. Gastrointestinal Muc5ac and Muc2 mucin O-glycan patterns reveal a regiospecific distribution. Am J Physiol - Gastrointest Liver Physiol 2013;305.

63. Arike L, Holmén-Larsson J, Hansson GC. Intestinal Muc2 mucin O-glycosylation is affected by microbiota and regulated by differential expression of glycosyltranferases. Glycobiology 2017;27:318–328.

64. Hasnain SZ, Dawson PA, Lourie R, et al. Immune-driven alterations in mucin sulphation is an important mediator of Trichuris muris helminth expulsion. PLoS Pathog 2017;13.

65. McDermott JR, Bartram RE, Knight PA, et al. Mast cells disrupt epithelial barrier function during enteric nematode infection. Proc Natl Acad Sci U S A 2003.

66. Helmby H. Human helminth therapy to treat inflammatory disorders- where do we stand? BMC Immunol 2015;16.

67. Kiss M, Burns H, Donnelly S, et al. Effectiveness of Helminth Therapy in the Prevention of Allograft Rejection: A Systematic Review of Allogeneic Transplantation. Front Immunol 2020;11.

Figure legends

Figure 1. Diet drives changes in mucin-degrading bacteria and alters worm infection. (A) Experimental timeline. Age-matched 18–23 weeks old germ-free (GF) C57BL/6 mice were gavaged with the synthetic 14-member gut microbiota (14SM) on two consecutive days. These colonized mice were maintained for six days on the fiber-rich (FR) diet, after which nearly half of the mice were switched to a fiber-free (FF) diet. The mice were maintained for 20 days on their respective diets, after which they were gavaged with *T. muris* eggs. The infection was observed for up to 30 days and on day 13, 15, 20, 25 and 30 post infection 4–5 mice were euthanized for final readouts. (B) Relative bacterial abundance at day 0, just before the infection, determined by qPCR on DNA extracted from fecal pellets. Red latin crosses denote known mucin-degrading bacteria. (C) Weekly assessed weights of *T. muris* infected mice. Error bars represent SEM and significance labels comparisons between FR and FF group as determined by an unpaired, two-tailed t-test. (D) Worm burdens assessed on the mice euthanized at day 13, 15, 20, 25 and 30 post infection. Error bars represent SEM; unpaired, two-tailed t-test. (E) Fecal Lipocalin-2 (LCN-2) levels assessed by ELISA before (day 0) and after infection with *T. muris* (13, 15, 20, 23, 30 DPI). Error bars represent SEM; unpaired t-test. ns, non-significant; *p<0.05; **p<0.01; ***p<0.001; ****p<0.0001.

Figure 2. Host transcriptomics supports chronic and acute outcome of worm infection. Analysis of data generated by RNA-seq of RNA extracted from colonic tissue at day 30 post infection (n = 4 per group). (A) Volcano plot of the distribution of all differentially expressed genes. (B) Barplot showing significantly up- or downregulated host pathways (Fiber Rich (FR)/Fiber Free (FF)) determined by Ingenuity Pathway Analysis (IPA). The higher the opacity of the bar, the more up- or downregulated the pathway. (C) Graphical summary generated by IPA showing the major upregulated genes and pathways as well as their interactions.

Figure 3. Maintenance or moderate increase of Th2 immunity leads to worm expulsion. (A) Relative cytokine expression of INFγ, IL-04 and IL-13 (Fiber-free versus Fiber-rich fed mice) determined by qPCR using RNA extracted from mesenteric lymph nodes and colonic tissue (colon) at 30 days post infection (n = 3-5). Error bars represent 95% confidence intervals; unpaired, two-tailed t-test. (B) Serum cytokine concentrations determined by LEGENDplex bead-based immunoassay at days 30 post infection. Error bars represent SEM; unpaired, two-tailed t-test. (C) Total IgE and total IgG1 concentrations determined by ELISA on mouse

serum. Error bars represent SEM; two-way ANOVA using a Šidák multiple comparison test. (D) Parasite-specific IgG1 and IgG2c concentrations determined by ELISA on mouse serum. Error bars represent SEM; two-way ANOVA using a Šidák multiple comparison test. (E) Serum mast cell protease 1 (MCPT1) concentrations determined by ELISA. Error bars represent SEM. Black significance labels denote comparisons between FR and FF groups. Red asterisk denotes significant comparison to day 0 within the FF group. Error bars represent SEM; Two-way ANOVA using a Šidák multiple comparison test; ns, non-significant; *p<0.05; **p<0.01; ***p<0.001; ****p<0.0001.

Figure 4. Mucin-generalist bacteria increase during worm clearance. (A) PCoA plot of the microbiome composition of all mice split by diet (left panel) or by day and diet (middle and right panels). PCs were selected based on Eigenvalues. (B) Microbial composition of the gut microbiota before the infection (day 0) and at day 13, 15, 20, 25 and 30 post infection (denoted by dotted lines). Relative bacterial abundances were determined by qPCR of DNA extracted from fecal pellets using primers specific to each bacterial strain. Red crosses denote known mucin-degrading bacteria. (C) Relative abundances of individual bacterial strains. Black significance labels denote comparisons between the Fiber-rich (FR) and Fiber-free (FF) groups on a specific day. Green asterisks denote significant comparisons to day 0 within the FR group. Red asterisks similarly denote significant comparisons to day 0 within the FF group. Error bars represent SEM; two-way ANOVA using a Šidák multiple comparison test. (D) Fold-change of mucin generalists (*Bacteroides caccae* and *Bacteroides thetaiotaomicron*) and mucin specialists *(Akkermansia muciniphila* and *Barnesiella intestinihominis*) normalized by their average day 0 relative abundance. Black significance labels denote comparisons between the FR and FF group on a specific day. Green asterisks denote significant comparisons to day 0 within the FR group. Red asterisks similarly denote significant comparisons to day 0 within the FF group. Error bars represent SEM; two-way ANOVA using a Šidák multiple comparison test. ns, non-significant; *p<0.05; **p<0.01; ***p<0.001; ****p<0.0001.

Figure 5. Increased mucin–microbiome interactions promote worm clearance. (A) Glycan-degrading enzyme activities of the gut microbiome determined by stool-based p-nitrophenyl glycoside-based enzyme assays. β-N-acetyl-glucosaminidase (NAG) and α-fucosidase (FUC) are key mucin-degrading enzymes, while β-glucosidase (GLUC) serves as a control for general glycan-degrading activity. Error bars represent SEM; Mann-Whitney test between Fiber-rich (FR) and Fiber-free (FF) groups. (B) Goblet cell counts per crypt of *T.*

muris infected mice determined by histological assessment of methacarn-fixed cecum sections. Error bars represent SEM; two-way ANOVA using a Šidák multiple comparison test. (C) Relative gene expression (FF/FR) at 30 days post infection of the 5 most significant activated pathways in the colonic tissue under FF conditions (n = 4 per group). Pathways are based on GO terms for biological processes and REVIGO was used to reduce redundant terms. ns, non-significant; *p<0.05; **p<0.01. †Adaptive immune response is based on somatic recombination of immune receptors built from immunoglobulin superfamily domains.

Figure 6. Model for clearance of *T. muris* following excessive microbial mucin foraging. Under homeostatic conditions there is a balance between bacterial fiber- and mucin-degradation. Deprivation of dietary fiber leads to an increased bacterial mucin-degrading activity of the gut microbiome, which is further increased after infection with *T. muris*. This increase is a result of the expansion of mucin-generalist bacteria around 20 DPI, which in turn opens up a growth niche for other bacteria such as *D. piger* and *E. rectale*, which can utilize the sulfate or simple mucin glycoproteins, respectively, resulting from the depolymerization of the complex host mucins by the mucin-generalist bacteria. In contrast to mucin-generalists, mucin-specialists drastically drop in abundance following worm hatching in Fiber-free (FF)-diet fed mice. In Fiber-rich (FR)-diet fed mice, the host develops a Th1 response characterized by an increase of Th1-type cytokines, particularly IFNγ, and the production of parasite specific IgG2 resulting in a chronic *T. muris* infection. In contrast, the excessive mucin foraging in FF-fed mice leads to a moderate Th2 response characterized by the secretion of Th2 cytokines, expression of parasite-specific IgG1 and increased degranulation of mast cells ultimately leading to the clearance of *T. muris* around 30 DPI.

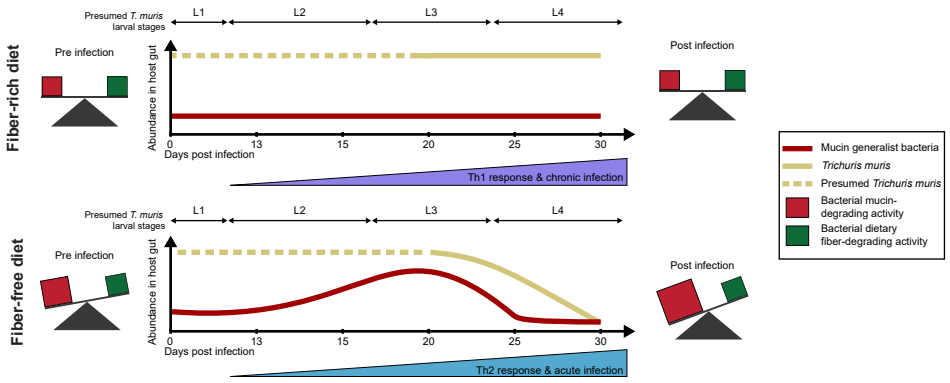

Graphical abstract

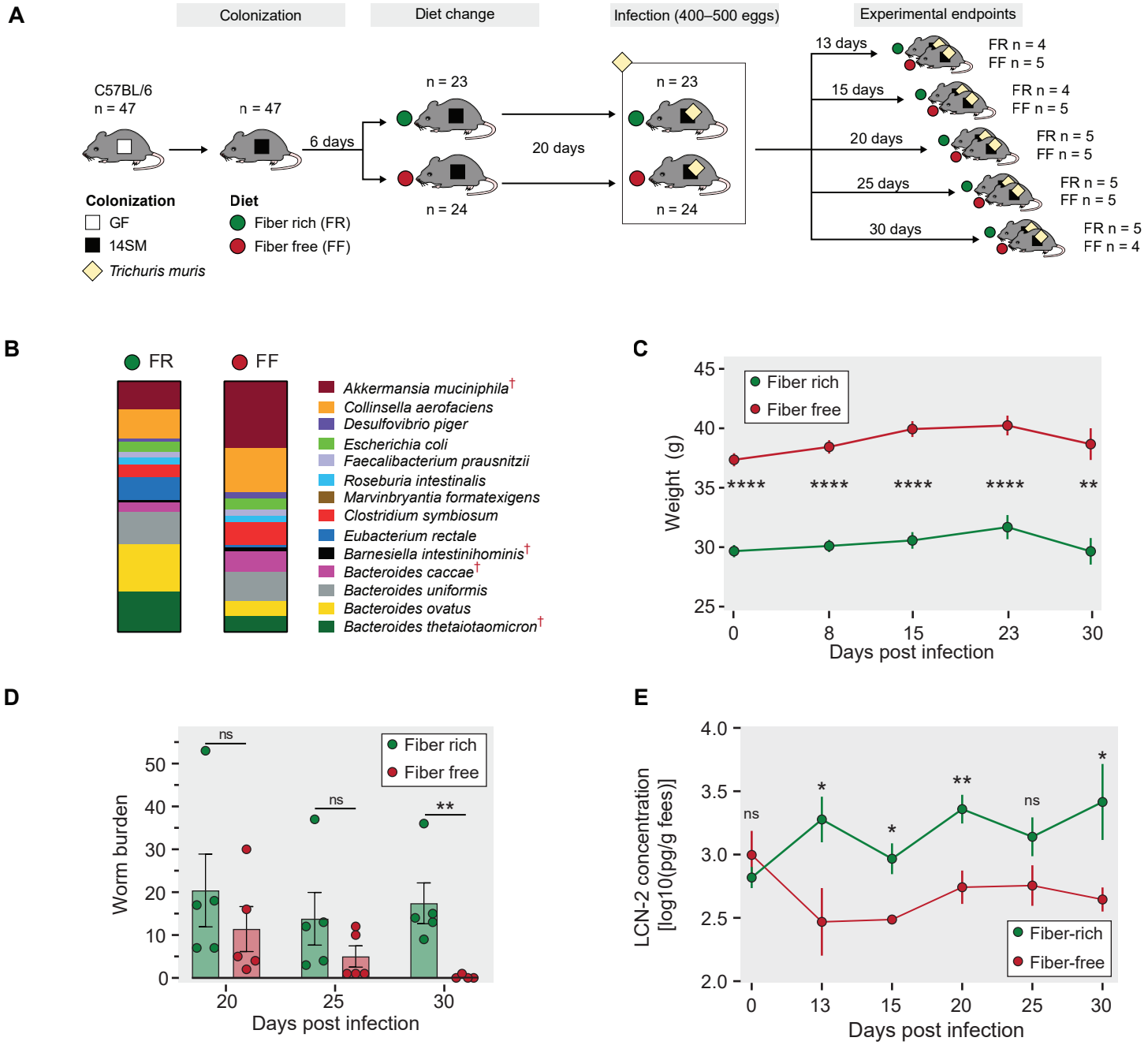
A
Colonization
Diet change
Infection (400–500 eggs)
Experimental endpoints
C57BL/6
n = 47
n = 47
6 days
n = 23
n = 24
20 days
n = 23
n = 24
13 days
15 days
20 days
25 days
30 days
FR n = 4
FF n = 5
FR n = 4
FF n = 5
FR n = 5
FF n = 5
FR n = 5
FF n = 5
FR n = 5
FF n = 4
Colonization
GF
14SM
Trichuris muris
Diet
Fiber rich (FR)
Fiber free (FF)
B
FR
FF
Akkermansia muciniphila†
Collinsella aerofaciens
Desulfovibrio piger
Escherichia coli
Faecalibacterium prausnitzii
Roseburia intestinalis
Marvinbryantia formatexigens
Clostridium symbiosum
Eubacterium rectale
Barnesiella intestinihominis†
Bacteroides caccae†
Bacteroides uniformis
Bacteroides ovatus
Bacteroides thetaiotaomicron†
C
Fiber rich
Fiber free
Weight (g)
45
40
35
30
25
****
****
****
****
**
0
8
15
23
30
Days post infection
D
Fiber rich
Fiber free
Worm burden
50
40
30
20
10
0
ns
ns
**
20
25
30
Days post infection
E
LCN-2 concentration [log10(pg/g fees)]
4.0
3.5
3.0
2.5
2.0
ns
*
*
**
ns
*
Fiber-rich
Fiber-free
0
13
15
20
25
30
Days post infection

Figure 1


A
Gsdmc2
Gsdmc4
Anxa8
Sval1
Gal3st2b
Dennd11
Gal3st2
Ighv5-16
Igkv1-117
Gm28382
Upregulated in FR
Upregulated in FF
Not significant
-log10(pvalue)
log2FoldChange
Upregulated in FF
Upregulated in FR
B
threshold
positive z-score
negative z-score
-log(p-value)
Interferon signaling
Neuroinflammation signaling pathway
MSP-RON signaling in macrophages pathway
Necroptosis signaling pathway
Role of hypercytokinemia/ hyperchemokinemia in the pathogenesis of influenza
Systemic lupus erythematosus in B cell signaling pathway
Osteoarthritis pathway
Th1 pathway
PD-1, PD-L1 cancer immunotherapy pathway
Role of PKR in interferon induction and antiviral response
Production of nitric oxide and reactive oxygen species in macrophages
Activation of IRF by cytosolic pattern recognition receptors
Dendritic cell maturation
PI3K/AKT signaling
White adipose tissue browning pathway
p38 MAPK signaling
HIF1α signaling
ERK/MAPK signaling
T cell exhaustion signaling pathway
Cardiac hypertrophy signaling (enhanced)
C
Th1 pathway
SAMSN1
Systemic lupus erythematosus in B cell signaling pathway
TNFSF10
IRF3
TRIM24
STAT1
IL21
Interferon signaling
Activation of cytotoxic T cells
MAVS
IRF5
IRF7
TNF
IFNG
IL27
Hematopoiesis of mononuclear leukocytes
SASH1
DDX58
IFNB1
IL1B
Lymphopoiesis
IL10RA
Antimicrobial response
DOCK8
IRF1
EBI3
Replication of RNA virus
IL1RN
Replication of virus
Cell death of macrophages
Cell death of stomach cancer cell lines
Apoptosis of stomach cancer cell lines
Apoptosis of neuroglia
Cytokine
Enzyme
Canonical pathways
Upregulated in fiber rich
Transcription regulator
Functions
Other
Upregulated in fiber free
Transmembrane receptor
Diseases
Direct interaction
Indirect interaction

Figure 2

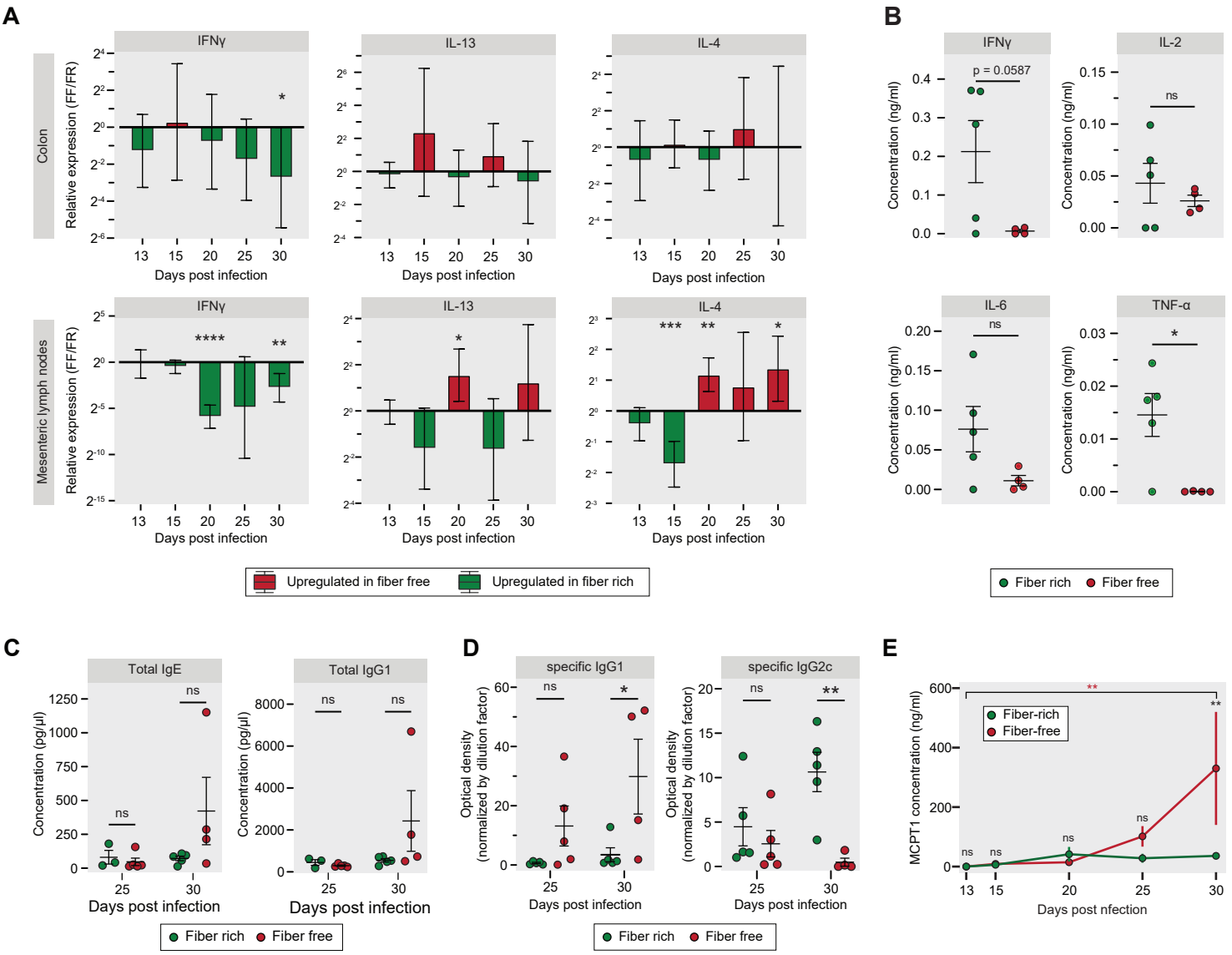
A
Colon
Mesenteric lymph nodes
Relative expression (FF/FR)
IFNγ
IL-13
IL-4
Days post infection
Upregulated in fiber free
Upregulated in fiber rich
B
IFNγ
IL-2
IL-6
TNF-α
Concentration (ng/ml)
p = 0.0587
ns
Fiber rich
Fiber free
C
Total IgE
Total IgG1
Concentration (pg/µl)
Days post infection
Fiber rich
Fiber free
D
specific IgG1
specific IgG2c
Optical density (normalized by dilution factor)
Days post infection
Fiber rich
Fiber free
E
MCPT1 concentration (ng/ml)
Fiber-rich
Fiber-free
Days post nfection

Figure 3

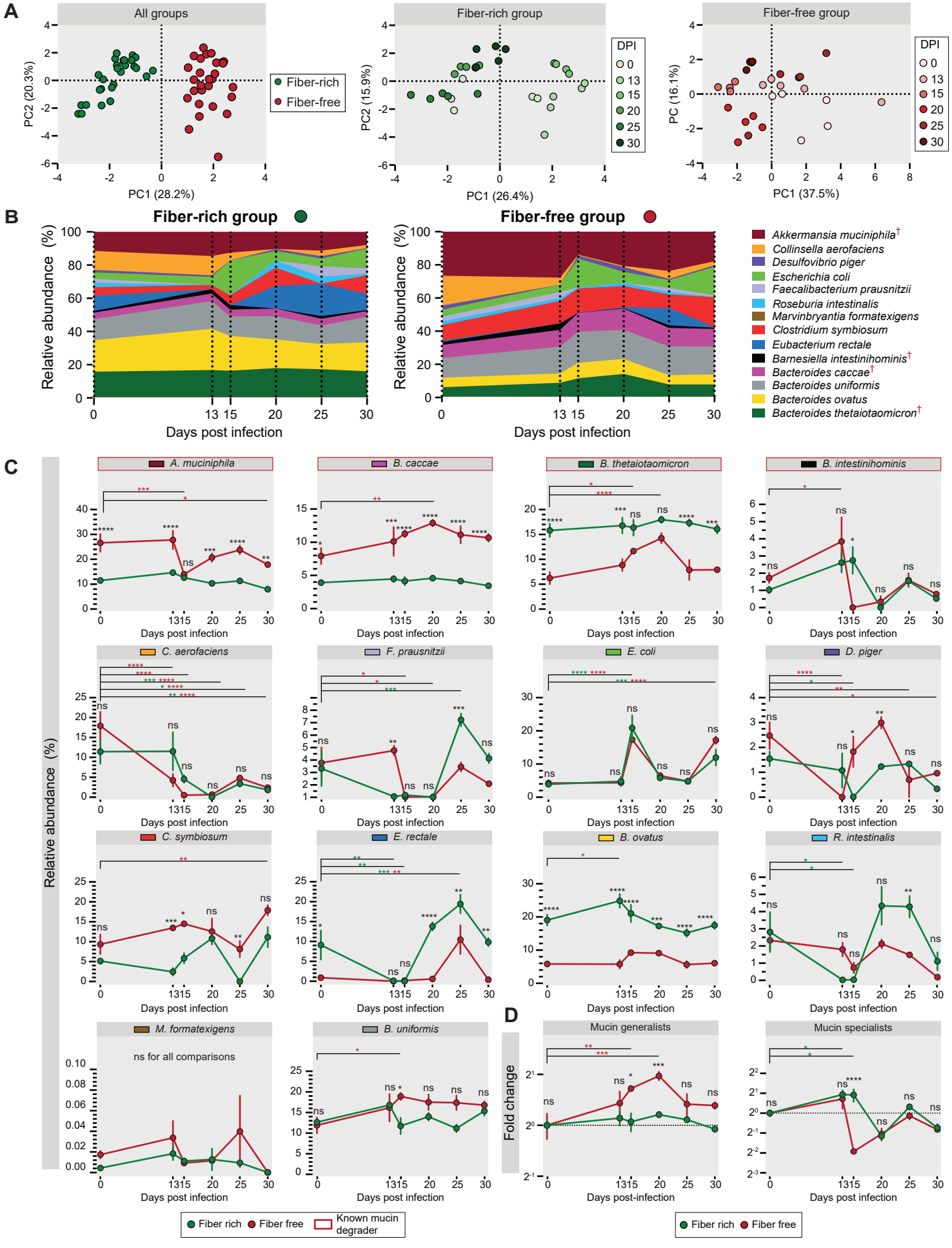
A
All groups
Fiber-rich group
Fiber-free group
PC2 (20.3%)
PC1 (28.2%)
PC2 (15.9%)
PC1 (26.4%)
PC (16.1%)
PC1 (37.5%)
Fiber-rich
Fiber-free
DPI
0
13
15
20
25
30
B
Fiber-rich group
Fiber-free group
Relative abundance (%)
Days post infection
Akkermansia muciniphila†
Collinsella aerofaciens
Desulfovibrio piger
Escherichia coli
Faecalibacterium prausnitzii
Roseburia intestinalis
Marvinbryantia formatexigens
Clostridium symbiosum
Eubacterium rectale
Barnesiella intestinihominis†
Bacteroides caccae†
Bacteroides uniformis
Bacteroides ovatus
Bacteroides thetaiotaomicron†
C
A. muciniphila
B. caccae
B. thetaiotaomicron
B. intestinihominis
C. aerofaciens
F. prausnitzii
E. coli
D. piger
C. symbiosum
E. rectale
B. ovatus
R. intestinalis
M. formatexigens
ns for all comparisons
B. uniformis
Relative abundance (%)
Days post infection
D
Mucin generalists
Mucin specialists
Fold change
Days post-infection
Fiber rich
Fiber free
Known mucin degrader

Figure 4

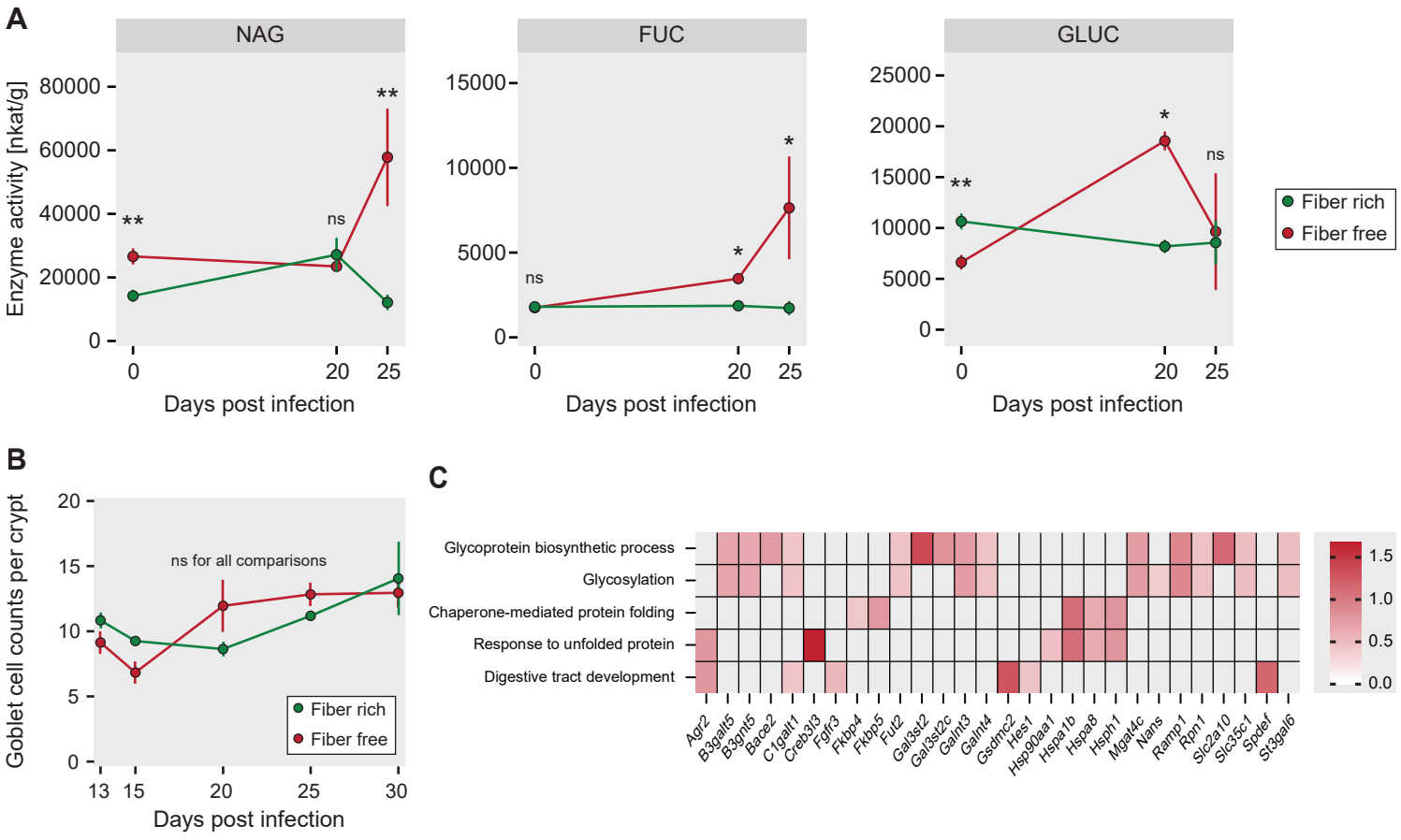
A
NAG
FUC
GLUC
Enzyme activity [nkat/g]
Days post infection
Fiber rich
Fiber free
B
Goblet cell counts per crypt
ns for all comparisons
C
Glycoprotein biosynthetic process
Glycosylation
Chaperone-mediated protein folding
Response to unfolded protein
Digestive tract development
Agr2
B3galt5
B3gnt5
Bace2
C1galt1
Creb3l3
Fgf3
Fkbp4
Fkbp5
Fut2
Gal3st2
Gal3st2c
Galnt3
Galnt4
Gsdmc2
Hes1
Hsp90aa1
Hspa1b
Hspa8
Hsph1
Mgat4c
Nans
Ramp1
Rpn1
Slc2a10
Slc35c1
Spdef
St3gal6

Figure 5

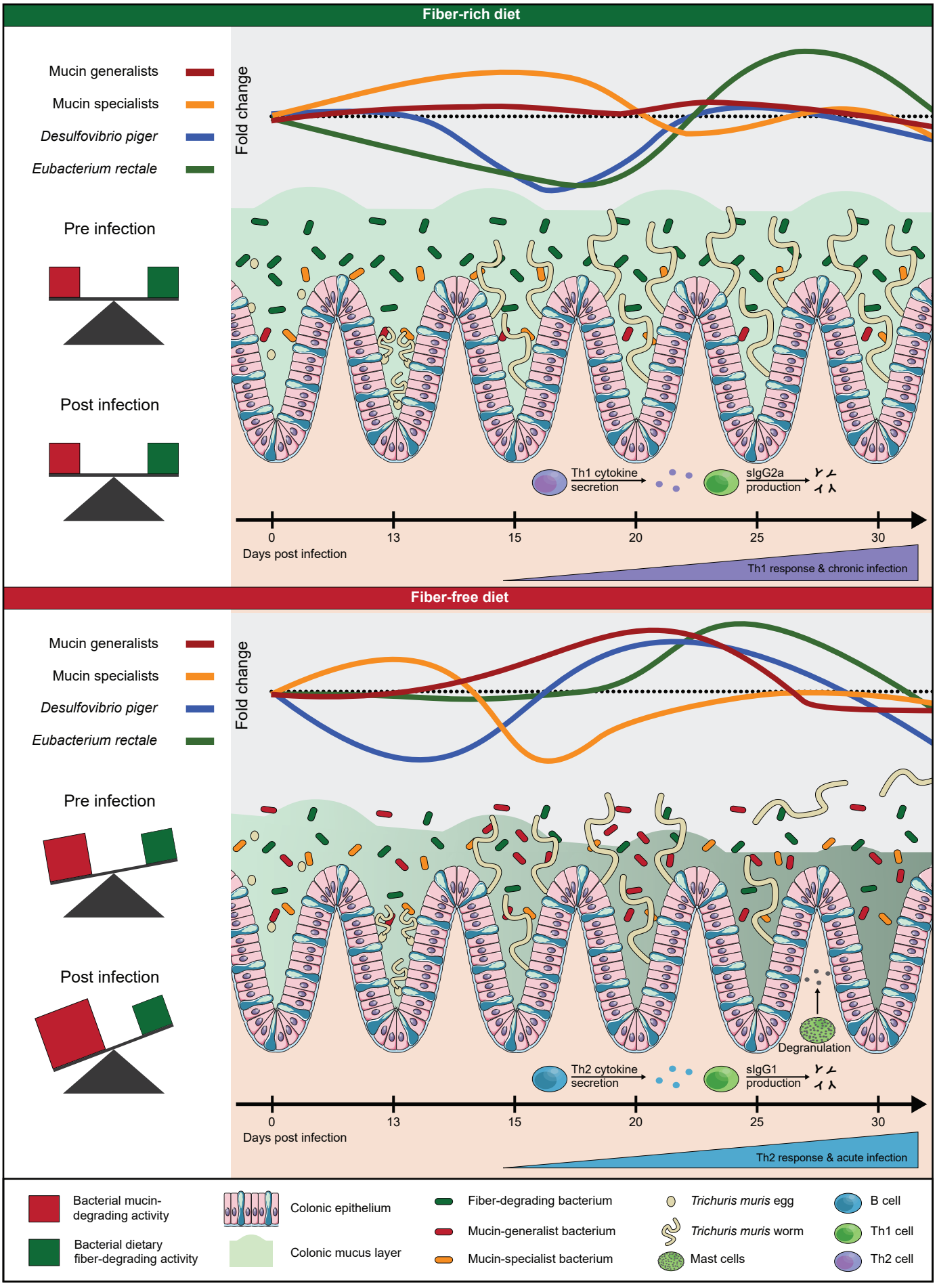
Fiber-rich diet
Mucin generalists
Mucin specialists
Desulfovibrio piger
Eubacterium rectale
Fold change
Pre infection
Post infection
Th1 cytokine secretion
sIgG2a production
0
13
15
20
25
30
Days post infection
Th1 response & chronic infection
Fiber-free diet
Mucin generalists
Mucin specialists
Desulfovibrio piger
Eubacterium rectale
Fold change
Pre infection
Post infection
Degranulation
Th2 cytokine secretion
sIgG1 production
0
13
15
20
25
30
Days post infection
Th2 response & acute infection
Bacterial mucin-degrading activity
Bacterial dietary fiber-degrading activity
Colonic epithelium
Colonic mucus layer
Fiber-degrading bacterium
Mucin-generalist bacterium
Mucin-specialist bacterium
Trichuris muris egg
Trichuris muris worm
Mast cells
B cell
Th1 cell
Th2 cell

Figure 6

Supplementary figure legends

Figure S1. Host gene expression on the FR diet is dominated by genes involved in Th1 response. Relative gene expression (FR/FF) at 30 days post infection of the 5 most significant activated pathways in the colonic tissue under FF conditions (n = 4 per group). Pathways are based on GO terms for biological processes and REVIGO was used to reduce redundant terms.

Figure S2. Cytokine transcript and protein abundances on different days post worm infection. (A) Relative cytokine expression of TNF-α, IL-5, IL-22 and IL-17a (fiber-free over fiber-rich fed mice) determined by qPCR of cDNA from RNA extracted from mesenteric lymph nodes (MLN) and colonic tissue (colon) at 13 and 30 DPI. Error bars represent 95% confidence intervals; unpaired, two-tailed t-test. (B) Serum cytokine concentrations of IL-22 and IL-5 at 30 DPI determined by LEGENDplex bead-based immunoassay. Error bars represent SEM; unpaired, two-tailed t-test. (C) Relative transcription factor expression of Tbet and GATA3 (Fiber-free over Fiber-rich fed mice) determined by qPCR using RNA extracted from mesenteric lymph nodes (MLN) and colonic tissue (colon) at 13–30 DPI. In the colon, GATA3 for all DPI and Tbet for 13 DPI were below the detection threshold. Error bars represent 95% confidence intervals; unpaired, two-tailed t-test; ns, non-significant; *p<0.05; **p<0.01.

Figure S3. Absolute abundances of cytokine transcripts on different days post worm infection. (A) Absolute cytokine and transcription factor expression as determined by qPCR using RNA extracted from mesenteric lymph nodes (MLN) and colonic tissue (colon) at 13, 15, 20, 25 and 30 DPI. Error bars represent SEM; unpaired, two-tailed t-test. (B) Absolute cytokine expression as determined by qPCR of using RNA extracted from mesenteric lymph nodes (MLN) and colonic tissue (colon) at 13 and 30 DPI. Error bars represent SEM; unpaired, two-tailed t-test. In the colon, GATA3 for all DPI and Tbet for 13 DPI were below the detection threshold. Error bars represent 95% confidence intervals; unpaired, two-tailed t-test; ns, non-significant; *p<0.05; **p<0.01; ***p<0.001; ****p<0.0001.

Supplementary table legends

Table S1. Relative gene expression (FR/FF) based differential expression analysis using DESeq2.

Table S2. Significantly upregulated pathways in FR diet based on gene oncology (GO) terms for biological processes.

Table S3. Significantly upregulated pathways in FF diet based on gene oncology (GO) terms for biological processes.

Table S4. RT-qPCR primers for genes encoding various cytokines, transcription factors and a reference (GAPDH).

Supplemental methods

Serum ELISA for total IgG1 and IgE

Serum ELISA for total IgG1 and IgE were performed as follows. Plate were coated overnight at room temperature using 0.5 µg/µl rat α mouse IgE purified UNLB (Imtec Diagnostics, 1130-01) or rat α-mouse IgG1 purified UNLB (Imtec Diagnostics, Ardmore, OK, United States; catalog no. 1144-01) capture antibody, respectively, diluted in 0.05 M carbonate/bicarbonate buffer (pH 9.6). Wells were washed three times using a washing buffer consisting of 1% Tween, 154 mM NaCl, 10 mM Trizma Base. 1% w/v of BSA in a TBS buffer (15 mM Trizma-acetate, 136 mM NaCl & 2 mM KCl) was used to block plates by incubating them for 2 hours at room temperature. Afterwards, plates were washed three times using the washing buffer. As controls, Mouse IgG1 Isotype Control UNLB (Imtec Diagnostics, Ardmore, OK, United States; catalog no 0102-01) or Mouse IgE Isotype Control (UNLB), Southern Biotech (Imtec Diagnostics, Ardmore, OK, United States; catalog no 0114-01) was used to generate two-fold serial dilutions. Serum samples were two-fold diluted from 1/40 to 1/1280 using the aforementioned TBS buffer with 0.1% w/v Tween-20 and 1% BSA. Plates were loaded the standards and samples were incubated for 90 minutes at room temperature. Another three wash steps were performed before loading a 1/500 dilution of the 2nd antibody, Goat anti-mouse IgG1-AP, Southern Biotech (Imtec diagnostics, Ardmore, OK, United States; catalog no 1071-04) or Goat anti-mouse IgE-AP, Southern Biotech (Imtec diagnostics, Ardmore, OK, United States; catalog no 1110-04), respectively. The final three wash steps were performed before loading the substrate solution consisting of 0.5 mg/ml phosphate substrate (Sigma-Aldrich, St. Louis, MO, United States; catalog no. S0642-200 TAB) in 1 mM AMP and 0.1 mM $MgCl_2 \bullet 6H_2O$. Plates were incubated for 1 hour at 37°C before they were read at 405 nm using a SpectraMax ABS PLUS spectrophotometer (Molecular Devices, San Jose, CA, United States).

RNA extraction from mesenteric lymph nodes and colonic tissue

Serum ELISA for total IgG1 and IgE were performed as follows. Plate were coated overnight at room temperature using 20 µl/well of 0.5 µg/µl rat α mouse IgE purified UNLB (Imtec Diagnostics, 1130-01) or rat α-mouse IgG1 purified UNLB (Imtec Diagnostics, Ardmore, OK, United States; catalog

no. 1144-01) capture antibody, respectively, diluted in 0.05 M carbonate/bicarbonate buffer at pH 9.6. Wells were washed three times using 100 µl/well of a washing buffer consisting of 1% Tween, 154 mM NaCl, 10 mM Trizma Base. Then plates were blocked by incubating them for 2 hours at room temperature with 75 µl of blocking buffer consisting of 1% w/v of BSA in a TBS buffer (15 mM Trizma-acetate, 136 mM NaCl & 2 mM KCl). Afterwards, plates were washed three times using the washing buffer. As controls, Mouse IgG1 Isotype Control UNLB (Imtec Diagnostics, Ardmore, OK, United States; catalog no 0102-01) was used to generate a two-fold serial dilution from 1/500 to 1/512000 and Mouse IgE Isotype Control (UNLB), Southern Biotech (Imtec Diagnostics, Ardmore, OK, United States; catalog no 0114-01) was used to generate a two-fold serial dilution from 1/1000 to 1/1024000. Serum samples were two-fold diluted from 1/40 to 1/1280. The dilution buffer consisted of 0.1% w/v Tween-20 and 1% BSA in the aforementioned TBS buffer. Plates were loaded with 20 µl/well of the standards and diluted samples and incubated for 90 minutes at room temperature. Another three wash steps were performed before loading 20 µl/well of a 1/500 dilution of the 2nd antibody, Goat anti-mouse IgG1-AP, Southern Biotech (Imtec diagnostics, Ardmore, OK, United States; catalog no 1071-04) or Goat anti-mouse IgE-AP, Southern Biotech (Imtec diagnostics, Ardmore, OK, United States; catalog no 1110-04), respectively. The final three wash steps were performed before loading 40 µl/well of the substrate solution, which consists of 0.5 mg/ml phosphate substrate Sigma-Aldrich, St. Louis, MO, United States; catalog no. S0642-200 TAB) in a 1 mM AMP and 0.1 mM $MgCl_2 \bullet 6H_2O$. Plates were incubated for 1 hour at 37°C before they were read at 405 nm using a SpectraMax ABS PLUS spectrophotometer (Molecular Devices, San Jose, CA, United States).

RT-qPCR

Targeted analysis of cytokine and transcription factor expression was determined by RT-qPCR of RNA extracted from mesenteric lymph nodes (MLN) and colonic tissue (colon). The cDNA library was prepared by combining 500 µM dNTP Set (100 mM) Solution (Invitrogen, Waltham, USA), 2.5 µM Random Primers (Invitrogen), 100 ng/µl of RNA sample and 1ul of ddH2O per sample, followed by heating to 65°C for 5 min and incubation on ice for at least 1 min. Next, 1× SSIV Buffer, 100 mM DTT, 40 U RNaseOUT (Invitrogen, Waltham, USA), Recombinant Ribonuclease Inhibitor (Invitrogen, Waltham, USA), and 200 U Superscript IV Reverse Transcriptase (Invitrogen, Waltham, USA) was added to each sample and incubated at 23°C for 10 min. Samples were incubated at 50°C for 10 min, then heat-inactivated at 80°C for 10 min. A master mix consisting of 1× Buffer, 2.5 mM $MgCl_2$, 400uM dNTP, 1× SYBR Green I Nucleic Acid Gel Stain, 10,000× concentrate in DMSO

(Invitrogen, Waltham, USA), and 0.5 U Platinum *Taq* DNA Polymerase (Life Technologies, Carlsbad, USA), was added to 1 µl each cDNA sample along with 0.2 µM each of forward and reverse primers (the specific primers are listed in **Table S4)**. The PCR cycle consisted of pre-denaturation at 94°C for 5 min, followed by 40 cycles of 20 sec denaturation at 94°C, 50 sec annealing at 60°C, and 45 sec extension at 72°C. Samples were held at 72°C for 5 min post-extension and then a melting curve was generated by heating from 65°C to 95°C with 0.3°C interval increases over 15 sec.

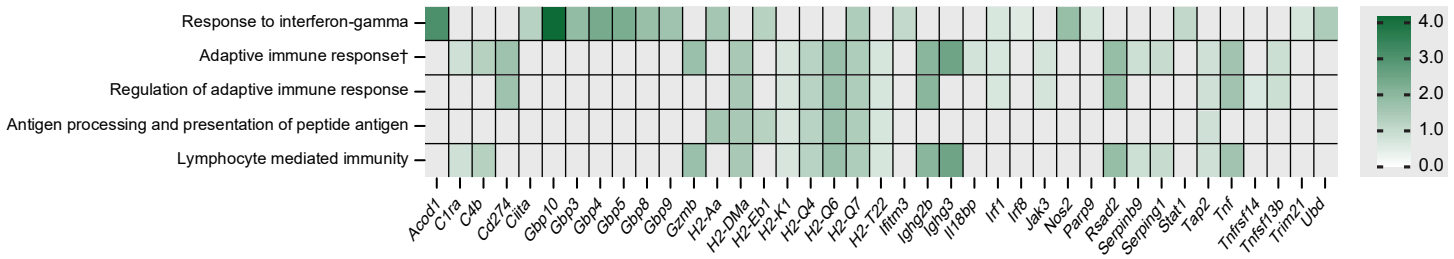
Response to interferon-gamma
Adaptive immune response†
Regulation of adaptive immune response
Antigen processing and presentation of peptide antigen
Lymphocyte mediated immunity
4.0
3.0
2.0
1.0
0.0
Acod1
C1ra
C4b
Cd274
Ciita
Gbp10
Gbp3
Gbp4
Gbp5
Gbp8
Gbp9
Gzmb
H2-Aa
H2-DMa
H2-Eb1
H2-K1
H2-Q4
H2-Q6
H2-Q7
H2-T22
Ifitm3
Ighg2b
Ighg3
Il18bp
Irf1
Irf8
Jak3
Nos2
Parp9
Rsad2
Serpinb9
Serping1
Stat1
Tap2
Tnf
Tnfrsf14
Tnfsf13b
Trim21
Ubd

Figure S1

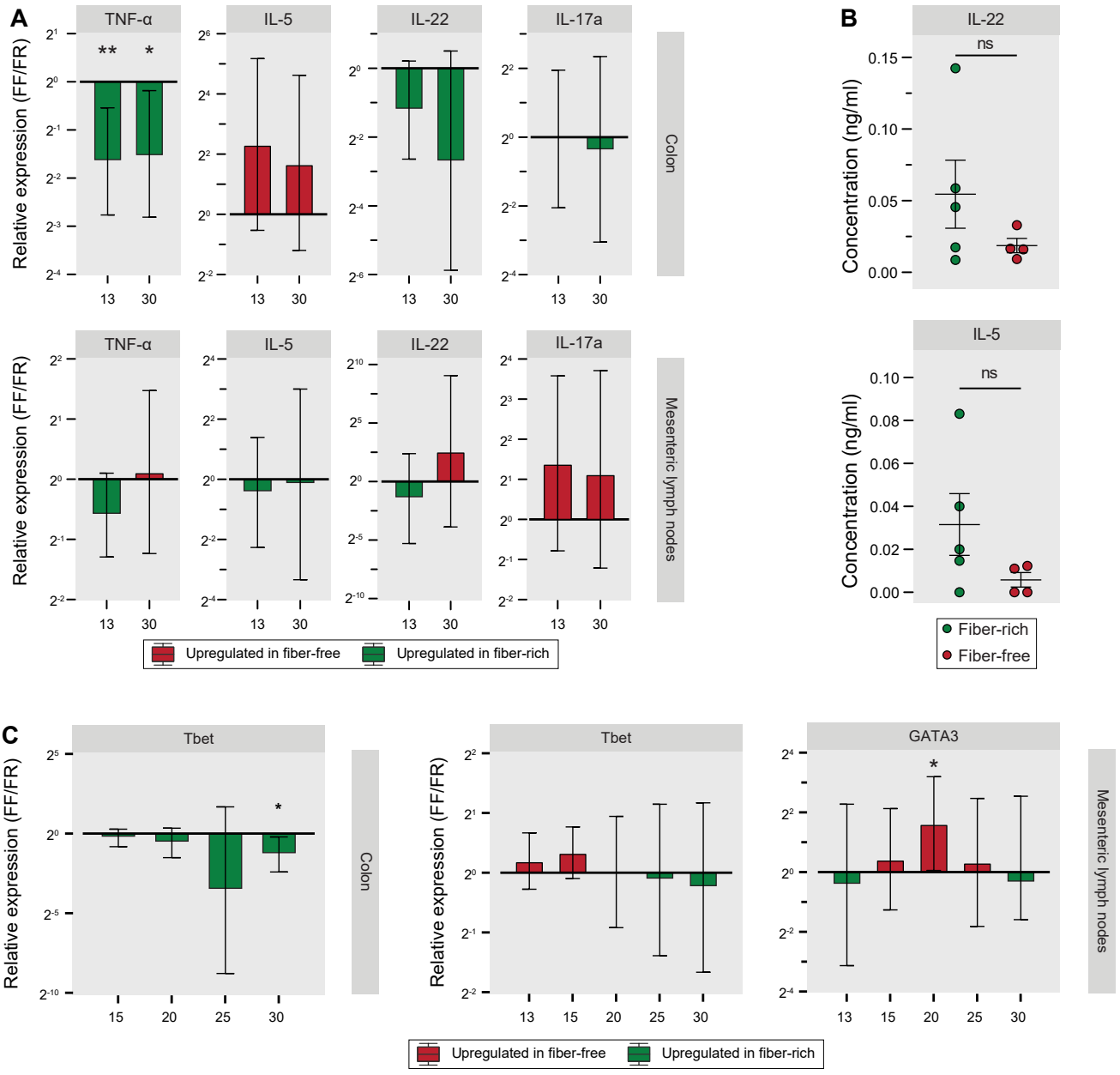
A
TNF-α
IL-5
IL-22
IL-17a
Relative expression (FF/FR)
Colon
Mesenteric lymph nodes
13
30
B
IL-22
IL-5
ns
Concentration (ng/ml)
Fiber-rich
Fiber-free
C
Tbet
GATA3
15
20
25
Upregulated in fiber-free
Upregulated in fiber-rich

Figure S2

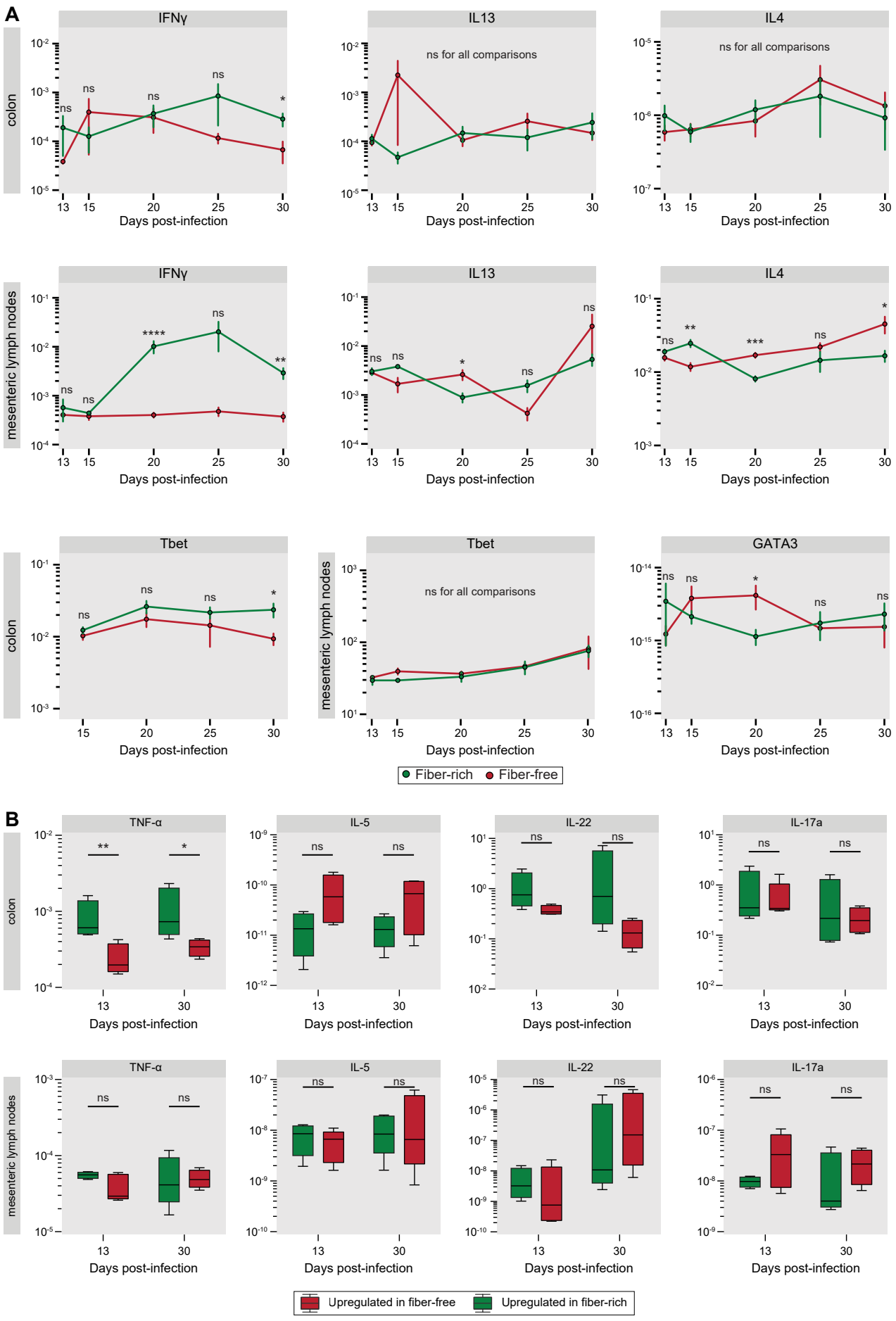
A
IFNγ
IL13
IL4
colon
mesenteric lymph nodes
Tbet
GATA3
ns for all comparisons
Days post-infection
Fiber-rich
Fiber-free
B
TNF-α
IL-5
IL-22
IL-17a
Upregulated in fiber-free
Upregulated in fiber-rich

Figure S3

6. Dietary-fiber deprivation induces lethal colitis in an IBD mouse model

6.1 Rationale

Autoimmune diseases, in particular inflammatory bowel disease (IBD), have been often linked with a thin mucus layer phenotype as well as the expansion of mucolytic bacteria. However, the cause effect relationship of this remains not fully explored. Therefore, we decided to investigate how dietary fiber deprivation might affect susceptibility to IBD. As dietary fiber deprivation leads to the expansion of mucolytic bacteria and the erosion of the mucus layer, we hypothesized that in a genetically susceptible host IBD could develop. Using our 14SM in an IL-10$^{-/-}$ mice, a murine model for IBD we determined that indeed the interaction of microbiome and diet in a genetically susceptible host can induce lethal colitis and that each of these three factors is essential for the development of the colitis. Furthermore, we showed that any of the four mucolytic bacteria in our community has the potential to induce this phenotype and that not a specific strain is required.

Personal contributions: I am an author of this research paper and had contributions to the initial design, the execution, and the data analysis. I performed most of the experiments and analysis for figure 1 with the exception of the analysis of figure 1D and 1E. I also performed the complete data analysis for figure 1C.

6.2 Results

Dietary-fiber deprivation induces lethal colitis in an IBD mouse model

[#]Gabriel V. Pereira[1], [#] Mathis Wolter[1,2,3], Austin Campbell[1], Nicholas A. Pudlo[1] , Kathryn A. Eaton[1], [*]Mahesh S. Desai[1,4], [#,*]Eric C. Martens[1*]

[1]Department of Microbiology and Immunology, University of Michigan Medical School, Ann Arbor, Michigan, USA

[2]Department of Infection and Immunity, Luxembourg Institute of Health, Esch-sur-Alzette, Luxembourg

[3]Faculty of Science, Technology and Medicine, University of Luxembourg, Esch-sur-Alzette, Luxembourg

[4]Odense Research C 30 enter for Anaphylaxis, Department of Dermatology and Allergy Center, Odense University Hospital, University of Southern Denmark, Odense, Denmark

[#]Authors contributed equally

*Correspondence to: emartens@umich.edu, Mahesh.Desai@lih.lu

[#]Lead author

Abstract

Inflammatory bowel disease (IBD) is a chronic inflammation, which is increasing in industrialized populations. Host genetics, diet and the gut microbiome are thought to be the major contributors to IBD. Nonetheless, the detailed mechanisms underlying IBD susceptibility remain to be determined. Using a gnotobiotic mouse model hosting a synthetic human gut microbiota, we show dietary fiber deprivation-induced microbial erosion of the protective colonic mucus layer leads to lethal colitis in mice with genetically ablated interleukin-10 production. Only in the presence of a gut microbiome which included mucus-degrading bacteria did the combination of genetic predisposition and fiber-deprivation lead to lethal colitis. Our results highlight the role of mucus-degrading bacteria in the development of IBD and offer insight into how diet could be leveraged to reduce susceptibility and possible induce remission.

Introduction

Inflammatory bowel disease (IBD) is a chronic inflammation of the gastrointestinal tract resulting from an inappropriate immune response (*1*). One major factor affecting the predisposition and development of IBD is host genetics, however, genetics are insufficient to fully explain the development of the disease (*2*). The hosts own gut microbiome—which usually helps maintaining the host's immune homeostasis (*3*)—is the origin of intestinal antigens targeted by the inappropriate immune response in IBD (*1*). In addition to genetics and the gut microbiome, diet has also been shown to play an important role in the rising IBD incidence and "westernized" diets, which generally are low on fiber, have the potential to enhance IBD susceptibility (*4*). Low fiber diets have the potential to shift the gut microbiome towards a more mucolytic composition, resulting in a thinning of the gut mucus layer (*5*) and increased mucus permeability (*6*). Considering that both the expansion of mucolytic bacteria (*7*, *8*) and an impaired mucus layer has been observed in patients suffering from IBD (*9*), we decided to investigate a potential direct link between IBD and diet–microbiome–mucus layer interactions. In order to study these interactions, we employed gnotobiotic mice with genetically ablated interleukin-10 production (IL-10$^{-/-}$) hosting our 14-member synthetic gut microbiome (*5*, *10*). The lack of IL-10 production makes these mice prone to spontaneously develop IBD-like colitis in the presence of gut microbes (*11*). Our results show that dietary fiber deprivation by itself is sufficient to trigger lethal colitis in a genetically susceptible host. Furthermore, we demonstrate that this effect is mediated by the gut microbiome.

Results

We gavaged the 14SM into germ-free IL-10$^{-/-}$ C57BL/6 mice which were kept on a fiber-rich diet (FR), that is normal mouse chow (**Fig. 1A)**. Importantly, this mouse strain has been reported to be more resistant to develop spontaneously colitis (*12*). The proper colonization of the mice was checked and 14 days later half of the mice per group were put on the fiber-free (FF) diet (**Fig. 1A)**. Afterwards the mice were observed closely in an open-ended manner (**Fig. 1A)**. Throughout the experiment, mice fed the FR diet did not show any weight loss or other signs of disease. In contrast, approximately 32 days after the initial 14SM gavage, the mice on the FF diet started to drastically lose weight leading to lethal colitis for over 75% of the mice by day 54 **(Fig 1B)**. As the gut microbiota plays an essential role in the development of IBD, we chose to assess the gut microbiota composition of these mice. The initial colonization of both groups was very similar, however, the diet switch to the FF diet leads to a clear divergence of the microbial abundances in both groups. Compared to the FR-fed mice, FF-fed mice were characterized by a reduction of fiber-degrading bacteria, such as *Eubacterium rectale* and *Bacteroides ovatus*, and an expansion of mucolytic bacteria, particularly

Bacteroides caccae **(Fig 1C)**. The expansion of mucolytic bacteria might lead to the erosion of the gut mucus layer, thus we assessed the gut mucus layer by histology. The mucus thickness of FR-fed mice was around 125 µm while FF showed a significantly thinner mucus layer of around 40 µM **(Fig. 1D)**. In addition to being thinner, the mucus layer of FF-fed mice was also less dense than the one of the FR-fed mice **(Fig. 1E)**. This data suggest a potential link between dietary fiber deprivation-induced microbial mucus layer erosion and IBD-like colitis susceptibility.

In order to establish if there is a causal link between these observations, we chose to assess whether our FF phenotype was driven by diet-microbiome interactions, diet-genotype interaction or a combination of both. To determine this we repeated the previous experiment with wild type (WT) 14SM colonized mice and germ-free IL-10$^{-/-}$ mice. None of these groups showed weight losses, which were similar to the 14SM-colonized IL-10$^{-/-}$ mice on the FF diet **(Fig. 2A)**. To further support this data we determined LCN-2 levels, a marker for low-level inflammation (*13*) which confirmed the observed lethal colitis phenotype in the 14SM colonized, FF-fed IL-10$^{-/-}$ mice and the absence thereof in all of the other groups **(Fig. 2B)**. In order to elucidate the role of the mucus-degrading members of our synthetic microbiota, we similarly repeated the previous experiments, but excluded all mucus-degrading bacteria (labelled 10) or all but one (labelled 10+*Bc*; 10+*Bt*; 10+*Bi*; 10+*Am*). Only the inclusion of *B. thetaiotaomicron* or *B. caccae* resulted in a weight loss, which was far lower than the one of the 14SM group **(Fig. 2C)**. In contrast, LCN-2 are slightly increased in all groups under FF conditions with the highest increase being observable in the 14SM group **(Fig. 2C)**. Taken together, these results suggest that each of the mucin-degrading bacteria does slightly increase the susceptibility to IBD-like colitis in a genetically susceptible host. This seems to be an additive effect resulting in the lethal colitis phenotype observed in the FF-fed, 14SM-colonized IL-10$^{-/-}$ mouse group.

Discussion

Due to the complex nature of the pathophysiology of IBD resulting from the high number of variables affecting it, deducing the mechanisms underlying the development of this disease remains challenging. Here we leveraged our 14SM gnotobiotic mouse model to show how diet can drive the development of IBD through modulation of the commensal, mucus-degrading bacteria in the gut.

The host benefits of dietary fiber fermentation by the gut microbiota have been well documented. The produced end-products like short-chain fatty acids (SCFAs) are critical for the intestinal immune homeostasis and the gut epithelial barrier integrity (*14*, *15*). Often only the lack of SCFA is considered when analyzing the health impact of the gut microbiome during dietary fiber deprivation, however, the full extent of potential ramifications is starting to emerge. For example, it has been shown that a

lack of dietary fiber also results in a microbiota mediated deterioration of the gut mucus layer (*5*, *6*) and such an eroded mucus layer is often observed in IBD patients (*9*). Here we were able to link both observations, showing that the microbial erosion of the gut mucus layer can induce lethal colitis in genetically susceptible mice. Furthermore, we show that this observation is not linked to specific taxa, but to a function, the mucin foraging capability of the bacteria. Nonetheless, the detailed mechanisms underlying mucin foraging and increased colitis susceptibility remains to be determined. Considering that colonic crypts are protected by sentinel goblet cells which trigger mucus secretion in response to high levels of bacterial Toll-like receptor ligands (*16*), we hypothesize that the close contact of the bacteria with the host epithelium is triggering the colitis.

Altogether, our data gives important insights in one of the mechanisms involved in the development of IBD. Given that people living in industrialized countries tend to consume less than the daily-recommended fiber (*17*), we also offer an explanation to why IBD might be more prevalent in these countries. Finally, we raise the question if the traditional employed, low fiber therapeutic diets for IBD employed could not be optimized by the inclusion of certain dietary fibers.

Material and methods.

Ethical statement.

All animal experiments in the were approved by the University of Michigan, University Committee for the Use and Care of Animals

Experimental design and dietary treatment.

For the infection experiments, 8- to 9-week-old, age-matched, germfree (GF) C57J/B6 mice were housed in ISOcages with up to five animals per cage. Sterile water and diets were provided ad libitum. Mice were gavaged with 0.2 ml of the synthetic human gut microbiota on three consecutive days. The gavage mix was prepared as described previously (*5*, *10*). Before and 14 days following the initial gavage, all mice were maintained on a standard mouse chow which we refer to as a fiber-rich (FR) diet. Afterwards, half of the mice were switched randomly to a fiber-free (FF) diet, while the rest were maintained on the FR diet. Instead of dietary fibers from plant sources, the FF contains increased glucose levels (*5*). Mice were monitored closely until one of the groups developed symptoms. Mice were euthanized by CO2 asphyxiation followed by cervical dislocation. Colons were excised and stored in Methacarn fixative for mucus thickness measurements. Cecal contents were flash frozen before being stored at −80°C for subsequent SCFA measurements.

Animal diets.

The fiber-rich diet was a standard, autoclaved rodent chow (LabDiet, St. Louis, MO, USA; catalog no. 5013). The fiber-free diet was TD.140343 (Envigo, Indianapolis, IN, USA) diet formulation, a modified version of the Harlan.TD08810 diet (Envigo, Indianapolis, IN, USA) described previously (*5*). The fiber-free diet lacks dietary fiber, which has been compensated by an increased glucose content; note that this diet also contains crystalline cellulose, although it cannot be degraded by any member of the SMs.

DNA extraction

DNA was extracted by phenol-chloroform extraction, followed by the purification using a DNeasy Blood and Tissue Kit (Qiagen, USA) according to the following protocol:
Samples were put in screw-cap tubes and ~250 µl glass beads (Sigma G1277, acid washed 212-300 µl), 500 µl of Buffer A (200mM NaCl, 200 mM Tris, 200mM EDTA), 210 µl of 20% SDS and 500 µl of Phenol:Chloroform (1:1). The mixture was then bead beaten for 2 minutes at room temperature. The samples were then centrifuged for 3 minutes at 18000 rcf at 4°C and the aqueous phase was recovered. 500 µl Phenol: Chloroform (1:1) were added to the recovered sample and mixed by inversion. The samples were then centrifuged once more centrifuged for 3 minutes at 18000 rcf at 4°C and the aqueous phase was recovered. A final time 500 µl Phenol: Chloroform (1:1) were added to the recovered sample and mixed by inversion. The samples were centrifuged a third time for 3 minutes at 18000 rcf at 4°C and the aqueous phase was recovered. 1/10 volume of 3 M sodium acetate and 1 volume of isopropanol were added to the recovered phase and mixed by inversion. Next, the samples were placed for 20 minutes at -80°C in order to precipitate the DNA. In order to recover the DNA the samples were centrifuged at 4°C for 20 minutes at maximum speed and the pellet was recovered. The pellet was washed using 1ml of room temperature 70% ethanol. To recover the pellet the sample was centrifuged for 3 minutes at max speed at room temperature. The supernatant was removed and the pellet dried for ~1 hour. Next, the pellet was resuspended in 100 µl ddH2O and further purified by using the DNeasy Blood & Tissue Kit (QIAGEN, USA) according to manufacturer's instruction.

16S sequencing and data analysis

The V4 region of the 16S rRNA gene was analyzed and library preparation was performed by the University of Michigan Microbial Systems Molecular Biology Lab as described previously by Kozich et al. (*18*). Raw sequences were analysed using Mothur (*19*) as described previously (*5*) and based on the MiSeq SOP (*18*). Analysis sequences were aligned to a custom database including only the 14 bacteria found in the 14SM. To screen for contamination, samples were also aligned to the SILVA database (*20*).

Lipocalin ELISA

Samples for the lipocalin enzyme-linked immunosorbent assay (ELISA) were prepared as described previously (4) and measured using the mouse lipocalin-2/NGAL DuoSet ELISA R&D system (Bio-Techne, Minneapolis, MN, USA; catalog no. DY1857) according to the manufacturer's instructions.

Mucus measurements

The slides were deparaffinized by submerging the slides in xylene (Sigma-Aldrich, USA) for five minutes, followed by another xylene incubation for five minutes. Afterward, the slides were dehydrated twice in 100% ethanol for 5 minutes. The slides were then quickly washed in Milli-Q water and antigens were retrieved by submerging in antigen retrieving solution (10 mM sodium citrate, pH 6.0). The submerged sections were heated to 90°C for 10 minutes and cooldown in room temperature for 20 minutes. Slides were quickly dipped three times in Milli-Q water and blotted to remove excess liquid. To better hold liquid, a PAP pen was used to draw around the tissue area for the subsequent steps. The sections were blocked by covering the tissue in blocking buffer (1:10 goat serum (Sigma, USA) in Tris-buffered saline (TBS; 500 mM NaCl, 50 mM Tris, pH 7.4) and incubated for an hour at room temperature. For the primary antibody staining, the tissue was covered with a 1:200 dilution of Mucin 2 antibody (H-300) (Santa Cruz Biotechnology, USA) in blocking buffer and incubated for two hours at room temperature. Following the incubation, the slides were rinsed three times in TBS, for five minutes each. The secondary antibody staining was performed by covering the tissue with a 1:200 dilution of Alexa Fluor 488 conjugated goat anti-rabbit IgG antibody (Thermo Fisher Scientific, USA) in blocking buffer for one hour at room temperature in dark. The tissue sections were washed twice in TBS for 5 minutes, gently blotted, and covered with ProLong Gold Antifade reagent with DAPI (Invitrogen, USA), covered with cover slips and sealed with nail polish. The slides were kept at room temperature for 24 hours in dark and then kept in 4°C until imaging. The mucus layer in the sections were visualized using a Zeiss Apotome by taking pictures across fecal pellets and stitching the images together to compose a single image. Mucus layer measurements were performed by using BacSpace as described by previously (*21*).

Statistical analyses.

Statistical analysis was performed using Microsoft Excel. (Microsoft, Washington, USA). Statistical significances are represented by asterisks as follows: *, $P < 0.05$; **, $P < 0.01$; ***, $P < 0.001$; and ****, $P < 0.0001$. Unless otherwise specified in the figure legend, for normal distributed values, unpaired two-tailed t tests were used, while for non-normal distributed values, a Mann-Whitney test was used. The specific test and the number of animals used for each experiment are detailed in the figure legends.

Bibiology

1. Y. Shan, M. Lee, E. B. Chang, The Gut Microbiome and Inflammatory Bowel Diseases. *Annu. Rev. Med.* (2022), doi:10.1146/annurev-med-042320-021020.
2. I. Loddo, C. Romano, Inflammatory bowel disease: Genetics, epigenetics, and pathogenesis. *Front. Immunol.* (2015), , doi:10.3389/fimmu.2015.00551.
3. D. P. Venegas, M. K. De La Fuente, G. Landskron, M. J. González, R. Quera, G. Dijkstra, H. J. M. Harmsen, K. N. Faber, M. A. Hermoso, Short chain fatty acids (SCFAs)mediated gut epithelial and immune regulation and its relevance for inflammatory bowel diseases. *Front. Immunol.* (2019), , doi:10.3389/fimmu.2019.00277.
4. A. Levine, R. Sigall Boneh, E. Wine, Evolving role of diet in the pathogenesis and treatment of inflammatory bowel diseases. *Gut* (2018), doi:10.1136/gutjnl-2017-315866.
5. M. S. Desai, A. M. Seekatz, N. M. Koropatkin, N. Kamada, C. A. Hickey, M. Wolter, N. A. Pudlo, S. Kitamoto, N. Terrapon, A. Muller, V. B. Young, B. Henrissat, P. Wilmes, T. S. Stappenbeck, G. Núñez, E. C. Martens, A Dietary Fiber-Deprived Gut Microbiota Degrades the Colonic Mucus Barrier and Enhances Pathogen Susceptibility. *Cell*. **167**, 1339-1353.e21 (2016).
6. B. O. Schroeder, G. M. H. Birchenough, M. Ståhlman, L. Arike, M. E. V. Johansson, G. C. Hansson, F. Bäckhed, Bifidobacteria or Fiber Protects against Diet-Induced Microbiota-Mediated Colonic Mucus Deterioration. *Cell Host Microbe*. **23**, 27-40.e7 (2018).
7. E. S. Wills, D. M. A. E. Jonkers, P. H. Savelkoul, A. A. Masclee, M. J. Pierik, J. Penders, Fecal microbial composition of ulcerative colitis and Crohn's disease patients in remission and subsequent exacerbation. *PLoS One* (2014), doi:10.1371/journal.pone.0090981.
8. S. Khan, S. Waliullah, V. Godfrey, M. A. W. Khan, R. A. Ramachandran, B. L. Cantarel, C. Behrendt, L. Peng, L. V. Hooper, H. Zaki, Dietary simple sugars alter microbial ecology in the gut and promote colitis in mice. *Sci. Transl. Med.* (2020), doi:10.1126/scitranslmed.aay6218.
9. S. Van Der Post, K. S. Jabbar, G. Birchenough, L. Arike, N. Akhtar, H. Sjovall, M. E. V. Johansson, G. C. Hansson, Structural weakening of the colonic mucus barrier is an early event in ulcerative colitis pathogenesis. *Gut* (2019), doi:10.1136/gutjnl-2018-317571.
10. A. Steimle, A. De Sciscio, M. Neumann, E. T. Grant, G. V. Pereira, H. Ohno, E. C. Martens, M. S. Desai, Constructing a gnotobiotic mouse model with a synthetic human gut microbiome to study host–microbe cross talk. *STAR Protoc.* **2**, 100607 (2021).
11. R. K. Sellon, S. Tonkonogy, M. Schultz, L. A. Dieleman, W. Grenther, E. Balish, D. M. Rennick, R. B. Sartor, Resident enteric bacteria are necessary for development of spontaneous colitis and immune system activation in interleukin-10-deficient mice. *Infect. Immun.* (1998), doi:10.1128/iai.66.11.5224-5231.1998.
12. L. M. Keubler, M. Buettner, C. Häger, A. Bleich, A multihit model: Colitis lessons from the

interleukin-10-deficient mouse. *Inflamm. Bowel Dis.* (2015), , doi:10.1097/MIB.0000000000000468.

13. B. Chassaing, G. Srinivasan, M. A. Delgado, A. N. Young, A. T. Gewirtz, M. Vijay-Kumar, Fecal Lipocalin 2, a Sensitive and Broadly Dynamic Non-Invasive Biomarker for Intestinal Inflammation. *PLoS One*. **7**, e44328 (2012).
14. E. E. Blaak, E. E. Canfora, S. Theis, G. Frost, A. K. Groen, G. Mithieux, A. Nauta, K. Scott, B. Stahl, J. van Harsselaar, R. van Tol, E. E. Vaughan, K. Verbeke, Short chain fatty acids in human gut and metabolic health. *Benef. Microbes* (2020), , doi:10.3920/BM2020.0057.
15. P. M. Smith, M. R. Howitt, N. Panikov, M. Michaud, C. A. Gallini, M. Bohlooly-Y, J. N. Glickman, W. S. Garrett, The microbial metabolites, short-chain fatty acids, regulate colonic T reg cell homeostasis. *Science (80-.).* (2013), doi:10.1126/science.1241165.
16. G. M. Birchenough, E. E. Nystrom, M. E. Johansson, G. C. Hansson, A sentinel goblet cell guards the colonic crypt by triggering Nlrp6-dependent Muc2 secretion. *Science (80-.).* **352**, 1535–1542 (2016).
17. European Food Safety Authority, Scientific Opinion on Dietary Reference Values for carbohydrates and dietary fibre. *EFSA J.* **8**, 1–77 (2010).
18. J. J. Kozich, S. L. Westcott, N. T. Baxter, S. K. Highlander, P. D. Schloss, Development of a Dual-Index Sequencing Strategy and Curation Pipeline for Analyzing Amplicon Sequence Data on the MiSeq Illumina Sequencing Platform. *Appl. Environ. Microbiol.* **79**, 5112–5120 (2013).
19. P. D. Schloss, S. L. Westcott, T. Ryabin, J. R. Hall, M. Hartmann, E. B. Hollister, R. A. Lesniewski, B. B. Oakley, D. H. Parks, C. J. Robinson, J. W. Sahl, B. Stres, G. G. Thallinger, D. J. Van Horn, C. F. Weber, Introducing mothur: Open-source, platform-independent, community-supported software for describing and comparing microbial communities. *Appl. Environ. Microbiol.* (2009), doi:10.1128/AEM.01541-09.
20. G. Kim, J. Bae, M. J. Kim, H. Kwon, G. Park, S. J. Kim, Y. H. Choe, J. Kim, S. H. Park, B. H. Choe, H. Shin, B. Kang, T. Magoč, S. L. Salzberg, C. Quast, E. Pruesse, P. Yilmaz, J. Gerken, T. Schweer, P. Yarza, J. Peplies, F. O. Glöckner, S. Trachtenberg, M. Reyman, M. A. van Houten, D. van Baarle, A. A. T. M. Bosch, W. H. Man, M. L. J. N. Chu, K. Arp, R. L. Watson, E. A. M. Sanders, S. Fuentes, D. Bogaert, A. Ramírez-Guzmán, Y. Taran, M. A. Armienta, The SILVA ribosomal RNA gene database project: Improved data processing and web-based tools. *Nucleic Acids Res.* (2019).
21. K. A. Earle, G. Billings, M. Sigal, J. S. Lichtman, G. C. Hansson, J. E. Elias, M. R. Amieva, K. C. Huang, J. L. Sonnenburg, Quantitative Imaging of Gut Microbiota Spatial Organization. *Cell Host Microbe* (2015), doi:10.1016/j.chom.2015.09.002.

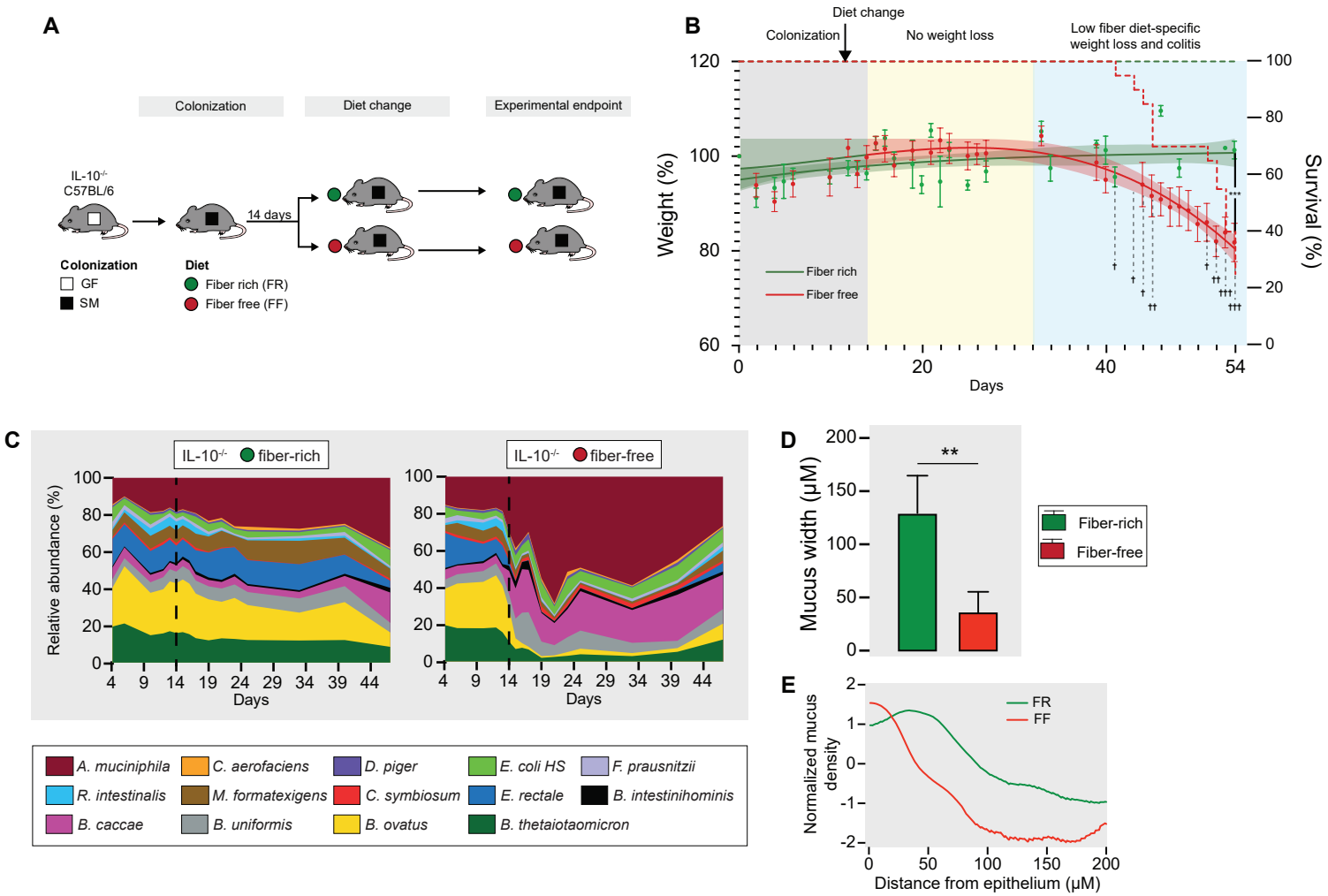

Figure 1. Dietary fiber-deprivation in a genetically susceptible host leads to lethal colitis. (A) Experimental timeline. Germ-free IL-10$^{-/-}$ mice were gavaged with the synthetic 14-member gut microbiota (14SM) on three consecutive days. These colonized mice were maintained for 14 days on the fiber-rich (FR) diet after which half of the mice were switched to a fiber-free (FF) diet. Mice were then observed for up to 54 days. (B) Weight loss (unbroken line) and survival curve (dotted line) of the 14SM colonized IL-10$^{-/-}$ mice. Error bars represent SEM; highlighted areas around the curves represent the 95% confidence interval; unpaired, two-tailed t-test; christian crosses represent the death of a mouse in the FF group; ***p<0.001. (C) Relative bacterial abundance throughout the experiment as determined by 16S gene sequencing on DNA extracted from fecal pellets. Dotted lines represent the day the FF group was put on the FF diet. (D) Mucus layer thickness determined by analysis of immunofluorescently stained colonic sections and quantified using BacSpace. Error bars represent SEM; unpaired, two-tailed t-test; **p<0.01. (E) Normalized mucus density versus distance from the epithelium determined by analysis of immunofluorescently stained colonic sections and quantified using BacSpace. For normalization, curves are mean-subtracted and divided by the standard deviation.

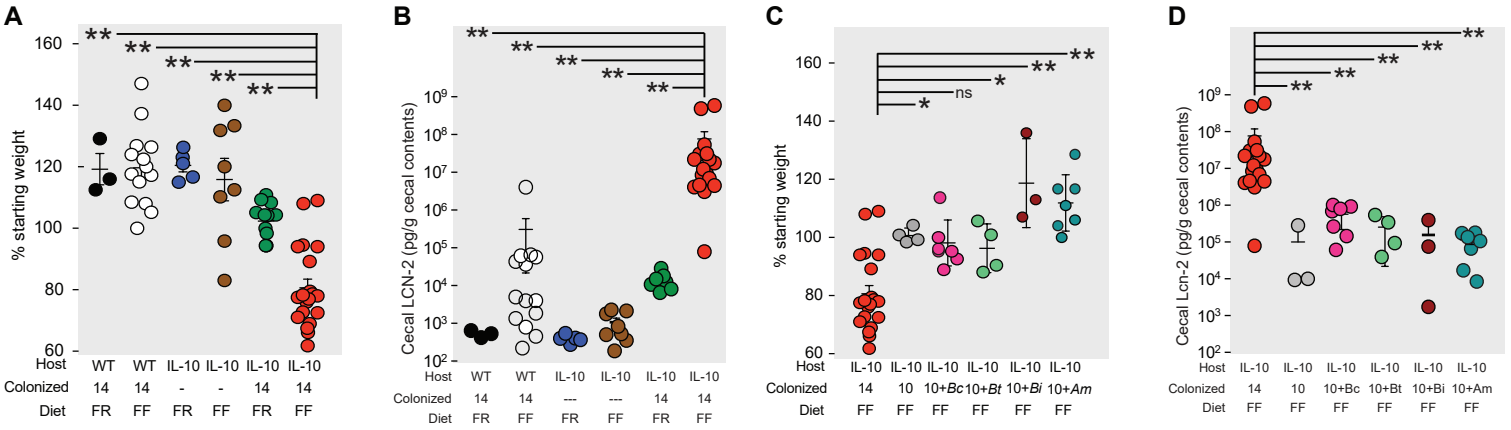

Figure 2. Development of spontaneous colitis is dependent on interaction of diet, genotype and mucolytic gut bacteria. (A) Final weights of 14SM colonized wild-type (WT) mice, germ-free IL-10$^{-/-}$ mice, and 14SM colonized L-10$^{-/-}$ mice on the FR or FF diet. Error bars represent SEM; unpaired, two-tailed t-tests. (B) Final cecal lipocalin-2 (LCN-2) levels of 14SM colonized wild-type (WT) mice, germ-free IL-10$^{-/-}$ mice, and 14SM colonized L-10$^{-/-}$ mice on the FR or FF diet. Error bars represent SEM; unpaired, two-tailed t-tests. (C) Final weights of colonized IL-10$^{-/-}$ mice on the FF diet. The group labelled as colonized with "10", hosts none of the 4 mucus degrading bacteria *Bacteroidetes caccae* (*Bc*), *Bacteroidetes thetaiotaomicron* (*Bt*), *Barnesiella intestinihominis* (*Bi*) and *Akkermansia muciniphila* (*Am*). Error bars represent SEM; unpaired, two-tailed t-tests. (D) Final cecal LCN-2 levels of colonized IL-10$^{-/-}$ mice on the FF diet. The group labelled as colonized with 10 hosts none of the 4 mucus degrading bacteria *B. caccae* (*Bc*), *B. thetaiotaomicron* (*Bt*), *B. intestinihominis* (*Bi*) and *A. muciniphila* (*Am*). Error bars represent SEM; unpaired, two-tailed t-tests. ns, non-significant; *p<0.05; **p<0.01.

7. Conclusion and perspective

The purpose of this thesis was to explore how the excessive degradation of the colonic mucus layer can affect susceptibility to different types of diseases. Most commonly the gut mucus layer's importance is studied using Muc2$^{-/-}$ models. However, the genetic ablation of the predominant gut mucus glycoprotein does not fully reflect the reality of how the mucus layer is eroded. By their nature, these models are limited to MUC2 glycoproteins and do not affect the other types of mucin. Furthermore, the mucin production is completely ablated in knockout models contrasting the natural degradation of the mucus layer by the gut microbiome. Here, we leveraged the fact that, in the 14SM gnotobiotic mouse model, dietary fiber-deprivation leads to an excessive degradation of the gut mucus layer. This results in a model which is far more reflective of the natural erosion of the mucus layer. However, it must be noted that the dietary fiber-deprived mice are characterized by an increased weight gain compared to Muc2$^{-/-}$ and wild type mice, a potentially important point to consider for certain disease models. The data presented in this thesis highlights how important it is to understand the complex diet-microbiome-host interactions, as depending on the context the susceptibility to the different diseases was completely different.

In the first chapters we focused on different enteric pathogens. Starting with **Chapter 3**, where we leveraged the ability to drop out different bacteria from our synthetic microbiota to show which strain is responsible for promoting the increased *C. rodentium* susceptibility observed under fiber free diet-induced mucus erosion. We showed how *A. muciniphila* alone is able to drive this phenotype, most likely by an excessive erosion of the protective gut mucus layer. *C. rodentium* needs to bypass the gut mucus layer in order to infect the host. Therefore,

the excessive erosion of the mucus layer in the presence of *A. muciniphila* seems to increase pathogen susceptibility by facilitating *C. rodentium* access to the host tissue. Neither host response nor *C. rodentium* transcriptome were able to uncover further underlying causes for the increased pathogen susceptibility. However, other alternative explanations can not be fully excluded and mechanisms such as as altered nutrient competition or cross-feeding with or without *A. muciniphila* should be explored in the future.

In **Chapter 4**, we explored how intracellular pathogens would be affected by an excessive degradation of the gut mucus layer. We were able to show that the natural erosion of the gut mucus layer had no visible impact on the susceptibility towards either *L. monocytogenes* or *S*. Typhimurium. Instead, our germ-free controls showed that the fiber-free diet itself was the major factor determining the outcome of the infection, with mice on the fiber-free diet surprisingly being more resistant to the infection. Intuitively, it might not surprising that an intracellular pathogen might be less affected by the gut mucus layer, however, our observation contrasts previously published results using Muc2$^{-/-}$ mice [1, 2]. The question remains whether the microbial erosion of the colonic mucus layer is insufficient to reproduce the effects observed in Muc2$^{-/-}$ mice or if the direct diet effects observed dominate the impact of the mucus layer. Reports on the impact of dietary fiber on *S*. Typhimurium and *L. monocytogenes* susceptibility vary with some types of fiber increasing pathogen susceptibility—similarly to our observation— [3–5] while others seem to decrease susceptibility [3]. This shows the importance of not equating every type of dietary fiber and highlights the need to further investigate how exactly these different fibers are metabolized by the gut microbiome.

In **Chapter 5**, we were able to similarly demonstrate that in contrast to Muc2$^{-/-}$ mice [6], a natural, microbial erosion of the mucus layer does not lead to a delayed *T. muris* clearance. Our work supports a model in which increased microbial activity promotes a Th2-driven worm clearance. In contrast, a balanced fiber and mucin degradation leads to an IFN-γ driven Th1 response resulting in a chronic infec-

tion. This observation is in accordance to the work of Myhill et al. [7], who showed that a high fiber diet containing inulin similarly shifts the immune response from a Th2 response to an IFN-γ driven Th1 response resulting in a chronic *T. muris* infection. Furthermore, the presence of the nematode had a major impact on the gut microbiome, with the microbial abundances seemingly shifting in correlation with the worm's larval stages. While there are numerous reports showing that *T. muris* alters the host's gut microbiota composition [7–12], our longitudinal characterization of a defined gut microbiota lets us infer functional changes resulting from the altered microbiota composition. We observed, that the microbiota shifts in resistant mice around the worm larval stages L3-L4 were characterized by an increased abundance of mucin generalist bacteria which appears to increase the overall mucolytic activity of the gut microbiome. Overall, our results let us suggest several mechanisms through which the excessive mucin foraging could potentially alter the host immune response such as mast cell activation [13] or modulation of the host's mucin glycosylation [14].

In **Chapter 6**, we shifted our focus from infectious to autoimmune diseases. Using the IL-10$^{-/-}$ mice which are a model for IBD, we demonstrate that an excessive erosion of the gut mucus layer in a genetically susceptible host results in spontaneous colitis without the need for any additional triggers. We show that this effect is not dependent on specific taxa, but that the capability of a species to degrade mucin seems to be sufficient to induce light colitis. Furthermore, this effect seems to stack additively as lethal colitis was only triggered in the presence of multiple mucolytic strains. As I have discussed in the section "Leveraging diet to engineer our gut microbiome" of my introduction, diet is a widely debated topic in the context of autoimmune diseases and particularly diet-microbiome interactions have been shifted into focus recently. Here, we demonstrated that dietary-fiber deprivation by itself was capable of triggering a severe autoimmune disease such as IBD in a genetically susceptible host. This observation is particularly interesting considering that IBD is on the rise in industrialized countries in which people

are known to generally consume less than the daily recommended amount of dietary fibers [15].

Overall, we were able to demonstrate that the mucolytic portion of the gut microbiota plays an essential role in modulating disease susceptibility to both infectious and autoimmune diseases. We show that the role of the microbial erosion of the gut mucus layer is highly dependent on the disease context as it can be either beneficial (*T. muris* model), negative (*C. rodentium* & IL-10$^{-/-}$ models) or irrelevant (*L. monocytogenes* & *S*. Typhimirum models). However, we also have to note the potential limitations of this work. First of all, while we tried to control as much as possible for direct diet effects, their effects still have to be considered. We mainly focused on the role of dietary fiber-deprivation in inducing a microbial erosion of the mucus layer, but it must be noted that the effect of low fibers might change the overall microbiome-host dynamics, independent of the mucus layer [16]. Furthermore, our fiber-free diet did contain increased amounts of glucose compared to the fiber-rich diet which could also affect the aforementioned dynamics and the disease susceptibility [17–20]. Additionally, working in a gnotobiotic model has the inherent risk to miss specific microbiota-pathogen or microbiota-host interactions due to the limited microbial community. However, strong similarities between our work and comparable studies using complex gut communities should alleviate most of these concerns [3, 7, 20, 21]. Even given these limitations, our work provides valuable insight in diet-microbiome-mucin interactions in the context of both infectious and autoimmune disease. Considering that dietary fiber consumption is overall high in developing countries, it is particularly interesting that *L. monocytogenes*, *S.* Typhimurium and *T. muris*, diseases generally more prevalent in these countries [22, 23], clear the infection more efficiently during fiber-deprivation. This could have important implications for the diet-supported treatment of these diseases. Similarly IBD was resisted by mice fed a diet rich on fiber, while the disease is on the rise in industrialized countries [24] where people generally eat less than the recommended daily value of fiber [15]. While many questions concerning the detailed mechanisms remain, we generated important

prerequisite knowledge for clinical settings in order to develop new or improve existing treatment strategies and in order to improve prevention strategies. Furthermore, our mechanistic insights might prove invaluable for the development of personalized treatments.

Bibliography

[1] Zhang T, Sasabe J, Hullahalli K, Sit B, Waldor MK. 2021. Increased listeria monocytogenes dissemination and altered population dynamics in Muc2-deficient mice. Infect Immun 89:e00667-20.

[2] Zarepour M, Bhullar K, Montero M, Ma C, Huang T, Velcich A, Xia L, Vallance BA. 2013. The mucin muc2 limits pathogen burdens and epithelial barrier dysfunction during salmonella enterica serovar typhimurium colitis. Infect Immun 81:3672–3683.

[3] Ebersbach T, Jørgensen JB, Heegaard PM, Lahtinen SJ, Ouwehand AC, Poulsen M, Frøkiær H, Licht TR. 2010. Certain dietary carbohydrates promote Listeria infection in a guinea pig model, while others prevent it. Int J Food Microbiol 140:218–224.

[4] Wotzka SY, Kreuzer M, Maier L, Arnoldini M, Nguyen BD, Brachmann AO, Berthold DL, Zünd M, Hausmann A, Bakkeren E, Hoces D, Gül E, Beutler M, Dolowschiak T, Zimmermann M, Fuhrer T, Moor K, Sauer U, Typas A, Piel J, Diard M, Macpherson AJ, Stecher B, Sunagawa S, Slack E, Hardt WD. 2019. Escherichia coli limits Salmonella Typhimurium infections after diet shifts and fat-mediated microbiota perturbation in mice. Nat Microbiol 4:2164–2174.

[5] Petersen A, Heegaard PMH, Pedersen AL, Andersen JB, Sørensen RB, Frøkiær H, Lahtinen SJ, Ouwehand AC, Poulsen M, Licht TR. 2009. Some putative prebiotics increase the severity of Salmonella enterica serovar Typhimurium infection in mice. BMC Microbiol 9:245.

[6] Hasnain SZ, Wang H, Ghia JE, Haq N, Deng Y, Velcich A, Grencis RK, Thornton DJ, Khan WI. 2010. Mucin Gene Deficiency in Mice Impairs Host Resistance to an Enteric Parasitic Infection. Gastroenterology 138:1763-1771.e5.

[7] Myhill LJ, Stolzenbach S, Mejer H, Jakobsen SR, Hansen TVA, Andersen D, Brix S, Hansen LH, Krych L, Nielsen DS, Nejsum P, Thamsborg SM, Williams AR. 2020. Fermentable Dietary Fiber Promotes Helminth Infection and Exacerbates Host Inflammatory Responses. J Immunol 204:3042–3055.

[8] Li RW, Wu S, Li W, Navarro K, Couch RD, Hill D, Urban JF. 2012. Alterations in the porcine colon microbiota induced by the gastrointestinal nematode Trichuris suis. Infect Immun https://doi.org/10.1128/IAI.00141-12.

[9] Broadhurst MJ, Ardeshir A, Kanwar B, Mirpuri J, Gundra UM, Leung JM, Wiens KE, Vujkovic-Cvijin I, Kim CC, Yarovinsky F, Lerche NW, McCune JM, Loke P. 2012. Therapeutic Helminth Infection of Macaques with Idiopathic Chronic Diarrhea Alters the Inflammatory Signature and Mucosal Microbiota of the Colon. PLoS Pathog https://doi.org/10.1371/journal.ppat.1003000.

[10] Holm JB, Sorobetea D, Kiilerich P, Ramayo-Caldas Y, Estellé J, Ma T, Madsen L, Kristiansen K, Svensson-Frej M. 2015. Chronic Trichuris muris infection decreases diversity of the intestinal microbiota and concomitantly increases the abundance of lactobacilli. PLoS One https://doi.org/10.1371/journal.pone.0125495.

[11] Rosa BA, Snowden C, Martin J, Fischer K, Kupritz J, Beshah E, Supali T, Gankpala L, Fischer PU, Urban JF, Mitreva M. 2021. Whipworm-Associated Intestinal Microbiome Members Consistent Across Both Human and Mouse Hosts. Front Cell Infect Microbiol https://doi.org/10.3389/fcimb.2021.637570.

[12] Houlden A, Hayes KS, Bancroft AJ, Worthington JJ, Wang P, Grencis RK, Roberts IS. 2015. Chronic Trichuris muris infection in C57BL/6 mice causes significant changes in host microbiota and metabolome: Effects reversed by pathogen clearance. PLoS One https://doi.org/10.1371/journal.pone.0125945.

[13] White EC, Houlden A, Bancroft AJ, Hayes KS, Goldrick M, Grencis RK, Roberts IS. 2018. Manipulation of host and parasite microbiotas: Survival strategies during chronic nematode infection. Sci Adv https://doi.org/10.1126/sciadv.aap7399.

[14] Hasnain SZ, Dawson PA, Lourie R, Hutson P, Tong H, Grencis RK, McGuckin MA, Thornton DJ. 2017. Immune-driven alterations in mucin sulphation is an important mediator of Trichuris muris helminth expulsion. PLoS Pathog https://doi.org/10.1371/journal.ppat.1006218.

[15] European Food Safety Authority. 2010. Scientific Opinion on Dietary Reference Values for carbohydrates and dietary fibre. EFSA J 8:1–77.

[16] Bachem A, Makhlouf C, Binger KJ, de Souza DP, Tull D, Hochheiser K, Whitney PG, Fernandez-Ruiz D, Dähling S, Kastenmüller W, Jönsson J, Gressier E, Lew AM, Perdomo C, Kupz A, Figgett W, Mackay F, Oleshansky M, Russ BE, Parish IA, Kallies A, McConville MJ, Turner SJ, Gebhardt T, Bedoui S. 2019. Microbiota-Derived Short-Chain Fatty Acids Promote the Memory Potential of Antigen-Activated CD8+ T Cells. Immunity https://doi.org/10.1016/j.immuni.2019.06.002.

[17] Jimenez AG, Ellermann M, Abbott W, Sperandio V. 2020. Diet-derived galacturonic acid regulates virulence and intestinal colonization in enterohaemorrhagic Escherichia coli and Citrobacter rodentium. Nat Microbiol https://doi.org/10.1038/s41564-019-0641-0.

[18] Henke MT, Kenny DJ, Cassilly CD, Vlamakis H, Xavier RJ, Clardy J. 2019. Ruminococcus gnavus, a member of the human gut microbiome associated with Crohn's disease, produces an inflammatory polysaccharide. Proc Natl Acad Sci U S A https://doi.org/10.1073/pnas.1904099116.

[19] Zhang S, Wang M, Wang X, Li H, Tang H, Li X. 2019. Salmonella infection leads to severe intestinal inflammation and increased CD4+FoxP3+ Treg cells in streptozotocin-induced hyperglycemic mice. Mol Med Rep https://doi.org/10.3892/mmr.2019.10195.

[20] Khan S, Waliullah S, Godfrey V, Khan MAW, Ramachandran RA, Cantarel BL, Behrendt C, Peng L, Hooper L V., Zaki H. 2020. Dietary simple sugars alter microbial ecology in the gut and promote colitis in mice. Sci Transl Med https://doi.org/10.1126/scitranslmed.aay6218.

[21] Neumann M, Steimle A, Grant ET, Wolter M, Parrish A, Willieme S, Brenner D, Martens EC, Desai MS. 2021. Deprivation of dietary fiber in specific-pathogen-free mice promotes susceptibility to the intestinal mucosal pathogen Citrobacter rodentium. Gut Microbes 13.

[22] WHO. 2015. World Health Organization. WHO Estimates of the Global Burden of Foodborne Diseases: Foodborne Disease Burden Epidemiology Reference Group 2007-2015. Encycl Parasitol.

[23] Pullan RL, Smith JL, Jasrasaria R, Brooker SJ. 2014. Global numbers of infection and disease burden of soil transmitted helminth infections in 2010. Parasites and Vectors 7:37.

[24] Alatab S, Sepanlou SG, Ikuta K, Vahedi H, Bisignano C, Safiri S, Sadeghi A, Nixon MR, Abdoli A, Abolhassani H, Alipour V, Almadi MAH, Almasi-Hashiani A, Anushiravani A, Arabloo J, Atique S, Awasthi A, Badawi A, Baig AAA, Bhala N, Bijani A, Biondi A, Borzì AM, Burke KE, Carvalho F, Daryani A, Dubey M, Eftekhari A, Fernandes E, Fernandes JC, Fischer F, Haj-Mirzaian A, Haj-Mirzaian A, Hasanzadeh A, Hashemian M, Hay SI, Hoang CL, Househ M, Ilesanmi OS, Balalami NJ, James SL, Kengne AP, Malekzadeh MM, Merat S, Meretoja TJ, Mestrovic T, Mirrakhimov EM, Mirzaei H, Mohammad KA, Mokdad AH, Monasta L, Negoi I, Nguyen TH, Nguyen CT, Pourshams A, Poustchi H, Rabiee M, Rabiee N, Ramezanzadeh K, Rawaf DL, Rawaf S, Rezaei N, Robinson SR, Ronfani L, Saxena S, Sepehrimanesh M, Shaikh MA, Sharafi Z, Sharif M, Siabani S, Sima AR, Singh JA, Soheili A, Sotoudehmanesh R, Suleria HAR, Tesfay BE, Tran B, Tsoi D, Vacante M, Wondmieneh AB, Zarghi A, Zhang ZJ, Dirac M, Malekzadeh R, Naghavi M. 2020. The global, regional, and national burden of inflammatory bowel disease in 195 countries and territories, 1990–2017: a systematic analysis for the Global Burden of Disease Study 2017. Lancet Gastroenterol Hepatol https://doi.org/10.1016/S2468-1253(19)30333-4.

8. Appendix

Below are the following publications to which I only contributed minorly.

— A Dietary Fiber-Deprived Gut Microbiota Degrades the Colonic Mucus Barrier and Enhances Pathogen Susceptibility, published in Cell.

— Deprivation of dietary fiber in specific-pathogen-free mice promotes susceptibility to the intestinal mucosal pathogen *Citrobacter rodentium*, published in Gut Microbes.

— *Akkermansia muciniphila* and *Parabacteroides distasonis* synergistically protect from colitis by enhancing the gut immunity, submitted to Gut.

Article

Cell

A Dietary Fiber-Deprived Gut Microbiota Degrades the Colonic Mucus Barrier and Enhances Pathogen Susceptibility

Graphical Abstract

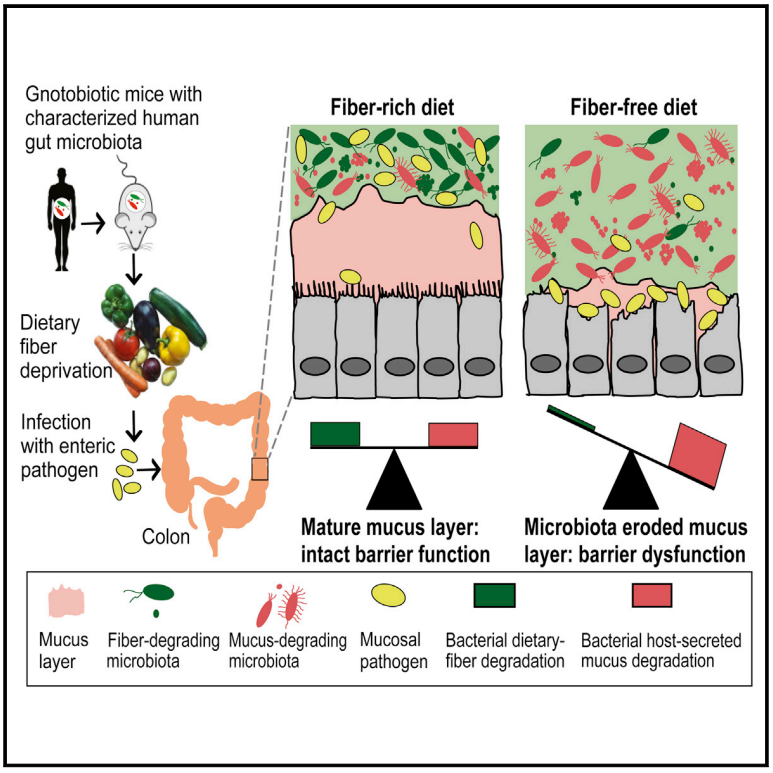

Authors

Mahesh S. Desai, Anna M. Seekatz, Nicole M. Koropatkin, ..., Thaddeus S. Stappenbeck, Gabriel Núñez, Eric C. Martens

Correspondence

mahesh.desai@lih.lu (M.S.D.), emartens@umich.edu (E.C.M.)

In Brief

Regular consumption of dietary fiber helps prevent erosion of the intestinal mucus barrier by the gut microbiome, blunting pathogen infection and reducing the incidence of colitis.

Highlights

- Characterized synthetic bacterial communities enable functional insights in vivo
- Low-fiber diet promotes expansion and activity of colonic mucus-degrading bacteria
- Purified prebiotic fibers do not alleviate degradation of the mucus layer
- Fiber-deprived gut microbiota promotes aggressive colitis by an enteric pathogen

Desai et al., 2016, Cell *167*, 1339–1353
November 17, 2016
http://dx.doi.org/10.1016/j.cell.2016.10.043

CellPress

Article

Cell

A Dietary Fiber-Deprived Gut Microbiota Degrades the Colonic Mucus Barrier and Enhances Pathogen Susceptibility

Mahesh S. Desai,[1,2,3,7,*] Anna M. Seekatz,[2] Nicole M. Koropatkin,[2] Nobuhiko Kamada,[2] Christina A. Hickey,[4] Mathis Wolter,[3] Nicholas A. Pudlo,[2] Sho Kitamoto,[2] Nicolas Terrapon,[5] Arnaud Muller,[6] Vincent B. Young,[2] Bernard Henrissat,[5] Paul Wilmes,[1] Thaddeus S. Stappenbeck,[4] Gabriel Núñez,[2] and Eric C. Martens[2,8,*]

[1]Luxembourg Centre for Systems Biomedicine, Esch-sur-Alzette 4362, Luxembourg
[2]University of Michigan Medical School, Ann Arbor, MI 48109, USA
[3]Department of Infection and Immunity, Luxembourg Institute of Health, Esch-sur-Alzette 4354, Luxembourg
[4]Washington University School of Medicine, St. Louis, MO 63110, USA
[5]Aix-Marseille Université, UMR 7257, 13288 Marseille, France
[6]Department of Oncology, Luxembourg Institute of Health, Luxembourg 1526, Luxembourg
[7]Present address: Department of Infection and Immunity, Luxembourg Institute of Health, Esch-sur-Alzette 4354, Luxembourg
[8]Lead Contact
*Correspondence: mahesh.desai@lih.lu (M.S.D.), emartens@umich.edu (E.C.M.)
http://dx.doi.org/10.1016/j.cell.2016.10.043

SUMMARY

Despite the accepted health benefits of consuming dietary fiber, little is known about the mechanisms by which fiber deprivation impacts the gut microbiota and alters disease risk. Using a gnotobiotic mouse model, in which animals were colonized with a synthetic human gut microbiota composed of fully sequenced commensal bacteria, we elucidated the functional interactions between dietary fiber, the gut microbiota, and the colonic mucus barrier, which serves as a primary defense against enteric pathogens. We show that during chronic or intermittent dietary fiber deficiency, the gut microbiota resorts to host-secreted mucus glycoproteins as a nutrient source, leading to erosion of the colonic mucus barrier. Dietary fiber deprivation, together with a fiber-deprived, mucus-eroding microbiota, promotes greater epithelial access and lethal colitis by the mucosal pathogen, *Citrobacter rodentium*. Our work reveals intricate pathways linking diet, the gut microbiome, and intestinal barrier dysfunction, which could be exploited to improve health using dietary therapeutics.

INTRODUCTION

The diet of industrialized nations has experienced a decrease in fiber intake, which for many is now well below the recommended daily range of 28–35 g for adults, and this deficit has been linked to several diseases (Burkitt et al., 1972; Sonnenburg and Sonnenburg, 2014). Fiber provides direct physical benefits, including increased fecal bulking and laxation (Burkitt et al., 1972). However, another feature of dietary fiber—a nutrient category that includes a broad array of polysaccharides that are not digestible by human enzymes—has also drawn it into the spotlight: it provides an important substrate to the community of microbes (microbiota) that inhabits the distal gut (Sonnenburg and Sonnenburg, 2014). Unlike humans, who produce ~17 gastrointestinal enzymes to digest mostly starch, our gut microbiota produces thousands of complementary enzymes with diverse specificities, enabling them to depolymerize and ferment dietary polysaccharides into host-absorbable short-chain fatty acids (SCFAs) (El Kaoutari et al., 2013). Thus, the physiology of the gut microbiota is geared toward dietary polysaccharide metabolism. At present, relatively little is known about how a fiber-deprived gut microbiota fulfils its energy demands and how low fiber-induced microbiota changes impact our health.

Apart from dietary fiber, an alternative energy source for the microbiota is the glycoprotein-rich mucus layer that overlies the gut epithelium as a first line of defense against both commensal microbes and invading pathogens (Johansson et al., 2013; McGuckin et al., 2011). The colonic mucus layer is a dynamic and chemically complex barrier composed largely of secreted mucin-2 glycoprotein (MUC2) (Johansson et al., 2008). Goblet cells secrete MUC2 as a disulfide cross-linked network that expands to form an inner layer, which is tightly adherent to the epithelium and is poorly colonized by commensal bacteria. As bacterial and host enzymes continuously hydrolyze the luminal edge of this layer, a looser outer layer is formed that supports a more dense and metabolically distinct community (Li et al., 2015). A key nutritional aspect of the mucus layer for gut bacteria is its high polysaccharide content, with up to 80% of the mucin biomass being composed of mostly *O*-linked glycans (Johansson et al., 2013). However, only a distinct subset of gut microbiota species has evolved the capacity to utilize this nutrient source (Hoskins and Boulding, 1981; Png et al., 2010).

The direct impact of fiber polysaccharides on the microbiota, combined with the ability of at least one nutritional generalist

(*Bacteroides thetaiotaomicron*) to shift from dietary polysaccharides to mucus glycan metabolism in the absence of fiber (Sonnenburg et al., 2005), suggests a connection between diet and the status of the colonic mucus barrier. Indeed, three previous reports have correlated reduced dietary fiber with thinner colonic mucus (Brownlee et al., 2003; Earle et al., 2015; Hedemann et al., 2009). Nevertheless, the underlying mechanisms with respect to involvement of the microbiota and, perhaps more importantly, consequences for the host remain largely unknown. Such knowledge is important as it could provide explanations for why deviations or imbalances in gut microbial community membership and physiology ("dysbiosis") correlate with several negative health outcomes, including pathogen susceptibility, inflammatory bowel disease (IBD), and colon cancer (Cameron and Sperandio, 2015; Flint et al., 2012; McKenney and Pamer, 2015). Finally, such knowledge could inform therapeutic and preventative strategies to correct these conditions.

The integrity of the mucus layer is critical for health. Genetic ablation of *Muc2* in mice brings bacteria into close contact with the epithelium, leading to inflammation and colon cancer (Van der Sluis et al., 2006). Additional studies have implicated reduced or abnormal mucus production or *O*-glycosylation in the development of intestinal inflammation (Fu et al., 2011; Larsson et al., 2011) and penetration of commensal bacteria in the inner mucus layer in murine models of colitis and ulcerative colitis patients (Johansson et al., 2014). Moreover, the mucus barrier—a reservoir of antimicrobial peptides and immunoglobulins—is the first structure that a mucosal pathogen must overcome to establish an infection (McGuckin et al., 2011). Given that the status of the mucus layer is precariously balanced between replenishment by goblet cells and degradation by gut bacteria, we hypothesized that a fiber-deprived microbiota would progressively forage on this barrier, leading to inflammation and/or increased pathogen susceptibility.

We aimed to investigate the mechanistic connections between chronic or intermittent dietary fiber deprivation on microbiota composition and physiology as well as the resulting effects on the mucus barrier. To create a model that facilitates functional interpretation, we assembled a synthetic gut microbiota from fully sequenced human gut bacteria in gnotobiotic mice. In the face of reduced dietary fiber, we examined changes in community physiology and susceptibility to *Citrobacter rodentium*, a murine pathogen that models human enteric *E. coli* infection (Collins et al., 2014). We demonstrate that a microbiota deprived of dietary fiber damages the colonic mucus barrier and promotes pathogen susceptibility. Our findings suggest a mechanism through which diet alters the activity of the gut microbiota and impacts health, which is important prerequisite knowledge for rationally designing future dietary interventions and therapeutics.

RESULTS

A Synthetic Human Gut Microbiota with Versatile Fiber Polysaccharide Degrading Capacity

Diet changes are known to rapidly affect the composition of the microbiota in humans and rodents (David et al., 2014; Faith et al., 2011; McNulty et al., 2013; Rey et al., 2013). However, the full complexity of the gut microbiota is a barrier to deriving detailed conclusions because sequence-based approaches (16S rRNA gene and meta-genomics/-transcriptomics) suffer from substantial functional uncertainty. Thus, to test our hypothesis that specific members within a fiber-deprived gut microbiota cause damage by increasingly foraging for nutrients in the protective mucus layer, we designed a synthetic microbiota (SM) containing 14 species of fully sequenced commensal human gut bacteria (Figure 1A). The selected species were chosen to represent the five dominant phyla and collectively possess important core metabolic capabilities (Figure S1A).

To provide an additional layer of functional knowledge about complex carbohydrate metabolism, we pre-evaluated our 14 species for growth in vitro on a panel of 42 plant- and animal-derived mono- and polysaccharides, including purified mucin *O*-glycans (MOGs) as sole carbon sources (Martens et al., 2011). These growth assays allowed us to determine that all major groups of dietary fiber and host mucosal polysaccharides could be used by one or more strains in our community as well as which bacteria target each glycan (Figures 1A, S1A, and S1B; Table S1). It is evident that the four mucin-degrading species fall into two categories: mucin specialists (*A. muciniphila* and *B. intestinihominis*), which only grow on MOGs as a sole polysaccharide source, and mucin generalists (*B. thetaiotaomicron* and *B. caccae*), which each grow on several other polysaccharides. Overall, our choice of species is physiologically and ecologically representative of the more complex native gut microbiota. Because our community is composed of bacteria with determined carbohydrate metabolic abilities, it allows us to address our central hypothesis in more precise, mechanistic detail.

To develop a gnotobiotic model, we assembled the SM in germfree mice, which were fed a standard fiber-rich (FR) laboratory diet that contains ~15% dietary fiber from minimally processed grains and plants (Figures 1B and 1C). Colonized animals were maintained on the FR diet for 14 days to monitor reproducibility and stability of community assembly (Figure 1B). All of the introduced species persisted in each mouse between 6 and 54 or 66 days of colonization depending on the length of the experiment (n = 37 total, two independent experiments; analyzed by both 16S rRNA sequencing [Table S2] and qPCR approaches [Table S3]). Individual mice exhibited reproducible SM assembly irrespective of caging, mouse gender, experimental replicate, or method of analysis (Figure S2; Tables S2 and S3). In addition to 29 germfree control animals, a total of four different gnotobiotic colonization experiments (51 SM-colonized mice in total; experiments 1–4) were performed according to the timeline shown in Figure 1B.

Both Chronic and Intermittent Fiber Deficiency Promotes Enrichment of Mucus-Degrading Bacteria

Although dietary changes are known to perturb microbiota composition, the impact of diet variation, especially chronic or intermittent fiber deficiency, on the activities and abundance of mucin-degrading bacterial communities has not been studied in functional detail. After validating stable SM colonization, three groups of mice were maintained by constant feeding of one of three different diets: fiber-rich (FR), fiber-free (FF), or prebiotic

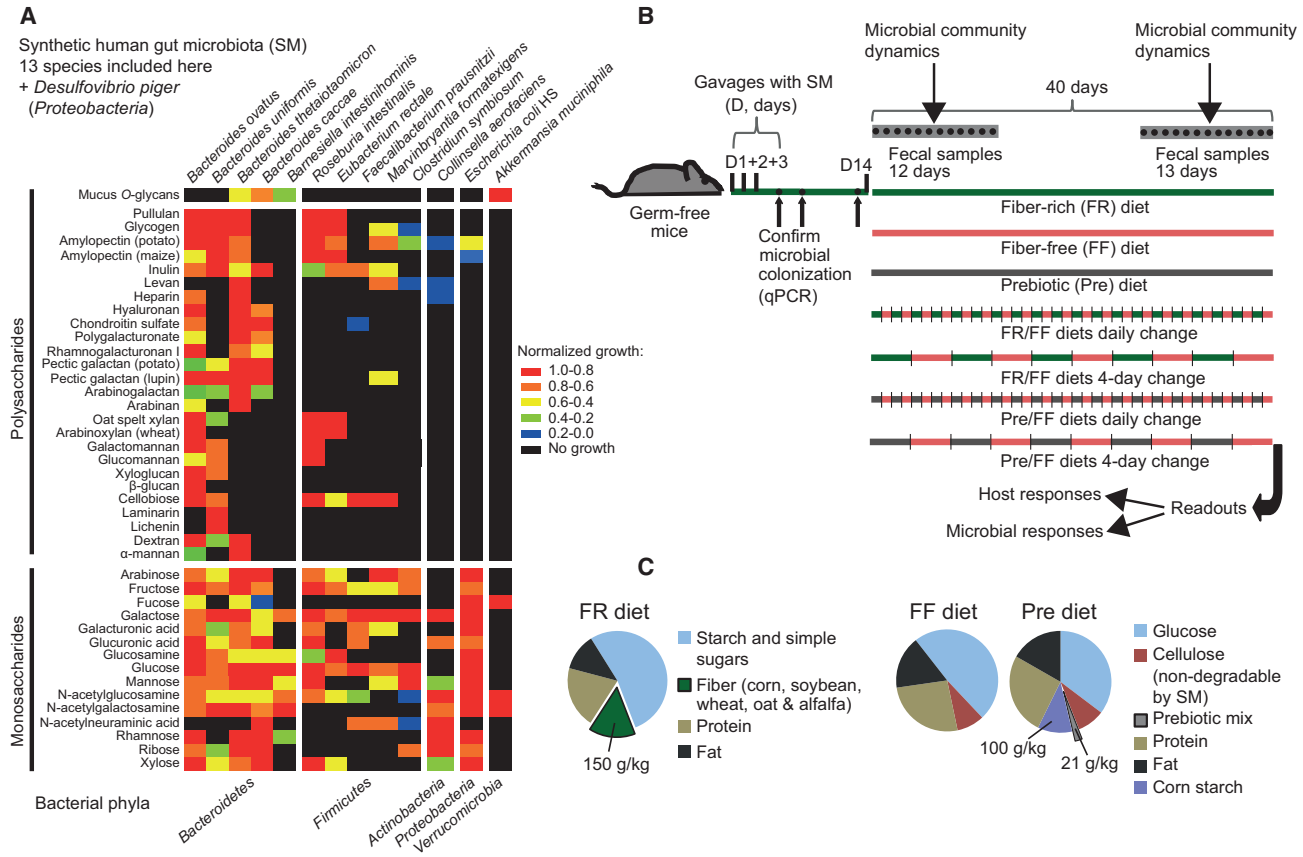

Figure 1. Carbohydrate Utilization by the Synthetic Human Gut Microbiota Members and Gnotobiotic Mouse Treatments

(A) Heatmap showing normalized growth values of 13/14 synthetic human gut microbiota (SM) members.

(B) Schematic of the gnotobiotic mouse model illustrating the timeline of colonization, feeding strategies, and fecal sampling.

(C) Compositions of the three distinct diets employed in this study (common additives such as vitamins and minerals are not shown). The prebiotic mix contained equal proportions of 14 host indigestible polysaccharides (see Table S1).

See also Figure S1.

(Pre). In contrast to the FR diet that contained naturally milled food ingredients with intact fiber particles, the Pre diet was designed to study the effect of adding a mixture of purified, soluble glycans, similar to those used in prebiotic formulations (Figure 2C). To imitate the fact that the human diet experiences fluctuating amounts of fiber from meal-to-meal, four other groups were alternated between the FR and FF or Pre and FF diets on a daily or 4-day basis (Figure 1B).

Fecal microbial community dynamics showed that in mice switched to the FF diet, several species rapidly and reproducibly changed in abundance (Figures 2A, 2B and S3). Four species—*A. muciniphila*, *B. caccae*, *B. ovatus*, and *E. rectale*—were highly responsive to diet change. *A. muciniphila* and *B. caccae* are able to degrade MOGs in vitro. *B. ovatus* and *E. rectale* cannot metabolize MOGs, but together can use a broad range of polysaccharides found in dietary fiber (Figure 1A). In the absence of fiber, the abundance of *A. muciniphila* and *B. caccae* increased rapidly with a corresponding decrease of the fiber-degrading species (Figure 2A). The Pre diet, which contains purified polysaccharides and is otherwise isocaloric with the FF diet, had a similar effect on community composition as the FF diet but separated slightly by PCoA ordination from FF, likely due to increased *Bacteroides* abundance (Figures 2A and 2B). Intriguingly, the abundances of the same four bacteria noted above fluctuated rapidly on a daily basis when the FR and FF diets were oscillated (Figures 2C and S3), corroborating their ability to respond dynamically to variations in dietary fiber. The increase in mucin-degrading species observed in fecal samples matched with cecal abundances at the end of the experiment (Figure 2D and panels to the right of plots in Figure 2A). Moreover, similar levels of mucin-degrading bacteria were quantified in the colonic lumen and mucus layer using laser capture microdissection (Figure 2E), indicating that proliferation of mucin-degrading bacteria in this model is a community-wide effect and not limited just to the mucus layer.

Many of the other bacteria (except *R. intestinalis* and *B. intestinihominis*) were sensitive to changes between the FR and FF diets on daily and 4-day bases, albeit to lower degrees (Figure S3B; Table S2). Two additional species especially sensitive to diet change were *Desulfovibrio piger* (increased on FF diet)

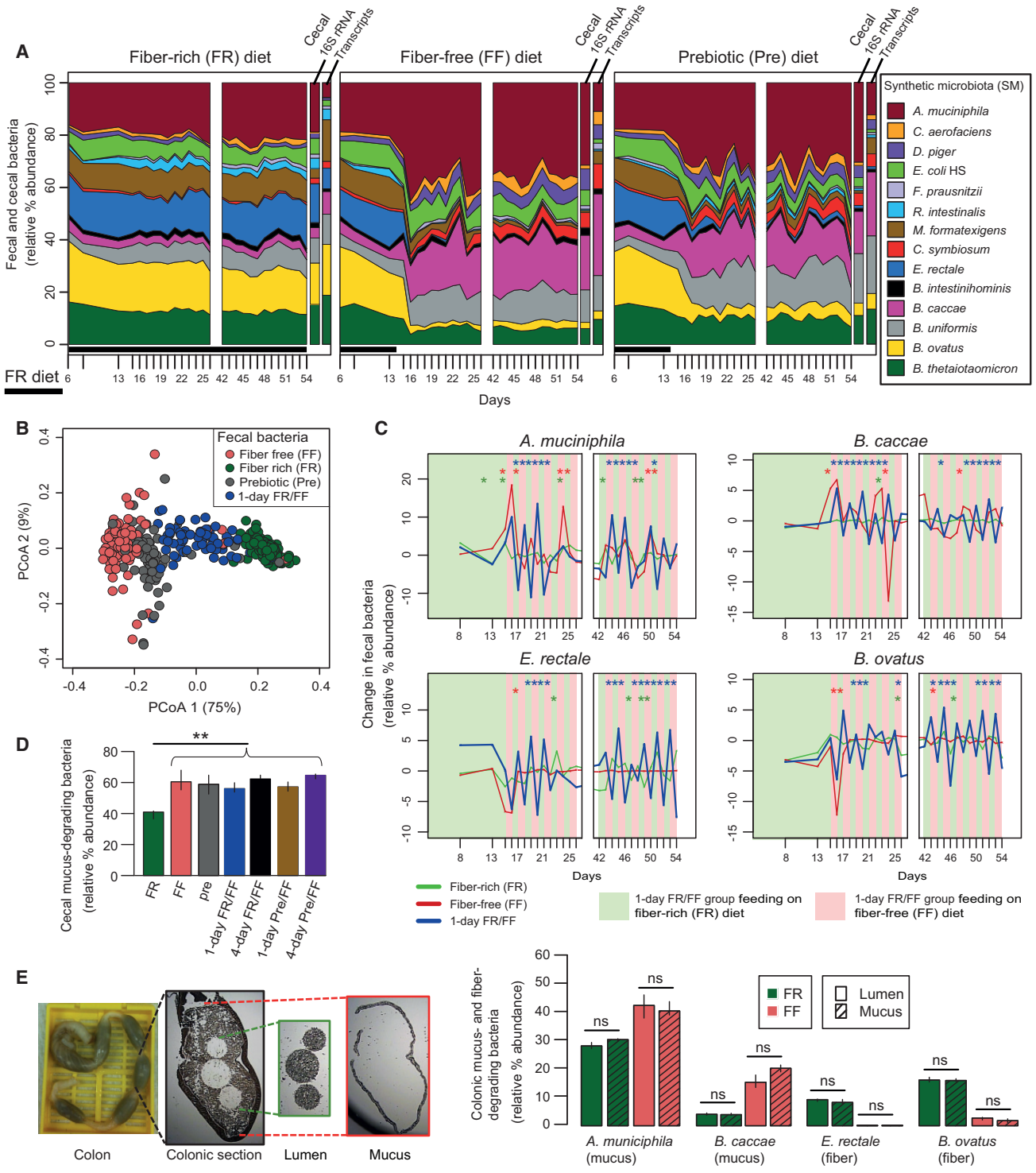

Figure 2. Complex Dietary Fiber Deficiency Leads to Proliferation of Mucus-Degrading Bacteria

(A) Stream plots exhibiting fecal (over time, Figure 1B) and cecal (end point) microbial community dynamics and average abundance of total species-specific transcripts from cecal RNA-seq transcriptome mapping at the endpoint; for transcript abundance n = 3 mice/group.

(B) Principal coordinate analysis (PCoA) based on bacterial community similarity.

(C) Changes in relative bacterial abundance over time in mice oscillated for 1-day increments between FR and FF feeding. Changes in FR and FF control groups are shown for comparison. Asterisks (colored according to the dietary group) indicate a statistically significant difference in the change of relative abundance from the previous day within each group. Student's t test.

(legend continued on next page)

and *Marvinbryantia formatexigens* (decreased on FF diet) (Figure S3A). Population changes in the groups oscillated between Pre and FF diets were similar to the abundances observed in FF only diet regimen (Table S2). Thus, despite the pure polysaccharides contained in the Pre diet exerting a clear physiological impact on the microbiota (discussed below), the amount and composition of the purified polysaccharides in this diet exert little effect on species composition.

Community Transcriptional and Enzymatic Readouts Demonstrate Enhanced Degradation of Mucus When Fiber Is Absent

Because mucin-degrading bacteria were higher on both the FF and Pre diets that lack naturally complex plant fiber, we reasoned that this increased abundance is due to their ability to degrade mucus as an alternative nutrient. To test this, we measured changes in transcripts encoding carbohydrate active enzymes (CAZymes) that enable gut bacteria to utilize dietary fiber and mucosal polysaccharides (cecal samples from all but the 4-day oscillation groups were analyzed).

Based on new or existing genome annotations of the 14 species in our synthetic community, a total of 1,661 different degradative CAZymes belonging to 96 different families were detected (glycoside hydrolase [GH], polysaccharide lyase [PL], and carbohydrate esterase [CE] families were counted). This number is close to the total number of families (122) that was identified in a larger survey of 177 human gut bacterial reference genomes (El Kaoutari et al., 2013), indicating that our synthetic community retains much of the metabolic potential toward carbohydrates that is present in a more diverse microbiota. Of the 96 enzyme families in our community, members of 38 families, plus M60-like proteases (pfam13402), a group of enzymes previously shown to degrade mucin glycoproteins (Nakjang et al., 2012), showed variable expression in either FR/FF or Pre/FF community transcriptome comparisons (Figure 3A). These differentially abundant degradative enzymes mapped to 770 different genes contributed from all species except *D. piger* (Table S4).

Our transcriptomic data show that in the mice fed the FR diet, transcripts belonging to enzyme families that target dietary fiber polysaccharides were more abundant. In contrast, in mice fed the FF diet, transcripts encoding enzyme families known to release sugars from host substrates, including mucin *O*-glycans, were elevated (Figure 3A). In line with our in vitro growth assays (Figure 1A) and the microbial community abundance data (Figure 2), we found that *B. ovatus* and *E. rectale* contributed a majority of CAZymes specific for plant polysaccharides (Figure 3A). The four in vitro mucin degraders were the major contributors to the degradation of host glycans and mucus in vivo. Additionally, transcripts encoding M60-like proteases (pfam13402) were also more highly expressed in FF conditions (Figure 3A). Expression of these putative mucin-targeting enzymes was primarily contributed by *B. caccae*, an organism that possesses 16 of these genes compared to just four in *A. muciniphila* and five in all other species combined. This observation suggests the tantalizing possibility that *B. caccae* is particularly equipped via its M60-like proteases to perform a key degradative step (cleavage of glycoprotein backbones) during mucin foraging and this ability may facilitate access to mucus carbohydrate structures by other bacteria.

In the group fed the Pre diet, similar transcripts as in the FR-fed group were elevated relative to FF, albeit to lower levels (Figure 3A bottom histogram). Furthermore, transcripts for the same bacterial enzymes presumed to target mucus in the FR/FF diet comparison were observed in the Pre/FF comparison. Additional RNA sequencing (RNA-seq) analyses of cecal transcriptomes from mice oscillated between FR/FF and Pre/FF on a daily basis (collected after 1 day on FF diet) provided similar results to those obtained for the FF only diet mice (Table S4). Our transcriptomic readouts corroborate the increased abundance of mucin-degrading bacteria observed in these mice (Figure 2D) and demonstrate that even intermittent fiber deficiency has the potential to alter the microbiota and favor mucin-degrading species.

To further connect the in vivo responses of *B. caccae* and *A. muciniphila* with degradation of mucin *O*-glycans, we performed additional transcriptional profiling of these two species on purified MOGs from porcine gastric mucus. We have previously shown that this mixture contains ~110 different structures (Hickey et al., 2015) that when metabolized by *B. thetaiotaomicron* stimulate a transcriptional response that overlaps substantially with genes expressed in vivo under fiber-restricted conditions (Martens et al., 2008). During growth on MOGs as the sole carbon source, *B. caccae* and *A. muciniphila* activated expression of 82 and 58 genes, respectively (Table S5). Based on a recalculation using a 5-fold cutoff of previous microarray data from growth in the same substrate, *B. thetaiotaomicron* activated expression of 166 genes (Martens et al., 2008). Next, we examined expression of these validated *O*-glycan-responsive genes (for *B. caccae*, *A. muciniphila*, and *B. thetaiotaomicron*) in the SM community from FF-fed mice compared to FR. In support of our hypothesis, validated *B. caccae* and *A. muciniphila* *O*-glycan-responsive genes were increased in the FF condition (Figure 3B). *B. caccae* expression was increased irrespective of normalization by reads mapped to the whole community (i.e., including increased *B. caccae* abundance) or to just the *B. caccae* genome (discounts abundance change and examines changes in expression).

Consistent with its specialization for *O*-glycans, *A. muciniphila* mostly showed increased expression of *O*-glycan-responsive genes proportional to its increased population size (from ~20% to ~40%), indicating that it does not shift its substrate utilization in comparison to the FR diet (Figure 3B; see also

(D) Additive relative abundances of four mucus-degrading bacteria (Figure 1A).
(E) Relative bacterial abundances in laser capture microdissected colonic lumen and mucus samples (images displayed on left). n = 3 mice/group.
Microbial community abundance data are based on Illumina sequencing of 16S rRNA genes (V4 region) and median values at each time point are shown; error bars in (D) and (E) denote interquartile ranges (IQRs). Unless specified, significance was determined using Kruskal-Wallis test and n = 4 for FR and FF groups, n = 3 for all other groups. All data in (A)–(E) are from experiment 1.
See also Figures S2 and S3 and Tables S2 and S3.

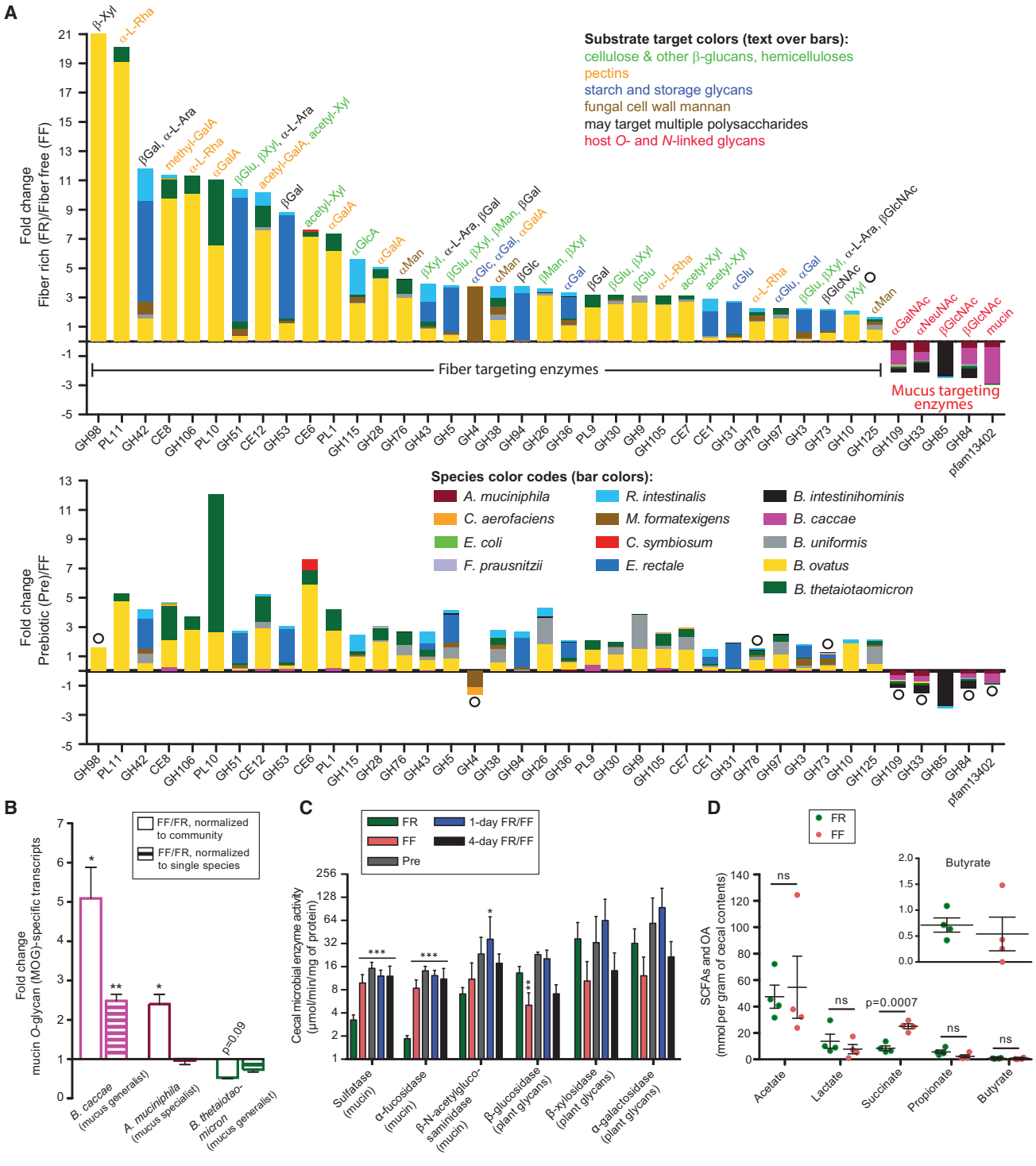

Figure 3. Diet-Specific Changes in Carbohydrate Active Enzyme Expression Reveal a Community Shift from Fiber to Mucus Degradation

(A) Positive and negative fold-changes in transcripts encoding carbohydrate active enzymes (CAZymes) between either FR/FF (top) or Pre/FF (bottom) comparisons. Only CAZyme families (x axis) in which >2-fold changes and $p < 0.05$ (Student's t test) were observed for all of the genes in that family in RPKM-normalized cecal community transcriptomes are shown as averages; open circles denote statistically insignificant differences. n = 3 mice/group, experiment 1. (B) Fold-change values of empirically validated (Table S5), MOG-specific transcripts of three mucus-degrading bacteria. n = 3 mice/group, experiment 1. Data are shown as average and error bars represent SEM. Student's t test.

(legend continued on next page)

Table S6E). The idea that *B. caccae* is capable of broader transcriptional shifts, compared to *A. muciniphila*, is further supported by global analysis of its gene expression changes between the FF and FR diets and 1-day alternations (Figure S4). In response to the FF diet, *B. caccae* showed increased in vivo expression of 230 genes, including 27 degradative enzymes; whereas, *A. muciniphila* only showed increased expression of 43 genes, including two enzymes (Figure S4). In contrast to previous monoassociation data (Sonnenburg et al., 2005), *B. thetaiotaomicron* mostly showed unchanged or slightly decreased expression of its known *O*-glycan utilization genes after a shift to FF (Figure 3B; Table S6B).

Colonic mucin *O*-glycans contain glycosidic linkages distinct from plant fibers and also covalently linked sulfate. In further support of increased bacterial degradation of the host mucus on the FF diet, we detected significantly increased bacterial enzymes targeting mucin linkages (sulfatase and α-fucosidase) in the mice subjected to the FF diet on either a chronic or intermittent basis (Figure 3C). In contrast, enzymes targeting linkages in fiber polysaccharides (β-glucosidase) were significantly reduced in the mice fed the fiber-deficient diets, while others involved in xylan and α-galactan degradation trended similarly without significance (Figure 3C). Despite the dramatic change in microbiota species abundance and transcriptional response, there was only one significant change (succinate) in SCFA and organic acids in the FF diet fed mice (Figure 3D). Overall, the transcriptomic and enzyme analyses support the conclusion that a fiber-deprived gut microbiota synergistically and progressively expresses CAZymes, sulfatases, and proteases to attack mucus polysaccharides when the diet lacks complex plant fiber.

Fiber Deprivation Leads the Gut Microbiota to Degrade the Colonic Mucus Barrier

The mucus layer is a dynamic barrier that is constantly replenished through the secretory activity of goblet cells (Johansson et al., 2013). We rationalized that if bacterial consumption of mucin-derived nutrients exceeds new production, the integrity of this critical barrier could be compromised. To explore this possibility, we performed blinded thickness measurements of the colonic mucus layer from proximal colon to rectum in each mouse using Alcian blue-stained sections (Figure 4A). We further validated thickness of the mucus layer by immunofluorescence staining of the Muc2 mucins using α-*Muc2* antibody (Figure 4B). To address the possibility that variations in thickness are directly influenced by the diets used, we measured mucus layer thickness in germfree mice fed the FR or FF diets.

Colonic mucus measurements revealed that mucus thickness was highest in the colonized group fed the FR diet (Figure 4C). In most other groups, including germfree (GF) controls, mucus thickness was significantly thinner than in colonized FR mice. The observation that GF mice have thinner colonic mucus is consistent with previous studies in gnotobiotic mice and rats (Petersson et al., 2011; Wrzosek et al., 2013), which found that microbial colonization or exposure to cues such as peptidoglycan or lipopolysaccharides is required for mucus production. Notably, mucus in SM-colonized FF diet mice was five to six times thinner than colonized mice fed the FR diet. From these data, we conclude that the mucus layer: (1) is initially thinner in GF mice regardless of diet, (2) begins expanding upon microbial colonization, but (3) is disproportionately eroded back to a thinner layer due to the increased mucus foraging activity by the microbiota in the context of the FF diet. A similar reduction in mucus thickness was observed in the Pre diet and both 4-day oscillation groups, while an intermediate thickness was observed in the 1-day FR/FF oscillation group (Figure 4C).

Next, we determined whether mucus production was altered in colonized mice fed the FF diet. We examined the abundance of transcripts encoding several key proteins involved in building and regulating the mucus barrier (Figure 4D): *Muc2 and Muc5ac*, two building blocks of colonic mucus; *Tff1 and Tff3*, goblet cell proteins that promote mucosal repair and protection; and *Klf3*, a transcription factor involved in barrier function. Our results show that the transcription of the major colonic mucin gene (*Muc2*) was slightly elevated in the colonized FF diet group, suggesting a compensatory response of the host to offset the increased bacterial mucus degradation in this group; whereas other genes (*Muc5ac*, *Tff1*, *Tff3*, and *Klf3*) remained statistically unchanged (Figure 4D). Qualitative visualization by Alcian blue (Figure 4A) staining supports the conclusion that the colonic tissue of FF-fed colonized mice contained similar numbers of goblet cells that have yet to secrete their glycoproteins.

As expected, degradation of the mucus layer by the fiber-deprived gut microbiota brought luminal bacteria closer to the intestinal epithelium (Figure 4B, inset), which could potentially trigger deleterious effects or other host compensatory responses. Histopathology (Figure S5A) and body weight measurements over time (Figure S5B) of mice from the groups with reduced mucus thickness did not reveal changes compared to the mice consuming the FR diet. However, measurements of three additional host parameters provided support for altered host responses in the face of mucus erosion: the first was fecal lipocalin—a neutrophil protein that binds bacterial siderophores and is associated with low-grade inflammation (Chassaing et al., 2015)—that was increased in the group of colonized mice fed the FF diet compared to those fed FR (Figure 4E). A second readout, colon length, revealed shorter colons in colonized FF fed mice and other SM colonized groups when compared to colonized FR fed mice or GF mice on either diet (Figure 4F). Additional analysis of host cecal tissue global transcriptional responses failed to reveal large-scale changes in the host; although, some compensatory responses were suggested by pathway analysis, which illuminated several immune responses as altered in the colonized FF fed mice (Figures 4G and S5C; Table S7). Collectively, the data described above indicate that fiber-restricted,

(C) Activities of cecal enzymes determined by employing *p*-nitrophenyl-linked substrates. n = 4 for FR and FF groups and n = 3 for other groups, experiment 1. Data are shown as average and error bars represent SD. One-way ANOVA, FR diet group versus other groups.

(D) Concentrations of organic acid (OA, succinate) and short-chain fatty acids (SCFA) determined from cecal contents. n = 4 mice/group; 2 mice/dietary group in two independent experiments (#2A and 3). Middle lines indicate average of the individual measurements shown and error bars represent SEM. Student's t test. See also Figure S4 and Tables S4, S5, and S6.

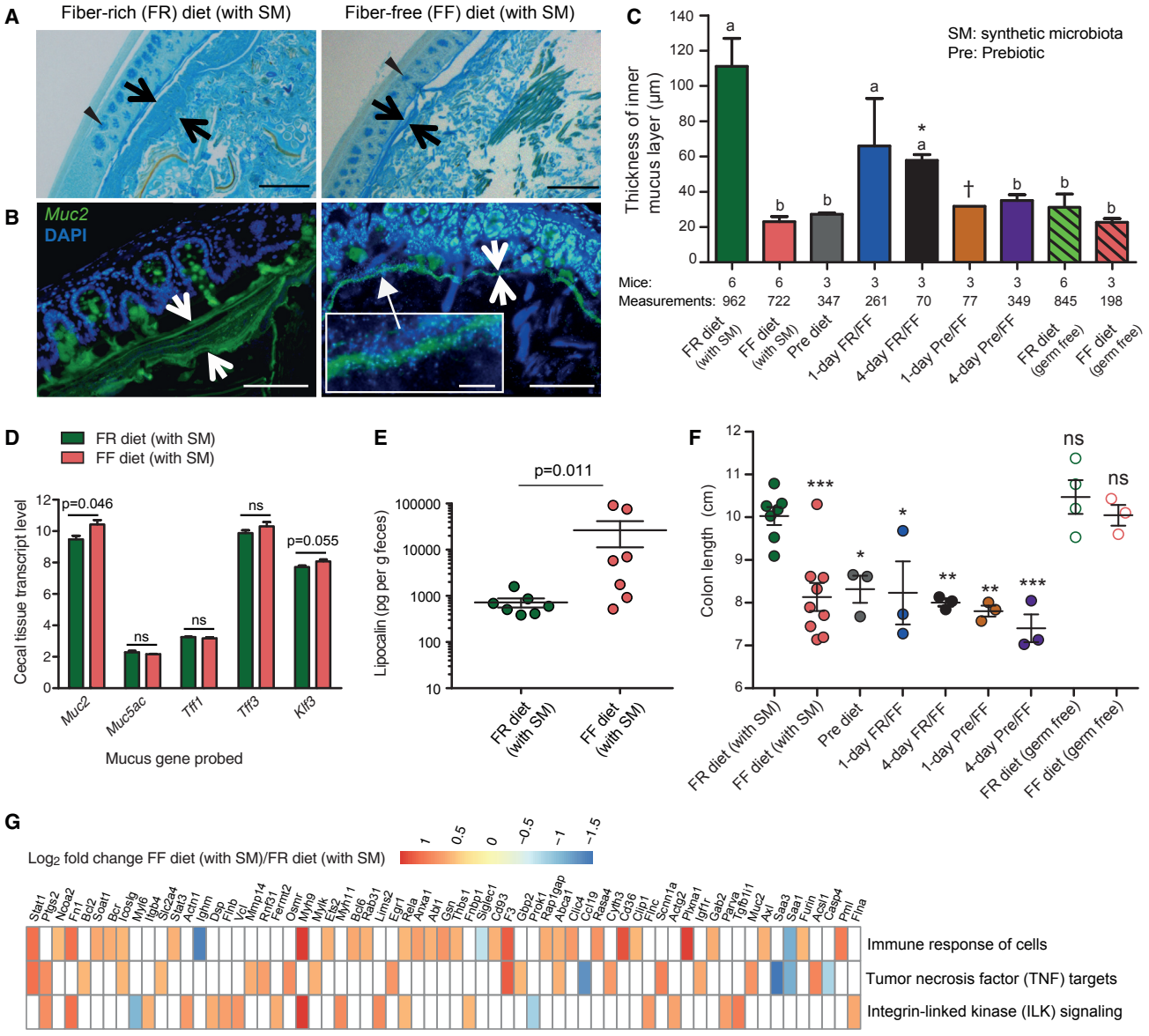

Figure 4. Microbiota-Mediated Erosion of the Colonic Mucus Barrier and Host Responses

(A) Alcian blue-stained colonic sections showing the mucus layer (arrows). Scale bars, 100 μm. Opposing black arrows with shafts delineate the mucus layer that was measured and triangular arrowheads point to pre-secretory goblet cells.

(B) Immunofluorescence images of colonic thin sections stained with α-Muc2 antibody and DAPI. Opposing white arrows with shafts delineate the mucus layer. Inset (FF diet group) shows a higher magnification of bacteria-sized, DAPI-stained particles in closer proximity to host epithelium and even crossing this barrier. Scale bars, 100 μm; inset, 10 μm.

(C) Blinded colonic mucus layer measurements from Alcian blue-stained sections. Mice in the FR and FF fed colonized groups (experiments 1 and 2A), and in the FR-diet fed germfree groups are from two independent experiments; all other colonized mice are from experiment 1. Asterisk and dagger indicate that colons of only two and one mice contained fecal masses, respectively. Data are presented as average and error bars represent SEM. Statistically significant differences are annotated with different letters $p < 0.01$. One-way ANOVA with Tukey's test.

(D) Microarray-derived transcript levels of genes involved in the production of colonic mucus (n = 4 for the FR diet group and n = 3 for the FF diet group). Data are from two independent experiments (#2A and 3). Values are shown as average and error bars represent SEM. Student's t test.

(E) Levels of fecal lipocalin (LCN2) measured by ELISA in the FR and FF diet fed groups (day 50, Figure S6A; experiment 2A). n = 7 mice/group. Middle lines indicate average of the individual measurements shown and error bars represent SEM. Mann-Whitney test.

(F) Colon lengths of mice subjected to different dietary treatments. Data for the FR (with SM) and FF (with SM) are representative of three independent experiments (experiments 1, 2A, and 3). Middle lines indicate average of the individual measurements shown and error bars represent SEM. One-way ANOVA, FR diet group (with SM) versus other groups.

(legend continued on next page)

colonized mice experience erosion of the mucus barrier and some altered intestinal responses, albeit without overt signs of disease.

A Fiber-Deprived Gut Microbiota Promotes Heightened Pathogen Susceptibility

Because the mucus layer is a critical barrier against both commensal microbes and invading pathogens, we next hypothesized that the reduction in thickness associated with microbiota activity during low-fiber conditions would increase pathogen susceptibility. To test this idea, we chose the attaching/effacing pathogen *Citrobacter rodentium* (*Cr*) because it must traverse the mucus layer to access the epithelium and cause colitis (Collins et al., 2014). Toward this point, a previous study demonstrated that mice genetically lacking the dominant colonic mucin glycoprotein (*Muc2*$^{-/-}$), but not wild-type mice, develop lethal colitis following infection with *Cr*, highlighting that the mucus layer is an important initial barrier to this pathogen (Bergstrom et al., 2010).

Therefore, we recreated the previously observed diet-modulated thick and thin mucus layer phenotypes in gnotobiotic mice and infected both groups with *Cr* (Figure S6A). To control for diet-specific effects on *Cr* pathogenesis in the absence of our SM, we infected two additional groups consisting of germ-free (GF) mice fed a priori (~4 weeks before infection) the same FR or FF diets. We collected fecal samples each day post *Cr* infection to measure changes in pathogen colonization by both selective plating for *Cr* and 16S rRNA gene analysis (Figures 5A, 5B, and S6A). In the two groups colonized by the synthetic microbiota, *Cr* levels gradually increased but were significantly higher beginning at day 2 in mice fed the FF diet and remained ~10-fold higher thereafter.

The dramatic diet-specific increase of *Cr* levels in SM-colonized mice fed the FF diet was accompanied by weight loss that was specific to this group (Figure 5C). Importantly, both GF+*Cr* groups that had high pathogen levels (Figure 5A) failed to exhibit similar weight loss, illuminating that the pathogen alone is insufficient for this effect on either diet. The higher pathogen burdens in colonized mice fed the FF diet were associated with multiple signs of morbidity such as hunched posture and inactivity. Notably, by 10 days post infection, 60% of the mice from the SM colonized FF group had to be euthanized due to ≥20% loss of body weight (Figure 5D). Mice in the other three groups did not show similar morbidity.

Histological scoring of the cecal and colonic tissue revealed that the SM-colonized FF diet group experienced inflammation that covered a significantly more expansive surface area (Figures 5E–5G). An exception was the descending colon/rectum, which showed larger areas of inflamed tissue in both FR and FF groups; although, the FF group was still significantly higher and 100% affected. When the tissue was inflamed, the level of hyperplasia was similar across all four groups (Figure S6B). Importantly, there were overall lower levels of inflamed tissue in both of our GF+*Cr* control groups. To determine if increased mucus production post infection could explain the lower disease observed in the GF+*Cr* groups, we measured thickness of the colonic mucus and found that *Cr* triggered only a slight increase in GF mucus thickness; whereas the thick mucus layer associated with the FR diet in the context of microbiota colonization persisted (Figures S7A and S7B).

Based on the above results, we further hypothesized that the increased area of inflamed tissue in FF mice was due to earlier and increased pathogen access due to the microbiota-degraded mucus layer. To test this idea, we infected the same four treatment groups (SM-colonized or GF mice, fed either FR or FF diets) with a luciferase-expressing *Cr* strain (Figure 6A). At 4 days post infection, we sacrificed all mice and conducted bioluminescent imaging of the colons after flushing out the luminal contents. In support of our hypothesis, and despite having similar levels of fecal *Cr* in FR- and FF-fed SM mice (Figure 6B), we saw significantly higher pathogen signal adherent to the colonic tissue of SM colonized mice fed the FF diet as compared to those fed FR (Figures 6C and 6D). The higher levels of attached *Cr* in FF fed SM mice were further validated by transmission electron microscopy, revealing increased appearance of the attaching and effacing lesions, pedestals and loss of microvilli that is typically associated with *Cr* infection (Figure 6E). Notably, GF+*Cr* mice on either diet displayed similarly high adherent bacterial signal as the FF-fed SM mice (Figures 6D and S7C). Taken together, these results suggest that the pathogen can more quickly traverse the thin colonic mucus layers in GF mice (irrespective of diet) and SM-colonized mice fed the FF diet. However, the commensal microbiota is also required in the context of increased pathogen access to elicit more severe disease, possibly by provoking co-inflammatory responses.

DISCUSSION

The health benefits of fiber consumption have been purported for decades, yet the influence of many different chemical and physical forms of fiber polysaccharides on the gut microbiota and the ways through which gut bacteria digest, sequester, and share these chemically complex nutrients, are just now being unraveled in detail (Cuskin et al., 2015; Rakoff-Nahoum et al., 2016). Aside from loss of beneficial SCFA production, microbiota-mediated mechanisms that connect low fiber intake to poor gastrointestinal health have not been described. Using a gnotobiotic mouse model, our study provides a mechanism by which a diet deficient in complex plant fiber triggers a synthetic gut microbiota to feed on the colonic mucus layer that acts as a primary barrier against invading pathogens (Figure 7). Our findings reveal important implications regarding how our immediate diet history may modify susceptibility to some enteric diseases.

Our approach highlights the power of using a tractable synthetic human gut microbiota, in which the individual members can be characterized or manipulated to support functional

(G) Changes in the host cecal transcriptome between FR and FF diet conditions. Heatmap shows statistically significant fold changes of genes identified from ingenuity pathway analysis (false discovery rate [FDR] < 0.05 and absolute Log_2 fold-change > 0.5). n = 4 for the FR diet group and n = 3 for the FF diet group; data are from two independent experiments (#2A and 3).
See also Figure S5 and Table S7.

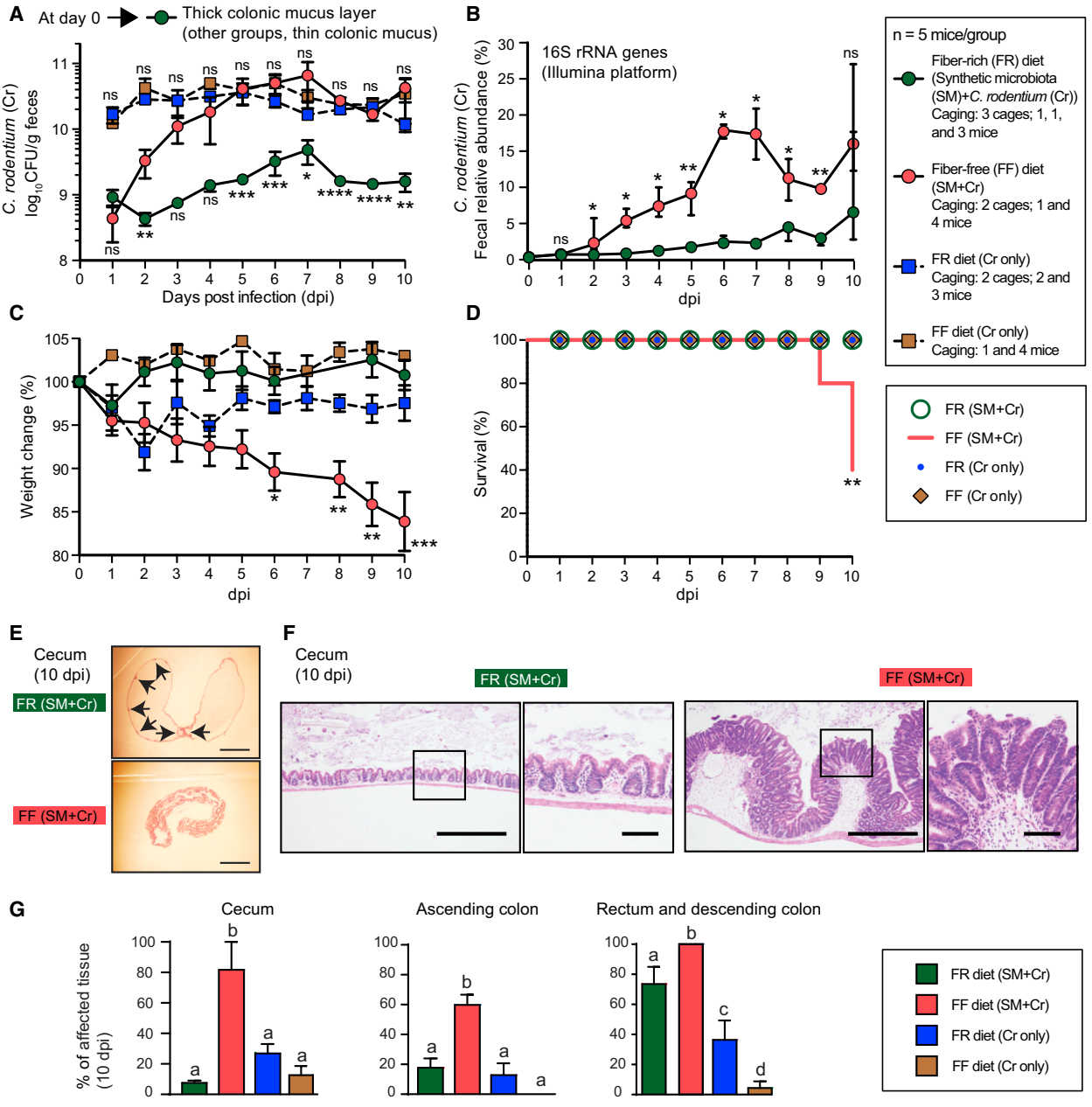

Figure 5. Fiber-Deprived Gut Microbiota Contributes to Lethal Colitis by *Citrobacter rodentium*

(A) Fecal *C. rodentium* levels over time. Data are shown as average and error bars represent SEM. Student's t test; FR (SM+Cr) group versus FF (SM+Cr) group (bottom statistics labels) and FR (Cr) versus FF (Cr) (top statistics labels). Data in (A)–(G) are from experiment 2B.

(B) Relative abundance of *C. rodentium* in fecal samples over time. Data are shown as median and error bars represent IQR. Wilcoxon test.

(C) Weight changes in the four groups of mice. Values are shown as average and error bars represent SEM. One-way ANOVA, FF diet group (with SM) versus other groups.

(D) Survival curves for the four groups of mice. One-way ANOVA with Tukey's test.

(E) Representative images of unflushed ceca after H&E staining highlighting major differences in hyperplasia (indicated with arrows in the FR group, where hyperplasia is patchy and infrequent). Scale bars, 5 mm.

(F) Images of representative H&E-stained colonic thin sections depicting differences in hyperplasia between two groups. Scale bars, low power, 500 μm; high power, 50 μm.

(G) Measurements of inflamed tissue area in different intestinal segments. n = 5 mice/group except that n = 4 mice were used for FF (SM+Cr) group. Values are shown as mean and error bars represent SEM. Statistically significant differences are shown with letters within each intestinal segment; $p < 0.0002$. One-way ANOVA with Tukey's test.

See also Figures S6 and S7 and Table S2.

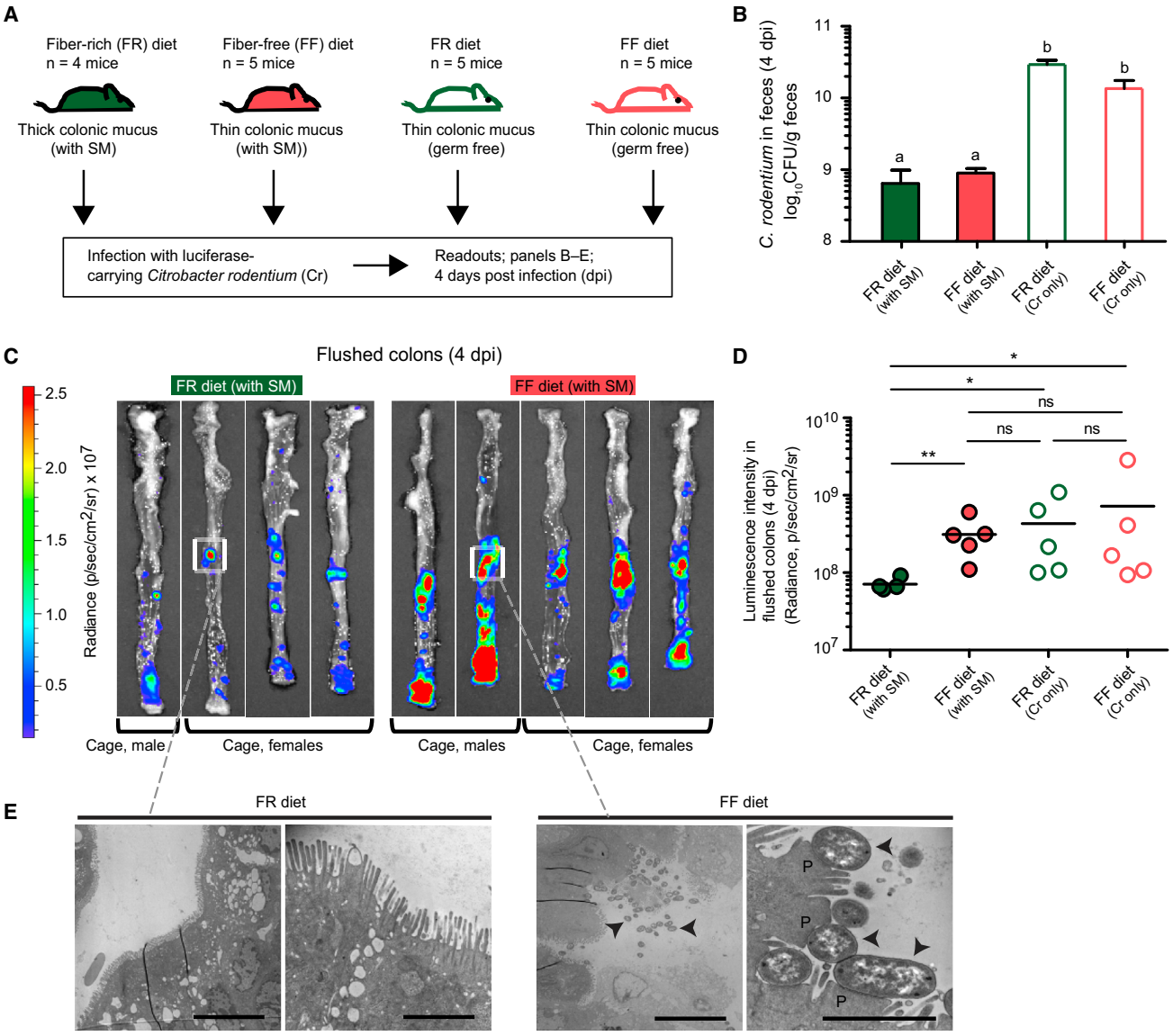

Figure 6. Fiber-Deprived Gut Microbiota Promotes Faster *C. rodentium* Access to the Colonic Epithelium

(A) Experimental setup for luminescent *C. rodentium* experiment (experiment 4).

(B) Fecal burdens of *C. rodentium* at 4 dpi. Data are shown as averages and error bars represent SEM; statistically significant differences are shown with different letters ($p < 0.001$). One-way ANOVA with Tukey's test.

(C) Bioluminescence images of flushed colons showing the location and intensity of adherent *C. rodentium* colonization.

(D) Quantified bioluminescence intensities of *C. rodentium* from (C) and Figure S7C. Middle lines indicate average of the individual measurements shown. Kruskal-Wallis one-way ANOVA with Dunn's test.

(E) Transmission electron microscopy images of the representative colonic regions from flushed colons; arrowheads denote individual *C. rodentium* cells and "P" denotes epithelial pedestals in high power/FF image. Scale bars, low power views 10 μm and high power views 2 μm.

See also Figure S7.

interpretations. We demonstrate that fiber deficiency allows the subset of mucin-degrading bacteria to increase their population and express mucin-degrading CAZymes to access mucin as a nutrient. While the ability to annotate CAZyme functions is well developed vis-a-vis many other metabolic functions that are important in the microbiome (El Kaoutari et al., 2013), there are still substantial ambiguities in connecting such predictions with precise catalytic roles. Here, we not only leverage knowledge of the substrate and enzyme specificities associated with some of the well-studied species in our SM (Table S4 and references therein), but we also employ new in vitro growth and transcriptional profiling experiments for key mucus-degrading bacteria (*B. caccae* and *A. muciniphila*). Our results point out a poignant example of how this evolving "bottom up" approach

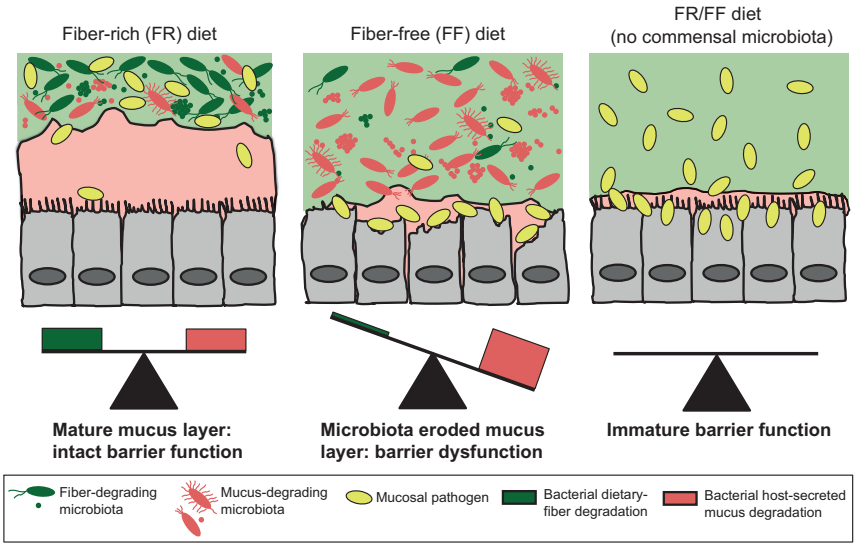

Figure 7. Model of How a Fiber-Deprived Gut Microbiota Mediates Degradation of the Colonic Mucus Barrier and Heighted Pathogen Susceptibility

Schemes derived from results shown in Figures 1, 2, 3, 4, 5, 6 illustrating the balance between fiber degradation and mucus degradation in FR diet-fed mice; whereas an FF diet leads to proliferation of mucus-degrading bacteria and microbiota-mediated degradation of the colonic mucus layer. The latter results in more severe colitis by *C. rodentium*.

can increasingly resolve functional resolution in complex microbial systems: only very recently, the single *B. ovatus* GH98 enzyme that is increased in the FR diet (leftmost bar, Figure 3A, top) was shown unequivocally to be an *endo*-β-xylosidase (Rogowski et al., 2015). Prior to this finding, the GH98 family was only known to contain blood group antigen-cleaving *endo*-α-galactosidases—a function that could have confusingly been associated with mucus *O*-glycan metabolism instead of its proper target, the plant fiber xylan.

Our results shed important light on the nature and amount of fiber that is required for the health of the colonic mucus layer. The prebiotic diet, which contains purified soluble fibers that are similar to common prebiotics (e.g., inulin, arabinoxylan, β-glucan), could not mitigate microbial erosion of the mucus barrier, despite having a clear impact on the cecal community transcriptome. Because the FR diet contains complex plant fiber in its natural form (intact plant cell walls) and at higher concentration (~15% versus 10% in the Pre diet), we cannot determine which variable (form or amount) is most important. However, the defined FF diet provides an ideal platform to which purified polysaccharides and even individual food items can be added to separately test both of these parameters for their ability to alleviate mucus degradation. Such an approach could help to design dietary therapeutics and next-generation prebiotics and will be particularly powerful given our existing knowledge of which polysaccharides the non-mucin-degrading species target (Figure 1A) and our ability to implant new species with other defined functionalities in the SM.

The present work highlights that the gut microbiota plays significant positive and negative roles in the pathogenesis of *C. rodentium*. Whereas we previously showed that the presence of a microbiota blocks colonization by *C. rodentium* unless it possesses virulence traits (Kamada et al., 2012), here, we demonstrate that diet-specific modulation of the gut microbiota can facilitate pathogen colonization and a fiber-deprived microbiota enhances disease susceptibility. Because the colonic mucus layer is an early barrier that a pathogen must transit (Collins et al., 2014), our data illustrate that a fiber-deprived microbiota has profound effects on the susceptibility to a gastrointestinal pathogen via reduction of this barrier. The contribution of mucus degradation to heightened pathogen susceptibility in our study is surprisingly parallel to a previous report that found a similar level of lethal colitis in mice with a genetically ablated ($Muc2^{-/-}$) mucus layer (Bergstrom et al., 2010). From this perspective, it is striking that a dietary alteration in wild-type mice can imitate the phenotype of a mutation as severe as *Muc2* loss. Given that *Muc2* knockout mice experience inflammation and eventual colorectal cancer, it is reasonable to conclude that prolonged diet-driven mucus layer loss could result in similar outcomes. In this context, it is worth noting that higher levels of mucolytic bacteria have been found in IBD patients (Png et al., 2010). In light of our observations that mice subjected to intermittent (daily or 4-day) dietary fiber deprivation exhibit thinner mucus, it will be critical in future studies to investigate the impact of periodic fiber deprivation, which is more like real human dietary habits, on the status of the mucus layer and the many downstream health effects that may be connected to mucus barrier dysfunction.

Taken together, our findings support a model in which dynamic interactions between dietary fiber and metabolism of a synthetic microbiota composed of commensal bacteria influence the status of the colonic mucus layer and susceptibility to pathogens that traverse this barrier (Figure 7). The current findings are likely applicable to gut microbial communities with higher numbers of species: three previous studies (see also the Introduction) involving rats with native microbiota and mice with transplanted human gut microbiota found a correlation between fiber-deficient diets and thinner colonic mucus layer. However, it remains to be investigated whether a thin colonic mucus layer together with a complex microbiota would contribute to enhanced pathogen susceptibility or how this effect might vary between individual microbial communities. Moreover, to understand whether microbial degradation of the colonic mucus is required for its secretion by the host in order to achieve a thicker mucus layer, future experiments need to address the effects on the mucus thickness after exclusion of the four validated mucus degraders from our synthetic microbiota. Finally, because the strains used here are of human origin,

and given the significant structural overlap between human and murine mucin (including glycosylation) (Johansson et al., 2013) and that *C. rodentium* uses similar pathogenesis mechanisms as human pathogenic *E. coli* strains, it is likely that such diet-induced disease susceptibility would extend to humans. Because *E. coli* infections are associated with high morbidity (Kaper et al., 2004) and health-care cost, our study emphasizes the need to consider a dietary perspective in fully understanding their transmission. With this in mind, efforts to find the optimal combinations of natural or prebiotic fiber polysaccharides and the minimum intake required to restore the integrity and resilience of the colonic mucus layer should be paramount.

STAR★METHODS

Detailed methods are provided in the online version of this paper and include the following:

- KEY RESOURCES TABLE
- CONTACT FOR REAGENT AND RESOURCE SHARING
- EXPERIMENTAL MODEL AND SUBJECT DETAILS
  - Gnotobiotic Mouse Model and Diet Treatments
  - *Citrobacter rodentium* Infection
  - Formulation of the Synthetic Microbiota
- METHOD DETAILS
  - Experimental Design
  - Sample Processing for Animal Experiments
  - Purification of Mucin *O*-Glycans
  - Bacterial Growth Assays in a Custom Carbohydrate Array
  - *Citrobacter rodentium* quantification
  - Extraction of Nucleic Acids
  - Bioluminescence Imaging and Transmission Electron Microscopy
  - Laser Capture Microdissection
  - Illumina Sequencing and Data Analysis
  - Microbial RNA-Seq and CAZyme Annotation
  - *p*-Nitrophenyl Glycoside-Based Enzyme Assays
  - Thickness Measurements of the Colonic Mucus Layer
  - qPCR
  - Quantification of Short-Chain Fatty Acids
  - Immunofluorescence Staining
  - ELISA for Fecal Lipocalin
  - Tissue Histology
  - Mouse Microarray Analyses
- QUANTIFICATION AND STATISTICAL ANALYSIS
  - Statistical Analyses
- DATA AND SOFTWARE AVAILABILITY
  - Accession Numbers

SUPPLEMENTAL INFORMATION

Supplemental Information includes seven figures and seven tables and can be found with this article online at http://dx.doi.org/10.1016/j.cell.2016.10.043.

AUTHOR CONTRIBUTIONS

M.S.D., E.C.M., P.W., T.S.S., and G.N. conceived the study. M.S.D. and E.C.M. designed the study. M.S.D. performed the experiments. M.S.D., A.M.S., and E.C.M. analyzed data. M.S.D., A.M.S., C.A.H., and E.C.M. prepared figures. M.S.D. and E.C.M. primarily wrote and edited the manuscript. M.S.D., N.M.K., and N.A.P. carried out bacterial in vitro growth assays. G.N., N.K., and S.K. assisted with *C. rodentium* infection and luminescence experiments. M.W. assisted with mucus measurements. C.A.H. and T.S.S. conducted blinded histology scoring. A.M. analyzed microarray data. N.T. and B.H. provided CAZy annotations. All authors discussed the results and provided comments on the manuscript.

ACKNOWLEDGMENTS

We thank Lansing C. Hoskins for critical comments on this manuscript and the germfree animal facility of the University of Michigan for expert support. We also thank Markus Ollert and Rudi Balling for their encouragement and advice. This work was supported by Luxembourg National Research Fund (FNR) INTER Mobility (13/5624108) and CORE (C15/BM/10318186) grants to M.S.D.; Luxembourg Ministry of Higher Education and Research support (DM-Muc) to M.S.D.; FNR ATTRACT (A09/03), CORE (11/1186762), and European Union Joint Programming in Neurodegenerative Diseases (INTER/JPND/12/01) grants to P.W.; NIH R01 (GM099513) grant to E.C.M.; and financial support from the University of Michigan Host Microbiome Initiative and Center for Gastrointestinal Research (DK034933).

Received: May 13, 2016
Revised: August 13, 2016
Accepted: October 21, 2016
Published: November 17, 2016

REFERENCES

Bergstrom, K.S.B., Kissoon-Singh, V., Gibson, D.L., Ma, C., Montero, M., Sham, H.P., Ryz, N., Huang, T., Velcich, A., Finlay, B.B., et al. (2010). Muc2 protects against lethal infectious colitis by disassociating pathogenic and commensal bacteria from the colonic mucosa. PLoS Pathog. *6*, e1000902.

Brownlee, I.A., Havler, M.E., Dettmar, P.W., Allen, A., and Pearson, J.P. (2003). Colonic mucus: secretion and turnover in relation to dietary fibre intake. Proc. Nutr. Soc. *62*, 245–249.

Burkitt, D.P., Walker, A.R.P., and Painter, N.S. (1972). Effect of dietary fibre on stools and the transit-times, and its role in the causation of disease. Lancet *2*, 1408–1412.

Cameron, E.A., and Sperandio, V. (2015). Frenemies: signaling and nutritional integration in pathogen-microbiota-host interactions. Cell Host Microbe *18*, 275–284.

Chassaing, B., Koren, O., Goodrich, J.K., Poole, A.C., Srinivasan, S., Ley, R.E., and Gewirtz, A.T. (2015). Dietary emulsifiers impact the mouse gut microbiota promoting colitis and metabolic syndrome. Nature *519*, 92–96.

Collins, J.W., Keeney, K.M., Crepin, V.F., Rathinam, V.A.K., Fitzgerald, K.A., Finlay, B.B., and Frankel, G. (2014). Citrobacter rodentium: infection, inflammation and the microbiota. Nat. Rev. Microbiol. *12*, 612–623.

Cuskin, F., Lowe, E.C., Temple, M.J., Zhu, Y., Cameron, E.A., Pudlo, N.A., Porter, N.T., Urs, K., Thompson, A.J., Cartmell, A., et al. (2015). Human gut Bacteroidetes can utilize yeast mannan through a selfish mechanism. Nature *517*, 165–169.

David, L.A., Maurice, C.F., Carmody, R.N., Gootenberg, D.B., Button, J.E., Wolfe, B.E., Ling, A.V., Devlin, A.S., Varma, Y., Fischbach, M.A., et al. (2014). Diet rapidly and reproducibly alters the human gut microbiome. Nature *505*, 559–563.

Earle, K.A., Billings, G., Sigal, M., Earle, K.A., Lichtman, J.S., Hansson, G.C., Elias, J.E., Amieva, M.R., Huang, K.C., and Sonnenburg, J.L. (2015). Quantitative imaging of gut microbiota spatial resource quantitative imaging of gut microbiota spatial organization. Cell Host Microbe *18*, 478–488.

Edgar, R.C., Haas, B.J., Clemente, J.C., Quince, C., and Knight, R. (2011). UCHIME improves sensitivity and speed of chimera detection. Bioinformatics *27*, 2194–2200.

El Kaoutari, A., Armougom, F., Gordon, J.I., Raoult, D., and Henrissat, B. (2013). The abundance and variety of carbohydrate-active enzymes in the human gut microbiota. Nat. Rev. Microbiol. *11*, 497–504.

Faith, J.J., McNulty, N.P., Rey, F.E., and Gordon, J.I. (2011). Predicting a human gut microbiota's response to diet in gnotobiotic mice. Science *333*, 101–104.

Flint, H.J., Scott, K.P., Louis, P., and Duncan, S.H. (2012). The role of the gut microbiota in nutrition and health. Nat Rev Gastroenterol Hepatol. *9*, 577–589.

Fu, J., Wei, B., Wen, T., Johansson, M.E.V., Liu, X., Bradford, E., Thomsson, K.A., McGee, S., Mansour, L., Tong, M., et al. (2011). Loss of intestinal core 1-derived O-glycans causes spontaneous colitis in mice. J. Clin. Invest. *121*, 1657–1666.

Gibson, G.R., Cummings, J.H., and Macfarlane, G.T. (1991). Growth and activities of sulphate-reducing bacteria in gut contents of healthy subjects and patients with ulcerative colitis. FEMS Microbiol. Lett. *86*, 103–112.

Hedemann, M.S., Theil, P.K., and Bach Knudsen, K.E. (2009). The thickness of the intestinal mucous layer in the colon of rats fed various sources of non-digestible carbohydrates is positively correlated with the pool of SCFA but negatively correlated with the proportion of butyric acid in digesta. Br. J. Nutr. *102*, 117–125.

Hickey, C.A., Kuhn, K.A., Donermeyer, D.L., Porter, N.T., Jin, C., Cameron, E.A., Jung, H., Kaiko, G.E., Wegorzewska, M., Malvin, N.P., et al. (2015). Colitogenic Bacteroides thetaiotaomicron antigens access host immune cells in a sulfatase-dependent manner via outer membrane vesicles. Cell Host Microbe *17*, 672–680.

Hoskins, L.C., and Boulding, E.T. (1981). Mucin degradation in human colon ecosystems. Evidence for the existence and role of bacterial subpopulations producing glycosidases as extracellular enzymes. J. Clin. Invest. *67*, 163–172.

Irizarry, R.A., Hobbs, B., Collin, F., Beazer-Barclay, Y.D., Antonellis, K.J., Scherf, U., and Speed, T.P. (2003). Exploration, normalization, and summaries of high density oligonucleotide array probe level data. Biostatistics *4*, 249–264.

Johansson, M.E.V., and Hansson, G.C. (2012). Preservation of mucus in histological sections, immunostaining of mucins in fixed tissue, and localization of bacteria with FISH. Methods Mol. Biol. *842*, 229–235.

Johansson, M.E.V., Phillipson, M., Petersson, J., Velcich, A., Holm, L., and Hansson, G.C. (2008). The inner of the two Muc2 mucin-dependent mucus layers in colon is devoid of bacteria. Proc. Natl. Acad. Sci. USA *105*, 15064–15069.

Johansson, M.E.V., Sjövall, H., and Hansson, G.C. (2013). The gastrointestinal mucus system in health and disease. Nat. Rev. Gastroenterol. Hepatol. *10*, 352–361.

Johansson, M.E.V., Gustafsson, J.K., Holmén-Larsson, J., Jabbar, K.S., Xia, L., Xu, H., Ghishan, F.K., Carvalho, F.A., Gewirtz, A.T., Sjövall, H., and Hansson, G.C. (2014). Bacteria penetrate the normally impenetrable inner colon mucus layer in both murine colitis models and patients with ulcerative colitis. Gut *63*, 281–291.

Kamada, N., Kim, Y.-G., Sham, H.P., Vallance, B.A., Puente, J.L., Martens, E.C., and Núñez, G. (2012). Regulated virulence controls the ability of a pathogen to compete with the gut microbiota. Science *336*, 1325–1329.

Kaper, J.B., Nataro, J.P., and Mobley, H.L.T. (2004). Pathogenic Escherichia coli. Nat. Rev. Microbiol. *2*, 123–140.

Kozich, J.J., Westcott, S.L., Baxter, N.T., Highlander, S.K., and Schloss, P.D. (2013). Development of a dual-index sequencing strategy and curation pipeline for analyzing amplicon sequence data on the MiSeq Illumina sequencing platform. Appl. Environ. Microbiol. *79*, 5112–5120.

Larsson, J.M.H., Karlsson, H., Crespo, J.G., Johansson, M.E.V., Eklund, L., Sjövall, H., and Hansson, G.C. (2011). Altered O-glycosylation profile of MUC2 mucin occurs in active ulcerative colitis and is associated with increased inflammation. Inflamm. Bowel Dis. *17*, 2299–2307.

Li, H., Limenitakis, J.P., Fuhrer, T., Geuking, M.B., Lawson, M.A., Wyss, M., Brugiroux, S., Keller, I., Macpherson, J.A., Rupp, S., et al. (2015). The outer mucus layer hosts a distinct intestinal microbial niche. Nat. Commun. *6*, 8292.

Loubinoux, J., Bronowicki, J.-P., Pereira, I.A.C., Mougenel, J.-L., and Faou, A.E. (2002). Sulfate-reducing bacteria in human feces and their association with inflammatory bowel diseases. FEMS Microbiol. Ecol. *40*, 107–112.

Martens, E.C., Chiang, H.C., and Gordon, J.I. (2008). Mucosal glycan foraging enhances fitness and transmission of a saccharolytic human gut bacterial symbiont. Cell Host Microbe *4*, 447–457.

Martens, E.C., Lowe, E.C., Chiang, H., Pudlo, N.A., Wu, M., McNulty, N.P., Abbott, D.W., Henrissat, B., Gilbert, H.J., Bolam, D.N., and Gordon, J.I. (2011). Recognition and degradation of plant cell wall polysaccharides by two human gut symbionts. PLoS Biol. *9*, e1001221.

McGuckin, M.A., Lindén, S.K., Sutton, P., and Florin, T.H. (2011). Mucin dynamics and enteric pathogens. Nat. Rev. Microbiol. *9*, 265–278.

McKenney, P.T., and Pamer, E.G. (2015). From hype to hope: the gut microbiota in enteric infectious disease. Cell *163*, 1326–1332.

McNulty, N.P., Wu, M., Erickson, A.R., Pan, C., Erickson, B.K., Martens, E.C., Pudlo, N.A., Muegge, B.D., Henrissat, B., Hettich, R.L., and Gordon, J.I. (2013). Effects of diet on resource utilization by a model human gut microbiota containing Bacteroides cellulosilyticus WH2, a symbiont with an extensive glycobiome. PLoS Biol. *11*, e1001637.

Nakjang, S., Ndeh, D.A., Wipat, A., Bolam, D.N., and Hirt, R.P. (2012). A novel extracellular metallopeptidase domain shared by animal host-associated mutualistic and pathogenic microbes. PLoS ONE *7*, e30287.

Petersson, J., Schreiber, O., Hansson, G.C., Gendler, S.J., Velcich, A., Lundberg, J.O., Roos, S., Holm, L., and Phillipson, M. (2011). Importance and regulation of the colonic mucus barrier in a mouse model of colitis. Am. J. Physiol. Gastrointest. Liver Physiol. *300*, G327–G333.

Png, C.W., Lindén, S.K., Gilshenan, K.S., Zoetendal, E.G., McSweeney, C.S., Sly, L.I., McGuckin, M.A., and Florin, T.H.J. (2010). Mucolytic bacteria with increased prevalence in IBD mucosa augment in vitro utilization of mucin by other bacteria. Am. J. Gastroenterol. *105*, 2420–2428.

Qin, J., Li, R., Raes, J., Arumugam, M., Burgdorf, K.S., Manichanh, C., Nielsen, T., Pons, N., Levenez, F., Yamada, T., et al.; MetaHIT Consortium (2010). A human gut microbial gene catalogue established by metagenomic sequencing. Nature *464*, 59–65.

Rakoff-Nahoum, S., Foster, K.R., and Comstock, L.E. (2016). The evolution of cooperation within the gut microbiota. Nature *533*, 255–259.

Rey, F.E., Gonzalez, M.D., Cheng, J., Wu, M., Ahern, P.P., and Gordon, J.I. (2013). Metabolic niche of a prominent sulfate-reducing human gut bacterium. Proc. Natl. Acad. Sci. USA *110*, 13582–13587.

Ritchie, M.E., Phipson, B., Wu, D., Hu, Y., Law, C.W., Shi, W., and Smyth, G.K. (2015). limma powers differential expression analyses for RNA-sequencing and microarray studies. Nucleic Acids Res. *43*, e47.

Rogowski, A., Briggs, J.A., Mortimer, J.C., Tryfona, T., Terrapon, N., Lowe, E.C., Baslé, A., Morland, C., Day, A.M., Zheng, H., et al. (2015). Glycan complexity dictates microbial resource allocation in the large intestine. Nat. Commun. *6*, 7481.

Schloss, P.D., Westcott, S.L., Ryabin, T., Hall, J.R., Hartmann, M., Hollister, E.B., Lesniewski, R.A., Oakley, B.B., Parks, D.H., Robinson, C.J., et al. (2009). Introducing mothur: open-source, platform-independent, community-supported software for describing and comparing microbial communities. Appl. Environ. Microbiol. *75*, 7537–7541.

Schneider, C.A., Rasband, W.S., and Eliceiri, K.W. (2012). NIH Image to ImageJ: 25 years of image analysis. Nat. Methods *9*, 671–675.

Sonnenburg, E.D., and Sonnenburg, J.L. (2014). Starving our microbial self: the deleterious consequences of a diet deficient in microbiota-accessible carbohydrates. Cell Metab. *20*, 779–786.

Sonnenburg, J.L., Xu, J., Leip, D.D., Chen, C.-H., Westover, B.P., Weatherford, J., Buhler, J.D., and Gordon, J.I. (2005). Glycan foraging in vivo by an intestine-adapted bacterial symbiont. Science *307*, 1955–1959.

Sonnenburg, J.L., Chen, C.T.L., and Gordon, J.I. (2006). Genomic and metabolic studies of the impact of probiotics on a model gut symbiont and host. PLoS Biol. *12*, e413.

Van der Sluis, M., De Koning, B.A., De Bruijn, A.C., Velcich, A., Meijerink, J.P., Van Goudoever, J.B., Büller, H.A., Dekker, J., Van Seuningen, I., Renes, I.B., and Einerhand, A.W. (2006). Muc2-deficient mice spontaneously develop colitis, indicating that MUC2 is critical for colonic protection. Gastroenterology *131*, 117–129.

Wickham, H. (2011). The split-apply-combine strategy for data. J. Stat. Softw. *40*, 1–29.

Wrzosek, L., Miquel, S., Noordine, M.-L., Bouet, S., Joncquel Chevalier-Curt, M., Robert, V., Philippe, C., Bridonneau, C., Cherbuy, C., Robbe-Masselot, C., et al. (2013). Bacteroides thetaiotaomicron and Faecalibacterium prausnitzii influence the production of mucus glycans and the development of goblet cells in the colonic epithelium of a gnotobiotic model rodent. BMC Biol. *11*, 61.

STAR★METHODS

KEY RESOURCES TABLE

REAGENT or RESOURCE	SOURCE	IDENTIFIER
Antibodies		
Alexa Fluor 488 goat anti-rabbit IgG	Life Technologies	Cat#A11008
Mucin 2 antibody (H-300)	Santa Cruz Biotechnology	Cat#sc-15334
Chemicals, Peptides, and Recombinant Proteins		
4-nitrophenyl N-acetyl-β-D-glucosaminide	Sigma-Aldrich	Cat#N9376
4-nitrophenyl α-D-galactopyranoside	Sigma-Aldrich	Cat#N0877
4-nitrophenyl β-D-glucopyranoside	Sigma-Aldrich	Cat#N7006
4-nitrophenol	Sigma-Aldrich	Cat#73560
Acetic acid	Acros Organics	Cat#222140010
Adenine	Sigma-Aldrich	Cat#A2786
Alanine	Sigma-Aldrich	Cat#A7469
Alcian blue	Sigma-Aldrich	Cat#A5268
Alginate	Sigma-Aldrich	Cat#180947
Ammonium chloride	Sigma-Aldrich	Cat#A0171
Ammonium sulfate	Thermo Fisher Scientific	Cat#A702
Arginine	Sigma-Aldrich	Cat#A8094
Asparagine	Sigma-Aldrich	Cat#A4159
Aspartic Acid	Sigma-Aldrich	Cat#A93100
Barley β-glucan (Barliv Betafiber)	Cargill	Cat#BBF-100
Beef extract	Sigma-Aldrich	Cat#B4888
Biotin	Sigma-Aldrich	Cat#B4501
Boric acid	Sigma-Aldrich	Cat#B6768
Calcium chloride	Sigma-Aldrich	Cat#C1016
Calcium pantothenate	Sigma-Aldrich	Cat#P2250
Cellulose	International Fiber Corporation	Solka-Floc
Chloroform	Sigma-Aldrich	Cat#496189
Chondroitin sulfate	Federal Laboratories	Cat#CSP1K
cOmplete, Mini, EDTA-free Protease Inhibitor Cocktail	Sigma-Aldrich	Cat#000000004693159001
Copper(II) sulfate pentahydrate	Sigma-Aldrich	Cat#C7631
Corn starch / amylopectin	Sigma-Aldrich	Cat#10120
Cyanocobalamin	Sigma-Aldrich	Cat#V2876
Cysteine	Sigma-Aldrich	Cat#C7352
Cytosine	Sigma-Aldrich	Cat#C3506
DAPI	Sigma-Aldrich	Cat#D9542
Dextran	Sigma-Aldrich	Cat#31389
Dipotassium phosphate	Thermo Fisher Scientific	Cat#BP363-500
EDTA	Sigma-Aldrich	Cat#ED4SS
Ethanol	Decon Labs	Cat#2701
Fiber-Free diet	Teklad/Envigo	Cat#TD.130343
Folic acid	Sigma-Aldrich	Cat#F7876
Fructose	Sigma-Aldrich	Cat#F0127
Galactose	Sigma-Aldrich	Cat#G0625
Glucomannan	Konjac Foods	Konjac Glucomannan Powder
Glucose	Sigma-Aldrich	Cat#158968

(*Continued on next page*)

Continued

REAGENT or RESOURCE	SOURCE	IDENTIFIER
Glutamine	Sigma-Aldrich	Cat#G8540
Glutaraldehyde	Electron Microscopy Sciences	Cat#16537
Guanine	Sigma-Aldrich	Cat#G11950
Guar gum galactomannan	Sigma-Aldrich	Cat#G4129
Glutamic Acid	Sigma-Aldrich	Cat#G1501
Hematin	Sigma-Aldrich	Cat#H3281
Histidine	Sigma-Aldrich	Cat#H8000
Hydrochloric Acid	Sigma-Aldrich	Cat#320331
Inulin	Cargill	Oliggo-Fiber Instant Inulin
Iron(II) sulfate heptahydrate	Sigma-Aldrich	Cat#215422
Isobutyric acid	Alfa Aesar	Cat#79-31-2
Isoleucine	Sigma-Aldrich	Cat#I2752
Isopropanol	Sigma-Aldrich	Cat#278475
Isovaleric acid	Alfa Aesar	Cat#503-74-2
Laboratory Autoclavable Rodent Diet - 5010	LabDiet	Cat#0001326
Larch arabinogalactan	Megazyme	Cat#P-ARGAL
Leucine	Sigma-Aldrich	Cat#L8000
Lysine	Sigma-Aldrich	Cat#L5501
Lysozyme	Thermo Fisher Scientific	Cat#BP535-1
Magnesium chloride anhydrous	Sigma-Aldrich	Cat#M8266
Magnesium sulfate anhydrous	Sigma-Aldrich	Cat#M7506
Magnesium sulfate heptahydrate	Sigma-Aldrich	Cat#M5921
Manganese(II) sulfate monohydrate	Mallinkrodt	Cat#6192
Mannose	Acros Organics	Cat#150600
Menadione	Sigma-Aldrich	Cat#M5625
Methanol anhydrous	Thermo Fisher Scientific	Cat#A412-1
Methionine	Sigma-Aldrich	Cat#M9625
Mucin from porcine stomach	Sigma-Aldrich	Cat#M1778
N-acetyl glucosamine	Sigma-Aldrich	Cat#A3286
Nicotinic acid	Sigma-Aldrich	Cat#N4126
Osmium tetroxide	Electron Microscopy Sciences	Cat#19100
p-Aminobenzoic acid	Sigma-Aldrich	Cat#A9878
Pancreatic digest of casein	BioWorld	Cat#30620060-1
Phenol	Sigma-Aldrich	Cat#P4557
Phenol:Chloroform:Isoamyl Alcohol (pH 8.05)	Thermo Fisher Scientific	Cat# 15593031
Phenol:Chloroform:Isoamyl Alcohol (pH 4.3)	Fisher Scientific	Cat#BP1754I-400
Phenylalanine	Sigma-Aldrich	Cat#P2126
p-nitrophenyl α-L-fucopyranoside	Sigma-Aldrich	Cat#N3628
p-nitrophenyl β-D-xylopyranoside	Sigma-Aldrich	Cat#N2132
Polygalacturonic acid	Sigma-Aldrich	Cat#P3850
Potassium 4-nitrophenyl sulfate	Sigma-Aldrich	Cat#N3877
Potassium chloride	Sigma-Aldrich	Cat#P9333
Potassium dihydrogen phosphate	Thermo Fisher Scientific	Cat#P284
Potato pectic galactan	Megazyme	Cat#P-PGAPT
Proline	Sigma-Aldrich	Cat#P5607
Propionic acid	Acros Organics	Cat#149300010

(*Continued on next page*)

Continued

REAGENT or RESOURCE	SOURCE	IDENTIFIER
Propylene oxide	Electron Microscopy Sciences	Cat#20412
Pyridoxine HCl	Sigma-Aldrich	Cat#P9755
Resazurin	Acros Organics	Cat#418900010
Retrievagen A	BD Biosciences	Cat#550524
Rhamnogalacturonic acid	Megazyme	Cat#P-RHAM1
Riboflavin	Sigma-Aldrich	Cat#R7649
RNAprotect	QIAGEN	Cat#76506
SDS	Sigma-Aldrich	Cat#L3771
Serine	Sigma-Aldrich	Cat#84959
Sodium acetate	Sigma-Aldrich	Cat#S2889
Sodium bicarbonate	Sigma-Aldrich	Cat#S5761
Sodium chloride	Sigma-Aldrich	Cat#S7653
Sodium citrate	Sigma-Aldrich	Cat#S1804
Sodium hydroxide	Sigma-Aldrich	Cat#S8045
Sodium lactate	Thermo Fisher Scientific	Cat#S326-500
Sodium molybdate dehydrate	JT Baker Chemical Company	Cat#3764
Sugar beet arabinan	Megazyme	Cat#p-ARAB
Tamarind xyloglucan	Carbomer	Cat#4-00634
Thiamine HCl	Sigma-Aldrich	Cat#T4625
Thioctic acid	Sigma-Aldrich	Cat#T5625
Threonine	Sigma-Aldrich	Cat#T8625
Thymine	Sigma-Aldrich	Cat#T0895
Tris	Thermo Fisher Scientific	Cat#BP152
Triton X-100	Sigma-Aldrich	Cat#T9284
TRIzol	Invitrogen	Cat#15596026
Tryptone	Thermo Fisher Scientific	Cat#BP1421
Tyrosine	Sigma-Aldrich	Cat#T3754
Uracil	Sigma-Aldrich	Cat#U1128
Valeric acid	Alfa Aesar	Cat#109-52-4
Valine	Sigma-Aldrich	Cat#V0500
Wheat arabinoxylan	Megazyme	Cat#P-WAXYL
Xylene	Sigma-Aldrich	Cat#296333
Xylene Substitute	Sigma-Aldrich	Cat#A5597
Xylose	Sigma-Aldrich	Cat#X3877
Yeast extract	Fluka Analytical	Cat#70161
Zinc sulfate heptahydrate	JT Baker Chemical Company	Cat#4382
Critical Commercial Assays		
AccuPrimeTaq DNA Polymerase, high fidelity kit	Thermo Fisher Scientific	Cat#12346086
Affymetrix Mouse Gene ST 2.1 strips	Affymetrix	Cat#902120
Arcturus PicoPure DNA Extraction Kit	Arcturus	Cat#KIT0103
DNeasy Blood & Tissue Kit	QIAGEN	Cat#69506
epMotion 5075 TMX	Eppendorf	Cat#960020033
High-sensitivity DNA analysis kit	Agilent	Cat#5067-4626
KAPA SYBRFAST qPCR kit	KAPA Biosystems	Cat#KK4600
KAPA Library Quantification Kit for Illumina platforms	KAPA Biosystems	Cat# KK4824
Mouse Lipocalin-2/NGAL DuoSet ELISA kit	R & D Biosystems	Cat#DY1857

(*Continued on next page*)

Continued

REAGENT or RESOURCE	SOURCE	IDENTIFIER
Pierce Microplate BCA Protein Assay Kit	Thermo Fisher Scientific	Cat#PI23252
PowerSoil Isolation Kit	MoBio Laboratories	Cat#12888
Qubit RNA Assay Kit	Thermo Fisher Scientific	Cat#Q32852
Ribo-Zero rRNA Removal Kits (Bacteria)	Illumina	Cat#MRZB12424
RNeasy Protect Bacteria Mini Kit	QIAGEN	Cat #74524
SequalPrep Normalization Plate Kit, 96-well	Thermo Fisher Scientific	Cat#A1051001
TURBO DNase kit	Ambion	Cat#AM1907
Deposited Data		
16S rRNA gene sequences and metadata	NCBI BioProjectID; NCBI SRA	PRJNA300261;SRP065682
Mouse microarray data	NCBI Geo	GSM2084849–55
RNA-Seq data	NCBI BioProjectID	NCBI: SRP092534, SRP092530, SRP092478, SRP092476, SRP092461, SRP092458, SRP092453
Experimental Models: Organisms/Strains		
Akkermansia muciniphila: DMS 22959, type strain	DSMZ	Cat#DMS 22959
Bacteroides caccae: DSM 19024, type strain	DSMZ	Cat#DSM 19024
Bacteroides ovatus: DSM 1896, type strain	DSMZ	Cat#DSM 1896
Bacteroides thetaiotaomicron: DSM 2079, type strain	DSMZ	Cat#DSM 2079
Bacteroides uniformis: ATCC 8492, type strain	ATCC	Cat#ATCC 8492
Barnesiella intestinihominis: YIT11860	DSMZ	Cat#DSM 21032
Citrobacter rodentium: DBS100	David Schauer, Massachusetts Institute of Technology	N/A
Citrobacter rodentium: DBS120	David Schauer, Massachusetts Institute of Technology	N/A
Clostridium symbiosum: DSM 934, type strain, 2	DSMZ	Cat#DSM 934
Collinsella aerofaciens: DSM 3979, type strain	DSMZ	Cat#DSM 3979
Desulfovibrio piger: ATC 29098, type strain	ATCC	Cat#ATC 29098
Escherichia coli HS	ATCC	N/A
Eubacterium rectale: DSM 17629, A1-86	DSMZ	Cat#DSM 17629
Faecalibacterium prausnitzii: DSM 17677, A2-165	DSMZ	Cat#DSM 17677
Marvinbryantia formatexigens: DSM 14469, type strain, I-52	DSMZ	Cat#DSM 14469
Roseburia intestinalis: DSM 14610 type strain, L1-82	DSMZ	Cat#DSM 14610
Sequence-Based Reagents		
16S rRNA gene Illumina sequencing primers	Kozich et al., 2013	Table S2B
qPCR primers	This paper	Table S3A
Software and Algorithms		
Arraystar	DNAStar	http://www.dnastar.com/t-sub-products-genomics-arraystar.aspx
Gen5	Biotek	http://www.biotek.com/products/microplate_software/gen5_data_analysis_software.html

(*Continued on next page*)

Continued

REAGENT or RESOURCE	SOURCE	IDENTIFIER
ImageJ	Schneider et al., 2012	http://imagej.net/Welcome
Microsoft Excel	Microsoft	https://products.office.com/en-us/excel
Mothur v1.33.3	Schloss et al., 2009	http://www.mothur.org/
Multi-array average (RMA) method	Irizarry et al., 2003	http://www.bioconductor.org/
Prism v5.04	GraphPad Software	http://www.graphpad.com/scientific-software/prism/
QIAGEN's Ingenuity Pathway Analysis	QIAGEN	http://www.ingenuity.com/products/ipa
R	The R Foundation	https://www.r-project.org/
R - Limma package	Ritchie et al., 2015	https://bioconductor.org/packages/release/bioc/html/limma.html
R - Plyr package	Wickham, 2011	http://cran.r-project.org/web/packages/plyr/index.html
UCHIME	Edgar et al., 2011	http://drive5.com/usearch/manual/uchime_algo.html
Other		
Acid-washed glass beads (212-300 μm)	Sigma-Aldrich	Cat#G1277
Anaerobic chamber	Coy manufacturing	Vinyl Type A + Type B
Biostack automated plate handling device	Biotek Instruments	BIOSTACK2WR
Bioluminescence reader	Xenogen	IVIS200
Breathe-Easy polyurethane membrane	Biversified Biotech	Cat#BEM-1
Flat bottom 96-well plates	Costar	
General Laboratory Homogenizer	Omni International	
Microdissection instrument	Arcturus	Veritas Microdissection Instrument
Millex-GV Syringe Filter Unit, 0.22 μm, PVDF, 4 mm, ethylene oxide sterilized	EMD Millipore	Cat#SLGV004SL
Mini-BeadBeater-16	Biospec Products	Cat#607
Powerwave HT absorbance reader	Biotek Instruments	PowerWaveHT
Synergy HT absorbance reader	Biotek Instruments	Synergy HT
Upright fluorescence microscope	Olympus	BX60
Transmission electron microscope	Philips	Philips CM-100

CONTACT FOR REAGENT AND RESOURCE SHARING

Further information may be obtained from the Lead Contact Eric C. Martens (Email: emartens@umich.edu; address: University of Michigan Medical School, Ann Arbor, Michigan 48109, USA).

EXPERIMENTAL MODEL AND SUBJECT DETAILS

Gnotobiotic Mouse Model and Diet Treatments

All animal experiments followed protocols approved by the University of Michigan, University Committee for the Use and Care of Animals. Germfree male and female wild-type Swiss Webster mice were colonized at 8–9 weeks of age and none of these mice were involved in any previous experiments/treatments. Mice were housed alone or in groups as appropriate for gender, litter and diet requirements and provided ad libitum with autoclaved distilled water and the diets described below.

Identities and culture purity of the bacterial species in the synthetic gut microbiota were confirmed by sequencing their 16S rRNA genes, followed by comparison to sequences in public databases. Bacteria were grown in their respective media (Table S1) for community assembly or in vitro growth evaluation on carbohydrates. Each individual bacterial member of the SM was grown anaerobically (atmosphere 85% N_2, 10% H_2, 5% CO_2) in its respective medium (Table S1) at 37°C with final absorbance (600nm) readings ranging from about 0.5 to 1.0. Bacterial cultures were mixed in equal volumes and each individual inoculum sealed in its own tube with anaerobic headspace. Each mouse was gavaged with 0.2 mL of this mixture (freshly prepared each day) for three consecutive days at nearly the same time of the day.

Fiber-free (FF) and Prebiotic (Pre) diets were sterilized by gamma irradiation and the Fiber-rich (FR) diet (LabDiet 5010; autoclavable rodent diet) was sterilized by autoclaving. The FF diet was manufactured by Teklad/Envigo (WI, USA) and, as previously

described (TD.140343) (Kamada et al., 2012), consisted of a modified version of Harlan TD.08810 in which starch and maldodextrin were replaced with glucose. The Pre diet was a new formulation based on the FF diet with 2.1% of a purified polysaccharide mixture (Table S1) added along with 10% cornstarch (each replacing an equivalent amount of glucose).

On day 14 after colonization (Figure 1B), mice were randomly assigned to groups by a technician, who was not aware of the details of the treatment groups. The mice were sometimes caged separately even within individual groups. For dietary oscillations, mice from their respective cage were transferred to a different cage with another diet. Bedding was replaced in each cage before the mice were transferred. To minimize the potential for circadian effects, the oscillation was carried out at nearly the same time of the day (±1.0 hr between different days) and fecal samples were collected just prior to their transfer to another cage containing a different diet. The fecal samples were immediately stored at −20°C until further use.

Citrobacter rodentium Infection

A kanamycin (Km)-resistant wild-type *C. rodentium* strain (DBS120) and a luciferase-expressing strain of *C. rodentium* (DBS100; resistant to ampicillin (Amp)) were used (Kamada et al., 2012). Each mouse was gavaged with 0.2 mL of culture grown aerobically overnight at 37°C (~10^9 CFU grown in Luria-Bertani broth without antibiotics). The exact same culture was used to gavage all mice in a single experiment to rule out effects of growth variation on pathogenesis. For experiments with luciferase expressing *C. rodentium*, mice were fed the FF diet for nearly the same duration (39 days instead of 42) as for the other experiment (Experiment 2B, Figure 5), prior to infecting them with *C. rodentium*. For the experiment with germfree (GF) mice, two groups of mice were separately pre-fed the FR and FF diets for ~4 weeks prior to infection with luciferase-expressing *C. rodentium* or the wild-type *C. rodentium*.

Formulation of the Synthetic Microbiota

We selected 12/14 bacterial species (Figure 1A) from the list of the most common/frequent 75−89 species in the human gut (Qin et al., 2010). Moreover, the selection of 14 species was based in part on carbohydrate utilization abilities of a larger pool of ~350 strains that were screened on the same platform as shown in Figure 1A (K. Urs, N.A.P., and E.C.M., unpublished data). Based on the in vitro assays, our synthetic microbiota (SM) is not biased toward mucin-degrading bacteria, as only 4/14 species possess this ability (Figure 1A).

METHOD DETAILS

Experimental Design

A total of four gnotobiotic animal experiments (Experiments 1−4; also mentioned in figure legends) were performed – details of the experimental replication are provided in the corresponding figure legends. Both male and female mice were randomly used depending on the availability of animals. Gnotobiotic Experiment 1 contained 2 male mice in Fiber-rich (FR) group, 2 male mice in Fiber-free (FF) group and 1 male mouse in Prebiotic (Pre) group; all other animals in Gnotobiotic Experiment 1 were females. Gnotobiotic Experiment 2A and 2B had all male mice. All animals in Gnotobiotic Experiment 3 were females. Gender details of the animals in gnotobiotic Experiment 4 are shown in Figure 6 (both males and females were used). For infection with wild-type *C. rodentium* in germfree (GF) mice, all male mice were used. Gender details of GF mice used for infection with luciferase-expressing *C. rodentium* are included in Figure S7 (both males and females were used). Finally, all GF mice used for measurement of the colonic mucus layer (Figure 4C) were females. The researchers were not blinded to the identities of the treatment groups; however, the technician who assigned individual gnotobiotic animals to different treatment groups was not aware of the experimental details. Measurements of the colonic mucus layer were single blinded (see details below in the relevant section). The pathologist who devised the inflammation-scoring rubric was not blinded, and the pathologist who performed the histology scoring and the technician who performed electron microscopy were blinded for the identities of the treatment groups (see below for details of the methods). No data were excluded from the final analysis.

Sample size estimations were performed as follows in consultation with a statistician. Based on previous studies it was assumed an effect size (ratio of mean difference to within group standard deviation) of 3 would be reasonable for readouts such as mucus layer measurements, enzyme assays and measurement of transcript changes. With 3 animals in each group and a 5% significance level, two-sided, this would yield a power of 78% for the t test. Therefore, for some of the feeding groups (those alternated between different diets), 3 animals were used. However, for other feeding groups that were more important for the central research question of the study (e.g., constant feeding on Fiber-rich (FR) and Fiber-free (FF) diets), at least 4 animals were used to obtain higher power. For *C. rodentium* infection experiments, in most cases 5 animals per group were used based on results of our previous study (Kamada et al., 2012).

Sample Processing for Animal Experiments

All animals were killed using CO_2 asphyxiation followed by cervical dislocation. The gastrointestinal tracts were quickly removed. The colons were gently separated, by cutting at the cecum-colon junction and the rectum, and immediately preserved in Carnoy's fixative (dry methanol:chloroform:glacial acetic acid in the ratio 60:30:10) with slight modifications to a previous protocol (Johansson and Hansson, 2012). Note that the Carnoy's fixative was made fresh with anhydrous methanol, chloroform and glacial acetic acid. The colons were fixed in Carnoy's solution for 3 hr followed by transfer to fresh Carnoy's solution for 2−3 hr. The colons were

then washed in dry methanol for 2 hr, placed in cassettes and stored in fresh dry methanol at 4°C until further use. Cecal contents from each animal were divided into replicates; instantly flash-frozen in liquid nitrogen and were stored at −80°C until further use. Immediately after squeezing out the cecal contents, the cecal tissues were transferred in separate screw-cap tubes and were rapidly flash-frozen in liquid nitrogen, followed by their storage at −80°C until further use. Lengths of colons were measured immediately after fixation in Carnoy's solution by photographing the colons in a reference cassette of identical size, followed by length measurement in ImageJ.

Purification of Mucin *O*-Glycans

Mucin *O*-glycans were purified from porcine gastric mucus as previously described in Martens et al. (2008), albeit with several modifications. Porcine gastric mucin (Type III, Sigma, USA) was suspended at 2.5% w/v in 100 mM Tris (pH 7.4): the mixture was immediately autoclaved for 5 min to increase solubility and reduce potential contaminating glycoside hydrolase and polysaccharide lyase activity, then cooled to 55°C. Proteinase K (Invitrogen, USA) was added to a final concentration of 0.1 mg/ml and the suspension was incubated at 55°C for 16−20 hr with slow shaking. The proteolyzed solution was subsequently centrifuged at 21,000 x g for 30 min at 4°C to remove insoluble material, and NaOH and $NaBH_4$ were added to final concentrations of 0.1 M and 1 M, respectively. This solution was incubated at 65°C for 18 hr to promote selective release of *O*-linked glycans (mucin *O*-glycans and GAGs) from mucin glycopeptides by alkaline β-elimination. The pH was subsequently decreased to 7.0 with HCl and the neutralized mixture centrifuged at 21,000 x g for 30 min at 4°C, and then filtered through a 0.22 μm filter (Millipore) to remove remaining insoluble material. The filtrate was exhaustively dialyzed (1 kDa cutoff) against deionized distilled H_2O to remove salts and contaminating small molecules. The collected mucosal glycans were further fractionated using anion exchange chromatography by passing them twice over a DEAE-Sepharose (Sigma) column (325 mL bed volume; equilibrated in 50 mM Tris 7.4; gravity flow). The flow through (neutral fraction) was collected and the column washed with 1L of 50 mM Tris, pH 7.4. This fraction was used in all growth experiments and was further prepared by dialyzing against ddH_2O (1 kDa cutoff), lyophilized and resuspended in ddH_2O at 20 mg/ml.

Bacterial Growth Assays in a Custom Carbohydrate Array

All species except *Desulfovibrio piger* were evaluated in a custom carbohydrate array (n = 2 replicate cultures per glycan); *D. piger* failed to grow in any of the tested minimal media, but is not predicted to have extensive carbohydrate-degrading capacity based on its small genomic complement of only 30 carbohydrate active enzymes. The custom carbohydrate array was formulated according to Martens et al., 2011, but with a few modifications included in the following protocol: flat bottom 96-well plates (Costar) were used, to which 100 μL of a 2x concentrated solution (prepared in Milli-Q water) of each of the sterilized carbohydrate stocks (Table S1) were added. The plates were then transferred to the anaerobic chamber (10% H_2, 5% CO_2 and 85% N_2) and were allowed to equilibrate with the anaerobic atmosphere for ~3−4 hr. Growth assays for all carbohydrates were carried out in non-adjacent duplicates and all growth arrays contained two non-adjacent water only negative controls that were checked to ascertain that other medium components without added carbohydrates did not yield detectable growth. The cultures for the inoculation were grown overnight in their respective minimal media (MM)/regular growth media at 37°C under an anaerobic atmosphere (10% H_2, 5% CO_2 and 85% N_2). MM for some bacterial species were used from previous studies, and for other members of the synthetic microbiota, MM with novel formulations were devised (see Table S1 for compositions of all growth media used in this study). MM were pre-reduced in the anaerobic chamber overnight by loosening the lids of the glass bottles containing the MM. 1 mL of the culture was centrifuged and the pellet was recovered – note that the centrifugation was performed inside the anaerobic chamber. The pellet was washed 2 times in the respective MM in order to remove carried over carbohydrates from the culture media and was then resuspended in 1 ml, 2x concentrated MM without any carbohydrates. This 1 mL culture was used to inoculate 50 mL of 2x concentrated MM without carbohydrates at a 1:50 ratio. 100 μL of the resulting cultures were then added to the individual wells of the carbohydrate solutions in the 96-well plates, resulting in 200 μL of final volumes. A gas permeable, optically clear polyurethane membrane (Diversified Biotech, USA) was then used to seal the well plates under the same anaerobic atmosphere. Next, the well plates were loaded in a Biostack automated plate-handling device (Biotek Instruments, USA) placed inside the anaerobic chamber, which was coupled with a Powerwave HT absorbance reader (Biotek Instruments, USA).

Absorbance values were measured at 600nm (A_{600}) at an interval of 10 min over 96 hr for all species, except for *Akkermansia muciniphila*, for which the absorbance was measured over 144 hr, owing to its relatively slow growth on mucin *O*-glycans (Figure S1B). To construct the heatmap containing relative growth values (Figure 1A), absorbance data of all bacterial species were normalized as follows: only carbohydrate growth assays for which both replicate cultures produced an increase in absorbance of more than 0.1 were scored as positive (all other values were set to 0). Next, the maximum change in absorbance was normalized within each individual species by setting its best growth to 1.0 and normalizing all other positive growths to this maximum value (normalized values were thus between 0 and 1.0). Finally, growth on each substrate was normalized across species by setting the maximum (previously normalized) growth value on that substrate to 1.0 and then adjusting the growth values for other strains on that same substrate relative to the maximum value, yielding final normalized values between 0 and 1.0. Both raw and normalized values are provided in Table S1.

To perform RNA-Seq analysis on pure cultures, *A. muciniphila* and *Bacteroides caccae* were grown anaerobically in their respective minimal media (Table S1). *A. muciniphila* was grown separately on two different substrates N-acetylglucosamine (5 mg/ml final concentration) and purified mucin *O*-glycans (10 mg/ml final concentration). Cultures of *A. muciniphila* were grown to mid-log phase

(A_{600} values between 0.45–0.6). Cultures of *B. caccae* were grown separately on glucose and mucin *O*-glycan as the carbon sources (10 mg/ml final concentration for both sugars) to mid-log phase (OD values between 0.7–0.8). Cultures of both species were treated with RNAprotect (QIAGEN, USA) according to the manufacturer's instructions. The RNAprotect treated bacterial pellets were stored at −80°C until extraction of RNA. Two replicate cultures per glycan (with closely matching ODs) were performed for each of the two bacterial species.

Citrobacter rodentium quantification

To determine the CFUs of *C. rodentium*, freshly collected fecal samples were weighed and homogenized in cold phosphate-buffered saline and were plated on LB agar plates with 50 μg/ml Km (for strain DBS120) or 200 μg/ml Amp (for strain DBS100) at serial dilutions up to 10^{-9}. The plates were incubated aerobically overnight at 37°C. Killing of *E. coli* HS, the only facultative anaerobe in our SM, to Km and Amp was confirmed by plating it on LB agar with Km or Amp.

Extraction of Nucleic Acids

DNA from fecal samples was isolated using the MoBio PowerSoil Isolation Kit (MoBio Laboratories, USA) adapted for use in the epMotion 5075 TMX or the DNA extraction protocol used for *Collinsella aerofaciens* (mentioned below). DNA was extracted from the bacterial pure cultures using DNeasy Blood & Tissue Kit (QIAGEN, USA), except that the following bead beating and phenol–chloroform extraction protocol, was employed to better extract DNA from *C. aerofaciens*: 1–2 mL of the overnight grown culture was centrifuged and the resulting pellet was combined with acid-washed glass beads (212–300 μm; Sigma-Aldrich, USA), 500 μl Buffer A (200 mM NaCl, 200 mM Tris, 20 mM EDTA), 210 μl SDS (20% w/v, filter-sterilized) and 500 μl phenol:chloroform:isoamyl alcohol (25:24:1, pH 8.05; Thermo Fisher Scientific, USA). A Mini-BeadBeater-16 (Biospec Products, USA) was used to disrupt the bacterial cells for 5 min at room temperature, which was followed by cooling the samples for 1–2 min on wet ice. The samples were then centrifuged and the aqueous phase was recovered. An equal volume of phenol:chloroform:isoamyl alcohol (25:24:1) was added to the aqueous phase and was mixed with the aqueous phase by gentle inversion. After centrifugation (12,000 rpm, 4°C, 3 min), the aqueous phase was recovered. Next, 500 μl of pure chloroform was added to the aqueous phase, mixed by inversion and the tubes were centrifuged (12,000 rpm, 4°C, 3 min). The aqueous phase was transferred into fresh tubes and 1 volume of −20°C chilled 100% isopropanol and 1/10 volume 3 M sodium acetate (pH 5.2) were added to the aqueous phase. The samples were mixed by gentle inversion and incubated at −20°C for 1 hr, centrifuged for 20 min (12,000 rpm, 4°C) and the supernatants were discarded. The pellets were washed in 70% ethanol (v/v, prepared in nuclease-free water), air-dried and then resuspended in nuclease-free water. The resulting DNA extracts were purified by using DNeasy Blood & Tissue Kit (QIAGEN, USA).

RNA was extracted from cecal contents using a standard phenol–chloroform method with bead beating as mentioned earlier (Sonnenburg et al., 2006), but with a few modifications: 1 mL of RNAprotect (QIAGEN, USA) stored at room temperature was added to 200–300 mg of cecal contents stored at −80°C, followed by thawing the cecal samples on wet ice. After the cecal contents were thawed, 250 μl acid-washed glass beads (212–300 μm; Sigma-Aldrich, USA) were added to the samples. Next, 500 μl of a solution of Buffer A (200 mM NaCl, 200 mM Tris, 20 mM EDTA), 210 μl of 20% SDS (filter sterilized) and 500 μl of phenol:chloroform:isoamyl alcohol (125:24:1, pH 4.3; Fischer Scientific, USA) were added to the samples. The mixture was then bead beaten (instrument same as above) for 5 min and centrifuged at 4°C (3 min at 13000 rpm). The aqueous phase was recovered and mixed with 500 μl of the aforementioned phenol:chloroform:isoamyl alcohol solution. Afterward, the mixture was centrifuged again at 4°C (3 min at 13,000 rpm) and the aqueous phase was recovered. 1/10 volume of a 3M sodium acetate (pH: 5.2) and 1 volume of −20°C chilled ethanol were added to the aqueous phase. The resulting solution was then mixed by gentle inversion and incubated for 20 min on ice. Afterward, the mixture was centrifuged at 4°C (20 min at 13,000 rpm). The pellet was recovered and washed twice in 500 μl of cold 70% ethanol. The mixture was centrifuged at 4°C (5 min at 13,000 rpm) and the RNA pellet was recovered, air-dried and then resuspended in nuclease-free water. The RNA extracts were then purified using an RNeasy Mini kit (QIAGEN, USA) according to the manufacturer's protocol. During extraction of RNA from the cecal contents, a portion (~100–200 μl) of homogenized material was removed immediately after bead beating and stored at −80°C for extraction of DNA. To extract DNA from these cecal-content derived samples, DNA extraction protocol described above (used for *C. aerofaciens*) was used, except that bead beating and inclusion of glass beads were skipped. RNA was extracted from the RNAprotect-treated cell pellets of bacterial pure cultures of *B. caccae* using RNeasy Protect Bacteria Mini Kit. For extraction of RNA from RNAprotect-treated cell pellets of *A. muciniphila*, the RNA extraction protocol used for cecal contents (see above) was used, except that the samples were not treated with RNAprotect after thawing. RNA was extracted from cecal tissue by thawing the samples in the presence of RNAprotect (as described above for cecal contents), followed by homogenization (OMNI International) involving metal beads. RNA was then extracted with Trizol (Invitrogen, USA) according to manufacturer's instructions. All RNA extracts were subjected to digestion of DNA using TURBO DNase (Ambion, USA) according to the manufacturer's instructions.

Bioluminescence Imaging and Transmission Electron Microscopy

For bioluminescence imaging of the luciferase-expressing *Citrobacter rodentium*, GI tracts were removed and luminal contents were gently flushed with a syringe by passing phosphate-buffered saline (PBS) through the colon. The GI tracts were then cut open flat and rinsed in PBS to remove loosely attached luminal contents. Bioluminescence was visualized (identical exposure across all samples) and photographed using the IVIS200, Xenogen system. The colonic tissue sections showing highest luciferase intensity (from both

Fiber-rich (FR) and Fiber-free (FF) diet fed colonized mice) were then immediately fixed in 2.5% glutaraldehyde prepared in 0.1 M Sorensen's buffer (pH 7.4). Thereafter, the samples were treated with 1% osmium tetroxide in 0.1 M Sorensen's buffer and were sequentially dehydrated in graded alcohols and propylene oxide, followed by infiltration in Spurrs or Epon. Ultrathin sections of the tissue samples were made using a diamond knife, stained and were visualized with a transmission electron microscope (Philips CM-100).

Laser Capture Microdissection

To perform laser capture microdissection (LCM) on colonic thin sections, 4 and 3 fecal masses were analyzed for the Fiber-rich (FR) and Fiber-free (FF) groups, respectively. Colonic thin sections that were deposited on microscope slides were deparaffinized in xylene followed by dehydration by isopropanol (see details in the immunofluorescence staining protocol below). The sections were stored overnight in a container with Drierite dessicant (Drierite, USA). LCM was carried out using a Veritas Microdissection instrument (Arcturus, USA). DNA was extracted from the microdissected samples using the Arcturus Pico Pure DNA extraction kit and the accompanying protocol. In order to perform Ilumina sequencing, 16S rRNA genes were amplified from the LCM-derived samples using a low biomass-optimized touch down PCR protocol as follows: denaturation at 95°C for 2 min; a total of 20 cycles with a touchdown program: denaturation at 95°C for 20 s, extension at 72°C for 5 min, annealing starting at 60°C for 15 s which decreased 0.3°C per cycle; a total of 20 cycles: extension at 72°C for 5 min, annealing at 55°C 15 s and extension at 72°C for 5 min; final extension at 72°C for 5 min. Note that a 5 min extension was used in order to reduce chimera development. Library preparation and sequencing were carried out using similar protocols described for fecal and cecal samples (see below).

Illumina Sequencing and Data Analysis

PCR and library preparation were performed by the University of Michigan Microbial Systems Molecular Biology Lab as described by Kozich et al. (2013). The V4 region of the 16S rRNA gene was amplified using the dual-index primers described by Kozich et al. (2013) with a few modifications to the PCR assay, which are included in the following protocol. Each of these dual-index primers contains an Illumina adaptor, an 8-nt index sequence, a 10-nt pad sequence, a 2-nt linker, and the V4 primers F515 and R806. These primer sequences are listed in Table S2. For the PCR assays, 5 μL of each of the 4 μM primers, 0.15 μL AccuPrime High Fidelity Taq polymerase (Thermo Fisher Scientific, USA), 2 μL of 10x AccuPrime PCR II buffer (Thermo Fisher Scientific, USA), 11.85 μL of sterile PCR-grade water and 1 μL of the DNA template were mixed. The PCR cycles started with a 2 min of denaturation at 95°C, followed by 30 cycles each consisting of 95°C for 20 s, 55°C for 15 s and 72°C for 5 min, followed by a final step of 72°C for 10 min. The amplicons were normalized to the lowest concentration of the pooled plates using a SequalPrep normalization plate kit (Thermo Fisher Scientific, USA). A KAPA Library Quantification kit for Illumina platforms (Kapa Biosystems, USA) was used to determine the library's concentration and an Agilent Bioanalyzer high-sensitivity DNA analysis kit (Agilent, USA) was employed to determine the amplicon size. The amplicons were sequenced using an Illumina MiSeq with a MiSeq Reagent 222 kit V2 (Illumina, USA). The libraries were prepared following the Illumina protocol for 2nM libraries: 'Preparing Libraries for Sequencing on the MiSeq' (part 15039740, Rev. D).

Raw sequences were analyzed using mothur (v1.33.3) (Schloss et al., 2009). The following control samples were included: 1) DNA extracted from the fecal samples collected from germfree mice, 2) a mixture of extracted DNA from pure cultures of the members of the synthetic microbiota (DNA samples from each strain were mixed in equal amounts) and 3) PBS negative controls during DNA extraction and PCR amplification. Following sequence barcode-trimming, sequences were aligned to a custom reference database, consisting of the V4 16S rRNA region from each of the 14 bacterial members and *C. rodentium*. UCHIME (Edgar et al., 2011) was used to remove sequence chimeras. The R package 'vegan' was used to calculate the principal coordinates analysis (PCoA) from the Bray-Curtis dissimilarity index based on phylotype classification of the 14 bacterial members. Standard R commands and the R package 'plyr' (Wickham, 2011) were used to generate median values of relative abundance or change in relative abundance over time, and the Wilcoxon signed-rank test (two-sample comparisons) or the Kruskal-Wallis test (multiple groups) was used to determine significance as indicated due to the nonparametric distribution of relative abundance data. R was used to visualize relative abundance of bacterial members in different groups, over time as streamplots, or in heatmaps. Change in relative abundance over time was determined by subtracting the relative abundance of the specified microbial member from the day prior within each animal, over time. Change in relative abundance followed a parametric distribution, and Student's t tests were used to calculate significant differences in the change of relative abundance between diet groups. The R package 'ggplots' was used to generate heatmaps visualizing the Percent of Maximum Abundance (POMA) as previously described (McNulty et al., 2013). For this, the relative abundance of the different species was normalized by their maximum abundance observed for a given species across all time-points from the given animal. A detailed list of commands used to analyze the data, including the commands used in mothur, are included in https://github.com/aseekatz/mouse.fiber. Raw sequences have been deposited in the Sequence Read Archive under the study accession and Bioproject identifiers (SRA: SRP065682 and PRJNA300261).

Microbial RNA-Seq and CAZyme Annotation

Microbial RNA-Seq was performed on pure cultures of *A. muciniphila* and *B. caccae* that were grown separately on mucin *O*-glycans and on the respective simple sugars (see above). For *Bacteroides thetaiotaomicron*, gene expression data from previous studies was utilized (Martens et al., 2008; Sonnenburg et al., 2005). To perform RNA-Seq on cecal samples, 3 samples each (out of 4) were randomly selected from Fiber-rich (FR) and Fiber-free (FF) diet groups and all three samples each from the Prebiotic diet (Pre), FR–FF

daily oscillation and Pre−FF daily oscillation groups were utilized. To remove ribosomal RNA, samples were subjected to Ribo-Zero rRNA Removal Kits (Bacteria) (Epicenter, Illumina, USA) according to the manufacturer's instructions. The resulting residual mRNA concentrations were quantified using Qubit RNA Assay Kit (Life Technologies, USA).

Libray preparation and sequencing of RNA-Seq libraries was carried out using the Illumina HiSeq platform and TruSeq adaptors. Samples were multiplexed in groups of 24 per lane (see Tables S4, S5, and S6 for quantification of reads mapped to each sample). The resulting data in fastq file format were demultiplexed and mapped to the respective species genomes or community metagenomes using RPKM normalization and default parameters, and were further analyzed for fold-change and statistics (moderated t test with Benjamini-Hochberg correction) within the Arraystar software package (DNAStar, USA). Mapping reads to all genes in the 14 species community was intended to retain the contributions of community member abundance shifts while mapping only to individual genomes was intended to normalize abundance shifts of the same species between conditions and isolate gene expression changes between conditions. The diet-specific behavior of known *B. thetaiotaomicron* and *B. ovatus* genes involved in fiber polysaccharide degradation (Table S6) was used as internal validation that biologically relevant changes in gene expression were indeed being detected. As stated above, three biological replicates were analyzed for each of the in vivo dietary conditions used.

p-Nitrophenyl Glycoside-Based Enzyme Assays

p-Nitrophenyl glycoside-based enzyme assays were carried out on cecal samples stored at −80°C. The cecal samples were thawed on wet ice and 500 μl buffer (50 mM Tris, 100 mM KCl, 10 mM $MgCl_2$; pH 7.25) was added to 22−67 mg of cecal contents. The buffer additionally contained the following additives: lysozyme (tiny amount of powder/100 mL buffer), TritonX (100 μl, 12%/100 mL buffer), DNases (tiny amount of powder/100 mL buffer) and protease inhibitor (one tablet of EDTA-free, Protease Inhibitor Cocktail, Roche, USA/100 mL buffer). After adding the buffer to cecal samples, the samples were sonicated with an ultrasonic processor for 45 s (9 cycles of 5 s sonication followed by a break of 10 s; 35% amplitude; using a tapered microtip of 3 mm) on ice. Sonicated samples were subjected to centrifugation (10,000 g, 10 min, 4°C). Supernatants (~400 μl) were carefully pipetted and were stored at −20°C until further use. The following nitrophenyl-linked substrates (Sigma-Aldrich, USA) were employed: Potassium 4-nitrophenyl sulfate, 4-nitrophenyl α-D-galactopyranoside, 4-nitrophenyl N-acetyl-β-D-glucosaminide, 4-nitrophenyl β-D-glucopyranoside, p-nitrophenyl α-L-fucopyranoside and *p*-nitrophenyl β-D-xylopyranoside. Protein concentrations in the supernatants were determined using Pierce Microplate BCA Protein Assay Kit (Thermo Scientific, USA). Some samples were diluted with the buffer (same buffer as above) to obtain a homogeneous range of protein concentrations across all samples. 5 μg of total protein was used in the 150 μl reactions inside flat-bottom, 96-well plates (Costar) with 10 mM nitrophenyl-based substrate in the buffer (same buffer as above). Absorbance measurements (405 nm) were started immediately in a plate reader (Biotek, USA) at 37°C and absorbance values were recorded every minute for 6−12 hr duration depending on linearity of the kinetic curve. The enzyme activities were determined by plotting a standard curve of known concentrations of 4-nitrophenol and measuring the OD values at 37°C.

Thickness Measurements of the Colonic Mucus Layer

Post Carnoy's fixation, the methanol-stored colon samples (see above) were embedded in paraffin and thin sections (~5 μm) were cut and deposited on glass slides. Alcian blue staining was performed by the following protocol: 1) deparaffinization and hydration to distilled water, 2) Alcian blue solution for 30 min, 3) washing in running tap water for 2 min, 4) rinsing in distilled water, 5) dehydration with 95% alcohol (2X changes) and treatment with absolute alcohol (2X changes), 3 min each, 6) clearance in xylene (3X changes), 3 min each 7) cover with coverslip. To measure the thickness of the colonic inner mucus layer, thousands of partially overlapping photographs were taken from nearly the entire length of each colon based from the Alcian blue stained slides after cross-validation using anti-Muc2 staining (Figures 4A and 4B main text). The images captured all of the available fecal masses of all mice, although this number was variable and there were generally fewer colonic fecal masses in mice fed the FF diet alone or in any combination. Image sample names were blinded by M.S.D. and M.W., and the thickness of the colonic sections were then measured by E.C.M. using ImageJ. Only regions in which the mucus layer was sandwiched between epithelium on one side and luminal contents on the other were used; care was taken to measure regions that represented the average thickness in each blinded image; 2−3 measurements per image were taken and averaged over the entire usable colon surface. See Figures 4A and 4B for representative images in which the region measured as the inner mucus layer is delineated in both Alcian blue and anti-Muc2 staining.

Measurements in *Cr* infected mice were conducted exactly as described for non-infected mice above, with the exception that only distal colon−rectal tissue was considered as this was uniformly a site at which inflammation was high and *C. rodentium* would be present. Since only sections in which luminal contents that could be visualized adjacent to the mucus layer were considered, only a few measurements were obtained for a single SM-colonized infected mouse fed the FF diet due to the fact that all mice in this group were extremely morbid and not eating.

qPCR

In addition to Illumina sequencing of the 16S rRNA genes (V4 region), as a second approach to quantifying relative bacterial abundance in fecal samples, phylotype-specific bacterial primers were designed. The primers were designed against randomly selected genes that were checked for homology against the other 13 species in each case. These primer sequences are listed in Table S3A. The primers were tested for specificities against the target strain by comparing the primer and target gene sequences against sequences in public databases. Moreover, specificity of each primer was validated by the following three approaches: 1) by

quantitative PCR (qPCR) against target species genome and melting curve analysis (for a single peak), 2) by qPCR for each primer set against a non-target template comprising of genomic DNA from the 13 bacterial species in our synthetic microbiota, 3) by performing qPCR against DNA extracted from the fecal samples of germfree mice feeding on the Fiber-rich diet. qPCR was carried out in 384 wells (with each plate including known concentrations of template DNA included to plot a standard curve). The qPCR analyses were performed using KAPA SYBR FAST qPCR Kits (KAPA Biosystems, USA) on Applied Biosystems (ABI) Real Time PCR instrument (ABI, USA). The amount of DNA was quantified by plotting a standard curve of varying DNA concentrations of the target template.

Quantification of Short-Chain Fatty Acids

Cecal samples stored at −80°C were used to quantify short-chain fatty acids (SCFAs). Samples were first thawed on wet ice. Then, an equivalent amount of Milli-Q water was added (100 ul per 100 mg of material) to cecal contents (≥0.05 g) and the samples were thoroughly homogenized by vortexing for 1 min. The samples were then centrifuged at 13,000 g for at least 3 min (or for a longer time depending on time required to obtain a tight pellet). The supernatant was pipetted and filtered through a 0.22 μm filter (Millex-gv 4mm SLGV004SL). Samples were kept on ice or frozen until quantification of SCFAs by high-performance liquid chromatography (HPLC). Some samples were diluted to obtain enough liquid to inject onto the HPLC, or in certain cases they were diluted so that they could be filtered. A Shimadzu HPLC with an Agilent HP-87X column was utilized for separating compounds, with a mobile phase of 0.01 N H_2SO_4, a flow rate of 0.6 ml/min, and a column temperature of 50°C. A UV detector set to a wavelength of 214 nm was used to measure concentrations.

Immunofluorescence Staining

The immunofluorescence staining for Muc2 mucin was performed on the colonic thin sections after several modifications to the protocols from Johansson and Hansson, 2012 and an immunohistochemistry/tissue section staining protocol from BD Biosciences, USA (http://www.bdbiosciences.com). The sections were deparaffinized by dipping in 50 mL Falcon conical tubes filled with xylene (Sigma-Aldrich, USA) for 5 min, followed by transfer to another tube with fresh xylene for 5 min – care was taken to completely immerse the tissue material in the liquid (also in the subsequent steps). This was followed by two dehydration steps of 5 min each using 100% isopropanol contained in conical tubes. The slides were then washed by dipping in conical tubes containing Milli-Q water. The antigens were retrieved by placing the slides in a glass beaker with enough BD Retrievagen A (pH 6.0; BD Biosciences, USA) to cover the slides. The sections were then heated by microwaving and holding at about 89°C for 10 min (microwaving was repeated during this time, as required). The slides were then cooled for 20 min at room temperature. Afterward, the slides were washed 3 times with Milli-Q water. Excess liquid was gently blotted away and a PAP pen was used to draw a circle around the tissue area, in order to better hold liquid on the tissue area during subsequent steps. Blocking was performed by immersing the slides into blocking buffer (1:10 dilution of goat serum (Sigma, USA) in 1x Tris-buffered Saline (TBS; 500 mM NaCl, 50 mM Tris, pH 7.4)) and incubating them at room temperature for 1 hr. For the primary antibody staining, the tissue sections were covered in a 1:200 dilution Mucin 2 antibody (H-300) (original concentration: 200 μg/ml; Santa Cruz Biotechnology, USA) in the aforementioned blocking buffer and incubated for 2 hr at room temperature. After the incubation step, the excess liquid was blotted away and the slides were rinsed 3 times in 1x TBS (in conical tubes) for 5 min each. The secondary antibody staining was performed by covering the tissue sections with a 1:200 dilution of Alexa Fluor 488 conjugated goat anti-rabbit IgG antibody (original concentration: 2 mg/ml; Thermo Fisher Scientific, USA) in blocking buffer and the sections were incubated for 1 hr at room temperature in dark. The excess liquid was blotted away and the sections were rinsed twice for 5 min each using TBS. Next, the sections were stained for 5 min at room temperature in dark using a 10 μg/ml of DAPI solution diluted in 1x TBS (Sigma-Aldrich, USA). The sections were then rinsed with Milli-Q water and blotted dry. Finally, the sections were covered with ProLong Gold Antifade Mountant (Invitrogen, USA), covered with coverslips and the edges of the coverslips sealed with nail polish. The slides were kept at room temperature in dark for at least 24 hr and then visualized by Olympus BX60 upright fluorescence microscope (Olympus, USA).

ELISA for Fecal Lipocalin

Frozen fecal samples (−20°C) were used to determine the levels of fecal Lipocalin (LCN-2). The assays were performed within 30 days of sample collection. The samples were prepared as mentioned previously (Chassaing et al., 2015), with a few modifications in the sample prepration protocol: fecal samples stored at −20°C were thawed on wet ice and 6.9−67.7 mg of samples were separated in fresh tubes, to which 0.5 mL of 1% (v/v) Tween 20 (Sigma-Aldrich, USA) prepared in PBS was added. To get a homogeneous suspension, the samples were vortexed for 20 min. The suspension was then centrifuged at 4°C for 10 min at 12000 rpm. Next, the supernatant was carefully recovered and stored at −20°C until the analysis. To measure the LCN-2 levels, a mouse Lipocalin-2/NGAL DuoSet ELISA kit (R & D Biosystems, USA) was employed and the manufacturer's protocol was followed.

Tissue Histology

To perform histology analyses on GI tracts of *C. rodentium* infected mice: first the intestinal segments (cecum and colon together) were fixed in Carnoy's fixative for 3 hr, followed by transfer to fresh Carnoy's fixative overnight. Next, the samples were washed in 100% methanol (2x) for 30 min each, which was followed by washing in 100% ethanol (2x) for 20 min each. The samples were then stored in 100% ethanol at 4°C until further use. After 100% ethanol washes, the intestinal tissue samples were divided into 3 sections for histology: cecum, ascending colon, and the descending colon/rectum. These sections were embedded, processed

and cut by an experienced histology core (Washington University, USA), and then stained with hematoxylin and eosin (H and E) prior to analysis. An unblinded experienced pathologist (T.S.S.) examined the slides from each of the groups to determine a viable readout. The best readout was determined to be the extent of epithelial area showing crypt hyperplasia. After a scoring rubric was devised, an independent blinded evaluator (C.A.H.) then measured the total length of each intestinal segment with a ruler in millimeters. Areas of increased crypt hyperplasia were then determined by microscopy and the lengths of these areas were measured as a percentage of the total epithelial length on a single slide.

Mouse Microarray Analyses

Mouse microarrays were carried out with Affymetrix Mouse Gene ST 2.1 strips. Expression values for each gene were calculated using a robust multi-array average (RMA) approach (Irizarry et al., 2003). Linear models were fitted to the data by employing the limma bioconductor package in R version 3.1.1. Note that selected probesets had a fold change greater than 1.5 and an FDR adjusted p value of 0.05 or less. Data were analyzed through the use of QIAGEN's Ingenuity Pathway Analysis (IPA, QIAGEN Redwood City, http://www.ingenuity.com) using the default parameters. Input data correspond to significantly detected genes with FDR < 0.05 and absolute log Fold-Change > 0.5. ILK signaling was the number 1 canonical pathway detected (p value = 8.33E-07). TNF targets corresponded to the number 1 (overlap p value = 2.64E-06) upstream regulator detected by IPA. The category 'Immune response of cells' was predicted as the most significantly activated (p value = 6.83E-06 and Z-score = 2.316) in the inflammatory response category.

QUANTIFICATION AND STATISTICAL ANALYSIS

Statistical Analyses

All experimental analyses were conducted in consultation with a statistician. Unless otherwise stated in individual method sections above, all statistical analyses were performed using Prism 5.04 (GraphPad Software, Inc.), except statistics for colony forming units (CFU) for *C. rodentium* (Figure 5A) were performed in Excel. Statistically significant differences are shown with asterisks as follows: *$p < 0.05$, **$p < 0.01$, ***$p < 0.001$ and ****$p < 0.0001$; whereas, ns indicates comparisons that are not significant. Numbers of animals (n) used for individual experiments, details of the statistical tests used and pooled values for several biological replicates are indicated in the respective figure legends. A two-tailed t test was employed in all cases. Since generally the microbiome data did not follow a normal distribution, for these data a nonparametric test such as the Wilcoxon test was used. An exception was the data in Figure 2C, which generally followed a normal distribution and hence a t test was used (see details in the section: Illumina sequencing and data analysis). For the other data that appeared normally distributed, a t test was used; otherwise, a non-parametric (Mann-Whitney) test was used (for example for Figure 4E). Finally, ANOVA (parametric) and Kruskal-Wallis (nonparametric) methods were used to describe differences between more than two groups. For data in Figure 6D, a non-parametric approach with Dunn's test and involving pairwise comparisons was employed.

DATA AND SOFTWARE AVAILABILITY

Accession Numbers

Data from this study have been deposited in the NCBI Short-Read Archive (SRA) and Gene Expression Omnibus (GEO) databases under the following accession and/or BioProjectID identifiers: 16S rRNA gene sequences and metadata (SRA: SRP065682, PRJNA300261); RNA-seq data (NCBI: SRP092534, SRP092530, SRP092478, SRP092476, SRP092461, SRP092458, SRP092453); mouse microarray data (GEO: GSM2084849-55). The commands used to analyze the 16S rRNA gene data can be found online at the following link: https://github.com/aseekatz/mouse.fiber.

Supplemental Figures

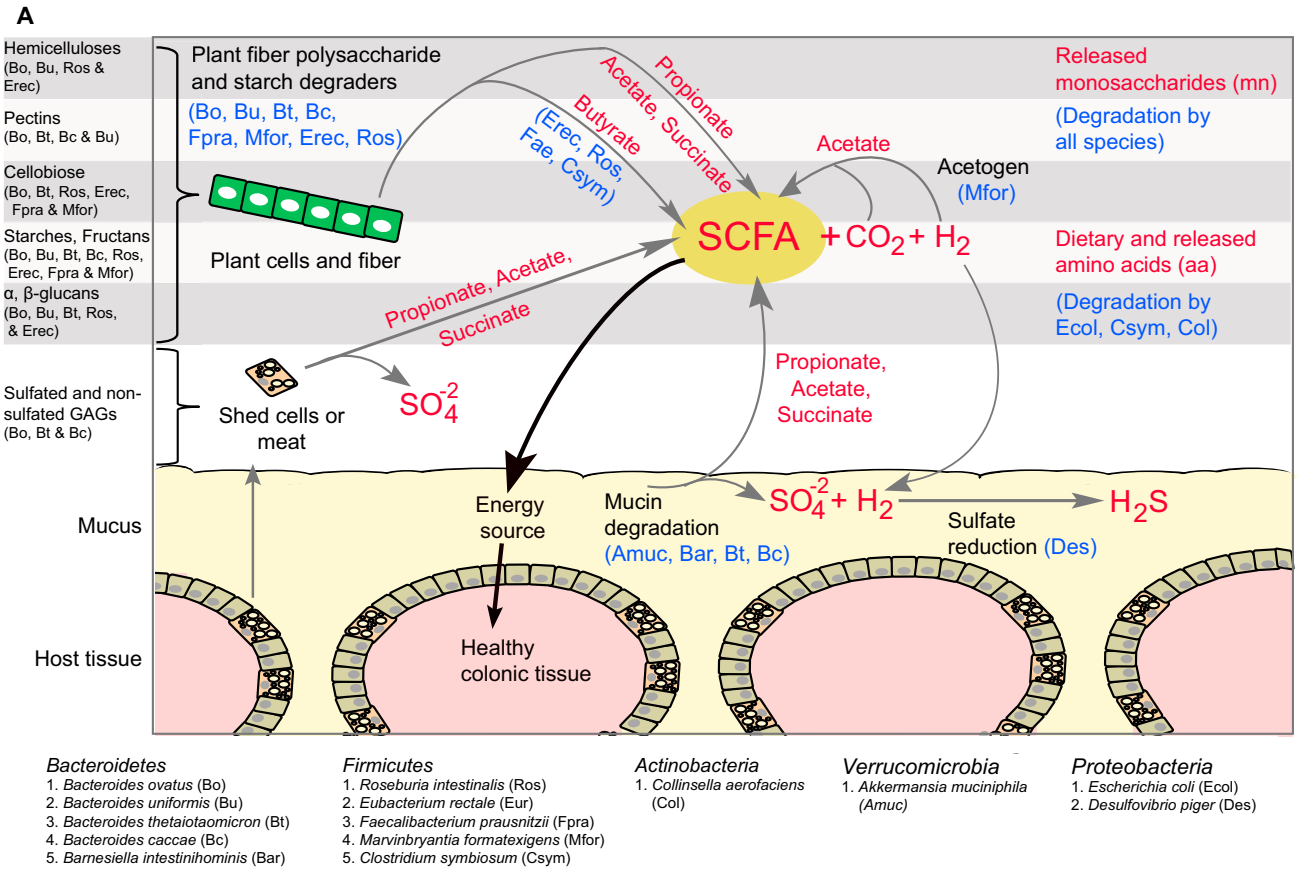

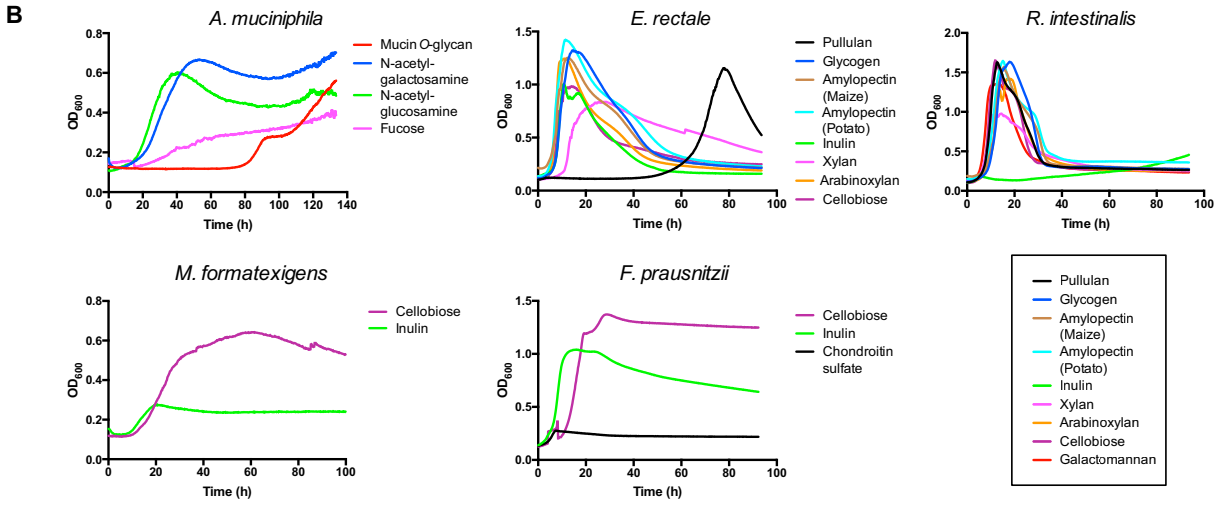

Figure S1. Versatile Metabolic Abilities Contributed by Members of the Human Gut Synthetic Microbiota (SM), Related to Figure 1

(A) A schematic displaying abilities of the SM to degrade a wide variety of dietary and host-derived polysaccharides and possible metabolic interactions between members of the SM. GAGs, Glycosaminoglycans.

(B) Representative growth curves of selected members of the SM on several polysaccharides and glycans as sole carbon sources (n = 2 for each glycan; values are shown as averages). The absorbance was measured every 10 min. See Table S1 for raw and normalized growth values and growth media descriptions for the 13 members of the SM evaluated for carbohydrate growth ability (all except *D. piger*).

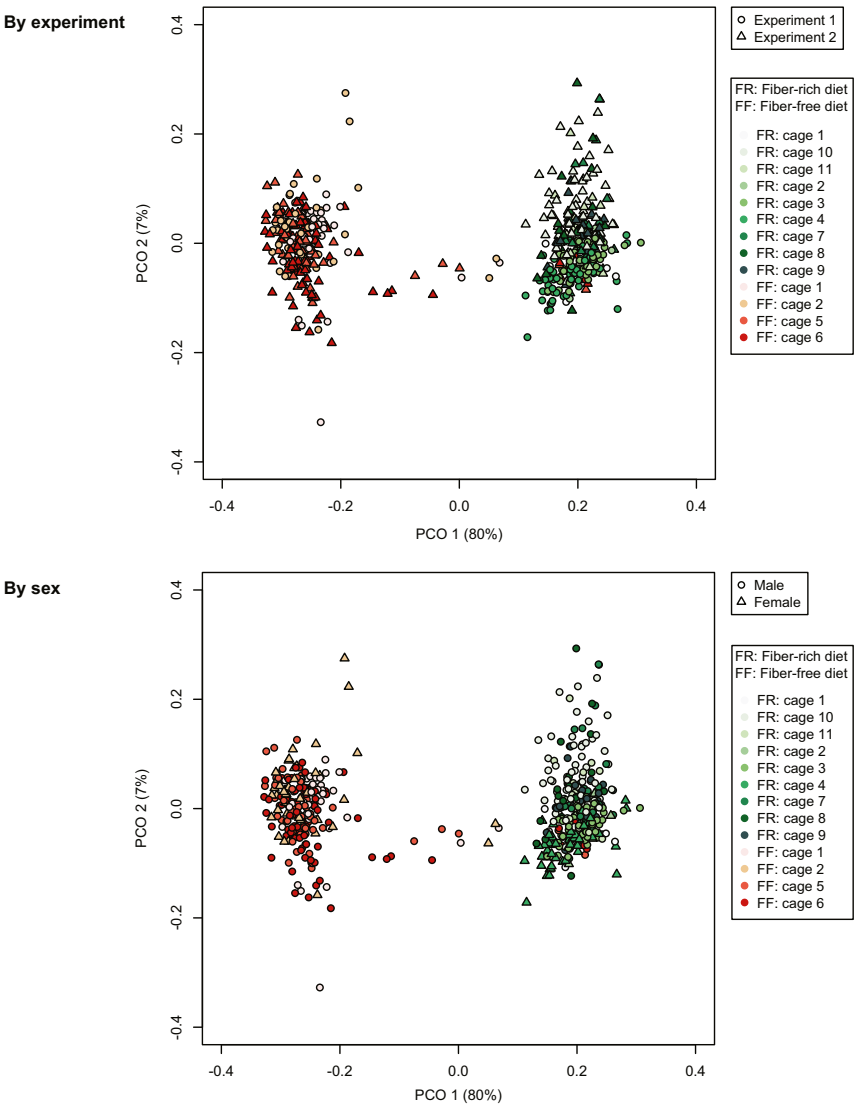

Figure S2. PCoA Plots Demonstrating Clustering of Fecal Bacterial Communities over Time in Two Feeding Regimens, Related to Figure 2

Principal coordinates analysis (PCoA) of microbial community dissimilarity (Bray-Curtis) in fecal samples (collected according to Figure 1B) as determined by 16S rRNA-based sequencing (V4 region). Samples from both *Experiments 1* and *2* are shown, with samples coded by experiment (top panel) or sex (bottom panel) and by cage (legend) (*Experiment 1*: n = 4 mice/group; *Experiment 2*: n = 7 mice/group).

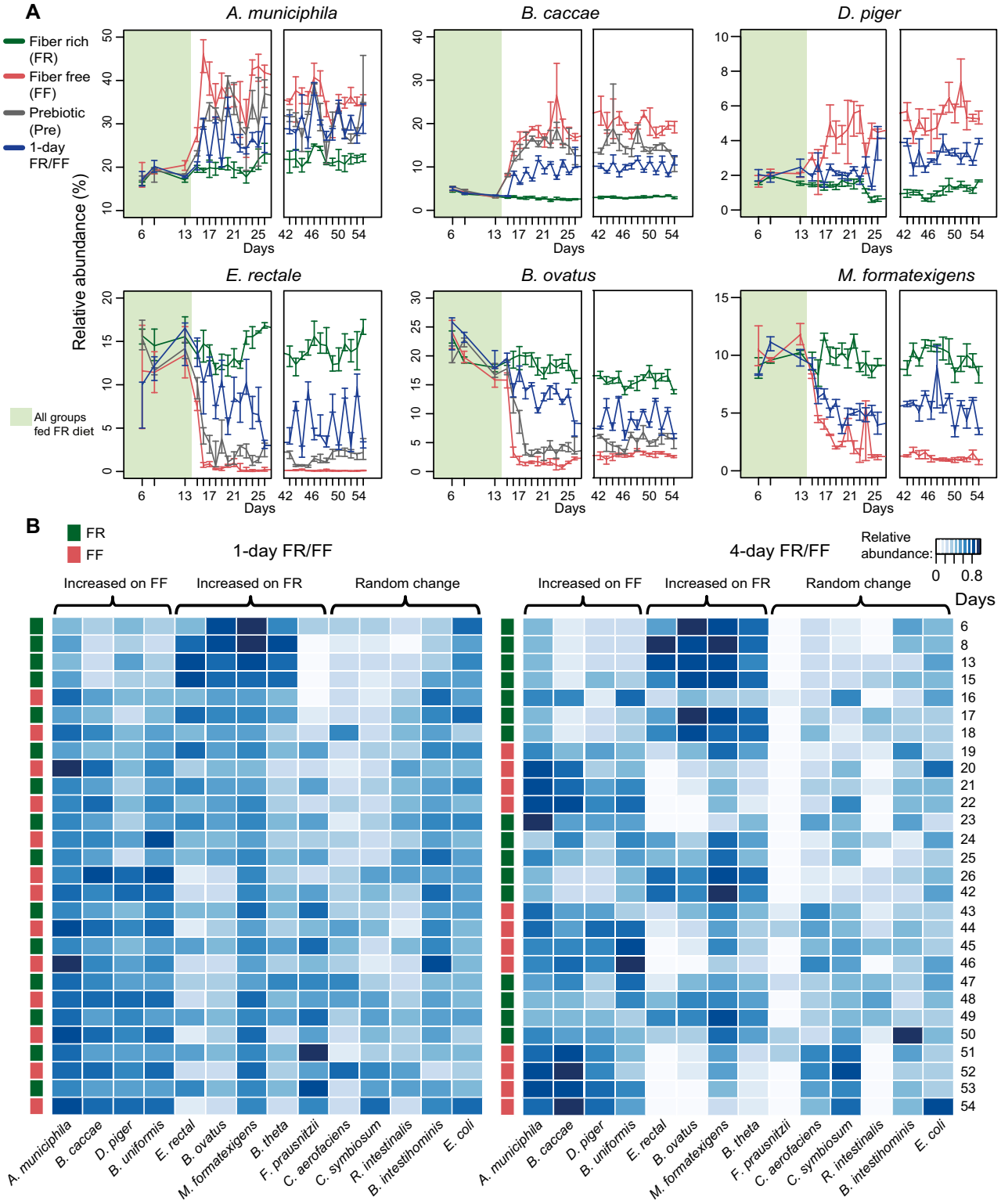

Figure S3. Fecal Microbial Community Dynamics in Mice from Distinct Dietary Feeding Groups, Related to Figure 2

(A) Relative abundance of indicated bacteria in mice over time subjected to various dietary regimes as determined by Illumina-based 16S rRNA sequencing (*Experiment 1*). An explanation for the inverse relationship between the relative abundances of *D. piger* and *M. formatexigens* on FR and FF diets is their

(legend continued on next page)

competition for the same electron donor (hydrogen). The increased proliferation of mucin-degrading bacteria in the FF diet indicates higher degradation of sulfated mucin *O*-glycans, which is supported by transcriptomic and enzyme assay data shown in Figure 3. The corresponding release of additional sulfate would preferentially feed the sulfate-reducer *D. piger*, leading to production of the toxic metabolite hydrogen sulfide (Figure S1A). Increased *D. piger* has also been observed in IBD patients (Gibson et al., 1991; Loubinoux et al., 2002), which could result from enhanced sulfate release by mucinolytic bacteria. Values are shown as medians ± IQR. n = 4 for FR and FF groups; n = 3 for Pre and 1-day FR/FF groups.

(B) Heatmap showing Percent of Maximum Abundance (POMA) values of all species for two of the feeding groups from Illumina-based sequencing (see Figure 1B); n = 3 mice/group (*Experiment 1*; according to timeline in Figure 1B). See also Table S2.

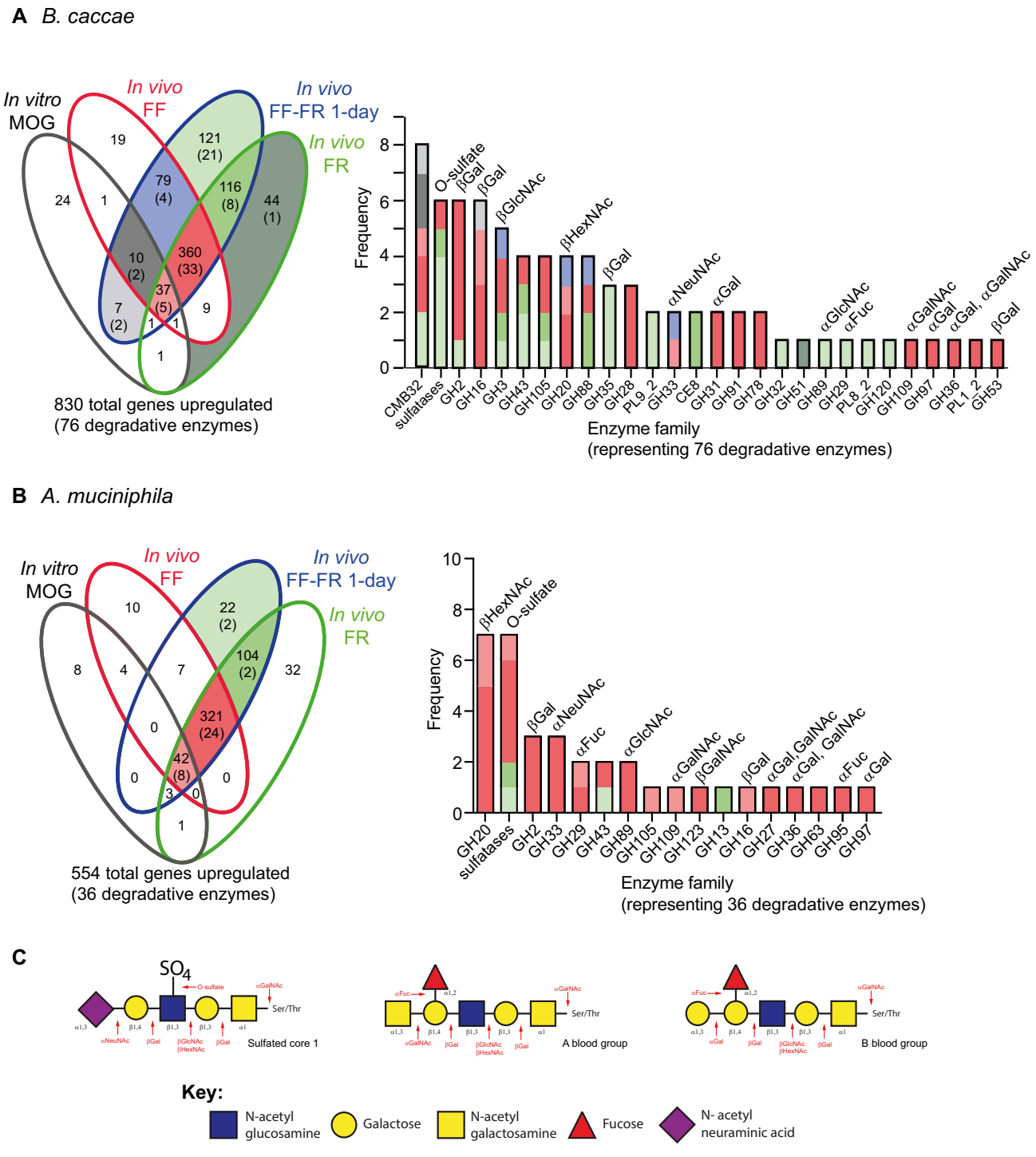

Figure S4. Dynamic Changes in Transcriptional Profiles of *B. caccae* and *A. muciniphila* In Vivo and In Vitro, Related to Figure 3

Figures are based on RNA-Seq measurements of *B. caccae* (A) and *A. muciniphila* (B) responses in vitro (minimal medium with simple sugars or MOG) and in vivo (constant feeding or daily alternation of FR and FF diets). In vivo samples are from the entire cecal community at the end of *Experiment 1*. Gene transcripts that were increased > 5-fold relative to the corresponding simple sugar references are included for each bacterium. Venn diagrams show overlap and differences of the transcripts between various groups. Numbers indicate the total differentially regulated gene count for a given sector, while number in parentheses denote numbers of carbohydrate-degrading enzymes (glycoside hydrolase, polysaccharide lyase or carbohydrate esterase families counted toward this number; sulfatases and carbohydrate binding module, CBM, families were not counted). Note that *A. muciniphila* shows less regulatory versatility as manifest by most of its upregulated enzymes being confined to the core (dark pink) sector containing all of the in vivo samples. This suggests that MOG only triggers a small percentage

(legend continued on next page)

of this species' *O*-glycan degrading responses in vitro; although 8 enzymes were also triggered in vitro. The corresponding histograms display frequencies of related enzyme families (shown with matching colors to their respective Venn sectors). Possible mucin-related degradative functions are given above each family-specific histogram bar. For in vitro samples, n = 2 for each MOG and simple sugar grown condition; for in vivo samples, n = 3 mice/group (*Experiment 1*).
(C) Schematic mucin *O*-glycan structures, from among $\sim 10^2$ that can be found on human and murine Muc2, with the sites at which various enzymes noted in (A) and (B) would be expected, or are known, to cleave. See also Tables S4 and S5 for in vivo and in vitro transcript data.

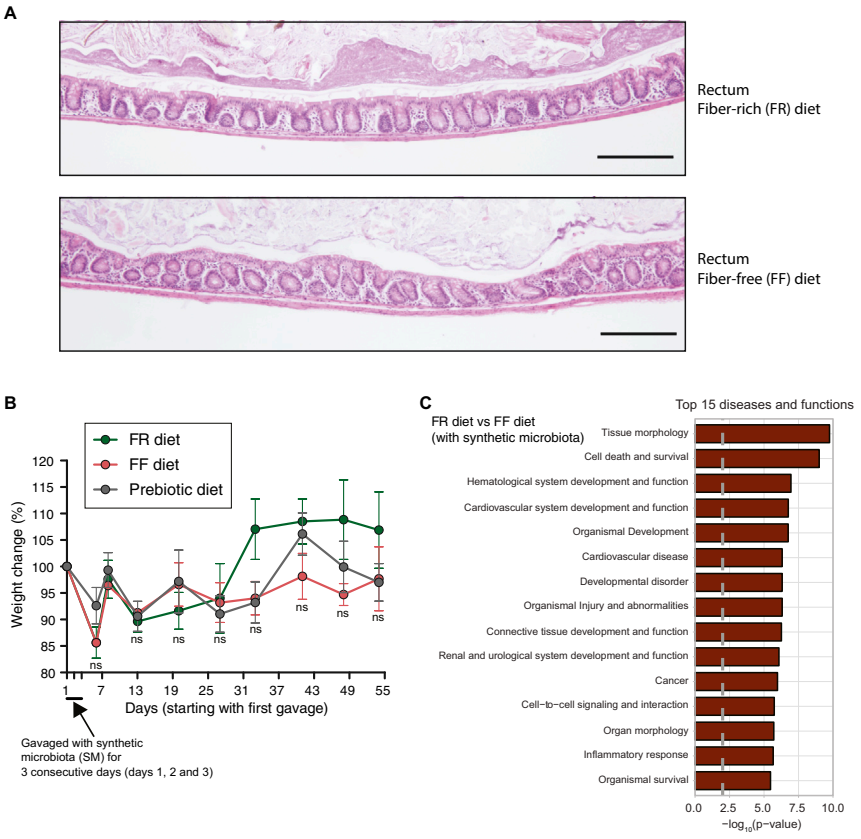

Figure S5. Histology Images, Body Weights, and Additional Cecal Tissue Transcriptional Responses of Gnotobiotic Mice Fed Fiber-Rich (FR) and Fiber-Free (FF) Diets, Related to Figure 4

(A) Depictive histology images (Hematoxylin and Eosin of colonic thin sections) showing no overt signs of inflammation between the two dietary regimens (*Experiment 1*), in the absence of *C. rodentium*. Scale bars, 500 μm.

(B) Weight change in mice over time. Values are shown as averages ± SEM; n = 4 for FR and FF groups; and n = 3 for Pre group (*Experiment 1*). ns, not significant; One-way ANOVA with Tukey's test.

(C) Top 15 altered diseases and functions between two dietary regimens detected by Ingenuity Pathway Analysis of microarray data (cecal tissue mRNA). n = 4 for the FR diet group and n = 3 for the FF diet group (*Experiments 2A and 3*).

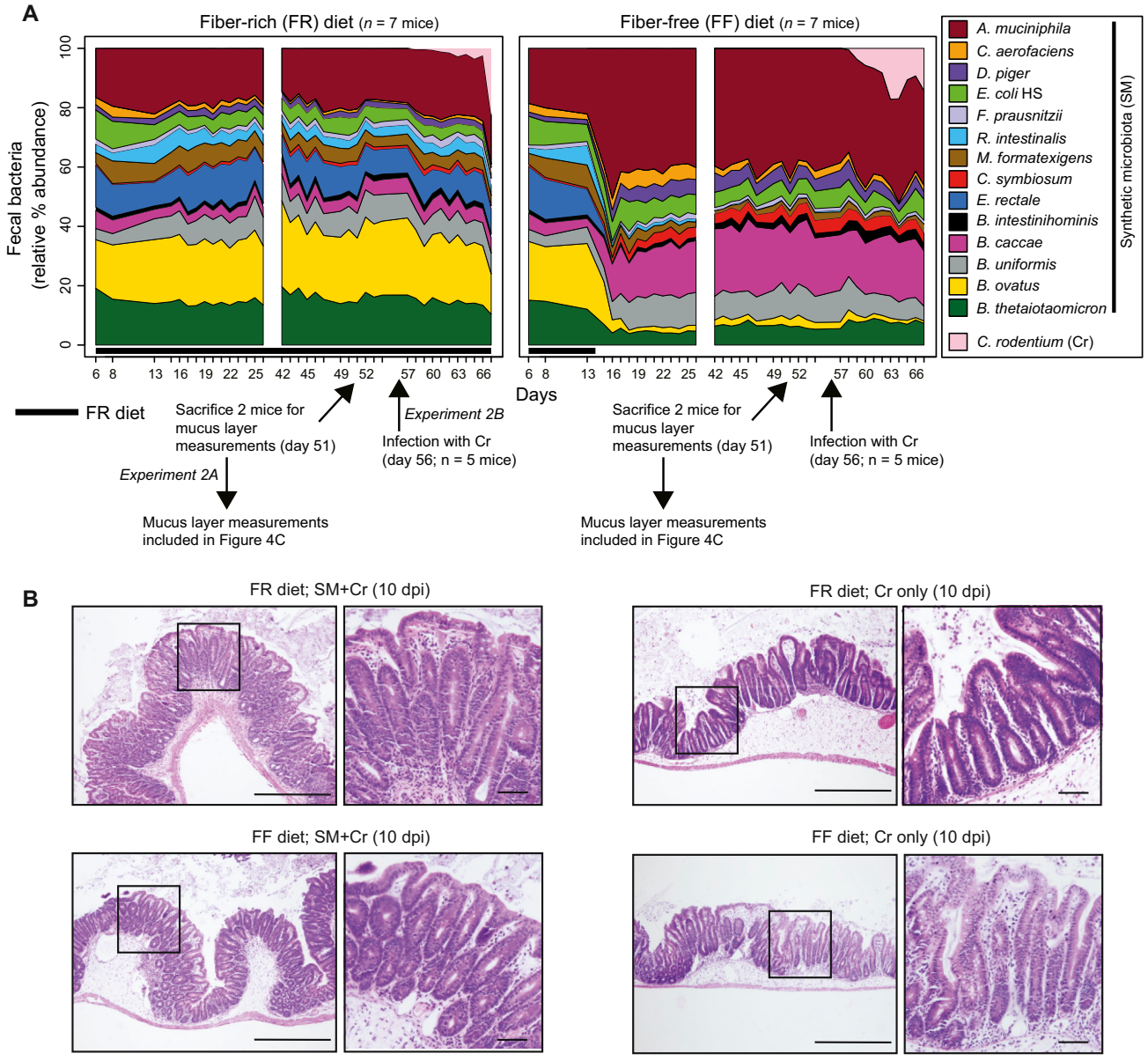

Figure S6. Microbial Community Structure Pre- and Post-*Citrobacter rodentium* Infection and Severity of Colitis Post-*C. rodentium* Infection, Related to Figure 5

(A) Stream plots illustrating fecal microbial community dynamics over time. Stream plots are based on Illumina sequencing of the V4 region of 16S rRNA genes (*Experiment 2A,B*); see Figure 1B for timeline. See Table S2 for % relative abundance of each species in individual mice. Experimental setup for the gnotobiotic experiments *2A* and *2B* is also shown.

(B) Histological images illustrating the similar severity of *C. rodentium*-associated hyperplasia in SM-colonized mice from different feeding groups or germfree animals only exposed to pathogen. The images are Hematoxylin and Eosin (H and E) stained sections of unflushed cecal tissue all at 10 dpi (*Experiment 2B*). Scale bars, 500 μm; higher power inset bars, 50 μm.

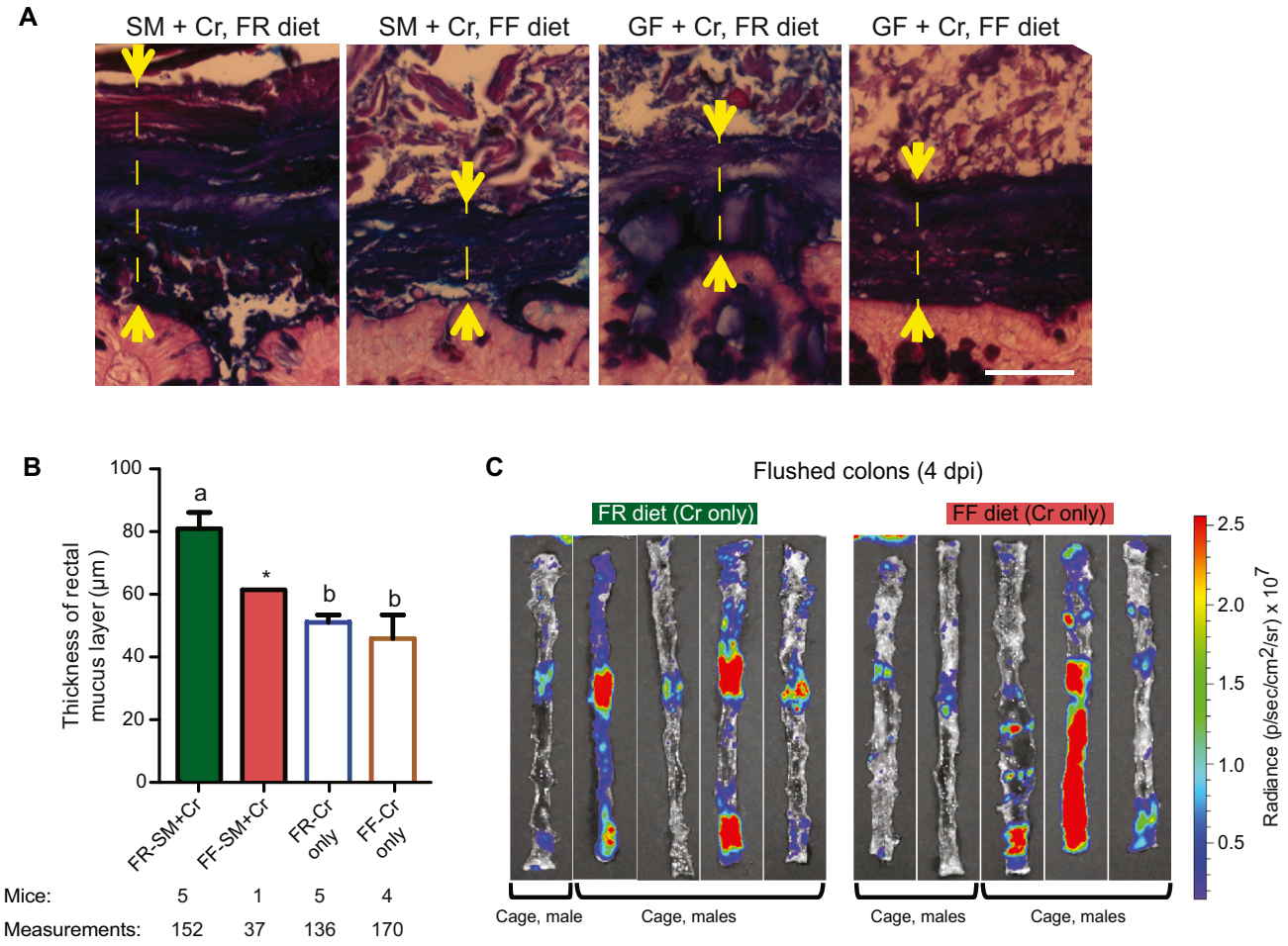

Figure S7. Thickness of the Rectal Mucus Layer Post-*Citrobacter rodentium* Infection and Bioluminescence Images of Flushed Colons Showing Colonization Intensity of Luciferase-Expressing *C. rodentium*, Related to Figures 5 and 6

(A) Periodic acid-Schiff (PAS)-Alcian Blue (AB) stained colonic thin sections showing the mucus layer (shown with opposing arrows with shafts) in recta of different groups of mice at 10 dpi (*Experiment 2B*). Scale bar, 50 µm.

(B) Mucus layer measurements in the recta of mice from PAS-AB stained thin sections (exemplified in A). Asterisk indicates that the FF-SM group had only one mouse, whose rectal mucus layer could be measured, because the other mice from this group were severely affected with colitis. Data are shown as average ± SEM; statistically significant differences are shown with different alphabets ($p < 0.01$); One-way ANOVA with Tukey's test.

(C) Flushed colons showing intensity of adherent, luciferase-expressing *C. rodentium* in germ free (GF) mice pre-fed the FR and FF diets and infected with the pathogen (that is mice without the synthetic microbiota).

GUT MICROBES
2021, VOL. 13, NO. 1, e1966263 (15 pages)
https://doi.org/10.1080/19490976.2021.1966263

Taylor & Francis
Taylor & Francis Group

RESEARCH PAPER

OPEN ACCESS Check for updates

Deprivation of dietary fiber in specific-pathogen-free mice promotes susceptibility to the intestinal mucosal pathogen *Citrobacter rodentium*

Mareike Neumann[a,b], Alex Steimle[a], Erica T. Grant[a,b], Mathis Wolter[a,b], Amy Parrish[a,b], Stéphanie Willieme[a], Dirk Brenner[a,c,d], Eric C. Martens[e], and Mahesh S. Desai[a,c]

[a]Department of Infection and Immunity, Luxembourg Institute of Health, Esch-sur-Alzette, Luxembourg; [b]Faculty of Science, Technology and Medicine, University of Luxembourg, Esch-sur-Alzette, Luxembourg; [c]Odense Research Center for Anaphylaxis, Department of Dermatology and Allergy Center, Odense University Hospital, University of Southern Denmark, Odense,, Denmark; [d]Immunology & Genetics, Luxembourg Centre for System Biomedicine (Lcsb), University of Luxembourg, Belval, Luxembourg; [e]Department of Microbiology and Immunology, University of Michigan Medical School, Ann Arbor, Michigan, USA

ABSTRACT

The change of dietary habits in Western societies, including reduced consumption of fiber, is linked to alterations in gut microbial ecology. Nevertheless, mechanistic connections between diet-induced microbiota changes that affect colonization resistance and enteric pathogen susceptibility are still emerging. We sought to investigate how a diet devoid of soluble plant fibers impacts the structure and function of a conventional gut microbiota in specific-pathogen-free (SPF) mice and how such changes alter susceptibility to a rodent enteric pathogen. We show that absence of dietary fiber intake leads to shifts in the abundances of specific taxa, microbiome-mediated erosion of the colonic mucus barrier, a reduction of intestinal barrier-promoting short-chain fatty acids, and increases in markers of mucosal barrier integrity disruption. Importantly, our results highlight that these low-fiber diet-induced changes in the gut microbial ecology collectively contribute to a lethal colitis by the mucosal pathogen *Citrobacter rodentium*, which is used as a mouse model for enteropathogenic and enterohemorrhagic *Escherichia coli* (EPEC and EHEC, respectively). Our study indicates that modern, low-fiber Western-style diets might make individuals more prone to infection by enteric pathogens via the disruption of mucosal barrier integrity by diet-driven changes in the gut microbiota, illustrating possible implications for EPEC and EHEC infections.

ARTICLE HISTORY
Received 2 June 2021
Revised 29 July 2021
Accepted 3 August 2021

KEYWORDS
Microbiome; mucin; mucus layer; *citrobacter rodentium*; dietary fiber; SPF mice

Introduction

Typical diets in Western societies are characterized by a fiber intake below the recommended amount of 28–38 g per day.[1] Such a reduced consumption of fiber is a possible explanation for the imbalances in gut microbial communities, which have been associated with various diseases such as inflammatory bowel disease (IBD) and colorectal cancer.[2] Furthermore, several studies have shown a link between Western-style diets (WSD) and enteric pathogenic infections in mice.[3–5] Specifically, bacterial metabolites derived from dietary fiber fermentation are known to impact disease severity of enteropathogenic infections.[6] As shown in mouse models, apart from maintaining immune homeostasis by producing certain metabolites like short-chain fatty acids (SCFAs) from dietary fiber digestion,[7,8] the intestinal microbiome confers colonization resistance against invading enteric pathogens by enhancing mucosal barrier integrity[9] or by competing for the same nutritional resources.[10] However, knowledge of how deprivation of dietary fiber impacts susceptibility to a mucosal pathogen by the altered gut microbial ecology remains uncovered.

The murine mucosal pathogen *Citrobacter rodentium* forms attaching and effacing (A/E) lesions on the intestinal mucosa of the host and is often used as a model for human enteropathogenic and enterohemorrhagic *Escherichia coli* (EPEC and EHEC, respectively) infections.[11] Thus, *C. rodentium* allows further study of how deprivation of dietary fiber impacts the complex ecological interactions between the gut microbiome, enteropathogens and the host. This, in turn, can aid in understanding the associations of Western-style dietary patterns with increased susceptibility to enteric pathogens.[12] The lessons learned from

CONTACT Mahesh S. Desai mahesh.desai@lih.lu Department of Infection and Immunity, Luxembourg Institute of Health, Esch-sur-Alzette 4354, Luxembourg

such a model could furthermore inform strategies for designing customized diets to reduce the burden of enteric infections.

We previously showed that, when gnotobiotic mice colonized with a 14-member synthetic human gut microbiome (14SM) are fed a fiber-free diet, a community-wide proliferation of mucin-degrading bacteria causes erosion of the intestinal mucus barrier.[13] This leads to lethal colitis by the rodent mucosal pathogen *C. rodentium*.[13] It was uncertain whether our results from a gnotobiotic mouse model could be observed within specific-pathogen-free (SPF) mice, since the pathogen should face increased colonization resistance from a native, complex gut microbiota. Here, we investigated whether increased susceptibility to *C. rodentium* can be observed in fiber-deprived SPF mice and whether accompanying alterations in the gut homeostasis might contribute to the virulence of this mucosal pathogen.

Methods

Ethical statement

The animal experiments were approved by the Animal Welfare Structure of the Luxembourg Institute of Health (protocol number: DII-2017-14) and by the Luxembourgish Ministry of Agriculture, Viticulture and Rural Development (national authorization number: LUPA 2018/09). All experiments were performed according to the "Règlement grand-ducal du 11 janvier 2013 relatif à la protection des animaux utilisés à des fins scientifiques" based on the "Directive 2010/63/EU" on the protection of animals used for scientific purposes. The mice were housed in a specific-pathogen-free (SPF) facility according to the conditions stated in the recommendations of the Federation of European Laboratory Animal Science Association (FELASA).

Experimental design and dietary treatment

A total of fifty 6- to 8-week-old, female C57BL/6J mice purchased from Charles River Laboratories (Saint Germain Nuelles, 69210, France) were used for the experiments reported in this study. All mice were bred and housed in the same breeding room at Charles River Laboratories and were derived from the same colony. After the arrival of all mice in the same transport box, mice were housed in the same individually ventilated cage (IVC) rack with up to five animals per cage. Throughout the experiments, all animals were exposed to 12 hours of light daily. Sterile water and diets were provided ad libitum. Upon arrival, all mice were maintained on a standard mouse chow, which we henceforth call a fiber-rich (FR) diet, for seven days. After the seven days of settling time, the cages were randomly allocated to one of the two dietary groups. The first group of five cages was maintained on the FR diet (n = 25), while the second group of five cages was switched to a fiber-free (FF) diet (n = 25) for 36–40 days. Fecal samples were collected from both groups (FR, n = 10 and FF, n = 10) before the diet switch (d00) to confirm similar microbial colonization using 16S rRNA gene analyses and during the feeding period (D08 and D22) to analyze changes in microbial abundances. Prior to sacrificing and to infection with *Citrobacter rodentium* (D36), fecal samples were collected from all fifty mice for various readouts such as lipocalin (Lcn2) quantification (FR, n = 25 and FF, n = 25), p-nitrophenyl glycoside-based enzyme assay (FR, n = 4 and FF, n = 4), and 16S rRNA gene sequencing (FR, n = 10 and FF, n = 10). After the feeding period, 10 mice (FR, n = 5 and FF, n = 5) were euthanized by cervical dislocation for mucus layer measurements, histological evaluation, colon length measurements and short-chain fatty acid quantification (cecal contents). Nine animals (FR, n = 4 and FF, n = 5) were maintained on the two diets for a total of 70 days to control for diet-specific weight alterations. Twenty animals were infected with approximately 2×10^8 colony-forming units (CFUs) of kanamycin-resistant, wild-type *C. rodentium* strain (DBS 120) via intragastric gavage of 0.2 ml bacterial culture (FR, n = 10 and FF, n = 10; five mice per cage). The same inoculum of *C. rodentium* was used to gavage all mice in both dietary groups. Fecal samples were collected daily following the infection. Mice were scored daily (none, mild, moderate, or severe) for the following criteria: reduced grooming habits resulting in dull coat, weight loss, activity, diarrhea, constipation, anorexia, hunched back position, and dehydration. The same scoring was also used for uninfected animals maintained on the two diets for

70 days. Animals were euthanized if three of the criteria were scored as moderate, one of the physical appearance criterions was scored as severe, or if the animals lost >20% of their initial body weight (measured on the day of infection, before the intragastric gavage of *C. rodentium*).

Animal diets

The fiber-free (FF) diet was manufactured by SAFE diets (Augy, France), as previously described,[13] and was synthesized according to a modified version of the Harlan TD.08810 diet. The fiber-rich (FR) diet (4.23% crude fiber) is the standard mouse chow in the local animal facility (Special Diets Service; Essex, UK; product code: 801722). The FF diet and the FR diet were both sterilized using 9 kGy gamma irradiation.

Mucus layer measurements and histological evaluation

After euthanizing the animals by cervical dislocation, the gastrointestinal tracts were dissected, the colons were rapidly separated and fixed in methacarn solution for five hours (60% dry methanol, 30% chloroform, 10% glacial acetic acid) and then stored in 100% methanol until further processing. Samples were infiltrated with paraffin in a tissue processor, embedded in paraffin and subjected to either Alcian blue or hematoxylin and eosin (H&E) staining on thin colonic sections (5 µm). Alcian blue-stained sections were used for the mucus layer measurements, as described previously.[13] Samples were deparaffinized in xylene (2x) for 8 min and 5 min, hydrated in 96%, 80%, and 70% ethanol (5 min each) and transferred to distilled water (30 sec). Samples were stained in Alcian blue solution (30 min) and washed under running tap water (2 min), briefly rinsed in distilled water (30 sec), and dehydrated with 96% alcohol (2x) for 1.5 min and 2 min. Samples were transferred to isopropanol (5 min) and treated with xylene (2x) for 5 min each and covered with a coverslip. Partially overlapping tile pictures over the entire colon length were taken by M. N. using a Zeiss Axio Observer Z1 Inverted Phase Contrast Fluorescence Microscope with the Zen software. The mucus layer measurements were performed in a single-blinded fashion by A. P. using ImageJ. Depending on the size of the fecal pellet, between 100 and 1300 measurements were performed and the average mucus layer thickness was calculated for each animal by averaging the measurements. H&E-stained sections were used for blinded histological scoring. Samples were deparaffinized as described above and stained with hematoxylin solution (5 min), washed in distilled water (30 sec) and transferred to running tap water (5 min). Samples were counterstained with 1% aqueous eosin (5 min), washed under running tap water (4 min), dehydrated as described above and covered with a coverslip. Histological scoring was performed with a validated scale[14] of 0–3 with "0" representing no inflammation, "1" representing mild inflammation, "2" representing moderate inflammation and "3" representing severe inflammation. A total of 12 categories for histomorphological scores were used[14] to evaluate 4–5 consecutive colonic regions and microscopic fields to determine the averages per group (e.g. infiltration of inflammatory cells, crypt hyperplasia, goblet cell loss, and distortion of colonic architecture; please see [14] for detailed criteria about histomorphological scores).

Citrobacter rodentium growth and fecal quantification

C. rodentium was cultured aerobically from a cryostock on LB-agar plates supplemented with 50 µg/ml kanamycin. A single colony was incubated in Luria-Bertani (LB) broth without antibiotic supplementation at 37°C for 22 hours. The culture was then diluted in phosphate-buffered saline (PBS) to reach the concentration of approximately 2×10^8 CFU per 0.2 ml, which was verified by plating on LB-agar plates supplemented with 50 µg/ml kanamycin. Fecal sampling to determine *C. rodentium* CFUs was performed daily and samples were processed immediately. CFU detection continued to be performed daily for FF-fed mice until day 47 post infection, whereas no further CFU detection was performed for FR-fed mice upon pathogen clearance. The samples were weighed, homogenized in 1 ml cold PBS, and 10 µl of the fecal suspensions was plated in serial dilutions on LB-agar plates supplemented with 50 µg/ml kanamycin. The plates

were incubated aerobically overnight at 37°C and the emerging colonies from the appropriate dilutions, ranging from 10^4 to 10^{12}, were counted. For CFU analysis of sacrificed animals, fresh cecal contents were collected and processed immediately, as described above.

Lipocalin ELISA

A total of n = 50 samples (FR, n = 25; FF, n = 25) were used for this experiment. Lipocalin (Lcn2) concentration was determined for fecal samples stored at –20°C. Ice-cold PBS with 1% Tween 20 (500 µl) was added to fecal pellets , followed by homogenization for 20 min at 4°C on a thermomixer. Samples were then centrifuged for 10 min at 18 000 × g at 4°C. Supernatants were stored at –20°C and Lcn2 detection was performed using the Mouse Lipocalin-2/NGAL DuoSet Elisa, R&D Systems (Bio-Techne), according to the manufacturer's instructions.

Colon length measurements

Colons fixed in methacarn solution (see above) were transferred to a histology cassette and stored in 100% methanol. The lengths of colons were measured as previously described .[13]

Intestinal fatty acid analysis

Flash-frozen cecal contents (30–100 mg) stored at –80°C were homogenized using five ceramic beads (1.4 mm) per tube with 500 µl stock solution IS (2-Ethylbutyric acid, 20 mmol/L) per 50 mg of cecal content (VK05 Tough Micro-Organism Lysing Kit). Samples were homogenized at 4 500 × g for 30 sec at 10°C (Precellys 24 Homogenizer) and centrifuged for 5 min at 21 000 x g and 4°C. Further processing of the homogenate and measurements of SCFAs were then performed using high-performance liquid chromatography (HPLC), as previously described.[15]

P-Nitrophenyl glycoside-based enzyme assays

Frozen fecal samples were stored and processed according to an established protocol.[16] The activity of three host mucus targeting bacterial enzymes, β-*N*-acetylglucosaminidase, sulfatase, α-fucosidase, and two dietary plant fiber glycan-targeting bacterial enzymes, α-galactosidase, and β-glucosidase were investigated. Details about bacterial enzymes, their biological substrate and the chemical substrate used for activity detection can be found in Table 1.

Illumina sequencing of 16S rRNA genes and data analysis

Fecal samples were stored at –20 C° until bacterial DNA extraction and library preparations, which were performed as previously described.[13] The cited protocol is a modified version of the protocol by Kozich et al. in which the V4 region of the 16S rRNA gene is amplified using dual-index primers.[17] Raw sequences have been deposited in the European Nucleotide Archive (ENA) under the study accession number PRJEB44016. The raw sequences were processed using the program mothur (v1.33.3)[18] according to the MiSeq SOP published on the mothur website.[17,19] Probabilistic modeling to cluster the microbial communities in metacommunities was performed in mothur based on the Dirichlet multinomial mixtures method.[20] Alignment and classification of the sequences was done using the SILVA reference database (release 132).[21] Chimeric sequences were removed using the VSEARCH tool. Microbial abundance figures were generated using the following packages in RStudio 4.0.2: phyloseq 1.34.0,[22] ggplot2 3.3.3,[23] vegan 2.5.7,[24] forcats 0.5.1.[25] Alpha diversity analyses were

Table 1. Bacterial enzymes and chemical substrates used for activity detection.

Bacterial enzyme	Biological substrate	Chemical substrate used for activity detection	Supplier
Sulfatase	Host mucus glycans	Potassium 4-nitrophenyl-sulfate	Sigma Aldrich, Cat#N3877
β-*N*-Acetyl-glucosaminidase	Host mucus glycans	4-Nitrophenyl N-acetyl-β-D-glucosamidine	Sigma Aldrich, Cat#N9376
α-Fucosidase	Host mucus glycans	4-Nitrophenyl α-L-fucopyranoside	Sigma Aldrich, Cat#N3628
α-Galactosidase	Dietary plant fiber glycans	4-Nitrophenyl α-D-galacto-pyranoside	Sigma Aldrich, Cat#N0877
β-Glucosidase	Dietary plant fiber glycans	4-Nitrophenyl β-D-gluco-pyranoside	Sigma Aldrich, Cat#N7006

performed on unfiltered data. The Principal Coordinates of Analysis (PCoA) plot is based on Bray-Curtis dissimilarity index, after filtering out taxa not seen at least 10 times in at least 20% of the samples. The spatial means of the FR diet-fed mice and FF diet-fed mice clusters at the end of the feeding period were significantly different by PERMANOVA using adonis ($p = 0.001$), although a significant betadisper test ($p = 0.001$) means that this finding could be an artifact of the heterogenous dispersions. The heatmap was generated based on the top 50 significant OTUs determined using DESeq2 1.30.1;[26] all OTUs shown are significant based on an adjusted p-value < 0.01. The heatmap shows log2 fold-change for data rarefied to the minimum library size and filtered (minimum 10 counts in 20% of samples) displaying the fold-changes in abundance of each OTU, relative to the average abundance of that OTU in the comparator dietary group. Samples where the read count is zero are presented as infinitely negative values. In cases where all samples in a group had zero read counts, all samples with a non-zero value in the comparator group are then infinitely positive relative to the other group's zero average count. Adjusted p-values were obtained using the Benjamini-Hochberg procedure to correct for multiple comparisons.

Results and discussion

Six to eight-week-old, age-matched specific-pathogen-free (SPF) female C57BL/6J mice were maintained on a mouse chow, which, with a fiber content of 4.23% crude fiber, we consider to be a fiber-rich (FR) diet. Ten animals were switched to a fiber-free (FF) diet and were continuously fed the FF diet for a 36–40 days "feeding period" (Figure 1a). As controls, the remaining C57BL/6J mice were maintained on the FR diet. The FR diet contained naturally milled food ingredients with crude plant fiber sources, such as corn, soybean, and wheat, whereas the isocaloric FF diet lacked such plant polysaccharides and instead contained increased levels of glucose.[13] Throughout the feeding period, the FF-fed mice did not exhibit any physiological irregularities (data not shown) or weight loss.

Fiber deprivation leads to an increase in potential mucus-degrading bacterial taxa in SPF mice

Before, during and at the end of the feeding period (d00, d08, d22 and d36), 16S rRNA gene sequencing (Illumina MiSeq platform) was performed in two independent experiments using DNA extracted from the mouse fecal samples. The results were compared to the FR-fed mice to evaluate changes in microbiome composition in response to diets with different fiber content (Figure 1b**–d**). Alpha diversity between groups was not significantly different using the Chao 1 richness estimate or by Shannon and inverse Simpson indices, which account for the evenness of the detected taxa (data not shown). Principal Coordinates of Analysis (PCoA) based on Bray-Curtis dissimilarity (Figure 1b) confirmed similar microbial composition before the diet switch (d00) and statistically significant clusters by diet during the feeding period (d08 and d22 after diet switch). The PCoA furthermore revealed significant diet-specific clustering by PERMANOVA ($p = 0.001$) after 36 days of feeding. Although the dispersion was significantly different between the diets at d36 ($p = 0.001$), it is reasonable to conclude that the spatial medians are indeed significantly different since the design is balanced.[27] On the phylum-level, *Proteobacteria* and *Firmicutes* were significantly higher among FF-fed mice, whereas *Bacteroidetes* was enriched in FR-fed mice (Figure 1c). Family-level analysis revealed heterogeneous changes within the *Bacteroidetes* phylum, as *Muribaculaceae* and *Prevotellaceae* were enriched in FR-fed mice, but *Rikenellaceae, Marinifilaceae*, and *Tannerellaceae* were higher among FF-fed mice (Figure 1d). *Firmicutes* belonging to *Peptostreptococcaceae, Streptococcaceae*, and *Clostridiales* Family XIII, were higher among FF-fed mice, as were *Proteobacteria* belonging to *Burkholderiaceae* and *Desulfovibrionaceae* families (Figure 1d). An expansion of *Proteobacteria* has been associated with intestinal epithelial dysfunction.[28] *Peptostreptococcaceae* have been found to be enriched in patients with colorectal cancer[29] and has been associated with a decrease in mucus layer thickness.[30] Furthermore, increased levels of *Bacteroidetes* over *Firmicutes*, as shown in FR-fed animals (Figure 1d), has been previously

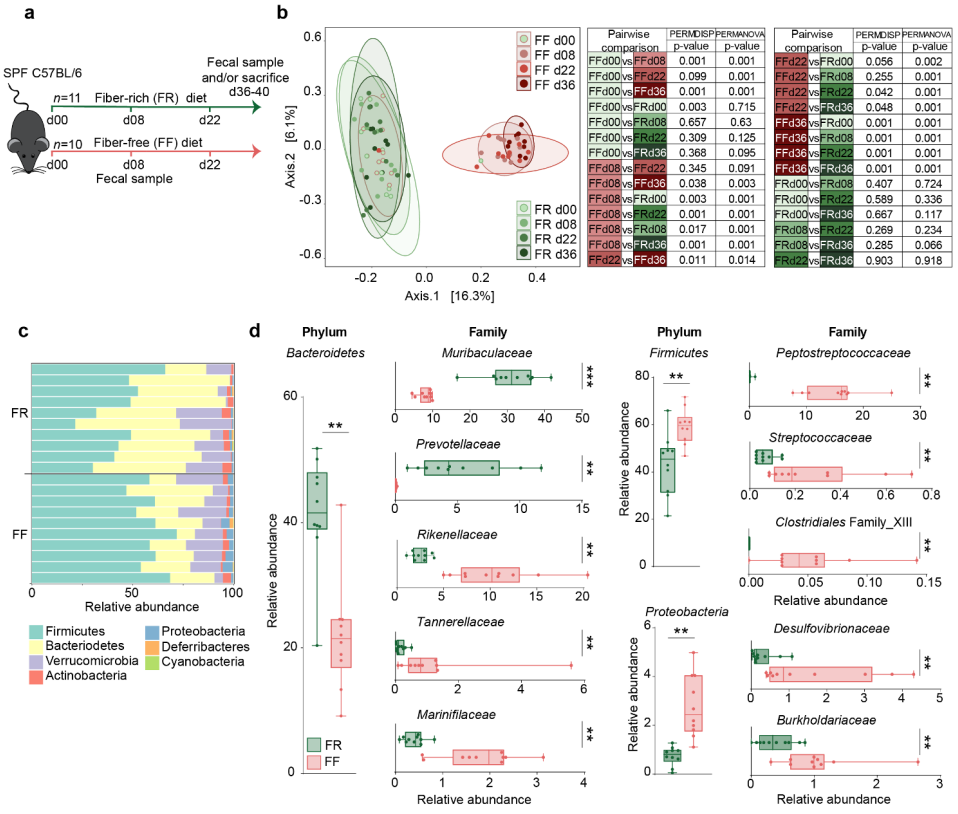

Figure 1. Fiber deprivation in mice harboring a complex microbiome results in changes in bacterial families. Green: FR-fed mice; Red: FF-fed mice. * = $p < 0.05$; ** = $p < 0.01$; *** = $p < 0.001$. **(a)** Experimental schedule. 6 to 8 week-old female specific-pathogen-free (SPF) C57BL/6J mice were continued on a fiber-rich (FR) diet or switched to a fiber-free (FF) diet for a feeding period of 36–40 days. Fecal samples were collected before diet switch (d00) and at d08, d22 and d36 after the diet switch. At the end of the 36–40 days feeding period, mice were sacrificed for various readouts. FR, $n = 11$ and FF, $n = 10$. **(b)** Left: Principal coordinates analysis (PCoA) of the fecal microbial communities of FR and FF mice before the diet switch (d00), on d08, d22 and after 36 days of feeding the two different diets, based on Bray-Curtis dissimilarity index. Ellipses represent 95% confidence interval for each group. Right: Statistical analysis between all dietary groups on d00, d08, d22 and d36 after diet switch. The difference in spatial means of FR and FF diet clusters was significant by PERMANOVA testing using adonis ($p = 0.001$), however, the dispersions (PERMDISP) were also significantly different using a permuted betadisper function ($p = 0.001$). FR, $n = 10$ and FF, $n = 10$. Adjusted p-values were obtained using the Benjamini-Hochberg procedure to correct for multiple comparisons. **(c)** Barplot of relative microbial abundances of the bacterial phyla after 36 days of feeding among FR- ($n = 10$) and FF-fed ($n = 10$) mice. **(d)** Boxplots displaying significant changes in the relative abundance (%) of *Bacteroidetes, Firmicutes* and *Proteobacteria* between FR- ($n = 10$) and FF-fed ($n = 10$) mice. Boxplots display significant changes in relative abundance (%) of bacterial families between FR- and FF-fed animals, sorted by their corresponding phylum (left). Whiskers display minimum and maximum. Mann–Whitney test, two-tailed.

linked with a decreased *C. rodentium* susceptibility.[31] Analysis of log2 fold-change on an OTU level using DESeq2 reveals discrete changes between the dietary conditions (Figure 2). We exclude a cage effect based on the Dirichlet multinomial mixtures method,[20] which identified only two microbial community clusters that correspond to the diet. These clusters are evident in the phylogenetic tree of the heatmap, depicting samples from individual animals and their corresponding cages (Figure 2). An upregulation of specific OTUs belonging to the bacterial genera *Lachnospiraeceae, Ruminococcaceae*, and *Oscillibacter* could be detected in fiber-deprived animals compared to the control group (Figure 2). An increased abundance of *Lachnospiraeceae* spp. has previously been reported to be associated with the increased susceptibility to adherent-invasive *Escherichia coli* (AIEC) infection.[32] Furthermore, *Ruminococcaceae* spp.[33] *Lachnospiraceae* spp., *Clostridiales* spp., *Desulfovibrionales* spp., and *Oscillibacter* spp. have been shown to correlate with the production of branched chain fatty acids (BCFAs), such as isovaleric and isobutyric acid.[34]

Figure 2. Fiber deprivation in mice harboring a complex microbiome results in changes in bacterial families with no detectable cage effect. At the top of the heatmap, a phylogenetic tree displays clustering by diet (FR = green, FF = red). Green numbers (cages 1 and 2) and lines indicate cages of FR-fed mice. Red numbers (cages 3 and 4) and lines indicate cages of FF-fed mice. FR, $n = 10$, FF, $n = 10$ with $n = 5$ animals per cage. The heatmap displays fold-changes in abundance of top 50 operational taxonomic units (OTUs) that were identified as significantly different between FR- and FF-fed mice using DESeq2, based on the adjusted p-value; FR, $n = 10$, FF, $n = 10$. Adjusted p-values were obtained using the Benjamini-Hochberg procedure to correct for multiple comparisons. The $\log_2$-transformed fold-change of each OTU (rows) in each sample (columns) is calculated relative to the average abundance of the other group. OTUs labeled with green squares to the left are enriched in FR-fed mice, wheras OTUs labeled with red squares are enriched in FF-fed mice.

In line with these and previous results, we investigated whether dietary fiber deprivation resulted in altered intestinal fatty acid concentrations by measuring levels of SCFAs (acetate, butyrate, propionate, and valerate) and BCFAs (isobutyrate and isovalerate) in cecal contents of FR-fed and FF-fed mice at the end of the feeding period. We detected significantly increased levels of the SCFAs acetate, propionate and butyrate in FR-fed mice compared to FF-fed mice, while amounts of all detected BCFAs were significantly lower compared to fiber-deprived mice (Figure 3a). While SCFAs are generated largely by the microbial fermentation of dietary fibers,[35] intestinal BCFAs are mainly the result of bacteria-mediated dietary protein metabolism.[36]

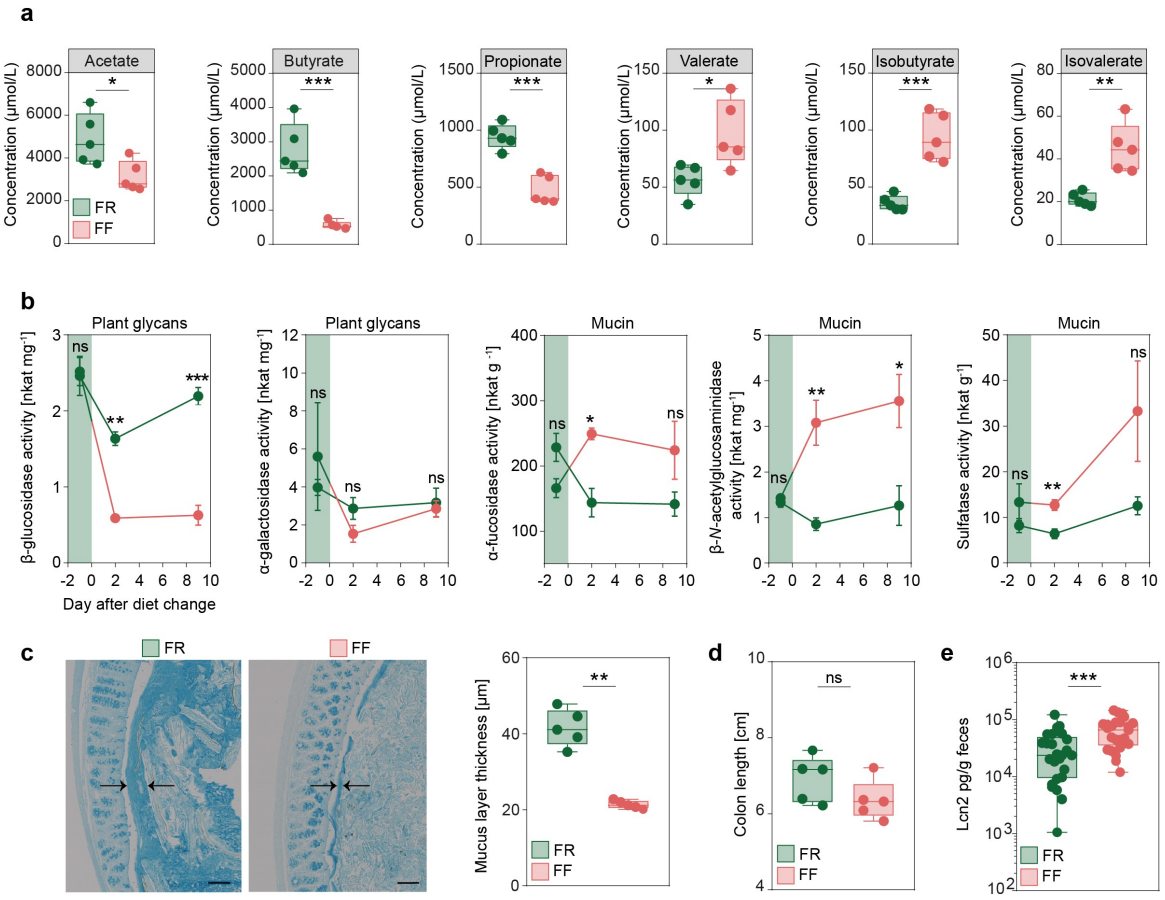

Figure 3. Fiber deprivation in mice harboring a complex microbiome results in changes in bacterial enzyme activity and levels of mucosal barrier integrity markers. Green: FR-fed mice; Red: FF-fed mice. * = $p < 0.05$; ** = $p < 0.01$; *** = $p < 0.001$. **(a)** SCFA and BCFA concentrations in cecal contents in µmol/L after 40 days of feeding in FR- ($n = 5$) and FF-fed ($n = 5$) animals. Unpaired t-test, two-tailed. **(b)** Results for *p*-nitrophenyl glycoside-based enzyme assay from fecal samples of FR-fed ($n = 4$) and FF-fed ($n = 4$) animals. Evaluation of five different bacterial enzymes. Plant glycans: β-glucosidase, α-galactosidase. Mucin: α-fucosidase, β-*N*-acetylglucosaminidase, and sulfatase at three different time points. Day 1 before diet switch to FF diet, day 2 after diet switch to FF diet and day 9 after diet switch to FF diet. Green area indicates FR feeding period before diet switch to FF diet. Error bars represent SEM. Unpaired t-test, two-tailed. **(c)** Left panel: Alcian blue-stained 5 µm thin sections of the colonic mucus layer of FR-fed and FF-fed animals. Black arrows indicate thickness of the colonic mucus layer. Scale bar = 100 µm. Right panel: Statistical analysis of mucus layer measurements of FR-fed ($n = 5$) and FF-fed ($n = 5$) animals. Mann–Whitney test, two-tailed. **(d)** Colon length in FR- ($n = 5$) and FF-fed ($n = 5$) mice after 40 days of feeding. Mann–Whitney test, two-tailed. **(e)** Levels of lipocalin in fecal supernatant, normalized on fecal weight for FR- ($n = 25$) and FF-fed ($n = 25$) animals after 36–40 days of feeding. Mann–Whitney test, two tailed.

Among other microbial protein fermentation products, such as phenol, biogenic amines, hydrogen sulfide and *p*-cresol,[37] BCFAs are associated with an increased colonic epithelial cell permeability *in vitro*,[38] whereas SCFAs are reported to maintain mucosal barrier integrity by increasing mucin-2 glycoprotein (MUC2) expression,[39] enhancing colonic tight-junction assembly,[40] and stimulating antimicrobial peptide secretion.[41] Furthermore, changes in intestinal butyrate concentration is known to affect susceptibility of *C. rodentium*[42] and oral administration of butyrate ameliorates *C. rodentium*-induced inflammation via enhanced IL-22 production.[43]

Additionally, specific species within the *Rikenellaceae* (*Alistipes*),[44,45] *Lachnospiraceae*[46,47] and *Muribaculaceae*[45] families are thought to possess the capacity to degrade mucus. Thus, in line with our 14SM model,[13] our results suggest that the deprivation of dietary fiber may also increase mucus-degrading populations in the SPF mice containing their native gut microbiota. An increase in

Desulfovibrionaceae family (Figure 1d) is consistent with the significant increase of *Desulfovibrio piger* (family: *Desulfovibrionaceae*), which was previously observed in fiber-deprived 14SM-colonized gnotobiotic mice.[13] An increase in these sulfate-reducing bacteria indicates higher availability of sulfate groups that are used as an electron acceptor by this group of bacteria. A possible source of this increased sulfate could be the terminal sulfate groups on the colonic mucin-associated glycans.[10]

A dietary fiber-deprived gut microbiota erodes the colonic mucus layer in SPF mice

Given the relevance of mucus erosion on pathogen-susceptibility of fiber-deprived mice in a gnotobiotic mouse model,[13] we evaluated whether the increase in these potentially mucus-degrading taxa resulted in the increased activities of microbial enzymes that are involved in the degradation of host-secreted colonic mucus. We studied activities of five different enzymes in the mouse fecal samples before, and after a switch to the FF diet. Our results show a significant increase in the activities of three microbial enzymes, namely α-fucosidase, β-*N*-acetylglucosaminidase and sulfatase (Figure 3b), that are involved in colonic mucus degradation. Conversely, the activity of β-glucosidase, an enzyme involved in the degradation of plant glycans, was significantly decreased in the FF-fed animals.

To assess the impact of the increased activities of these mucus-specific enzymes on the mucus layer, we performed measurements of the colonic mucus layer thickness, using fixed colonic tissue samples stained with Alcian blue.[13] The mucus measurements revealed significantly decreased mucus layer thickness in fiber-deprived mice compared to the FR-fed mice (Figure 3c). Taken together, decreased SCFA levels and reduced mucus layer thickness suggest impairment of the intestinal mucosal barrier in fiber-deprived mice.

In order to evaluate inflammatory reactions in the colonic tissue in response to the potential mucosal barrier impairment in the FF-fed mice, we measured colon lengths and the levels of lipocalin (Lcn2), a sensitive marker capable of detecting low-grade inflammation, in fecal contents of the FR- and FF-fed mice after the feeding period. There was a trend toward reduced colon lengths in the FF-fed animals compared to the FR-fed animals (Figure 3d), athough this was not statistically significant. Fecal Lcn2 levels, however, were significantly increased in fiber-deprived mice (Figure 3e), indicating an increased inflammatory tone in FF-fed mice without pronounced colonic inflammation. Furthermore, histopathological evaluation[14] of colonic hematoxylin/eosin-stained sections did not reveal significant differences between FR- and FF-fed mice (histology data not shown; average histological score for FR-fed mice 0.017 (SD, 0.058) and for FF-fed mice 0.12 (SD, 0.232); Mann–Whitney test, two tailed, $p = 0.342$). These observations were in line with the previous observation in our gnotobiotic mouse model[13] and prompted us to investigate whether the diet-induced alterations in the microbiome composition and its associated effects on the markers of mucosal barrier integrity impacted the susceptibility of fiber-deprived mice to infection with *C. rodentium*.

Deprivation of dietary fiber in SPF mice promotes susceptibility to C. rodentium

To test our hypothesis, we infected FF-fed and control FR-fed mice with *C. rodentium*. Weight and general appearance were monitored daily for up to 47 days post infection (dpi), and fecal *C. rodentium* (*Cr*) colony forming units (CFUs) were assessed until all animals cleared the pathogen or had to be euthanized (Figure 4a). FR and FF animals without infection showed no significant weight differences in two dietary groups for up to 70 days after switch to the FF diet (Figure 4b). The FF-fed animals infected with *Cr* demonstrated significantly higher weight loss compared to the FR-fed animals, with several animals requiring euthanasia owing to >20% weight loss (Figure 4c). In line with the observed weight loss, survival curves of infected animals fed the two different diets showed only a 40% survival rate in FF-fed mice, whereas 100% of the mice in the FR-fed group survived (Figure 4d).

Moreover, FF-fed mice showed overall delayed *Cr* clearing capacities and elevated CFUs in fecal samples until 23 dpi (Figure 4e). While the FR-fed mice showed rapidly decreasing CFUs after 11 dpi and all mice of this group cleared the pathogen completely by 19 dpi (Figure 4e), the FF-fed mice took longer (24 dpi) to clear the pathogen.

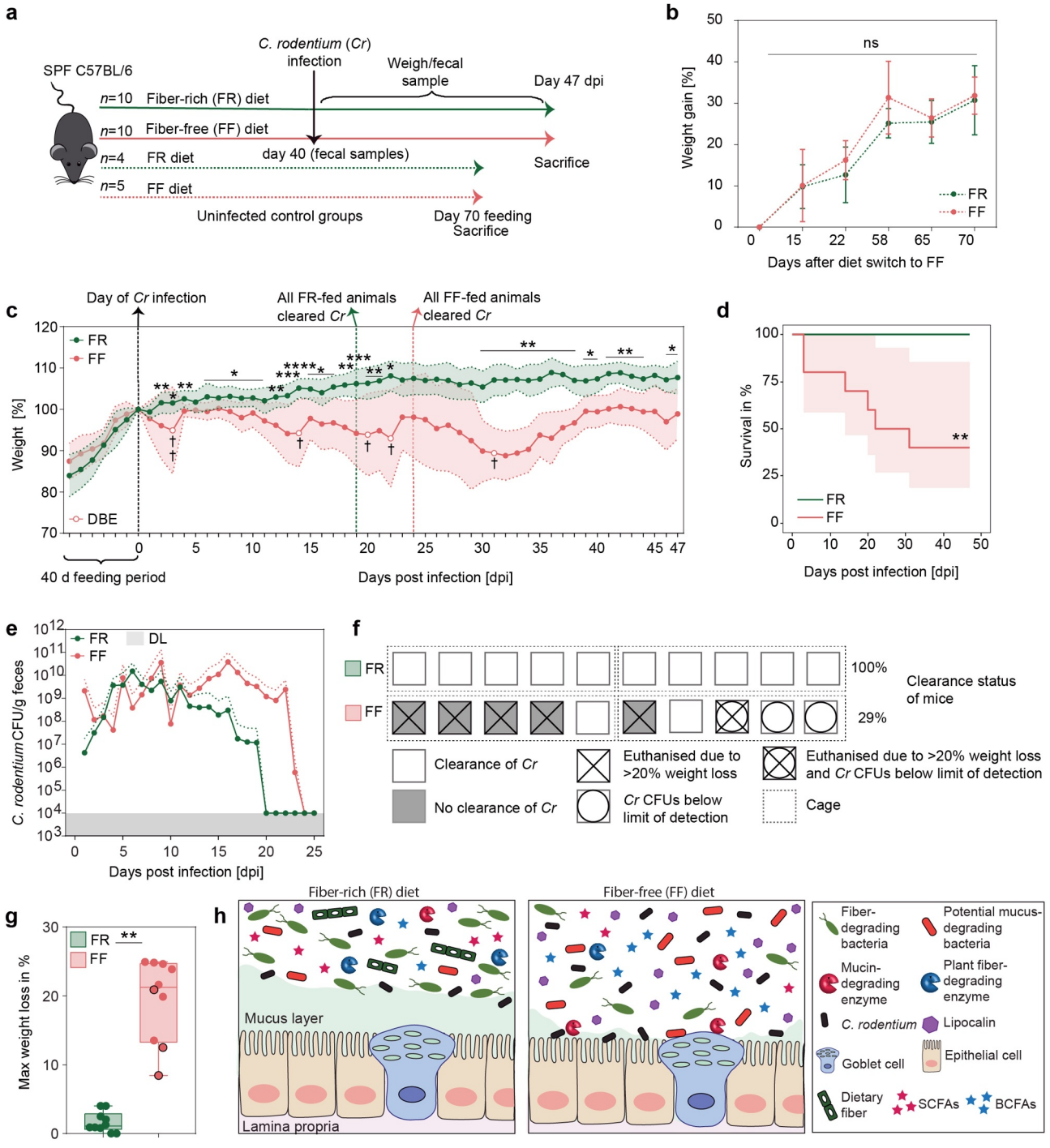

Figure 4. Fiber-deprivation in mice is associated with a higher susceptibility to *C. rodentium* infection. Green: FR-fed mice; Red: FF-fed mice. * = $p < .05$; ** = $p < 0.01$; *** = $p < 0.001$; **** = $p < 0.0001$. **a)** Experimental schedule. Animals were fed the FR diet or the FF diet (FR, $n = 10$ and FF, $n = 10$) for 40 days and infected via intragastric gavage with 2×10^8 colony forming units (CFU) in 0.2 ml culture of *C. rodentium* (*Cr*). Fecal samples were collected before the infection and used for various readouts. Animals were monitored daily for 47 days post infection (dpi). Mice were euthanized when they lost 20% of the body weight compared to the initial day of infection. Dotted red and green arrow: animals (FR, $n = 4$ and FF, $n = 5$) were fed the respective diets as uninfected control groups for 70 days. **(b)** Mean weight in percent of FR-fed and FF-fed animals over a time period of 70 days after the diet switch. FR: $n = 4$ and FF: $n = 5$. Green and red error bars represent SD. ns = not significant. MannâWhitney test, two-tailed **(c)** Left of zero: Mean weight as a percent of reference weight to the day of diet switch of FR-fed ($n = 15$; 5 animals used for earlier readouts without infection) and FF-fed ($n = 15$; 5 animals used for earlier readouts without infection) animals during the 40-days feeding period. Dotted black line at d0: day of *Cr* infection and reference weight. Right of zero: Mean weight as a percent of reference weight (d0) in FR-fed ($n = 10$) and FF-fed ($n = 10$) animals after the infection with *Cr*. Dotted green or red line: all FR- or FF-fed animals cleared *Cr*, respectively. White circles indicate time points where animals had to be euthanized due to weight loss beyond 20%, compared to the reference weight (d0). Black cross

indicates number of animals that had to be euthanized. DBE = death before experimental endpoint. Red and green areas represent SD. Mann–Whitney test, two-tailed. **(d)** Cumulative number of individuals at risk over time among FR- ($n = 10$) and FF-fed ($n = 10$) animals infected with *Cr*. Log-rank test. Red area represents confidence interval. **(e)** *Cr* CFUs per gram fecal content of FR- ($n = 10$) and FF-fed ($n = 10$) animals. For days where CFUs were below the detection limit of 10^4 CFUs, the detection limit of 10^4 CFUs was used. No CFUs values were included if no fecal samples could be obtained or if an animal had to be euthanized. Red and green dotted lines represent SD. DL = detection limit of 10^4 CFUs. **(f)** Graphic representation of the clearance rates of *Cr* susceptible animals, FR, $n = 10$ and FF, $n = 10$. Animals and treatment groups sorted by their caging (5 animals/cage) (dotted lines) and dietary experimental groups. Each symbol represents one mouse with the respective clearance status and *Cr* susceptibility. **(g)** Maximal weight loss of each individual animal in percent (FR, $n = 10$ and FF, $n = 10$). Maximal weight loss is displayed in percent of the day during the experiment where the highest weight loss was detected. Black circles: Animals displaying *Cr* CFUs below limit of detection throughout the experiment. Wilcoxon matched-pairs signed rank test. Two-tailed. **(h)** Graphical summary on diet-driven changes within gut homeostasis on *Cr* susceptibility. Left: Homeostatic conditions in FR-fed mice. Right: Changes in dietary fiber-deprived mice within gut homeostasis. Far right: Legend.

Although three FF animals failed to show detectable CFUs, one out of these three FF animals had to be euthanized on 31 dpi due to weight loss (Figure 4c), suggesting that fiber deprivation acts in favor of a lethal *Cr* phenotype even when CFUs are below the detection limit. These results suggest that dietary fiber deprivation is associated with a delayed *Cr* clearance (Figure 4e) as well as reduced rates of clearance (Figure 4f) and an overall higher weight loss (Figure 4g). The infection by *Cr* is usually self-limiting in healthy mice because the commensal gut bacteria are able to outcompete the pathogen by competing for nutritional resources, such as monosaccharides.[48,49]

A lethal infection phenotype like the one we observed in the FF-fed wild-type mice has typically been observed in mice lacking essential genes that protect from *Cr* clearance and invasion, such as *Muc2*[50] or genes encoding the cytokines IL-10 and IL-22.[51,52] Our previous[13] and current studies show that such a lethal phenotype could be generated in wild-type mice merely by eliminating plant fibers from the diet. Given that $Muc2^{-/-}$ mice exhibit a similar lethal phenotype to *Cr*,[50] it is plausible that the fiber-deprived gut microbiota-led erosion of the mucus layer contributes to the pathogenicity. Nevertheless, germ-free mice, which naturally possess a thinner mucus layer, on either the FR and FF diets do not exhibit a lethal colitis following the *Cr* infection on either the FR or FF diet.[13] Thus, together with our previous study,[13] the current study further supports the role of a fiber-deprived, mucus-eroding gut microbiota in driving susceptibility to *Cr*. Notably, no systemic spread of *Cr* into other organs, such as liver or spleen, could be detected in FF-fed mice that had to be euthanized due to >20% weight loss (data not shown). These results indicate a local impact of *Cr* in the cecum and colon, possibly driven by differences in the microbiota composition and microbial mucus erosion, that drives the lethal phenotype.

Conclusion

Our results indicate a crucial role of fiber intake on the maintenance of mucosal barrier integrity governed by the microbial ecology of the native, complex mouse microbiome, which plays an important role in protecting against infection with a mucosal pathogen. Different microbiota compositions, in mice from distinct mouse facilities, are responsible for a variable colitis phenotype to *Cr* infection.[42] Here, we show that mice possessing the same starting microbiota (Figure 1b), when fed a fiber-deprived diet, undergo a change in the composition and function of the gut microbiota (Figure 1c-Figure 3), which collectively contributes to a lethal phenotype to *Cr* (Figure 4).

A recent study showed that the WSD as compared to a standard grain-based chow (GBC) impedes the initial colonization of *Cr*, although WSD leads to alterations in the gut microbiota in such a way that *Cr* cannot be outcompeted by the microbiota;[53] hence, *Cr* in the mice fed WSD cannot be cleared or the clearance is delayed. Here, we observed a similarly delayed clearance of *Cr* in mice fed the FF diet. However, the difference in the phenotype we observe in the FF diet and the one observed in the WSD-fed mice could be rooted in important differences in the composition of these two diets. While the WSD contains nearly twice the amount of %kcal derived from fat as compared to the FF diet (60% vs. 34.1%), the FF diet contains more than twice the calories derived from

carbohydrates as compared to the WSD (42.4% vs 20%). Other reasons for differences in the *Cr* infection phenotypes observed with the FF diet and the WSD could be related to the differences in the native mouse gut microbiota and/or differences in the initial pathogen CFU gavaged in the mice.

Compositional differences between the FR and FF diets other than the fiber content, such as increased amounts of simple sugar in the FF diet, raise a caveat in directly associating the lethal phenotype observed in FF-fed mice with the absence of plant fiber. Although we cannot rule out potential effects of other compositional differences between the FR and FF diets, using our 14SM community, we have documented that the two diets lead to a major impact on the fiber- versus mucin-utilization dynamics of the gut microbiota.[13] Furthermore, our current data clearly show that the FF diet leads to enhanced mucin degradation by the gut microbiota, which occurs as a result of fiber deprivation. As SCFAs are derived abundantly from microbial fermentation of dietary fiber,[35] the decreased butyrate levels of FF-fed mice compared to the control group can be linked to the dietary fiber deprivation. Butyrate provides up to 80% of the required energy for colonocytes to maintain colonic homeostasis.[54,55] The decreased butyrate levels in FF-fed mice might lead to a more vulnerable mucosal barrier, thereby contributing to the increased lethal phenotype when challenged with an enteric pathogen. Thus, it is likely that the absence of plant fiber in the FF diet plays a crucial role on the lethal phenotype observed in this study.

Further investigations are needed to determine specific dietary strategies and/or usage of various reduced microbial communities in gnotobiotic mouse models to understand which specific bacterial taxa, their associated bacterial enzymes or microbial cross-talk with the host immune system modulate susceptibility to *Cr* infection. A follow-up study to the current one needs to utilize various reduced synthetic communities, such as removing some or all four mucus degraders from our 14SM model,[13] to better understand the mechanisms of how mucin-degrading bacteria possibly erode the mucus layer and contribute to the lethal phenotype of *Cr* under fiber deprivation. Removing specific pathogen-promoting and mucus-degrading bacterial species could aid to understand if targeted microbiome modulations could be a tool to prevent severe disease outcomes. Such future studies would also facilitate the understanding whether the changes observed here (mucus reduction, changes in microbial metabolites, and elevated inflammation) independently contribute to the lethal phenotype of *Cr* or whether a combination of such changes is essential in order to drive susceptibility to *Cr*.

Although the burden of intestinal pathogenic infections is increased and is often more lethal in developing countries compared to westernized countries,[56] further studies elaborating the connection between a WSD and enteric infections could help to prevent associated diseases such as irritable bowel syndrome[57] and tackle emerging antibiotic overuse.[58] Our findings underline the importance of increased dietary fiber consumption in WSD in order to strengthen colonization resistance and barrier integrity within the host against possible enteric infections by EPEC and EHEC.

Acknowledgments

Work in the authors' laboratory was supported by the following grants to M.S.D.: Luxembourg National Research Fund (FNR) CORE grants (C15/BM/10318186 and C18/BM/12585940). M. N. and A.P. and were supported by the FNR AFR bilateral grant (15/11228353) and FNR AFR individual grant (11602973), respectively. E.T.G. was supported by the FNR PRIDE grant (17/11823097) and the Fondation du Pélican de Mie et Pierre Hippert-Faber under the aegis of the Fondation de Luxembourg. D.B. is supported by the FNR-ATTRACT program (A14/BM/7632103). E.C.M. was supported by grants from the US National Institutes of Health (DK118024 and DK125445).

Declarations

Availability of data and materials

Most of the data generated or analysed during this study are included in this article. Please contact author for data requests.

Disclosure statement

The authors declare that they have no competing interests.

ORCID

Mahesh S. Desai http://orcid.org/0000-0002-9223-2209

Authors' contributions

Conceptualization, M.N., D.B., E.C.M., and M.S.D.; Experiments, M.N., M.W., S.W., and A.P.; Investigation, M.N., A.S., E.T.G., and M.S.D.; Resources, M.N., S.W., E.T.G, M.W., A.P., A.S., E.C.M., and M.S.D.; Writing – Original Draft, M.N., A.S., and M.S.D; Writing – Review & Editing, M.N., A.S., E.T.G., A.P., M.W., E.C.M. and M.S.D.; Supervision, M.S.D.; Funding Acquisition, M.S.D.

References

1. EFSA. Panel on dietetic products n, allergies. scientific opinion on dietary reference values for carbohydrates and dietary fibre. EFSA Journal 2010;8:1462.
2. Makki K, Deehan EC, Walter J, Bäckhed F. The impact of dietary fiber on gut microbiota in host health and disease. Cell Host Microbe. 2018;23(6):705–715. doi:10.1016/j.chom.2018.05.012.
3. Mefferd CC, Bhute SS, Phan JR, Villarama JV, Do DM, Alarcia S, Abel-Santos E, Hedlund BP. A high-fat/high-protein, atkins-type diet exacerbates Clostridioides (Clostridium) difficile infection in mice, whereas a high-carbohydrate diet protects. mSystems. 2020;5(1):e00765-19.
4. Wotzka SY, Kreuzer M, Maier L, Arnoldini M, Nguyen BD, Brachmann AO, Berthold DL, Zünd M, Hausmann A, Bakkeren E, et al. Escherichia coli limits salmonella typhimurium infections after diet shifts and fat-mediated microbiota perturbation in mice. Nature Microbiology. 2019;4(12):2164–2174. doi:10.1038/s41564-019-0568-5.
5. Agus A, Denizot J, Thévenot J, Martinez-Medina M, Massier S, Sauvanet P, Bernalier-Donadille A, Denis S, Hofman P, Bonnet R, et al. Western diet induces a shift in microbiota composition enhancing susceptibility to adherent-invasive e. coli infection and intestinal inflammation. Scientific Reports. 2016;6(1):19032. doi:10.1038/srep19032.
6. Jacobson A, Lam L, Rajendram M, Tamburini F, Honeycutt J, Pham T, Van Treuren W, Pruss K, Stabler SR, Lugo K, et al. A gut commensal-produced metabolite mediates colonization resistance to salmonella infection. Cell Host & Microbe. 2018;24(2):296–307.e7. doi:10.1016/j.chom.2018.07.002.
7. Lin L, Zhang J. Role of intestinal microbiota and metabolites on gut homeostasis and human diseases. BMC Immunol. 2017;18(1):2. doi:10.1186/s12865-016-0187-3.
8. Smith PM, Howitt MR, Panikov N, Michaud M, Gallini CA, Bohlooly YM, Glickman JN, Garrett WS. The microbial metabolites, short-chain fatty acids, regulate colonic treg cell homeostasis. Science. 2013;341(6145):569–573. doi:10.1126/science.1241165.
9. Buffie CG, Pamer EG. Microbiota-mediated colonization resistance against intestinal pathogens. Nature Reviews Immunology. 2013;13(11):790–801. doi:10.1038/nri3535.
10. Martens EC, Neumann M, Desai MS. Interactions of commensal and pathogenic microorganisms with the intestinal mucosal barrier. Nat Rev Microbiol. 2018;16(8):457–470. doi:10.1038/s41579-018-0036-x.
11. Mullineaux-Sanders C, Sanchez-Garrido J, Hopkins EGD, Shenoy AR, Barry R, Frankel G. *Citrobacter rodentium*–host–microbiota interactions: immunity, bioenergetics and metabolism. Nature Reviews Microbiology. 2019;17(11):701–715. doi:10.1038/s41579-019-0252-z.
12. Cao Y, Liu J, Zhu W, Qin N, Ren X, Zhu B, Xia X. Impact of dietary components on enteric infectious disease. Critical Reviews in Food Science and Nutrition 2021:1-26.
13. Desai MS, Seekatz AM, Koropatkin NM, Kamada N, Hickey CA, Wolter M, Pudlo NA, Kitamoto S, Terrapon N, Muller A, et al. A dietary fiber-deprived gut microbiota degrades the colonic mucus barrier and enhances pathogen susceptibility. Cell. 2016;167(5):1339–53 e21. doi:10.1016/j.cell.2016.10.043.
14. Erben U, Loddenkemper C, Doerfel K, Spieckermann S, Haller D, Heimesaat MM, Zeitz M, Siegmund B, Kühl AA. A guide to histomorphological evaluation of intestinal inflammation in mouse models. International Journal of Clinical and Experimental Pathology. 2014;7:4557–4576.
15. Greenhalgh K, Ramiro-Garcia J, Heinken A, Ullmann P, Bintener T, Pacheco MP, Baginska J, Shah P, Frachet A, Halder R, et al. Integrated in vitro and in silico modeling delineates the molecular effects of a synbiotic regimen on colorectal-cancer-derived cells. Cell Rep. 2019;27(5):1621–1632.e9. doi:10.1016/j.celrep.2019.04.001.
16. Steimle A, Grant ET, Desai MS. Quantitative assay to detect bacterial glycan-degrading enzyme activities in mouse and human fecal samples. STAR Protocols. 2021;2(1):100326. doi:10.1016/j.xpro.2021.100326.
17. Kozich JJ, Westcott SL, Baxter NT, Highlander SK, Schloss PD. Development of a dual-index sequencing strategy and curation pipeline for analyzing amplicon sequence data on the Miseq illumina sequencing platform. Applied and Environmental Microbiology. 2013;79(17):5112–5120. doi:10.1128/AEM.01043-13.
18. Schloss PD, Westcott SL, Ryabin T, Hall JR, Hartmann M, Hollister EB, Lesniewski RA, Oakley BB, Parks DH, Robinson CJ, et al. Introducing mothur: open-source,

platform-independent, community-supported software for describing and comparing microbial communities. Applied and Environmental Microbiology. 2009;75 (23):7537–7541. doi:10.1128/AEM.01541-09.
19. Schloss PD, MiSeq SOP 2019; https://mothur.org/wiki/miseq_sop/ 23.10.2019 Accessed 26 Jul. 2021.
20. Holmes I, Harris K, Quince C, Gilbert JA. Dirichlet multinomial mixtures: generative models for microbial metagenomics. PLOS ONE. 2012;7(2):e30126. doi:10.1371/journal.pone.0030126.
21. Quast C, Pruesse E, Yilmaz P, Gerken J, Schweer T, Yarza P, Peplies J, Glöckner FO. The SILVA ribosomal RNA gene database project: improved data processing and web-based tools. Nucleic Acids Research. 2013;41 (D1):D590–6. doi:10.1093/nar/gks1219.
22. McMurdie PJ, Holmes S, Watson M. phyloseq: an R package for reproducible interactive analysis and graphics of microbiome census data. PLOS ONE. 2013;8 (4):e61217. doi:10.1371/journal.pone.0061217.
23. Wickham H. ggplot2: elegant graphics for data analysis. Springer-Verlag New York: New York; 2016.
24. Oksanen J, Blanchet FG, Friendly M, Kindt R, Legendre P, McGlinn D, et al. vegan: community ecology package. R package version 2.5-7. 2020; https://CRAN.R-project.org/package=vegan 26 Jul .2021.
25. Wickham H forcats: tools for working with categorical variables (Factors). R package version 0.5.1. 2021; https://CRAN.R-project.org/package=forcats 26 Jul .2021
26. Love MI, Huber W, Anders S. Moderated estimation of fold change and dispersion for RNA-seq data with DESeq2. Genome Biology. 2014;15(12):550. doi:10.1186/s13059-014-0550-8.
27. Anderson MJ, Walsh DCI. PERMANOVA, ANOSIM, and the mantel test in the face of heterogeneous dispersions: what null hypothesis are you testing? Ecological Monographs. 2013;83(4):557–574. doi:10.1890/12-2010.1.
28. Litvak Y, Byndloss MX, Tsolis RM, Bäumler AJ. Dysbiotic proteobacteria expansion: a microbial signature of epithelial dysfunction. Current Opinion in Microbiology. 2017;39:1–6. doi:10.1016/j.mib.2017.07.003.
29. Ahn J, Sinha R, Pei Z, Dominianni C, Wu J, Shi J, Goedert JJ, Hayes RB, Yang L. Human gut microbiome and risk for colorectal cancer. JNCI: Journal of the National Cancer Institute. 2013;105(24):1907–1911. doi:10.1093/jnci/djt300.
30. Wlodarska M, Willing B, Bravo D, Finlay B. Phytonutrient diet supplementation promotes beneficial Clostridia species and intestinal mucus secretion resulting in protection against enteric infection. Scientific Reports. 2015;5(1):9253. doi:10.1038/srep09253.
31. BP W, Vacharaksa A, Croxen M, Thanachayanont T, Finlay BB, Bereswill S. Altering host resistance to infections through microbial transplantation. PLOS ONE. 2011;6(10):e26988. doi:10.1371/journal.pone.0026988.
32. Chassaing B, Koren O, Carvalho FA, Ley RE, Gewirtz AT. AIEC pathobiont instigates chronic colitis in susceptible hosts by altering microbiota composition. Gut. 2014;63(7):1069–1080. doi:10.1136/gutjnl-2013-304909.
33. Aguirre M, Eck A, Koenen ME, Savelkoul PH, Budding AE, Venema K. Diet drives quick changes in the metabolic activity and composition of human gut microbiota in a validated in vitro gut model. Research in Microbiology. 2016;167(2):114–125. doi:10.1016/j.resmic.2015.09.006.
34. Kortman GAM, Dutilh BE, Maathuis AJH, Engelke UF, Boekhorst J, Keegan KP, Nielsen FGG, Betley J, Weir JC, Kingsbury Z, et al. Microbial metabolism shifts towards an adverse profile with supplementary iron in the TIM-2 in vitro model of the human colon. Frontiers in Microbiology. 2016;6:1481. doi:10.3389/fmicb.2015.01481.
35. El Kaoutari A, Armougom F, Gordon JI, Raoult D, Henrissat B. The abundance and variety of carbohydrate-active enzymes in the human gut microbiota. Nat Rev Microbiol. 2013;11(7):497–504. doi:10.1038/nrmicro3050.
36. NE D, Willing BP. Microbial fermentation of dietary protein: an important factor in diet□microbe□host interaction. Microorganisms. 2019;7.
37. Yao CK, Muir JG, Gibson PR. Review article: insights into colonic protein fermentation, its modulation and potential health implications. Alimentary Pharmacology & Therapeutics. 2016;43(2):181–196. doi:10.1111/apt.13456.
38. Hughes R, Kurth MJ, McGilligan V, McGlynn H, Rowland I. Effect of colonic bacterial metabolites on Caco-2 cell paracellular permeability in vitro. Nutr Cancer. 2008;60(2):259–266. doi:10.1080/01635580701649644.
39. Burger-van Paassen N, Vincent A, Puiman PJ, van der Sluis M, Bouma J, Boehm G, van Goudoever J, van Seuningen I, Renes I. The regulation of intestinal mucin MUC2 expression by short-chain fatty acids: implications for epithelial protection. Biochem J. 2009;420(2):211–219. doi:10.1042/BJ20082222.
40. Peng L, Li Z-R, Green RS, Holzman IR, Lin J. Butyrate enhances the intestinal barrier by facilitating tight junction assembly via activation of AMP-activated protein kinase in Caco-2 cell monolayers. J Nutr. 2009;139 (9):1619–1625. doi:10.3945/jn.109.104638.
41. Zhao Y, Chen F, Wu W, Sun M, Bilotta AJ, Yao S, Xiao Y, Huang X, Eaves-Pyles TD, Golovko G, et al. GPR43 mediates microbiota metabolite SCFA

regulation of antimicrobial peptide expression in intestinal epithelial cells via activation of mTOR and STAT3. Mucosal Immunology. 2018;11(3):752–762. doi:10.1038/mi.2017.118.
42. Osbelt L, Thiemann S, Smit N, Lesker TR, Schröter M, EJC G, Schmidt-Hohagen K, Pils MC, Mühlen S, Dersch P, et al. Variations in microbiota composition of laboratory mice influence *Citrobacter rodentium* infection via variable short-chain fatty acid production. PLOS Pathogens. 2020;16(3):e1008448. doi:10.1371/journal.ppat.1008448.
43. Yang W, Yu T, Huang X, Bilotta AJ, Xu L, Lu Y, Sun J, Pan F, Zhou J, Zhang W, et al. Intestinal microbiota-derived short-chain fatty acids regulation of immune cell IL-22 production and gut immunity. Nature Communications. 2020;11(1):4457. doi:10.1038/s41467-020-18262-6.
44. Bomar L, Maltz M, Colston S, Graf J, Handelsman J. Directed culturing of microorganisms using metatranscriptomics. mBio. 2011;2(2):e00012–11. doi:10.1128/mBio.00012-11.
45. Pereira FC, Wasmund K, Cobankovic I, Jehmlich N, Herbold CW, Lee KS, Sziranyi B, Vesely C, Decker T, Stocker R, et al. Rational design of a microbial consortium of mucosal sugar utilizers reduces *Clostridiodes difficile* colonization. Nature Communications. 2020;11(1):5104. doi:10.1038/s41467-020-18928-1.
46. Bell A, Brunt J, Crost E, Vaux L, Nepravishta R, Owen CD, Latousakis D, Xiao A, Li W, Chen X, et al. Elucidation of a sialic acid metabolism pathway in mucus-foraging *Ruminococcus gnavus* unravels mechanisms of bacterial adaptation to the gut. Nat Microbiol. 2019;4(12):2393–2404. doi:10.1038/s41564-019-0590-7.
47. Crost EH, Tailford LE, Monestier M, Swarbreck D, Henrissat B, Crossman LC, et al. The mucin-degradation strategy of *Ruminococcus gnavus*: the importance of intramolecular trans-sialidases. Gut Microbes. 2016;7:302–312. doi:10.1080/19490976.2016.1186334.
48. Kamada N, Kim YG, Sham HP, Vallance BA, Puente JL, Martens EC, Nunez G. Regulated virulence controls the ability of a pathogen to compete with the gut microbiota. Science. 2012;336(6086):1325–1329. doi:10.1126/science.1222195.
49. Fabich AJ, Jones SA, Chowdhury FZ, Cernosek A, Anderson A, Smalley D, McHargue JW, Hightower GA, Smith JT, Autieri SM, et al. Comparison of carbon nutrition for pathogenic and commensal *escherichia coli* strains in the mouse intestine. Infect Immun. 2008;76(3):1143–1152. doi:10.1128/IAI.01386-07.
50. Bergstrom KS, Kissoon-Singh V, Gibson DL, Ma C, Montero M, Sham HP, Ryz N, Huang T, Velcich A, Finlay BB, et al. Muc2 protects against lethal infectious colitis by disassociating pathogenic and commensal bacteria from the colonic mucosa. PLoS Pathog. 2010;6(5):e1000902. doi:10.1371/journal.ppat.1000902.
51. Dann SM, Le C, Choudhury BK, Liu H, Saldarriaga O, Hanson EM, Cong Y, Eckmann L. Attenuation of intestinal inflammation in interleukin-10-deficient mice infected with *Citrobacter rodentium*. Infect Immun. 2014;82(5):1949–1958. doi:10.1128/IAI.00066-14.
52. Zheng Y, Valdez PA, Danilenko DM, Hu Y, Sa SM, Gong Q, Abbas AR, Modrusan Z, Ghilardi N, de Sauvage FJ, et al. Interleukin-22 mediates early host defense against attaching and effacing bacterial pathogens. Nat Med. 2008;14(3):282–289. doi:10.1038/nm1720.
53. An J, Zhao X, Wang Y, Noriega J, Gewirtz AT, Zou J, Baumler AJ. Western-style diet impedes colonization and clearance of Citrobacter rodentium. PLoS Pathog. 2021;17(4):e1009497. doi:10.1371/journal.ppat.1009497.
54. Gasaly N, Hermoso MA, Gotteland M. Butyrate and the fine-tuning of colonic homeostasis: implication for inflammatory bowel diseases. International Journal of Molecular Sciences. 2021;22(6):3061. doi:10.3390/ijms22063061.
55. Donohoe DR, Garge N, Zhang X, Sun W, O'Connell TM, Bunger MK, Bultman S. The microbiome and butyrate regulate energy metabolism and autophagy in the mammalian colon. Cell Metab. 2011;13(5):517–526. doi:10.1016/j.cmet.2011.02.018.
56. Fletcher SM, McLaws ML, Ellis JT. Prevalence of gastrointestinal pathogens in developed and developing countries: systematic review and meta-analysis. Journal of Public Health Research. 2013;2(1):42–53. doi:10.4081/jphr.2013.e9.
57. Card T, Enck P, Barbara G, Boeckxstaens GE, Santos J, Azpiroz F, Mearin F, Aziz Q, Marshall J, Spiller R, et al. Post-infectious IBS: defining its clinical features and prognosis using an internet-based survey. United European Gastroenterology Journal. 2018;6(8):1245–1253. doi:10.1177/2050640618779923.
58. Aslam B, Wang W, Arshad MI, Khurshid M, Muzammil S, Rasool MH, Nisar MA, Alvi RF, Aslam MA, Qamar MU, et al. Antibiotic resistance: a rundown of a global crisis. Infection and Drug Resistance. 2018;11:1645–1658. doi:10.2147/IDR.S173867.

Akkermansia muciniphila and *Parabacteroides distasonis* synergistically protect from colitis by enhancing the gut immunity

Joana Gaifem[1,2], Ana Mendes-Frias[1,2], Mathis Wolter[3,4], Maria Jose Garzón[5,6], Carles Ubeda[5,6], Cristina Cunha[1,2], Agostinho Carvalho[1,2], António Gil Castro[1,2], Mahesh S. Desai,[3,7], Fernando Rodrigues[1,2], Ricardo Silvestre[1,2,#]

[1]Life and Health Sciences Research Institute (ICVS), School of Medicine, University of Minho, Braga, Portugal
[2]ICVS/3B's – PT Government Associate Laboratory, Braga/Guimarães, Portugal
[3]Department of Infection and Immunity, Luxembourg Institute of Health, Esch-sur-Alzette, Luxembourg
[4]Faculty of Science, Technology and Medicine, University of Luxembourg, Esch-sur-Alzette, Luxembourg
[5]Departamento de Genómica y Salud, Centro Superior de Investigación en Salud Pública – FISABIO, Valencia, Spain
[6]Centers of Biomedical Research Network (CIBER) in Epidemiology and Public Health, Madrid, Spain
[7]Odense Research Center for Anaphylaxis, Department of Dermatology and Allergy Center, Odense University Hospital, University of Southern Denmark, Odense, Denmark

Corresponding Author
Ricardo Silvestre
Life and Health Sciences Research Institute (ICVS), School of Medicine, University of Minho, Braga, Portugal; ICVS/3B's–PT Government Associate Laboratory, Braga/Guimarães, Portugal; e-mail: ricardosilvestre@med.uminho.pt

Objective: Gut microbiota majorly contributes as an environmental variable; however, little is known about which specific members of the microbiome aid in the intestinal epithelial barrier function to protect from disease. We aim therefore to clarify how interactions between commensal bacteria may promote protection against inflammatory bowel disease (IBD).

Design: Chemically-induced colitis was assessed in mice from different animal facilities. 16S rRNA sequencing was performed on the stools to characterize the microbiota composition. Pinpointed bacteria were then administered to mice by oral gavage. Colonic epithelial barrier integrity was assessed by qPCR and histochemistry. Immune profile was assessed by flow cytometry.

Results: We serendipitously found that mice in one facility showed remarkable resistance to disease development, which was associated with increased markers of epithelial barrier integrity. Importantly, we show that *Akkermansia muciniphila* and *Parabacteroides distasonis* were significantly increased in the microbiota of resistant mice. After colonization of susceptible mice with the two bacterial species, we demonstrated that *A. muciniphila* and *P. distasonis* synergistically drive a protective effect in both acute and chronic models of colitis by boosting the frequency of ILC3 cells in the colon and by improving gut epithelial integrity.

Conclusion: We revealed a combined effort of commensal microbes in offering protection against severe intestinal inflammation, by shaping the gut immunity and by enhancing intestinal epithelial barrier stability. Our study highlights the beneficial role of gut bacteria in dictating intestinal homeostasis, which is an important step towards employing microbiome-driven therapeutic approaches for the management of IBD.

What is already known on this topic:

It is widely known the contribution of the gut microbiome to the balance between homeostasis and inflammation. Nevertheless, the etiology of inflammatory bowel disease, which is known to be influenced by genetics, immune response and environmental cues, remains unclear. Therefore, unlocking novel players involved in the dictation of a protective gut, namely in the microbiota component, is crucial to develop novel strategies to tackle IBD.

What this study adds:

Herein, we revealed a synergistic interaction between two commensal bacterial strains, *Akkermansia muciniphila* and *Parabacteroides distasonis*, which induce protection against both acute and chronic models of colitis induction, by enhancing epithelial barrier integrity and promoting ILC3 in the colonic mucosa.

How this study might affect research, practice or policy:

This study provides a novel insight on how commensal bacteria can beneficially act to promote intestinal homeostasis, which may open new avenues towards the use of microbiome-derived strategies to tackle IBD.

INTRODUCTION

The gastrointestinal tract harbours a vast community of microbes, from bacteria to fungi and viruses, that have coevolved and developed mutualistic interactions with the host. These microorganisms play a role in the complex environment that is found in the intestine, such as the occupation of niches thus avoiding pathogen colonization and by the synthesis of vitamins, metabolites and other nutrients that are only accessible to the host through microbial metabolism[1]. Besides acting as a defence mechanisms against infections, several pathogen recognition receptors sense and respond to the microbiota in a beneficial relationship with the host towards homeostasis and thus mediate the interaction with the intestinal epithelial barrier[1]. In turn, the presence of the intestinal epithelial barrier avoids the excessive contact between microorganisms and the immune cells[2]. In this sense, the interaction between the microbiota, the intestinal barrier function and the immune system must be fine-tuned in order to keep gut homeostasis. Thus, alterations affecting this dynamic interaction may trigger intestinal inflammation, such as inflammatory bowel disease (IBD)[3].

IBD is a chronic, debilitating disorder from the gastrointestinal tract that comprises both Crohn's disease (CD) and ulcerative colitis (UC). This disease poses a major clinical challenge since there is still lack of knowledge regarding its etiopathology, which in turn hampers the development of efficient therapies[4]. Notwithstanding, it is well established that the development of an exacerbated immune response towards the gut microbiota, often enhanced by genetic susceptibility factors, is the main cause for the occurrence of this disease[4,5]. Throughout the years, several reports have demonstrated how commensal bacteria can be beneficial or detrimental for gut homeostasis, such as *Faecalibacterium prausnitzii* or *Bacteroides fragilis*, respectively[6,7]. However, some of these studies are circumscribed to the phylum level, therefore lacking the precision needed to pinpoint its specific players[8,9]. Moreover, it is unknown if interactions between different commensal bacteria may have any role on IBD development besides the impact that single microbes could have on disease progression. The findings collected in this work have shown that *A. muciniphila* and *P. distasonis* can play an important role in promoting protection against ulcerative colitis. In addition, this work revealed that the beneficial effect driven by *A. muciniphila* can be amplified by the co-colonization with *P. distasonis*, reinforcing the importance of studying the intricate interactions between microbiota players, rather than focusing on single microbe probiotics, in order to develop new microbiome-based therapies to tackle IBD.

METHODS

Model of chemically induced colitis

C57BL/6 mice (7 to 9 weeks old) were given sodium dextran sulfate (DSS; 3% (w/v), molecular weight approximately 40000 Da; TdB Consultancy) in the drinking water *ad libitum* for 7 days. Clinical signs of colitis were monitored daily and measured by the disease activity index (DAI; Table 1). For chronic colitis model, 2% DSS was given in the drinking water for 5 days in two subsequent phases with an interval of 3 weeks. Detailed methods of experiments and analysis can be found in online supplemental methods.

Analysis of gut structure and immune cell quantification

In vivo intestinal permeability was assessed by the serum quantification of gavage fed fluorescein isothiocyanate (FITC) labeled dextran. Colon inflammation was assessed blindly by a pathologist using a graduated semi quantitative system (Table 2). Mucin- and claudin-encoding genes *Muc1*, *Muc2*, *Muc13* and *Cldn3*, *Cldn4* and *Cldn7*, respectively as well as *Cdh1* were quantified by quantitative real-time PCR (qRT-PCR) (Table 3). Lamina propria leukocytes (LPL) were isolated and the immune cell populations were quantified following the gating strategy presented in Supplemental Figure 1. The levels of IL-10, IL-17A/F and IL-22 were measured by ELISA using commercially available kits (Biolegend), according to manufacturer's instructions. Detailed methods of experiments and analysis can be found in online supplemental methods.

Microbiota modulation

Ampicillin (1 mg/mL), streptomycin (1 mg/mL), vancomycin (0.5 mg/mL) and neomycin sulfate (1 mg/mL) were given to C57BL/6 mice for microbiota depletion. Fecal microbiota transplant (FMT) was performed after antibiotic treatment as using a disease remission model as represented in Figure 3A-C, respectively. A $2x10^8$ CFU *A. muciniphila* (Am) and *P. distasonis* (Pd) suspensions were administered daily by oral gavage for 12 days. Detailed methods of experiments and analysis can be found in online supplemental methods.

Metagenomic analysis and bacterial quantification

Mice stools were collected and subjected to the the MiSeq platform from Illumina and analyzed with mothur. Absolute abundance of bacteria was performed by quantification of bacterial copy number in stool DNA samples using specific primers for Am and Pd (Table 3). Detailed methods of experiments and analysis can be found in online supplemental methods.

Statistical analysis

Data are presented as mean ± standard deviation (SD). For multiple group comparisons t-test or one-way ANOVA test with a Tukey multiple-comparison posttest were performed, while for multiple group comparisons with repeated measures two-way ANOVA test with a Tukey multiple-comparison posttest was applied. Detailed methods of experiments and analysis can be found in online supplemental methods.

RESULTS

Mice from different animal facilities display different susceptibility to chemically induced colitis

To characterize the immune response associated with IBD development, we chemically induced colitis in wild-type C57BL/6 mice by DSS treatment for seven days (Figure 1A). All parameters associated to disease progression, such as weight loss, stool consistency and presence of blood in stools were monitored daily and scored according to the Disease Activity Index (DAI). Unexpectedly, we observed that wild-type C57BL/6 mice did not display major clinical signs of disease development even when exposed to a prolonged treatment (Figure 1B; from now on referred to as resistant). To study this unexpected phenotype, colitis was induced using a similar protocol on wild-type C57BL/6 mice housed in a different animal facility. These mice developed colitis, following the expected disease course, with an average DAI score of 8 (out of 10) at day 7 post DSS administration (Figure 1B; from now on referred to as susceptible). Upon examination, susceptible mice had short, thick colons, consistent with significant colon pathology (Figure 1C). Histological analysis of the colons, comprising ulceration, crypt shortening or ablation and the presence of inflammatory infiltrates, showed a severe histopathology in the susceptible group when compared to those without severe disease progression (Figure 1D-E). The total number of goblet cells were also different between susceptible and resistant mice under homeostatic conditions, with a massive reduction of goblet cells and mucus layer only observed in susceptible mice after DSS-induced colitis (Figure 1F-G). Hence, despite being genetically identical and subjected to the same experimental protocol, mice from different animal facilities showed a different response to the induction of colitis.

Resistant mice exhibit an upregulation of genes associated with epithelial barrier function and a distinct gut immunity

Since the two groups of mice have the same genetic background but a divergent phenotype upon colitis induction, we hypothesized that alterations in the stability and function of the intestinal epithelial barrier could be associated with the observed phenotype. Alterations in the expression of tight and adherens junction proteins, such as claudins, were described in IBD patients, reinforcing the relevance of the integrity of the intestinal epithelial barrier in this pathology[10]. Other important component of the epithelial barrier is the mucus layer constituted by mucin glycoproteins produced and secreted by goblet cells, which prevents the direct contact of luminal microorganisms[11]. Under homeostatic conditions the transcriptional

levels of mucin-encoding genes (*Muc1*, *Muc2* and *Muc13*) as well as E-cadherin- and claudin-encoding genes (*Cdh1; Cldn2*, *Cldn3*, *Cldn4* and *Cldn7)* were significantly upregulated in resistant mice when compared to the susceptible group (Figure 2A-B). These data suggest an hyperactivation of epithelial barrier-associated proteins in the resistant group, which may allow the epithelial barrier to sustain an inflammatory insult. Although exacerbated intestinal permeability is known to be a hallmark in IBD and is found in IBD patients[12], no significant differences were found in the intestinal permeability among the two groups of mice at homeostasis (Figure 2C).

To determine whether the protective phenotype observed in resistant mice was driven by an altered gut immunity, the immune environment in the gut of both susceptible and resistant mice prior to colitis induction was evaluated considering the cytokine levels. IL-10 was found increased in resistant mice (Figure 2D), which goes in line with the protective phenotype displayed by these mice. Additionally, resistant mice also presented higher levels of IL-17A and IL-22 when compared to susceptible mice (Figure 2D). Both IL-17A and IL-22 can be produced by a myriad of immune cells present in the gut, namely T helper 17 (Th17) cells and ILC3 and may have either proinflammatory or tissue-protective properties depending on the context[13–15]. We observed that susceptible and resistant mice have a divergent frequency of both ILC3 and Th17 cells in the gut at homeostatic conditions, with resistant mice displaying a significantly higher frequency of ILC3 and, inversely, lower frequency of Th17 cells, when compared to susceptible mice (Figure 2E-F). Since ILC3 are one of the major producers of IL-22 in the gut and play a pivotal role in the maintenance of gut homeostasis[16], these results suggest that the increased frequency of ILC3 cells at steady state may be contributing to a healthier intestinal environment in resistant mice.

Microbiome modulates protection against colitis development

To determine if the protective phenotype upon colitis induction was driven by a distinctive microbiota composition, a fecal microbiota transplant (FMT), with fecal contents from resistant mice, was performed into antibiotic-induced microbiota-depleted susceptible mice (Figure 3A). Susceptible mice were previously treated with a mixture of antibiotics for 5 weeks to deplete the native gut microbiota. The efficacy of the microbiota depletion was assessed throughout the antibiotic treatment (Supplemental Figure 2). After this, the susceptible group received a fecal suspension from resistant mice for three consecutive days. Three weeks after FMT, mice were submitted to DSS treatment for colitis induction and the DAI was compared with susceptible and resistant mice without FMT. A clear protection against

colitis induction was observed (Figure 3B). These data, mirroring the resistant group as reflected by their similar DAI, support the key role of gut-microbiome in the protective phenotype against colitis development.

In order to understand the protective effect in a relapse-remission model of colitis, disease was induced in susceptible mice and, upon remission of the disease, mice received FMT from the resistant mice by oral gavage during five days. No antibiotic treatment was administered in this setting. Two weeks after FMT, mice were again challenged with colitis (Figure 3C). Mice treated with fecal contents from resistant mice displayed only mild symptoms of colitis, contrary to the control group that only received the vehicle (PBS) (Figure 3D). FMT-treated mice displayed significantly fewer signs of pathology than the control group as well as higher amount of goblet cells per crypt (Figure 3E-G).

Akkermansia and _Parabacteroides_ species are significantly increased in the gut microbiota community of mice protected against colitis induction

16S rRNA gene analysis of the gut microbiota composition was performed on the stools of mice, both susceptible and resistant, in homeostatic conditions. A distinct microbiota signature was found when comparing resistant and susceptible mice, with these clustering separately in an unsupervised multivariate analysis (Figure 4A-B). The resistant group of mice presents a significant reduction of richness (Figure 4C) and species diversity (Figure 4D), which was unexpected since the decrease in number and diversity is often associated with disease[17]. To pinpoint which bacterial species could be underlying the protective phenotype against colitis, susceptible mice that received FMT from resistant mice were also included in the microbiota analysis. No major alterations were observed on the susceptible group before or after the FMT regarding number and diversity of species. Yet, very clear shifts in the relative abundance of a limited number of genera, such as *Akkermansia*, suggest that minority populations could be responsible for the protective phenotype (Figure 4A-D). Indeed, from the 129 genera identified, 6 were found to be significantly different between resistant and susceptible mice, while 7 were found significantly different between susceptible mice and susceptible mice that received FMT ($p<0.05$; FDR<0.05; Table 4). These hits were also validated using ANCOM-BC test (Supplemental Tables 1-2). *Akkermansia* and *Parabacteroides* genera were pinpointed as our candidates given their significantly increased number of copies when a resistant phenotype was observed (for *Akkermansia*, the relative abundance was of 1.29%, 12.07% and 15.55% in susceptible, resistant and susceptible+FMT groups, respectively; for *Parabacteroides*, the relative abundance was of 0.14%, 5.66% and

0.78% in susceptible, resistant and susceptible+FMT groups, respectively). A Basic Local Alignment Search Tool (BLAST) analysis of the 16S RNA gene sequences pinpointed *Akkermansia muciniphila* and *Parabacteroides distasonis* as the representative species for each genus.

To confirm that *A. muciniphila* and *P. distasonis* were increased in mice that showed protection against colitis induction, we examined the absolute abundance of these bacteria. As expected, *A. muciniphila* and *P. distasonis* were significantly increased in both resistant and susceptible mice after FMT, when compared to susceptible mice (Figure 4E-F). The abundance of *A. muciniphila* and *P. distasonis* in resistant mice is, on average, 500000 and 15000 times higher, respectively, than in susceptible mice, while for susceptible mice after FMT the abundance of *A. muciniphila* and *P. distasonis* was 3000000 and 7000 times higher, respectively, than before receiving FMT. Overall, this result confirms the significant representation of these two species in the intestinal microbiota of mice protected against colitis, pointing to a possible effect of these bacteria, alone or in combination, in creating a very particular immunological environment that allows the intestine to sustain an insult.

Akkermansia muciniphila **and** ***Parabacteroides distasonis*** **act synergistically towards a decreased colitis severity**

To assess the protective properties of *A. muciniphila* and *P. distasonis* in controlling inflammation in the chemically-induced colitis, susceptible mice were supplemented with bacteria for 12 days before colitis induction with 3% DSS (Figure 5A). Administration of *A. muciniphila* or *P. distasonis* alone was not able to reduce colitis. In contrast, administration of *P. distasonis* in addition to *A. muciniphila* significantly reduced the level of colitis as compared with control mice (Figure 5B). Although no major alterations were found in terms of goblet cell numbers (Figure 5C-D), the histological analysis showed that mice supplemented with both *A. muciniphila* and *P. distasonis* (Am+Pd) displayed less architectural damage and inflammation, with a histological score lower than the control group and Pd (Figure 5C-E). This points towards a beneficial effect of the combination of *A. muciniphila* with *P. distasonis* in controlling the inflammation associated with acute colitis.

The protective effect of the combination of *A. muciniphila* with *P. distasonis* was also evaluated in a relapse-remission chronic model of colitis, in which susceptible mice were supplemented with these bacteria by oral gavage during 12 days between 2 cycles of DSS induction (Figure 5F). We observed that supplementation with *A. muciniphila*, alone (Am) or in combination with *P. distasonis* (Am+Pd), was able to partially protect the mice from the

second cycle of DSS-induced colitis, conversely the supplementation of *P. distasonis* alone (Pd) was insufficient (Figure 5G). The best performance overall was indeed for *A. muciniphila*, alone or in combination with *P. distasonis*, as it is shown by the decreased area under the curve (AUC) (Figure 5H). *A. muciniphila* and the combination of both bacteria also led to an increased goblet cell count when compared to the control and Pd groups (Figure 5I-J). No statistical differences were found in the histological analysis, despite the tendency of *A. muciniphila* and *A. muciniphila* with *P. distasonis* towards a lower score of pathology (Figure 5I-K). Our results suggest that the combination of both bacteria is more effective in inducing protection against acute inflammatory events, with *A. muciniphila* supplementation standing out during chronic inflammation.

Supplementation with *Akkermansia muciniphila* shapes gut immunity by promoting ILC3 population in the gut

It is known that microbiota interact with the immune system, either directly or by producing signals that in turn will regulate the response of immune populations, such as ILC3[18]. To understand whether supplementation with *A. muciniphila* is indeed interfering with the gut immune response, the immune profile was characterized upon bacterial supplementation. Mice supplemented with *A. muciniphila*, alone or in combination with *P. distasonis* showed improved epithelial barrier integrity (Supplemental Figure 3) and increased ILC3 frequencies when compared with the control group (Figure 6A). This is accompanied with an increase in IL-17-producing ILC3 (Figure 6B) and a tendency, although not significant, in IL-22-producing ILC3 (Figure 6C). On the other hand, supplementation with *P. distasonis* (Pd) leads to an increase in Th17 and IL-17-producing Th17 frequency when compared with the control and Am treatment (Figure 6D-E). No major alterations were found in the frequencies of Th17-producing IL-22 cells (Figure 6F). Indeed, the number of copies of *A. muciniphila* was found to be positively correlated with ILC3 levels in the gut (Figure 6G). Th17 and ILC3 have a crucial, yet dichotomic profile in managing homeostasis and inflammation, with Th17 being highly involved in intestinal inflammation and ILC3 being an important player in promoting gut homeostasis[19,20]. This, together with observations in which *A. muciniphila* and *A. muciniphila* with *P. distasonis* exerted a beneficial impact on colitis development, suggests that *A. muciniphila* is able to shape gut immunity towards a more homeostatic immune profile, conferring some degree of protection against an inflammatory event.

We observed that *A. muciniphila* had a protective action against colitis development, benefiting in the acute model by the presence of *P. distasonis.* In this sense, we questioned if *P. distasonis* had any positive effect on the colonization by *A. muciniphila*. Although *A. muciniphila* abundance increases along the time due to the supplementation, it is strikingly increased when administered in combination with *P. distasonis* (Figure 6H). This suggested a symbiotic relationship between *A. muciniphila* and *P. distasonis* that may be the responsible factor for the increased beneficial effect observed when the two bacterial species are combined. In support of this, we found that the quantity of *A. muciniphila* was inversely correlated with the DAI (Figure 6I), which supports the protective effect observed in supplemented mice.

Altogether, these results suggest that *A. muciniphila* exerts a protective effect on colitis development by promoting an increase in ILC3 in the gut, thus controlling inflammation, and *P. distasonis* positively contributes to its colonization.

DISCUSSION

Alterations in composition of gut microbiota are known to occur in several human diseases[17,21,22]. A profound impairment in gut microbial composition occurs in IBD that largely contributes to the development and/or the severity of the disease[17,23]. A growing body of evidence has been stating the great involvement of microbiota to dictate protection or susceptibility to develop IBD, leading to an increased attention on the development of novel microbiota-derived therapies to tackle a disease which current treatments are not equally effective for all patients. Targeting the intestinal microbiota itself is not new; several approaches have already been described, such as fecal microbiota transplantation to control *Clostridium difficile* infection[24], or the use of specific strains of probiotics[8,25]. Nevertheless, the major aim in using microbiota modulation as a reliable strategy to treat or prevent IBD is the need of an effective immunomodulatory effect either locally or at the periphery. For this, a particular combination of players is pivotal for the ability to suppress proinflammatory strains and promote those that create a more tolerant immune environment. Thus, it is important to identify protective commensal bacteria and understand their ability to modulate immune cell populations to move forward as a potential therapeutic approach for IBD.

Here, we have revealed that the enrichment in *A. muciniphila* and *P. distasonis* bacteria in the gut exerts protection in both acute and chronic models of colitis induction. This microbial signature is concomitant with an increase in ILC3 frequency in the gut and with increased gut epithelial integrity, creating a balanced intestinal environment that is more prone to control inflammation and protect against severe forms of colitis. While a potential protective effect has been placing *A. muciniphila* as a promising probiotic to tackle intestinal inflammation[26], conflicting reports in murine experimental models[27,28] and IBD patients[29,30] have been disputing the *P. distasonis* role, being associated with enhanced or attenuated colitis development[31]. *A. muciniphila* is a strict anaerobe mucin-degrading bacterium that represents around 1-5% of the human intestinal microbial composition[32]. It is able to degrade mucin, leading to the production of the short-chain fatty acids propionate and acetate, which contributes for the regulation of host biological processes, including gut immune response[33,34]. *A. muciniphila* has been pinpointed as a promising player to induce intestinal protection. Lower abundances of *A. muciniphila* were described in IBD patients[35], where were correlated with higher inflammatory scores[36]. Despite several studies pointing towards a protective role of *A. muciniphila* in controlling intestinal inflammation, the exact mechanisms by which this bacterium hampers disease progression are still not fully understood. *A.*

muciniphila supplementation have been shown to reduce NLRP3 inflammasome in DSS-induced acute colitis [37], and to be partially responsible for the beneficial role of metformin in a mouse model of UC[38]. It was also described that *A. muciniphila* administration was able to reduce inflammation driven by DSS treatment in mice, not only by regulating the colonic and serum levels of inflammatory cytokines such as TNF-α and IL-6, but also by imposing alterations on the gut microbiota community and rescuing microbiota dysbiosis derived from DSS administration[39]. Our work has revealed that the administration of *A. muciniphila* alone or in combination with *P. distasonis* leads to an increase of ILC3 and IL-17^{+}-ILC3 that associates with control of colitis in mice, reinforcing the interaction between microorganisms in the gut and their contribution to a protective immune response. ILC3 are particularly relevant in the regulation of intestinal homeostasis by the production of IL-17, IL-22 and granulocyte-macrophage colony-stimulating factor (GM-CSF) at steady state[20]. It is known that both UC and CD patients display alterations in ILC3 populations, namely in their ability to produce IL-22, which may be linked to the enhanced epithelial damage found in these patients[40,41]. How the immune subsets respond to the divergent environmental cues, such as microbiota composition, needs to be further clarified. For instance, it is described that short-chain fatty acids (SCFA) produced by intestinal microbiota have the ability to induce ILC3 and also IL-22 production via AKT-STAT3 signalling pathway[42]. This reinforces the need of studying the impact of microbiota-derived metabolites in the modulation of intestinal homeostasis. Anyway, we have shown that the increased frequency of ILC3 in the gut may be largely shaped by the amount of *A. muciniphila* present in the gut, in a dose-dependent manner, unveiling a novel interaction between microbiota and immune response that needs to be explored in the future to disclose a protective strategy to avoid or control gut inflammation.

It was previously demonstrated that *A. muciniphila* and *Parabacteroides* can synergistically be involved in the prevention of epilepsy by the decrease in gammaglutamylation of amino acids and increase of hippocampal GABA/glutamate ratios, subsequently preventing seizures[43]. This is quite relevant since previous studies focusing on the effects of each one of these bacteria in intestinal inflammation have not addressed the possibility of the combination of both in promoting intestinal protection, which supports the novelty of this work. In fact, we observed the tolerant effect of *A. muciniphila* in controlling colitis induction in mice, but interestingly we found that this effect was even more pronounced when combined with *P. distasonis*. While we observed an advantageous and accelerated *A. muciniphila* gut colonization in the presence of the aerotolerant *P. distasonis,* the mechanisms by which this symbiotic interaction is established is an important topic for future studies. Yet,

the metabolism of these bacteria may be the key to answer this question. It is described that *P. distasonis* is able to synthesize acetate and succinate[44]. It is also known that *A. muciniphila* is a major propionate producer, mainly via mucin fermentation[45,46]. It is also described that the production of propionate by *A. muciniphila* can be promoted by vitamin B12 that is used as a cofactor in the conversion of succinate to propionate via methylmalonyl-CoA synthase[47]. Thus, we can hypothesize that this synergistic effect of the combination of *A. muciniphila* and *P. distasonis* may be explained by a commensal feeding mechanism in which *P. distasonis* may be providing an extra source to *A. muciniphila* for propionate production, benefiting its metabolism and colonization.

The *A. muciniphila* and *P. distasonis* co-supplementation had also a positive impact on the intestinal epithelial barrier. Mice enriched with *A. muciniphila* and *P. distasonis* displayed an upregulation of genes involved in the maintenance of epithelial barrier stability, such as mucins and claudins, increased number of goblet cells, and decreased histological and disease score upon colitis induction when compared with susceptible mice. These results point out that the presence of these bacteria prepare the epithelial barrier to better sustain an inflammatory insult. This goes in line with previous data that highlight the capacity of *A. muciniphila* to promote intestinal epithelial barrier integrity by its capacity to strengthen enterocyte monolayer *in vitro*[48] and by releasing extracellular vesicles with anti-inflammatory properties that promote gut protection[49].

Bacterial composition in the gut can rapidly fluctuate due to environmental cues, imposing a huge challenge in the identification of specific beneficial microbes to intestinal health. Within this work, we pinpointed two specific bacterial species that, when combined, are able to promote intestinal protection by shaping gut immunity towards a more tolerant, homeostatic environment. It would be important to dissect the mechanisms underlying the protective effect of these combined microbes with disease severity and gut immunity. The observed protective phenotype observed is directly dependent on the levels of these bacteria in the gut, which rapidly decrease if the supplementation is stopped. In this sense and based on the local and systemic protective effect described for *A. muciniphila*, it would be crucial to study how stable is the supplementation with a mixture containing these bacteria and its ecologic and functional impact in other microbial populations to assess its full potential as a probiotic. In addition, to ensure if bacterial supplementation as a probiotic can have a long-lasting effect or, at least, more effective in controlling the inflammatory processes associated with IBD, is a key factor that must be thoroughly studied. Overall, and despite the need of more complementary studies, this work provided a solid contribution in supporting role of the gut

456 microbiota in IBD development and prevention, undoubtedly a major topic to explore new
457 strategies to tackle IBD.
458
459

REFERENCES

1 Hooper L V, Littman DR, Macpherson AJ. Interactions between the microbiota and the immune system. *Science* 2012;**336**:1268–73. doi:10.1126/science.1223490

2 Groschwitz KR, Hogan SP. Intestinal barrier function: molecular regulation and disease pathogenesis. *J Allergy Clin Immunol* 2009;**124**:2–3. doi:10.1016/j.jaci.2009.05.038

3 Nalle SC, Turner JR. Intestinal barrier loss as a critical pathogenic link between inflammatory bowel disease and graft-versus-host disease. *Mucosal Immunol* 2015;**8**:720–30. doi:10.1038/mi.2015.40

4 Danese S, Fiocchi C. Ulcerative colitis. *N Engl J Med* 2011;**365**:1713–25. doi:10.1056/NEJMra1102942

5 Maloy KJ, Powrie F. Intestinal homeostasis and its breakdown in inflammatory bowel disease. *Nature* 2011;**474**:298–306. doi:10.1038/nature10208

6 Zamani S, Hesam Shariati S, Zali MR, *et al.* Detection of enterotoxigenic Bacteroides fragilis in patients with ulcerative colitis. *Gut Pathog* 2017;**9**:53. doi:10.1186/s13099-017-0202-0

7 Qiu X, Zhang M, Yang X, *et al.* Faecalibacterium prausnitzii upregulates regulatory T cells and anti-inflammatory cytokines in treating TNBS-induced colitis. *J Crohns Colitis* 2013;**7**:e558-68. doi:10.1016/j.crohns.2013.04.002

8 Schroeder BO, Birchenough GMH, Ståhlman M, *et al.* Bifidobacteria or Fiber Protects against Diet-Induced Microbiota-Mediated Colonic Mucus Deterioration. *Cell Host Microbe* 2018;**23**:27-40.e7. doi:10.1016/j.chom.2017.11.004

9 Vester-Andersen MK, Mirsepasi-Lauridsen HC, Prosberg M V, *et al.* Increased abundance of proteobacteria in aggressive Crohn's disease seven years after diagnosis. *Sci Rep* 2019;**9**:13473. doi:10.1038/s41598-019-49833-3

10 Chelakkot C, Ghim J, Ryu SH. Mechanisms regulating intestinal barrier integrity and its pathological implications. *Exp Mol Med* 2018;**50**:1–9. doi:10.1038/s12276-018-0126-x

11 Pelaseyed T, Bergström JH, Gustafsson JK, *et al.* The mucus and mucins of the goblet cells and enterocytes provide the first defense line of the gastrointestinal tract and interact with the immune system. *Immunol Rev* 2014;**260**:8–20. doi:10.1111/imr.12182

12 Michielan A, D'Incà R. Intestinal Permeability in Inflammatory Bowel Disease: Pathogenesis, Clinical Evaluation, and Therapy of Leaky Gut. *Mediators Inflamm* 2015;**2015**:628157. doi:10.1155/2015/628157

13 Robinette ML, Colonna M. Immune modules shared by innate lymphoid cells and T cells. *J Allergy Clin Immunol* 2016;**138**:1243–51. doi:10.1016/j.jaci.2016.09.006

14 Rutz S, Eidenschenk C, Ouyang W. IL-22, not simply a Th17 cytokine. *Immunol Rev* 2013;**252**:116–32. doi:10.1111/imr.12027

15 Zhang X, Liu S, Wang Y, *et al.* Interleukin-22 regulates the homeostasis of the intestinal epithelium during inflammation. *Int J Mol Med* 2019;**43**:1657–68. doi:10.3892/ijmm.2019.4092

16 Vivier E, Artis D, Colonna M, *et al.* Innate Lymphoid Cells: 10 Years On. *Cell* 2018;**174**:1054–66. doi:10.1016/j.cell.2018.07.017

17 Manichanh C, Rigottier-Gois L, Bonnaud E, *et al.* Reduced diversity of faecal microbiota in Crohn's disease revealed by a metagenomic approach. *Gut* 2006;**55**:205–11. doi:10.1136/gut.2005.073817

18 Lehmann FM, von Burg N, Ivanek R, *et al.* Microbiota-induced tissue signals regulate ILC3-mediated antigen presentation. *Nat Commun* 2020;**11**:1794. doi:10.1038/s41467-020-15612-2

19 Yen D, Cheung J, Scheerens H, *et al.* IL-23 is essential for T cell-mediated colitis and promotes inflammation via IL-17 and IL-6. *J Clin Invest* 2006;**116**:1310–6. doi:10.1172/JCI21404

20 Mortha A, Chudnovskiy A, Hashimoto D, *et al.* Microbiota-dependent crosstalk between macrophages and ILC3 promotes intestinal homeostasis. *Science* 2014;**343**:1249288. doi:10.1126/science.1249288

21 Ley RE, Bäckhed F, Turnbaugh P, *et al.* Obesity alters gut microbial ecology. *Proc Natl Acad Sci U S A* 2005;**102**:11070–5. doi:10.1073/pnas.0504978102

22 Ahn J, Sinha R, Pei Z, *et al.* Human gut microbiome and risk for colorectal cancer. *J Natl Cancer Inst* 2013;**105**:1907–11. doi:10.1093/jnci/djt300

23 Matsuoka K, Kanai T. The gut microbiota and inflammatory bowel disease. *Semin Immunopathol* 2015;**37**:47–55. doi:10.1007/s00281-014-0454-4

24 Gianotti RJ, Moss AC. Fecal Microbiota Transplantation: From Clostridium difficile to Inflammatory Bowel Disease. *Gastroenterol Hepatol (N Y)* 2017;**13**:209–13.

25 Le B, Yang SH. Efficacy of Lactobacillus plantarum in prevention of inflammatory bowel disease. *Toxicol reports* 2018;**5**:314–7. doi:10.1016/j.toxrep.2018.02.007

26 Cani PD, de Vos WM. Next-Generation Beneficial Microbes: The Case of Akkermansia muciniphila. *Front Microbiol* 2017;**8**:1765. doi:10.3389/fmicb.2017.01765

27 Dziarski R, Park SY, Kashyap DR, *et al.* Pglyrp-Regulated Gut Microflora Prevotella falsenii, Parabacteroides distasonis and Bacteroides eggerthii Enhance and Alistipes finegoldii Attenuates Colitis in Mice. *PLoS One* 2016;**11**:e0146162.

528 doi:10.1371/journal.pone.0146162
529 28 Kverka M, Zakostelska Z, Klimesova K, *et al.* Oral administration of Parabacteroides
530 distasonis antigens attenuates experimental murine colitis through modulation of
531 immunity and microbiota composition. *Clin Exp Immunol* 2011;**163**:250–9.
532 doi:10.1111/j.1365-2249.2010.04286.x
533 29 De Cruz P, Kang S, Wagner J, *et al.* Association between specific mucosa-associated
534 microbiota in Crohn's disease at the time of resection and subsequent disease
535 recurrence: a pilot study. *J Gastroenterol Hepatol* 2015;**30**:268–78.
536 doi:10.1111/jgh.12694
537 30 Noor SO, Ridgway K, Scovell L, *et al.* Ulcerative colitis and irritable bowel patients
538 exhibit distinct abnormalities of the gut microbiota. *BMC Gastroenterol* 2010;**10**:134.
539 doi:10.1186/1471-230X-10-134
540 31 Ezeji JC, Sarikonda DK, Hopperton A, *et al.* Parabacteroides distasonis: intriguing
541 aerotolerant gut anaerobe with emerging antimicrobial resistance and pathogenic and
542 probiotic roles in human health. *Gut Microbes* 2021;**13**:1922241.
543 doi:10.1080/19490976.2021.1922241
544 32 Derrien M, Collado MC, Ben-Amor K, *et al.* The Mucin degrader Akkermansia
545 muciniphila is an abundant resident of the human intestinal tract. *Appl Environ*
546 *Microbiol* 2008;**74**:1646–8. doi:10.1128/AEM.01226-07
547 33 Everard A, Belzer C, Geurts L, *et al.* Cross-talk between Akkermansia muciniphila and
548 intestinal epithelium controls diet-induced obesity. *Proc Natl Acad Sci U S A*
549 2013;**110**:9066–71. doi:10.1073/pnas.1219451110
550 34 Derrien M, Van Baarlen P, Hooiveld G, *et al.* Modulation of Mucosal Immune
551 Response, Tolerance, and Proliferation in Mice Colonized by the Mucin-Degrader
552 Akkermansia muciniphila. *Front Microbiol* 2011;**2**:166. doi:10.3389/fmicb.2011.00166
553 35 Png CW, Lindén SK, Gilshenan KS, *et al.* Mucolytic bacteria with increased prevalence
554 in IBD mucosa augment in vitro utilization of mucin by other bacteria. *Am J*
555 *Gastroenterol* 2010;**105**:2420–8. doi:10.1038/ajg.2010.281
556 36 Earley H, Lennon G, Balfe Á, *et al.* The abundance of Akkermansia muciniphila and its
557 relationship with sulphated colonic mucins in health and ulcerative colitis. *Sci Rep*
558 2019;**9**:15683. doi:10.1038/s41598-019-51878-3
559 37 Qu S, Fan L, Qi Y, *et al.* Akkermansia muciniphila Alleviates Dextran Sulfate Sodium
560 (DSS)-Induced Acute Colitis by NLRP3 Activation. *Microbiol Spectr*
561 2021;**9**:e0073021. doi:10.1128/Spectrum.00730-21

562 38 Ke H, Li F, Deng W, *et al.* Metformin Exerts Anti-inflammatory and Mucus Barrier
563 Protective Effects by Enriching Akkermansia muciniphila in Mice With Ulcerative
564 Colitis. *Front Pharmacol* 2021;**12**:726707. doi:10.3389/fphar.2021.726707
565 39 Bian X, Wu W, Yang L, *et al.* Administration of Akkermansia muciniphila Ameliorates
566 Dextran Sulfate Sodium-Induced Ulcerative Colitis in Mice. *Front Microbiol*
567 2019;**10**:2259. doi:10.3389/fmicb.2019.02259
568 40 Buela K-AG, Omenetti S, Pizarro TT. Cross-talk between type 3 innate lymphoid cells
569 and the gut microbiota in inflammatory bowel disease. *Curr Opin Gastroenterol*
570 2015;**31**:449–55. doi:10.1097/MOG.0000000000000217
571 41 Bhatt B, Zeng P, Zhu H, *et al.* Gpr109a Limits Microbiota-Induced IL-23 Production To
572 Constrain ILC3-Mediated Colonic Inflammation. *J Immunol* 2018;**200**:2905–14.
573 doi:10.4049/jimmunol.1701625
574 42 Chun E, Lavoie S, Fonseca-Pereira D, *et al.* Metabolite-Sensing Receptor Ffar2
575 Regulates Colonic Group 3 Innate Lymphoid Cells and Gut Immunity. *Immunity*
576 2019;**51**:871-884.e6. doi:10.1016/j.immuni.2019.09.014
577 43 Olson CA, Vuong HE, Yano JM, *et al.* The Gut Microbiota Mediates the Anti-Seizure
578 Effects of the Ketogenic Diet. *Cell* 2018;**173**:1728-1741.e13.
579 doi:10.1016/j.cell.2018.04.027
580 44 Sakamoto M, Benno Y. Reclassification of Bacteroides distasonis, Bacteroides
581 goldsteinii and Bacteroides merdae as Parabacteroides distasonis gen. nov., comb. nov.,
582 Parabacteroides goldsteinii comb. nov. and Parabacteroides merdae comb. nov. *Int J*
583 *Syst Evol Microbiol* 2006;**56**:1599–605. doi:10.1099/ijs.0.64192-0
584 45 Derrien M, Vaughan EE, Plugge CM, *et al.* Akkermansia muciniphila gen. nov., sp.
585 nov., a human intestinal mucin-degrading bacterium. *Int J Syst Evol Microbiol*
586 2004;**54**:1469–76. doi:10.1099/ijs.0.02873-0
587 46 Ouwerkerk JP, van der Ark KCH, Davids M, *et al.* Adaptation of Akkermansia
588 muciniphila to the Oxic-Anoxic Interface of the Mucus Layer. *Appl Environ Microbiol*
589 2016;**82**:6983–93. doi:10.1128/AEM.01641-16
590 47 Belzer C, Chia LW, Aalvink S, *et al.* Microbial Metabolic Networks at the Mucus Layer
591 Lead to Diet-Independent Butyrate and Vitamin B(12) Production by Intestinal
592 Symbionts. *MBio* 2017;**8**. doi:10.1128/mBio.00770-17
593 48 Reunanen J, Kainulainen V, Huuskonen L, *et al.* Akkermansia muciniphila Adheres to
594 Enterocytes and Strengthens the Integrity of the Epithelial Cell Layer. *Appl Environ*
595 *Microbiol* 2015;**81**:3655–62. doi:10.1128/AEM.04050-14

49 Ashrafian F, Behrouzi A, Shahriary A, *et al.* Comparative study of effect of Akkermansia muciniphila and its extracellular vesicles on toll-like receptors and tight junction. *Gastroenterol Hepatol from bed to bench* 2019;**12**:163–8.

ACKNOWLEDGEMENTS

This work was supported by the Northern Portugal Regional Operational Programme (NORTE 2020), under the Portugal 2020 Partnership Agreement, through the European Regional Development Fund (FEDER) (NORTE-01-0145-FEDER-000013) and the Fundação para a Ciência e Tecnologia (FCT) (contracts CEECIND/00185/2020 to RS, CEECIND/03628/2017 to AC, CEECIND/04058/2018 to CC, 2021.07836.BD to AF and PD/BD/106053/2015 to JG via InterUniversity Doctoral Programme in Ageing and Chronic Disease – PhDOC). This work was also supported by the following grants in the laboratory of M.S.D.: Luxembourg National Research Fund (FNR) CORE grants (C15/BM/10318186 and C18/BM/12585940) and PID2020-120292RB-I00 from MICINN and PCIN-2015-094 from InfectERA-ERANET-Acciones de Programación Conjunta Internacional grant to CU.

FIGURE LEGENDS

Figure 1. Mice from different animal facilities display distinct susceptibility to colitis development. (A) C57BL/6 mice from two different animal houses were administered with dextran sulfate sodium (DSS) 3% in the drinking water and were monitored daily. **(B)** Disease progression was assessed by scoring the disease activity index (DAI) throughout the experiment. **(C)** Representative colons were imaged and colon length was measured at day 7, after excision. **(D)** Histological analysis of hematoxylin & eosin staining of mice prior and after colitis induction. **(E)** Colitis scores were obtained by the histological evaluation of colon samples at day 7. **(F)** Alcian blue/periodic acid Schiff staining of the colonic tissues for goblet cells and mucus analysis. **(G)** Quantification of goblet cell numbers per crypt. For susceptible mice at day 7, no intact crypts were found; ND – not detected. Data is presented as mean ± standard deviation (SD). Statistically significant values are: *$p < 0.05$; **$p < 0.01$; ***$p < 0.001$; ****$p < 0.0001$.

Figure 2. Resistant mice display alterations on epithelial barrier function and gut immunity. (A-B) Expression of *Muc1*, *Muc2*, *Muc13* (A), and *Cldn2*, *Cldn3*, *Cldn4*, *Cldn7* and *Cdh1* (B) was analyzed by qPCR in homeostatic conditions. **(C)** Intestinal permeability in homeostasis was measured after administration of FITC-Dextran by oral gavage and quantified in the serum after four hours of administration. **(D)** The production of IL-10, IL-17 and IL-22 (pg cytokine/mg colon) was quantified in colonic extracts at homeostatic conditions. **(E-F)** Frequencies of Th17 cells (E) and ILC3 (F) in the gut of susceptible or resistant mice, under homeostatic conditions. For (E-F) each dot corresponds to a pool of 3 mice. Data is presented as mean ± standard deviation (SD). Statistically significant values are: *$p < 0.05$; **$p < 0.01$; ****$p < 0.0001$.

Figure 3. Fecal microbiota transplant (FMT) from resistant mice is able to prevent the development of acute colitis and avoid relapse in chronic colitis in susceptible mice. (A) Susceptible mice were treated with antibiotic for 5 weeks and then received fecal contents from resistant mice by oral gavage during 3 days. After 3 weeks to allow colonization, mice were challenged with DSS 3% for 7 days. **(B)** Disease progression was assessed by scoring the disease activity index (DAI) throughout the experiment. Images are representative of at least three independent experiments; n=5 per group. **(C)** Susceptible mice were treated with DSS 2% for five days. After remission, mice received FMT from resistant mice by oral gavage for

5 days. Control group was treated with the vehicle (PBS). Two weeks later, both groups were given DSS 2% as previously. **(D)** Disease progression was assessed by scoring the disease activity index (DAI) throughout the experiment. **(E)** Histological analysis of hematoxylin & eosin and Alcian blue/periodic acid-Schiff stainings of the colonic tissues from mice that received FMT or PBS at 7 weeks of treatment. **(F)** Colitis scores were obtained by the histological evaluation of colon samples at week 7. **(G)** Quantification of goblet cell numbers per crypt. Images are representative of at least three independent experiments; n=5 per group. Data is presented as mean ± standard deviation (SD). Statistically significant values are: *p < 0.05; **p < 0.01; ***p < 0.001; ****p < 0.0001.

Figure 4. Metagenomic characterization of resistant and susceptible mice revealed a distinct microbiota composition. (A) Principal coordinates analysis (PCoA) of susceptible, resistant and susceptible+FMT mice regarding intestinal microbiota composition. Resistant vs susceptible: *p*=0.001; resistant vs susceptible+FMT: *p*=0.005; susceptible vs susceptible+FMT: *p*=0.006. **(B)** Relative abundance of bacterial genera identified from DNA from stool samples of susceptible, resistant mice and susceptible+FMT mice; *A. muciniphila* and *P. distasonis* are marked by purple and beige arrows, respectively. **(C)** Number of operational taxonomic units (OTUs) and **(D)** diversity of species found in susceptible, resistant and susceptible + FMT mice. **(E)** Absolute abundance quantification of *A. muciniphila* and **(F)** *P. distasonis* in susceptible, resistant and susceptible + FMT mice. Images are representative of at least three independent experiments; n=5/6 per group. Data is presented as mean ± standard deviation (SD). Statistically significant values are *p < 0.05; **p < 0.01; ****p < 0.0001.

Figure 5. The combination of *Akkermansia muciniphila* and *Parabacteroides distasonis* attenuates colitis development. (A) Mice were supplemented with *Akkermansia muciniphila* (Am), *Parabacteroides distasonis* (Pd) or the combination of both (Am+Pd) during 12 days by daily oral gavage, followed by administration of 3% DSS for 7 days. **(B)** Disease progression was assessed by scoring the disease activity index (DAI) throughout the experiment. **(C-E)** Quantification of goblet cell numbers per crypt after colitis induction, as well as colitis scores obtained by the histological evaluation of colon samples after DSS treatment. N=5 per group. **(F)** A relapse-remission experiment was performed in which susceptible mice were subjected to colitis induction with 2% DSS for 5 days. After recovery, mice were supplemented with *Akkermansia muciniphila* (Am), *Parabacteroides distasonis* (Pd) or the combination of both

(Am+Pd) during 12 days by daily oral gavage, followed by a second cycle of colitis induction. Control mice (unsupplemented) received PBS as vehicle. **(G)** Disease progression was assessed by scoring the disease activity index (DAI). * in black corresponds to comparison between control and Am+Pd. * in blue corresponds to comparison between Am and Am+Pd. * in yellow corresponds to comparison between Pd and Am+Pd. $ in blue corresponds to comparison between control and Am. x corresponds to comparison between Am and Pd. **(H)** Area under the curve (AUC) was calculated based on the disease course upon colitis induction. **(I-K)** Quantification of goblet cell numbers per crypt after colitis induction, as well as colitis scores obtained by the histological evaluation of colon samples after DSS treatment. N=5 per group. Data is presented as mean ± standard deviation (SD). Statistically significant values are: *p < 0.05; **p < 0.01; ***p < 0.001; ****p < 0.0001.

Figure 6. Supplementation with *Akkermansia muciniphila* leads to increase frequencies of ILC3 in the colon and tissue integrity. (A-F) Frequencies of ILC3 (A), IL-17-producing ILC3 (B), IL-22-producing ILC3 (C), Th17 cells (D), IL-17-producing Th17 (E) and IL-22-producing Th17 (F) in the colon of control mice and mice supplemented with *Akkermansia muciniphila* (Am), *Parabacteroides distasonis* (Pd) or the combination of both (Am+Pd). **(G)** Correlation between the number of copies of Am with the frequencies of ILC3 in the colonic tissue. **(H)** Absolute abundance of *Akkermansia muciniphila*, alone (Am) or in combination with *Parabacteroides distasonis* (Am+Pd) in the colon of supplemented mice. **(I)** Correlation between the number of copies of Am with the disease activity index (DAI). Data is presented as mean ± standard deviation (SD). Statistically significant values are: *p < 0.05; **p < 0.01; ***p < 0.001; ****p < 0.0001.

Table 1. Disease activity index (DAI) scores.

Score	Weight loss	Stool consistency	Bleeding
0	No loss	Normal	No blood
1	1-5%	Mild-soft	Brown color
2	6-10%	Very soft	Reddish color
3	11-15%	Diarrhea	Bloody stool
4	16-20%		Gross bleeding
5	> 20%		

The final score is obtained by the sum of each parameter.

Table 2. Parameters for histological analysis of colitis severity.

Score	Epithelial hyperplasia and goblet depletion	Leukocyte infiltration in the Lamina Propria	Affected area	Markers of severe inflammation
0	None	None/rare	None	None
1	Minimal	Increased	1/3	Increased
2	Mild	Confluent	2/3	Confluent
3	Marked	Transmural	All	Transmural

The final score is obtained by the sum of individual scores. Markers of severe inflammation included ulceration and crypt abscesses.

Table 3. List of primers used for PCR.

Primer ID	Forward sequence (5'→ 3')	Reverse sequence (5'→ 3')
Cdh1	CACCTGGAGAGAGGCCATGT	TGGGAAACATGAGCAGCTCT
Cldn2	GGCTGTTAGGCACATCCAT	TGGCACCAACATAGGAACTC
Cldn3	AAGCCGAATGGACAAAGAA	CTGGCAAGTAGCTGCAGTG
Cldn4	CGCTACTCTTGCCATTACG	ACTCAGCACACCATGACTTG
Cldn7	AGGGTCTGCTCTGGTCCTT	GTACGCAGCTTTGCTTTCA
Muc1	CCCTATGAGGAGGTTTCGGC	AAGGGCATGAACAGCCTACC
Muc2	TCCTGACCAAGAGCGAACAC	ACAGCACGACAGTCTTCAGG
Muc13	CTGGCAGCTACATGAGCACT	GAACTACCCACGGTCACCAA
Ubq	TGGCTATTAATTATTCGGTCTGCAT	GCAAGTGGCTAGAGTGCAGAGTAA
Am	CAGCACGTGAAGGTGGGGAC	CCTTGCGGTTGGCTTCAGAT
Pd	TGCCTATCAGAGGGGGATAAC	GCAAATATTCCCATGCGGGAT

Table 4. Most significant hits found in the metagenomic analysis (*p* value<0.05; false discovery rate (FDR) <0.05); comparison is made by resistant *versus* susceptible mice and susceptible+FMT *versus* susceptible mice. FC = fold change.

Increased in resistant mice (*vs* susceptible)				Increased in susceptible+FMT mice (*vs* susceptible)			
Genus	**Log2FC**	***p* value**	**Adjusted *p* value**	**Genus**	**Log2FC**	***p* value**	**Adjusted *p* value**
*Clostridium*_XlVa	2.0492	0.00002002	0.00138125	*Akkermansia*	3.5844	0.0000225	0.00153222
Akkermansia	3.2186	0.00131297	0.01132440	*Parabacteroides*	2.4413	0.00028237	0.00860324
Parabacteroides	5.2930	0.00204649	0.01283708	*Clostridium*_XI	4.3576	0.00037956	0.00860324
Lactococcus	2.8413	0.00559808	0.02425864	*Bacteroides*	1.1833	0.00085129	0.01447191
Ureaplasma	7.4717	0.00755823	0.03067753	*Olsenella*	1.6756	0.00342211	0.02908795
Bacteroides	3.2818	0.00835472	0.03202644	*Clostridium*_XlVb	1.5458	0.00918029	0.04855569
				Coprococcus	2.0000	0.00928271	0.04855569

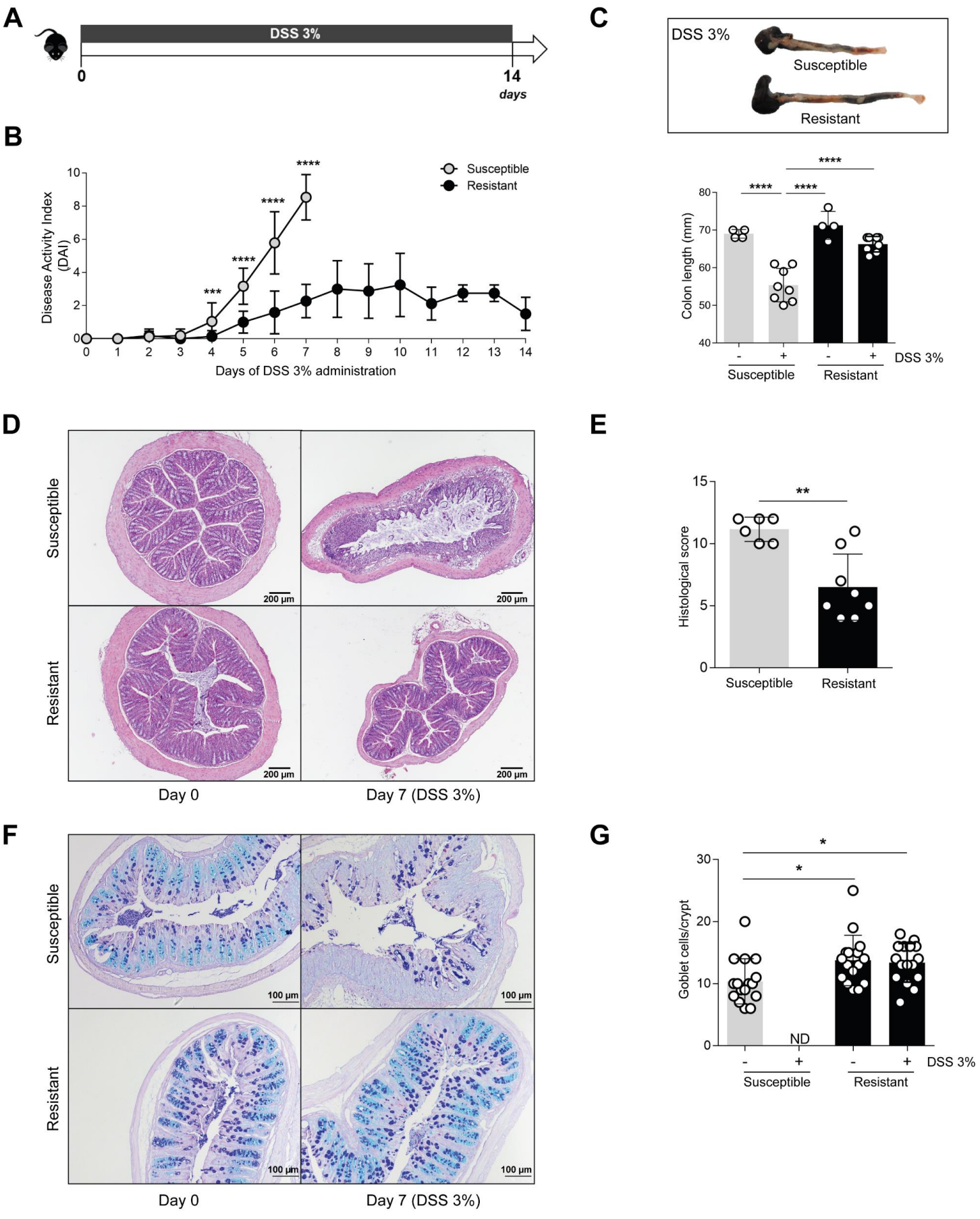
A
DSS 3%
0
14
days
B
Disease Activity Index (DAI)
Susceptible
Resistant
***
****
****
****
Days of DSS 3% administration
C
DSS 3%
Susceptible
Resistant
Colon length (mm)
****
****
****
DSS 3%
Susceptible
Resistant
D
Susceptible
Resistant
200 µm
Day 0
Day 7 (DSS 3%)
E
Histological score
**
Susceptible
Resistant
F
Susceptible
Resistant
100 µm
Day 0
Day 7 (DSS 3%)
G
Goblet cells/crypt
*
*
ND
DSS 3%
Susceptible
Resistant

Figure 1

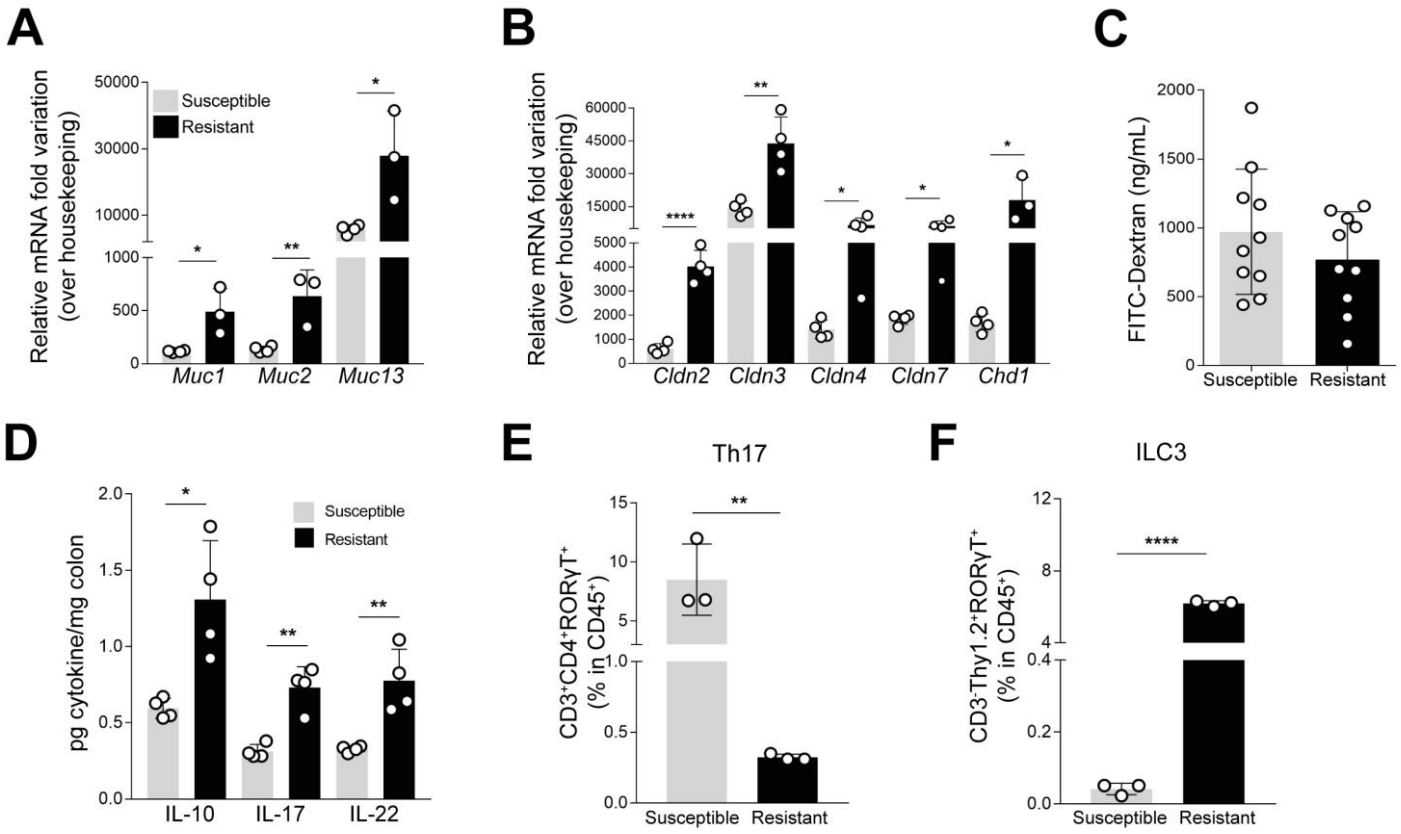
A
Relative mRNA fold variation (over housekeeping)
Susceptible
Resistant
Muc1
Muc2
Muc13
B
Relative mRNA fold variation (over housekeeping)
Cldn2
Cldn3
Cldn4
Cldn7
Chd1
C
FITC-Dextran (ng/mL)
Susceptible
Resistant
D
pg cytokine/mg colon
IL-10
IL-17
IL-22
E
Th17
CD3+CD4+RORγT+ (% in CD45+)
F
ILC3
CD3-Thy1.2+RORγT+ (% in CD45+)

Figure 2

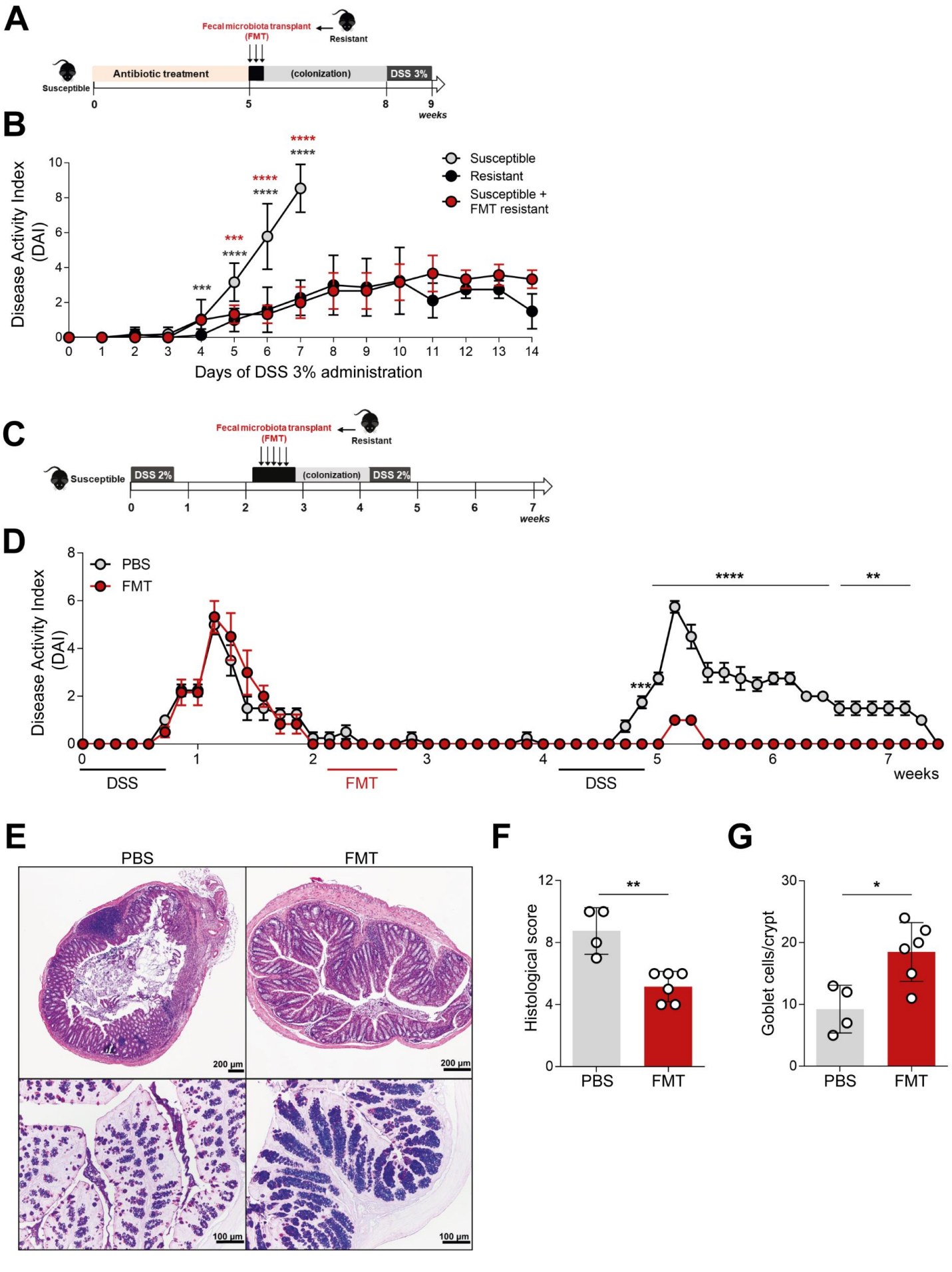
A
Fecal microbiota transplant (FMT)
Resistant
Susceptible
Antibiotic treatment
(colonization)
DSS 3%
0
5
8
9
weeks
B
Disease Activity Index (DAI)
Susceptible
Resistant
Susceptible + FMT resistant
Days of DSS 3% administration
C
Fecal microbiota transplant (FMT)
Resistant
Susceptible
DSS 2%
(colonization)
DSS 2%
weeks
D
Disease Activity Index (DAI)
PBS
FMT
DSS
FMT
DSS
weeks
E
PBS
FMT
200 µm
100 µm
F
Histological score
PBS
FMT
G
Goblet cells/crypt
PBS
FMT

Figure 3

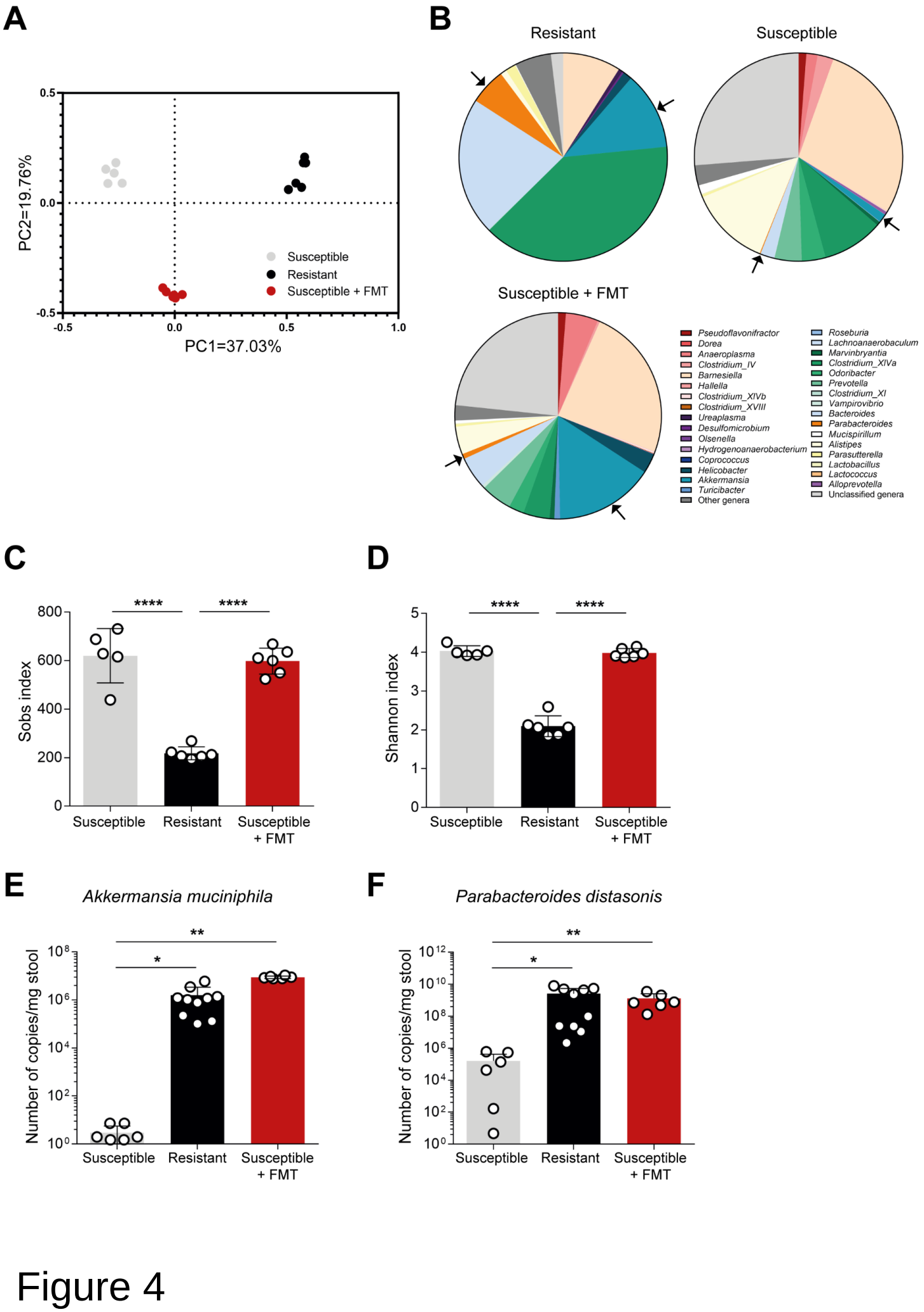
A
PC2=19.76%
PC1=37.03%
Susceptible
Resistant
Susceptible + FMT
B
Resistant
Susceptible
Susceptible + FMT
Pseudoflavonifractor
Dorea
Anaeroplasma
Clostridium_IV
Barnesiella
Hallella
Clostridium_XIVb
Clostridium_XVIII
Ureaplasma
Desulfomicrobium
Olsenella
Hydrogenoanaerobacterium
Coprococcus
Helicobacter
Akkermansia
Turicibacter
Other genera
Roseburia
Lachnoanaerobaculum
Marvinbryantia
Clostridium_XIVa
Odoribacter
Prevotella
Clostridium_XI
Vampirovibrio
Bacteroides
Parabacteroides
Mucispirillum
Alistipes
Parasutterella
Lactobacillus
Lactococcus
Alloprevotella
Unclassified genera
C
Sobs index
D
Shannon index
Susceptible
Resistant
Susceptible + FMT
E
Akkermansia muciniphila
F
Parabacteroides distasonis
Number of copies/mg stool

Figure 4

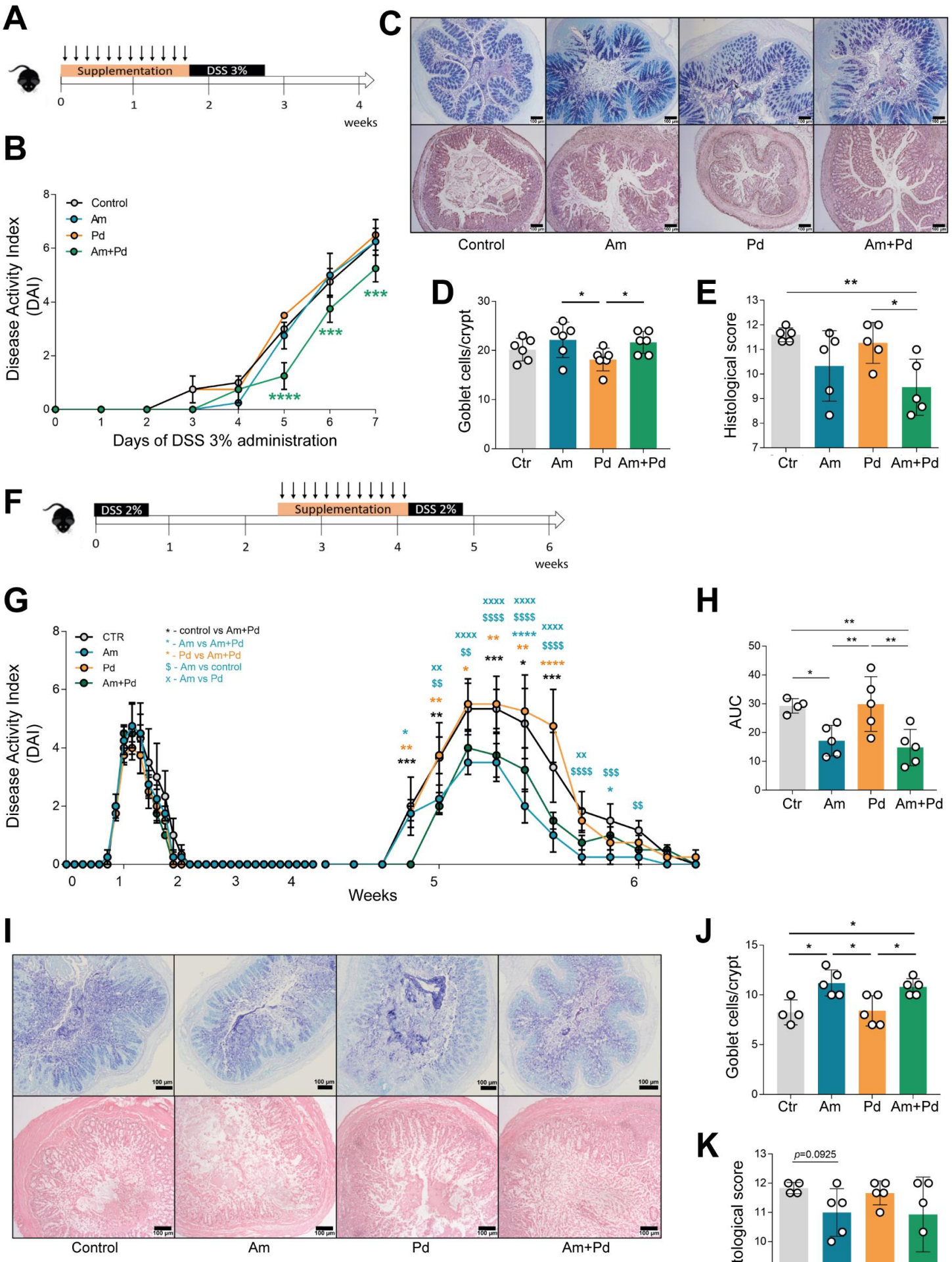
A
Supplementation
DSS 3%
0
1
2
3
4
weeks
B
Control
Am
Pd
Am+Pd
Disease Activity Index (DAI)
Days of DSS 3% administration
***
***
****
C
Control
Am
Pd
Am+Pd
D
Goblet cells/crypt
Ctr
Am
Pd
Am+Pd
E
Histological score
Ctr
Am
Pd
Am+Pd
F
DSS 2%
Supplementation
DSS 2%
0
1
2
3
4
5
6
weeks
G
CTR
Am
Pd
Am+Pd
* - control vs Am+Pd
* - Am vs Am+Pd
* - Pd vs Am+Pd
$ - Am vs control
x - Am vs Pd
Disease Activity Index (DAI)
Weeks
H
AUC
Ctr
Am
Pd
Am+Pd
I
Control
Am
Pd
Am+Pd
J
Goblet cells/crypt
Ctr
Am
Pd
Am+Pd
K
p=0.0925
Histological score
Ctr
Am
Pd
Am+Pd

Figure 5

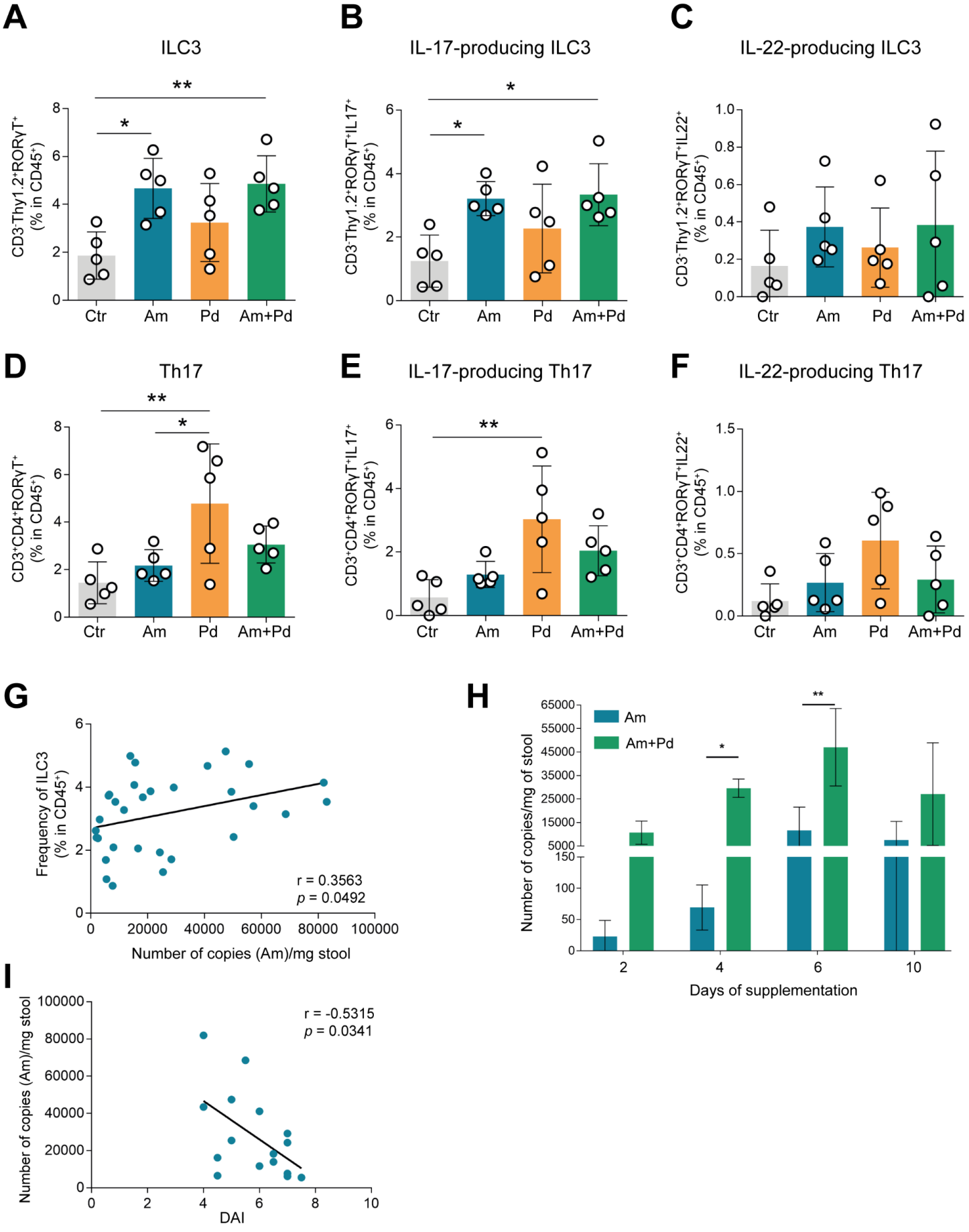
A
ILC3
CD3⁻Thy1.2⁺RORγT⁺ (% in CD45⁺)
Ctr
Am
Pd
Am+Pd
B
IL-17-producing ILC3
CD3⁻Thy1.2⁺RORγT⁺IL17⁺ (% in CD45⁺)
C
IL-22-producing ILC3
CD3⁻Thy1.2⁺RORγT⁺IL22⁺ (% in CD45⁺)
D
Th17
CD3⁺CD4⁺RORγT⁺ (% in CD45⁺)
E
IL-17-producing Th17
CD3⁺CD4⁺RORγT⁺IL17⁺ (% in CD45⁺)
F
IL-22-producing Th17
CD3⁺CD4⁺RORγT⁺IL22⁺ (% in CD45⁺)
G
Frequency of ILC3 (% in CD45⁺)
r = 0.3563
p = 0.0492
Number of copies (Am)/mg stool
H
Am
Am+Pd
Number of copies/mg of stool
Days of supplementation
I
Number of copies (Am)/mg stool
r = -0.5315
p = 0.0341
DAI

Figure 6

SUPPLEMENTAL METHODS

Mice

C57BL/6 mice used in this study were derived from two different animal facilities, one group purchased from Charles River Laboratories (France) and the other group was previously originated from the same commercial enterprise, but was housed and bred at ICVS Animal Facilities, under specific pathogen-free (SPF) conditions (4-6 mice/cage). Mice were euthanized by CO_2 inhalation with efforts to minimize suffering. All experimental procedures were performed in accordance with the relevant guidelines and regulations. Animal studies were approved by the Ethical Council for Life and Health Sciences at the University of Minho (SECVS 003/2018) and licensed by the Portuguese National Authority for Animal Health (DGAV) with reference DGAV0421/000/000/2020.

Colitis induction

Mice 7 to 9 weeks of age were given sodium dextran sulfate (DSS; 3% (w/v), molecular weight approximately 40000 Da; TdB Consultancy) in the drinking water *ad libitum* for 7 days. Clinical signs of colitis were monitored daily and measured by the disease activity index (DAI; Table 1), using a graded score adapted from both Cardoso *et al* and Gaifem *et al* [1,2]. Mice were euthanized at the end of each experiment or earlier, if the symptoms of clinical disease reached one of these endpoints: more than 20% weight loss, diarrhea or gross bleeding. For chronic colitis model, 2% DSS was given in the drinking water for 5 days in two subsequent phases with an interval of 3 weeks.

Histological analysis

Samples from colons were fixed in 4% paraformaldehyde and 5 μm paraffin-embedded sections were stained with hematoxylin and eosin. Inflammation was assessed blindly by a pathologist using a graduated semi quantitative system as described below (Table 2) [1]. Staining of colon sections with Alcian Blue/Periodic Acid-Schiff (AB/PAS) was performed to evaluate polysaccharide structures. The number of goblet cells were blindly evaluated for each experimental condition. Only intact crypts, cut longitudinally from crypt opening to bottom, were quantified. Images were captured using an Olympus BX61 microscope and recorded with a digital camera (DP70) using Cell^P software. Image analysis was performed using Fiji (ImageJ) software.

FITC-dextran intestinal permeability assay

In vivo intestinal permeability was assessed by administration of fluorescein isothiocyanate (FITC) labeled dextran. Food and water were withdrawn for 8 hours. Mice were administered 44 mg/100 g body weight of FITC-labelled dextran (TdB Consultancy; 4 kDa) by oral gavage. Serum was collected four hours later and fluorescence intensity was measured by spectrophotofluorimetry (excitation: 485 nm; emission: 528 nm).

RNA extraction, cDNA and quantitative real-time PCR (qRT-PCR)

Total RNA was isolated from colonic samples using TripleXtractor (Grisp) with mechanical disruption of the tissues on ice, followed by conversion into cDNA by reverse transcription with Xpert cDNA synthesis kit (Grisp). qRT-PCR was performed using KAPA SYBR FAST Universal (Roche) on a Bio-Rad CFX6 Real-Time System C1000 Thermal Cycler (Bio-Rad). Specific oligonucleotides for mouse mucin-encoding genes *Muc1*, *Muc2* and *Muc13*, for claudin-encoding genes *Cldn2*, *Cldn3*, *Cldn4* and *Cldn7*, and for *Cdh1* (E-cadherin) are shown in Table 3. Expression levels were normalized to ubiquitin (*Ubq*) and relative expression was determined based on the ΔCt method, as follows: $2^{(\text{housekeeping gene mRNA expression - Target gene mRNA expression})} \times 100000$.

Lamina propria leukocyte (LPL) isolation and flow cytometry analysis

To isolate lamina propria leukocytes (LPL), colons were flushed with Ca- and Mg-free PBS with 25 mM HEPES (Gibco), 50 mM sodium bicarbonate (Sigma-Aldrich) and 5% fetal bovine serum (FBS; Gibco). Colon fragments of 0.5-1 cm were incubated in Ca- and Mg-free Hank's Balanced Salt Solution (HBSS; Gibco) containing 1.3 mM EDTA (Sigma-Aldrich), 25 mM HEPES, 50 µg/mL penicillin/streptomycin (Gibco) and 2 mM L-Glutamine (Gibco), under 200 rpm agitation at 37ºC for 40 minutes, followed by an incubation in RPMI 1640 medium (Gibco) supplemented with 0.15 mg/mL collagenase D (Roche), 10% FBS, 25 mM HEPES, 50 µg/mL penicillin/streptomycin and 2 mM L-Glutamine for 40 minutes under 200 rpm agitation at 37ºC. Tissue was dissociated and filtered through a 70 µm cell strainer (BD Biosciences). Cell suspension was centrifuged, the pellet was resuspended in 40% Percoll (GE Healthcare), laid over 80% Percoll and centrifuged at 600g for 20 minutes at 20ºC. Cells retained in the interface were collected, washed in RPMI containing 2% FBS and recovered.

Cells were stimulated with 50 ng/mL phorbol myristate acetate (PMA), 500 ng/mL ionomycin calcium salt and 10 µg/mL brefeldin A for 4 hours at 37ºC (from Sigma-Aldrich). Cells were stained with eBioscience™ Fixable Viability Dye eFluor™ for viability control, followed by surface and intracellular staining using the eBioscience™ Foxp3 / Transcription Factor Staining Buffer Set as per manufacturer's instructions. Surface staining was performed with anti-mouse CD45 (clone 30-F11), CD90.2 (Thy1.2; clone 53-1.2), CD3 (clone 145-2C11), CD4 (clone GK1.5), CD19 (clone 6D5),

CD11c (clone N418) and CD11b (clone M1/70) for 30 minutes at 4ºC. Intracellular staining was performed for RORγT (clone B2D), IL-17A (clone TC11-18H10.1) and IL-22 (clone Poly5164), for 30 minutes at 4ºC. All antibodies were purchased to Biolegend and eBioscience. Gating strategy is presented in Supplemental Figure 1. Cell analysis was performed on a BD LSRII (Becton Dickinson, USA). Data were analyzed using FlowJo software (Tree Star, USA).

Cytokine quantification by ELISA

Colonic tissues were weighted and lysed using a homogenizer in ice-cold PBS containing protease inhibitors (Roche). Protein concentrations were quantified using the Pierce BCA protein assay kit (Bio-Rad). The levels of IL-10, IL-17A/F and IL-22 were measured by ELISA using commercially available kits (Biolegend), according to manufacturer's instructions.

Bacterial cultures

Akkermansia muciniphila (DMS 22959) was grown in mYCFA medium[3] under anaerobic conditions in a vinyl anaerobic chamber (Coy Laboratory Products, USA). Cells were grown to an OD of 1.0 before they were pelleted by centrifugation at 4°C for 10 min at 5000g. Cells were resuspended in fresh mYCFA to reach an OD of 0.05 and then sealed anaerobically in 2 ml screw-cap tubes. The cultures were transported at ambient temperature by overnight express from Luxembourg to Portugal, where they were incubated for 30–60 minutes at 37°C before administration. This results into a culture with approximately $2x10^9$ CFU/ml.

Parabacteroides distasonis bacteria (DSM 29491), purchased to DSMZ (Germany), was cultured with Columbia Agar plates with 5% sheep blood (Biolife) under anaerobic conditions using an anaerobic jar (Deltalab) with Anaerogen 2.5L (Thermo Scientific). Frozen stocks were made in PBS with 25% glycerol. Every stock was diluted and plated to quantify the colony forming units (CFUs).

Microbiota modulation

Antibiotic treatment for microbiota depletion. C57BL/6 mice were given ampicillin (1 mg/mL), streptomycin (1 mg/mL), vancomycin (0.5 mg/mL) and neomycin sulfate (1 mg/mL) in the drinking water for 4 weeks. All antibiotics were purchased from Sigma-Aldrich. Microbiota depletion was assessed throughout the treatment by aerobic and anaerobic culture of intestinal contents in Columbia agar plates with 5% sheep blood at 37ºC. The number of CFUs were counted and the number of bacteria per mg of feces were calculated.

Fecal microbiota transplant (FMT). Fresh fecal contents from resistant mice were directly collected to a sterile 2 mL capped microtube, resuspended in ice-cold PBS (Gibco) and centrifuged (800g for 5 minutes) to remove residual clumps. A 150 µL/day of the resuspended material was given by oral gavage to mice from the susceptible group. FMT was performed after antibiotic treatment as using a disease remission model as represented in Figure 3A and 3C, respectively.

Bacterial administration. A. muciniphila and *P. distasonis* suspensions were prepared in sterile PBS with a final density of $2x10^9$ CFU/mL. According to the group, mice received daily $2x10^8$ CFU of each strain in 100µL of PBS by oral gavage for 12 days. The control group received the same amount of PBS.

Metagenomic analysis and bacterial quantification

Genomic DNA from feces was extracted using the QIAamp Fast DNA Stool Mini Kit (Qiagen) according to manufacturer's instructions plus an additional membrane disruption step using glass beads as previously described [4]. After quantification of genomic DNA by spectrophotometry at 260 nm, 16S rRNA gene was amplified and sequenced using the MiSeq platform from Illumina and analyzed with mothur as previously described [5]. Sequences were trimmed using the sliding-window technique, such that the minimum average quality score over a window of 20 bases never dropped below 30. Sequences were trimmed from the 3'-end until this criterion was met. Then, trimmed forward and reverse paired-end sequences were assembled using fastq-join [6], applying default parameters. Assembled paired-end sequences larger than 400 bp were kept for the subsequent analysis. Sequences were aligned to the 16S rRNA gene using the SILVA reference alignment as the template [7], and the Needleman-Wunsch algorithm with the default scoring options. Potentially chimeric sequences were removed using Uchime [8]. To minimize the effect of sequencing errors in overestimating microbial diversity [9], rare abundance sequences that differ in 1% from a high abundance sequences were merged to the high abundance sequence using the pre.cluster option in Mothur [10]. Since different numbers of sequences per sample could lead to a different diversity (i.e., more Operational Taxonomic Units-OTUs could be obtained in those samples with higher coverage), we rarefied all samples to the number of sequences obtained in the sample with the lowest number of sequences (i.e. 27287). Sequences were grouped into OTUs using Vsearch [11], with the abundance based agc method. Sequences with distance-based similarity of 97% or greater were assigned to the same OTU. Shannon index was obtained at the OTU level with Mothur.

Phylogenetic classification of sequences was performed for each sequence using the Bayesian classifier algorithm described by Wang and colleagues with the bootstrap cutoff 60% [12].

Classification was assigned to the genus level when possible; otherwise the closest level of classification to the genus level was given, preceded by "unclassified; UC".

Absolute abundance of bacteria was performed by quantification of bacterial copy number in stool DNA samples using specific primers for *A. muciniphila* (Am) and *P. distasonis* (Pd) (Table 3). Values were interpolated from a standard curve obtained by different copy numbers of the targeted sequence belonging to each bacterium. The targeted sequence for *A. muciniphila* or *P. distasonis* was cloned into pJET1.2 by CloneJET PCR Cloning Kit (Thermo Scientific) and used as template for the qPCR standard curve.

Statistical analysis

For multiple group comparisons t-test or one-way ANOVA test with a Tukey multiple-comparison posttest were performed, while for multiple group comparisons with repeated measures two-way ANOVA test with a Tukey multiple-comparison posttest was applied. For microbiota analysis data, a t-test was initially applied to identify bacterial genera whose relative abundance was increased in resistant and FMT treated mice as compared to susceptible mice. Subsequently, we verified the obtained results by applying an approach recently developed specifically for studying microbiome data: analysis of composition of microbiomes with bias correction (ANCOM-BC) test [13]. ANCOM-BC was applied using the R package ANCOMBC. Since the number of samples per group was not large (N=5-6), a conservative variance estimate of the test statistic was used as recommended. To adjust for multiple hypothesis testing, for both ANCOMBC and t-test, we used the FDR approach by Benjamini and Hochberg implemented in the fdr.R package [14]. Only taxa with at least 10 counts were included in the analysis. q values (FDR) lower than 0.05 were considered significant. PCoA analysis was performed using the Bray-Curtis distances (OTU level) between pair of samples that were calculated using the package vegan from R. In order to analyze community-level differences in the microbiome among groups of samples, a non-parametric test, permutational multivariate analysis of variance (PERMANOVA), was applied using the adonis function from the R vegan package. Images are representative of at least 3 independent experiments. Data are presented as mean ± standard deviation (SD). Statistically significant values are: * $p < 0.05$; ** $p < 0.01$; *** $p < 0.001$; **** $p < 0.0001$.

References:

1 Cardoso A, Gil Castro A, Martins AC, *et al.* The Dynamics of Interleukin-10-Afforded Protection during Dextran Sulfate Sodium-Induced Colitis. *Front Immunol* 2018;**9**:400. doi:10.3389/fimmu.2018.00400

2 Gaifem J, Gonçalves LG, Dinis-Oliveira RJ, *et al.* L-threonine supplementation during colitis onset delays disease recovery. *Front Physiol* 2018;**9**. doi:10.3389/fphys.2018.01247

3 Steimle A, De Sciscio A, Neumann M, *et al.* Constructing a gnotobiotic mouse model with a synthetic human gut microbiome to study host-microbe cross talk. *STAR Protoc* 2021;**2**:100607. doi:10.1016/j.xpro.2021.100607

4 Djukovic A, Garcia-Garcera M, Martínez-Paredes E, *et al.* Gut colonization by a novel Clostridium species is associated with the onset of epizootic rabbit enteropathy. *Vet Res* 2018;**49**:123. doi:10.1186/s13567-018-0617-8

5 Rechenberger J, Samaras P, Jarzab A, *et al.* Challenges in Clinical Metaproteomics Highlighted by the Analysis of Acute Leukemia Patients with Gut Colonization by Multidrug-Resistant Enterobacteriaceae. *Proteomes* 2019;**7**. doi:10.3390/proteomes7010002

6 Aronesty E. Command-line tools for processing biological sequencing data. 2011.https://github.com/ExpressionAnalysis/ea-utils

7 Pruesse E, Quast C, Knittel K, *et al.* SILVA: a comprehensive online resource for quality checked and aligned ribosomal RNA sequence data compatible with ARB. *Nucleic Acids Res* 2007;**35**:7188–96. doi:10.1093/nar/gkm864

8 Edgar RC, Haas BJ, Clemente JC, *et al.* UCHIME improves sensitivity and speed of chimera detection. *Bioinformatics* 2011;**27**:2194–200. doi:10.1093/bioinformatics/btr381

9 Huse SM, Welch DM, Morrison HG, *et al.* Ironing out the wrinkles in the rare biosphere through improved OTU clustering. *Environ Microbiol* 2010;**12**:1889–98. doi:10.1111/j.1462-2920.2010.02193.x

10 Schloss PD, Westcott SL, Ryabin T, *et al.* Introducing mothur: open-source, platform-independent, community-supported software for describing and comparing microbial communities. *Appl Environ Microbiol* 2009;**75**:7537–41. doi:10.1128/AEM.01541-09

11 Rognes T, Flouri T, Nichols B, *et al.* VSEARCH: a versatile open source tool for metagenomics. *PeerJ* 2016;**4**:e2584. doi:10.7717/peerj.2584

12 Wang Q, Garrity GM, Tiedje JM, *et al.* Naive Bayesian classifier for rapid assignment of rRNA sequences into the new bacterial taxonomy. *Appl Environ Microbiol* 2007;**73**:5261–7. doi:10.1128/AEM.00062-07

13 Lin H, Peddada S Das. Analysis of compositions of microbiomes with bias correction. *Nat Commun* 2020;**11**:3514. doi:10.1038/s41467-020-17041-7

14 Benjamini Y, Hochberg Y. Controlling The False Discovery Rate - A Practical And Powerful Approach To Multiple Testing. *J R Stat Soc, Ser B* 1995;**57**:289–300. doi:10.2307/2346101

Supplemental Table 1. Most significant hits found in the metagenomic analysis using the ANCOM-BC test for susceptible and resistant mice groups.

Feature	ANCOMBC. pval	ANCOMBC. adjpval.fdr	mean. Resistant	mean. Susceptible	log2FC
Odoribacter	8.46E-185	5.92E-183	0	3.69260087	-11.796541
Ureaplasma	2.50E-157	5.83E-156	0.64682816	0	9.28526621
Flavonifractor	3.47E-77	6.07E-76	0.00122158	0.88247151	-8.6108253
Clostridium_IV	2.49E-45	3.48E-44	0	2.48836442	-11.227297
Helicobacter	8.81E-44	1.03E-42	1.40482037	0.0014659	9.13286018
Prevotella	3.72E-29	3.26E-28	0	4.23205189	-11.993209
Pseudoflavonifractor	1.14E-28	8.85E-28	0.00061079	1.2079012	-9.5178152
Lactococcus	6.09E-24	4.26E-23	0.02259928	0	4.50872692
Clostridium_XI	2.82E-23	1.79E-22	0.11116405	0	6.75567307
Escherichia_Shigella	1.98E-19	9.88E-19	4.96512381	0.00659655	9.34530766
Bacteroides	2.46E-19	1.15E-18	21.4167919	2.19884927	3.28331061
Alloprevotella	7.85E-18	3.23E-17	0	0.45442885	-8.7769168
Clostridium_XlVb	2.72E-17	1.06E-16	0	0.09528347	-6.5355041
Anaeroplasma	4.56E-17	1.68E-16	0	1.73782387	-10.709641
Clostridium_XlVa	4.37E-13	1.46E-12	39.2152551	9.47264265	2.04945619
Parabacteroides	6.11E-13	1.94E-12	5.65715054	0.14072635	5.31877011
Oscillibacter	7.56E-13	2.30E-12	0.00061079	1.02686261	-9.2837743
Parasutterella	1.27E-08	3.55E-08	1.57828514	0.33422509	2.23593966
Akkermansia	3.01E-08	8.11E-08	12.0661854	1.29292337	3.22122696
Desulfovibrio	1.27E-07	3.18E-07	0.47030943	0.08282332	2.49070848
Insolitispirillum	1.48E-07	3.56E-07	0.00671871	0	2.90122185
Desulfomicrobium	9.03E-06	1.91E-05	0.25714321	0	7.95795556
Holdemania	0.000225865	0.00045173	0	0.25213472	-7.9296935
Vampirovibrio	0.000288407	0.000560791	0	0.03811339	-5.2367177
Alistipes	0.000447334	0.000846308	0.95100231	12.5678895	-3.7226946
Tannerella	0.000937811	0.001683251	0.0140482	0.0058636	1.12818827

Supplemental Table 2. Most significant hits found in the metagenomic analysis using the ANCOM-BC test for susceptible and susceptible+FMT mice groups.

Feature	ANCOMBC. pval	ANCOMBC. adjpval.fdr	mean. Susceptible	Mean. Susceptible+FMT	log2FC
Helicobacter	1.37E-59	9.87E-58	0.0014659	3.07838898	-10.492168
Clostridium_XI	1.30E-36	3.11E-35	0	0.0714626	-6.7463616
Alloprevotella	9.61E-33	1.73E-31	0.454428849	0	9.40378673
Clostridium_XVIII	3.19E-10	3.83E-09	0.002198849	0.0641331	-4.4966201
Anaerostipes	7.90E-10	8.12E-09	0.128999157	0.00427554	4.71203865
Holdemania	2.39E-08	2.15E-07	0.252134716	0	8.55563492
Ureaplasma	1.66E-07	1.33E-06	0	0.02748562	-5.3891913
Coprococcus	2.25E-07	1.62E-06	0	0.01099425	-4.1179972
Eubacterium	1.48E-06	9.70E-06	0.063033679	0.00061079	5.63420602
Akkermansia	3.00E-06	1.80E-05	1.29292337	15.5489183	-3.5874184
Clostridium_IV	5.95E-06	3.29E-05	2.488364423	0.34265401	2.85793674
Olsenella	9.53E-05	0.000489875	0.00073295	0.01038346	-2.9762839
Clostridium_XlVb	0.000115277	0.000553331	0.095283468	0.28523961	-1.5751336
Turicibacter	0.000123892	0.000557514	0.064499579	0.88320446	-3.7615325
Alistipes	0.000215537	0.000823978	12.56788947	4.36715897	1.52483063
Dorea	0.000217439	0.000823978	0.016124895	0.00183237	2.7457358
Tannerella	0.000405591	0.001460128	0.005863598	0.04764173	-2.8860669
Parabacteroides	0.001121515	0.003608068	0.140726353	0.78059149	-2.466045
Flavonifractor	0.001152577	0.003608068	0.882471507	0.41289503	1.09452695

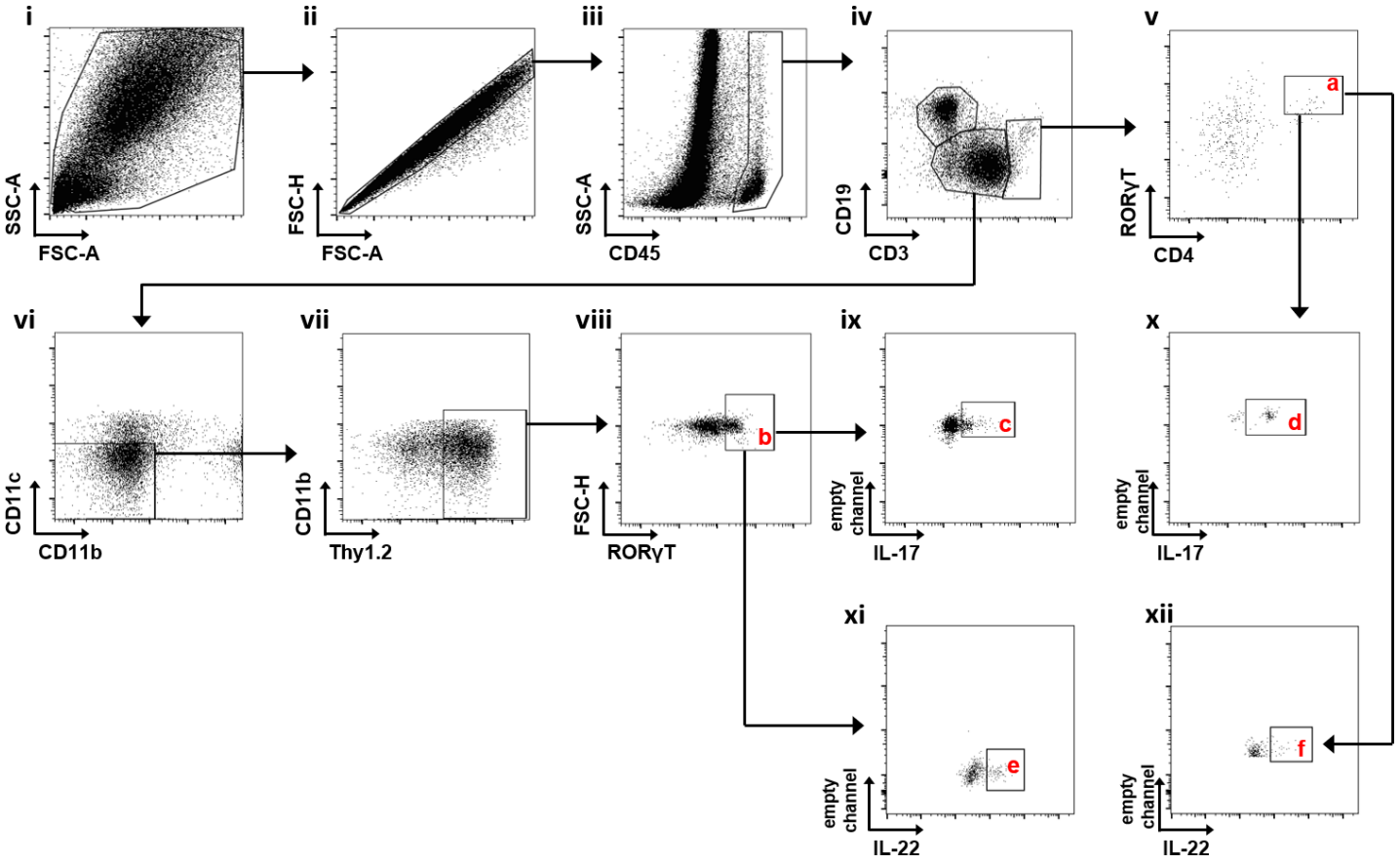

Supplemental Figure 1. Representative plots showing gating strategy used for the identification of Th17 cells and ILC3. Cells were selected by forward scatter (FSC) and side scatter (SSC) profile (i) and excluding doublets (ii). After gating hematopoietic cells by CD45 expression (iii), cells were distinguished by the expression of CD3 (iv). Th17 cells were identified as CD3+CD4+RORγt+ cells (v; a). ILC3 were identified as CD45+CD3-CD19-CD11b-CD11c-Thy1.2+RORγt+ (viii; b). IL-17-producing cells within ILC3 and Th17 were identified in (ix; c) and (x; d), respectively. IL-22-producing cells within ILC3 and Th17 were identified in (xi; e) and (xii; f), respectively.

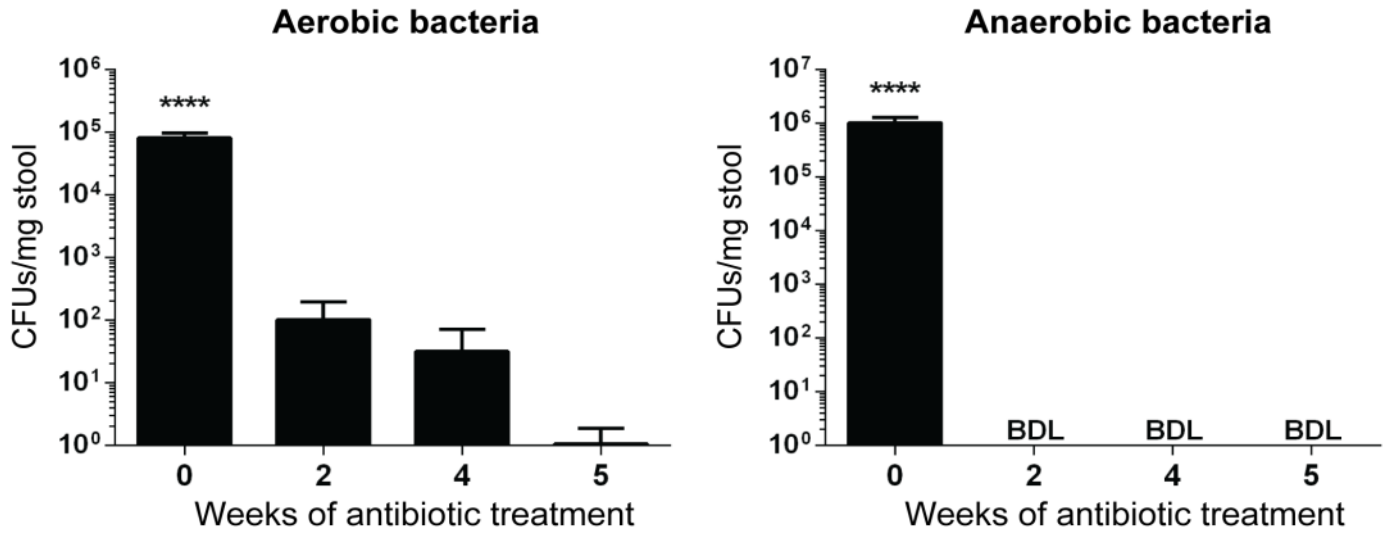

Supplemental Figure 2. Rate of microbiota depletion during antibiotic treatment, assessed by quantification of aerobic and anaerobic bacteria colony-forming units (CFU) in stool.

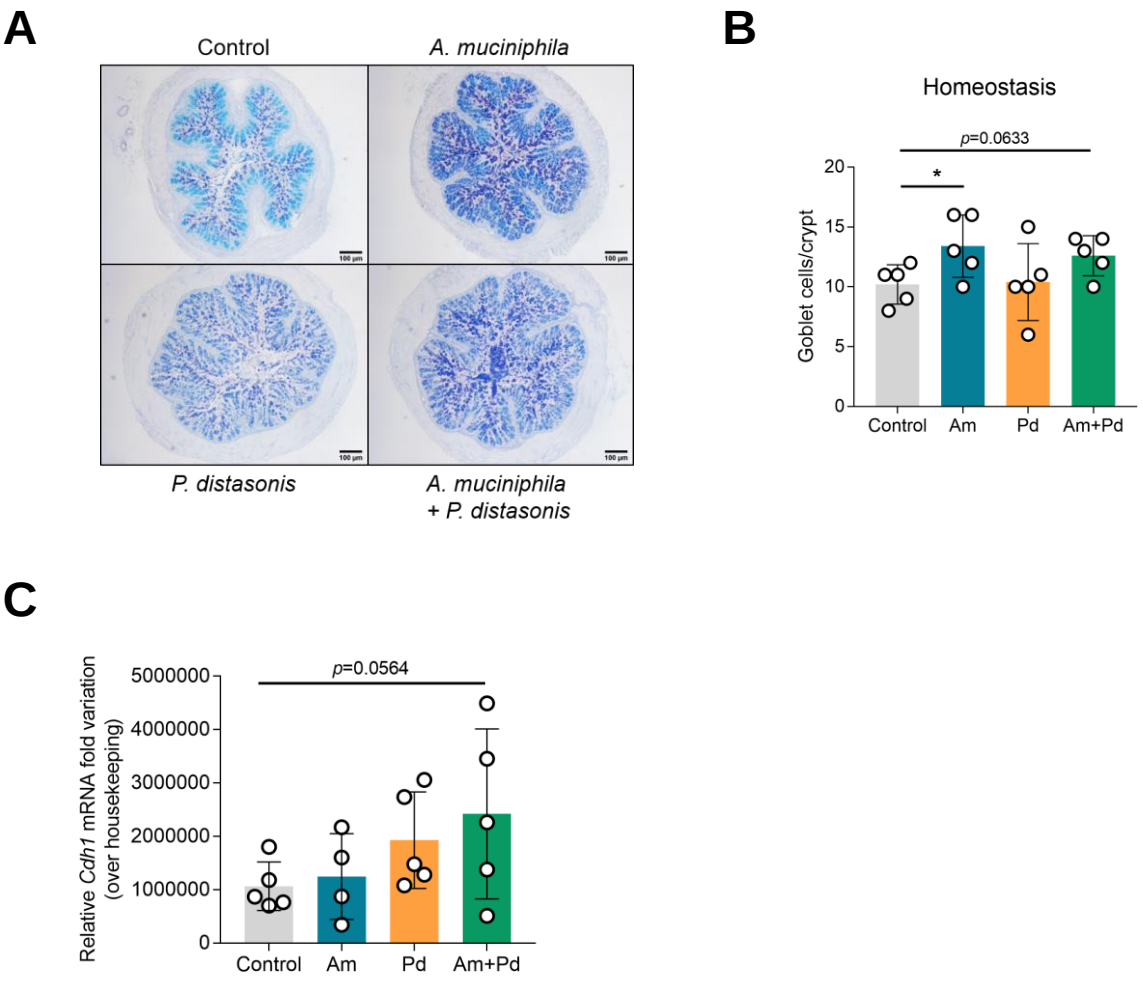

Supplemental Figure 3. (A-B) Quantification of goblet cell numbers per crypt in mice supplemented and non-supplemented, at homeostasis. **(C)** Expression of *Cdh1* in colonic tissue from mice supplemented and non-supplemented, at homeostasis, was analysed by qPCR. N=5 per group. Data is presented as mean ± standard deviation (SD). Statistically significant values are: *p < 0.05; **p < 0.01.